LEABHARLANN CHOLÁISTE NA TRÍONÓIDE, BAILE ÁTHA CLIATH | TRINITY COLLEGE LIBRARY DUBLIN
Ollscoil Átha Cliath | The University of Dublin

Terms and Conditions of Use of Digitised Theses from Trinity College Library Dublin

Copyright statement

All material supplied by Trinity College Library is protected by copyright (under the Copyright and Related Rights Act, 2000 as amended) and other relevant Intellectual Property Rights. By accessing and using a Digitised Thesis from Trinity College Library you acknowledge that all Intellectual Property Rights in any Works supplied are the sole and exclusive property of the copyright and/or other IPR holder. Specific copyright holders may not be explicitly identified. Use of materials from other sources within a thesis should not be construed as a claim over them.

A non-exclusive, non-transferable licence is hereby granted to those using or reproducing, in whole or in part, the material for valid purposes, providing the copyright owners are acknowledged using the normal conventions. Where specific permission to use material is required, this is identified and such permission must be sought from the copyright holder or agency cited.

Liability statement

By using a Digitised Thesis, I accept that Trinity College Dublin bears no legal responsibility for the accuracy, legality or comprehensiveness of materials contained within the thesis, and that Trinity College Dublin accepts no liability for indirect, consequential, or incidental, damages or losses arising from use of the thesis for whatever reason. Information located in a thesis may be subject to specific use constraints, details of which may not be explicitly described. It is the responsibility of potential and actual users to be aware of such constraints and to abide by them. By making use of material from a digitised thesis, you accept these copyright and disclaimer provisions. Where it is brought to the attention of Trinity College Library that there may be a breach of copyright or other restraint, it is the policy to withdraw or take down access to a thesis while the issue is being resolved.

Access Agreement

By using a Digitised Thesis from Trinity College Library you are bound by the following Terms & Conditions. Please read them carefully.

I have read and I understand the following statement: All material supplied via a Digitised Thesis from Trinity College Library is protected by copyright and other intellectual property rights, and duplication or sale of all or part of any of a thesis is not permitted, except that material may be duplicated by you for your research use or for educational purposes in electronic or print form providing the copyright owners are acknowledged using the normal conventions. You must obtain permission for any other use. Electronic or print copies may not be offered, whether for sale or otherwise to anyone. This copy has been supplied on the understanding that it is copyright material and that no quotation from the thesis may be published without proper acknowledgement.

Explorations of miRNA Expression in the Mammalian Retina

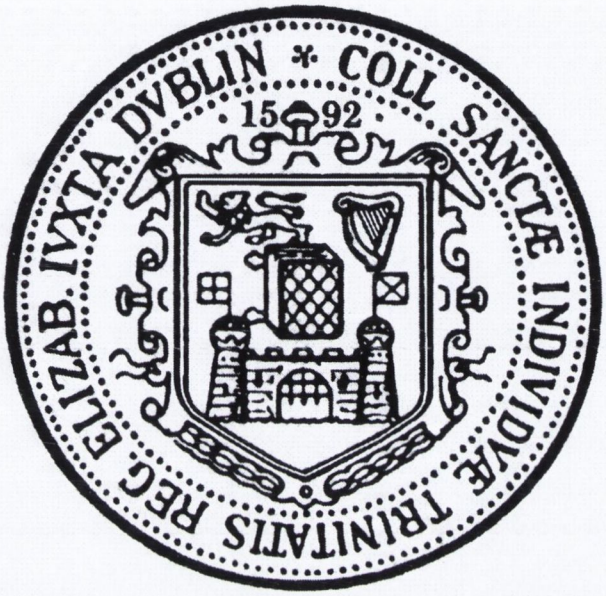

A thesis submitted to the University of Dublin for the Degree of Doctor of Philosophy

By

Carol Jane Loscher

April 2009

Under the supervision of Prof. Jane Farrar

Department of Genetics
Trinity College Dublin
Ireland

TRINITY COLLEGE
10 AUG 2009
LIBRARY DUBLIN
THOSIS
8856

Declaration

This thesis has not been previously submitted to this or any other university for the examination of a higher degree. The work presented here is entirely my own except where noted. This thesis may be made available for consultation within the university library. It may be photocopied or lent to other libraries for the purpose of consultation.

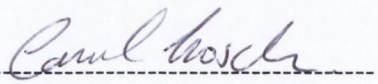

Carol Loscher

April 2009

Acknowledgements

Firstly, I would like to thank my supervisor Prof. Jane Farrar for granting me the opportunity to carry out my PhD with her, but most importantly for her guidance and encouragement which she continually offered, especially the supportive hot chocolates during the last few months. Similarly, I must also sincerely thank Dr. Arpad Palfi for his help in the lab and particularly his patience. Thanks must also go to all the members of the Ocular Genetics Unit, both past and present, who through their knowledge, support and laughter have made my time in the lab such an enjoyable and fruitful experience. In addition I also greatly appreciate the financial support granted to me by the Health Research Board under the Integrated PhD Neuroscience programme, directed by Prof. Marina Lynch.

Special and heartfelt thanks must also go to all the members of Room 3.14 in TCIN for giving me a home away from home; I couldn't have imagined the last 4 years without your friendship and streams of laughter; Wen for introducing me to wasabi peas and shredded dried pork, Gill for her tea, chats and sing-star superstar performances, and Sally for her humour and high spirits!

I would also like to give a special thanks to my parents, John and Moira for their untold love, tolerance and support, which they have given to me, not just during the duration of my PhD but for the all the times I have needed them over the years. My two sisters, Jen and Sofie, also deserve special praise, thank you. Last and by no means least, I would like to thank Andrew for his advice, hugs, and most of all his understanding which he has provided in bounds over the last 5 years.

Abstract

MicroRNAs (miRs) are an abundant class of non-coding RNAs which, for the most part were undiscovered until early this decade (Lagos-Quintana *et al.* 2001; Lee *et al.* 2001). Mature miR transcripts are small (~22 nucleotides) RNAs that control eukaryotic gene expression at the post-transcriptional level by interacting with target mRNAs, which either results in mRNA cleavage or translational repression (Bartel 2004). Tissue-specific expression of miRs is well documented, however, a clear understanding of the functions of the majority of miRs remains elusive. MiRs are known to participate in a wide range of developmental and physiological processes, and perturbed miR expression has been shown to occur in cancer and other diseases (Alvarez-Garcia *et al.* 2005; Bandres *et al.* 2006). This Ph.D. thesis describes the exploration of retinal miR expression and possible involvement of miRs in retinal disease, specifically in the mouse models of retinitis pigmentosa (RP). RP is a group of inherited retinal degenerations which leads to blindness typically by middle age, due to the loss of rod and cone photoreceptors which die by apoptosis. The primary genetic cause for many forms of RP have been identified.

Characterising the miR expression profile in the retina is essential to elucidate miR involvement in retinal-specific functions and Chapter 3 describes the examination of miR expression in the mouse retina by microarray analysis, in comparison to other brain and other tissues. Specifically a number of miRs are identified which are preferentially expressed in the retina, suggesting that these miRs may possibly be involved in regulating retinal-specific functions.

Given the emerging results from other fields of miR research, in which perturbed levels of miR expression were identified in disease states, including neuronal diseases (Kosik *et al.* 2005; Bilen *et al.* 2006), a key aim of the research undertaken for this Ph.D. study was to investigate if miRs are also altered in retinal disease, focusing on mouse models RP. Chapter 4 of this thesis describes miR expression in the retina of a rhodopsin-linked mouse model of RP carrying a rhodopsin mutation, the P347S mouse, using microarray and qPCR analysis. Significantly altered expression of four miRs was identified in the retina from the P347S RP model, specifically miR-1 and -133 expression was significantly increased in expression by approximately 3-fold while miR-96, -182 and -183 expression were decreased by up to 2-fold. The findings presented in Chapter 4 are expanded upon in Chapter 5, which examines if the alterations of miR expression observed in the P347S RP model, extend to other mouse models of RP. Notably these findings demonstrate that a common signature of miR expression is observed in a number of RP models independent of the causative RP gene, involving the specific upregulation of miR-1, -133 and -142, and a decrease in expression of miR-96, -182, and -183. Of note, the expression of these miRs specifically in rod photoreceptor cells is also detailed in Chapter 5, in an effort to eliminate any ambiguity which may exist regarding the altered cell composition of the degenerating retina. Interestingly the signature of miR expression that is observed in the retinas of RP mouse models can be attributed to specific alterations of miR

expression in rod photoreceptor cells. These findings are significant, and represent the first identification of altered miR expression in RP, and indeed any ocular disease.

While the photoreceptors of these models of RP undergo a moderately slow rate of degeneration, it was of interest to examine whether perturbed miR expression is also common to faster degenerating mouse models of RP such as the P23H mouse. Notably, as described in Chapter 6, the signature of miR expression was not observed in these faster degenerating RP models. The study highlights the rather limited utility of these mouse models in the context of exploration of miR profiles in retinal disease due to the rapid rate of photoreceptor degeneration in these animal models.

In order to examine the roles played by retinal miRs, and of the six miRs identified as differentially expressed in RP, an important starting point involves the use of bioinformatic tools to generate a list of miR targets, as detailed in Chapter 7. The incorporation of additional filtering steps to commonly used target prediction methods, was undertaken in an attempt to produce a robust list of biologically relevant targets. The target prediction findings presented in Chapter 7 provide the basis for future empirical validation of these targets *in vitro* and *in vivo*. Indeed the validation of miR targets is vital to gain an understanding of the retinal roles of miRs, which can be examined by overexpression and inhibition of retinal miRs *in vitro*. In Chapter 8 and 9 the design and construction of miR expression vectors is described, providing a means to overexpress miRs *in vitro*, and using non-viral delivery *in vivo*. The preliminary studies detailed in Chapter 8 and 9 demonstrate the ability to overexpress miRs both *in vitro* and *in vivo*, providing the ground-work for future experiments in which these constructs may be further explored, such as target validation, and retinal function of miRs.

In summary, this PhD thesis describes the evaluation of miR expression in the retina, and particularly in retinal disease using mouse models of RP. In addition, bioinformatic tools have been utilised to examine the potential targets that may be regulated by retinal miRs, some of which are altered in expression in disease states. In addition preliminary work has been undertaken to generate miR overexpression constructs and to evaluate these constructs *in vitro* and *in vivo,* which should provide the basis for the future detailed evaluation of miR overexpression *in vitro in cell culture* and *in vivo* in the mammalian retina.

Abbreviations

Autosomal dominant RP: adRP
Autosomal recessive RP: arRP
Base pair: bp
c. elegans : *Caenorhabditis elegans*
Chr: Chromosome
Cytomegalovirus: CMV
Digoxigenin: DIG
Double distilled H_2O: ddH_2O
Drosophila: *Drosophila melanogaster*
Dulbecco's modified Eagle medium: D-MEM
Electroretinogram : ERG
Enhanced green fluorescent protein : EGFP
Escherichia coli: E.coli
Exportin-5: Exp-5
Ganglion cell layer: GCL
Gram: g
High performance liquid chromatography: HPLC
In Situ Hybridisation: ISH
Inner nuclear layer: INL
Inner plexiform layer: IPL
Inner segment: IS
Leber congenital amaurosis: LCA
Litre: L
Microlitre: µl
microRNA: miR
MRE: miR recognition elements
Non-Coding RNAs: ncRNAs
Nucleotide: nt
Optical Density: OD
Outer nuclear layer: ONL
Outer plexiform layer : OPL
Outer segment: OS
Piwi-associated RNA: piRNA
Postnatal: P
Precursor-miRNA: pre-Mir
Primary miRNA: pri-Mir
Quantitative Reverse transcription PCR: qPCR
Retinal degeneration slow: RDS
Retinal pigment epithelium: RPE
Retinitis pigmentosa: RP
Rhodopsin (human): RHO
Rhodopsin (mouse): rho
RNA Interference: RNAi
RNA polymerase II: Pol II

Small interfering RNA: siRNA
Small temporal RNA: stRNA
Small nucleolar RNA: snoRNA
Standard Error of the Mean: S.E.M.

Table of Contents

	Page
Chapter 1: General Introduction	**1**
1.1 Introduction	**3**
1.2: Eye and Vision	**4**
1.2.1. The Retina	5
1.2.2 Photoreceptor cells	5
1.2.3. Phototransduction	6
1.3. Retinitis Pigmentosa	**7**
1.3.1 Symptoms and Genetics	8
1.3.2. Mechanisms of Photoreceptor cell death	9
1.3.3. Therapeutic strategies for the treatment of RP	13
1.4. Non-Coding RNAs (ncRNAs)	**15**
1.4.1. Discovery of microRNAs	16
1.4.2. Genomic Location of miRs	17
1.4.3. miR Biogenesis	18
1.4.4. MiRNA Effector Mechanism	21
1.5. Tissue Specific Expression of miRs	**25**
1.6. Development and Cell identity	**26**
1.7. Physiological and Pathophysiological Roles of miRs	**28**
1.8. Aim	**29**
Chapter 2: Materials and Methods	**41**
2.1: Materials Used	**43**
2.1.1. Buffers and Stock Solutions for Cloning	45
2.1.2: Buffers and stock solutions for mammalian cell culture experiments	46
2.1.3: Buffers and stock solutions for In Situ Hybridisation	47
2.1.4. Animals	49
2.1.5: Oligonucleotides Synthesis:	50
2.1.6: Cell lines	50

2.2 General Methods **50**
2.2.1. Restriction Enzyme Digests 50
2.2.2. Phenol/Chloroform Extraction of DNA 51
2.2.3. Ethanol Precipitation of DNA 51
2.2.4. Agrose Gel Electrophoresis and DNA extraction 51
2.2.5. Competent Cell Preparation of E. coli XL1B 52
2.2.6. Transformations 52
2.2.7 Plasmid DNA Mini-Preparations 53
2.2.8 Large-scale Plasmid Purification 53
2.2.9. Glycerol Stocks of Bacteria 54
2.2.10. Quantification of DNA and RNA 54
2.2.11. Capillary Sequencing 54
2.3. General RNA Techniques **56**
2.3.1 Ribonuclease (RNAase)-Free Conditions 56
2.3.2. RNA Extraction from Animal Tissues and Cultured Cells 56
2.3.3. Quantitative real-time RT-PCR (qPCR) 58
2.3.4. In Situ Hybridisation (ISH) 61
2.3.5. MicroRNA Microarray Expression Profiling 64
2.4. Mammalian Tissue Culture Techniques **68**
2.5. Fluorescent Activated Cell Sorter (FACS) analysis **70**
2.6. Database Resources **71**
2.7. Animal Tissue Collection **72**
2.8. Histology and Microscopy **73**
2.9. Immuno-histochemistry **73**
2.10. Statistical Analysis **74**

Chapter 3: Examination of miR Expression in the Retina **79**
3.1. Introduction **81**
3.2. Materials and Methods **83**
3.2.1. Experimental Animals 83
3.2.2. RNA Isolation 83

3.2.3. MiR Microarray Experiment 83
3.2.4. Micorarray Data Analysis 84
3.2.5. Quantitative Real-Time RT-PCR (qPCR) 84
3.2.6. *In Situ* Hybridisation (ISH) 85
3.2.7 Microscopy 85
3.2.8. Statistical Analysis 85
3.3. Results **87**
3.3.1 Microarray analysis of miR expression in wild type Retina 87
3.3.2. Validation of retinal miR Expression by qPCR 89
3.3.3. Spatial localisation of retinal miR expression 90
3.3.4. Summary 91
3.4. Discussion **93**
3.5. Conclusion **98**

Chapter 4: Examination of miR expression in the Retina of P347S-rhodopsin mouse model of RP **107**
4.1. Introduction **109**
4.2. Materials and Methods **111**
4.2.1. Experimental Animals 111
4.2.2. RNA Isolation 111
4.2.3. miR Microarray Experiments 111
4.2.4 Microarray Data Analysis 112
4.2.5. Quantitative Real-Time RT-PCR (qPCR) 112
4.2.6. Histology and Microscopy 113
4.2.7. Statistical Analysis 113
4.3. Results **115**
4.3.2: Retinal Histology of P347S RP model 115
4.3.2. Comparison of miR expression in wild type retinas by microarray analysis 116
4.3.3. Altered miR expression profile in P347S retina 116
4.3.4. Validation of Altered miR Expression by qPCR 117

4.3.5. miR cluster analysis 119
4.3.6. Summary 120
4.4. Discussion **121**
4.5. Conclusion **124**

Chapter 5: Exploration of Common Signature of Retinal Degeneration in mouse models of RP **135**

5.1. Introduction **137**
5.2. Materials and Methods **139**
5.2.1. Experimental Animals 139
5.2.2. RNA Extraction 139
5.2.3. Micorarray Experiment 139
5.2.4. Micorarray Data Analysis 140
5.2.5. FACS 140
5.2.6. Quantitative Real-Time RT-PCR (qPCR) 140
5.2.7. Histology and Microscopy 141
5.2.8. Immunocytochemistry Analysis 141
5.2.9. Statistical Analysis 141
5.3. Results **143**
5.3.1: Outer Nuclear Layer Thickness Analysis in rho- and rds-linked mouse models of RP 143
5.3.2. Microarray Analysis of miR expression in rho-linked RP mouse models 144
5.3.3. qPCR analysis of miR expression in rho- and rds-linked RP mouse models 145
5.3.4. Generation of RGFP expressing RP models 147
5.3.5. Histological analysis and FACS of retinas of RGFP+/- mouse models 147
5.3.6: qPCR of GFP-positive and GFP-negative cells from RGFP+/- mouse models 148

5.4 Discussion **151**

5.5 Conclusion **156**

Chapter 6: miR Expression in the Retina of Fast Degenerative Models of RP **169**

6.1. Introduction **171**

6.2. Materials and Methods **173**

6.2.1. Experimental Animals 173

6.2.2. RNA Extraction 173

6.2.3. Micorarray Experiment 173

6.2.4. Micorarray Data Analysis 174

6.2.5. Quantitative Real-Time RT-PCR (qPCR) 174

6.2.6. Statistical Analysis 174

6.3. Results **175**

6.3.1. Pro23His and *rd1* RP animal models 175

6.3.2. Genotyping P23H animals 175

6.3.3. Microarray analysis of miR expression in P5 P23H and rho-/- mutant models 176

6.3.4. qPCR analysis of miR signature in P23H and rho-/- whole-eyes at P5 178

6.3.5. qPCR analysis of miR signature in *rd1* retinas at P11 179

6.4. Discussion **181**

6.5. Conclusion **184**

Chapter 7: Target Prediction of Retinal miRs **193**

7.1. Introduction **195**

7.2. Materials and Methods **199**

7.2.1. Collection of retinal expressed genes 199

7.2.2. MiR Target Prediction 200

7.2.3 Filtering of Targets 202

7.2.4. MiR Accessibility Analysis (ΔG Analysis) 202

7.2.5 Comparison of targets predicted for miR clusters 203
7.3. Results **205**
7.3.1. miRanda target prediction for miR-1, -133, -96 and -183 205
7.3.2. miR Target Prediction using three prediction methods and ΔG Analysis 205
7.3.2. Common Targets predicted for clustered miRs using miRanda 207
7.4. Discussion **209**
7.5. Conclusion **216**

Chapter 8: Design and Construction of miR Expression Vectors and *In Vitro* Analysis **263**
8.1. Introduction **265**
8.2. Materials and Methods **269**
8.2.1. Vector Construction 269
8.2.2. DNA dsOligo Design 270
8.2.3. Vector Construction 271
8.2.4. Transfection of miR Constructs in HeLa cells 272
8.2.5. Quantitative real time RT-PCR 273
8.2.6. Statistical Analysis 274
8.3. Results **275**
8.3.1. miRNA Expression Vector Design 275
8.3.2. Expression of miR-constructs in HeLa cells 276
8.3.3. Analysis of PTK9 suppression by miR-1 277
8.4: Discussion **279**
8.5. Conclusion **282**

Chapter 9: Evaluation of miR expression Constructs *In Vivo* **297**
9.1. Introduction **299**
9.2. Materials and Methods **301**
9.2.1. Concentration of DNA constructs 301
9.2.2. Sub-retinal Injection and electroporation of miR constructs 301

9.2.3. Histology and Microscopy 302
9.2.4. miR In Situ Hybridisation 302
9.2.5. FACS Analysis 302
9.2.6. Statistical Analysis 303
9.3. Results **305**
9.3.1. Histology of retinas electroporated with miR-expression constructs 305
9.3.2 In-Situ Hybridisation of retinas electroporated with miR-expression constructs 305
9.3.3. FACS analysis of electroporated retinas and miR expression analysis by qPCR 306
9.4. Discussion **307**
9.5. Conclusion **311**

Chapter 10: General Discussion **319**

Bibliography **335**

Appendices **363**

Appendix 1 **365**
A.1.1. Primer Sequences 365
A.1.2. pcDNA6.2-EmGFP Construct 366
A.1.3. Human PTK 9 (Protein tyrosine kinase 9) mRNA transcript sequence 368

List of Figures

Page

Chapter 1

Figure 1.1: Basic Structure of the Eye 33

Figure 1.2: Retina and Visual Cortex 34

Figure 1.3: Retinal histology of a wild-type mouse retina at light microscope level 35

Figure 1.4: Schematic representation of a rod photoreceptor 36

Figure 1.5: Phototransduction cascade 37

Figure 1.6: Growth in miR Research 38

Figure 1.7: Model of miR biogenesis 39

Figure 1.8: Transcriptional variations of intronic and intergenic miRs 40

Figure 1.9: Model for Mirtonic miR Biogenesis Pathway 41

Table 1.1: List of causative genes of RP 42

Chapter 2

Figure 2.1: miR RT-PCR using stem-loop primer and TaqMan Probe 75

Figure 2.2: LOWESS Normalisation 76

Figure 2.3: Scatter plot of normalised Cy3 and Cy5 signals 77

Table 2.1: Worked Example of $\Delta\Delta C_T$ PCR analysis 78

Table 2.2: Hybridisation Temperature of In Situ Hybridisation Probe 79

Chapter 3

Figure 3.1: Hierarchical clustering of miRs in Retina, Brain and mouse Platform 99

Figure 3.2: Volcano plots of miR expression in wt retina versus brain & platform 100

Figure 3.3: Comparative expression of selected miRs 101

Figure 3.4: Comparative expression of selected miRs 102

Figure 3.5: qPCR Validation of relative expression of selected miRs 103

Figure 3.6: qPCR Validation of relative expression of selected miRs 104

Figure 3.7: miR ISH analysis in the mouse retina (*let-7*, miR-181a, and -182) 105

Figure 3.8: miR ISH analysis in the mouse retina (miR-183 and sense miR-159) 105

Table 3.1: miRs Expressed in the Retina 106

Chapter 4

Figure 4.1: Comparative histology of 1-month-old c57 and P347S retinas 127
Figure 4.2: Volcano plots of miR expression in P347S and wild-type retinas 128
Figure 4.3: Heat Map and Hierarchical clustering of miRs in c57 and P347S retina 129
Figure 4.4: Differentially expressed miRs between c57 versus P347S retinas 130
Figure 4.5: Differentially expressed miRs between c57 versus P347S retinas 131
Figure 4.6: Differentially expressed miRs between c57 versus P347S retinas 132
Figure 4.7: Differentially expressed miRs between c57 versus P347S retinas 133
Table 4.1: miR Cluster Analysis 134

Chapter 5

Figure 5.1: Retinal Histology of rho- and rds-linked RP mouse models 159
Figure 5.2: Volcano plots of miR expression in Rho-/-, R347 and wild-type retinas 160
Figure 5.3: Hierarchical clustering of miRs in 129 wild type and Rho-/- retina 161
Figure 5.4: Retinal miR signature in rho- and rds-linked RP mouse models 162
Figure 5.5: Retinal miR signature in rho- and rds-linked RP mouse models 163
Figure 5.6: MiR expression in the RGFP+/- Retina 164
Figure 5.7: Histological and FACS analysis of RGFP-Δ307 and -R347 retinas 165
Figure 5.8: Histological analysis of GFP-positive cells from RGFP retina 166
Figure 5.9: MiR expression signature in rod & non-rod cells of Δ307& R347 retinas 167
Figure 5.10: Comparative miR expression in rod vs non-rod cells in RGFP retinas 168

Chapter 6

Figure 6.1: Genotype of P23H animals 187
Figure 6.2: Volcano plots of miR expression in Rho-/- and P23H whole-eyes 188
Figure 6.3: Hierarchical clustering of miRNAs in Rho-/- and P23H whole-eyes 189

Figure 6.4: Relative miR Expression in Rho-/- and P23H whole-eyes 190
Figure 6.5: qPCR Validation of miR expression in Rho-/- and P23H whole-eyes 191
Figure 6.6: Relative expression of selected miRs in wt 129, wt C3H and *rd1* retinas 192

Chapter 7

Figure 7.1: Venn diagrams of miRanda-predicted targets for clustered miRs 218
Figure 7.2: Schematic representation of miR target prediction strategy 219
Table 7.1: Overview of retinal miR targets predicted by miRanda 220
Table 7.2: miRanda predicted Retinal Target Transcripts for miR-1, -133, -96 & -183 221
Table 7.3: Targets Predicted using miRanda, TargetScan and Pictar Algorithms 222
Table 7.4.A: Overlapping Target Predictions for miR-96 using miRanda, TargetScan and PicTar Algorithms 223
Table 7.4.B: Overlapping Target Predictions for miR-182 using miRanda, TargetScan and PicTar Algorithms 230
Table 7.4.C: Overlapping Target Predictions for miR-183 using miRanda, TargetScan and PicTar Algorithms 236
Table 7.5.A: Overlapping Target Predictions for miR-1 using miRanda, TargetScan and PicTar Algorithms 241
Table 7.5.B: Overlapping Target Predictions for miR-133 using miRanda, TargetScan and PicTar Algorithms 246
Table 7.5.C: Overlapping Target Predictions for miR-142 using miRanda, TargetScan and PicTar Algorithms 250
Table 7.6: Summary of *in silico* target predictions for miR-96,-182, -183 and miR-1, 133, and -142 using miRanda and PicTar algorithms 252
Table 7.7.A: Common targets predicted for miR-1 and –133 253
Table 7.7.B: Common targets predicted for miR-1 and –142 254
Table 7.7.C: Common targets predicted for miR-133 and –142 255
Table 7.8.A: Common targets predicted for miR-96 and -182 256

Table 7.8.B: Common targets predicted for miR-96 and –183 258
Table 7.8.C: Common targets predicted for miR-183 and –182 260

Chapter 8

Figure 8.1: Overview of miR Expression Plasmid Construction 284
Figure 8.2: Overview of miR vector Design (pcDNA-6.2-EmGFP-miR-1-1 vector) 285
Figure 8.3: MiR Oligo Design 286
Figure 8.4: Transfection of miRNA Constructs in HeLa cells 287
Figure 8.5: Overexpression of pcDNA-miR constructs in HeLa cells 288
Figure 8.6: Endogenous miR expression in HeLa cells 289
Figure 8.7: Overview of design of pcDNA-6.2-EmGFP-miR-182 vector 290
Figure 8.8: Overview of design of pcDNA-6.2-EmGFP-miR-182 shRNA vector 291
Figure 8.9: Overview of design of pcDNA-6.2-EmGFP-miR-29c vector 292
Figure 8.10: Overview of design of pcDNA-6.2-EmGFP-miR-29c shRNA vector 293
Figure 8.11: Overexpression of pcDNA-miR constructs in HeLa cells 294
Figure 8.12: PTK9 Suppression in HeLa cells 295
Figure 8.13: PTK9 (TWF1) Target Prediction by TargetSan 296

Chapter 9

Figure 9.1: Histological sections of retinas electroporated with miRNA constructs 313
Figure 9.2: miRNA In Situ Hybridisation of electroporated retinas 314
Figure 9.3: FACS Analysis of Electroporated Retinas 315
Figure 9.4: qPCR analysis of miR expression 316
Figure 9.5: Electroporation Procedure and Apparatus for *in vivo* electroporation 317

Chapter 1

Introduction

1.1. Introduction

Retinitis Pigmentosa (RP) is a group of hereditary retinal degenerative diseases, that affects an estimated 1.5 million patients worldwide (Weleber and Gregory-Evans 2001). The disease results in photoreceptor death, initially resulting in night blindness followed by progressive loss of colour vision. While no current therapies exist, great advances have been made in the last two decades including identification of the causative mutant genes for RP and the development of novel therapeutic strategies, including gene therapy aiming to correct the initial genetic defect and thereby hopefully slow disease progression.

In recent years microRNAs (miRs), an abundant group of small endogenous non-coding RNAs have been identified, predicted to constitute between 1-4% of genes in the human genome and negatively regulating gene expression in animals, plants and viruses (Lai et al. 2003; Esquela-Kerscher and Slack 2006). For the most part, miRs were undiscovered until early this decade (Lagos-Quintana et al. 2001; Lee and Ambros 2001), however since their discovery the field has expanded dramatically facilitated by advances in RNA Interference (RNAi) research, proving to be a vibrant and exciting research area of untold potential. MiRs are known to participate in a wide range of developmental and physiological pathways, and perturbed expression has been shown to occur in cancer and other diseases (Alvarez-Garcia and Miska 2005; Bandres et al. 2006). There has been a great deal of progress made in the identification of novel miRs and in the understanding of both miR biogenesis and effector functions. Indeed miRs are predicted to target 30% or more of all animal protein coding genes (Brennecke et al. 2005; Grun et al. 2005; Krek et al. 2005; Lewis et al. 2005) and understanding the roles of these miRs in physiological states is therefore vital. Additionally, a key issue in miR research is to understand the involvement of miRs in disease, undeniably offering a vast opportunity for the future development of novel therapeutic strategies.

At the outset of this PhD thesis very little information was attainable relating to miR expression in the retina, or indeed in the eye. However studies identifying novel miRs and a number of global miR profiling studies suggested that subsets of miRs were discretely expressed in particular tissues, and that related tissues had similar miR

profiles compared to those that were functionally distinct (Lagos-Quintana et al. 2002; Babak et al. 2004; Liu et al. 2004; Sempere et al. 2004). As this clearly indicated that miRs could mediate discrete organ/tissue-specific functions, it was of immense interest to characterise miR expression in the retina. Fascinating reports were also emerging depicting the involvement of miRs in cancer and other diseases (Wienholds et al. 2005), which prompted the examination of altered retinal expression of miRs in the diseased RP retina. Although the main causative genes of inherited RP are known, miRs could potentially participate in mechanisms mediating or altering the disease process, offering primarily a greater understanding of the disease process and potentially a therapeutic strategy for treating the condition.

1.2. Eye and Vision

Sight, the ability to perceive and interpret light, is one of the most precious human senses, fundamental to our perception of colour and objects in three-dimensional space, while also impacting tremendously on our behaviour, mood and alertness. The nature and complexity of vision perception has been a source of intrigue for scientists for hundreds of years and in the 17th century the role of the retina in the detection of light was realized, not the cornea as was previously thought. An unlikely pioneer of microbiology Anthony von Leeuwenhoek, in 1675 observed that "soft globules" present at the back of the eye were involved in the reception of light, later confirmed in 1835 by Gottfired Treviranous, a comparative biologist, who noted that "cylinders" were present in the retinas of birds, animals, amphibians and fish. It wasn't until the mid 19th century that Muller and Schultze distinguished between rods and cone photoreceptors, their outer and inner segments and defined the layers of the retina (Finger 2001).

These seminal discoveries, along with further anatomical findings and advances in optics, paved the way for the current understanding of vision; the focusing of light by the lens onto the retina followed by the stimulation of photoreceptor neurons that signal through retinal neurons and the optic nerve, via the thalamus, to the visual cortex where images are perceived. (Figure 1.1 and 1.2)

1.2.1. The Retina

As correctly identified by Leeuwenhoek and Treviranous, the photoreceptors are fundamental to vision, by means of detecting the presence of photons reaching the retina and translating these signals into electrical messages required for perception. The retina is an outgrowth of the diencephalon, consisting of the neural retina and retinal pigment epithelium (RPE), and as such many similarities between the eye and the brain exist. Indeed the structure of the neural retina, which consists of discrete layers (Figure 1.3) reflects that of other sensory organs by which a stimulus is perceived by a specialized cell type, which synapse onto first and second order neurons, prior to transmission to the brain. The highly specialized photoreceptor neurons respond to light, and comprise the outer segment (OS), inner segment (IS) and outer nuclear layer (ONL) of the retina (Figure 1.3). The photoreceptor neurons synapse in the outer plexiform layer (OPL) with bipolar and horizontal cells, the nuclei of which are located in the inner nuclear layer (INL), and the bipolar cells conduct visual information through the INL and project into the second synaptic zone, the inner plexiform layer (IPL), which terminates on amacrine and ganglion cells. The ganglion cell layer (GCL) contains the ganglion cell nuclei, whose axons leave the eye as the optic nerve and transmit signals via the thalamus, to the visual cortex (Figure 1.2). The RPE is the outermost layer and has important functions that are vital for photoreceptor survival, including phagocytosis of outermost photoreceptor disks and regeneration of visual pigment, while fundamentally acting as a protective barrier from the choroidal circulation supplying the outer retina (Davson 1980).

1.2.2 Photoreceptor cells

Vertebrates depend on photoreceptors for vision, and in humans classically two types of photoreceptors exist, rods and cones, that are specialized for monochromatic vision in low light (scotopic vision) and trichromatic vision in daylight (photopic vision) respectively (Newell 1996; Fu and Yau 2007). The rod photoreceptors are extremely sensitive to light and can produce electrical responses to single photons, conversely cones are much less sensitive, but are far superior to rods, in the ability to resolve fine spatial detail (acuity), owing to the high density of cones in the fovea, and a lower degree of convergence on ganglion cells (Figure 1.1). Rods comprise about

95% of photoreceptors cells (~120 million cells) of the human retina with cones accounting for the remainder (Curcio et al. 1990; Applebury et al. 2000). The distribution of cones and rods differ throughout the retina, cones are predominantly located in the central region of the retina, while rods are dispersed in the peripheral retina. Recently, a photosensitive subtype of ganglion cells was identified, which unlike other ganglion cells depolarize in response to light, independent of rod or cone activation, and are currently thought to regulate circadian rhythms (Berson et al. 2002).

Both rods and cones share the same basic structure (Figure 1.4), however differences in size and shape exist. Each photoreceptor can be divided into five main parts consisting of: 1) an outer segment (OS) which contains hundreds of flattened membranous disks of which the visual pigment is the main protein constituent, 2) a connecting cilium required for intracellular transport of proteins products to the OS, and 3) an inner segment (IS) containing the mitochondria and organelles required for protein synthesis, 4) the cell body of the photoreceptor, containing the nucleus and 5) the synaptic terminal (Figure 1.4.).

1.2.3. Phototransduction

The mechanism, by which rod and cone photoreceptors mediate a nerve impulse in response to the absorption of light, is called phototransduction. These mechanisms have been studied for over 130 years, starting with the discovery of the rod pigment, rhodopsin (Luo et al. 2008). Rhodopsin is the most highly expressed protein in rod photoreceptors, accounting for 80% of their outer segment disk membranes and is replaced every 10 days (Nathans 1992; Briscoe et al. 2004). Indeed rhodopsin is the only visual pigment in rod photoreceptors, while 3 types of cones, each containing different visual pigments (S-opsin; L-opsin; M-opsin), mediate colour vision in humans based on the different wavelength of light absorbed by each pigment. Both rod and cone pigments are composed of an opsin (G-protein-coupled receptor (GPCR)) and a chromophore 11-cis-retinal, a vitamin-A derivative (Molday 1998).

Light striking the retina (Figure 1.5) activates Rhodopsin (R) by causing isomerisation of 11-*cis*-retinal to all-*trans*-retinal. The activated rhodopsin (R*) triggers the GDP/GTP exchange of the protein transducin (T), and in turn the activated

transducin (T*) activates phosphodiesterase (PDE). This results in the hydrolysis of cyclic guanosine monphospate (cGMP), and the closure of cGMP-gated cation channels (Na^+/Ca^{2+}), resulting in hyperpolarisation and lessening glutamate release at the photoreceptor synapse. The reaction is terminated by a succession of reactions, initiating with the deactivation of rhodopsin by rhodopsin kinase. This leads to the restoration of cytoplasmic cGMP levels, cGMP-gated channels reopen, and the photoreceptor returns to a depolarized state with a steady state release of glutamate. The all-*trans*-retinal chromophores are recycled in the RPE and returned to combine with the rod-opsin as 11-*cis*-retinal, reforming rhodopsin (Fu and Yau 2007; Shichida and Morizumi 2007; Luo et al. 2008).

1.3. Retinitis Pigmentosa

As the retina plays such a significant role in vision, it is undeniable that retinal disease, while not life threatening, has a severe and detrimental impact on a patient's life. Retinal dystrophies are a heterogeneous group of diseases involving retinal degeneration that leads to either partial or complete blindness. Retinitis Pigmentosa (RP) is one such disease affecting an estimated 1.5 million patients worldwide (Weleber and Gregory-Evans 2001), and is the leading cause of visual handicap among working populations in developed countries.

Our understanding of RP, the cause and the pathological mechanisms, have greatly advanced since Donders first coined the term in 1855. Even before the first RP gene was mapped in 1984 (Bhattacharya et al. 1984), it was evident that the disease was heterogeneous displaying a wide variation in severity, age of onset, mode of inheritance and phenotype. Since then great advances have been made, stimulated by the identification of causative genetic mutations and aided significantly by both technological advances in molecular biology and our knowledge of the human genome.

1.3.1 Symptoms and Genetics

The most common symptoms of RP patients are initially night blindness and progressive visual field loss resulting in blindness. The rate of disease progression is variable, somewhat dependent on the age of onset and the severity of RP. Primary RP can be categorized into three main subgroups, 1) rod-cone degenerations, in which diffuse degeneration of rod photoreceptors initially occurs followed by cone degeneration, 2) cone-rod degenerations which display an early loss of cone-mediated central vision prior to rod loss and 3) congenital onset RP (Phelan and Bok 2000). There are however other secondary RP diseases where other organs are affected, i.e. Usher's syndrome, and Bardet-Biedl syndrome.

The rod-cone degenerations are the most common forms of RP, however clinical features can vary between patients and even among family members carrying the same mutation (Kalloniatis and Fletcher 2004). Typically the first symptom of RP is night blindness that is usually noticeable during childhood. Enchantingly the first description of night blindness by Dr. Peter Parham in 1684 provides a genuine sense of the experience of RP sufferers (Winstanley 2001):

> ..the patient "*saw acutely and strenuously by day and was just like a post when sun set. When twilight came on he was as blind as a beetle, sees nothing, runs against gates, posts, rails (anything either higher, lower, or level to his eyes). In doors he tumbles over stools and runs his head against doors.*" – Dr. Peter Parham, Norwich, 1684

However undoubtedly the greatest impact on a patient's vision is the progressive loss of mid-peripheral visual fields, which eventually leads to a loss of central vision and complete blindness typically in the 4th or 5th decade.

These symptoms correspond with ophthalmoscopic findings, which mainly include abnormal pigmentation as the disease name suggests, as pigment is deposited following photoreceptor cell death. Narrowing of the retinal arterioles occurs, and the characteristic "bone spicule" appearance is observed, due to deposition of pigment in the walls of sclerosed retinal vessels. In advanced cases the optic nerve may also appear waxy and pale and the central retina atrophied (Heckenlively 1988).

RP is a genetically heterogeneous disease, which can be inherited in an autosomal dominant, recessive, X-linked recessive, digenic or mitochondrial mode, and currently mutations in approximately 40 genes are implicated in disease pathology (RetNet). The functions of the proteins encoded by these genes include structural and cytoskeletal proteins, transcription factors, splicing factors, and proteins involved in vitamin A metabolism (Table 1.1). Additionally, the causative mutated genes often encode proteins involved in phototransduction, including rhodopsin (McWilliam et al. 1989; Farrar et al. 1990), phosphodiestease (Huang et al. 1995), and a cGMP-gated channel (Dryja et al. 1995). Rhodopsin was the first gene implicated in autosomal dominant RP (adRP) and accounts for ~30-40% of adRP cases with up to 100 mutations identified in the rhodopsin gene to date (RetNet). RDS-peripherin is another gene frequently mutated in RP accounting for 5% of adRP cases, which encodes a tetraspanin glycoprotein involved in maintaining structure integrity of the rod outer segments (Farrar et al. 1991; Farrar et al. 1991; Farjo and Naash 2006; RetNet). RDS localises to the rim periphery of the photoreceptor outer segments, and by complexing with ROM-1, a homolog of RDS, plays a role in disk membrane formation during rod outer segment morphogenesis (Farjo and Naash 2006). Mutations in this protein can also cause macular degeneration, and other retinal dystrophies (Farjo and Naash 2006). Interestingly other cases of adRP involve mutations in genes that are ubiquitously expressed, but only retinal symptoms are observed. This includes the gene IMPDH1, which encodes inosine monophosphate dehydrogenase type 1 (Bowne et al. 2002; Kennan et al. 2002), that catalyzes a key step in guanine nucleotide biosynthesis (Tam et al. 2008), and also genes encoding pre-mRNA splicing factors (PRPF31 (Vithana et al. 2001; Sullivan et al. 2006), PRPF3 (Chakarova et al. 2002), PRPF8 (McKie et al. 2001). While great progress has been made in characterizing RP genes, a number of genes implicated in RP disease remain to be identified. For a comprehensive review of retina dystrophies and the genes involved refer to the RetNet database (RetNet).

1.3.2. Mechanisms of Photoreceptor cell death

Photoreceptor degeneration in human retinal dystrophies and related animal models, suggest that photoreceptors die by a final common pathway, apoptosis (Chang et al. 1993; Portera-Cailliau et al. 1994). Apoptosis is a regulated mode of cell death

that is essential for normal development and tissue homeostasis (Jacobson et al. 1997; Danial and Korsmeyer 2004), but abnormal regulation can contribute to disease, most prominently cancer (Hanahan and Weinberg 2000; Ghobrial et al. 2005), neurological diseases (Yuan and Yankner 2000), as well as retinal degeneration (Chang et al. 1993; Yuan et al. 2005). In RP the cellular effect of genetic mutations and environmental stressors can cause oxidative stress, for example, the rate of retinal degeneration in some dystrophies accelerates upon exposure to light (Organisciak et al. 2003; Kennan et al. 2005). Together with altered photoreceptor metabolism, these stressors can induce caspase-dependent and caspase-independent apoptosis (Thornberry 1998; Susin et al. 1999; Sanges et al. 2006; Marigo 2007). However the pathological mechanisms, stemming from the initial genetic mutation to the activation of apoptosis, are not well understood, but are likely to vary depending on the role of the mutated protein.

As rhodopsin mutations account for up to 30-40% of adRP cases, and 8-10% of all RP cases in the United States (Berson 1996; RetNet), understanding the mechanisms by which cell death is initiated has been a major focus of research (Briscoe, et al 2004). The dominance in rhodopsin-linked adRP, could in principle be due to dominant-negative, loss of function or gain-of-function mutations (Wilson and Wensel 2003), however as the heterozygous rhodopsin-knockout mouse does not display severe photoreceptor degeneration, loss-of-function mutations alone are not likely to cause adRP (Humphries et al. 1997). Rhodopsin-linked RP can be classified into two main groups based on the consequence of the rhodopsin mutations; this categorization in principle can be applied to other mutations causing RP (Mendes, 2004). A small number of rhodopsin-mutants cause the rhodopsin to fold correctly but other rhodopsin-mutants display defects in transport to the rod outer segment (Class I), or fold incorrectly and are accumulated abnormally in the endoplasmic reticulum (Class II) (Mendes et al. 2005).

An example of a class I mutants is the proline-347-serine (P347S; (Dryja et al. 1990)) mutation in the carboxyl terminus of rhodopsin, which alters the post-Golgi trafficking of rhodopsin to the developing disc membranes (Sung et al. 1994; Li et al. 1996; Deretic et al. 1998). Rhodopsin localises to the rod outer segments, and the mutation does not affect the response of rhodopsin to light, efficiently binding to 11-cis retinal to form active rhodopsin. Indeed in the early phases of disease the P347S mouse model displays relatively normal electroretinograms (ERGs) and no

accumulation of mutant rhodopsin at the site of synthesis and processing, however shortened outer segment discs and accumulation of rhodopsin-containing vesicles is evident near the connecting cilium (Li et al. 1996). Rhodopsin is normally transported in post-Golgi vesicles to the apical section of the inner segment prior to transport through the cilium to form new disc membranes. Mutations in the C-terminal of rhodopsin impair post-Golgi transport during rod outer segment morphogenesis (Deretic et al. 1998; Deretic et al. 2005) resulting in extracellular accumulation of rhodopsin-containing vesicles. It is thought that this process accounts for the shortened rod outer segments in a mouse model of the disease (Li et al. 1996), due to the loss of rhodopsin to the extracellular space or congestion of the machinery required for efficient rhodopsin synthesis and transport. Perturbed rhodopsin transport in P347S rhodopsin-mutants eventually leads to initiation of photoreceptor death (Li et al. 1996).

However the majority of rhodopsin mutations fall into the class II category of mutations, which results in the misfolding of rhodopsin protein. Misfolded rhodopsin is not always capable of binding to 11-cis retinal, and may be inefficiently transported to the rod OS membrane disks, accumulating in the endoplasmic reticulum (ER) (Sung et al. 1994; Illing et al. 2002; Mendes et al. 2005). The ER organelle takes part in the processing of proteins, calcium homeostasis and persistent ER stress can lead to the activation of cell death (Baumann and Walz 2001). The proline-23-histidine (P23H) rhodopsin mutation is an example of a class II mutation, which is the most common mutation causing RP in the United States (Dryja et al. 1990). The mechanism of photoreceptor death is incompletely understood however in culture, mutant opsins are prone to misfolding and aggregation. It is thought that mutant opsins are retained in the ER, as misfolding can result in the inefficient transport of these proteins to the plasma membrane. The accumulation of misfolded protein and retention of protein in the ER is likely to induce ER stress that results in the activation of the unfolded-protein response (UPR), a cellular stress response that attempts to up-regulate the cells capacity to fold proteins (Rutkowski and Kaufman 2004). This system is activated in tandem with ER-associated protein degradation (ERAD) in response to misfolded proteins, which are ubiquitinated and transported out of the ER where they are degraded by the proteasome, a protein degrading complex (McCracken and Brodsky 2000). UPR and ERAD cooperate together to eliminate misfolded proteins from the ER, however if the system becomes overwhelmed, protein aggregation occurs resulting in further

cytotoxicity and initiating a cascade that results in apoptosis. Indeed protein aggregation (Bence et al. 2001) and P23H rhodopsin expression in HEK 293 cells (Illing et al. 2002) have been shown to impair the function of this pathway and may potentially have a dominant negative effect by interfering with the normal processing of rhodopsin. Photoreceptor apoptosis is also observed in the P23H *Drosophila melanogaster (drosophila)* model, which demonstrates that aggregation of mutant rhodopsin in the ER activates URP associated MAPK kinases, p38 and JNK (Galy et al. 2005). Indeed the neuronal accumulation and aggregation of ubiquitinylated proteins in inclusion bodies, is a hallmark of most neurodegenerative diseases, suggestive of a common pathway in neuronal degeneration (Yuan and Yankner 2000; Soto and Estrada 2008; Winderickx et al. 2008).

As stated above, mutations in many genes other than rhodopsin can cause RP (Table 1.1). For example, other non-rhodopsin genetic mutations that result in RP are those in the RDS and PDEβ genes. The RDS (retinal degeneration slow) gene is an important structural protein involved in rod outer segment morphogenesis, and mutations implicated in RP appear to disturb rod outer segment formation resulting in shorter outer segments, which ends in both rod and cone photoreceptor death. The exact mechanism by which the mutations cause photoreceptor cell death is unknown however, animal studies suggest abnormalities in photoreceptor energy metabolism and intercellular interactions can lead to the accumulation of lipofuscin, a byproduct of RPE phagocytosis and a biomarker for cellular aging and oxidative stress (Delori et al. 1995) (Boon et al. 2008). The *RD1* form of RP results from a mutation in the phosphodiesterase PDEβ, and causes autosomal recessive RP. The PDEβ mutation encodes a non-functional β-subunit of the PDE enzyme that is critically involved in phototransduction. Curiously, a spontaneous mouse model "*rd*" was discovered by Keeler in 1924, who had identified mice without rods, termed "rodless (*r*)" (Keeler 1924). Keeler's entire mouse stock was destroyed in 1939, and any other stocks that carried the mutant allele were also likely lost by the end of WWII. Rodless mice displaying similar retinal histology to those identified by Keeler, were later caught in Switzerland in 1951. These mice were termed "retinal degeneration (*rd*)" and for many decades it was not know whether the mice identified by Keeler (*r*) was equivalent to the "*rd*" mice. However, endearingly this question was eventually laid to rest in 1993 by sequence analysis of DNA extracted from 70-year-old histological

sections and matching mutations in the PDEβ gene were identified in the "*r*" and "*rd*" mice (Pittler et al. 1993). Interestingly, it was only after the mutation of PDEβ had been identified in the spontaneous *rd1* mouse that PDEβ mutations were identified in human RP suffers. Homozygous *rd1* mice develop rods that then undergo rapid degeneration as early as postnatal day 10 (Komeima et al. 2007) however, the mechanism that leads to this degeneration is not fully established. Nevertheless it is thought that cell death may occur as a result of permanently raised cGMP levels, which could disrupt the electrochemical gradient of the photoreceptor cell resulting in raised intracellular calcium levels. Indeed photoreceptor apoptosis in *rd1* mice was demonstrated to be calcium-dependant, involving caspase-12 and apoptosis inducing factor (AIF) (Doonan et al. 2005; Sanges et al. 2006) and recently ER stress mediated apoptosis has been implicated in *rd1* mouse photoreceptors (Yang et al. 2007). Clearly, mutations in many different genes can lead to photoreceptor degeneration which clinically falls under the umbrella term RP (Table 1.1). The possible modes of action of some of these mutations have been discussed here however, it is clear that for many mutations the precise mode of action remains elusive.

1.3.3. Therapeutic strategies for the treatment of RP

Currently there are no adequate therapies for the treatment of RP, however remarkable advances have been made in recent years, including the publication of results from three individual human clinical trials, employing gene therapy to treat the rare form of RP, Leber's Congenital Amaurosis (LCA) (Bainbridge and Ali 2008; Hauswirth et al. 2008; Maguire et al. 2008). Impaired vision of an LCA suffer occurs from birth, and can be caused by a number of mutations in various genes, one of which is the RPE65 gene. Work by Jene Bennett, and colleagues at the Scheie Eye Institute in the University of Pennsylvania, delivered a replacement RPE65 transgene sub-retinally using a recombinant adeno-associated virus (AAV). The initial results from this trial and two others by Robin Ali and William Hauswirth demonstrate similar findings, namely a modest improvement of vision in dim light, and most importantly no adverse effects of AAV therapy were observed (Bainbridge and Ali 2008; Hauswirth et al. 2008; Maguire et al. 2008). Given the childhood onset of LCA, further trials aim to treat younger patients who may hopefully derive the greatest benefit from this therapy.

The findings from these clinical trials are extremely exciting and represent the pinnacle of ocular gene-therapy, accounting for in excess of 20 years research and opening up opportunities for gene therapeutic approaches for additional forms of RP, and indeed other retinal disorders.

The strategy employed in this study involves the delivery of a functional replacement gene, which may be applied to other autosomal recessive mutations such as RD1 (PDEβ), however other strategies are required for autosomal dominant diseases. Currently a suppression-replacement strategy is being investigated to treat rhodopsin-linked RP, in which the expression of rhodopsin is suppressed using RNA interference (RNAi) and a replacement transgene is introduced, which is refractory to RNAi. This cleverly overcomes the heterogeneity that exists in rhodopsin mutations and recent *in vivo* studies in mice have demonstrated its potential (O'Reilly et al. 2007). Separate to gene therapy, other strategies are currently under investigation to decrease the rate of photoreceptor cell loss including the delivery of antioxidants (Komeima et al. 2007), neurotrophic factors (Thanos and Emerich 2005; Komeima et al. 2006; MacDonald et al. 2007) and targeting apoptotic mechanisms (Doonan et al. 2005; Marigo 2007).

Animal models of human disease are of great benefit to further our understanding of retinal function in health and disease, crucial for the generation of novel treatments (Chader 2002). There are several naturally occurring models for recessive RP, including the retinal degeneration slow (*rds*; (Sanyal et al. 1980)) retinal degeneration (*rd*1; (Pittler and Baehr 1991)) mouse models that have facilitated the identification of causative mutations in humans. Aided by advances in genetic engineering technology, gene targeting has been used to generate transgenic mouse models of adRP, including for example a model carrying a single base pair deletion at codon 307 of the rds gene (Δ307) (McNally et al. 2002). Likewise rhodopsin mutations Pro347Ser (Li et al. 1996) and Pro23His (Olsson et al. 1992) have been used to generate rodent models of RP. Indeed for some forms of RP larger animal models are available, including naturally occurring mutations in chicken (Burt et al. 2003), cat (Narfstrom and Nilsson 1987) and dog (Aquirre et al. 1978; Aguirre et al. 1998), and the transgenic pig RP model (Petters et al. 1997). The utilisation of animal models in research studies provides an invaluable tool for elucidating the mechanisms of disease pathology and gaining a full appreciation of altered cellular responses during disease.

In addition animal models can be used for pre-clinical testing of therapeutics, for example the safety and therapeutic response of the LCA gene therapy trialed in humans, were initially tested in the Briard dog RPE65 LCA animal model (Le Meur et al. 2007).

As clearly outlined, huge gaps exist in our understanding of the disease process, from gene mutation to photoreceptor cell death, and extensive studies are required to complete this picture. Indeed devoid of this knowledge, the most efficient and beneficial therapeutic targets may not be realized. It is in this light that the involvement of miRs in retinal disease is fascinating, and in view of recent findings that link miRs to neurodegenerative diseases (Bilen et al. 2006; Stark et al. 2008), investigation of miR involvement in the retina and in RP warrants attention.

1.4. Non-Coding RNAs (ncRNAs)

Recently the focus of genetic research has shifted from the function of protein-coding DNA, to non-coding DNA initially termed "junk DNA". These areas of the genome often transcribe non-coding RNAs (ncRNAs), which appear to significantly regulate the output of the mammalian genome (Mattick and Makunin 2005). There are numerous types of ncRNAs, from long ncRNAs (Ponjavic et al. 2007), to small ncRNAs such as microRNAs (miRs), piwi-intearcting RNAs (piRNAs), short interfering RNAs (siRNAs), small nucleolar RNAs (snoRNAs) and small double-stranded RNAs (Doi et al. 2003; Carninci et al. 2005; Girard et al. 2006; Mattick and Makunin 2006; Ponjavic et al. 2007). siRNAs, miRNAs, and piRNAs all are termed small regulatory RNAs and appear to predominantly suppress gene expression by post-transcriptional silencing (Doi et al. 2003; Bartel 2004; Aravin et al. 2006; Lau et al. 2006). The precise mechanism in which ncRNAs affect gene expression is currently unknown, however emerging studies point towards their role as vital regulators of cellular processes (Stefani and Slack 2008), in addition to potential roles in disease (Alvarez-Garcia and Miska 2005). As the studies undertaken in this thesis focus the involvement of miRs in the retina, miRs are discussed below in relation to their biosynthesis, effector mechanisms and function.

1.4.1. Discovery of microRNAs

Initially miRs were identified as heterochronic genes, genes that controlled the temporal dimension of development in animals (Lee et al. 1993; Lau et al. 2001). Interestingly the initial discovery of the role played by miRs emanated from a novel finding where mutations in the heterochronic genes, lin-14, lin-28, and lin-29, were recognised to alter the timing of vulva precursor cell division in the nematode *Caenorhabditis elegans* (*c.elegans*) (Ambros and Horvitz 1984). In 1993 the gene lin-4 was successfully cloned and sequenced by a group of colleagues from Harvard University, Rosalind Lee, Rhonda Feinbaum and Victor Ambros, signalling the first discovery of a miR gene (Lee et al. 1993). Lin-4 was identified as a non-protein coding gene, which encoded two small transcripts of ~22nt and ~61 nt. These transcripts contained complementary sequences to the 3'untranslated region (3'UTR) of the lin-14 mRNA, suggesting that the level of LIN-14 protein was negatively regulated via an antisense RNA-RNA interaction. Seminal work by Wightman *et al.*, (1993) exposed the posttranscriptional nature of miR regulation, by illustrating that the 3'UTR sequence of the lin-14 mRNA transcript was the sole sequence requirement to permit antisense regulation by the lin-4 RNA (Wightman et al.). Also by monitoring both protein and mRNA levels of LIN-14, it was demonstrated that the translation of lin-14 mRNA was regulated by lin-4, without affecting mRNA transcript levels (Wightman et al. 1993). However for the next seven years, the discovery of lin-4 as a regulatory RNA was a novel finding confined to nematodes, as no homologous genes were identified in other species.

However in 2001, the small regulatory RNA let-7 was discovered in *c.elegans*, which was demonstrated to negatively regulate the expression of the heterochronic gene, lin-41, by binding to complementary sites in the 3'UTR of the mRNA transcript (Lau et al. 2001; Lee and Ambros 2001). The importance of this finding was only realised by the discovery of homologous genes to let-7 in other species, including human, *drosophila*, and zebrafish, which consequently led to the explosion of interest in these small temporal RNA (stRNAs) molecules, as they were termed (Pasquinelli et al. 2000). In the following year, a large number of these stRNAs were discoverd in humans, mouse, *drosophila* and *c.elegans,* and with all authors in agreement these small novel RNAs were termed miRs (Lagos-Quintana et al. 2001; Lau et al. 2001; Lee and Ambros 2001). An annotation system was also established for

the classification of experimentally identified miRs based on both expression and biogenesis criteria, furthermore naming conventions for miRs and mir genes were also described (Ambros et al. 2003). Since 2001, a vast wealth of information regarding miRs has been uncovered (Figure 1.6), with a current total of 8273 mature miR products identified in primates, rodents, birds, fish, worms, flies, plants and viruses (Griffiths-Jones 2004; miRBase).

1.4.2. Genomic Location of miRs

The location of miR genes, in intergenic and intronic segments of DNA has been identified, interspersed throughout all chromosomes in humans except chromosome Y. Initially it was thought that the majority of miR genes resided in intergenic non-coding regions, each miR representing individual transcriptional units (Lee et al. 2002; Cai et al. 2004; Lee et al. 2004). However this idea has been reversed in recent years and up to ~70% of miR loci are now thought to reside in the intronic regions of host genes, predominantly in the sense orientation (~75%) (Cai et al. 2004; Rodriguez et al. 2004; Kim and Kim 2007). By combining data from the genome and expressed sequence tag (EST) databases, Rodriguez predicted that ~55% of intronic miRs are located in protein coding genes, while the remaining ~45% are embedded in non-coding RNAs (Rodriguez et al. 2004). MiRs can also be located in close proximity on the genome as clusters and are frequently co-transcribed as polycistronic primary transcripts (Stefani and Slack 2008). Currently it is estimated that 50% of all miRs exist as clusters (Kim and Nam 2006). The maximum distance separating miRs in clusters is still unknown, however it is believed to range from 0.1kb to 50kb (Baskerville and Bartel 2005; Megraw et al. 2007). Evidence suggests that in some cases miR clusters result from ancient gene duplication events, as in the case for two miR-17-92 cluster paralogs in mammals: the miR-106b-25 cluster (located on human chromosome 7) and the miR-106a-363 cluster (located on the X chromosome) (Mendell 2008).

MiRs exhibit a large degree of conservation across species however, variations in mature miR sequences, copy number, and genomic location exist. The timing of miR expression, and spatial location to a lesser extent, also vary across species, more pronounced across disparate species (Ason et al. 2006). An example of this has

recently been highlighted in miRs expressed in mouse and zebrafish CNS, as ~50% of miRs displayed different expression patterns between species despite sequence conservation (Bak et al. 2008).

1.4.3. miR Biogenesis

A two-step maturation process of miRs was initially hypothesized, based on the initial observation that a 696 bp DNA fragment provided the functional effect of the lin-4 transcript (Lee et al. 1993), and further processing of this transcript was illustrated to result in the smaller ~61 nt and ~22 nt fragments (Lee et al. 2002). Additionally *in silico* analysis of the secondary structure also indicated that the ~70 nt fragment forms a stem-loop structure containing bulges (Lau et al. 2001; Lee and Ambros 2001). The mechanisms involved in the main maturation pathway of miRs have been identified (Figure 1.7). Initially the miR gene is transcribed as a longer precursor molecule termed primary-miR (pri-miR; ~70 nt) that is cleaved by the RNAse III enzyme Drosha to form a precursor-miR stem-loop structure (pre-miR). The pre-miR is actively transported to the cytoplasm by the Ran-GTP and Exportin-5 pathway (Lund et al. 2004), where it is further cleaved by the RNAse III enzyme Dicer. The resulting ~22 nt miR/miR* duplex is incorporated into a ribonucleoprotein complex termed (miRNPs) (Mourelatos et al. 2002; Tang 2005), which mediates post-transcriptional regulation of gene expression (Bartel 2004; Denli et al. 2004; Engels and Hutvagner 2006) (Figure 1.7). The identification of the intricate mechanisms behind these two processing steps was aided by the parallel expansion of RNA interference (RNAi) research, which undergoes similar Dicer processing steps (Lee et al. 2004; Tijsterman and Plasterk 2004)

1.4.3.1. Transcription of primary miRs

The majority of primary-miRs (pri-miRs) are transcribed by RNA polymerase II (Pol II) (Faller, 2008), which is one of the most tightly regulated classes of the RNA polymerases. Indeed analysis of the pri-miR sequence of miR-155 (Tam 2001), let-7 (Bracht et al. 2004), and a number of clustered and isolated human miRs (Cai et al.

2004), illustrated that the pri-miR transcript are usually several kilobases long, contain a 5' 7-methyl guanylate (m7G) cap, and a 3' poly(A) tail. As mentioned above, ~55% of intronic miRs are located in protein coding genes, and as such these miRs are thought to be co-transcribed with the host gene as part of a longer transcriptional unit (Figure 1.8). Therefore the expression of these miRs is thought to be regulated by the transcription of the host gene, and miR transcripts are additionally spliced prior to Drosha processing (Baskerville and Bartel 2005) In contrast intergenic miRs belong to individual transcriptional units (Figure 1.8) (Zhou et al. 2007). However to date very little is known about the promoters of these miRs, and indeed the promoter regions have only been located for a number of mammalian miRs, including the intergenic miR gene hsa-mir-23a-27a-24-2 (Lee et al. 2004) and hsa-mir-371-372-373 (Houbaviy et al. 2005). Additionally the miR promoter region has been identified experimentally for the miR-155/BIC gene, which appears to contain similar transcription elements to RNA polymerase II sites in protein coding genes (Tam 2001; Lee et al. 2004; Chung et al. 2006). However a recent study illustrated that a number of human miRs are transcribed by RNA polymerase III (Borchert et al. 2006). It is therefore likely that while Pol II transcribes the majority of miRs, some are indeed transcribed by Pol III.

1.4.3.2 Processing of pri-miR and pre-miR

The processing of pri-miR sequences in the nucleus, to produce a pre-miR double stranded miR duplex, is thought to occur by two separate pathways, the classical major miR pathway mediated by Drosha (Figure 1.7), and the recently identified spliceosome pathway (Figure 1.9) (Okamura et al. 2007; Ruby et al. 2007).

In the major miR maturation pathway the pri-miR transcript is cleaved into a precursor-miR (pre-miR) intermediate by the protein Drosha. Drosha, a nuclear RNase III enzyme, forms a complex with the protein partner, Pasha in drosophila and DGCR8 (DiGeorge Critical Region gene 8) in humans, to form the Microprocessor Complex (Denli et al. 2004; Gregory et al. 2004; Han et al. 2006), which is responsible for the nuclear processing of the pri-miR transcript in the major miR maturation pathway (Figure 1.7).

An alternative miR-processing pathway has recently been identified which bypasses the Drosha-mediated processing step, but involves a splicing and debranched process to produce the pre-miR molecule (Figure 1.9) (Okamura et al. 2007; Ruby et al. 2007). It is thought that this pathway processes a novel class of miRs, termed 'mirtrons', which have been found in flies, nematodes and mammals, identified as short introns with the potential to form hairpin structures but reported to lack the lower portion of the stem structure and the flanking single stranded RNA segments of a traditional pri-miR structure. Similar to other introns, 'mirtrons' are bordered by 5' and 3' splicing sites, contain branch point sequences and are transcribed by RNA Pol II. The splicesome generates a pre-miR in the lariat form, which is linearised by the debranching enzyme, to form a pre-miR hairpin structure (Figure 1.9) (Berezikov et al. 2007; Okamura et al. 2007; Ruby et al. 2007).

The pre-miR that results from either processing pathways is treated identically. The pre-miR is exported from the nucleus to the cytoplasm by Exportin-5 (Exp-5) and the Ran-GTP cofactor, where the pre-miR is cleaved to yield a miR duplex by the RNase III enzyme Dicer (Lund et al. 2004). The understanding of miR biogenesis and function has been greatly aided by RNAi research, as the RNase II protein Dicer was found to process small interfering RNAs (siRNAs) which are similar in size to that of the mature miRs (Bernstein et al. 2001; Hammond 2007). The involvement of Dicer in miR processing was first shown in *c.elegans*, where the inactivation of the gene encoding a homolog of *drosophila* dicer (*drc-1*) resulted in development phenotypes similar to *lin-4* and *let-7* mutants (Grishok et al. 2001). Indeed further studies demonstrated that when dicer function was reduced or inactivated in *c.elegans* and humans, the longer ~70nt RNA transcript accumulated while the ~22nt RNAs lessened (Grishok et al. 2001; Ketting et al. 2001; Hutvagner and Zamore 2002). Thereby definitively demonstrating that the longer RNA was the precursor-miR (pre-miR) transcript which was processed by dicer into the ~22nt mature miR.

Dicer is a class III RNase enzyme that contains, two RNase III-like domains (RIIIDs), one double-stranded RNA binding domain (dsRBD), a long N-terminus containing a RNAhelicase/ATPase domain, and a RNA binding module PAZ domain (Zhang et al. 2002; Macrae et al. 2006). Dicer cleaves dsRNA fragments non-specifically, possessing only a preference for the terminus of dsRNA molecule to produce small RNA duplexes (Zhang et al. 2002; Macrae et al. 2006). Dicer cleavage

results in the production of mature miRs, ~21-27nt long with 2-nt 3' overhangs at both end (Zhang et al. 2002; Macrae et al. 2006), the discrete size resulting from the manner by which Dicer processes dsRNA. It is important to note that Drosha effectively determines the full mature miR sequence, directly by generating one end of the mature miR, which indirectly determines the location of Dicer cleavage (Figure 1.7).

1.4.4. MiRNA Effector Mechanism

1.4.4.1 miRNP Complex

As mentioned above, the expansion of the RNAi field has greatly facilitated the understanding of the mechanism by which mature miRs negatively regulate their targets, as both siRNAs and miRs mediate their action by incorporation into similar assemblies of multiprotein complexes, RNA-induced silencing complex (RISC) (Briscoe et al. 2004) and ribonucleoproteins (miRNPs) respectively (Mourelatos et al. 2002). Dicer processing produces an miR:miR* intermediate duplex which appears to unwind when loaded into the miRNP complex. It appears that the more thermodynamically stable miR strand at the 5' end is degraded (miR*), while the remaining miR strand (miR) is stabilized by binding to the Ago-2 protein (Khvorova et al. 2003; Schwarz et al. 2003; Maniataki and Mourelatos 2005; Zeng 2006). The mature miR strand specifically guides the miRNP complex to load onto the miR recognition elements (MREs) on target mRNA transcripts, aided by the Ago-2 protein (Kirino and Mourelatos 2008). The Ago-2 protein is a member of the argonaute family, and is the key component of the miRNP complex, along with Ago1, Ago3 and Ago4 (Hammond et al. 2001; Mourelatos et al. 2002; Meister et al. 2004; Pillai et al. 2004). The Ago-2 protein has been shown to complex with Dicer, and is thought to facilitate the transfer of the mature miR to the miRNP complex (Hammond et al. 2001; Tahbaz et al. 2004; Chendrimada et al. 2005).

Depending on the degree of complementary of the miR and mRNA target sequence, translational repression (Olsen and Ambros 1999) or mRNA degradation of the mRNA target occurs (Elbashir et al. 2001; Hutvagner and Zamore 2002). Suppression of the target mRNA by either method requires a high degree of base-pairing of the mRNA transcript with the "seed region" of the miR, residues 2-8

(Doench and Sharp 2004; Brennecke et al. 2005). However mismatches or bulges within this seed region, the accessibility of the sequence surrounding the MRE sites, and the distance separating the MRE binding sites, can all interfere with the mechanism and efficiency of suppression (Aleman et al. 2007; Grimson et al. 2007).

1.4.4.2: Target mRNA degradation and translation repression

MiRs are known to mediate their effects by altering mRNA turnover (Lim et al. 2005), suppressing protein translation (Lee et al. 1993; Wightman et al. 1993) and possibly by methylation of target genes (Weber et al. 2007; Kanno et al. 2008). However the classical mechanisms of miR-mediated protein repression, involving mRNA degradation and translation suppression, have recently been opened for debate (Behm-Ansmant et al. 2006; Pillai et al. 2007; Standart and Jackson 2007).

Target mRNA degradation occurs when the miR strand is highly complementary to the mRNA transcript resulting in endonuclease cleavage of target mRNA sequences, thought to be mediated by the Ago-2 enzyme, the only Ago protein of the miRNP complex with RNase H activity (Meister et al. 2004; Forstemann et al. 2007). Consequently, cleavage of the target mRNA is less likely to occur when miR:mRNA transcripts are imperfectly paired, due to the physical restrictions imposed by mismatched bulges (Standart and Jackson 2007). As most miRs form imperfect base pairs with mRNA targets, it seems unlikely that this mechanism plays a major role in miR target suppression (Liu et al. 2005). Nevertheless miR-mediated decreases in target mRNA levels are widespread (Lim et al. 2005; Baek et al. 2008; Selbach et al. 2008), suggesting another mechanism facilitates target mRNA degradation. Wu *et al.*, (2006) has recently demonstrated that miRs with imperfect complementarity to their target mRNA, can increase decay rates of target mRNA by accelerating mRNA deadenlyation (Wu et al. 2006). Deadenylation is the first step of mRNA turnover in eukaryotes, and shortening of the poly(A) tail is followed by decapping of the m7G-cap and degradation of the mRNA body by 3'-5' and 5'-3' exonucleases (Parker and Song 2004; Behm-Ansmant et al. 2006; Valencia-Sanchez et al. 2006). The rate of degradation appears to be dependent on the stability of the miR:mRNA, as bulges in the duplex are thought to disrupt this degradation process (Behm-Ansmant et al. 2006; Aleman et al. 2007). It is thought that this process occurs in processing bodies (P-

bodies), cytoplasmic foci that contain the required enzymes for mRNA decay (Pillai 2005; Nilsen 2007).

Imperfect pairing of the miR:mRNA transcript results in translational repression of the mRNA transcript (Elbashir et al. 2001; Kiriakidou et al. 2007). The current view is that translational repression is mediated prior to the initiation of translation (Kiriakidou et al. 2007; Pillai et al. 2007), and/or during the elongation and termination steps of translation (Kim et al. 2004; Nelson et al. 2004; Petersen et al. 2006). Recent studies by Kirakidou et al (2007) support this mechanism, suggesting that the Ago-2 protein component of the miRNP complex prevents the initiation of translation, by loading the complex onto the MRE site and concurrently binding to the m7G-Cap of the target transcript, thereby preventing the recruitment of the translation initiation factor eIF4E (Kiriakidou et al. 2007; Mathonnet et al. 2007). EIF4E is a cap-binding protein that facilitates ribosome interaction with the mRNA, the removal of which has been shown to promote mRNA degradation (Ramirez et al. 2002). This model provides a simple method of inhibition of translation initiation that is in agreement with the original proposal by Pillai et al (Pillai 2005). However results illustrating that miRs co-purify with polyribosomes, the active site of translation, is suggestive of a translation inhibition mechanism that occurs subsequent to translation initiation (Kim et al. 2004; Liu et al. 2005). Petersen et al (2007) suggest that miR binding results in a premature exit of ribosomes from the target mRNA, perhaps mediated by the association of termination factors (Petersen et al. 2006). Together these studies offer a broad mechanism by which cap-dependent mRNA translation is repressed by miRs, occurring at distinct steps in the process of translation. However the specific mechanisms required for the suppression of individual miR-mRNA combinations have yet to be elucidated (Nelson et al. 2004).

While translation inhibition and mRNA degradation of target mRNA can act independently of each other, it is currently speculated that these two mechanisms occur sequentially (Wu et al. 2006; Pillai et al. 2007). As the translational status of mRNA is known to directly affect mRNA stability, it is suggested that mRNA decay occurs as a result of translational repression, rather than a primary effect of miR (Parker and Song 2004; Pillai et al. 2007). Indeed this argument is strengthened by recent global expression studies examining miR-mediated effects at both the mRNA and protein level, indicating that most targets that are repressed at the protein level are also

repressed at the mRNA level (Baek et al. 2008; Selbach et al. 2008). It is suggested that repressed mRNA transcripts are transferred to P-bodies, facilitated by Ago-2 containing miRNP complex (Liu et al. 2005; Pillai 2005), where miR decay is thought to occur. Indeed Argonaute proteins, miRs and repressed mRNAs have all been identified in P-bodies (Pillai 2005; Valencia-Sanchez et al. 2006). Alternatively P-bodies may act as temporary storage sites for repressed mRNA transcripts that are later released and translated, illustrated in the case of CAT-1 transcripts that were shown to localize to P-bodies when repressed by miR-122 but repression could be reversed by cell stress (Bhattacharyya et al. 2006).

The degree of repression of target mRNAs, is related to the number of MRE sites in the 3'UTR of the target gene (Doench and Sharp 2004; Petersen et al. 2006), demonstrated at the protein level by Selbach *et al.*, (2008) as targets with a single MRE displayed weak translation repression of usually 1.5-2-fold (Selbach et al. 2008). However other factors such as the extent of miR pairing outside seed regions, secondary structure of the mRNA, and protein binding sites on the mRNA may all affect the degree of miR mediated repression (Farh et al. 2005).

1.4.4.3. miR Target Recognition and Prediction

As plant miRs exhibit high levels of complementarity with target transcripts the identification of mRNA targets is straightforward (Jones-Rhoades, 2004), which contrasts strongly with the nature of target identification in mammals due to the diverse nature of target binding. The exact manner by which a miR identifies the mRNA target is ill-defined, however it is known to depend on the level of complementarity of miR sequences to target site sequences, and hindered by the presence of G:U base pairs bulges (Brennecke et al. 2005). Many bioinformatic approaches attempting to identify genome-wide targets have emerged, based on sequence complementarity, favorable thermodynamics and conservation of mRNA target sites for miRs in related species. The main miR target prediction algorithms used are miRanda (Enright et al. 2003), Pictar (Krek et al. 2005) and TargetScan (Lewis et al. 2003), all of which differ on the criteria used to score the complementarity of the miR:mRNA seed region, but converge on examination of the thermodynamic stability of binding sites (Maziere and Enright 2007). These three

prediction models inherently contain false-positives, yet they represent the top miR prediction algorithms, with target-prediction sensitivity values ranging between 65% and 68% based on knowledge of experimentally verified targets stored in the TarBase database (Sethupathy et al. 2006).

However predicting the roles of miR in animal function are further complicated as single genes can be regulated by multiple miRs acting in a coordinated manner (mir-17-92 cluster) (Mendell 2008), while conversely single miRs can simultaneously target a large number of target transcripts. This highlights the potential for miR involvement in complex regulatory networks and cellular pathways that affect physiological states in tissue-specific ways.

1.5. Tissue Specific Expression of miRs

One of the first reports of tissue specific expression of miRs was a study by the Tuschl lab which examined the expression of miRs in a number of different tissues by tissue-specific cloning experiments, as interestingly methods did not exist at the time to identify these ~22nt RNAs by in situ hybridization (Lagos-Quintana et al. 2002). The study identified 34 novel mouse miRs, and moreover a number of tissue-specific miRs were identified in the various tissues, in particular miR-1 in the heart, miR-122 in the liver, and mir-143 in the spleen (Lagos-Quintana et al. 2002). Later a subset of miRs enriched in the brain was uncovered by northern blot analysis (Sempere, et al., 2004). With the emergence of miR array technologies (Sun et al. 2004; Shingara et al. 2005) and high specificity *in situ* hybridization techniques (Kloosterman et al. 2006), subsets of tissue-specific miRs have emerged. These subsets represent a wide range of tissues, largely involving brain tissue (Krichevsky et al. 2003; Miska et al. 2004), heart muscle (Baskerville and Bartel 2005; Zhao et al. 2005; Chen et al. 2006), skeletal muscle (Baskerville and Bartel 2005; Chen et al. 2006) and hematopoietic stem cells (Monticelli et al. 2005).

The enriched expression of subsets of miRs in defined tissues is likely regulated by tissue-specific signaling, which controls the transcription and processing of mature miRs by complex regulatory pathways (Baskerville and Bartel 2005; Obernosterer et al. 2006; Kim and Kim 2007). Indeed specific regulatory circuits have

been elucidated that contribute to cell determination, involving the transcription of distinct miRs by tissue-specific transcriptional activators, displaying both positive and negative feedback loops. For instance in haematopoietic cells, miR –223 expression is regulated by the two transcription factors NF1-A and C/EBPalpha, which compete for binding sites on the miR promoter (Fazi et al. 2005). NF1-A induces a low level of miR-223 expression and is itself a target for miR-223, however displacement by C/EBPalpha upregulates miR-223 expression promoting differentiation to granulocytic lineage.

1.6. Development and Cell identity

Spatially and temporally coordinated expression of subsets of miRs characterizes development and physiological conditions of defined tissues, and as such miRs are thought to play critical roles in both cell differentiation and maintenance of tissue identity (Kosik and Krichevsky 2005; Kim and Nam 2006). Indeed miRs are known to mediate effects in a broad range of physiological functions, including embryogenesis, development, homeostasis, and the physiological processes of most organs.

The most obvious participation of miRs in development was observed in animals lacking *Dicer* expression, mediated by targeted-selected inactivation of the *Dicer1* gene in both mice and zebrafish (Bernstein et al. 2003; Wienholds et al. 2003; Giraldez et al. 2005). The *dicer-1* mouse mutant resulted in lethality at embryonic day 7.5, and in zebrafish the deletion, while not affecting axis formation, resulted in disorganized spatial distribution of cells during the positioning of the 3 embryonic germ layers, somitogenesis, and brain and heart development (Bernstein et al. 2003; Giraldez et al. 2005). Both of these examples point toward the essential roles of *Dicer-1*, and indirectly miRs, in vertebrate development. The emergence of tissue-specific *dicer-1* mutants, using cre-mediated recombination of loxP sites, will greatly facilitate the identification of tissue specific roles mediated by miRs (Harfe 2005). Studies have identified individual miRs involved in fine-tuning organ development, for example the miR-17-92 cluster plays important regulatory roles in mammalian heart and lung

development (Mendell 2008), and the miR *bantam* and miR-14 regulate tissue growth and cell death during *drosophila* development (Brennecke et al. 2003; Xu et al. 2003).

The effects of both bantam and miR-14 are anti-apoptotic in nature (Xu et al. 2003; Leaman et al. 2005) and indeed a vast number of miRs appear to regulate cell growth and apoptosis in mammalian cells (Cheng et al. 2005). It is not surprising that miRs that appear to regulate apoptosis are implicated in a number of cancer types. The miR-17-92 cluster of miRs mediate anti-apoptotic effects and are overexpressed in a diverse number of cancers, ranging from solid tumours of the breast, colon, lung, and pancreas to haematopoietic cancers (He et al. 2005; Volinia et al. 2006). Cooperative interaction of a number of miRs from the miR-17-92 cluster mediates an oncogenic effect, by targeting the transcription factor E2F that is implicated in apoptosis and cell-cycle activation (Stanelle and Putzer 2006; Zhang et al. 2007). Conversely miRs with pro-apoptotic effects are likely to function as tumour-suppressor genes, in agreement with the finding that a wide-range of miRs are downregulated in tumors compared to normal tissue (Hwang and Mendell 2006). For example miR-34, -15 and -16 promote the activation of the intrinsic apoptotic pathway by direct suppression of the anti-apoptotic protein *Bcl-2*, linking the reduced expression of mir-15 and –16 in patients with B-cell chronic lymphocytic leukaemia (Cimmino et al. 2005; Bommer et al. 2007; Chang et al. 2007).

Consistent with the idea that miRs play a critical role in cell differentiation and in the maintenance of cell identity is the finding that miRs regulate cells of the immune system (Monticelli et al. 2005). Ectopic expression of miR-181 in hematopoietic progenitor cells preferentially directs B-cell lineage differentiation, while miR-223 and -142 promotes T-cell fates (Chen et al. 2004). MiRs are also involved in the receptor-signaling pathway of the innate immune response, mediated by Toll-like receptors. This was demonstrated by the NFκB-dependent up-regulation of miR-146, -155 and –132 in response to bacterial challenge by LPS, repressing the expression of the adaptor molecules IRAK1, TRAF6 (Taganov et al. 2006). Notably miR-146 expression is significantly overexpressed in psoriasis, a chronic inflammatory disease of the skin involving the local infiltration of inflammatory cells (Sonkoly et al. 2008).

1.7. Physiological and Pathophysiological Roles of miRs

Separate from the involvement of miRs in development and maintenance of cell identity, miRs are thought to mediate a range of tissue-specific roles in the adult, including neuronal synaptic plasticity (Kosik 2006), circadian-rhythm regulation (Cheng et al. 2007), cardiac excitability (Yang et al. 2008)), pancreatic insulin secretion (Poy et al. 2004) as well as angiogenesis (Suarez et al. 2008). Specifically miR-1 and –133 are enriched in skeletal and cardiac muscle (Sempere et al. 2004; Zhao et al. 2005) and display tissue specific roles. For example in both of these tissues, miR-1 and -133 appear to fine-tune regulatory pathways, including muscle progenitor differentiation and proliferation, and cardiomyocyte apoptosis (Chen et al. 2006; Xu et al. 2007; Callis and Wang 2008). Also in mature neurons the brain-enriched miR-134 is thought to regulate neuronal transmission and synaptic plasticity, by regulating dendritic spine development (Schratt et al. 2006), while interestingly rhythmic expression of miR-129 and –132 in the suprachiasmatic nuclei (SCN) of the hypothalamus is implicated in circadian-rhythm regulation (Cheng et al. 2007).

Given the vast number of miRs and the abundant effects that they mediate (each miR is predicted to have >100 targets), it is not surprising that miRs are also implicated in disease processes (Lewis et al. 2005). Indeed correlations between miR expression and human disease have been observed, miR dysregulation is evident in an ever-increasing range of disorders, including muscle disorders (Care et al. 2007; Eisenberg et al. 2007; Yang et al. 2008), inflammatory skin conditions (Sonkoly et al. 2008), various forms of cancer (Zhang et al. 2007) and neuronal diseases (Hebert and De Strooper 2007; Kim et al. 2007; Li et al. 2008; Stark et al. 2008).

As the retina comprises of neuronal cell types, the implication of miRs in neuron-specific functions is particularly fascinating. Indeed miRs play critical role in zebrafish brain morphogenesis (Giraldez et al. 2005) and a subset of brain-specific miRs have been identified, including miR-124, -9, -125, -128, -134 and –135 (Miska et al. 2004; Sempere et al. 2004). Indeed two of these miRs, miR-124 and miR-9, affect neural lineage differentiation in embryonic stem cell-derived cultures (Smirnova et al. 2005; Krichevsky et al. 2006), in consensus with the observation that overexpression of miR-124 in HeLa cells shift the gene expression profile towards a brain mRNA expression profile (Lim et al. 2005). Similarly the involvement of miRs in eye

morphogenesis was demonstrated by early studies of *drosophila* and zebrafish dicer-1 mutants, in which the eye failed to develop correctly (Brennecke et al. 2003; Xu et al. 2003; Giraldez et al. 2005).

miRs are another set of contenders that are potentially involved in the complex pathophysiological mechanisms underlying neuronal diseases. Notably, Fragile-X Mental Retardation Syndrome was the earliest disease in which miRs were ever implicated (Jin et al. 2004) and since then evidence has been mounting associating miRs with a range of other neuronal disorders including spinocerebellar ataxia (Lee et al. 2008), psychiatric disorders (Stark et al. 2008), autism (Abu-Elneel et al. 2008), Alzheimer's disease (Hebert et al. 2008), Tourette's syndrome (Abelson et al. 2005), and Parkinson's disease (Kim et al. 2007). The involvement of miRs in neurodegenerative diseases is of particular interest, as correlations may exist in the degenerating retina. In conditionally floxed dicer-1 mice, the absence of miR expression in the hippocampus and cortex (Davis et al. 2008), cerebellum (Schaefer et al. 2007), and striatal neurons (Cuellar et al. 2008) all resulted in neuronal degeneration, highlighting the role of miRs in regulating apoptosis. Also emerging results from studies examining miR involvement in distinct neuronal diseases, suggesting that miR dysregulation may also potentially regulate the disease processes in both Alzheimer's disease and spinocerebellar ataxia (Hebert et al. 2008; Lee et al. 2008). Both of these diseases result in neuronal cell death due to the toxic build up of protein products, Ataxin-1 and Aβ fragments respectively, in the affected neurons. Recent studies demonstrate that miRs may regulate the buildup of these proteins, and considering the commonalities that exist in the mechanisms of neurodegeneration in these diseases and in degenerating involving photoreceptor neurons (e.g. RP); it is intriguing to consider whether miRs may similarly be involved in photoreceptor cell death.

1.8. Aim

At the outset of the studies undertaken for this Ph.D., there was no published research findings specifically relating to the expression or roles of miRs in the retina, however, a few studies were published highlighting a potential involvement of miRs in

eye development (Brennecke et al. 2003; Xu et al. 2003; Giraldez et al. 2005). One report relating to miR expression in the adult eye was presented as part of the seminal work by the Tuschl lab, in which novel miRs were characterised by cloning from various mouse tissues serendipitously including eye tissue. The following novel miR were identified in the adult mouse eye miR-129b, -181, -182, -183, -184, -185, -186, and –204, providing the first glimpse of the retinal-enriched mammalian miR expression profile (Lagos-Quintana et al. 2003). This study provided the foundation for the research presented in this Ph.D. thesis, which was further stimulated by the expansion of research in this area and facilitated by technological advances in miR research.

Characterising the retinal miR expression profile is essential to elucidate miR involvement in retinal-specific functions, as well as their potential involvement in disease. As the expression of a large percentage of miRs are enriched in discrete tissues (Landgraf et al. 2007), it is hypothesised that the expression of a subset of miRs may be enriched in the retina. The study described in this Ph.D thesis therefore aims to establish the miR expression profile in the retina, and to examine the spatial expression pattern among heterogenous cell types. It is theorised that the expression of retinal enriched miRs may overlap with miRs expressed in the brain, and in addition the expression of discrete subsets of miRs may be limited to defined retinal cell types. Alternatively, as miRs are implicated in a number of neuronal diseases, in which they appear to regulate the disease process (Kosik and Krichevsky 2005; Bilen et al. 2006), it is hypothesised that miR expression is altered in retinal disease. A further objective is therefore to analyse miR expression in the retina of mouse models of the inherited retinal degenerative disease, RP, and specificially within photoreceptor cells, the cell type primarily affected by this disease. Although many of the genetic causes implicated in RP are well-defined, miRs may modulate the disease process, perhaps altering the rate of retinal degeneration.It is therefore possible that miR inhibition and/or activation may show great promise in the future treatment of retinal degeneration.

In this thesis the miR expression profile of the adult retina is obtained, in comparison to both brain and non-neuronal tissues. Furthermore the evaluation of miR expression in the degenerating retina is examined in a number of mouse models of RP, including the specific analysis of miR expression in photoreceptor cells. Bioinformatic

prediction tools are used to predict target genes that may be regulated by retinal miRs, and candidate targets for each miR are highlighted from this study. Finally miR expression constructs are constructed, providing a means to overexpress miRs *in vitro,* in addition to the non-viral delivery of these expression constructs *in vivo*. The key findings of this study include the identification and assignment of retinal-preference for a number of retinal miRs. Significantly, a common profile of miR dysregulation is observed in the mouse models of RP analysed that can be attributed to specific alterations of miR expression in photoreceptors. Notably the findings presented in this Ph.D thesis represent novel findings, and the first demonstration of altered miR expression in ocular disease.

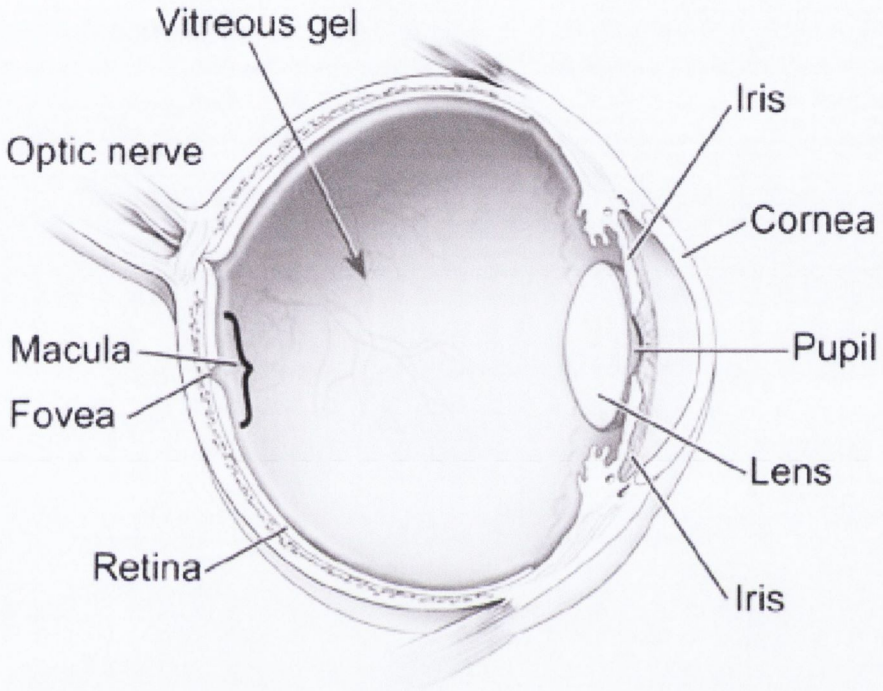

Figure 1.1: Basic Structure of the Eye: This representative image indicates the major components of the eye. The cornea is a protective layer, additionally involved in focusing light. The lens is a clear layer behind the pupil which focuses light onto the retina, and the iris can alter contract and relax altering the amount of light entering through the pupil. The retina lines the back of the eye and contains photoreceptor cells, which respond to light. The Macula is an oval yellow spot in the central part of the retina, which contains a high concentration of cone photoreceptors, responsible for high acuity colour vision; the fovea is the central most part of the macula. Peripheral areas of the retina surrounding the macula, contain a higher proportion of rod photoreceptors, and are involved in vision in dim-light. The Vitreous gel provides structural support to the eyeball. From http://www.nei.nih.gov/index.asp

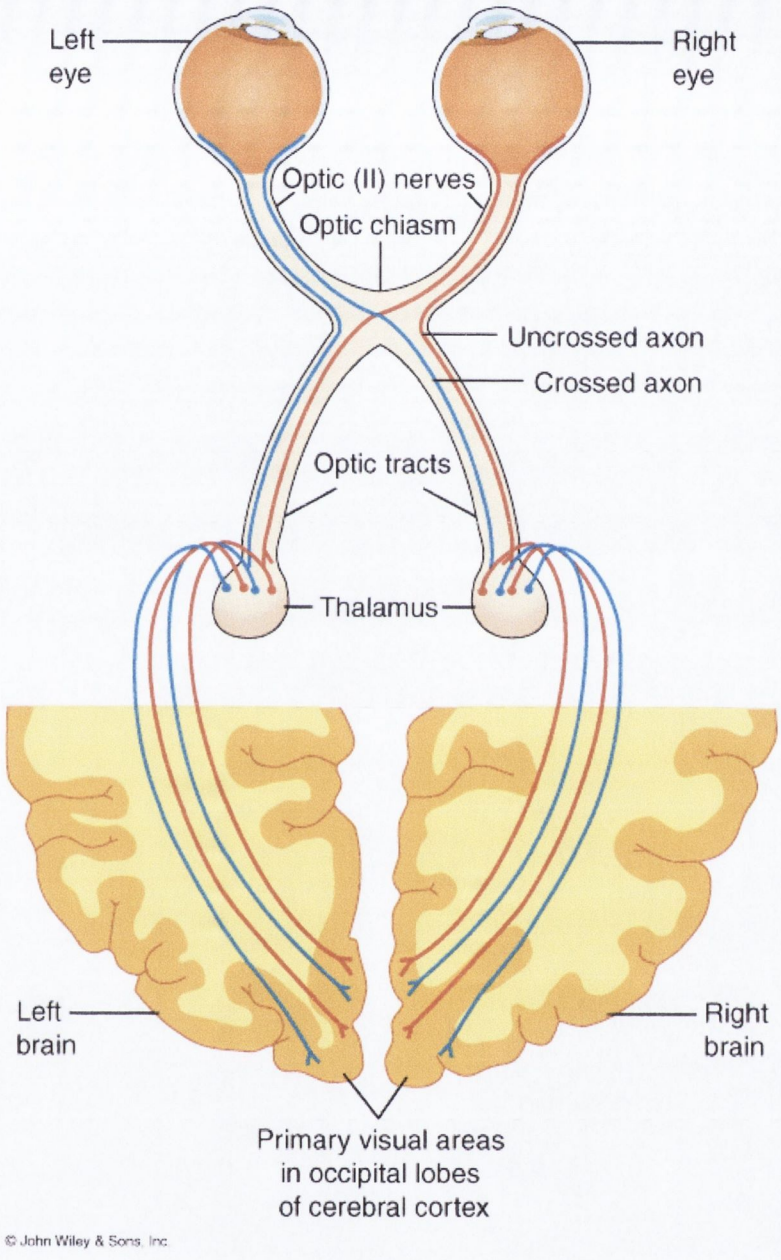

Figure 1.2: Schematic representation of the the pathways of nerve impulses from the retina of the eye to the visual cortex. Signals are transmitted from the retina to the brain, initially through retinal neurons, in which the ganglion cell axons combine to form the optic nerve. The optic nerve leaves the eye and passes through the optic chiasm forming the optic tract, which synapses on the lateral geniculate nucleus of the thalamus. A collection of axons from the thalamus, termed optic radiations, relay the signal to the visual cortex in the occipital lobe of the brain. From www.lrn.org/Graphics/Senses/figure%208.4.gif

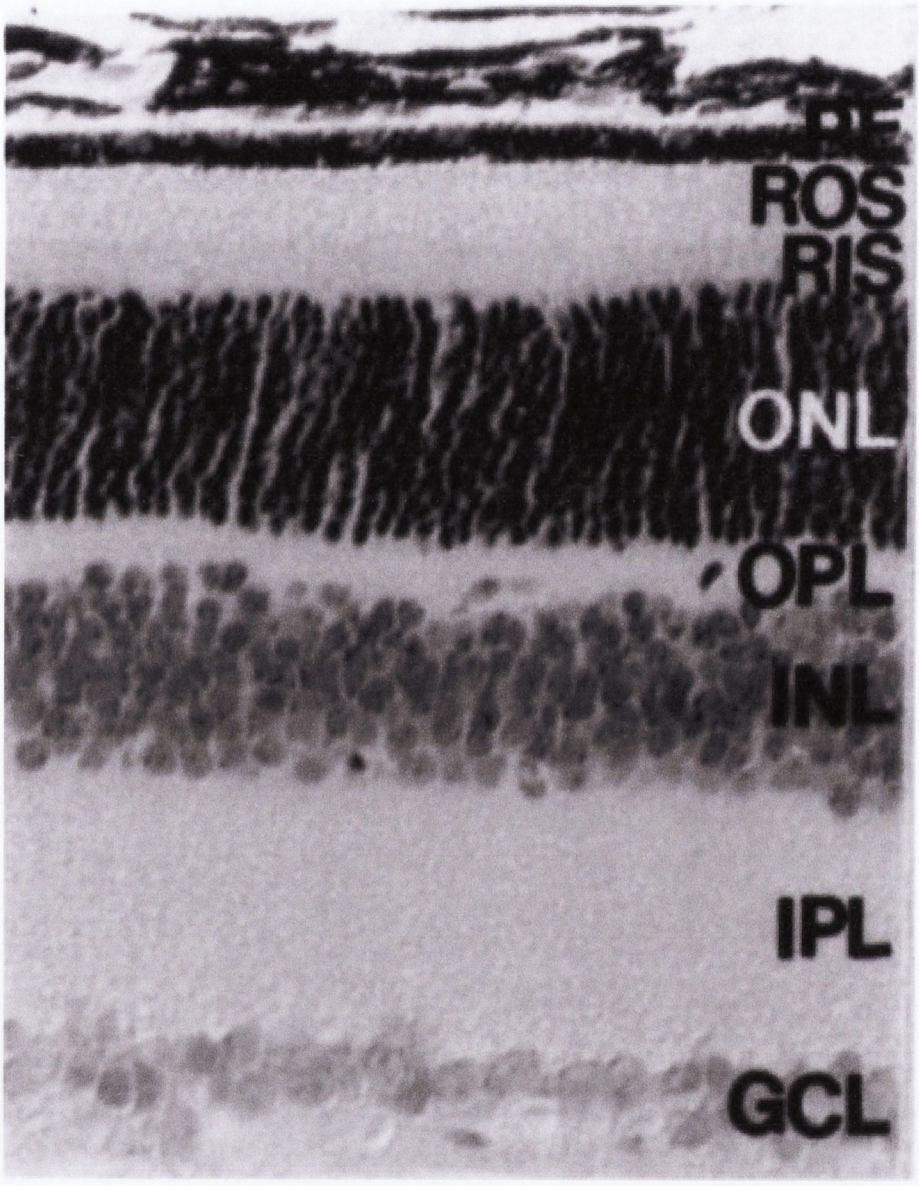

Figure 1.3. Retinal histology of a wild-type mouse retina at light microscope level: The layers of the retina are identified and abbreviated as follows: retinal pigment epithelium (RE), rod outer segments (ROS), inner segments (RIS), outer nuclear layer (ONL), outer plexiform layer (OPL), inner nuclear layer (INL), inner plexiform layer (IPL) and ganglion cell layer (GCL). From (Farrar *et al.* 2002).

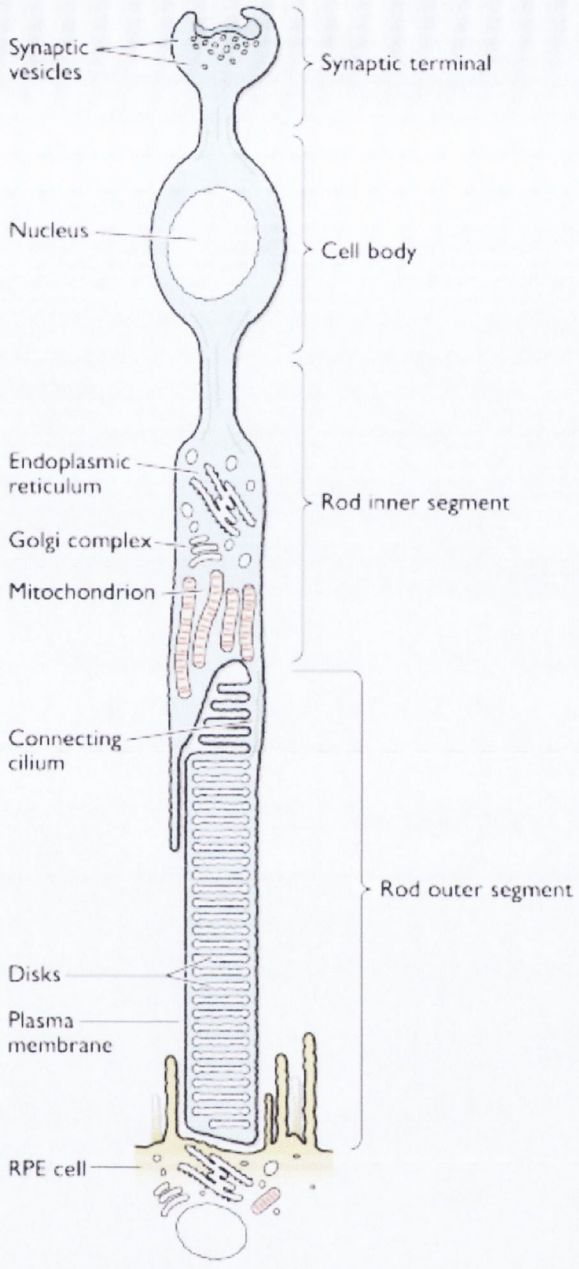

Figure 1.4. Schematic representation of a rod photoreceptor: The five main structures are the outer segment, the connecting cilium, the inner segment, cell body, and the synaptic terminal. Adapted from (Pierce 2001)

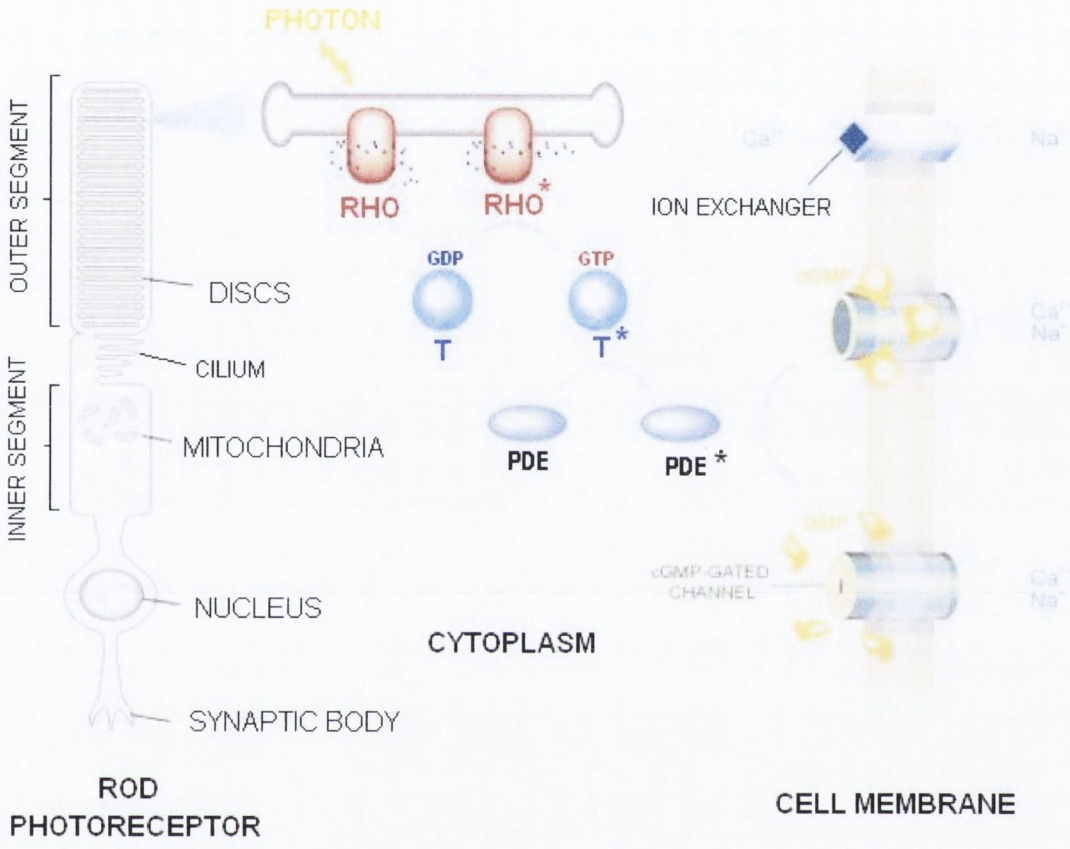

Figure1.5. Summary of the main processes involved in the phototransduction cascade: Rhodopsin is indicated by RHO, transducin by T, phosphodiesterase by PDE, and '*' indicates the activated state. Light striking the retina activates Rhodopsin (R) by causing isomerisation of 11-*cis*-retinal to all-*trans*-retinal. The activated rhodopsin (R*) triggers the GDP/GTP exchange of the protein transducin (T), and in turn the activated transducin (T*) activates phosphodiesterase (PDE). This results in the hydrolysis of cyclic guanosine monphospate (cGMP), and the closure of cGMP-gated cation channels (Na^+/Ca^{2+}), resulting in hyperpolarisation and lessening glutamate release at the photoreceptor synapse. From (Farrar *et al.* 2002).

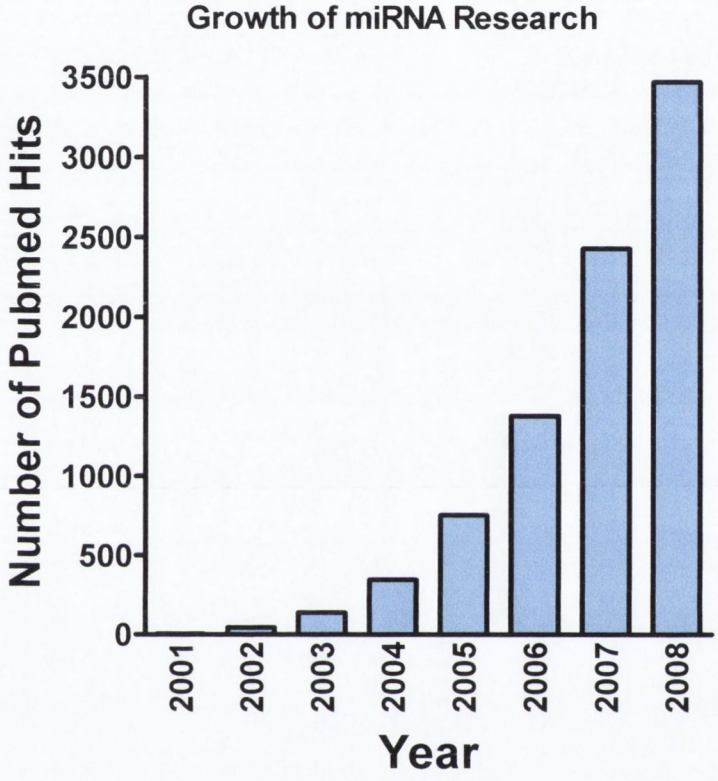

Figure 1.6: Growth in miR Research: Bars represent the quantity of scientific manuscripts published on the topic miRs since their discovery. Numbers are based on 'PubMed' database hits, using the keywords "microRNA" and the relevant year (PubMed).

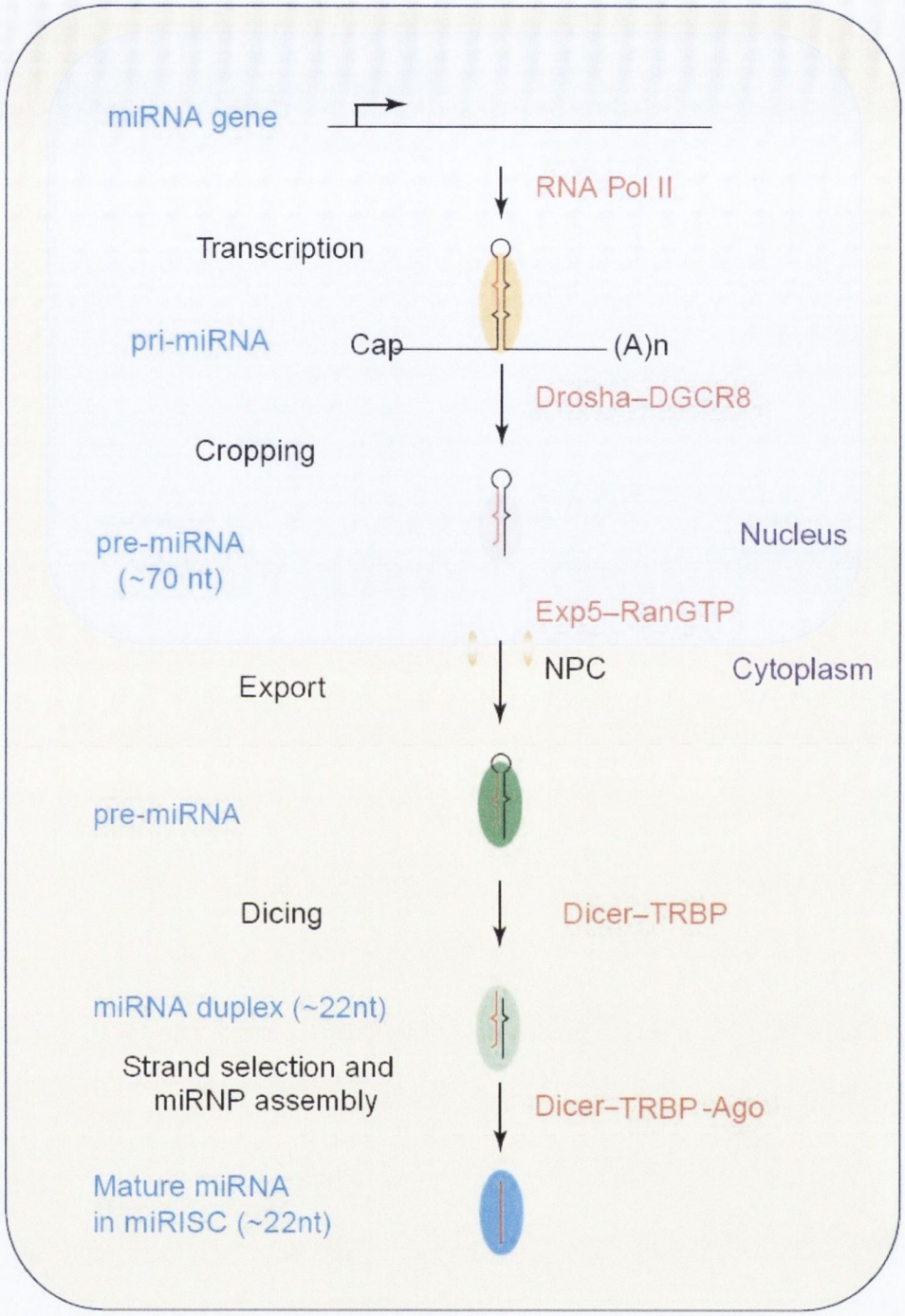

Figure1.7. Model of miR biogenesis: miR genes are transcribed by an RNA polymerase II (Pol II) to generate the primary transcripts (pri-miRs). Cropping of the pri-miR sequence is mediated by Drosha-DGCR8 complex in the nucleus. The pre-miR product is transported to the cytoplasm by Exportin 5 (Exp5-RanGTP). In the cytoplasm the RNase III Dicer processes the transcript to product mature miR intermediate duplexes, aided by the RNA-binding proteins, TRBP and Argonaute (Ago). The duplex is loaded into a miRNP protein complex where the passenger strand miR* is degraded, and the sense miR strand guides target mRNA regulation (Kim *et al.* 2006).

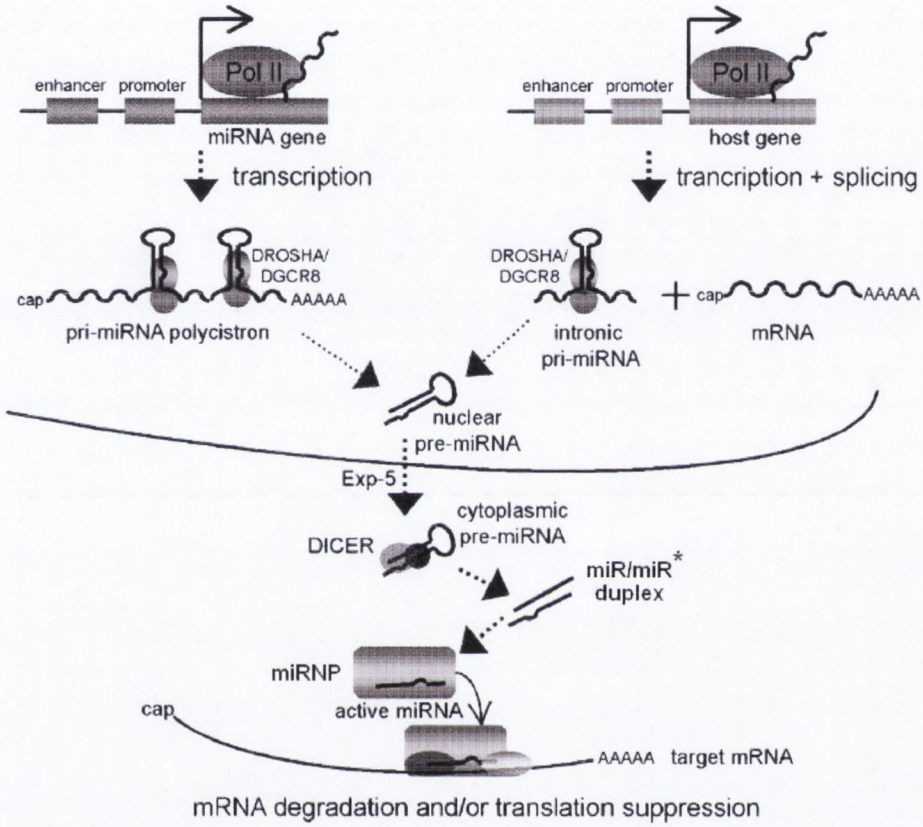

Figure 1.8. Transcriptional variations of intronic and intergenic miRs: Variations of miR transcription and processing exist, depending on the genomic location of the miR gene. Intergenic miRs, located within individual transcriptional units, are transcribed as pri-miRs, followed by Drosha processing. In contrast intronic miRs, embedded in host genes, are co-transcribed with the host transcripts. These transcripts are spliced, and the resulting pri-miR is then processed by Drosha. These pre-miR resulting from drosha-mediated cleavage, are exported from the nucleus by Exportin-5, and further processed by Dicer, to generate mature miRs (~21nt). Following unwinding of the miR/miR* intermediate duplex, the mature miR (miR) is incorporated into the miRNP, and negatively regulates target genes by post-transcriptional repression. From (Guil *et al.* 2008)

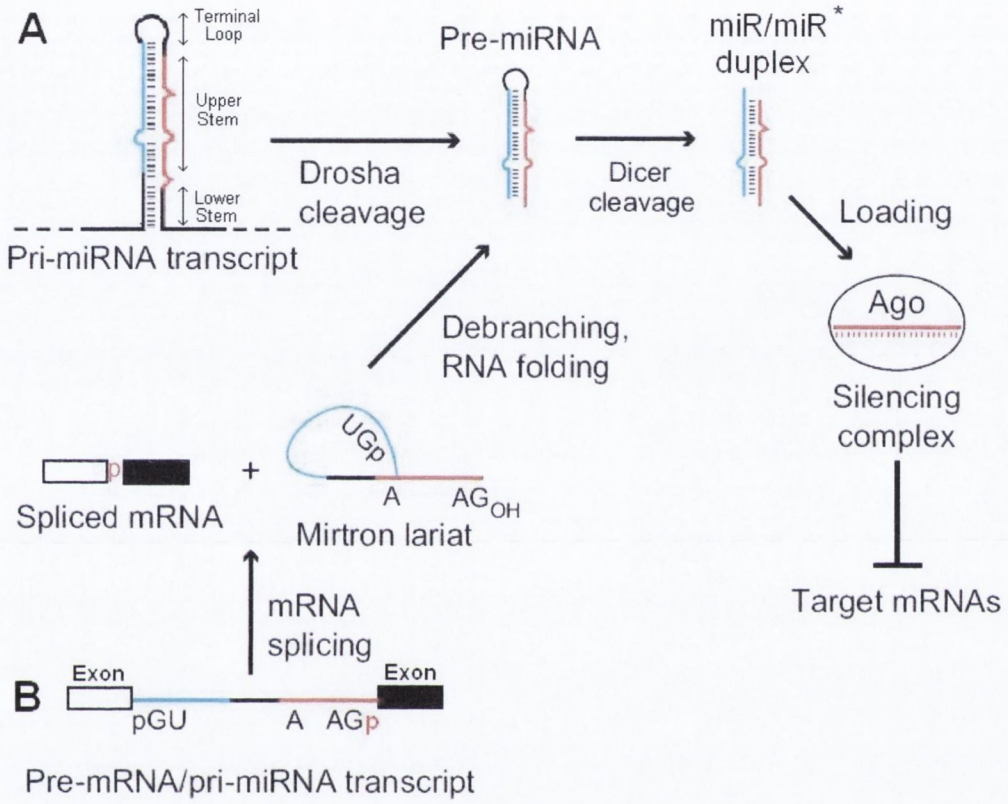

Figure 1.9. Model for Mirtonic miR Biogenesis Pathway: (A) Indicates the classical pathway of Drosha cleavage of pri-miR transcripts to form pre-miR transcripts. **(B)** However the processing of mirtrons, short introns with hairpin potential, is mediated by splicing and disbranching into pre-miRs, independent of Drosha processing. Mammalian mirtrons differ to pri-miRs as they lack a lower stem and single-stranded segments at the base. The pre-miRs produced by either pathway are transported to the cytoplasm for processing into mature miRs by the RNase III Dicer. Mir effector functions are mediated by incorporation of the mature miR strand into the silencing complex. Adapted from (Ruby *et al.* 2007)

Table 1.1 List of causative genes of Retinitis Pigmentosa and their functional involvement in the retina	
Functional category	**Gene name**
Phototransduction cascade	Rhodopsin (RHO); S-antigen (arrestin)(SAG); cyclic nucleotide gated channel α/β-subunit (CNGA1; CNGB1); phosphodiesterase 6 α/β-subunit (PDE6A; PDE6B); guanylate cyclase activator 1; β-subunit (GUCA1B)
Structural, cytoskeletal and membrane proteins	ATP-binding cassette subfamily A, member 4 (ABCA4); retinal degeneration slow/peripherin (RDS); rod outer segment protein 1 (ROM1); semaphorin 4A (SEMA4A); Crumbs homolog 1 (CRB1); retinitis pigmentosa 1 (RP1); usher 2A (USH2A)
Transcription factors	Neural retina leucine zipper (NRL); cone-rod homeobox (CRX); nuclear receptor subfamily 2, group E3 (NR2E3)
Splicing factors	Pre-mRNA processing factor 31 homolog (PRPF31); pre-mRNA processing factor 8 homolog (PRPF8); pre-mRNA processing factor 3 homolog (PRPF3); retinitis pigmentosa 9 (RP9)
Vitamin A metabolism	Retinal pigment epithelium 65 kDa protein; cellular retinaldehyde-binding protein; lecithin retinol acyl transferase (LRAT); RPE-retinal G-protein-coupled receptor (RGR)
RPE phagocytosis	c-mer protooncogene receptor tyrosine kinase (MERTK)
Neuronal cell viability	Ceramide kinase-like protein (CERKL)
Other cellular functions	Carbonic anhydrase 4 (CA4); inosine monophosphate dehydrogenase 1 (IMPDH1); retinitis pigmentosa GTPase regulator (RPGR, RP3); retinitis pigmentosa 2 (RP2); topoisomerase I binding arginine/serine-rich protein (TOPORS); tubby-like protein 1 (TULP1)

Table 1.1. List of causative genes of RP, and the function of these genes in relation to vision. Adapted from (Kannabiran 2008).

Chapter 2

Materials and Methods

2.1. Materials Used

2.1.1. Buffers and Stock Solutions for Cloning

1 M Tris (pH 8.0): 48.44 g tris-base (MW 121.14 g; Sigma-Aldrich, St. Louis, MO, USA) was dissolved in 300 ml of ddH_2O and the pH was adjusted to a pH of 8.0 using concentrated HCl. Once the desired pH was reached, ddH_2O was added to obtain a volume of 400 ml, followed by autoclaving for 15 minutes at 121°C.

0.5 M EDTA (pH 8.0): 74.44 g of disodium ethylenedeamine tetraacetate.$2H_2O$ (MW 186.12 g; Sigma-Aldrich) was added to 300 ml of ddH_2O. The solution was thoroughly mixed using a magnetic stirrer, the pH adjusted to 8.0 using NaOH. The final volume was increased to 400 ml using ddH_2O and autoclaved for 15 minutes at 121°C.

0.3 M Sodium Acetate: 98.44g of sodium acetate (MW 82.03; Sigma-Aldrich) was added to 300 ml of ddH_2O. Solutions with a pH of pH 7.0 and pH 4.6 were obtained using HCl. ddH_2O was used to achieve the final volume of 400 ml and the solutions were autoclaved for 15 minutes at 121°C.

Tris-acetate-EDTA electrophoresis buffer (50xTAE): 242 g of tris base (MW 121.14; Sigma-Aldrich) was weighed out and dissolved in approximately 750 ml ddH_2O. 57.1 ml of glacial acetic acid and 100 ml of 0.5 M EDTA (pH 8.0) was added and the solution adjusted to a final volume of 1 L. The pH of this buffer is not adjusted and should be about 8.5. This stock solution can be stored at room temperature and diluted to 1 X TAE with ddH_2O prior to use.

LB Media: 10 g tryptone (1.0%), 5 g yeast extract (0.5%) and 10g NaCl (1.0%) were added to 600 ml ddH_2O The pH was adjusted to 7.0 and made up to 1 L using ddH_2O before autoclaving.

LB Agar: 10 g tryptone (1.0%), 5 g yeast extract (0.5%), 10 g NaCl (1.0%) and 15 g agar (1.5%) was added to 600 ml of H_2O. The pH was adjusted to 7.0 and made up to 1 L using ddH_2O before autoclaving.

Antibiotics:

Antioboitic	Stock Solution	Working Concentration
Tetracycline:	20 mg/ml in 50% ethanol	50 μg/ml
Spectinomycin:	20 mg/ml in sterile ddH_2O	50 μg/ml

Spectinomycin solutions were filter-sterilised using a 0.22 μm filter prior to use.

E. Coli Lysis Solution 1: 50mM Tris pH 8.0, 25% sucrose and 2mM EDTA pH 8.0 were combined with 200 ml sterile ddH_2O.

M-STET: 50 mM Tris pH 8.0, 5% Sucrose, 50 mM EDTA pH 8.0, 5% triton X-100 were combined with 200 ml using sterile ddH_2O.

Annealing Buffer: 100mM Tris pH 8.0, 10 mM EDTA pH 8.0 and 1M NaCl.

10 X Tris-EDTA (TE): 0.1 M Tris pH 8.0 and 10 mM EDTA stock solution was made up to the volume required and pH adjusted to 8.0 and diluted to 1X TE for use.

2.1.2. Buffers and stock solutions for mammalian cell culture experiments

1x Sterile PBS (Lonza, Basel, Switzerland).

Dulbecco's Modified Eagle's Medium+: 500 ml Dulbecco's Modified Eagle's Medium (Lonza, Basel, Switzerland) was supplemented with 50 ml foetal calf serum (Invitrogen, Carlsbad, CA, USA), 5 ml sodium pyruvate (100 mM; Lonza) and 5ml L-glutamine (200 mM; Lonza).

Freezing Media: 20% DMSO (Sigma, D-8779), 20% DMEM, 60% foetal calf serum.

2.1.3. Buffers and stock solutions for *In Situ* Hybridisation

RNAase-Free H_2O (DEPC-H_2O): ddH_2O was treated with 0.1% of deithylpyrocarbonate (DEPC; Sigma-Aldrich), as it is an effective RNase inhibitor (Sambrook et al. 1989). The mixture was stirred to ensure the globules of DEPC were dissolved and left overnight at room temperature. The treated ddH_2O was then autoclaved for 15 minutes at 121°C, to sterilise the water but also to deactivate DEPC, which hydrolyses to form ethanol and carbon dioxide.

20 X Saline-Sodium Citrate (SSC) Buffer: 70.12 g NaCl and 35.28 g sodium citrate were added to 300 ml ddH_2O and dissolved. The pH was adjusted with NaOH to pH 7.0 and DEPC treated. The final 10X solution was diluted with DEPC-H_2O for use at the desired concentration.

10 X Phosphate buffered saline (PBS): 32 g NaCl, 0.8 g KCl, 5.76 g Na_2HPO_4 and 0.96 g KH_2PO_4 were dissolved in 300 ml of ddH_2O, and the pH adjusted to 7.4 using HCl. The solution was made up to 400 ml and DEPC treated as outlined in section 2.2.3. The solution was used at a working concentration of 1X, by dilution with DEPC-treated H_2O.

1 M Tris: 48.44 g tris-base was dissolved in DEPC-treated ddH_2O. The solution was pH adjusted to 9.5 using HCl and the volume increased to 400 ml with DEPC-treated H_2O. Note: Tris solutions cannot directly be DEPC treated as tris interacts with DEPC, preventing it from inactivating RNase.

0.5 M EDTA: 74.44 g EDTA disodium ethylenedeamine tetraacetate.$2H_2O$ (MW 186.12 g; Sigma-Aldrich) was added to 300 ml of ddH_2O. The solution was stirred vigeroulsy on a magnetic stirrer until dissolved. The pH was adjusted to 8.0 using NaOH, DEPC-treated and autoclaved.

PBS-Tween: Tween-20 (Sigma-Aldrich) was added to DEPC-treated PBS to make a stock solution of 5% tween solution or a working solution of 0.05% solution for blocking stages of the *in situ* hybridisation protocol.

4% Paraformaldehyde: 50 ml of 10X PBS was added to 400 ml of DEPC H_2O and the solution heated to 65°C on a heated plate. When the temperature was reached the heat was turned off and 20 g of powdered paraformaldehyde (Sigma; P-6148) was

added and stirred constantly using a magnetic stirrer. NaOH was added to aid solubilisation of the paraformaldehyde, and when fully dissolved the PFA was placed on ice. The pH was adjusted to 7.4 using HCl and the final volume of 500 ml was reached using DEPC H_2O.

Pre-Hybridisation Buffer: Both of the pre-hybridisation buffers outlined below are mixtures of high-molecular weight polymers capable of saturating non-specific binding sites.

Heparin Hybridisation Buffer

Final Concentration		Stock	25ml
50%	formamide	100%	12.5 ml
5X	SSC	20X	6.2 ml
0.1%	Tween	5%	0.5 ml
9.2 mM	citric acid	1M	230 µl
50 ug/ml	heparin	50mg/ml	25 µl
500 ug/ml	yeast tRNA	50mg/ml	250 µl

Denhart's Hybridisation Buffer

Final Concentration		Stock	25 ml
50%	formamide	100%	12.5 ml
5X	SSC	20X	6.2 ml
10%	dextran sulphate	50%	5 ml
1X	denhart's reagent	50X	0.5 ml
500ug/ml	yeast tRNA	50mg/ml	250 µl

The pre-hybridisation buffers were aliquoted into 1.5 ml and frozen at -80°C.

Note: Both heparin (GE Healthcare; Chalfont St. Giles, Buckinghamshire, UK) and yeast tRNA (Sigma-Aldrich) solutions were made to a concentration of 50 mg/ml in 4X SSC. Heparin and yeast tRNA solutions were used as blocking agents in the pre-hybridisation and hybridisation buffers. 25 g of dextran sulfate was dissolved in 50 ml of DEPC H_2O (0.5 g/ml). It was heated to 65°C to allow the dextran sulphate to go into solution.

Blocking Buffer: 2% sheep serum (Sigma-Aldrich) and 2mg/ml Bovine Serum Albumin (BSA; Sigma-Aldrich) in PBS-Tween (0.05% Tween).

Alkaline Phosphatase (AP) Buffer: 100 mM Tris (40 ml of 1M Tris, pH 9.5), 100 mM NaCl (400 ml of 1M NaCl) and 50 mM $MgCl_2$ (2 ml of 1M $MgCl_2$) were mixed with 300 ml DEPC-treated ddH_2O. The pH was adjusted to 9.5, and made up to 400 ml with DEPC-treated H_2O.

2.1.4. Animals

Animals were held under specific pathogen free (SPF) housing conditions and kept on a 12 hour light/12 hour dark cycle. Animals welfare and conditions complied with the Association for Research in Vision and Opthalmology (ARVO) statement regarding the use of animals in Ophthalmic and Vision Research and the European Communities (Amendment of Cruelty to Animals Act, 1876) Regulations, 2001 and 2005 (Wolfensohn and Lloyd 2003).

The strains of mice used were as follows:

1) Wild-type (wt) C57BL/6J mice from Harlan Laboratories, Oxfordshire, UK.
2) Wt 129 mice from Charles River Laboratories, Wilmington, MA, USA.
3) Wt C3H mice from Charles River Laboratories, Wilmington, MA, USA.
4) Wt BalbC mice from Trinity College, Dublin, Ireland.
5) Transgenic Rhodopsin-GFP mice from Prof. John Wilson, Texas, USA (Chan et al. 2004)

The mouse models of retinal degenerations used in this study are as follows, where autosomal dominant (adRP) and autosomal recessive RP (arRP) forms of RP are denoted.

1)	Rho-/-	Rhodopsin	Knock Out	arRP	(Humphries et al. 1997)
2)	P347S	Rhodopsin	P347S tg	adRP	(Li et al. 1996)
3)	P23H	Rhodopsin	P23H tg	adRP	(Olsson et al. 1992)
4)	Δ307	Peripherin/rds	Deletion	adRP	(McNally et al. 2002)
5)	Rds-/-	Peripherin/rds	Null	adRP	(Sanyal et al. 1980)
6)	Rd	PDEß	Null	arRP	(Pittler and Baehr 1991)

2.1.5. Oligonucleotides Synthesis

Oligonucleotides were supplied by Sigma-Genosys (Pampisford, Cambridgeshire, UK). Primers were ordered purified by high performance liquid chromatography (HPLC). They were resuspended in ddH_2O at a final stock concentration of 100 μM and diluted appropriately for use.

2.1.6. Cell lines

HeLa human epitheloid cervix carcinoma cell line were purchased from ATTC (Teddington, Middlesex, UK)

2.2. General Methods

2.2.1. Restriction Enzyme Digests

Restriction enzyme digests were typically carried out in a final reaction volume of 20-50 μl depending on the quantity of DNA being cleaved. The enzyme concentration for each reaction was between 2-5 Units per 1 μg DNA, and the appropriate buffer was used at a 1X concentration. Unless otherwise stated by the manufacturer, the reactions were incubated for 2 hrs at 37°C. All restriction digestion enzymes and buffers were obtained from New England Biolabs (Frankfurt, Germany).

2.2.2. Phenol/Chloroform Extraction of DNA

DNA samples were mixed with equal volumes of buffer saturated phenol (pH 7.5), vortexed for 30 seconds and centrifuged at 13,200 rpm for 5 minutes using a Micromax Centrifuge (Thermo-Electron, Waltham, MA, USA). The upper aqueous phase containing the DNA was transferred to a fresh epindorff and an equal volume of phenol/chloroform was added, vortexed and centrifuged as above. An equal volume of chloroform was then added to the aqueous phase, and centrifuged as before. The aqueous phase was removed and DNA extracted by ethanol precipitation.

2.2.3. Ethanol Precipitation of DNA

To precipitate the DNA, 0.1X volume of 3 M Sodium Acetate (pH 7.0), and 3X volume of 100% ethanol was added to the DNA solution. Samples were mixed and left at room temperature for 30minutes, and centrifuged at 13,200 rpm for 15 minutes (Micromax; Thermo-Electron). The supernatant was removed and the DNA pellet was washed in 80% ethanol. Following centrifugation for 15 minutes at 13,200 rpm the pellet was allowed to air dry before final resuspension in ddH_2O or PBS, depending on the downstream application required.

2.2.4. Agrose Gel Electrophoresis and DNA extraction

DNA was visualised on 1-2 % agarose gels, prepared by heating agrose in 1X-TAE buffer. Higher percentage gels are used to provide a better separation of small DNA bands (< 200 bp). The agarose solution was allowed to cool before the addition of ethidium bromide (0.5 μg/ml) used to allow visualisation of DNA under U.V. light. Subsequently the solution was poured into the casting blocks with combs and allowed to set. To load the gel, the combs were removed and the gel immersed in 1X TAE in the gel rig (Bio-Rad Laboratories; Hercules, CA, USA). Prior to loading each DNA sample was mixed with 0.1X loading dye, either bromophenol blue or xylene cyanol depending on the size of the DNA band to be visualised. Bromophenol blue and xylene cyanol migrate in a 1% gel at 400-500 bp and 4-5 Kb respectively. The DNA was loaded into the wells of the gel along with a DNA size marker (100 bp and 1Kb;

New England Biolabs). A current of 80 mA was applied to the gel, with the DNA migrating to the positive pole. DNA was visualised using a UV light source on the Gene Genius Gel Documentation System with GeneSnap software (Syngene, Cambridge, UK).

DNA fragments were extracted from agrose gels using the QIAquick® Gel Extraction Kit (Qiagen, Hilden, Germany). The desired DNA band was excised from the gel under U.V. light using a clean, sharp scalpel. DNA was extracted from the gel following the manufacturer's instructions.

2.2.5. Competent Cell Preparation of *E. coli* XL1B

A 1 ml overnight culture of *E.coli* strain XL1B was used to inoculate 25 ml LB selective media (containing 50 μg/ml tetracycline) and the bacteria were cultured until the optical density reading (OD_{600}) reached 0.45 to 0.5 (equals approximately 10^8 cells/ml). The cells were spun at 3,000 rpm for 10 minutes (GS-6 Centrifuge; Beckman Coulter, Fullerton, CA, USA), and the supernatant discarded. The cells were washed in 25 ml of $MgCl_2$ (100 mM; 4°C) and centrifuged for a further 10 minutes. The supernatant was discarded and the cells resuspended in 25 ml $CaCl_2$ (100 mM; 4°C). The cells were left on ice for 20 minutes, followed by 10 minutes of centrifugation and resuspension in 2.5 ml of 100 mM $CaCl_2$ (4°C).

2.2.6. Transformations

10 μl of the each ligated DNA solution was diluted in 90 μl of $CaCl_2$ (100 mM) and added to 200 μl of competent cells. The samples were left on ice for 30 minutes and then heat-shocked at 42°C for 2 minutes, and then returned to ice. 2.7 ml of LB media (see section 2.1.1) was added to each of the samples, and the samples were incubated at 37°C for 1 hour shaking at 225 rpm. 200 μl of each transformation was plated onto LB agar plates containing tetracycline (50 μg/ml) and spectinomycin (50 μg/ml), and incubated at 37°C overnight.

2.2.7. Plasmid DNA Mini-Preparations

10 ml of selective LB media was inoculated with a single colony and incubated at 37°C shaking overnight at 225 rpm to achieve a log phase of growth and to maximise plasmid retrieval. The media was spun at 3,200 rpm (GS-6) for 10 minutes and the supernatant poured off. The cells were resuspended in 60 µl of lysis solution 1 (see section 2.1.1.) and 20 µl of fresh lysozyme (40 mg/ml in 250 mM Tris-HCl pH 8.0) was added. The samples were incubated on ice for 10 minutes prior to the addition of 550 µl of M-STET solution (see section 2.1.1) and incubated at room temperature for 10 minutes. The samples were placed in boiling water for 1.5 minutes and then centrifuged at 13,200 rpm (MicroMax; Thermo-Electron) for 30 minutes. The pellet containing cell debris was removed and 1 µl of RNace-IT riobonuclease cocktail (Stratagene Inc., La Jolla, CA, USA) was added to the lysate and incubated at 37°C for 15 minutes. An equal volume of buffer saturated phenol (pH 8.0) was added, vortexed and centrifuged at 13,200 rpm for 5 minutes (MicroMax; Thermo-Electron). The top aqueous layer was removed to a new tube and 0.6X volume of isopropanol was added to the samples, which were left at room temperature for 15 minutes. The samples were centrifuged for 10 minutes and then supernatant poured off. The DNA pellet was washed with 80% Ethanol and allowed to air dry, and finally resuspended in 50-100 µl of sterile ddH_2O.

2.2.8. Large-scale Plasmid Purification

The Qiagen High Speed Plasmid Maxi Kit (Qiagen, Hilden, Germany) was used for all large-scale plasmid purifications according to the manufacturer's instructions. Briefly, colonies derived from a single bacterial clone were used to seed 2 ml of LB containing tetracycline (50 µg/ml) and spectinomycin (50 µg/ml). These cultures were grown for 8 hours at 37°C and 1 ml of the media was used to seed 200 ml of LB media, which was incubated overnight in an orbital shaker at 225 rpm at 37°C. The culture was centrifuged at 5,000 rpm for 15 minutes (Sorvall RC-5B Centrifuge; Beckman Coulter, Inc., Fullerton, CA, USA) and the pellet was purified using components of the Qiagen High Speed Plasmid Maxi Kit to produce 1 ml of high quality DNA.

2.2.9. Glycerol Stocks of Bacteria

Colonies derived from a single bacterial clone were used to inoculate 1ml of LB media and appropriate antibiotics, and grown overnight in an orbital shaker at 225 rpm at 37°C. 0.5 ml of sterile glycerol was added to the culture and vortexed. The sample was then frozen rapidly in liquid nitrogen and transferred to the –80°C freezer for long-term storage. To recover the bacteria, the frozen culture was scraped with a sterile inoculation loop and immediately streaked onto the surface of an agar plate containing the appropriate antibiotics. The plate was then incubated at 37°C overnight.

2.2.10. Quantification of DNA and RNA

Isolated nucleic acids (DNA and RNA) were quantified using the NanoDrop™ 1000 Spectrophotometer (Thermo Scientific, Wilmington, DE, USA) by measuring the absorbance at a wavelength of 260 nm (A260). After a blank measurement was made with ddH_2O, 1 µl of each sample was loaded onto the optical surface and the measurement readout (ng/ml) was displayed. The Beer Lambert Law is used to relate the amount of light absorbed at 260 nm to the concentration of dsDNA (50 $\mu g/OD_{260}$) and RNA (40 $\mu g/OD_{260}$), based on the different extinction coefficients of both nucleic acids. The ratio between the readings A260/A280 was used to determine the purity of the DNA and RNA sample. A ratio of 1.8 and 1.9-2.1 was achieved for pure DNA and RNA samples respectively.

2.2.11. Capillary Sequencing

Sequencing was performed using the ABI 310 Genetic Analyser (Applied Biosystems, Foster City, CA, USA) and the BigDye Terminator Cycle Sequencing Kit (Applied Biosystems). 250 ng of DNA, 2 pmol primer, 2 µl BigDye Terminator mix and 0.4 µl 5x Buffer were made up to a volume of 10 µl using ddH_2O. The reaction was cycled 35 times as follows: 96°C for 30 seconds, 50°C for 15 seconds, and 60°C for 4 minutes. After the PCR reaction the samples were precipitated using with 70% ethanol and 3 µl 3 M NaAc pH 4.6. The pellet was washed in 80% ethanol, air-dried and resuspended in 25 µl of Formamide Buffer (95% deionised formamide, 10 mM

EDTA, pH 8.0). The sample was denatured at 94°C for 2 minutes and then chilled on ice to maintain the DNA products in a denatured state. The samples were loaded and sequenced on an ABI 310 Genetic Analyser and the'ABI Prism 310 Collection' and 'Sequencing Analysis 3.1.4.' software was used to collect and analyse the sequence data. Sequencing was undertaking with the assistance of Alex McKee of the Smurfit Institute of Genetics, Trinity College Dublin.

2.3. General RNA Techniques

2.3.1 Ribonuclease (RNAase)-Free Conditions

As RNA is very susceptible to degradation it was very important that RNase-free conditions were maintained. Contaminating RNases were removed from glassware by autoclaving at high temperatures (180°C) for several hours or by soaking overnight in 5mM NaOH containing 0.1% Triton-X (Sigma). RNase-free pipette tips (Axygen Biosciences, Union City, California, USA), eppendorfs (Thermo Fischer Scientific,Waltham, MA, USA), solutions, and buffers were employed when RNA was being analysed. Clean gloves were worn at all times, and lab benches were cleaned using RNase Away (Sigma) and wiped down with 70% ethanol.

2.3.2. RNA Extraction from Animal Tissues and Cultured Cells

Most commercial RNA extraction kits do not recover RNA smaller than ~ 200 nucleotides. Due to this, the following two RNA extraction kits were utilised which specialise in purifying RNA while also recovering small RNAs from tissue and cultured cells; mirVana™ RNA Isolation kit (Ambion Inc., Texas, USA) and the miRNeasy Mini Kit (Qiagen, Hilden, Germany).

2.3.2.1. mirVana™ RNA Isolation Kit

The manufacturer's instructions were followed for extracting RNA using the mirVana™ RNA Isolation kit (Ambion Inc., Texas, USA), which is based on a phenol:chloroform RNA extraction, and total RNA purification using a glass-fibre binding procedure. For RNA extraction from animal tissue, 1 ml of lysis solution was added per 0.1 g of tissue, and the tissue was homogenised thoroughly on ice. The cells were homogenised using a pipette and the homogenised lysate collected. The lysis solution stabilises the RNA while also inactivating RNases. Equal volumes of acid-phenol:chloroform were used in the organic extraction, and the aqueous phase containing the RNA was collected. A glass-fibre filter was used for the final

purification of RNA. 1.25x volumes of 100% ethanol were used to immobilise the RNA on the glass-filter and the RNA was washed on the filter in a series of wash steps. The RNA was then eluted using 50 µl-100 µl of nuclease-free H_2O.

2.3.2.2. miRNeasy Mini Kit

The manufacturer's instructions were followed for both RNA extraction from animal tissue and cultured cells. The RNA extraction kit is based on a phenol/gudanidine lysis of cells and purification on a silica membrane. The QIAzol Lysis reagent contains phenol and guanidine thiocyanate and was used to lyse the cells and also to inhibit RNases. For extraction of RNA from animal tissue 700 µl of lysis reagent was added to fresh tissue (< 50 mg), and the tissue homogenized using a pipette .To extract RNA from cultured cells (< $1x10^7$ cells), the media was removed and 700 µl of the QIAzol Lysis Reagent was added directly to the cells. The cell lysate was transferred to a tube and homogenised by vortexing. Following homogenisation of the samples in the lysis reagent, the RNA was separated from the DNA and protein by an organic extraction, via the addition of chloroform. After centrifugation the upper aqueous phase, containing the RNA, was extracted and precipitated onto the RNeasy Mini spin column using 1.5X volumes 100% ethanol. This column system allowed RNA from up to 18 nt in size to attach, and contaminants were removed by a successive wash steps. The high quality RNA was then eluted from the column using Nuclease-free water.

During this protocol an optional DNase step was employed to ensure the removal of DNA from the sample when necessary for certain downstream applications. The RNase-Free DNase Set (Qiagen, Hilden, Germany) was used to provide an on-column digestion of DNA during the RNA purification protocol. After RNA immobilisation onto the filter column, ~30 Units of DNase I was added to each sample with the specified buffer, and digested for 2 hrs at 37°C. The RNA purification protocol stated above was then recommenced.

RNA concentration and purity was determined by measuring the absorbance at 260 nm (A260) and A260/A280 ratio respectively, using the NanoDrop™ 1000 Spectrophotometer (Thermo Scientific, Wilmington, DE, USA) (see section 2.2.10.)

2.3.3. Quantitative real-time RT-PCR (qPCR)

Quantitative real-time RT-PCR (qPCR) of both mRNA and miRNA transcripts, was performed using both the one-step Quantitech Sybr Green RT-PCR kit, (Qiagen, Hilden, Germany) and the two-step ABI miRNA TaqMan Assays (Applied Biosystems, Foster City, CA, USA).

2.3.3.1. miRNA Quantification using Two-Step real-time RT-PCR

ABI Taqman microRNAs Assays were used for all quantitative real-time RT-PCR of miRNAs. The Taqman microRNAs Assays are designed to sensitively detect and accurately quantify mature miRNAs, with a dynamic range of greater than 6 orders of magnitude. These assays are highly specific for individual miRs with single base pair discrimination and are designed to detect only the mature form of the miRNA and not the precursor sequence.

The TaqMan miRNA assays employ a two-step protocol. The initial step involves the reverse transcription (RT) of the total RNA samples into cDNA, using miR specific stem-loop primers. The second step involves the amplification of PCR products from the cDNA samples, which uses miRNA specific TaqMan MGB probes (Figure 2.1).

The primers used for the RT step are stem-loop primers, which include novel features. The stem structure of the stem-loop primer prevents the hybridisation of the probe with miRNA precursor sequences, while the ability of the primer to anneal to the 3' portion of the miR, allowing for the high specificity and sequence discrimination (Figure 2.1) (Schmittgen et al. 2008).

The high sensitivity and specificity of the assay is largely due to the forward PCR primer and TaqMan MGB probe. The TaqMan MGB probes contain three interesting features: 1) a 5' linked reporter FAM dye, 2) a 3' minor groove binder (MGB), and 3) a 3' non-fluorescent quencher (NFQ). During the PCR cycles the MGB probe anneals to the complementary sequence of the cDNA, between the forward and reverse primer target site. In the intact state, the probe does not fluoresce as the reporter FAM dye is suppressed by the proximity of the quencher dye. However

as the PCR process continues, the DNA polymerase cleaves the probes that are hybridized to the targeted cDNA. This cleavage results in the separation of the reporter dye from the quencher dye, and the FAM reporter dye is able to fluoresce and be detected by the Real-Time PCR machine. Due to the specific requirements for cleavage of the MGB probe (i.e. probe must be complementary and also amplified by the PCR) only specific amplification is detected (Figure 2.1)

Each RT reaction was performed using a single miR specific stem-loop RT primer and components from the TaqMan MicroRNA Reverse Transcription Kit (ABI). The RNA levels of the transcript under investigation were standardised to an internal controls, RNU19, RNU66, snoRNA-202, and snoRNA-234, which are all small nucleolar RNAs (ABI). The RNA samples were diluted to 2 ng/µl, and 5µl (10ng) of RNA was used in each 15 µl RT reaction, including 1.5 µl 10xRT-PCR buffer, 1µl of 50 U/µl MultiScribe RT enzyme, 0.15 µl 100x dNTP mix, 0.19 µl 20U/µl RNase-inhibitor, and 2µl 5x specific RT-primer. The reaction was made up to 15 µl with nuclease-free H_2O. The RT reactions were incubated on the T3000 Thermal Cycler (Biometra, Goettingen, Germany) as follows: 16°C for 30 minutes, 42°C for 30 minutes, 85°C for 5 minutes, and held at 4°C. Each PCR reaction was performed in a 96-well plate, using a unique set of PCR primers and TaqMan probes contained in the TaqMan miRNA assay. For each 20 µl reaction, 10 µl Universal PCR Master mix, 1 µl TaqMan Assay, 5 µl RT Product (diluted 1:60), and 4 µl nuclease-free water was added. The PCR reactions were incubated using the Applied Biosystems 7300 Real Time PCR System, at 95°C for 10 minutes, followed by 40 cycles of: 95°C for 15 seconds and 60°C for 60 seconds. All PCR reactions were performed in triplicate.

2.3.3.2. mRNA Quantification using Two-Step real-time RT-PCR

For qPCR of mRNA transcripts, individual TaqMan primers with TaqMan Gold Reverse Transcription Kit were used on the Applied Biosystems 7300 Real Time PCR System. A two-step RT-PCR was required for the use of specific TaqMan probes. A multiplex RT step was performed using the components of the TaqMan Gold Reverse Transcription Kit (ABI). RNA levels of the transcript of interest were standardised to the internal control gene 18S rRNA. The RT reaction was performed

using 100 ng of DNase treated total RNA (20 ng/µl), and added to 2 µl of 10X RT buffer, 4.4 µl of 25mM $MgCl_2$, 4 µl of 10X dNTP mix, 1 µl of Random Hexamer Primer, 0.4 µl of 20U/µl RNase inhibitor, 0.8 µl of 50 U/µl MultiScribe RT Enzyme, and nuclease-free H_2O to a final volume of 20 µl. The reactions were incubated on a thermocycler at 25°C for 10 minutes, 37°C for 60 minutes, 95°C for 5 minutes and held at 4°C. The PCR reaction was set up on a 96-well plate, using 4 µl RT product (diluted 1:5), 10 µl 2X PCR Master Mix (ABI), 1 µl TaqMan assay (ABI), and nuclease free water added to a final reaction volume of 20 µl. The PCR reactions were incubated at 95°C for 10 minutes, followed by 40 cycles of: 95°C for 15 seconds and 60°C for 60 seconds. The PCR reactions were performed in triplicate.

2.3.3.3. Quantification of mRNA using One-Step real-time RT-PCR

For qPCR of mRNA transcripts, primers for the target gene of interest were designed and used with the Quantitech Sybr Green RT-PCR Kit (Qiagen, Hilden, Germany) on the Applied Biosystems 7300 Real Time PCR System.

Primers were purified by high performance lipid chromatography (HPLC) and the RNA levels of the transcript of interest were standardised to an internal control genes: beta-actin and 18S rRNA. The forward and reverse primers were diluted in nuclease-free H_2O and used at a concentration of 10 pmol. Reactions were carried out at a final volume of 20 µl with 4.5 µl diluted RNA sample, 10 µl Master Mix, 0.3 µl RT enzyme, 1 µl of primer mix, 4.3 µl nuclease free H_2O. The samples were incubated on the 7300 Real Time PCR System (ABI), at 50°C for 30 seconds, 95°C for 15 minutes, and 35 cycles of 94°C for 15 seconds, 55°C for 30 seconds, and 72°C for 30 seconds.

2.3.3.4 RT-PCR Data Analysis

The comparative C_T (cycle threshold) method of PCR analysis was followed for all RT-PCR experiments as outlined by Livak and Schmittgen. (Livak and Schmittgen 2001). The Threshold Cycle (C_T) reflects the cycle number at which the

fluorescence generated within a reaction crosses the threshold. The Ct value assigned to a particular well thus reflects the point during the reaction at which a sufficient number of amplicons have accumulated, in that well, to be at a statistically significant point above the baseline.

This comparative C_T method is also known as the $2^{-\Delta\Delta CT}$ method and relies on the assumption that the PCR efficiency is close to 1 and the PCR efficiencies of the target transcript and internal control are similar. Data analysis of qPCR data involved a two-step processing of the raw C_T data. The first step normalised the C_T value of the transcript of interest to the internal control for each sample, termed the ΔC_T value.

I.e. ΔC_T = (C_T gene of Interest – C_T Internal Control)

The second step expressed the data for each sample relative to the control (untreated) sample, resulting in the $\Delta\Delta$ C_T value. To obtain a measure of the fold change, the data was transformed to a linear scale, as C_T data is expressed on a $\log_2$ scale. The following formula was used where sample A is the treated sample, and sample B is the untreated control:

$2^{-\Delta\Delta Ct}$ = (ΔC_T gene of interest – C_T internal Control) Sample A

– (ΔC_T gene of interest – C_T internal Control) Sample B.

A worked example is illustrated in Table 2.1, where miRNA expression of miR-182 in compared in wild type (wt) and transgenic (tg) animal tissues (Table 2.1)

2.3.4. *In Situ* Hybridisation (ISH)

2.3.4.1. RNAase-Free Conditions

Along with the general precautions for handling RNA (2.3.1.), it was also important for ISH to ensure that all solutions were free of contaminantion. All solutions used are treated with diethyl-pyrocarbonate (DEPC) to remove any RNase enzymes, and all glassware, instruments, and humidifier chambers were cleaned with RNase Away (Sigma-Aldrich) and 70% ethanol. See section 2.1.3 for information on the solutions used in for ISH.

2.3.4.2. Cryo-sectioning

Following dissection of mouse eyes, the eyes were fixed in 4% fresh paraformaldehyde for 2 hrs. The lens was then removed from the eye and the tissue washed twice in PBS for 5 min. The tissue was cryoprotected by immersing the tissue in a series of sucrose gradients (10%, 20%, 30% sucrose in PBS). On the day of the ISH protocol the eye was suspended in the OCT (Optimal Cutting Temperature) compound (Tissue Tek; Sigma-Aldrich) within plastic moulds. The tissue within the OCT was quickly frozen over isoproponal using liquid nitrogen, to allow for a slower rate of freezing. The tissue was then allowed to adjust to –20°C for 30 minutes before sectioning. Sections were taken using the Lecia CM 1900 Cryostat Machine (Meyer Instruments Inc., Houston, TX, USA) at a thickness of 12 μm.

2.3.4.3 APES (3-aminopropyltriethoxysilane)-coated slides

The covalent bonding of amino acids to the surface of glass microscope slides provides a net positive charge on the slide surface, which facilitates the adhesion of sections from animal tissues. Pre-washed glass microscope slides (Sigma-Aldrich) were placed in a slide rack, and washed in 1% Triton X-100 (Sigma-Aldrich) for 10 minutes before rinsing under running water for 10 minutes. The slides were placed in acetone for 10 minutes, followed by acetone containing 2% APES (3-aminopropyltriethoxysilane; Sigma-Aldrich) for 20 minutes. The slides were then rinsed in ddH_2O for 2X 10 minutes, and air-dried overnight at 60°C. Slides were stored in an RNase free container at room temperature until use.

2.3.4.4. ISH Protocol

5'-Digoxigenin (DIG)-labelled LNA-modified oligonucleotide ISH probes (Exiqon, Vedbaek, Denmark) were purchased for the following mouse miRs: miR-1, -9*, -26b, -96, -129-3p, -133b, -138, -182, -335, -451 and let-7d. The positive control miR-181a and negative control sense-miR-159 were used as controls. The manufacturers guidelines for the ISH protocol were followed and adapted to recommendations outlined by Obernosterer *et al.* (Obernosterer et al. 2007).

Following the collection of tissue sections on APES-coated slides, the sections were allowed to air dry for a maximum of 3 hrs prior to post-fixing in 4% paraformaldehyde. The sections were DEPC-treated for 15 minutes, washed twice in 1X PBS for 5 minutes, and incubated in pre-hybridisation buffer (see section 2.1.3.) for 2 hrs at the hybridisation temperature. The hybridisation temperature differed for each individual probe, determined to be 21°C lower than the melting temperature (T_m) of the probe (see Table 2.2). Hybridisation solution containing the specific LNA probe at 20 nM was added to the sections. The sections were covered with plastic coverslips (Sigma) and hybridised in a humidifier chamber at the specified hybridisation temperature for 16-18 hours. Hybridised sections were then washed twice with 50% formamide, 2XSSC for 30 minutes, at the hybridisation temperature. Following this the sections were placed in blocking buffer (2% Sheep Serum, 2 mg/ml BSA; see section 2.1.3) for 1 hour at room temperature, followed by incubation with anti-DIG-alkaline-phosphatase antibody-enzyme conjugate (Roche Applied Science, Indianapolis, IN, USA) overnight at 4°C at a concentration of 1:2000 (in 2% Sheep Serum, 2mg/ml BSA). Following successive washes in PBS-T, the sections were incubated with nitroblue tetrazolium and 5-bromo-4-chloro-3-indoyl phosphate substrate (NBT-BCIP; Roche Applied Science) at a concentration of 20 µl/ml in AP Buffer (see section 2.1.3). The colour reaction was allowed to develop for up to 4 days, depending on the miRNA expression level. The reaction was stopped by successive 5-minute washes in PBS. Nuclei were counterstained with 4',6-diamidine-2-phenylindole-dihydrochloride (DAPI; see section 2.8.), and sections mounted with Aqua-Poly/Mount (Polysciences Inc.,Warrington, PA, USA).

2.3.5. MiR Microarray Expression Profiling

Technical assistance was received from the microarray service companies, Ambion and Exiqon, which performed the miR micorarray profiling of total RNA provided to them, and the normalisation of the raw signals obtained from the arrays.

2.3.5.1. Tissue Collection and RNA Extraction

Retinal tissue, whole-eyes, and brain tissue were dissected from mice using sterilised RNase-free equipment following standard dissection techniques. The RNA was extracted as outlined in section 2.3.2.

2.3.5.2. miR Microarray Platforms

The miR profiling of the total RNA samples prepared from mouse tissue were outsourced to two miR microarray profiling companies, namely Ambion (Austin, Texas, USA) and Exiqon (Exiqon, Vedbaek, Denmark) both of which employ different microarray technologies i.e. mirVana™ miRNA Bioarray (Ambion) and miRCURY™ LNA (Locked Nucleic Acid) microRNA Array (Exiqon, Vedbaek, Denmark). LNA is a nucleic acid analogue, in which the ribose ring is modified and 'locked' in a conformation which increases the binding affinity of the LNA probes for complementary DNA or RNA sequences, resulting in a more stable duplex. LNA probes used for the detection of miRs, is beneficial due to the high sensitivity and specificity of these probes (Vester and Wengel 2004).

The mirVana™ miRNA Bioarray v.2 is a single-coloured microarray that profiles miRs using amine modified DNA probes. The v.2 array contained probes for 642 miRs (486 human, mouse and rat miRs and 156 Ambi-miRs) covering miRs annotated in Sanger miRBase release 8.0 (February, 2006).

The miRCURY™ microarray is a dual-coloured microarray, accommodating parallel hybridisation of a reference sample, allowing for direct comparison of data between arrays. Two versions of the miRCURY LNA™ microRNA Arrays were used

to accommodate additional miRs annotated in the updated releases of Sanger miRBase Database (miRBase) . The miRCURY LNA microRNA Array v.8.1 and v.9.2 were used, which probed for miRs annotated in miRBase v.8.1 (release date May 2006) and v.9.2 (release date May 2007) respectively. The miRCURY LNA microarray contained probes specifically for mouse miRs, and the v.8.1 and v.9.2 arrays probed for 489 miRs (343 mouse and 147 Exiqon miRs) and 494 miRs (420 mouse and 74 Exiqon miRs) respectively. In comparison to miRBase v.10.0 the coverage of the probe set used in the v.8.1 and v.9.2 array is 66% (385 of 579) and 74% (431 of 579) respectively.

Note that the hypothesised Exiqon (miRPlus) and Ambion (ambi-miR) miR sequences were not represented in the Sanger miR Database at the time of array manufacture. As a result of later releases of the miRBase database, some of these hypothesised miRs were revealed to be novel miR sequences. Note that all samples were outsourced to Ambion and Exiqon for miR profiling, and all samples and replicates were analysed on separate miR microarrays.

2.3.5.3 mirVana™ miR Microarray Protocol

Samples were checked for quality using the Agilent BioAnalyzer 2100 (Agilent Technologies, Inc., USA); ensuring that the RNA integrity score (Nairz et al.) was greater than 7.0. Total RNA (3–10 μg) extracted using the miRVana miRNA Isolation Kit (see section 2.2.2) was labelled using the mirVana miRNA Labeling Kit (Ambion). A 3' amine modified tail (20-50 nt) was added to the RNA using Poly(A) Polymerase, which allowed the Cy5 fluor to couple with the RNA to produce a fluorescent-labelled sample. The coupling of multiple fluorescent molecules to the 3' tail aided the sensitivity and accuracy the microarray data. The labelled samples were denatured and hybridised to the array for 12-16 hours at 42°C. 10 synthetic spike-in controls were used in each array to monitor bias within each microarray experiment. The miRNA spike-in controls were used at concentrations that spanned the dynamic range of the array intensity; each array contained 4 replicate probes complementary to each miRNA control sequence.

Low stringency washes were followed by a high stringency wash to remove non-specific binding to the array probes. The arrays were dried and images were acquired using the Axon® GenePix 4000B scanner (Molecular Devices, Sunnyvale, CA, USA) and GenePix software (Molecular Devices, Downingtown, PA, USA).

2.3.5.4. miRCURY™ LNA miR Microarray Protocol

The RNA sample quality was analysed on the Agilent Bioanalyser 2100 (RIN > 7.0) and RNA measurement were determined using the NanoDrop™ 1000 Spectrophotometer. Total RNA samples were labeled using the miRCURY™ LNA microRNA Array Power Labelling Kit (Exiqon, Vedbaek, Denmark), which includes a dephosphorylation step to minimise self-circularization and concatamerization of miRs, thus limiting dye bias. In total 1 μg of total RNA from experimental samples and reference sample were labelled in separate reactions with Cy3 and Cy5, respectively. The reference sample allows for direct comparison of array data between arrays, as the miR expression is expressed as a log ratio (Cy3/Cy5) relative to the miR contained in the reference sample. The reference sample was prepared by combining total RNA from 10 mouse tissues (including mouse brain, kidney, heart lung, liver, ovary, spleen, testicle, thymus and embryo) from the Mouse Assorted Total RNA Kit (Ambion). Spike-in controls were also added in various concentrations in both Cy3 and Cy5 labelling reactions that covered the full signal range. Each spike-in control had 32 replicates of capture probes on the array and was used to evaluate the labelling reaction, hybridization, and the performance of the array experiment. The Cy3 and Cy5 labelled samples were mixed pair-wise, denatured, and hybridised to the microarray at 56°C for 16 hours using a Tecan HS4800 hybridization station (Tecan, Grödig, Austria). Low stringency and high stringency washes were carried out and the microarrays dried. The microarray slides were scanned and stored in an ozone free environment (ozone level below 2.0 ppb) in order to prevent potential bleaching of the fluorescent dyes. The microarray slides were scanned using the Agilent G2565BA Microarray Scanner System (Agilent Technologies, Inc., USA) and the image analysis was carried out using the ImaGene 7.0 software (BioDiscovery, Inc., USA). The quantified signals were normalized using the global LOWESS (LOcally WEighted Scatterplot Smoothing) regression algorithm.

2.3.5.5. Microarray Data Analysis

Analysis of microarray data obtained using both array platofrms, was performed by the microarray profiling service companies, Exiqon and Ambion. The raw signal for each probe was obtained by subtracting the maximum of the local background and negative control signals from the foreground signal. The data was pre-processed to remove poor-quality spots and normalisation was used to remove any systematic bias.

Global normalisation of the miRVana microarrays was undertaken using the Variance Stabilization Normalization (VSN, (Huber et al. 2002)) method, while the Exiqon miR arrays were normalised by the global Lowess (LOcally WEighted Scatterplot Smoothing) regression algorithm (LOWESS, (Yang et al. 2002)). Normalisation attempts to correct for systematic bias in the data so that the true biological differences in gene expression can be more readily distinguishable, and to allow the comparison of expression differences across arrays. The types of systematic bias that can be introduced during array protocols include dye bias, scanner issues, and spatial bias. Normalised $\log_2$-transformed spot intensities and $\log_2$-transformed ratios were used for further analysis, as log transformation treats up-regulated and down-regulated genes symmetrically.

2.3.5.5.1. LOcally WEighted Scatterplot Smoothing (LOWESS)

In experiments where there are two fluorescent dyes used, the intensity dependent variation in dye bias can introduce variations in the collected data. Intensity-dependent dye bias is observed as a curvature on a M-A plot (Intensity Log Ratio (M) minus Intensity Level (A) plot). LOWESS normalisation merges two-colour data, by applying a smoothing adjustment that removes this variation resulting in a flat M-A plot (Figure 2.2 A). It does this by producing local estimates of the intensity log ratios (M) for various intensity levels (A), and adjusts each observed $\log_2$ ratio by subtraction of the calculated best-fit average $\log_2$ ratio. As illustrated in Figure 2.3., the normalised Cy3 and Cy5 values of the spike-in controls are strongly correlated, demonstrating that the normalised values do not display bias. (Figure 2.3.) . Spatial bias can also be introduced due to hybridisation artefacts or print tip variations during the printing of

each array. The spatial bias is removed by using individual LOWESS fits within each print tip group. After normalisation the log ratios from each print tip group is centred around zero (Figure 2.2 B).

2.3.5.5.2. Variance Stabilisation Model (VSM)

The variance of the spot intensity for each probe is dependent on the mean of the spot intensity. The log ratio reduces this dependence at high intensities; however at low intensities the variance is inflated. Variance stabilizing transformation is used to obtain a constant signal to noise ratio so that the difference statistic, Δh, exhibits a constant variance independent of the spot intensity. This replaces the log-ratio as a measure of differential gene expression, where Δh is the difference between the transformed data of the individual samples. For large intensities the values of Δh and the $\log_2$ ratio coincide, however for small intensities that are near the detection limit of the experiment, the values of Δh are contracted towards zero in comparison to those of the log-ratio (Huber et al. 2002; Lin et al. 2008). As a result the normalised $\log_2$-transformed spot intensities generated using this method are termed *generalised* $\log_2$ ratios ($g\log_2$).

2.4. Mammalian Tissue Culture Techniques

2.4.1. Sub-culturing mammalian cells

Adherent cells were grown in 10 cm tissue culture dishes (Nunclon) containing DMEM media at 37°C and 5% CO_2 in an incubator (Form Scientific) until 70-80% confluent. The media was removed using an aspirator and the cells were washed with 5 ml of phosphate buffered saline (PBS, Lonza). The PBS was removed and 1 ml of 2X EDTA-Trypsin (Sigma) was added to dissociate the cell monolayer and incubated at 37°C for 5 minutes. The detached cells were removed into a sterile tube and 10 ml of media was added to inhibit the activity of the trypsin. The cells were centrifuged at 1,000 rpm for 5 minutes and the pellet was resuspended in 5 mls of DMEM and 20 µl was removed for cell counting. Cells were sub-cultured 1:4 ($5x10^5$ cells) in new

dishes containing 10 mls media, which was renewed every 2-3 days. The passage number of the cells were updated and recorded following each sub-culturing procedure. All tissue culture procedures were carried out in a laminar airflow cabinet (ESI Securigarde 1200; Thermo Electron), with the exception of centrifugation and cell counting.

2.4.2. Haemocytomoeter cell counting

The edges of a coverslip were dampened and place over the counting area on a haemocytometer slide (Hawksley; Lancing, Sussex, UK) to achieve a secure seal. The cell sample was diluted 1:10, gently pippeted along the edge of the coverslip, resulting in the movement of liquid between the slide and the coverslip. The slide was viewed under the microscope using 100X magnification. The numbers of cells occupying four quadrants of the slide were counted, and the average number of cells per quadrant was calculated. The number of cells = average cell count x dilution factor x 10^4/ml.

2.4.3. Freezing cell stocks

Cells were grown to 70-80% confluency in 10 cm dishes, harvested and the pellets were resuspended in 2 mls DMEM (Sigma). 500 µl of the cell suspension was added to labelled cryotubes (Nunc, Rochester, NY, USA) containing an equal volume of 2X freezing solution (see section 2.1.4.). Cryotubes were frozen in a "Mister Frosty" freezing container (Nalgene, Rochester, NY) and stored at –80°C.

2.4.4. Transfection of cells with LipofectAMINE 2000

LipofectAMINE 2000 (Invitrogen, Carlsbad, CA, USA) is a polycationic lipid reagent that can be used to deliver nucleic acid molecules to cells. One day prior to transfection, cells were harvested, counted and plated on 6-well plates so that they would be approximately 90% confluence on the day of transfection. For the transfection of 4 µg of DNA, the DNA was diluted in 250 µl of serum-free media (Opti-MEM I, Invitrogen). 10 µl of the LipoFectAMINE 2000 reagent was diluted in

240 µl of serum-free medium (Opti-MEM I, Invitrogen) and complexed with the DNA for 5 minutes at room temperature. The diluted DNA and lipofectamine containing media were combined and incubated for 20 minutes at room temperature. 500 µl of the DNA-Lipid complexes were pippeted directly onto the cells and mixed gently by rocking the plate back and forth. The cells were incubated at 30°C and harvested 24 hrs later for total RNA isolation as outlined in section 2.3.2.2.

2.5. Fluorescent Activated Cell Sorting (FACS) analysis

2.5.1. Retinal dissociation

Retinas were collected in Hanks Balanced Salt Solution (HBSS; Lonza). The retinas were added to 1 ml of HBSS containing 1 mg/ml trypsin (Sigma-Aldrich) and 50 µg/ml DNase I (Sigma-Aldrich). The sample was incubated at 37°C for 20 minutes and gently homogenised using a pipette tip every 5 minutes. 2 mg/ml Trypsin Inhibitor (Roche Applied Science) was added to the sample, prior to centrifugation at 600 rpm for 5 minutes. The pellet was resuspended in HBSS containing 50 µg/ml of DNase I, and the sample was transported on ice to the UCD Facility for FACS analysis.

2.5.2. FACS

Technical assistance was received for the Fluorescent Activated Cell Sorting (FACS), from the FACS technicians Dr. Alfonso Blanco from the Flow Cytometry Core Facilities at University College Dublin and Dr. Barry Moran from the Biochemistry Department, Trinity College Dublin.

Prior to sorting with the BD FACSaria cell sorting system (BD Biosciences, San Jose, CA, USA) the cell suspension was filtered through a 50 µm Filcon Filters (Dakocytomation, Glostrup, Denmark). The sorter incorporated three lasers, which emit light at the following wavelengths; 488 nm (blue), 633 nm and 407 nm (violet). As cells flow past a focused laser beam the beam is deflected enabling the detection of two scatter signals, side scatter and forward scatter. Forward scatter is a measure of

cell size, and side scatter is a measure of cell granularity or general shape. A FITC optical filter was used to detection fluorescence and a non-fluorescent sample was used as a control, to enable the determination of the auto-fluorescence threshold. A sorting flow rate was chosen to maximise the purity of the final samples. Following sorting the cells were immediately concentrated on an Ultrafree-MC filter unit (Millipore, Bedford, MA, USA) at a concentration of < 200,000 cells/unit by centrifugation at 1,300 rpm for 1 minute. The filter units were frozen on dry ice for transportation, and stored at –20°C until further use.

2.6. Database Resources

2.6.1. Gene Sequence and Information Retrieval

The Sanger miRBase database was used for the sequence retrieval of all individual miRs, in addition to the examination the genomic location of these miR genes (miRBase).

Gene symbols were obtained from the Mouse Genome Informatics Database (MGI), the authoritative source of official names for mouse genes, alleles and strains (MGI_Database).

Entrez Gene, a database which provides gene-specific information of sequenced genes, was used to obtain Entrez Gene IDs and identifier information linked to these genes (Maglott et al. 2005).

UniGene is a database which provides information of the transcriptome, in which a unique UniGene entry represents a group of transcript sequences that appears to be transcribed from the same transcriptional unit (Sayers et al. 2008; UniGeneDatabase).

The data integration system, BioMart was additionally used to cross reference Gene IDs, and to retrieve information linking Gene IDs to other identifier information, such as the 3'UTR sequence and chromosomal coordinates (Durinck et al. 2005).

2.6.2. miRNA Target Prediction Software

MiR target prediction were undertaken using the target prediction software, miRanda (John et al. 2004), Pic-Tar (Krek et al. 2005), TargetScan (Lewis et al. 2003), and miRGator (Nam et al. 2008). In addition, the secondary structure of miR target sites were analysed using the software UNAFold (Markham and Zuker 2005; NEIBank). Tecnhical assistance was received from Dr. Karsten Hokamp, of the Smurfit Institute of Genetics, Trinity College Dublin.

2.6.3 Gene Expression Libraries

IDs of genes expressed in retina were downloaded from mouse eye libraries from UniGene and NEIBank, the Nationl Eye Institute database which contains genes expressed in the eye, including disease genes (Wistow 2002; Wistow et al. 2008; NEIBank).

2.6.4 Retinal Information Network

The retinal information network was commonly used to monitor newly identified retinal mutations (RetNet) .

2.6.5. Literature

The U.S. National Institutes of Health (NIH) archive of biomedical and life sciences journal literature, PubMed, was used to obtain the most up-to-date information used in the formulation of this thesis .

2.7. Animal Tissue Collection

Mice were sacrificed by CO_2 asphyxiation and standard dissection techniques were employed to dissect tissue from the brain and eye, including the retina.

2.8. Histology and Microscopy

Following dissection of the eye, the tissue was fixed in 4% paraformaldehyde for 4 hours at 4°C. Cryosectioning of eye tissue was undertaken as outlined in section 2.3.4.2 and sections placed on Poly-L-Lysine microscope slides (Polysciences Inc., Warrington, PA, USA). Nuclei were counterstained by using 4',6-diamidine-2-phenylindole-dihydrochloride (DAPI, Invitrogen). Sections were incubated in 300 mM DAPI solution in PBS for 1-5 minutes. The sample was washed twice in 1X PBS for 5 minutes, and mounted using aqueous mounting media (Sigma). Sections were analysed by bright field normal and phase-contrast as well as fluorescent microscopy using an Axiophot microscope (Carl Zeiss Ltd., Hertfordshire, UK) using the appropriate filters. Composite images were produced using the software Adobe Photoshop (Adobe Systems Europe Ltd., Glasgow, UK).

2.9. Immunocytochemistry

Following FACS analysis (section 2.5), the cells were fixed in 4% paraformaldehyde for 1 hour at 4°C. The cells were washed in 1xPBS and air-dried onto Poly-L-Lysine microscope slides. A water-resistant barrier was drawn around the sample using a PAP pen (Dako, Glostrup, Denmark). Each slide was incubated in 120 µl of blocking solution (10% goat serum, 0.3% Triton-X in PBS) for 2 hours at room temperature. The blocking solution was removed, and the sections were incubated in 120 µl of primary antibody overnight at 4°C. The following primary antibodies were used, mouse anti-RHO (1:100; from R.Molday) and rabbit anti-rod-transducin-alpha (1:100; Santa Cruz Biotechnology Inc., Santa Cruz, CA, USA), diluted in PBS containing 2% goat serum, and 0.1% Triton-X. the slides were washed for 4x 5 minutes in PBS and incubated with the secondary antibody (anti-mouse IgG-Cy3 and anti-rabbit IgG-Cy3) conjugated to Cy 3 dye (Invitrogen) (diluted 1:500 in 2% goat serum, 0.1 Triton-X, in PBS) for 2 hours at room temperature in a dark box. The slides were washed for 2x5 minutes in PBS, and then counter stained with DAPI (section 2.8), and washed for 2x5min in PBS and mounted using Aqua-Poly/Mount (Polysciences Inc., Warrington, PA, USA)

2.10. Statistical Analysis

Data from given sets were pooled, averaged and standard deviation (SD) values calculated. Statistical significance of differences between data sets was determined using either Student's two-tailed t-test, ANOVA, or Pearson's correlation; differences with $p<0.05$ were considered statistically significant. The statistical software package, GraphPad Prism 4, was used for all statistical analysis.

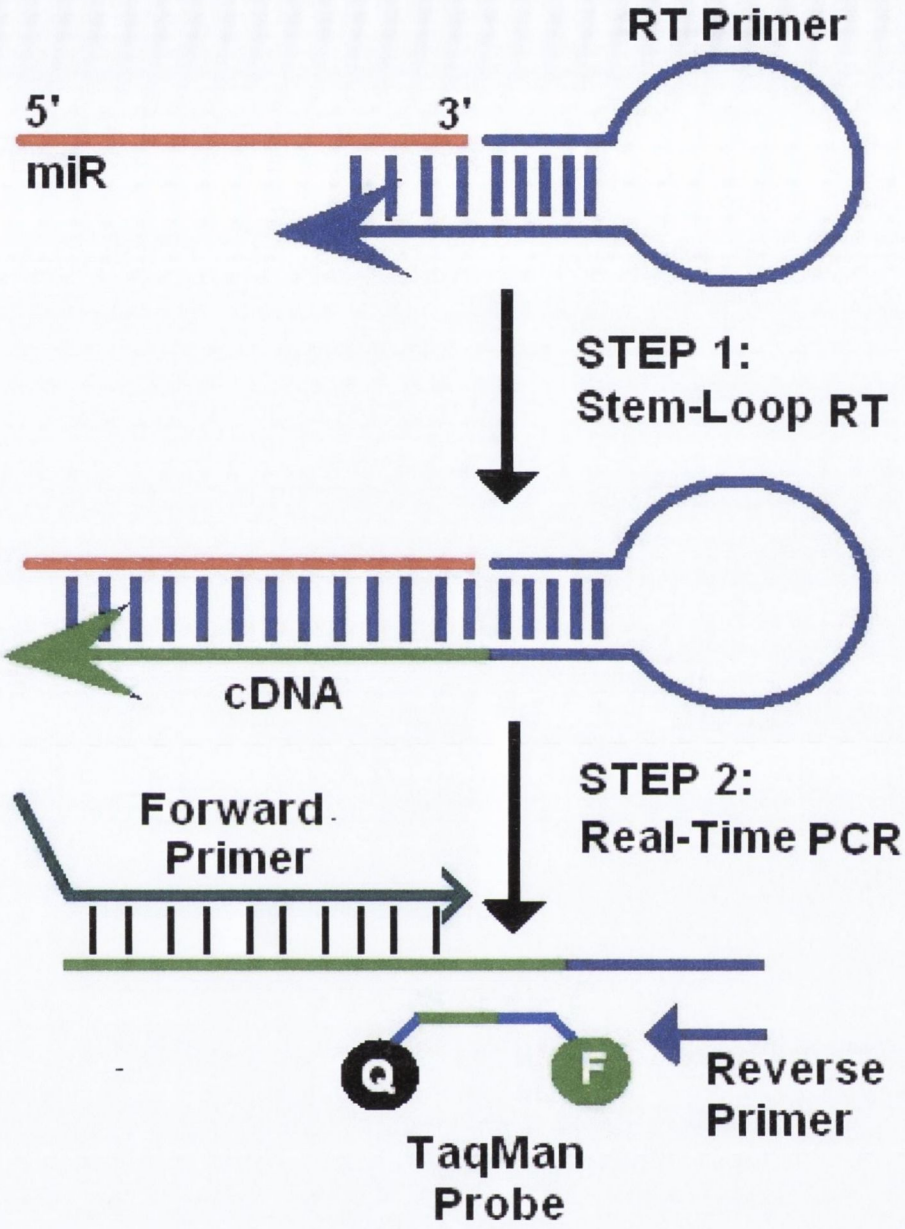

Figure. 2.1. Schematic representation of miR RT-PCR using stem-loop primer and TaqMan Probe: Reverse Transcription of the miR initiates by the specific binding of the stem-loop primer to the 3'- region of the miR, the primer is then extended during the RT reaction resulting in the formation of cDNA. The second step involves the amplification of the cDNA by means of forward and reverse primers. The TaqMan probe contains a 5' FAM dye (F) and a 3' non-fluorescent quencher (Q). During PCR cycles the probe anneals to the complementary sequence of cDNA, between the forward and reverse primer sites. The annealed probe does not fluoresce due to the presence of the quencher dye, but transcription by DNA Polymerase cleaves the hybridised probe and the FAM dye emits fluorescence. Adapted from Schmittgen et al., (2008).

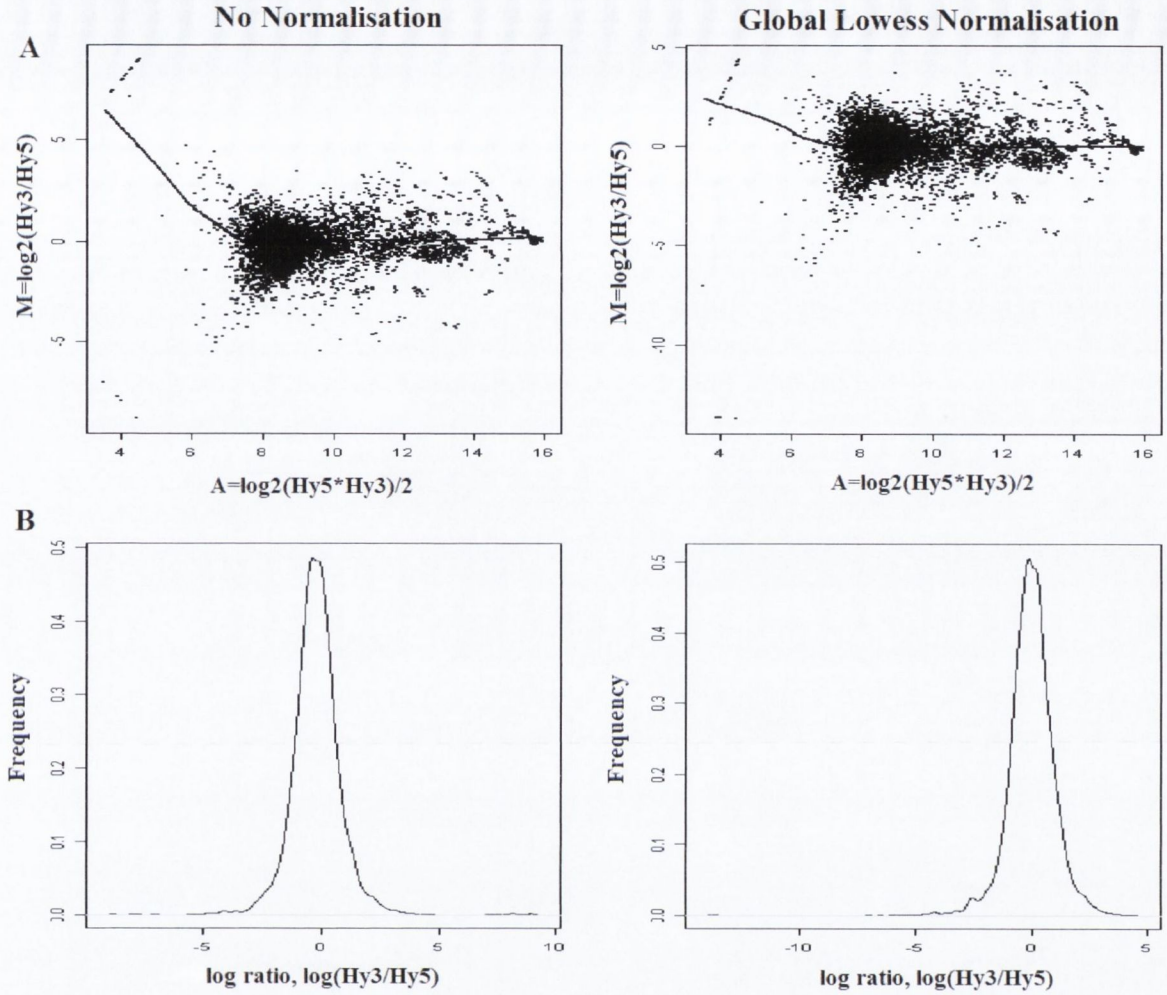

Figure 2.2: LOWESS Normalisation: **(A)** The M-A plot, where M is the intensity log ratio and A is the signal intensity level. With no normalisation the M-A plot is curved, due to dye bias. LOWESS normalisation smoothes the data by producing local estimates M for various A values, by subtraction of the calculated best-fit $\log_2$ ratio. This removes the effect of dye and spatial bias resulting in a flat M-A plot. **(B)** The Distribution Plot of Cy3/Cy5 ratios before and after normalisation, illustrates that normalisation has the effect of centering the Cy3/Cy5 $\log_2$ ratio on zero.

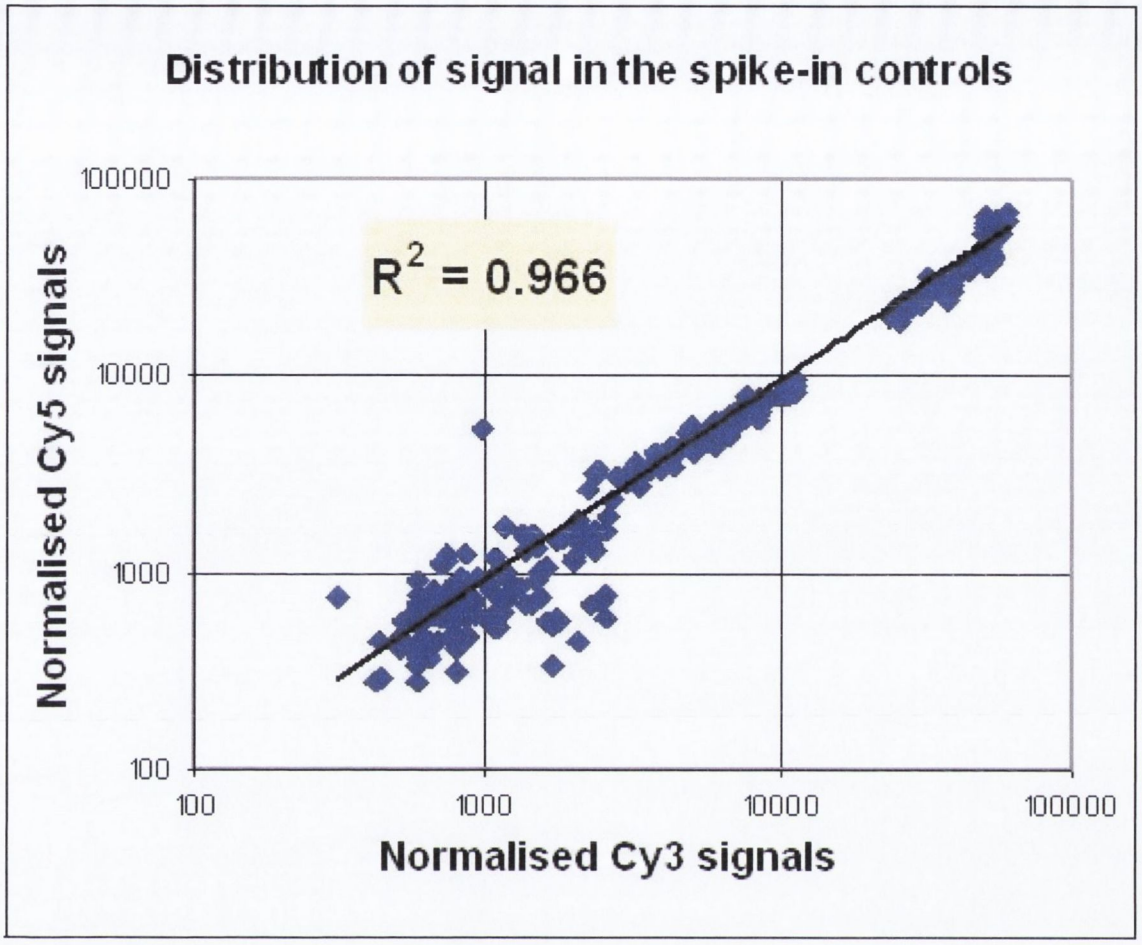

Figure 2.3: Scatter plot of normalised Cy3 and Cy5 signals from spike-in controls: This plot illustrates that the normalised Cy3 and Cy5 signals originating from spike-in controls. The normalised Cy3 and Cy5 values of the spike-in controls are strongly correlated by statistical correlation analyses (Pearson correlation); slope =0.95 and the R^2 value is 0.966. This demonstrates that normalisation using the LOWESS, eliminates bias which may exist, such as spatial or dye bias.

Well	Sample	Gene	Ct	ΔCt	Mean ΔCt	ΔΔCt	2^−ΔΔct	Mean Fold Change	S.D.
A1	Wt 1	miR-182	21.57	-1.60	-1.53	-0.07	1.05	1.00	0.10
A4	Wt 2	miR-182	21.94	-1.35		0.17	0.89		
A7	Wt 3	miR-182	21.51	-1.63		-0.10	1.07		
A10	Tg 1	miR-182	22.94	-0.39		1.13	0.46	0.51	0.05
B1	Tg 2	miR-182	23.35	-0.63		0.90	0.54		
B4	Tg 3	miR-182	23.06	-0.62		0.90	0.53		
C1	Wt 1	snoRNA-202	23.17		=(23.06 - 23.69)		=(0.9)-(-1.53)		
C4	Wt 2	snoRNA-202	23.29						
C7	Wt 3	snoRNA-202	23.14						
C10	Tg 1	snoRNA-202	23.34						
D1	Tg 2	snoRNA-202	23.98						
D4	Tg 3	snoRNA-202	23.69						

Table 2.1: Worked Example of $\Delta\Delta C_T$ PCR analysis: The average C_T value for each triplicate PCR is represented for each sample. The ΔC_T value is calculated for each sample by subtracting the C_T value of the internal control from the target of interest. The average ΔC_T value for the wt control group of samples is calculated, and subtracted from each ΔC_T value to obtain the $\Delta\Delta C_T$ value. The negative inverse log of this value is the fold change of the gene expression.

Table 2.2. Hybridisation Temperatures of ISH probes		
miR Probe	**T_m (°C)**	**T_m - 21°C**
miR-133b	81	60
miR-451	74	53
miR-1	64	43
miR-96	75	54
miR-335	67	46
miR-31	79	58
miR-9*	65	44
miR-138	70	49
let-7d	71	50
miR-129-3p	78	57
miR-182	72	51
miR-26b	65	44
miR-183	73	52
miR-181a	77	56
miR-159 sense	70	49

Table 2.2: Hybridisation Temperature of In Situ Hybridisation Probe: Column 1 contains a list of the name of each probe. The optimal hybridisation temperature is determined to be 21°C lower than the melting temperature of the probe (T_m - 21°C). Note that the miR-159 sense probe is a negative control.

Chapter 3

Examination of Retinal miR Expression

3.1. Introduction

As outlined in Chapter 1, the profiling of miRNA expression in various tissue types and diseases has been significantly facilitated by developments in miR detection technologies, specifically miR arrays (Babak et al. 2004; Miska et al. 2004; Sun et al. 2004; Shingara et al. 2005), LNA probes (Wienholds et al. 2003; Vester and Wengel 2004), and stem-loop primers (Chen et al. 2005). Using these technologies, sets of miRs have been found to be highly or specifically expressed in certain tissues, including miR-9, -124, -125, and -128 in brain, miR-1, -133, and -206 in heart and muscle, miR-122a in liver, and miR-142 and -150 in spleen (Lagos-Quintana et al. 2002; Lagos-Quintana et al. 2003; Miska et al. 2004; Sempere et al. 2004; Chen et al. 2005; Monticelli et al. 2005; Wienholds and Plasterk 2005). Indeed unsupervised hierarchical clustering methods can be used to successfully differentiate individual tissues, based on their miR expression profile (Lagos-Quintana et al. 2002; Babak et al. 2004). The extent of tissue-specific expression is supported by the recent publication of the miR expression library, which examined miR profiles of 26 different human and rodent organ systems and cell types, identifying that approximately 33% of miRs were expressed in a tissue-specific manner (Landgraf et al. 2007).

These findings suggest that miRs may play important roles in tissue specific events, such as cell differentiation and maintenance, while more ubiquitously expressed miRs, i.e. miR-17-92 and miR-15, -16 are perhaps involved in ubiquitous cell responses such as apoptosis and cell-cycle regulation (Xu et al. 2007). As outlined in Chapter 1 miRs play an important role in animal development, their expression pattern varying both temporally and spatially in the developing mouse and frog embryo, as identified by ISH detection (Kloosterman et al. 2006; Kloosterman et al. 2006). The significance of tissue-specific miR expression has been elegantly illustrated by the *in vitro* study by Lim *et al.,* (2005) in which overexpression of brain-specific miR-124 and muscle-specific miR-1 in HeLa cells, caused the expression profile of the cells to shift towards that of brain and muscle respectively, each miRs down regulating the expression of ~100 targets (Lim et al. 2005). The specific involvement of the muscle specific miRs, miR-1 and miR-133, in the regulation of skeletal muscle proliferation have been well elucidated (Chen et al. 2006). In contrast

the functional roles regulated by miRs in neuronal tissue, are only beginning to be understood (Smirnova et al. 2005; Leucht et al. 2008).

As a growing body of evidence suggests that miRs play an important role in tissue-specific regulation of gene expression (Ambros 2004; Bartel 2004; Kosik and Krichevsky 2005), it is therefore possible that miRs play a significant role in the retina, perhaps regulating retinal development and photoreceptor maintenance (Cepko et al. 1996; Hennig et al. 2008). It is therefore important to identify miRs which are preferentially expressed in the retina, which should assist in the identification of miRs with potential retinal specific roles. A number of miRs have been detected in the eye, using cloning and ISH techniques (Lagos-Quintana et al. 2003; Wienholds et al. 2005; Kloosterman et al. 2006) and miR expression in various components of the eye have also been examined, including the lens, cornea and retina (Ryan et al. 2006). Previously a role for miR-7 in *Drosophila* photoreceptor differentiation has been elucidated, mediated by epidermal growth factor receptor signalling (Li and Carthew 2005), and 13 miRs have been found to be differentially expressed during the development of the zebrafish eye (Wienholds et al. 2005). However, there was little available information on the global miR expression profile of the mouse retina at the start of this research.

The aim of the study described in this chapter, is therefore to generate the miR expression profile of the mouse retina using miR microarray technology and qPCR. Indeed it was of prime interest to identify 'retinal-specific' miRs by comparison with other tissues, and thereby identify subsets of miRs which are enriched in retinal tissue compared to that in the brain and other organs. For this reason, a detailed analysis of miR expression profiles in the mammalian retina was undertaken. Some of the key findings emerging from this study have been reported in (Loscher et al. 2007).

3.2. Materials and Methods

3.2.1. Experimental Animals

The wild type (wt) c57 mouse strain was used in these experiments and held under specific pathogen free (SPF) housing conditions (see section 2.1.4 for animal welfare). At one month of age mice were sacrificed by CO_2 asphyxiation.

3.2.2. RNA Isolation

For total RNA isolation retinas and brains were dissected immediately following CO_2 asphyxiation, and RNA was extracted using the mirVana™ RNA Isolation Kit (Ambion Inc., TX, USA) according to the manufacturer's procedures (see section 2.3.2). Tissue samples for total RNA were obtained in triplicates. For the wt c57 retinal sample, 6 retinas were pooled for each group. Individual brains from wt c57 animals were frozen in liquid nitrogen, homogenized in a pestle and mortar over dry ice and 50-100 μg of powdered tissue was used for RNA extraction. In order to represent the mouse body a mouse total RNA platform was prepared by pooling total RNA from 8 different mouse organs (mouse heart, kidney, liver, lung, ovary, spleen, testicle, and thymus) obtained from the Mouse Assorted Total RNA Kit (Ambion). Mouse Total RNA was derived from pooled tissues harvested from 8–10 week old Swiss Webster mice. In addition a reference RNA sample was used in this study to allow inter-array comparisons, which contained a pooled RNA from numerous tissues. The reference sample was prepared by combining total RNA from 10 mouse tissues (including mouse brain, kidney, heart lung, liver, ovary, spleen, testicle, thymus and embryo) from the Mouse Assorted Total RNA Kit (Ambion) (see section 2.3.5.4).

3.2.3. MiR Microarray Experiment

Wt c57 retina, wt c57 brain and mouse platform samples were outsourced to Exiqon for miR expression profiling. The miRCURY LNA miR Array v.8.1 (see section 2.3.5.2) was used in this experiment, which probed for miRs annotated in

miRBase v.8.1 (release date May 2006). This array probed specifically for 489 miRs (343 mouse and 147 Exiqon miRs), 66% (385 of 579) of which are annotated in miRBase v.10.0. Note however that the hypothesised Exiqon (miRPlus) miRs were not represented in the Sanger miR Database (miRBase) at the time of array manufacture.

In total, 3 total RNA sample were used to represent each tissue type; retina, brain and platform. Total RNA extracted in each retinal sample was obtained by pooling 6 retinas, while each brain sample contained total RNA extracted from 1 brain. Microarray profiling was undertaken using one array per biological replicate, and in total 9 miR arrays were used. As a single mixture of total RNA was used to make up the platform sample, only technical replicates were performed in this case. The total RNA was labelled with the fluor Cy3, while the reference RNA sample was labelled with Cy5. The reference total RNA sample was used to directly compare results obtained between each array as a Cy3/Cy5 ratio, thereby accounting for alterations in experimental conditions and array variability. All samples and biological replicates were analysed on separate miR microarrays as outlined in section 2.3.5.4.

3.2.4. Micorarray Data Analysis

Data was pre-processed and normalized using the global Lowess (LOcally WEighted Scatterplot Smoothing) regression algorithm as described in section 2.3.5.5. by the micorarray profiling company, Exiqon. Normalised $\log_2$-transformed Cy3/Cy5 ratios were used for further analysis.

3.2.5. Quantitative Real-Time RT-PCR (qPCR)

Two-step qPCR was performed using ABI's TaqMan miR Assay (Applied Biosystems, Foster City, CA, USA) according to manufacturer's instructions (see section 2.3.3.1). The TaqMan miR Assays for the following miRs were used: miR-1, -133, -183, -184, -96, -31, -335, -138, -129-3p, *let-7d.* The small nucleolar RNAs (snoRNAs), RNU19 (RNA, U19 small nucleolar) and RNU66 (RNA, U66 small nucleolar) were used as internal controls for normalisation. The data was analysed (see

section 2.3.3.4) and the log_2-transformed miR/control expression ratios were used for further analysis.

3.2.6. *In Situ* Hybridisation (ISH)

For *in situ* hybridization studies, eyes from 12 wt mice were dissected and fixed in 4% paraformaldehyde for 2 hr at 4°C (see section 2.3.4.). 5'-Digoxigenin (DIG)-labelled LNA-modified oligonucleotide ISH probes were purchased for the following mouse miRs: miR-1, -9*, -26b, -96, -129-3p, -133b, -138, -182, -335, -451 and *let-7d*. ISH probes for miR-181a and sense miR-159, were used as positive and negative controls respectively. The ISH protocol was carried out as detailed in section 2.3.4.4. A minimum of 6 slides were probed for each miR at a time, and this process was repeated when necessary. The probe specific melting temperature (T_m) and hybridisation temperature (T_m - 21°C) utilised in these experiments are listed in Table 2.1.

3.2.7 Microscopy

Nuclei were counterstained by using 4',6-diamidine-2-phenylindole-dihydrochloride (DAPI, Invitrogen) as outlined in section 2.8. All ISH sections were analysed by bright field normal and phase-contrast as well as fluorescent microscopy using an Axiophot microscope (Carl Zeiss Ltd., Hertfordshire, UK) using the appropriate filters. Composite images were created using Adobe Photoshop software (Adobe Systems Europe Ltd., Glasgow, UK).

3.2.8. Statistical Analysis

Data from given sets were pooled, averaged and standard deviation (SD) values calculated. Statistical significance of differences between data sets were determined by either Student's two-tailed t-test or ANOVA (Tukey's Multiple Comparison Test) using GraphPad Prism; differences with $p<0.05$ were considered statistically significant.

3.3 Results

3.3.1 Microarray analysis of miR expression in wild type Retina

MiR expression in the mouse c57 retina, brain and mouse platform were determined by microarray analysis, using Exiqon miRCURY LNA array v.8.1, performed by the miR profiling compnay, Exiqon. A benefit of the Exiqon array technology is the use of dual colour labelling which enables the parallel hybridization of a reference RNA sample and an experimental RNA sample. Unfortunately no commercial reference samples were available that contained defined amounts of synthetic miR that would allow the determination of absolute levels of miR expression. As a result, a reference RNA sample was created containing RNA from various mouse organs, ideally all miRs would be represented in this sample. The reference RNA sample was used in each array, labelled with Cy5, thereby controlling for inter-array variability as each Cy3/Cy5 ratio, for a given miR, is comparable between arrays. In this manner, a direct comparison of microarray data across arrays was obtained.

The mouse platform was prepared by pooling total RNA from 8 different mouse organs, representing the various levels of miR expression in other tissues. Substantial differences of miR expression profiles were observed in the comparison of miR expression in the retina, brain and mouse platform RNA samples, by microarray analysis. Indeed, the variation in expression levels spread greater than $\pm$ 6 on a $\log_2$ scale, best illustrated by the results of the two-way unsupervised hierarchical clustering (Figure 3.1) using $\log_2$(Cy3/Cy5) ratios. This clustering method uses statistical algorithms to organize genes according to similar patterns of gene expression, when no predefined expectations of the results are provided (unsupervised) (Eisen et al. 1998) . Here, miR profiles representing each RNA sample were organized based on miR gene expression, and those displaying the greatest degree of similarity were partitioned into clusters; from this heat-map it is evident that the miR expression profiles of the retina and brain samples exhibited a greater degree of similarity compared to the mouse platform samples (Figure 3.2).

The variation in miR expression between the retina versus brain samples (Figure 3.2A) and the retina versus mouse platform (Figure 3.2B) is displayed using volcano plots (Figure 3.2). These plots are constructed by plotting the log difference of

miR expression (Cy3/Cy5 ratios) between two groups on the X-axis ($\Delta\log_2$[group A-group B]), and the corresponding statistical significance of these differences on the Y-axis, expressed as the negative $\log_{10}$ of generated p-values (-ln[p-value]). In this manner, a p-value of 0.05 corresponds to a y-axis value of 1.3 (-ln[0.05]=1.3), and is indicated by a horizontal red line, while the vertical lines represent the magnitude of variation of miR expression between groups. As such, points plotted higher than 1.3 on the y-axis represent statistically significant differences in miR expression between both groups, and x-axis $\log_2$ values ±1, represent 2-fold alteration on a geometric scale; positive and negative values signifying a greater miR expression in group A and B respectively.

Utilising the Exiqon microarray, 104 out of 224 miR probes exhibited statistically significant ($p<0.05$) differences in miR expression between the retina versus brain samples. More specifically the expression of 47 miRs were changed by more than 2-fold ($p<0.05$) between both samples, illustrating the divergence in miR expression which exists between these two neuronal tissues (Figure 3.2A). As expected, miR expression in the mouse platform sample was markedly different to that of the retinal sample. Overall 152 out of 222 miR probes displayed variations in miR expression between retinal and mouse platform samples ($p<0.05$), of which 81 miRs revealed a greater than 2-fold ($p<0.05$) difference in expression (Figure 3.2B).

Based on the miR microarray data, a semi-quantitative comparison of expression levels of miRs in retina, brain and platform was undertaken, relative to mean $\log_2$ expression levels for each miR (Figure 3.3 and 3.4). The expression levels of 'retinal specific' miRs were examined, where 'retinal specificity' was based on previous studies (Lagos-Quintana et al. 2002; Wienholds et al. 2005; Ryan et al. 2006; Karali et al. 2007). Substantial variations of the expression levels of these miRs between retina and platform were detected, ranging from a value of more than 6 on a $\log_2$ scale for miR-183 and -96, and down to approximately a value of 1 on a $\log_2$ scale for miR-125b. Indeed of the documented 'retinal miRs', the high relative expression of miR-96, -182, -183, -29c and -9 in the retina are clearly visible in the heat map representation of the microarray data (Figure 3.1). Note however that the values obtained from the microarray data do not provide information about absolute miR expression levels. For example, while it is clear that miR-183 is expressed at higher

levels in the retina compared to other tissues analyses, the absolute level of miR-183 expression is not known.

Additional miRs that exhibited a 'retinal preference' were identified in this study (Figure 3.4). These novel findings are presented in the heat-map in Figure 3.1, which displays a high relative expression of miR-31, -26b, -106b, -335, -691, -let7-d, -129, -124, and -9* in the retina, compared to brain and platform RNA samples. Differences in miR expression levels, up to 4 on a $\log_2$ scale, were detected between retinal and platform samples (Figure 3.4). For example, miR-31, -106b, -26b, -691, -335, and - 129-3p showed a relatively high level of expression in the retina when compared to the brain or the platform samples (Figure 3.4B). On the other hand, the relative expression levels of miR-9*, -376a, -138, -338, and -136, while high in the retina compared to the platform, were expressed at even higher levels in the brain sample (Figure 3.4A). *Let-7d* demonstrated widespread miR expression in the retina, brain and mouse platform (Figure 3.4A).

3.3.2. Validation of retinal miR Expression by qPCR

Selected miRs depicted in Figure 3.3 and 3.4 were chosen and their relative expression levels quantified using qPCR in the retina, brain and mouse platform RNA samples (Figure 3.5 and 3.6). The RNA samples, on which miR expression was performed, were used for qPCR validation and each reaction was performed in triplicate, normalised to internal controls. Notably, a close correlation between qPCR and microarray data was found, however data resulting from qPCR analysis exhibited a higher dynamic range possibly due to the greater sensitivity of PCR. For example, a difference in miR-183 expression between the retina and platform samples was determined to be approximately 11 on a $\log_2$ scale by qPCR compared to approximately 6 by microarray analysis. In the case of miR-184, the disparity was more significant, with the corresponding $\log_2$ values of approximately 9 by qPCR versus 2 by microarray analysis (Figure 3.5)

In Figures 3.5 and 3.6, microarray and qPCR $\log_2$ values have been transformed into fold expression relative to retinal miR expression, which is set to 1. In this study miR-335, -31, and -129-3p were identified as miRs preferentially

expressed in the retina, and these findings were confirmed by qPCR (Figure 3.5A). MiR-335 and -129-3p exhibited a retinal expression level by qPCR that was 2-fold and 1.6-fold higher relative to the brain, and 14-fold and 250-fold higher compared to the platform sample, respectively ($p<0.001$). MiR-31 was expressed in the retina at approximately 9-fold higher than both brain and platform samples (Figure 3.5A). Additionally, previously identified 'retinal-specific' miRs, miR-183, -96 and -184, displayed the highest relative expression in the retina, compared to both brain and platform samples. Indeed miR-183 and -96 are expressed at approximately 1500-fold higher in the retina compared to the platform, and up to 180-fold higher when compared to the brain sample ($p<0.001$) (Figure 3.5B). MiR-184 displays the greatest degree of retinal specificity, as expression of miR-184 in the retina is 858-fold and 680-fold higher relative to the brain and platform samples, respectively as evaluated by qPCR ($p<0.001$) (Figure 3.5B).

MiR-1 and -133 were also identified as displaying a 1.2-fold higher retinal expression compared to the brain, however these miRs were expressed at vastly higher levels in the platform sample, by 35-fold and 19-fold respectively as evaluated by qPCR ($p<0.001$) (Figure 3.6A). The expression of miR-138 and *let-7d* were also examined by qPCR ($p<0.001$) (Figure 3.6B). MiR-138, while displaying a 7.9-fold higher retinal expression compared to the platform, exhibited a 5.33-fold higher expression in the brain compared to the retina. *Let-7d*, a ubiquitously expressed miR, was found to be expressed 1.27-fold and 2-fold higher in the retina than in the brain and platform sample ($p<0.01$) (Figure 3.6B).

3.3.3. Spatial localisation of retinal miR expression

The expression of miR-1, -9*, -26b, -96, -129-3p, -133, -138, -182, -335 and *let-7d* was explored by *in situ* hybridisation using LNA probes (Exiqon), and the expression of miR-181a (Figure 3.7 B) and sense miR-159 probes (Figure 3.8 A) were used as positive and negative controls respectively. It is notable that only the analysis of *let-7d*, miR-181a, miR-182, and miR-183 produced detectable signals (Figure 3.7 and 3.8). *Let-7* was expressed uniformly in the inner nuclear layer (INL) and labelling was also apparent in the ganglion cell layer (GCL, Figure 3.7A). MiR-181a was strongest in expression among these 4 miRs and was mainly localised in the inner part

of the INL, possibly corresponding to amacrine cells and in the GCL (Figure 3.7B). Interestingly miR-182 and -183 were detected in matching retinal locations displaying comparable signal intensities. Both miR-182 and -183 were detected at their highest intensity in the photoreceptor inner segments (Figure 3.7C and Figure 3.8A). Both miRs were also expressed to a lesser extent in the outer part of the INL and also between the ONL and INL, possibly in photoreceptor synapses (Figure 3.7C, and Figure 3.8B)

3.3.4. Summary

In summary, markedly different patterns of expressions between the retina, brain and mouse platform were determined by miR microarray profiling, and validated by qPCR. The results from the study suggest that retinal preference of miRs vary remarkably. Furthermore, preferential expression in the retina for additional miRs such as miR-31, -335 and -129-3p were newly identified, and validated by qPCR. The spatial location of miRs in the retina detected by ISH, suggests that miRs are expressed in a cell type-specific manner and additionally specific to subcellular compartments.

3.4 Discussion

The global expression profile of miRs in the mouse retina was determined, using the Exiqon miRCURY LNA array v.8.1., the most up-to-date array at the time of the study. In total 46% of miRs (228 out of 489) were expressed in the adult retina (Xu et al. 2007). The expression profile of miRs preferentially expressed in retinal was examined, compared to the brain and platform samples. MiRs which were previously described as being preferentially expressed in the retina (Ryan et al.; Karali et al.; Xu et al.), were identified and distinguished from miRs which were expressed at high levels in both the retina and brain, in addition to miRs which appeared to be predominantly expressed in non-neuronal tissue (Table 3.1).

Notably, the key finding of this study involved the identification of an additional 7 miRs (specifically miR-335, -31, -106b, -129-3p, -691 and -26b) which also revealed to exhibit 'retinal preference' by microarray analysis (Figure 3.4B). MiR-129-3p, -335 and -31 were preferentially expressed in the retina compared to the brain and platform sample, as validated by qPCR (Figure 3.5A). These findings are supported by recent studies, in which retinal preference for miR-335 and -31 was determined (Xu et al. 2007) and high levels of expression of miR-26b and miR-31 in the eye was observed (Ryan et al. 2006; Bak et al. 2008). Little is known about the expression pattern, targets or roles of these miRs. The expression of miR-31 has been established in the colon (Bandres et al. 2006), miR-106 in megakaryocytes (Garzon et al. 2006), and miR-691 in mouse embryo (Mineno et al. 2006). MiR-129-3p expression has been detected in embryonic brain tissue (Chen et al. 2007) and recently a role for miR-335 in neurogenesis has been demonstrated (Sathyan et al. 2007). Furthermore Xu *et al.,* (2007) demonstrated that peak expression of miR-335 in the eye occurs in the mouse embryo at embryonic day 14 (E14) (Xu et al. 2007). MiR-26b is expressed broadly in neuronal tissues (Lagos-Quintana et al. 2002), displaying a higher expression in astrocytes compared to neurons (Dostie et al. 2003; Smirnova et al. 2005) and recently it was demonstrated that expression of miR-26b was induced under hypoxic conditions (Kulshreshtha et al. 2007). The roles of these miRs in the retina, or indeed in the various tissues where they were originally isolated, are largely unknown.

Not surprisingly miR expression in the retina is more comparable to that of the brain, than the platform RNA sample. Indeed, preferential expression of miR-9*, 376a, -138, -338, -136 and *let-7d* was established in the retina compared to the mouse platform, however these miRs are predominately expressed at higher levels in the brain (Figure 3.4A). The majority of these miRs, miR-9*, -136, -138 and –338, have formerly been cloned from the hippocampus and cerebral cortex (Miska et al. 2004) and are found to be broadly expressed throughout the brain (Krichevsky et al. 2003; Babak et al. 2004; Schaefer et al. 2007). MiR-9* was initially described as miR-131 (Lagos-Quintana et al. 2002), but appears to be the sense strand of all three miR-9 predicted stem-loops (miRBase) and has been detected in the zebrafish sensory organs (Wienholds et al. 2005). miR-9* and miR-9 are expressed preferentially in the brain and are likely to mediate important roles in the CNS, however their downstream targets are likely to differ (Wienholds et al. 2005; Chen et al. 2007; Stark et al. 2007). *Let-7* family of miRs have important roles in regulating cell differentiation and proliferation, during development (Johnson et al. 2007).

Previously identified miRs, miR-9, -124 and –125 were also confirmed in this study, that display both high levels of retinal and brain expression and are characterised as 'neuronal-specific' miRs (Miska et al. 2004; Sempere et al. 2004; Smirnova et al. 2005; Kloosterman et al. 2006; Mishima et al. 2007). The retinal preference of miR-9 expression has formerly been identified in the retina (Xu et al. 2007), and additionally miR-9 is implicated in the development of sensory precursors in *drosophila* (Li and Carthew 2005). Recently an interesting study has highlighted miR-9 as an important mediator of neurogenesis, by regulating the fibroblast growth factor and *Her/HES* transcription factor signalling pathways (Leucht et al. 2008), both of which are involved in retinal development (Tomita et al. 1996; McCabe et al. 2006).

Inevitably miR expression in the retina is quite different from the mouse platform sample demonstrated clearly by muscle-specific miR-1 and miR-133, which are expressed at vastly higher levels in non-neuronal compared to neuronal tissue, however these miRs displayed a higher expression in the retina compared to the brain (Figure 3.6A).

The 'retinal-specific' expression of miR-204, -31, -29c, -181a, -184, and the cluster miR-96, -182, and -183 was confirmed in this study, in agreement with

previous findings (Table 3.1) (Lagos-Quintana et al. 2003; Tsonis et al. 2004; Wienholds et al. 2005; Makarev et al. 2006; Ryan et al. 2006; Karali et al. 2007; Xu et al. 2007). The expression of some of these miRs (miR-9, -29c, -96, -124a, -181a, -182, -183 and -204) have previously been localised in the mouse retina by ISH (Deo et al. 2006; Ryan et al. 2006; Karali et al. 2007; Xu et al. 2007), however ISH detection of other 'retina-specific' miRs, including miR -213, -216, and -217, were not detected (Ryan et al. 2006; Karali et al. 2007). Among the 11 ISH probes investigated in the current study, *let-7d*, miR-181a, -182 and -183, resulted in positive labelling in the retina. Nevertheless, these four miRs displayed an intricate pattern of expression suggesting marked cell type specificity and also differential intracellular targeting. The unsuccessful ISH detection of the other miRs tested is most likely due to a lower expression in absolute quantities. For example, despite miR-184 displaying a very high relative retinal expression, it was undetectable in the retina, however it appears to display a higher absolute expression in the lens and cornea and is detectable by ISH in these regions (Ryan et al. 2006). Other factors may also have prevented the detection of these miRs by ISH, such as secondary structure of the probe or target.

Regarding 'photoreceptor specific' expression, miR-182 and -183 appeared to be strongly and exclusively expressed in the rod photoreceptors, and miR-182 co-localised with rhodopsin expression in the OS of rod photoreceptors (Ryan et al. 2006; Karali et al. 2007; Xu et al. 2007). Results from the current study also indicate labelling in the outermost part of the INL, in line with recent results by Xu *et al.*, (2007) in which miR-96, -182 and -183 were also identified in interneurons of the inner nuclear layers. This was also confirmed, as expression of these miRs was detected in 4 month-old retinal degenerative 1 mice (*rd1*) (Chang et al. 2002), which possess no photoreceptors at this age (Xu et al. 2007). However, miR-182 was not observed to co-localise with bipolar cells, suggesting that miR-182 is expressed in other interneurons in the INL or in the synaptic terminals extending from photoreceptor cells (Karali et al. 2007).

In this study and in agreement with previous findings, miR-181a expression was identified in the retina displaying the strongest labelling in the innermost part of the INL, perhaps in association with amacrine cells, and in the GCL (Karali et al. 2007). The expression of *Let-7d* also paralleled that of miR-181a, but the intensity of the labelling was lower. The spatial expression of other 'retinal specific' miRs

confirmed in this study by microarray and qPCR analysis, have formerly been determined by ISH in the adult mouse retina. MiR-204 in expressed in a similar fashion to miR-181 and let-7, being strongly expressed in the innermost part of the INL and GCL (Karali et al. 2007). MiR-124a expression is strong in OS and IS of the photoreceptors, weak labelling of miR-9 was identified in the INL, while miR-29c is expressed throughout the retina appearing strongest in the IS of the photoreceptors and the outermost layer of the INL (Karali et al. 2007). The labelling patterns depicted by ISH indicate characteristic cell type specific expression and possible differential intracellular targeting of these miRs, i.e. to the cell body or in case of photoreceptor cells to the IS and synapse.

On the whole, these data confirm that retinal miRs display highly specific expression patterns using both comparative microarray studies and ISH (Table 3.2). The mechanisms that regulate this striking tissue specificity are ill defined, and indeed regulatory mechanisms must exist at the transcriptional and miR processing level. Indeed some circuits have been identified in muscle tissue, the muscle-specific transcriptional regulators serum response factor (SRF) and Myostatin-D (Myo-D), promote miR-1 and miR-133 expression, which also participate in negative feedback regulatory loops (Zhao et al. 2005; Chen et al. 2006). Indeed miR localised in the introns of protein-coding genes are also likely to be expressed in a tissue-specific manner, as miRs are thought to be co-transcribed with their host gene (Baskerville and Bartel 2005; Kim and Kim 2007). Of the 7 miRs revealed by this study to be preferentially expressed in the retina, miR-335, -106, -691 and -26b are intronic miRs of protein-coding genes; corresponding to Mest1 (mesoderm-specific transcript protein), Mcm7 (minichromosome maintenance deficient 7), Robo2 (roundabout homolog 2), and Ctdsp1 (Carboxy-terminal domain small phosphatase I) (miRBase) respectively. It is therefore possible that the expression of these miRs is determined by the transcription of the host gene.

MiR-138 and *let-7d*, two 'retinal-specific' miRs identified in this study, appear to be regulated post-transcriptionally. Fascinatingly miR-138 expression appears to be regulated by cytoplasmic factors involved in Dicer cleavage, as pre-miR-138 transcripts are expressed ubiquitously despite the neuronal-specific nature of mature miR-138 expression (Obernosterer et al. 2006). The expression of *let-7* appears to be regulated at the Drosha-processing stage, as *let-7* pri-miR expression remains constant

during development, despite the observation that mature *let-7* increases in differentiated cells (Bussing et al. 2008; Roush and Slack 2008). In addition *let-7* has recently been revealed to regulate Dicer expression by a negative feedback loop, thereby potentially regulating the expression of other tissue-specific miRs (Tokumaru et al. 2008).

As observed in this study, miR-96, -182 and -183 exhibit similar expression patterns in the adult retina, and parallel expression of these miRs have also been observed during mouse and zebrafish retinal development (Wienholds et al. 2005; Kloosterman et al. 2006; Xu et al. 2007). The similar patterns of expression of these miRs is likely due to the clustering of these miRs within 3.8kb of each other in the intergenic region on mouse Chr6q, and are likely transcribed as one polycistronic pri-miR transcript (Lagos-Quintana et al. 2003; Xu et al. 2007). This is consistent with the idea that transcriptional regulation is the main determinant of tissue-specific miR expression, however post-transcriptional regulation may account for the variations in absolute level of miRs expressed, for example retinal expression of miR-182 is labeled stronger by ISH than miR-183 and -96 (Ryan et al. 2006; Karali et al. 2007). The sequences of these three miRs are broadly conserved across species and each miR displays close sequence similarities in the seed region of the miR. It follows that these miRs may target similar mRNA transcripts, and this is further discussed in Chapter 7 in relation to miR target prediction.

In addition to the retina, miR-96, -182, and -183 expression appears to be common to a number of neurosensory cells, including the inner ear (Weston et al. 2006) and mouse dorsal root ganglia (Kloosterman et al. 2006), suggesting that these three miRs play important roles in the terminal differentiation and maintenance of mature sensory cells (Xu et al. 2007). This is supported by the identification of transcription binding sites, upstream of the sequence coding for miR-96, -182, and -183, for key transcription factors involved in neurosensory genes, including *CHX10* and *Pax2*, both of which regulate retinal development (Xu et al. 2007). During development, these miRs are suggested to play important roles in the differentiation of the rod photoreceptors, bipolar cells and muller glia cells, as the increase in retinal expression of miR-96, -182 and -183 closely parallels the differentiation of these retinal cells (Xu et al. 2007). In particular, miRs are believed to play long-term roles in retinal cell survival and function, demonstrated by the conditional retinal *Dicer*

knockout that displayed severe structural defects in the retina, including photoreceptor cell death, at 1 month (Damiani et al. 2008).

3.5. Conclusion

Data from this study combined with previous results demonstrate a widespread and intricate expression of miRs in the wild type mouse retina (See Table 3.1). A small subset of miRs exhibits a high degree of tissue specificity while others appear to be more ubiquitously expressed. A significant overlap between brain and retinal miR expression profiles was observed in this study. Despite the relatively small number of 'retinal-specific' miRs identified, the large number of targets and the coordinated manner in which miRs regulate gene expression would suggest that just a few miRs may play a central role in regulating retinal development and maintaining retinal structures and function. Data presented in this study contributes towards the understanding of the role of miRs in the mouse retina by characterising retinal miR expression. From this analysis, a number of miRs were highlighted with newly identified retinal preference. These data will aid in the identification of key miRs vital for retinal function. At present, knowledge of the function of miRs in the development and normal physiology of the retina is limited. Furthermore, it has become evident that miR profiles may be perturbed in certain disease states. Therefore it was of interest to explore whether altered retinal miR expression profiles characterise some forms of retinal degenerations. Exploring this question forms the basis of the work undertaken in Chapter 4 and 5.

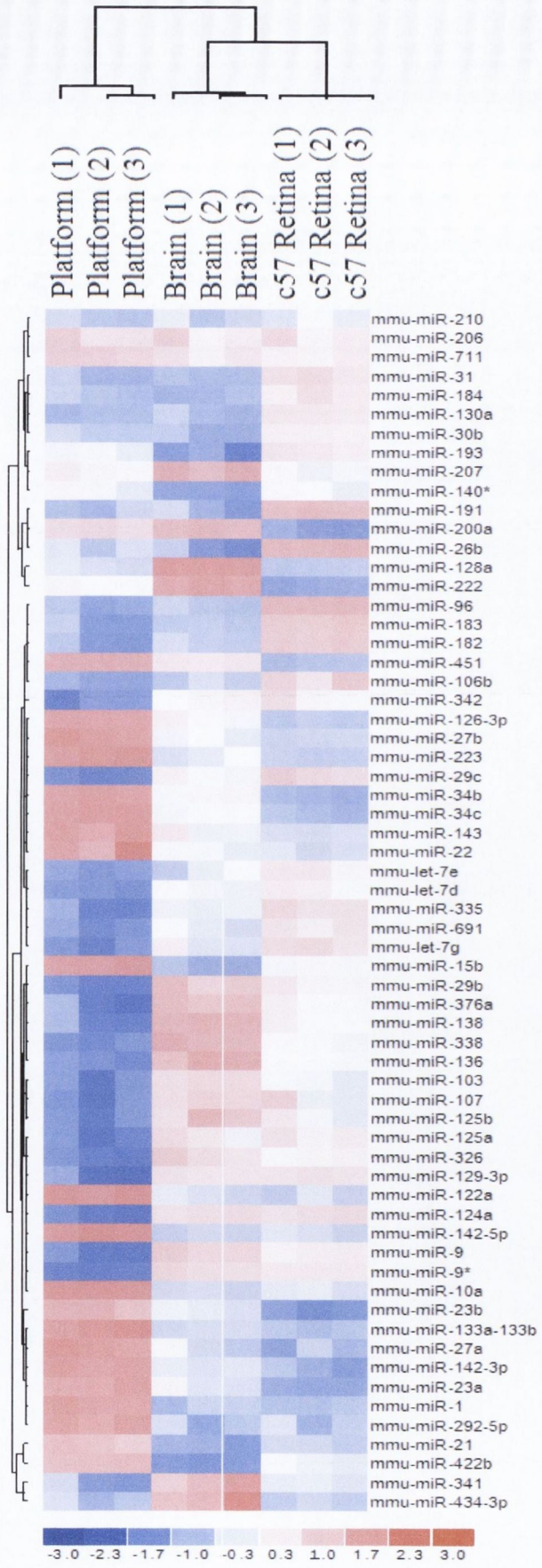

Figure 3.1: Heat Map and Hierarchical clustering of miRs in Retina, Brain and mouse Platform: The heat map diagram shows the result of the two-way unsupervised hierarchical clustering of miRs and the experimental groups; c57 retina, brain and mouse platform using Exiqon v8.1 microarrays. Each row represents a miR and with clusters indicated on the left, while each column represents a sample with clusters appearing at the top. The clustering was performed on a filtered set of $\log_2$(Cy3/Cy5) ratios, which displayed a high variability across samples (standard deviation >0.5). Clusters were generated using the average linkage method, a method which calculates the distance between clusters. The Cy5 labelled reference was used in each array, and provides a constant baseline to compare samples to. The color scale shown at the bottom illustrates the relative expression level of each miR across all samples ($\log_2$Cy3/Cy5). The red color represents a relative miR expression level greater than the mean, blue color represents a relative expression level lower than the mean. Log_2(Cy3/Cy5) ratios ± 1 correspond to a more than 2 fold up or down regulation, relative to the miR reference (Cy5).

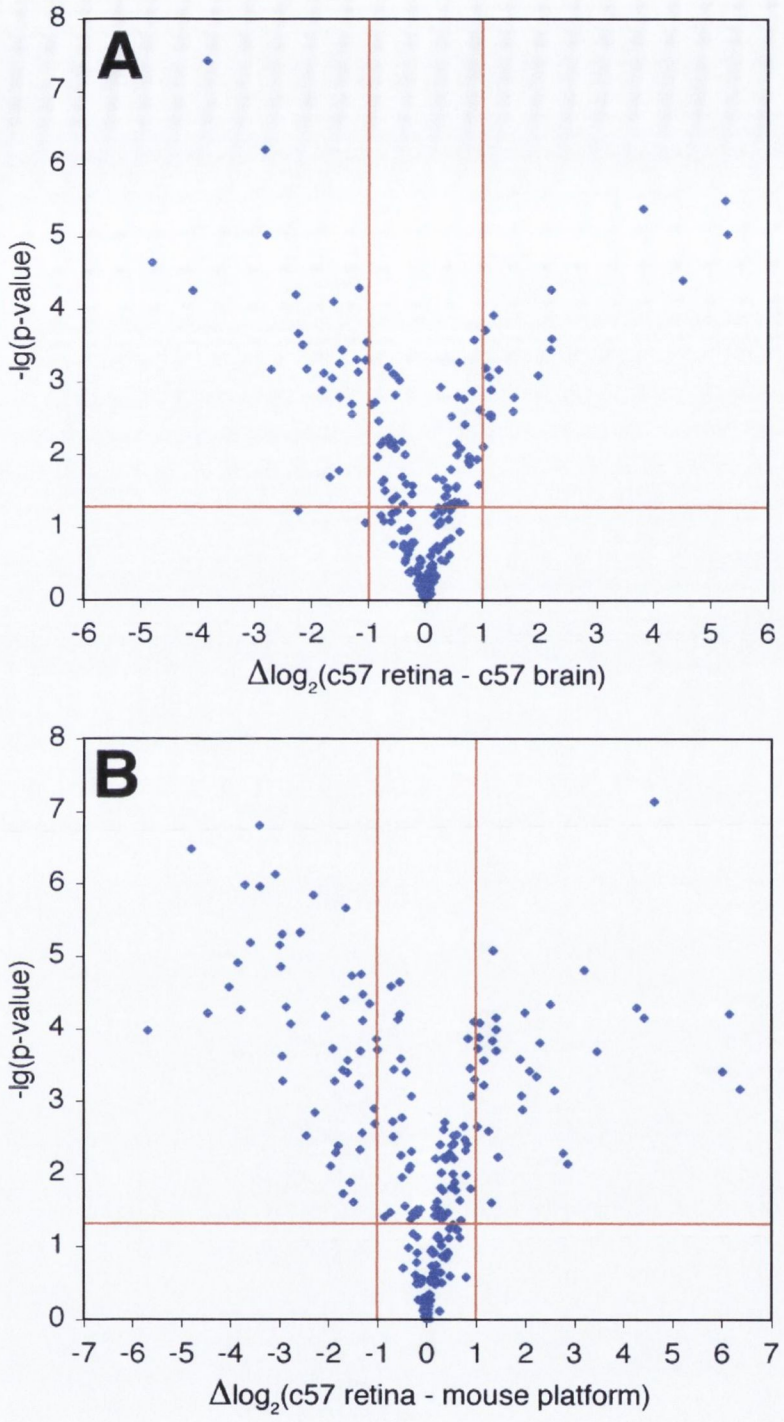

Figure 3.2: Volcano plots of miR expression in wild-type retina versus brain and mouse platform. Plots represent comparative miR expression profiles of **(A)** c57 retina versus c57 brain and **(B)** c57 retina versus mouse platform using Exiqon miR microarrays. X-axis indicate difference in expression level on a $\log_2$ scale, whereas the y-axis represents corresponding *p-values* (Student's *t*-test) on a negative log scale. A $-\log_{10}$ *p-value* of 1.30 (highlighted by the red horizontal line) corresponds to a *p-value* of 0.05 on a geometric scale, and therefore points above this line represent statistically significance variations of miR expression. The vertical red line was chosen arbitrarily, and represents differences in expression between samples of ±1 on a $\log_2$scale. Therefore the more lateral points, represent a greater magnitude of miR expression between the two groups analysed, and positive and negative values signify the group with higher or lower expression.

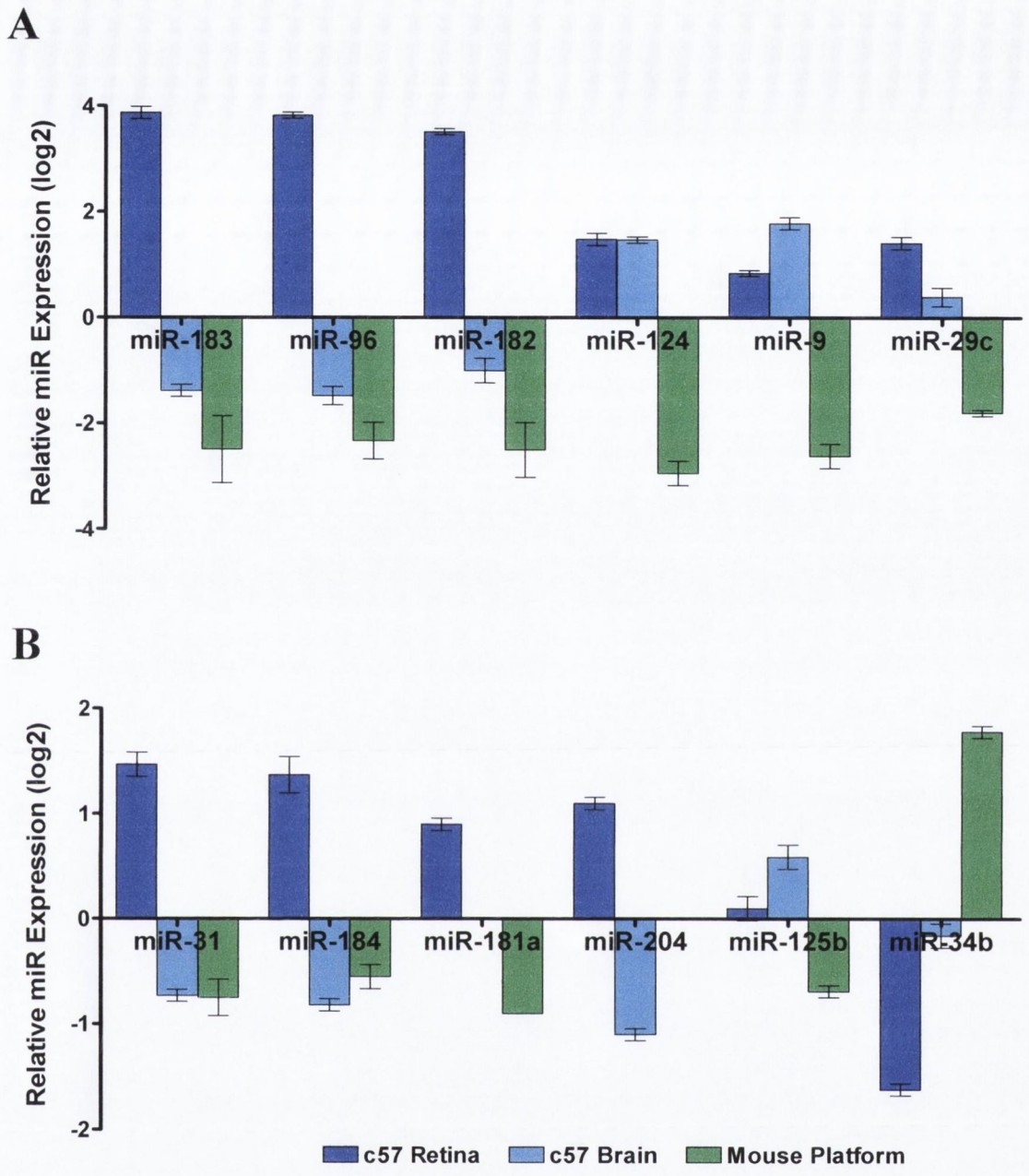

Figure 3.3: Comparative expression of selected miRs in the retina, brain, and mouse platform. The graph illustrates the relative expression level of miRs from microarray data, previously documented to be highly expressed in the retina. Bars represent deviations from mean expression levels for each miR on a $\log_2$ scale in c57 retina (dark blue), c57 brain (light blue), and mouse platform (green). Y-axes are to different scales. Error bars indicate S.E.M. Bars for miR-181a in brain and miR-204 in mouse platform are missing in panel B due to incomplete data, as the signal was below the background.

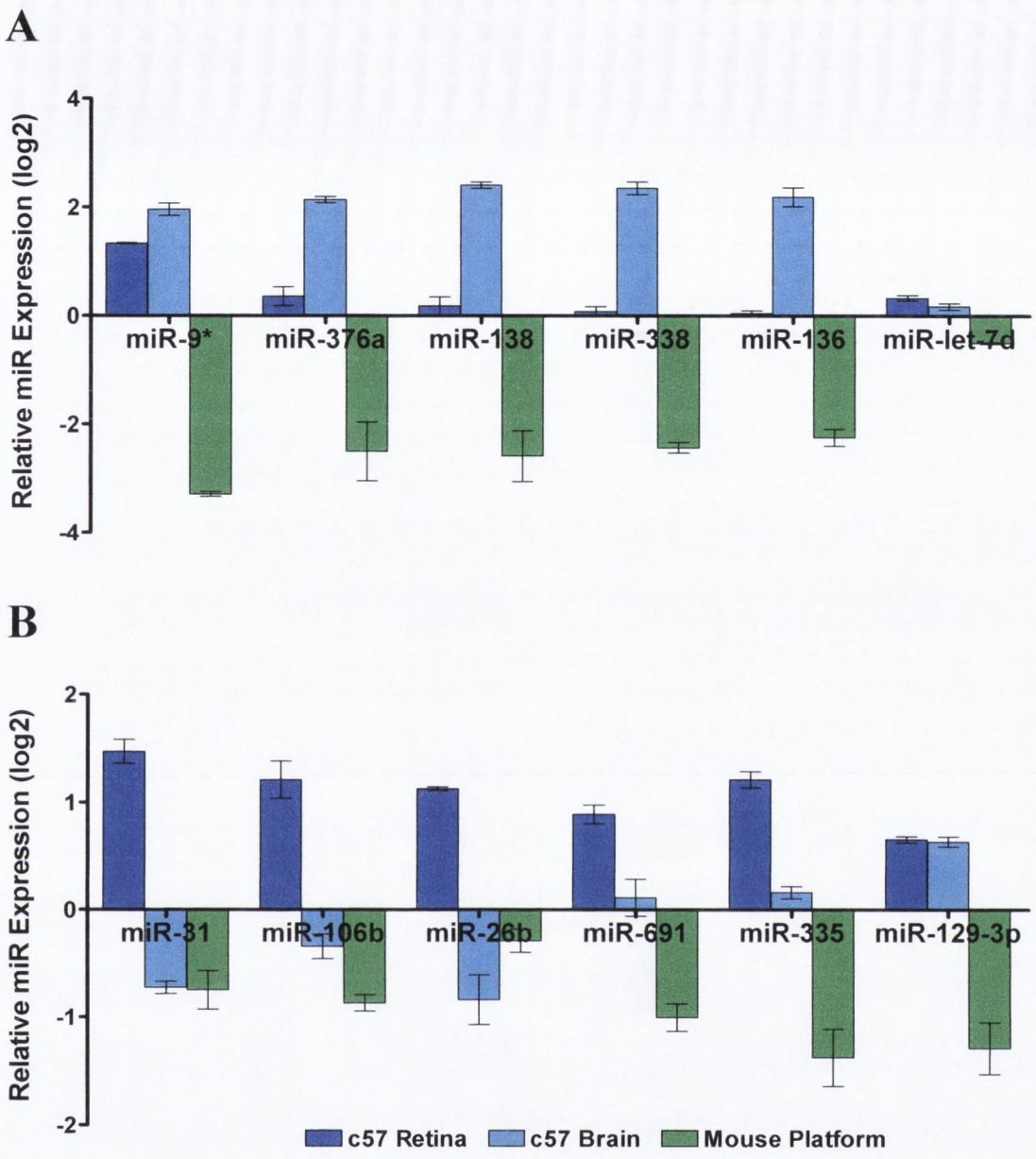

Figure 3.4: Comparative expression of selected miRs in the retina, brain, and mouse platform. The graph illustrates the relative expression level of miRs from microarray data, which were previously unknown to have a high relative expression in the retina. (**A**) miRs which are expressed at high levels in the retina and brain relative to mouse platform, and (**B**) miRs which are highly expressed in the retina compared to the brain and platform are depicted. Bars represent deviations from mean expression levels for each miR on a $\log_2$ scale in c57 retina (dark blue), c57 brain (light blue), and mouse platform (green). Note that columns are in descending order of difference between retinal and platform expression; Y-axes are to different scales. Error bars indicate S.E.M.

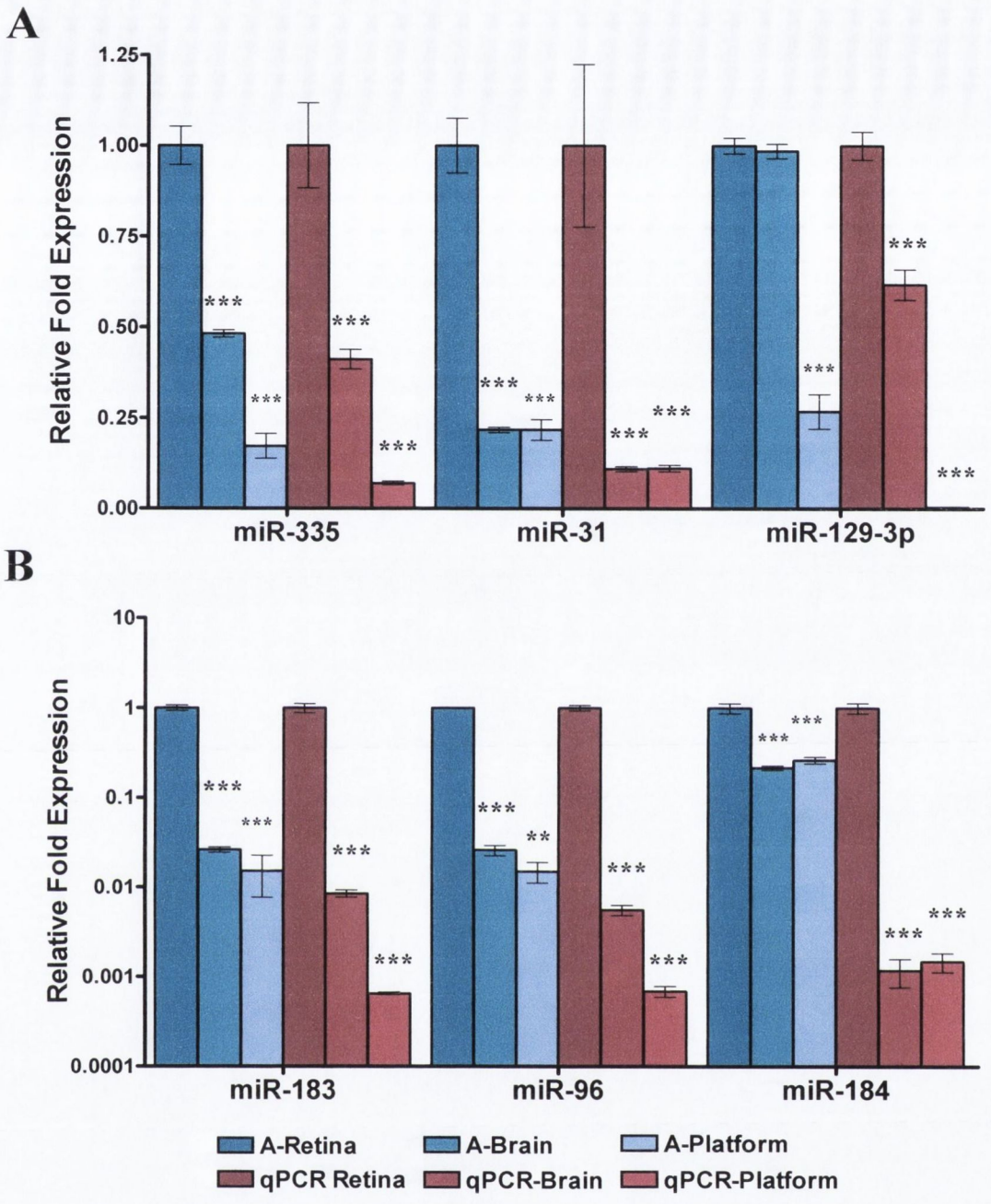

Figure 3.5: qPCR Validation of relative expression of selected miRs in the retina, brain, and mouse platform. The graph illustrates the relative expression level of miRs from microarray data (blue) and validation by qPCR (magenta). Bars represent fold expression relative to retinal samples on a linear scale in c57 retina (dark blue, dark magenta), c57 brain (lighter blue, lighter magenta), and mouse platform (light blue, light magenta). (**A**) Illustrates the expression of miR-335 and miR-32 which exhibit moderately high relative retinal expression compared to brain and mouse platform. **B** illustrated the expression of highly retinal specific miRs; miR-183, -96, and -184, relative to the brain and mouse platform (**B**). Note that the percentage miR expression data in figure B is plotted on a $\log_{10}$ scale. Retina miR expression compared to brain and mouse platform was analysed by ANOVA (Tukey's Multiple Comparison Test) and the statistical significance is indicated by *p-values* correspond to;(**) $p < 0.01$, and ***; $p < 0.001$. Error bars indicate S.E.M.

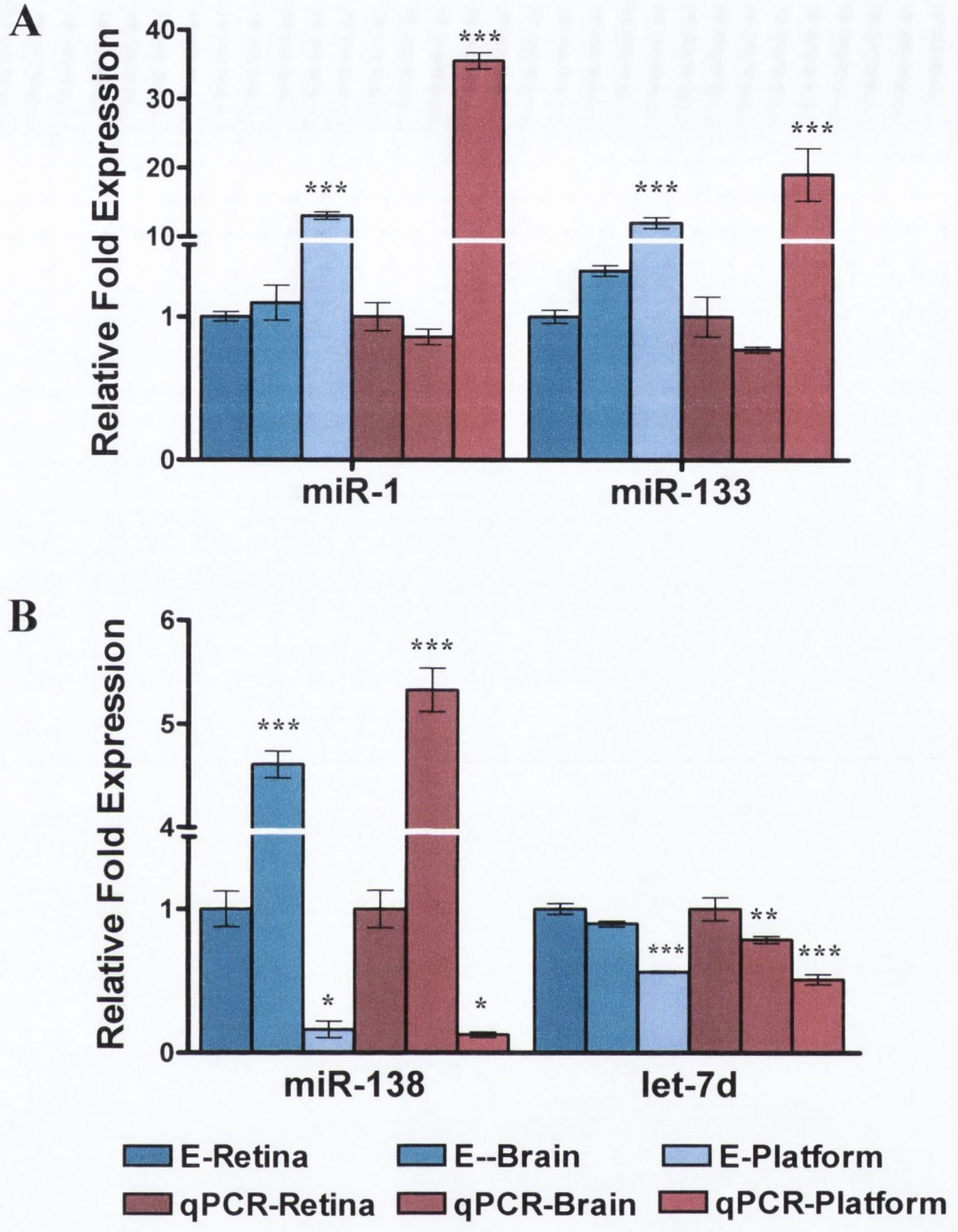

Figure 3.6: qPCR Validation of relative expression of selected miRs in the retina, brain, and mouse platform. The graph illustrates the relative expression level of miRs from microarray data (blue) and validation by Quantitative real-time RT-PCR (qPCR) (magenta). Bars represent fold expression relative to retinal samples on a linear scale in c57 retina (dark blue, dark magenta), c57 brain (lighter blue, lighter magenta), and mouse platform (light blue, light magenta). (**A**) Illustrates the expression of miR-1 and miR-133 which exhibit low relative retinal expression compared to mouse platform. (**B**) The expression of miRs (miR-138, -129, and –let7d) which have a high relative expression in the brain and retina compared to the mouse platform. Note that the y-axes are to different scales. Retina miR expression compared to brain and mouse platform was analysed by ANOVA (Tukey's Multiple Comparison Test) and the statistical significance is indicated by *p-values* correspond to; (*) $p < 0.05$, (**) $p< 0.01$, and ***; $p < 0.001$. Error bars indicate S.E.M.

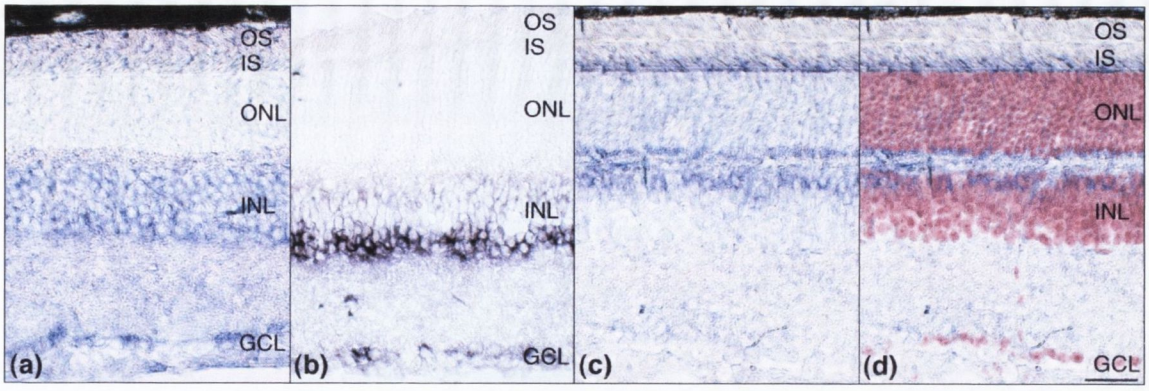

Figure 3.7: miR ISH analysis in the mouse retina (*let-7*, miR-181a, and -182) Eyes from one-month-old c57 animals were fixed in 4% paraformaldehyde, and 12 μm cryosections were *in situ* hybridized with 5'-digoxigenin labeled locked nucleic acid (LNA) microRNA (miR) probes for **(a)** let-7, **(b)** miR-181a, and **(c,d)** miR-182. A false-colored (magenta) 4',6-diamidine-2-phenylindole-dihydrochloride (DAPI) nuclear staining is overlaid on the miR-182 *in situ* hybridization (ISH) label (panel d) to indicate the position of the nuclear layers. Scale bar: 25 μm. GCL, ganglion cell layer; INL, inner nuclear layer; IS, photoreceptor inner segments; ONL, outer nuclear layer; OS, photoreceptor outer segments. Negative control, miR-159 ISH is displayed in Figure 3.8.

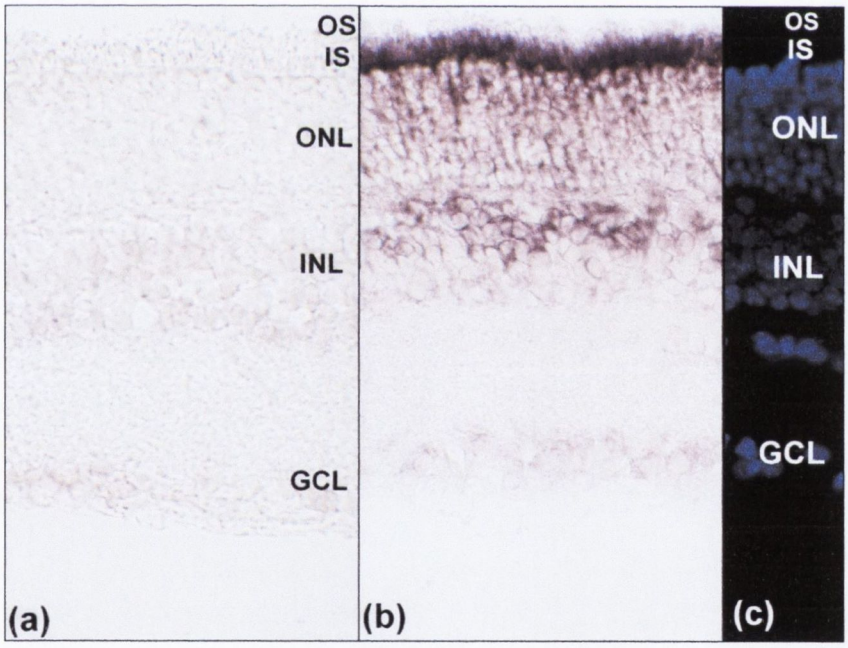

Figure 3.8: miR ISH analysis in the mouse retina (miR-183 and sense miR-159). Eyes from 1-month-old c57 animals were fixed in 4% paraformaldehyde, and 12 μm cryosections were *in situ* hybridized with 5'-digoxigenin labeled locked nucleic acid (LNA) microRNA (miR) probes for **(a)** sense miR-159 negative control and **(b)** miR-183. The adjacent **(c)** 4',6-diamidine-2-phenylindole-dihydrochloride (DAPI) nuclear staining indicates the position of the nuclear layers. GCL, ganglion cell layer; INL, inner nuclear layer; IS, photoreceptor inner segments; ONL, outer nuclear layer; OS, photoreceptor outer segments.

Table: 3.1. miRs Expressed in the Retina			
Tissue Expression Pattern	**miR**	**Expression**	**References:**
'Retinal-Preference'	miR-96	Retina	[1-5]
	miR-182	Retina	[1-7]
	miR-183	Retina	[1, 3-6]
	miR-184	Retina, Lens, Cornea,	[1-5, 7]
	miR-335	Retina	[4, 5]
	miR-31	Retina	[4, 5, 7]
	miR-129	Retina	[4, 5]
	miR-29c	Retina	[3-6]
	miR-181a	Retina	[2, 3, 7]
	miR-204	Retina, RPE, Lens	[1, 3, 6-8]
	miR-691	Retina	[5]
	miR-26b	Retina	[4, 5]
	miR-106b	Retina	[5]
'Neuronal-Preference'	miR-124	Retina	[3, 5, 6, 8-12]
	let-7	Retina	[5, 9, 11, 12]
	miR-125	Not determined	[3, 7, 10, 11]
	miR-9/9*	Retina	[1, 3, 5, 6]
	miR-376	Retina	[5]
	miR-128	Retina	[5]
	miR-338	Retina	[5]
	miR-136	Retina	[5]
'Non-Neuronal' miRs	miR-1	Retina	[5, 9]
	miR-133a	Retina	[5, 11]
	miR-34b	Retina, Eye	[3]
Undefined	miR-7	Retina, Lens	[4, 9, 10, 13]

Table 3.1: miRs expressed in the Retina as determined by microarray analysis and qPCR: MiRs are listed which displayed a 'Retinal-Preference' of expression, i.e. miRs which were expressed higher in the retina than the brain or non-neuronal sample. miRs displayed 'Neuronal-Preference' had a high relative expression in the brain and retina compared to the platform sample. 'Non-neuronal' miRs are miRs, while expressed in the retina, displayed a higher relative expression in the platform sample. Previous studies that support these findings are listed, the citation referring to the references below:

1. Bak, et al., RNA, 2008. 14(3): p. 432-44.
2. Lagos-Quintana, et al., RNA, 2003. 9(2): p. 175-9.
3. Wienholds, et al., Science, 2005. 309(5732): p. 310-1.
4. Xu, et al., J Biol Chem, 2007. 282(34): p. 25053-25066.
5. Loscher, C.J., et al., Genome Biol, 2007. 8(11): p. R24
6. Karali, et al., Invest Ophthalmol Vis Sci, 2007. 48(2): p. 509-15.
7. Ryan, et al., Mol Vis, 2006. 12: p. 1175-84.
8. Deo, et al., Dev Dyn, 2006. 235(9): p. 2538-48.
9. Arora, et al., Invest Ophthalmol Vis Sci, 2007. 48(9): p. 3962-7.
10. Frederikse, et al., Histochem Cell Biol, 2006. 126(1): p. 1-8.
11. Makarev, et al., Mol Vis, 2006. 12: p. 1386-91.
12. Tsonis, et al. Biochem Biophys Res Commun, 2007. 362(4): p. 940-5.
13. Li, and Carthew, Cell, 2005. 123(7): p. 1267-77.

Chapter 4

Examination of Retinal miR expression in the P347S-rho RP mouse model

4.1. Introduction

In Chapter 3 the global miR expression profile was identified in the mouse adult retina, and miR retinal preference was determined for miR-9*, -335, -31, -106, -129-3p, -691 and -26b in addition to previously characterised retinal miRs miR-96, -183, -182, -184, -124 and -204 (Ryan *et al.,* 2006; Karali *et al.,* 2007; Xu, S. *et al.,* 2007). The tight temporal and spatial expression of some of these miRs in the retina suggests an involvement in retinal-specific functions (Karali *et al.,* 2007; Xu, S. *et al.,* 2007). It has been frequently reported that miRs are involved in tissue development, where they regulate the differentiation and proliferation of progenitor cells (Harfe 2005; Chen *et al.,* 2006; Kosik 2006). However as the expression of many miR remain high, or even peak in adulthood, miRs are thought to mediate important roles in adult tissues too (Kim *et al.,* 2007; Damiani *et al.,* 2008).

In the adult retina miRs are believed to be required for the maintenance of retinal cell identity, and photoreceptor survival. This is supported by findings by Damiani *et al.,* (2008) in which photoreceptor cell death occurred following a global reduction of retinal miR expression by Dicer inactivation, using a floxed Dicer allele and the retinal Chx10Cre transgene, a homeobox gene expressed in retinal progenitor cells (Ceh10 homeodomain-containing homolog) (Rowan and Cepko 2004; Damiani et al. 2008). This is in agreement with other conditional dicer knockouts in mature neurons, in which a slow progressive degeneration was observed (Kim et al. 2007; Schaefer et al. 2007). Indeed the preservation of apical-basal polarisation of photoreceptors is crucial for sustaining vital interactions with Muller glia cells, on which the photoreceptors depend for both structural and metabolic support (van de Pavert *et al.,* 2004; Bringmann *et al.,* 2006). In the retinal dicer knockout both architectural and functional defects were observed in the retina at 1 month, displaying prominent rosette formation and altered laminar structure of the retina, coexisting with an impaired response to light (Damiani et al. 2008). This potential requirement of miRs to regulate pathways involved in sustaining photoreceptor function is attractive and encourages investigation of miR involvement in retinal disease.

As described in Chapter 1, retinitis pigmentosa (RP) is the most common form of inherited retinal degeneration affecting more than 1.5 million individuals worldwide

(Hartong et al. 2006). Notably, mutations in the rhodopsin gene (*RHO*), encoding a principal protein in photoreceptor outer segments are responsible for approximately 25% of autosomal dominant forms of RP (RetNet). Experimental data from animal models of RP and human patients suggests that photoreceptors die prematurely by apoptosis (Portera-Cailliau *et al.,* 1994; Marigo 2007). However, much less is known about the chain of events that leads from the different genetic mutations to eventual photoreceptor cell death, a process that can take decades in humans (Berson et al. 2002). Altered miR expression has been observed in many disease states, including neuronal diseases, in which alterations in the expression of specific miRs have been found to alter the rate of neuronal degeneration in polyglutamine-based neurodegenerative conditions and Alzheimer's disease (Bilen et al. 2006; Hebert et al. 2008; Lee et al. 2008). It is fascinating to examine if miRs are involved in either mediating these disease pathways, or alternatively acting independently to modulate disease progression, and evidence exists to support both of these mechanisms. In neuronal polyglutamate degenerations, miRs may mount a cell defence mechanism as miR expression appears to promote the survival of neurons in the presence of the toxic disease proteins, for example in Purkinje cells miR-101 targets the transcript for the disease protein ataxin-1 in spinocerebellar ataxia 1 (Bilen et al. 2006). As miRs appear to be important for long-term neuronal survival and the proposed involvement of miRs in the response of neuronal cells to toxic proteins products (Kim *et al.,* 2007), it is enticing to consider the role that miRs may play in photoreceptor degeneration in RP. MiRs, whose expression is significantly altered in RP, may play a role in the disease process and by identifying these miRs subsequent targets and the effect which these miRs exert over biological pathways, examined.

In this Chapter of the Ph.D. thesis, retinal miR expression is examined in a mouse model of RP carrying a mutant Pro347Ser *RHO* transgene (P347S) (Li et al. 1996) and compared to the expression profile of wild type mice. Notably, the results from the study provide the first evidence of modified miR expression profiles in retinal disease (Loscher et al. 2007).

4.2. Materials and Methods

4.2.1. Experimental Animals

Transgenic P347S (Li et al. 1996) and wt 129 and wt c57 mouse strains were used in these experiments. P347S animals carry a Pro347Ser mutation in the carboxyl terminal of *RHO*, a mutation identified in some autosomal dominant RP families (Dryja et al. 1990). To compensate for the extra *RHO* transgene these mice were maintained on a mouse rhodopsin +/- background (*Rho*+/-, (Farrar et al. 2002)) resulting a P347S+/- Rho+/- genotype. Mice used in these experiments were held under specific pathogen free housing conditions (see section 2.1.4). At one month of age mice were sacrificed by CO_2 asphyxiation.

4.2.2. RNA Isolation

For total RNA isolation retinas were dissected immediately and extracted using the mirVana™ RNA Isolation kit (Ambion Inc., TX, USA) according to the manufacturer's procedure (see section 2.3.2). Tissue samples for each animal breed (wt 129; wt c57; P347S) were obtained in triplicates, each sample containing pooled total RNA from 6 retinas. Therefore each group of animals was represented by RNA from a total of 18 retinas.

4.2.3. miR Microarray Experiments

Both of the miR microarray platforms, mirVana™ miRNA Bioarray v.2. (Ambion) and miRCURY™ LNA miR Array v.8.1. (Exiqon, Vedbaek, Denmark) were used in this experiment (see section 2.3.5.2). P347S, wt 129 and wt c57 retinal samples were analysed using the mirVana miR Bioarray v.2 and samples were outsourced to Ambion for miR profiling. No reference miR sample was used in this experimental set up, and individual experimental samples were labelled using Cy5. Three retinal RNA samples were used to represent each group (P347S, wt129, c57), and each biological replicate was analysed on one array as outlined in section 2.3.5.3.,

a total of 9 miR Bioarrays. Separate wt c57 and P347S retinal RNA samples were obtained and outsourced to Exiqon for miR pofiling using the Exiqon miRCURY LNA miR Array v.8.1 (see section 2.3.5.2). All experimental samples were labelled with the fluor Cy3 and a reference sample was provided and labelled with Cy5. In total 6 Exiqon LNA miR arrays were used in this study as outlined in section 2.3.5.4. Each RNA sample was analysed on one array representing three biological replicates (three retinal RNA samples representing each group P347S and c57), however no technical replicates were performed. One of the main advantages of using the Exiqon array was the ability to control for inter-array variability by means of a Cy5 reference RNA sample on each array, thereby allowing the direct comparison of miR expression profiles generated using the Cy3/Cy5 log ratio. In addition Exiqon arrays utilise LNA miR probes, which are thought to detect miRs with a greater sensitivity and specificity, than amine modified DNA probes, as used on the Ambion Bioarray (Vester and Wengel 2004).

4.2.4 Microarray Data Analysis

Global normalisation of the Ambion microarrays was undertaken using the Variance Stabilization Normalization (VSN) method (Huber et al. 2002) (see section 2.3.5.5) by the microarary profiling company, Ambion. The resulting *generalised* $\log_2$ ($glog_2$) values were used in further data analysis. Exiqon array data was pre-processed and normalized using the global Lowess (LOcally WEighted Scatterplot Smoothing) regression algorithm as described in section 2.3.5.5. by the microarary profiling company, Exiqon. Normalised $\log_2$-transformed Cy3/Cy5 ratios were used for further analysis

4.2.5. Quantitative Real-Time RT-PCR (qPCR)

Two-step qPCR was performed using ABI's TaqMan miR Assay (Applied Biosystems, Foster City, CA, USA) according to manufacturer's instructions (see section 2.3.3.1). The TaqMan miR Assays for the following miRs were used: miR-1, -133, -183, -96, -182, -206, -31, -335, -138, let-7d, -146, -451, and –489. The TaqMan

miR Assay RNU19 and snoRNA-202 were used as internal controls. The data were analysed (see section 2.3.3.4) and the log_2-transformed miR/control expression ratios were used for further analysis.

4.2.6. Histology and Microscopy

The eyes from 4 one-month-old wt c57 and P347 animals were dissected and fixed in 4% paraformaldehyde for 4 hr at 4°C. Following sucrose cryoprotection, frozen sections of the eyes at 12 μm thickness were obtained (see section 2.3.4.2). The nuclei were counterstained by using 4',6-diamidine-2-phenylindole-dihydrochloride (DAPI, Invitrogen) as outlined in section 2.8. Sections were analysed by bright field phase-contrast as well as fluorescent microscopy using an Axiophot microscope (Carl Zeiss Ltd., Hertfordshire, UK). Outer nuclear layer thickness was measured using microscopic images from sections in three planes 250 μm apart in the medial part of the eye using Adobe Photoshop Software (Adobe Systems Europe Ltd., Glasgow, UK).

4.2.7. Statistical Analysis

Data from given sets were pooled, averaged and standard deviation (SD) values calculated. Statistical significance of differences between data sets were determined by either Student's two-tailed t-test or ANOVA using the statistical software package, GraphPad Prism; differences with $p<0.05$ were considered statistically significant.

4.3. Results

4.3.2. Retinal Histology of P347S RP model

Given the emerging role of miRs in various diseases, it was hypothesised that perturbed miR expression may characterise or even contribute to some of the cellular events underlying the pathology observed in RP. To seek experimental evidence supporting this theory, miR expression profiles in retinas from an RP transgenic mouse model (P347S) (Li et al. 1996) and wild type mice were compared by microarray analyses, using two array technologies. Note also that both c57 wt and 129 wt retinas were used as controls, due to the mixed c57/129 background of the P347S mouse model. To reflect the adult miR expression pattern and to allow a valid comparison of retinas from P347S and wild type mice, animals at one month of age were chosen for the study. Retinal degeneration in the P347S animals is slower than in many other RP models, with little or no photoreceptor cell loss at 1 month, and 50% of photoreceptors remaining at 4-5 months of age (Li et al. 1996). It was important to quantify the degree of photoreceptor loss in the P347S model, to account for alterations in cellular composition of the retina. Figure 4.1 illustrates representative retinal histology of P347S (Figure 4.1A) and wild type c57 mice (Figure 4.1B) at one month. In the P347S retinal sections, the outer segments (OS) of the photoreceptors were compromised and the thickness of the outer nuclear layer (Chen et al. 2006) was decreased by up to 25% (Figure 4.1A) when compared to the wild type controls (Figure 4.1B). These values were used to justify a selection criterion for screening genuine variations in miR expression in the P347S retina, as changes resulting from the altered cellular makeup of the retina should not exceed the magnitude of photoreceptor cell loss, i.e. approximately ± 25%. In contrast, larger changes in retinal miR levels should reflect modifications that have occurred due to altered regulation of miR expression in the P347S mutant retina. Therefore a threshold of a 2-fold change (i.e. +100% and -50%) was set to screen for miRs that differed in expression between P347S and wild type mice.

4.3.2. Comparison of miR expression in wild type retinas by microarray analysis

Initially, the miR expression profiles in retinas of the two wild type mouse strains, c57 and 129 mice, were compared (Figure 4.2A) using the mirVana™ miRNA Bioarray v.2. Minor variations were detected between the two wild type retinas, as only 25 out of 642 miR probes on the mirVana microarray displayed significant ($p<0.05$) deviations. Note however, that the magnitude of these miR variations were all less than 2-fold, with a variance of less than ±1 on a $\log_2$ scale in the c57 vs. 129 plot (Figure 4.2A).

4.3.3. Altered miR expression profile in P347S retina

MiR expression profiles in retinas from P347S and wild type mice were compared by microarray analyses using two different miR platforms; the mirVana™ miRNA Bioarray v2 (Ambion, Austin, TX, USA) and miRCURY™ LNA miR Array v8.1 (Exiqon, Vedbaek, Denmark). These array platforms differed on the type of probes used (amine modified DNA, and locked nucleic acid), and also the number of miR probes contained on each array. The mirVana array probed for a total of 642 miRs (486 human, mouse and rat miRs and 156 Ambi-miRs), covering miRs annotated in the Sanger miRBase release 8.0, while the miRCURY LNA microarray contained probes for a total of 489 mouse miRs (343 mouse and 147 Exiqon miRs). Volcano plots were used to display the miR expression data from both array platforms (Figure 4.2). These plots were constructed by plotting the log difference of miR expression (Cy3/Cy5 ratios) between two groups on the X-axis ($\Delta\log_2$[group A- group B]), and the corresponding statistical significance of these differences on the Y-axis, expressed as the negative $\log_{10}$ of generated p-values (-ln[p-value]). In this manner, a p-value of 0.05 corresponds to a y-axis value of 1.3 (-ln[0.05]=1.3), and is indicated by a horizontal red line, while the vertical lines represent the magnitude of variation of miR expression between groups. As such, points plotted higher than 1.3 on the y-axis represent statistically significant differences in miR expression between both groups, and x-axis $\log_2$ values ±1, represent 2-fold alteration on a geometric scale; positive and negative values signifying a greater miR expression in group A and B respectively (Figure 4.2). As mentioned above the differences between the total number of miRs plotted in these volcano plots, resulted from the use of two different microarrays

platforms. Also as more than half of the probes in the Exiqon microarray did not detect target miRs in the samples, the actual number of plotted miRs was approximately 220 in the corresponding plots (Figure 4.2 D).

MiR expression in the P347S retina was compared to the wt c57 and wt 129 retinas using the mirVana Bioarrays (Figure 4.2 B, 4.2 C) and the miRCURY LNA arrays were also used to compare the wt c57 retina to P347 mutant model (Figure 4.2D). Each animal group was represented by a total of 3 pooled retinal RNA samples, each sample containing RNA from 6 retinas. As previously mentioned, a Cy5 labelled reference sample was used in the Exiqon arrays, thereby providing a baseline level of miR expression, allowing direct comparison of Cy3/Cy5 ratios across arrays for each miR. The data from these microarray analyses revealed marked alterations between the P347S and wild type miR profiles, in fact the variance in miR expression spread greater than ±6 on a $\log_2$ scale (Figure 4.2 B, 4.2 C, 4.2 D) compared to that of less than ±1 in the c57 vs. 129 plot (Figure 4.2A). Figure 4.2 B, 4.2 C and 4.2 D reveal statistically significant ($p<0.05$) changes of 63 out of 640, 75 out of 640 and 87 out of 154 probes respectively, between the P347S and wt retinas. Employing the same microarray chemistry (Ambion), the P347S vs. c57 (Figure 4.2 B) and P347S vs. 129 (Figure 4.2C) retinal plots are almost identical, with 8 and 9 miRs exhibiting a greater than 2-fold ($p<0.05$) changes between both samples. Using Exiqon's LNA technology 16 probes displayed higher than 2-fold alterations ($p<0.05$) between the P347S and c57 miR profiles (Figure 4.2 D). These variations are clearly presented in the heat map of the Exiqon microarray data, illustrating the results of two-way unsupervised hierarchal clustering method (Figure 4.3). It is notable that two array platforms yielded a number of miRs that displayed similar alterations in expression between the P347S mutant and wild type retinas; e.g. miR-1, -133 or –96 (highlighted in red, in Figures 4.2 B, 4.2 C and 4.2D).

4.3.4. Validation of Altered miR Expression by qPCR

In total 11 miRs were chosen for qPCR validation; some of which had previously been characterised as 'retinal specific' miRs (let-7d, miR-31, -335, -138, -96, and -183), while other miRs were selected that displayed a greater than 2-fold

difference ($p<0.05$) in expression between the P347S and wt mice (miR-1, -133, -96, -183, -184, -146, -451, and -489). A further criterion used in the selection was that the signal intensity of each miR probe was above background for all samples and replicates. Note that some of the miRPlus and Ambi-miRs, that achieved these criteria, were not included in further analysis as these miR sequences had not been validated as genuine miRs, and therefore did not correspond to valid entries in the Sanger miR Database (Griffiths-Jones *et al.,* 2006; miRBase).

In general, there was a good correlation among data from qPCR and the microarray studies (Figures 4.4-4.7). The expression levels of the miR-31, -335, *let-7d*, and -138 in wt and P347S retinal samples were examined by qPCR (Figure 4.4), as these miRs demonstrated a high relative expression in the retina (see Chapter 3). In the P347S retina, miR-31, -335 and let-7d, displayed a 1.5-fold, 1.9-fold and 1.5-fold greater expression compared to wt c57 retina ($p<0.05$) by either Ambion and/or Exiqon microarray analyses (Figure 4.4). However these alterations in miR expression were not verifiable by qPCR analysis (Figure 4.4). In addition the 'retinal specific' miR-138, was not differentially expressed in P347S versus c57 retinal samples ($p>0.05$), by microarray or qPCR analysis (Figure 4.4).

The expression levels of miR-146, -451, -489, and -184 were altered by more than 2-fold in the P347S versus c57 retina by either Ambion and/or Exiqon microarray analyses; specifically miR-129, -451, and -184 increased in expression by 2.6-fold, 2.5-fold, and 2.6-fold respectively, while miR-489 expression decreased by 3.8-fold (Figure 4.5). These altered miR profiles were validated by qPCR for miR-146 and -451, which increased by 2.1-fold ($p<0.001$) and 1.6-fold ($p<0.01$) respectively in P347S retina. In contrast, the microarray findings were not confirmed by qPCR for miR-489 and -184 ($p>0.05$) (Figure 4.5). This highlights the importance of microarray validation, as alterations of miR expression detected by microarray analyses were not always verifiable by qPCR. Alterations observed between both array platforms, may reflect the variation in technologies on which these platforms are based, in relation to sensitivity and specificity of miR detected. In addition inter-array variability should be minimised in the Exiqon array analyses, due to the incorporation of the Cy5 labelled reference sample which allows direct comparison of Cy3/Cy5 ratios.

The miRs that exhibited the greatest relative miR variation in expression between wt and P347S retinas were miR-1, -133, -96, and -183 (Figure 4.6). The expression of miR-96 and -183 decreased, by 2.7-fold and 2.2-fold ($p<0.001$) respectively, in mutant retinas by qPCR analysis (Figure 4.6). However the expression of miR-1 and 133, which are expressed at low levels in the retina, were raised in the P347S retinas by 3.7-fold and 4.48-fold ($p<0.001$) respectively (Figure 4.6). Notably, these results provided the first evidence of an altered miR expression profile in retinal disease (Loscher et al. 2007).

4.3.5: miR cluster analysis

Following analysis of the genomic location of the above miRs, it was noted that miR-96, -182 and -183 were clustered within 3.8 Kb on mouse chromosome 6, and were transcribed in the same direction as each other (Table 4.1) (Xu et al. 2007). MiR-1 and -133 are also clustered but in a more complex manner (Chen et al. 2006), owing to the presence of homologous miR sequences and varied chromosome (Chr) locations (Table 4.1). MiR-1-1 and miR-1-2 are located on Chr 2 and Chr 18 respectively, however the mature miR transcripts are identical, with minor variations existing in the precursor transcript of each miR. Likewise identical mature miR transcripts result from the processing of pre-miR-133a-1 (Chr 18) and pre-miR-133a-2 (Chr 2) (Table 4.1), however the mature miR transcripts of the homologous miRs, miR-133a and miR-133b (Chr 1), differ by 1 nt at the 3' end (For further information regarding annotation of miRs see (Ambros et al. 2003)).

Neighbouring miRs are often expressed in a similar pattern due to their co-transcription as polycistronic transcripts, prior to cleavage into multiple RNAs (Baskerville and Bartel 2005). The miR-96-182-183 cluster on Chr6 and the miR-1-133 cluster on Chr2, are intergenic miRs, and likely to be transcribed as polycistronic transcripts from their own transcriptional units (Baskerville and Bartel). However miR-1-133 cluster on Chr18 is an intronic miR gene, embedded in the intron of the host gene mind bomb-1 (Mib1), and as such the expression of these miRs may be regulated by host gene transcription (Kim and Kim 2007; miRBase). As miR-182 and -206 are members of the miR-133b-206 and miR-96-182-183 cluster respectively, the expression of miR-182 and -206 were also examined by qPCR, despite the

unaltered expression of these miRs reported by microarray data. The microarray data comparing P347S to c57 retinas using miRCURY LNA arrays, revealed a significant 3.2-fold reduction of miR-206 in P347S retinas (Figure 4.2D), contrasting with the earlier observations of increased expression of miR-1 and -133b expression (Figure 4.6). However no changes in miR-206 expression were detected by qPCR (Figure 4.7). Conversely, qPCR analysis revealed a 1.97-fold decrease in retinal miR-182 expression in P347S vs c57 retinas ($p<0.001$; Figure 4.7), mirroring the alterations observed in the expression of miR-96 and -183 (Figure 4.6).

4.3.6. Summary

A comparative analysis between P347S and wild type mouse retinas revealed a significant alteration in miR expression profiles in mutant mice, as evaluated by microarray analysis and validated by qPCR. Specifically, significant differences in retinal expression of the miR clusters, miR-1-133 and miR-96-182-183were observed between the *P347S-RHO* mutant and wild type mice, with a significant increase in expression of members of the miR-1-133 cluster and reduction in expression of members of the miR-96-182-183 cluster.

4.4. Discussion

In order to gain a better insight into the possible involvement of miRs in retinal degenerative diseases, such as RP, the retinal miR expression profiles of P347S and wild type mice were compared.

Significantly, the expression levels of more than 50 miRs were altered in the P347S RP model compared to both wt 129 and c57 retinas (Figure 4.2 B and C) as the P347S mouse model is bred on a mixed genetic background (c57/129). Notably the comparison of the miR expression profiles of wt c57 and 129 retinas only revealed minor variations in miR expression (Figure 4.2 A) and alterations of miR expression between P347S and both wt mouse models were similar (Figure 4.2 B and C). The most significant alterations in P347S mice were observed for miR-96, -183, -1 and -133, detected by microarray analysis and validated by qPCR. The expression of miR-96 and miR-183 was reduced by greater than 2.5-fold in P347S retinas compared to wild type mouse retinas, while on the other hand, miR-1 and -133 levels increased by more than 3-fold in RP retinas (Figure 4.6). A similar expression patterns was observed for members of these miRs as these genes are likely to be co-transcribed as a polycistronic pri-miR transcript, owing to the location of members of the miR-1-133 group and members of the miR-96-182-183 group, in close proximity to each other on Chr2/18 and Chr6, respectively (Baskerville and Bartel 2005; Xu et al. 2007; RetNet). As miR-182 is also within 3.6kb of the miR-96-183 cluster, the expression of miR-182 was also examined by qPCR, revealing a similar reduction of 3.2-fold expression in the P347S retina.

As discussed in Chapter 3, miR-96, -182, and -183 were identified to be remarkably 'retinal-specific', distinctly localised to the photoreceptor cells by ISH, and potentially also expressed in interneurons (Ryan *et al.,* 2006; Karali *et al.,* 2007; Xu, S. *et al.,* 2007). As observed in this study, the expression patterns of these miRs are similar, both temporally and spatially, owing to the probable co-transcription of these miRs (Karali et al.; Xu et al.). In addition, recent studies in the retina (Xu et al. 2007), inner ear (Weston et al.), and dorsal root ganglia (Kloosterman et al. 2006) suggest that miR-96, -182 and -183 may represent a conserved sensory organ-specific cluster of miRs. However there is currently little existing evidence regarding their role in the

adult retina, however as the expression of miR-96, -182, and -183 increases postnatally and levels are sustained in adulthood (Xu et al.), it is possible that these miRs may be involved in the maintenance of mature photoreceptor cells. A diurnal variation in the expression of miR-182 and -96 has been observed, suggesting a circadian variation of retinal gene expression (Xu et al. 2007). It is possible that these miRs regulate the apoptosis pathway, as overexpression of miR-182 and -183 in cell cultures, inhibited the extrinsic activation of caspase-3 mediated by death-receptor activation (Ovcharenko et al. 2007). Additionally, the adaptor protein FAAD which is involved in the death receptor signalling pathway, is a predicted target of miR-182 and -96 (Ovcharenko et al. 2007).

Similarly, miR-1 and -133 are clustered miRs (Table 4.1), and are therefore likely co-transcribed. In addition as the miR-1-133 cluster on Chr18 is embedded in the intronic region of the host gene Mib1, the expression of these miRs at this location is likely regulated by the transcription of Mib1; which is thought to be involved in neurogenesis (Kim and Kim 2007; Yoon et al. 2008; miRBase). In contrast, more evidence regarding the biological functions of miR-1 and -133 exists, and these miRs are classically defined as muscle-cell specific miRs expressed in both heart and skeletal muscle. Both of these miRs regulate cardiomyocyte apoptosis and skeletal muscle proliferation and differentiation (Chen et al. 2006; Xu et al. 2007; Callis and Wang 2008), mediating opposing effects in both of these processes. For example in skeletal muscle miR-1 promotes myogenesis while miR-133 enhances myoblast proliferation (Chen *et al.,* 2006; Xu, C. *et al.,* 2007). Attention has also been drawn to the involvement of miR-1 and -133 in cardiac disease by two high profile publications, demonstrating that overexpression of both miRs can produce arrhythmias (Yang et al. 2008), and a decreased expression of miR-1 and -133 was observed in cardiac hypertrophy, which could be attenuated by overexpression of these miRs (Care et al. 2007). Recently Kim and co-workers (Kim et al. 2007) have demonstrated that miR-133 is enriched in the midbrain dopaminergic neurons, promoting the idea that miR-133 may play important roles in neuronal cells, peripheral to their identified functions in muscle. Interestingly miR-133 expression was significantly reduced in Parkinson disease patient brains, suggestive of an important role in the maintenance of these neuronal cells (Kim et al. 2007). A reduction of miR-1 and miR-133 expression is observed in both cardiac hypertrophy and Parkinson's disease, however as both of

these miRs may mediate opposing roles in some tissues (Callis and Wang 2008), the significance of the increased expression observed in the P347S retina is difficult to interpret. As miR-1 and -133 are co-transcribed, it is proposed that the resulting cellular outcome may be determined by either miR, depending on the presence of additional transcriptional factors and activation of specific regulatory pathways (Chen *et al.,* 2006; Xu, C. *et al.,* 2007). Additionally, as observed in Chapter 3, the relative expression of miR-1 and -133 is low in the retina in comparison to other tissues.

Not all miRs with higher than 2-fold changes in expression between P347S and wild type mice were followed up for qPCR validation. Other miRs, such as miR-451 and -146a (from Ambion microarray data) or miR-21, -23 and -140 (from Exiqon microarray data) were left out from further analysis as these miRs displayed very low levels of expression in the retina compared to the mouse platform. It was deemed, that such low signal-to-background ratios might have interfered with detection of the genuine expression levels of these miRs. The screening criterion implemented in the study, i.e. the threshold of at least a 2-fold change between P347S and wild type mouse retinas, was chosen rather arbitrarily, but with the objective of highlighting real changes in miR expression. The expression of more than 50 miRs changed significantly, but by less than 2-fold, many of which may represent miRs whose intracellular expression might have also genuinely been altered in P347S retinas, however to date expression of these miRs have not been validated by qPCR.

In this study, the P347S transgenic model was selected for two reasons. *RHO*-linked RP is one of the most common types of RP, representing approximately 25% of all autosomal dominant inherited RP cases in human patients (Dryja et al. 1990). In principle, the P347S transgenic animal model therefore potentially mirrors cellular events of a very frequent form of human RP. In addition, P347S mice are very useful as the retinal degeneration in this mouse model is rather slow (Li et al. 1996) compared to other *RHO*-linked transgenic RP lines such as the Pro23His *RHO* mouse (Olsson et al. 1992). Slow degeneration in P347S mice provides a reasonable time frame for the mutant retina to develop into adulthood while maintaining a relatively normal histological structure and function, the latter demonstrated by normal electroretinography (Li et al. 1996). Notably, in this study a slightly faster degeneration in the P347S animals was detected compared to the original findings (Dryja et al. 1990). Nevertheless, a time point of 1 month was chosen for the analysis

because at this age P347S mice have a fully differentiated retina and despite the ongoing retinal degeneration only exhibit a minor decrease in photoreceptor cell numbers (up to 25%).

Regarding the potential alterations in expression of individual miRs due to the above changes in cell composition in the P347S retina, they should not exceed the percentage of photoreceptor cell loss (approximately ±25%). In light of this, it is unlikely that the significant changes observed in the expression of miR-96, -182, -183, -1, and -133, are due to the altered cellular composition of the P347S retina. In contrast, Xu and co-workers (Xu et al. 2007) used rd1 mice with severe retinal degeneration to demonstrate that the retinal expression of miR-96, -182 and -183 occurred in cells other than the photoreceptors. In this case, altered expression of these miRs between wild-type and mutant retina was most likely observed because of the significant shift in cellular constituents in the rd1 retina, due to a complete loss of photoreceptors. It is also worth noting, that the P347S animals are on a c57/129 mixed genetic background. While it is preferable to utilise mice on a pure genetic background, the process of generating such mice takes approximately 12 generations of mating. In relation to the current study it is notable that almost identical miR profiles between c57 versus 129 mice were observed, and similar variations in miR profiles occurred between c57 versus P347S mice and 129 versus P347S mice. This supports the view that the alterations observed in miR expression profiles between P347S and wild type mice, are a function of the presence of the *RHO* mutation in P347S mice, and not due to differences in genetic background.

4.5. Conclusion

Data from this study highlight the potential function of miRs in retinal disease, demonstrating for the first time that the miR expression profile is altered in retinal degeneration. Using a transgenic mouse model of a common form of human RP, widespread changes in the miR expression profile in the retina were detected. In particular, the expression of two 'retinal specific' miRs decreased significantly, while two non-'retinal specific' miRs, with a known role in muscle and perhaps involved in dopaminergic neurons and Parkinson's disease, increased extensively. At present, very

little is known about the function of miRs in retinal disease, however the results from this study suggest that the normal miR expression profile is perturbed in *RHO*-linked RP. Further studies are required to address the nature and types of cellular targets for these miRs and the underlying mechanisms regulated by these miRs. Identifying disease-related miRs in RP models may provide a better understanding of the pathophysiology of retinal degenerations and modulation of the expression of key miRs may potentially open future avenues for therapeutic development for retinopathies such as RP.

Given the identification of an altered miR expression profile in a retinal degeneration mouse model, it was of immense interest to ascertain whether these changes were specific to this form of RP or were common to other RP animal models. The work associated with addressing this question form the basis of the study described in Chapters 5 and 6 of this Ph.D. thesis.

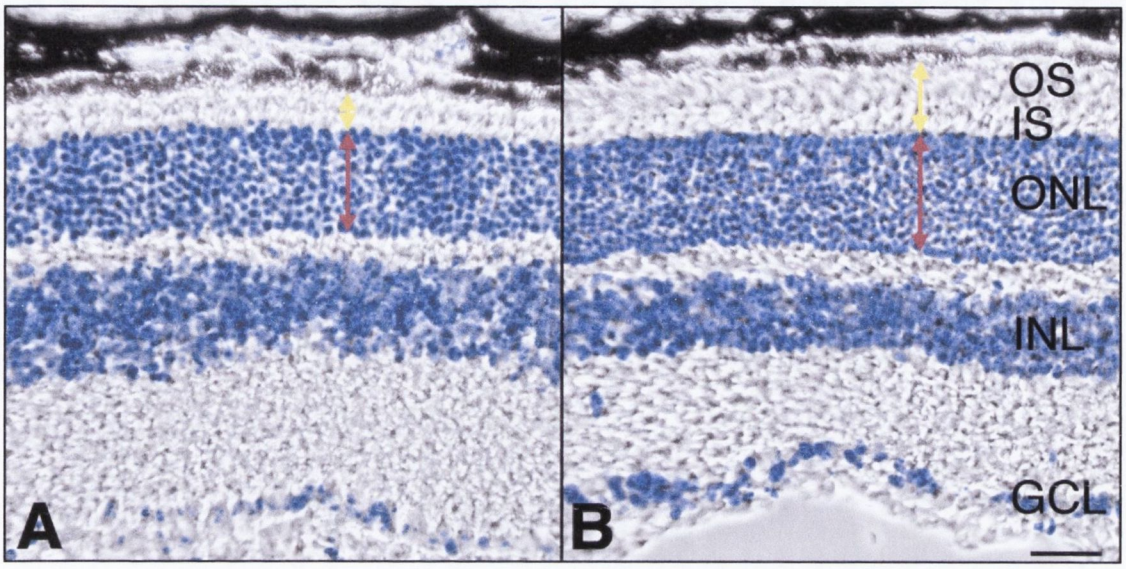

Figure 4.1: Comparative histology of 1-month-old c57 and P347S retinas. Eyes from 1-month-old c57 and P347S (mutant pro347ser *RHO* transgene) animals were fixed in 4% paraformaldehyde, 12 μm cryosections cut, and nuclei counterstained with 4',6-diamidine-2-phenylindole-dihydrochloride (DAPI). Phase contrast and fluorescent dark field (DAPI, false colored) microscopic images were overlaid to display histology of **(a)** P347S and **(b)** c57 retinas. Combined thicknesses of photoreceptor outer and inner segments (yellow arrows) and outer nuclear layer (magenta arrows) are indicated. Scale bar: 25 μm. GCL, ganglion cell layer; INL, inner nuclear layer; IS, photoreceptor inner segments; ONL, outer nuclear layer; OS, photoreceptor outer segments.

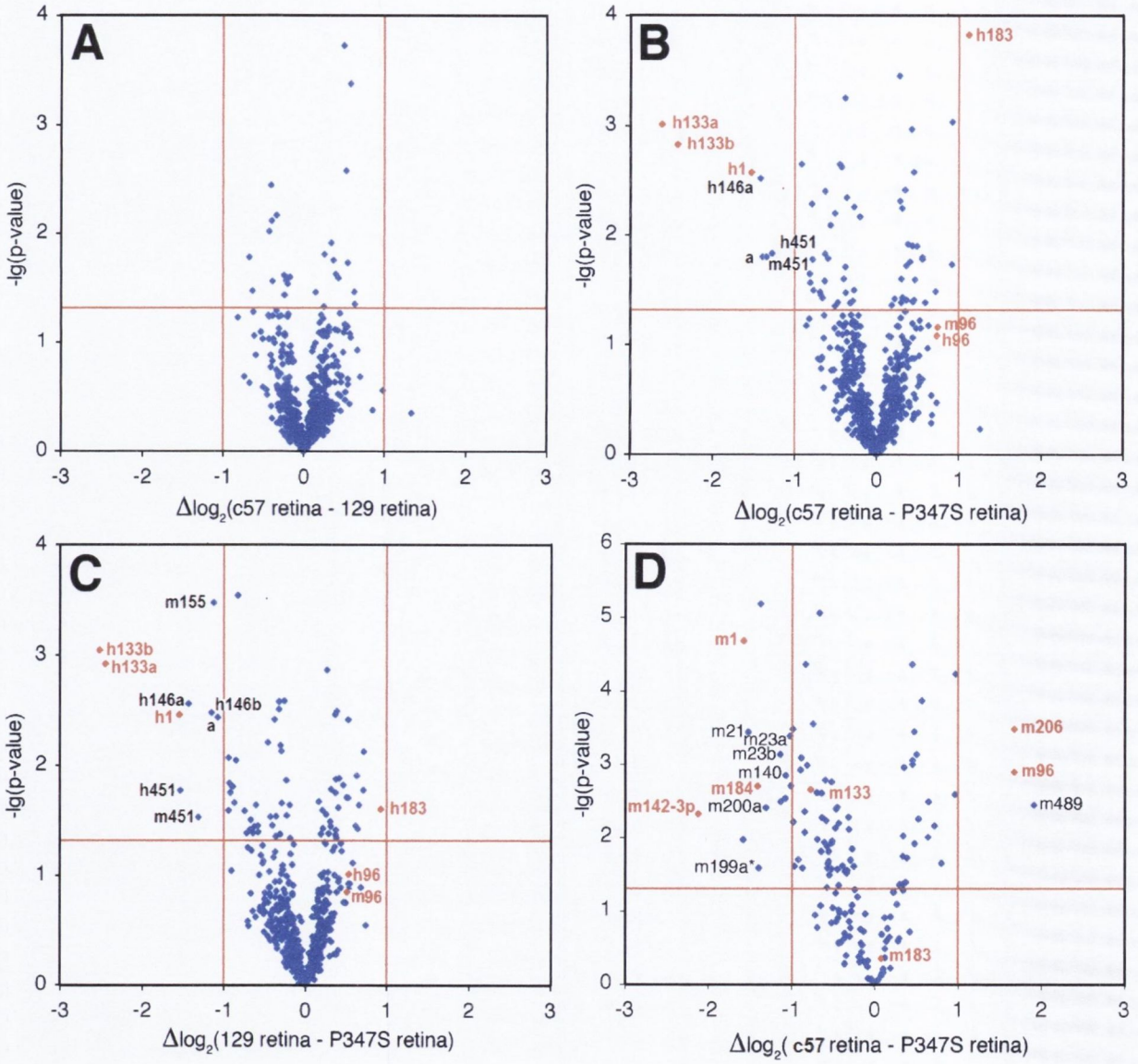

Figure 4.2: Volcano plots of miR expression in P347S and wild-type retinas. Plots represent comparative miR expression profiles of **(A)** c57 versus 129 retinas, **(B)** c57 versus P347S (mutant pro347ser *RHO* transgene) retinas, and **(C)** 129 versus P347S retinas using Ambion miR microarrays v2, **(D)** c57 versus P347S retinas using Exiqon miR microarrays v8.1. X-axis indicate difference of expression level on a $\log_2$ scale, while Y-axis represents corresponding *p-values* (Student's *t*-test) on a negative log scale. A $-\log_{10}$ *p-value* of 1.30 (highlighted by the red horizontal line) corresponds to a *p-value* of 0.05 on a geometric scale, and therefore points above this line represent statistically significance variations of miR expression. The vertical red line was chosen arbitrarily, and represents differences in expression between samples of ±1 on a $\log_2$scale. Therefore the more lateral points, represent a greater magnitude of miR expression between the two groups analysed, and positive and negative values signify the group with higher or lower expression.

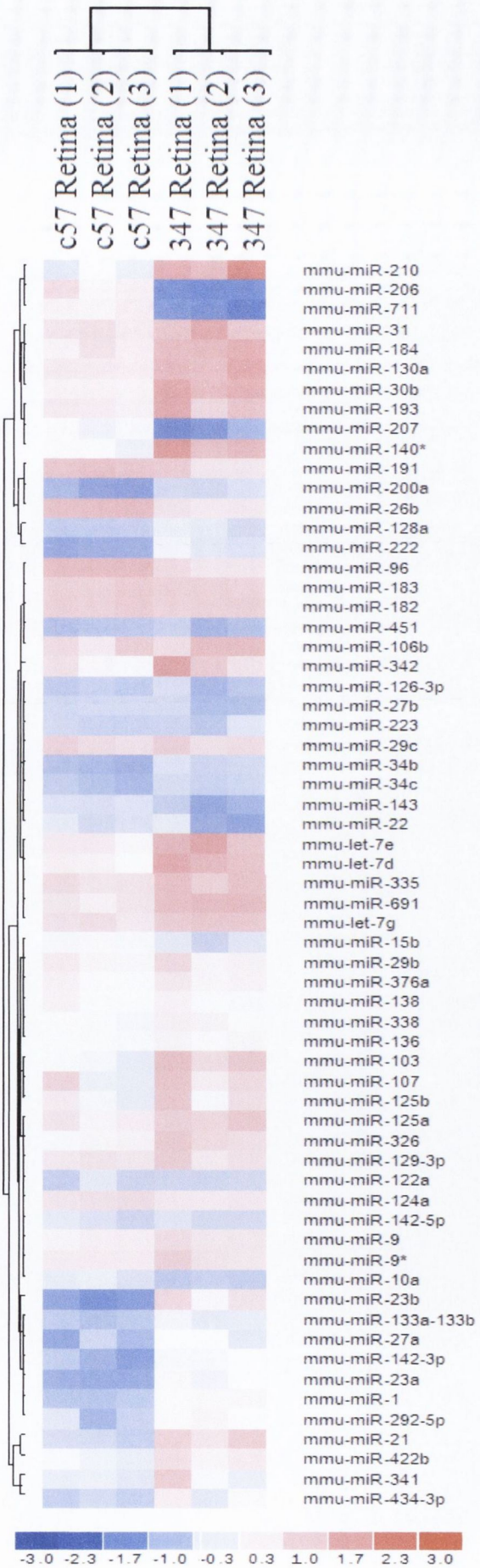

Figure 4.3: Heat Map and Hierarchical clustering of miRs in c57 and P347S retina: The heat map diagram shows the result of the two-way unsupervised hierarchical clustering of miRs and the experimental groups; c57 retina and P347S retinas, using Exiqon V8.1 microarrays. Each row represents a miRNA and with clusters indicated on the left, while each column represents a sample with clusters appearing at the top. The clustering was performed on a filtered set of $\log_2$(Cy3/Cy5) ratios, which displayed a high variability across samples (standard deviation >0.5). Clusters were generated using the average linkage method, a method which calculates the distance between clusters. The Cy5 labelled reference was used in each array, and provides a constant baseline to compare samples to. The color scale shown at the bottom illustrates the relative expression level of each miR across all samples (log2Cy3/Cy5). The red color represents a relative miR expression level greater than the mean, blue color represents a relative expression level lower than the mean. Log_2(Cy3/Cy5) ratios ± 1 correspond to a more than 2 fold up or down regulation, relative to the miR reference (Cy5).

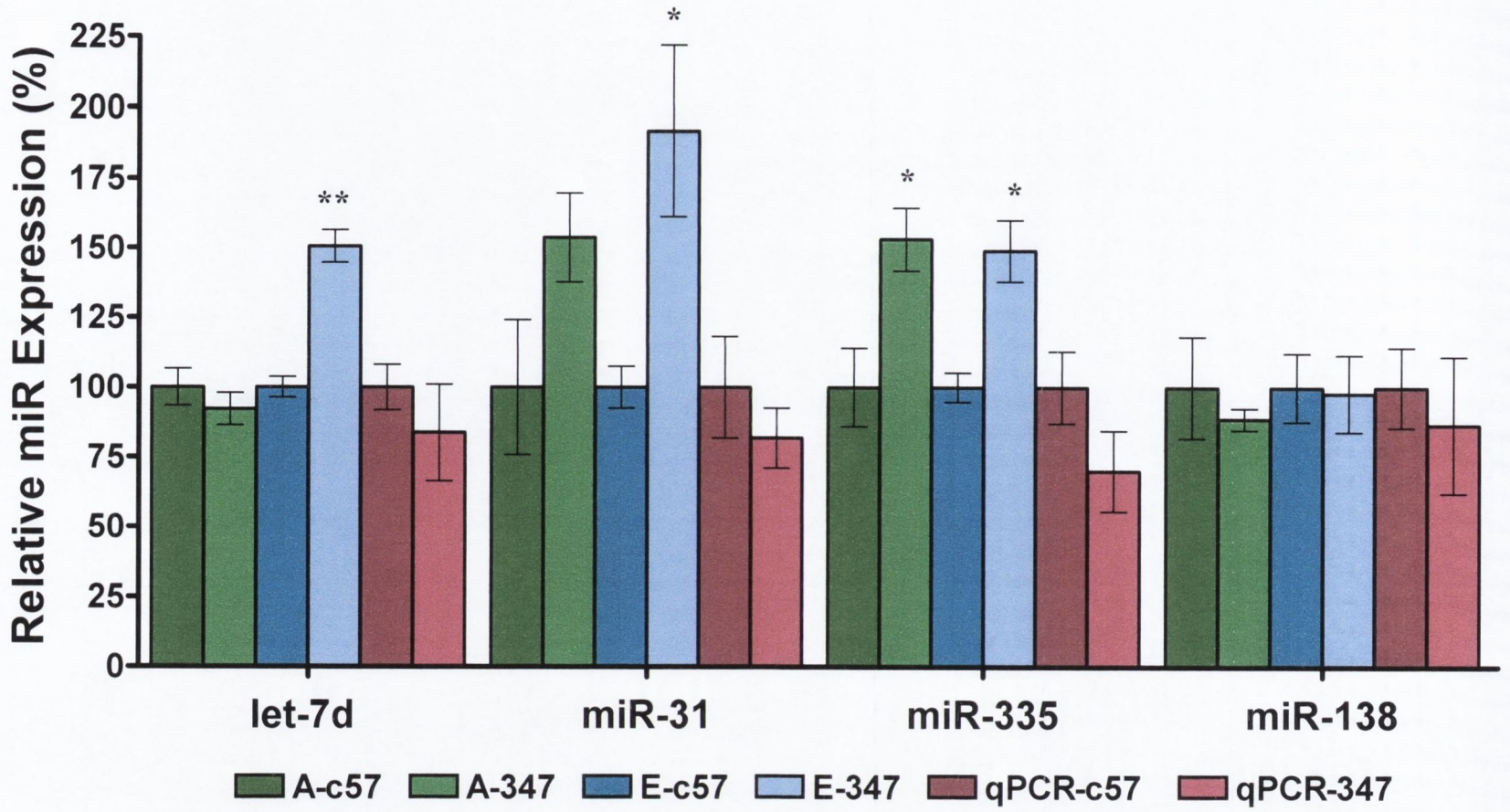

Figure 4.4: Differentially expressed miRs between c57 versus P347S retinas. Expressions of mouse miR let-7d, miR-31, -335, and -138, were analyzed using Ambion miR microarrays (green, 'A-' in legend), Exiqon miR microarrays (blue, 'E-' in legend), and quantitative real-time RT-PCR (magenta; 'qPCR'-in legend). Expression levels of each miR in P347S (mutant pro347ser *RHO* transgene; light green, light blue and magenta columns) is expressed relative to c57 retinas (taken as 100%; dark green, dark blue, and purple columns). Statistical analysis was performed using Students *t-test* analysis, and *p-values* correspond to; (*) $p < 0.05$, and (**) $p < 0.01$. Error bars indicate S.E.M.

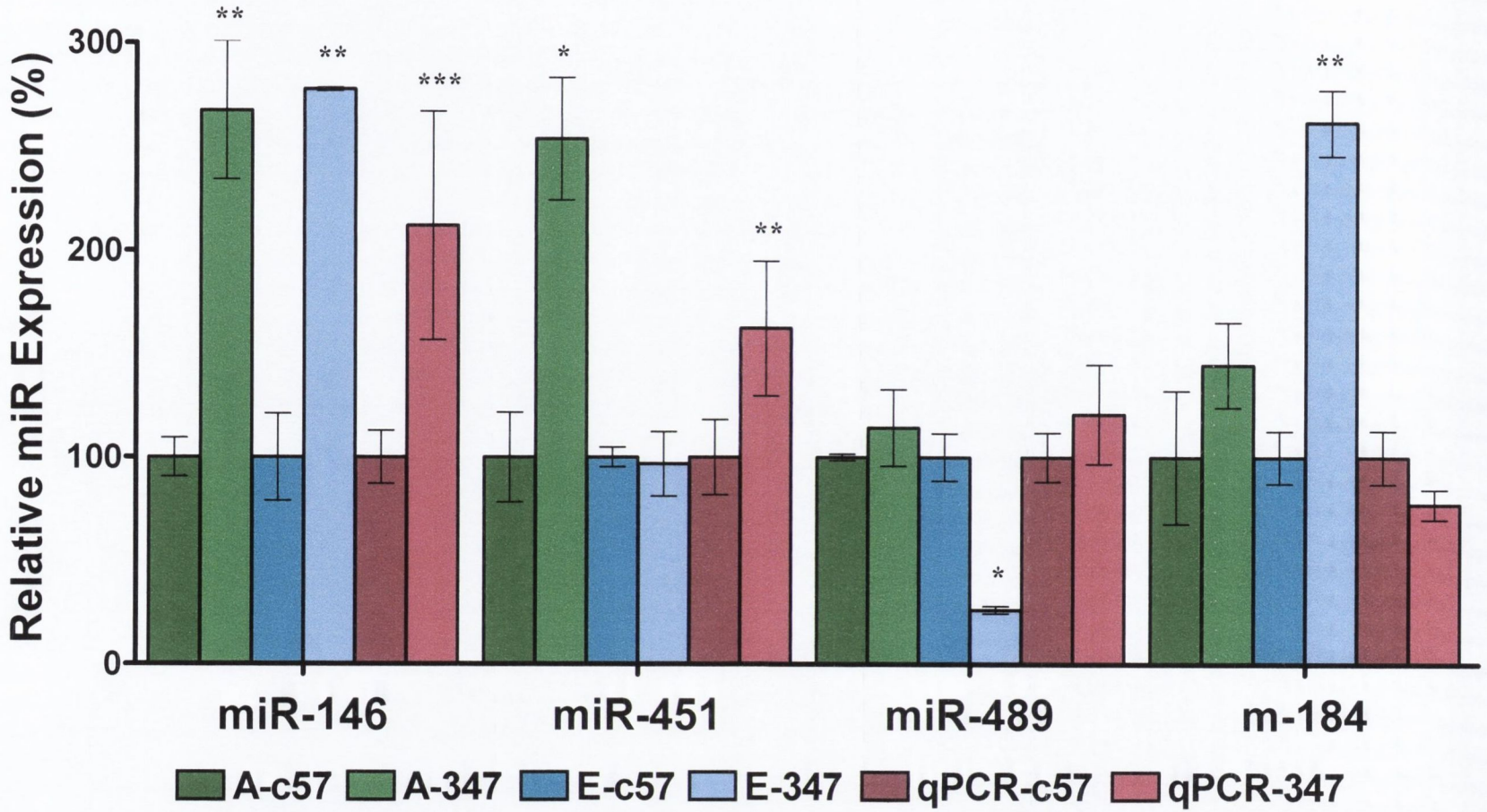

Figure 4.5: Differentially expressed miRs between c57 versus P347S retinas. Expressions of mouse miR-146, miR-451, and miR-489 were analyzed using Ambion miR microarrays (green, 'A-' in legend), Exiqon miR microarrays (blue, 'E-' in legend), and quantitative real-time RT-PCR (magenta; 'qPCR'-in legend). Expression levels of each miR in P347S (mutant pro347ser *RHO* transgene; light green, light blue and magenta columns) is expressed relative to c57 retinas (taken as 100%; dark green, dark blue, and purple columns). Statistical analysis was performed using Students *t-test* analysis, and *p-values* correspond to; (*) $p < 0.05$, (**) $p < 0.01$, and ***; $p < 0.001$. Error bars indicate S.E.M.

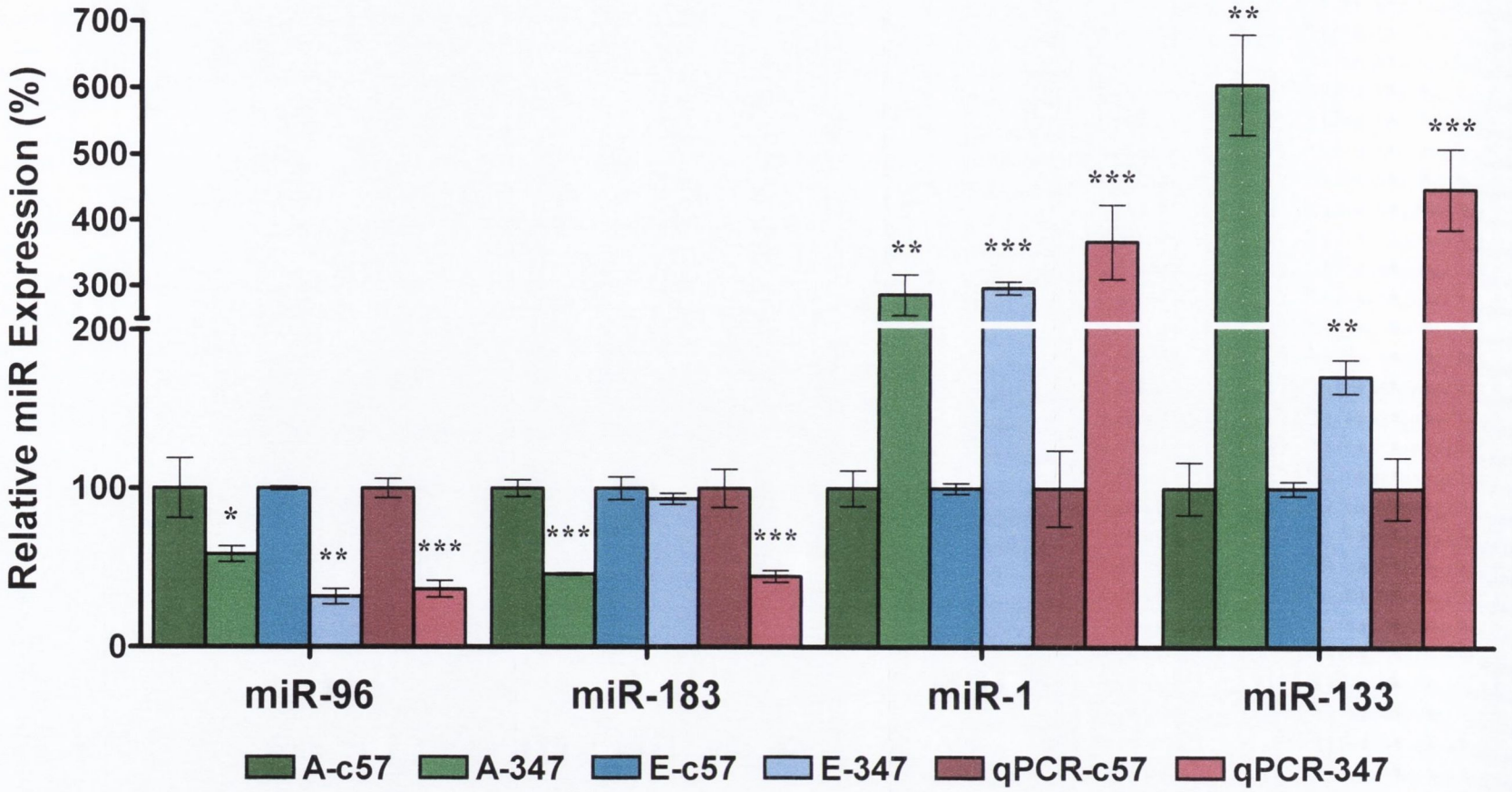

Figure 4.6: Differentially expressed miRs between c57 versus P347S retinas. Expressions of mouse miR-96, miR-183, miR-1 and miR-133 were analyzed using Ambion miR microarrays (green, 'A-' in legend), Exiqon miR microarrays (blue, 'E-' in legend), and quantitative RT-PCR (magenta; 'qPCR'-in legend). Expression levels of each miR in P347S (mutant pro347ser *RHO* transgene; light green, light blue and magenta columns) is expressed relative to c57 retinas (taken as 100%; dark green, dark blue, and purple columns). Note that the y-axis is discontinuous. Statistical analysis was performed using Students *t-test* analysis, and *p-values* correspond to; (*) $p < 0.05$, (**) $p < 0.01$, and ***; $p < 0.001$.. Error bars indicate S.E.M.

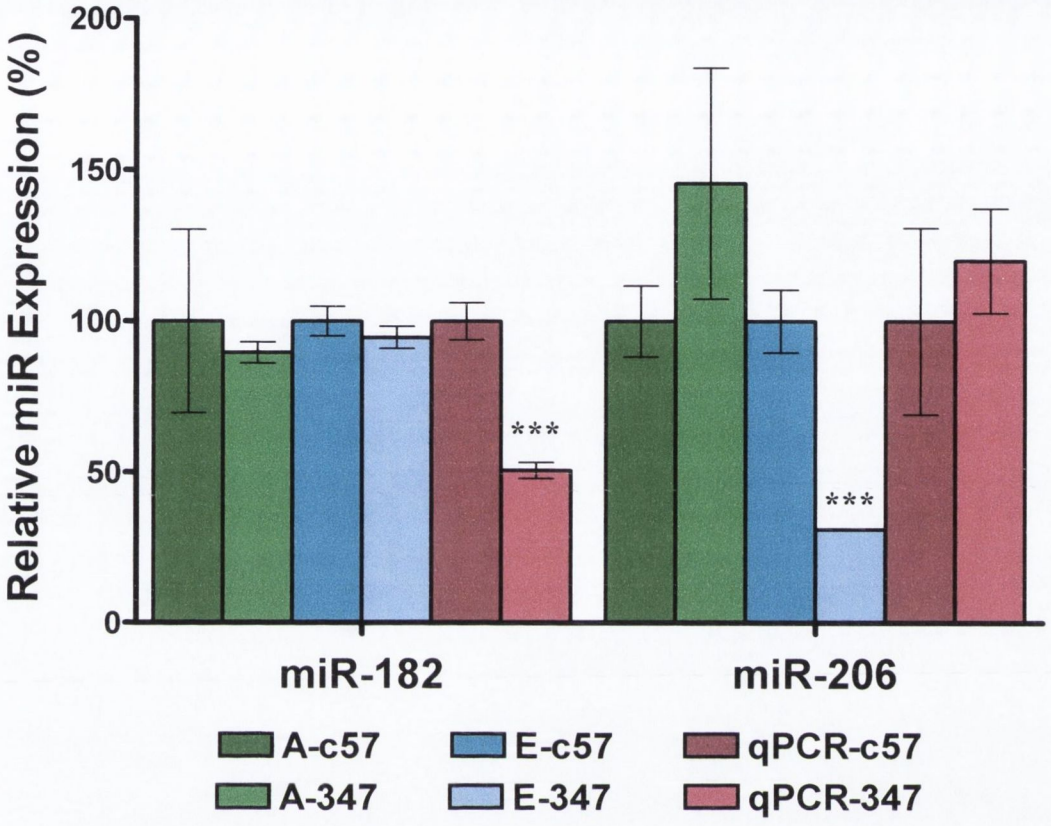

Figure 4.7: Differentially expressed miRs between c57 versus P347S retinas. Expressions of mouse miR-182 and miR-206 were analyzed using Ambion miR microarrays (green, 'A-' in legend), Exiqon miR microarrays (blue, 'E-' in legend), and quantitative real-time reverse transcription polymerase chain reaction (magenta; 'qPCR'-in legend). Expression levels of each miR in P347S (mutant pro347ser *RHO* transgene; light green, light blue and magenta columns) is expressed relative to c57 retinas (taken as 100%; dark green, dark blue, and purple columns). Note that the y-axis is discontinuous. Statistical significance was analysed by Students *t-test* analysis, and denoted by ***$p< 0.001$. Error bars indicate S.E.M.

Table 4.1: miR Clusters						
miRNA Name	Chr	Coordinates from:	to:	Pre-miR Size	Location	Cluster size
mmu-mir-182	6	30,115,918	30,115,992	74	Intergenic	3.8 Kb
mmu-mir-96	6	30,119,446	30,119,551	105	Intergenic	
mmu-mir-183	6	30,119,668	30,119,737	69	Intergenic	
mmu-mir-133a-1	18	10,782,897	10,782,983	86	Intronic	2.7 Kb
mmu-mir-1-2	18	10,785,479	10,785,550	71	Intronic	
mmu-mir-1-1	2	180,123,753	180,123,829	76	Intergenic	9.4 Kb
mmu-mir-133a-2	2	180133084	180133187	103	Intergenic	
mmu-mir-133b	1	20,672,850	20,672,968	118	Intergenic	3.9 Kb
mmu-mir-206	1	20,669,091	20,669,163	72	Intergenic	

Table 4.1: miR Clusters: Information is presented regarding the clustered miRs, miR-96-182-183 , -133-1 and 133-206, detailing the chromosome location and coordinates of these mir genes. The size of the pre-miR sequences is listed for individual miRs, in addition to the cluster size containing all miR members.

Chapter 5

Examination of Retinal miR expression in rho-linked and rds-linked RP mouse models

5.1. Introduction

A number of highly expressed miRs were previously identified in the retina (Ryan et al. 2006; Karali et al. 2007; Loscher et al. 2007; Xu et al. 2007), and Chapter 4 of the thesis describes the observation of an altered miR expression profile in the P347S rho-linked mouse model of RP (R347) (Li et al. 1996). This finding provides the first evidence of an altered miR expression in retinal disease, specifically miR-96, -182, and -183 expression was diminished, and miR-1 and -133 expression was enhanced (Loscher et al. 2007). However, the fundamental roles that these miRs, or other 'retinal-specific' miRs, may have in the adult or diseased retina are not yet understood (Arora et al. 2007; Xu et al. 2007).

As previously described, RP is an umbrella term for a large group of inherited retinal degenerations (RetNet), however despite the differences that exist in both symptoms and morphological findings, the majority or possibly all mutations are thought to result in photoreceptor loss by the final common pathway of programmed cell death (Portera-Cailliau et al. 1994; Sanges et al. 2006). However elucidating the series of cellular events that lead to photoreceptor cell death is of fundamental biological interest, and imperative in order to fully examine possible therapeutic strategies for RP. Indeed the alteration of miR expression observed in the R347 RP model may underlie some of these cellular events, mediated in response to mutant rhodopsin expression. As RP is characterised by both intergenic and intragenic mutational heterogeneity, it is relevant to consider whether these changes in miR expression are common to other forms of RP. Similar miR alterations may occur in photoreceptor cells in RP models, caused by other rhodopsin mutations, or alternatively by other mutant proteins, i.e. RDS/Peripherin. Indeed common miR profiles have been observed in other diseases, such as cancer (Bandres et al.) and skeletal muscle dystrophies, suggestive of a common role of miRs in disease pathology (Eisenberg et al. 2007). Intriguingly, in some cases miR expression has been observed to vary within disease states, demonstrating sufficient power to diagnostically discriminate between some disease subtypes (Neely et al. 2008) and also to reliably predict disease prognosis (Yu et al. 2008). It follows, that similar alterations of miR expression in the retina may occur in RP, independent of the causative gene or mutation.

Therefore the aim of this study was to determine whether the identified retinal miR expression signature observed in the R347 mouse model, was also present in other rhodopsin and rds/peripherin-linked mouse models of RP. For instance, the rho knockout (rho-/-) mouse line fails to form rod outer segments, exhibiting a severe retinal degeneration (Humphries et al. 1997). Additionally, mutations in the RDS/Peripherin gene are also causative of RP and other retinal dystrophies (RetNet), this gene encodes the photoreceptor specific protein rds/peripherin required for rod outer segment morphogenesis (Farjo and Naash 2006). Notably, transgenic mice carrying a deletion in codon-307 of the rds gene (Δ307) (McNally et al. 2002), model a similar human mutation responsible for a dominant form of RP (RetNet http://www.sph.uth.tmc.edu/Retnet/), and mice with a naturally occurring null mutation in this gene (rds-/-) (Sanyal et al. 1980) display progressive retinopathy.

As observed in Chapter 4 of this thesis, a reduction in the ONL thickness of the R347 retina was observed at one-month of age. It is unlikely that this degree of photoreceptor loss accounts for the magnitude of alterations observed for some miRs, however the altered cellular composition of the degenerating retina might contribute in part to the observed miR profile. Therefore, a further objective of the research described in this chapter of the thesis, is to clarify if genuine alterations in miR expression in retinal cells, account for the observed miR expression signature in RP models. By defining miR expression profiles specifically in photoreceptor cells, a valuable insight into miR expression changes occurring in the primary cell type affected in RP can be ascertained.

In this study a common signature of miR dysregulation has emerged in the analysed mouse RP retinas. Notably the observed variations in miR expression are unequivocally found in the rod photoreceptor cells of both the Δ307 and R347 mouse models of RP.

5.2. Materials and Methods

5.2.1. Experimental Animals

P347S-rhodopsin (R347; (Li et al. 1996)), Δ307-rds (Δ307; (McNally et al. 2002)), rho knockout (rho-/-;(Humphries et al. 1997)), rds null mutant (rds-/-; (Sanyal et al. 1980)), and the rhodopsin-GFP fusion knock-in mouse model (RGFP;(Chan et al. 2004)) were used in this experiment. Wt balb/C and wt 129 mice were used as experimental controls. The R347 and Δ307 models are bred on a rho+/- and rds+/- backgrounds respectively, thereby containing one mutant transgene and one wt rhodopsin/rds allele, mimicking possible genotypes of human RP. RGFP+/-Δ307+/- and RGFP+/-R347+/- mice were generated by crossing the R347 and Δ307 mouse models with the RGFP+/- mouse (Chan et al. 2004). The RGFP+/- mouse is a transgenic mouse expressing a fusion Rhodopsin-GFP protein, thereby efficiently labelling rod photoreceptor cells (Chan et al. 2004). These mice were bred under specific pathogen free (SPF) housing conditions (see section 2.1.4) and mice at one-month of age were sacrificed by CO_2 asphyxiation.

5.2.2. RNA Extraction

Total RNA was extracted using the Qiagen miRNeasy Mini Kit as outlined in section 2.3.2.2. Three retinal samples per mouse line were prepared by pooling six retinas per sample.

5.2.3. Microarray Experiment

Wt 129 retina and rho-/- retinal RNA samples were outsourced to Exiqon for miR profiling. The miRCURY LNA miR Array v.9.2 (see section 2.3.5.2) was used in this experiment, which probed for miRs annotated in miRBase v.9.2 (release date May 2007). This array probed specifically for 494 miRs (420 mouse and 74 Exiqon miRs), 74% (431 of 579) of which are annotated in miRBase v.10.0. Experimental RNA samples were labelled with Cy3 while the reference RNA sample was labelled with

Cy5. All samples and biological replicates were analysed on separate miR microarrays as outlined in section 2.3.5.4.

5.2.4. Microarray Data Analysis

Data was pre-processed and normalized using the global Lowess (LOcally WEighted Scatterplot Smoothing) regression algorithm as described in section 2.3.5.5. by the miR profiling company, Exiqon. Normalised log_2-transformed Cy3/Cy5 ratios were used for further analysis.

5.2.5. FACS

For FACS analysis, RGFP+/-, RGFP+/-Δ307+/- and RGFP+/-R347+/- mice at one-month of age were sacrificed and three samples were prepared representing each group, and two retinas were pooled per retinal sample. Retinas were dissociated using trypsin (see section 2.5.1) and cells analyzed and separated by FACS as described in section 2.5.2. with the technical assistance of Dr. Alfonso Blanco, University College Dublin. Total RNA was extracted from the Ultrafree-MC filter unit (Millipore) by adding 350 µl RNA lysis buffer (see section 2.3.2) to the filter unit. The buffer was passed through the filter by centrifugation at 6600 rpm for 2 minutes, and the filtrate reapplied to the filter unit and eluted 3 times to ensure complete lysis and collection of RNA. The Qiagen miRNeasy Mini Kit was used to extract the RNA from the filtrate according to manufacturers' instructions (see section 2.3.2.2).

5.2.6. Quantitative Real-Time RT-PCR (qPCR)

Two-step qPCR was performed using ABI's TaqMan miR Assay (Applied Biosystems, Foster City, CA, USA) according to manufacturer's instructions (see section 2.233.1). The TaqMan miR Assays for the following miRs were used: miR-1, -133, -142, -183, -96, -182, -21, -23b, -129-3p, -190, -489. Equal amounts of RNA (10 ng/reaction) were used in each RT reaction. SnoRNA-202 and -234, with strong correlation in their expressions across all samples (r^2=0.8958 and $p<0.0001$), were

used as internal controls. The data were analysed (see section 2.3.3.4) and the log_2-transformed miR/control expression ratios were used for further analysis.

5.2.7. Histology and Microscopy

To examine retinal histology, the eyes from one-month old animals were obtained, two eyes per animal models analysed. Eyes were fixed in 4% paraformaldehyde for 4 hr at 4°C. Following sucrose cryoprotection, frozen sections of the eyes at 12 μm thickness were obtained (see section 2.3.4.2). The nuclei were counterstained by using 4',6-diamidine-2-phenylindole-dihydrochloride (DAPI, Invitrogen) as outlined in section 2.8. Sections were analysed by bright field normal and phase-contrast as well as fluorescent microscopy using an Axiophot microscope (Carl Zeiss Ltd., Hertfordshire, UK) and the appropriate filters. Outer nuclear layer thickness was measured using microscopic images from sections in three planes 250 μm apart in the medial part of the eye using Adobe Photoshop Software (Adobe Systems Europe Ltd., Glasgow, UK).

5.2.8. Immunocytochemistry Analysis

The expression of rhodopsin and rod-transducin was examined using immunocytochemical analysis on FACS sorted cells. The cells were fixed and mounted onto Poly-L-Lysine microscope slides, and expression of rhodopsin and transducin was detected as detailed in section 2.8. The following primary antibodies were used, anti-RHO (1:100; from R.Molday) and rabbit anti-rod-transducin-alpha (1:100; Santa Cruz Biotechnology Inc.) in addition to the secondary antibodies, anti-mouse IgG-Cy3 (1:500) and anti-rabbit IgG-Cy3 (1:500) (Invitrogen).

5.2.9. Statistical Analysis

Analysis of statistical significance was performed using ANOVA, Student's *t-test* and Pearson's correlation using GraphPad Prism statistical software, and

variations in expression, corresponding to a *p-value* <0.05 were considered statistically significant.

5.3. Results

5.3.1: Outer Nuclear Layer Thickness Analysis in rho- and rds-linked mouse models of RP

The retinal miR expression of the previously reported miRs; miR-96, -182, -183, -1 and -133 (Chapter 3) and additionally miR-142, were explored in the current study. MiR-142 expression was also examined in this study, as it exhibited marked changes in expression in the previous microarray experiment (Chapter 4), where miR-142 expression was reduced 4.14-fold in the R347 retina, however these changes were not followed up at the time. The objective of this study was to test whether the reported miR expression signature detected in R347 (P347S) animals involving a rhodopsin mutation, characterized other photoreceptor-linked mouse models of RP. The models of RP used in this study were rho-/- (rho knockout; (Humphries et al. 1997)), R347 (P347S mutant in rho transgene, (Li et al. 1996)), Δ307+/- (deletion in *rds* transgene; (McNally et al. 2002) and rds-/- (null rds mutant) (Sanyal et al. 1980) models. Wild type 129 mice and balb/C mice were used as controls, as the above RP models are bred on a 129 background, with the exception of the rds-/- mouse, which is on a balb/C background.

As in previous experiments, an early time-point of one month of age was chosen for this study, to minimize the possibility that miR expression changes resulted from altered cell composition of the degenerating mouse retinas. The magnitude of retinal degeneration in these models was semi-quantitatively ascertained, by determining the thickness of the ONL in retinal histological sections of each mutant mouse line, relative to ONL thickness of wt 129 retinas. At this time-point, a similar level of retinal degeneration was observed in the rho-linked RP models, the R347+/- and rho-/- models exhibiting a 29.7 ± 3.3 % and 22.9 ± 3.2 % reduction in ONL thickness, respectively compared to wt 129 ONL thickness ($p<0.01$; Figure 5.1C, 5.1D, 5.1G). In contrast, the rds/peripherin-linked RP models displayed varying degrees of photoreceptor loss; the rds-/- and Δ307+/- models exhibiting a reduction of 31.8±3.6% and 7.7±3.7% of ONL thickness respectively, compared to wt 129 ONL thickness ($p<0.01$; Figure 5.1E, 5.1F, 5.1G). ONL thickness of wild type balb/C and

129 mice did not differ significantly from each other, with a relative ONL thickness of 104.488±4.8% and 100.0± 4.6% respectively ($p>0.05$; Fig. 5.1A, 5.1B, 5.1G).

5.3.2. Microarray Analysis of miR expression in rho-linked RP mouse models

Microarray analysis was undertaken by the miR profiling company Exiqon, to compare the global miR expression profile of rho-/- animals to wt 129 mouse mutants using Exiqon miRCURY LNA arrays v9.2, and concurrently compared to R347 data from previous experiments using Exiqon miRCURY LNA array v8.1 (Figures 5.2, 5.3). Three RNA samples were obtained for each of the three mouse models analysed, wt 129, R347 and rho-/- mouse models, and each retinal RNA sample comprised of RNA pooled from 6 retinas As two versions of the miRCURY array were used to create these plots (Figure 5.2 B, 5.2 C) only data from 108 probes are illustrated, compared to 211 probes for direct comparison of results using v9.2 array (Figure 5.2 A). This disparity is due to the large number of miRs, which were added or modified in the v9.2 platform, and therefore could not be directly compared. Note also that for the rho-/- vs. 129 retina comparisons using the v9.2 array (Figure 5.2 A), only 43% of miR probes (211 out of the 494) provided $\log_2$Cy3/Cy5 ratios above background in both samples.

Comparison of miR expression in rho-/-, R347 and wt 129 retinas by microarray analysis is presented in Figure 5.2. The expression levels of 4 miRs, miR-133a, -133b, -1, and -689 were increased 2-fold in rho-/- retinas compared to 129 retinas (Figures 5.2A, 5.3). These alterations in miR expression were reflected in the R347 vs. 129 plot, where miR-133a, -133b, and -1 were also significantly increased in R347 by greater than 4-fold (Figure 5.2B). Additionally the expression levels of miR-199a, -142, -21, and -23c were significantly raised, while miR-206, -489, and -129 were reduced by ± 2-fold in the R347 retina (Figure 5.2B). The key variations between rho-/- and R347 retinas are highlighted in Figure 5.2C; specifically miR-1, -133, and -142 are reduced to a greater extent in the R347 retina, while decreased expression of miR-206, -489 and -199 is only observed in the R347 retina.

5.3.3. qPCR analysis of miR expression in rho- and rds-linked RP mouse models

The retinal expressions of miR-1, -133, -142, -96, -182, and -183 miRs were analysed by qRT-PCR in the rho-linked (R347+/-, rho-/-) and rds/peripherin-linked (Δ307+/-, rds-/-) mice. Interestingly, a common trend in retinal miR expression profiles was observed among the analysed mouse models ($p<0.01$ by ANOVA; Fig. 5.4). The relative expression of miR-1, -133 and -142 was increased between 207.0±45.0% to 533.1±22.1% compared to wt 129 retinas (Fig. 5.4 A), while expression of miR-96, -182 and -183 decreased between 21.8±5.7% to 50.9±6.1%, in the mutant retinas compared to wild type controls (Fig. 5.4 B).

The magnitude of up-regulation of miR-1 and -133 was very similar across all mutant models. For example miR-1 expression increased between 274.9±32.3% to 533.1±22.1% and miR-133 expression increased between 279.3±26.3% to 495.65±11.9%; the highest and lowest increases were detected in retinal RNA samples of R347 and Δ307+/- mouse models respectively. Additionally, miR-142 expression was also raised in the four mouse models of RP analyses, between 207.0±45.0% in the rds-/- model and up to 392.3±25.2% in the retinas of the R347 mouse model. The relative expression of miR-1, -133, and -142 was significantly higher in the retina of the R347+/- mouse model compared to the rho-/- model, by 107.7±24%, 89.3±21.6% and 168.9±24% respectively ($p<0.001$). In contrast, a similar magnitude of expression of miR-1, -133 and -142 was observed in the retinas of rds-linked mouse models of RP (Figure 5.4A).

The magnitude of miR-96, -182 and -183 expression was comparable among all models; specifically the expression of miR-96 was decreased between 31.8±4.9% to 48.0±2.4%, miR-182 expression was decreased between 21.8±5.7% to 50.9±6.1%, and miR-183 between 24.4±8.3% to 37.3±6.3% (Figure 5.4B). The greatest reduction of which was observed in the R347+/- and rds-/- retinal samples compared to the wt 129 retina; where expression of miR-96 was reduced by 48.0±2.4% and 44.0±7.8%; miR-182 by 47.8±1.0% and 50.9±6.1%, and miR-183 by 37.1±4.4% and 37.3±6.3% respectively. Lower alterations of miR-96, -182, and -183 expression were observed in the rho-/- retinal samples, corresponding to a reduction in expression of 34.3±3.2%, 39.4±3.1% and 24.6±4.6% of respectively (Figure 5.4B). Note also that the basal expression of miR-1, -133, -96 and -183 was significantly lower in wild type balb/C

retinas compared to the wt 129 mice; for example miR-96 expression was reduced by 15.1±10.3% ($p<0.05$), while miR-133 expression was reduced by 70.0±8.6% ($p<0.01$), as analysed by ANOVA ($p<0.05$)(Fig. 5.4B). This finding is relevant, as the rds-/- model is bred on a balb/C background, and as such miR expression in the rds-/- model is compared to the balb/C model.

The miR expression profiles of miR-21, -23b, -129, -190, and -489 were also examined by qPCR in rho- and rds-linked models of RP. These miRs were chosen as microarray data revealed that their expression levels were altered in R347 or rho-/- models compared to 129 wt retinas (Figure 5.2). The expression profile varied considerably for each of these miRs, and very few similarities were observed among the mutant models (Figure 5.5). The R347+/- mouse model displayed altered miR profiles of miR-21 and -23b, where expression was increased by 28.0±14.6% and 39.9±14.8% respectively, compared to wt 129 retinal samples (Figure 5.5A). The rho-/- mouse model did not mirror these changes, as a decrease in expression of miR-129 by 31.4±3.5% was the only statistically significant alteration in this animal model ($p<0.01$; ANOVA; Figure 5.5B). (Note that there was a trend for reduced expression of miR-21 and -489 in rho-/- retinal samples, by 15.8±4.3% and 11±8.5% respectively; however these changes were not statistically significant by ANOVA analysis). In the rds-linked RP models few alterations in expression were observed for these 5 miRs. No significant differences were observed in the Δ307+/- model, however the expression of miR-21, -23b was increased in the rds-/- model compared to the balb/C retinal samples, by 30.5±14.3% and 38.8±14.6 % respectively ($p<0.01$). However it should be noted that expression levels in the rds-/-model were compared to balb/C retinal samples, in which the expression of 4 of the 5 miRs were reduced significantly in the balb/C model compared to wt129 retina ($p<0.05$) (Figure 5.5).

It is important to note that the R347 is on a mixed c57/129 background as discussed in Chapter 4; however miR expression profiles obtained using microarrays, reveal similar miR profiles between the two strains of mice. Wt balb/C mice were used in this analysis as the rds-/- mouse is on a balb/C background. Therefore, for some of the results involving small changes in miR expression profiles, the changes may in part be a function of the lack of uniformity in genetic background between the animal models being evaluated. Nevertheless, many of the changes observed in miR

expression, far exceed those observed between balb/C and 129 mice, and therefore are likely to represent genuine changes in miR expression profiles.

5.3.4. Generation of RGFP expressing RP models

To clarify whether the above changes in miR expression resulted from alterations in cell composition of the degenerating retina or were due to an altered miR expression in retinal cells, RGFP mice with expression of GFP restricted to rod photoreceptors were used (Chan et al. 2004). R347 and Δ307 mouse models were crossed onto the RGFP background, producing RGFP+/-R347+/- and RGFP+/-Δ307+/- models. Initially, to ensure that RGFP did not interfere with retinal expression of miR-1, -133, -142, -96, -182, and -183, the expression levels of these miRs were compared in retinal RNA samples of RGFP+/- and wild type 129 mice (Figure 5.6). Minor variations in expression of the above six miRs were identified in the RGFP mice; miR-133 and -183 expression was reduced by 26.3±15.6% and 13.4±8.9% respectively. However the expression of miR-142 was raised by 48.6±15.6% in RGFP+/- mice compared to wild type 129 mice (Figure 5.6).

5.3.5. Histological analysis and FACS of retinas of RGFP+/- mouse models

Retinas from resulting RGFP+/-Δ307+/- and RGFP+/-R347+/- mice along with RGFP+/- and wild type 129 (controls) mice were analysed by histology and FACS (Fig. 5.7). For histological analysis, sections were taken from two eyes for each animal model analysed (Figure 5.7) and counterstained with DAPI. A strong expression of GFP in the outer segments of photoreceptor cells and the ONL was detected by histology in retinas of mice with RGFP+/- genotypes compared to retinas in wild type 129 mice (Fig. 5.7 A, B, E, F, I, J, M and N). In order to elucidate the rod photoreceptor-specific expression pattern of the above six miRs, RGFP+/-Δ307+/- and RGFP+/-R347+/- mice were generated. Histological analysis of the retinas of mice with the RGFP background, reveal a strong GFP fluorescence in rod photoreceptors (Fig. 5.7 D, H, L and P). FACS analysis was undertaken, and three retinal samples were prepared to represent each animal model, each sample containing the retinal cells

from two retinas. Three retinal obtained from the RGFP+/- , RGFP+/-Δ307+/- and RGFP+/-R347+/- mice were dissociated and the retinal cell preparations were separated by FACS based on the detection of GFP-fluorescent. For each retinal sample analysed by FACS (9 in total), a GFP-positive and GFP-negative sample were obtained, representing rods and non-rods respectively. Similar scatter plots for all four mouse lines were obtained (Fig. 5.7 C, G, K and O).

The GFP-positive cells resulting from FACS of RGFP+/- mice were fixed and placed onto microscope slides. The nuclei were counterstained with DAPI, and rhodopsin, and rod-transducin-alpha expression was examined by immunocytochemisty and fluorescent microscopy (Figure 5.8). Indeed all of the GFP-positive cells co-stained for rod-transducin-alpha (Figure 5.8C) and rhodopsin (Figure 5.8G), demonstrating that the sorted cells were indeed rod photoreceptor cells. DAPI staining was detected in the majority of GFP-positive cells, confirming the presence of nuclei (Figure 5.8D, 5.8H). This successfully verified that the sorted GFP-positive cells were rod photoreceptor cells (Figure 5.8).

5.3.6. qPCR of GFP-positive and GFP-negative cells from RGFP+/- mouse models

MiR expression levels of sorted cell populations from RGFP+/-Δ307+/- and RGFP+/-R347+/- mice were compared to those from wild type RGFP+/- mice by qPCR. A total of three GFP-positive and three GFP-negative samples were obtained for each animal model, and miR expression was detected in these samples by qPCR. qCR was undertaken in triplicate and normalised to the internal controls, snoRNA202 and snoRNA234. The levels of expression of the six analysed miRs, miR-1, -133, -142, -96, -182, and -183, were significantly altered in the GFP-positive and GFP-negative sorted cells, as determined by qPCR (Fig. 5.9).

Expression levels of miR-1, -133 and -142 were vastly increased in rod photoreceptors of RGFP+/-Δ307+/- mice by 1698.4±365.2%, 1406.7±207.1% and 527.9±163.3% respectively, and in RGFP+/-R347+/- mice by 2144.8±369.7%, 2043.9±147.8% and 882.8±283.3% respectively ($p<0.001$; Fig. 5.9A). In non-rod cells, miR-1 and -133 were significantly reduced in expression in RGFP+/-R347+/- mice, by 63.2±17.9% and 73.4±9.2% respectively ($p<0.05$), while no significant alterations

were observed in the RGFP+/-Δ307+/- mice (Fig. 5.9A).

In RGFP+/-R347+/- mice, miR-96, -182, and -183 expression was significantly lower in both rod photoreceptors by up to 38.6±4.0% ($p<0.001$), and non-rod cells by up to 62.6±7.0% ($p<0.001$; Fig. 5.9B). In RGFP+/-Δ307+/- mice, the expression of miR-96 and -183 increased slightly in rod photoreceptors by 17.6±11.2% ($p<0.05$) and 18.9±5.4% ($p<0.01$) respectively, while miR-96 expression decreased by up to 27.8±5.3% in non-rod cells ($p<0.001$; Fig. 5.9B).

MiR expression in rod photoreceptors relative to non-rod cells was compared to gain a greater insight into the alterations in miR expression that were observed (Figure 5.10). MiR expression levels in rod photoreceptors and non-rod cells in wild type RGFP+/- retinas are illustrated in Fig. 5.10A. The expression levels of miR-96, -182 and -183 were approximately 2-fold higher in rod photoreceptors (2.0±0.03-fold, 2.24±0.04-fold and 1.86±0.01-fold respectively; Fig. 5.10A), while conversely the expression of miR-1, -133 and -142 were significantly higher in non-rod cells by up 3.8±1.46-fold, 5.4±1.55-fold, and 33.2±13.3-fold respectively (Fig. 10A).

In contrast to the findings in the RGFP+/- mouse, the miR expression in GFP-positive cells in the RGFP+/-Δ307+/- and RGFP+/-R347+/- retinas were all raised significantly, compared to the non-rod cells. MiR-1, -133 and -142 expression was significantly lower in the non-rod cells of the RGFP+/-Δ307+/- model by 4.56-fold, 19.7-fold, and 3.5-fold respectively (Figure 5.10B), while expression of these miRs in RGFP+/-R347+/- retinas were lower in the non-rod cells by 58.3-fold, 77.0-fold and 12.7-fold respectively (Figure 5.10C). The expression of miR-96, -182 and -183 in rods and non-rods of RGFP+/-Δ307+/- and RGFP+/-R347+/- mouse models, reflects the miR alterations observed in the RGFP+/- mouse and in Figure 5.9. Expression of miR-96, -182, and -183 in non-rod cells remains lower compared to rod photoreceptors in the RGFP+/-Δ307+/- model, by 3.3-fold, 2.8-fold, and 3.1-fold respectively; and in the RGFP+/-R347+/- model, by 3.3-fold, 2.5-fold and 2.2-fold respectively (Figure 5.10).

5.4. Discussion

In order to examine if the altered miR expression profile identified in the R347 RP retina, extended to other mouse models of RP models, miR expression was examined in two rho- and two rds-linked RP mouse lines. These models were mated in order to represent possible genotypes of patients with both dominant (R347+/- and Δ307+/-) and recessive (rho-/- and rds-/-) forms of RP.

Notably a common signature of altered miR expression was revealed in the RP mice analysed, in agreement with the initial results described in Chapter 4 in the R347 retina. Specifically the retinal expression of 6 miRs was examined; miR-1, -133, and -142 expression was increased between 207.0±45.0% to 533.1±22.1%, while miR-96, -182, and -183 expression was reduced between 21.8±5.7% to 50.9±6.1% in the four models analysed. An increased magnitude of retinal up-regulation of miR-1, -133 and -142 was observed in the R347 retina compared to the rho-/- model, while similar levels of expression were observed among the rds-linked models. Comparable magnitudes of miR-96, -182, and -183 expression were observed among all four models, with the rds-/- and R347 models displaying the greatest reduction of miR expression. Other miRs were also examined that did not display a common signature of miR expression, for example miR-21 and -23b expression was similarly increased by 30% and 40% respectively in rds-/- and R347 models, a finding which was not observed in the Δ307 or rho-/- models. Additionally miR-129 expression was exclusively decreased in the rho-/- sample, by 31.4% (Figure 5.5).

The miR expression profiles in the retinas of the mouse models used in this study were examined at one-month, allowing sufficient time for full retinal development, while ensuring a minimal degree of retinal degeneration. The rates of photoreceptor degeneration of each RP model are broadly similar at the time point examined, the ONL thickness decreased by 23-32% in the rho-/-, R347 and rds-/- models, however in contrast only an 8% reduction in ONL was observed in the Δ307 model, with a less severe retinal degeneration (Fig 5.1.G) (McNally et al.). In the rhodopsin knockout mouse (rho-/-), the absence of rhodopsin expression leads to morphological and structural changes of the rod photoreceptors, which fail to form rod outer segments. Apoptosis of rod photoreceptors is continuous until degeneration is

complete at three months and appears to peak at postnatal day 24 (p24) (Humphries et al. 1997; Hobson et al. 2000; Liang et al. 2004). As previously described the rds gene also encodes an important structural protein required in rod outer segment morphogenesis, as the interaction of rds with Rom-1 (rod outer segment membrane protein 1) is involved in membrane fusion and rod outer segment assembly (Farjo and Naash 2006). The role of rds is clearly observed in the naturally occurring null mutant rds-/- and Δ307-rds models. The rds-/- mouse is inefficient at forming rod outer segment structures, and rhodopsin-containing vesicles accumulate at the tip of the cilium in photoreceptor cells (Sanyal et al. 1980; Farjo and Naash 2006). The rds-/- mouse displays a slow rate of retinal degeneration that is not thought to be complete until after one-year (Sanyal et al. 1980), this slow rate of degeneration is accompanied by a reduced ERG response at 6-7 months, which is severely diminished or absent at one year (Reuter and Sanyal 1984). In agreement with previous studies, a slower rate of retinal degeneration was observed in the heterozygous Δ307 RP mouse model, which is representative of a similar mutation observed in patients with adRP (McNally et al. 2002). A one base-pair frameshift mutation at codon 307 in the rds gene, results in a shorter protein product affecting the C-terminus, which leads to a slow progressive form of retinal degeneration. The rod outer segment structure is disrupted in the Δ307-rds mouse, with almost complete loss of the ONL by 10 months (McNally et al. 2002). Indeed animal models of RP, such as those used in this study, are crucial for eye research, to understand the pathways involved in retinal degeneration, and for the identification of novel therapeutic targets (Chader 2002; Fauser et al. 2002).

Due to the nature of the degenerating retina, it is possible that the observed retinal miR signature is partially due to changes in cellular composition of the retina. However in principle these changes should not exceed the percentage of the photoreceptor cell loss observed in the ONL, i.e up to 31.8% (Fig. 5.1. G). Therefore it is unlikely that partial loss of photoreceptors accounts for up to a 533.1% increase of miR-1, -133 and -142 expression in the retina; rather, *bona fide* alterations in miR expression may possibly underlie events of tissue remodelling during neurodegeneration. In contrast to the substantial changes in expression profiles observed for miR-1, -133 and -142, the expression levels of miR-96, -182 and -183 in the retinal analysis decreased by 24.6-50.9%, a value that is similar to the reduction in thickness of the ONL (Fig. 5.1. G).

In order to resolve this ambiguity, Δ307 and R347 RP models were derived on an RGFP background that enabled the separation of rod photoreceptors from the remaining retinal cells, by dissociation and subsequent FACS analysis of the retina. The qPCR analysis of miR expression on FACS purified retinal cells from wild type RGFP+/- retinas, demonstrates that miR-1, -133 and -142 are preferentially expressed in the non-rod cell population by up to 3.8±1.4-fold, 5.4±1.5-fold, and 33.2±13.3-fold respectively (Fig. 10A), a finding that was not previously known. On the other hand, it was established that miR-96, -182 and -183 are expressed at higher levels in rod than in non-rod cells in the wild type retina by approximately 2-fold for all three miRs. This is in agreement with previous studies examining the spatial localisation of these miRs by ISH (Ryan et al. 2006; Karali et al. 2007; Xu et al. 2007). However as miR-96, -182 and -183 exhibit strong labelling in photoreceptor cells, by ISH, a greater magnitude of expression of miR-96, -182, and -183 was expected in the sorted rod-photoreceptor cells compared to the non-rod cells. This can be rationalised, as interneurons are also believed to express these miRs (Xu et al.). Additionally it is possible that photoreceptor segments (which display for example a very high level of miR-182 expression) are lost during trypsin dissociation of the retina (required for FACS analysis), therefore decreasing the detectable pool of these miRs.

Examining miR expression specifically in the rod photoreceptor cells and non-rod cells was central in determining if the expression of the 6 miRs analysed were genuinely altered in retinal cells. Interestingly, the increase detected in retinal expression of miR-1, -133, and -142 (up to 533.1%; Fig. 5.4A) in RP mice can be attributed to an enhanced expression of these miRs (up to 2144.8%) in rod photoreceptors (at least in RGFP+/-Δ307+/- and RGFP+/-R347+/- mice), as expression of these miRs does not increase in non-rod cells (Fig. 5.9A). Notably the discrepancy between the magnitude of miR up-regulation values in the retinal and rod-specific samples, may be explained by the lower basal expression of miR-1, -133 and -142 in rods, and the concomitant decrease in expression of miR-1 and -133 in non-rods in the R347 retinas. Further analysis of RGFP+/-R347+/- mice demonstrates that the decreased retinal expression of miR-96, -182 and -183 (Fig. 5.4B) is due, at least in part, to a *bona fide* decrease in expression of these miRs in rods, as expression of these miRs reduced by up to 38.6±4.0% (Fig. 5.9B). In contrast, the lower retinal expression of these miRs in Δ307 mice cannot be attributed to a reduced expression in rods, as

miR-96 and -183 expression increased slightly in rod photoreceptors by 17.6±11.2% and 18.9±5.4% respectively. The observed differential regulation of miR-96, -182 and -183 in rod photoreceptors of Δ307 and R347 mice may represent different stages of degeneration, as the Δ307 model displays a less severe retinopathy at the time point examined (Fig. 5.1). The expression levels of some of these miRs were reduced in non-rod cells by up to 62.6±7.0% in the RGFP+/-347+/- and 27.8±5.3% in the RGFP+/-Δ307+/- mouse models (Fig. 5.9B). However, as this population of non-rod cells also includes different cell types, our data does not demonstrate conclusively whether these changes are due to genuine alterations in miR expression within these cells or rearrangements of cell composition (Fig. 5.9). By combining the rod-specific expression of RGFP in wild type and RP mice with subsequent FACS of retinal cells, miR expression could be examined in retinal cell subtypes. Notably, a differential expression of miRs in cell populations of the wild type retina was demonstrated, and in particular an altered expression of miRs in rod photoreceptors was observed in both models of RP; both of which are novel findings (Loscher et al. 2008).

In wild type balb/C mice compared to wild type 129 mice, expression levels of miR-96, -182, -183, and miR-1, -133 and -142 were reduced between 18.3% to 70.0% respectively. Slight differences in expression of these miRs were detected in RGFP+/- retinas when compared to wild type 129 retinas, most notably miR-142 expressed was increased by 48.6±15.6% in RGFP+/- mice compared to wild type 129 mice. The significance and role of these findings are not clear. Comparable global miR expression profiles in wild type 129 and c57 mice were described in Chapter 4, and similar differential expressions of miR-142 were observed between wt and RP models, bred on both wt 129 and RGFP+/- backgrounds.

As mentioned previously, the similarities of miR-1-133, and miR-96-182-183 expression is likely due to the clustered nature of these miRs in the genome, however the mechanisms responsible for deregulation of miRs in RP are unknown. It is possible that miR expression is altered post-transcriptionally in disease as demonstrated in tumour samples, in which pri-miR levels correlate to mature miR expression in normal tissue but not in tumour samples (Thomson et al. 2006).

The functions of the discussed six miRs in the retina and other tissues have yet to be fully elucidated. As previously described miR-96, -182 and -183 belong to a sensory

organ-specific cluster, have a high relative expression in the retina (Arora et al. 2007; Xu et al. 2007) and may be involved in circadian rhythm regulation (Xu et al. 2007). The clustered miRs, miR-1 and –133 have potential roles in heart and skeletal muscle (Care et al. 2007), while miR-142 is a 'hematopoietic- specific' miR, primarily expressed in B and T lymphocytes (Chen et al. 2004; Ramkissoon et al. 2006). Therefore miR-142 is implicated in immune response, and raised miR-142 expression were detected lung inflammation (Moschos et al. 2007) (Caspi 2006; Wu et al. 2007).

MiR-1, -133, and -142 are expressed at low levels in the retina relative to other tissues (see Chapter 3), and appear to be preferentially expressed in non-rod cells, however to date the roles of these miRs in the retina are ill-defined. Interestingly miR-96, -182 and -183 expression is similarly downregulated in the hypoxic retina as determined by microarray analysis (Shen et al. 2008), and therefore these miRs may play an important role in the response to low oxygen levels. Similarly, a miR signature of colorectal cancer has been determined, in which the expression of miR-96, -182, -183, and -142 was increased by approximately 300% in colorectal cell lines, and miR-133 expression was decreased by 50%. These miRs are suggested to regulate apoptosis, by mediating oncogenic and tumor suppressor activities (Bandres et al. 2006). The common pattern of miR expression identified in this study, in four mouse models of retinal degeneration, therefore suggests that these miRs may be involved in cellular processes that occur independently of the genetic mutation or disease gene. Such possibilities include a cellular defence mechanism, apoptosis regulation or indeed early phases of retinal remodelling triggered by photoreceptor degeneration. Neural remodelling of the retina coincides with photoreceptor loss, commencing with subtle changes in neuronal structure and followed by a protracted global reorganisation of the remaining neural retina (Jones et al. 2003; Marc et al. 2003).

However in addition to global changes consistently observed in all four mouse models evaluated, some alterations of miR expression were specific to the disease model being analysed, which may reflect variations in the underlying pathogenesis of each disease state. For example, miR-21 and -23b expression was solely increased in the R347 and rds-/- retina, while conversely miR-129 expression was exclusively decreased in the rho-/- model compared to wt control (Fig 5.5). Significantly, miR-21 and -23b expression is induced under hypoxic conditions in the retina (Shen et al. 2008), and also in a number of breast and colon cancer cell lines (Kulshreshtha et al.

2007). In RP, retinal vessel atrophy can result in hypoxia (Penn et al. 2000), inducing the expression of the cytokine erythropoietin (EPO). EPO mediates both neuro-protective and anti-apoptotic effects (Penn et al. 2000; Junk et al. 2002), capable of protecting photoreceptors from light-induced degeneration and acute ischemic insults (Grimm et al. 2002; Junk et al. 2002). It is intriguing to suggest that these miRs may be implicated in this neuro-protective process; however both miR-21 and -23b are only two of a whole host of miRs differentially regulated in the hypoxic retina (Shen et al. 2008). Individually miR-23b is also raised in the signature of cardiac hypertrophy and thought to mediate important roles in proliferation (van Rooij et al. 2006), while miR-21 is consistently up-regulated in cancer, and is suggested to be involved apoptosis and proliferation in neuronal glioblastoma cells (Chan et al. 2005; Papagiannakopoulos et al. 2008)

It is likely that differences in miR expression among RP models reflect processes specific to disease subtypes, whereas common alterations are likely to reflect broader processes. It will be of interest to further examine if these alterations extend to other retinal degenerative models of RP, such as the Pro23His rhodopsin mouse model (P23H; (Olsson et al. 1992) and the naturally occurring Retinal Degeneration 1 RP mouse model (rd1; (Pittler and Baehr 1991), both of which display rapid rates of retinal degeneration.

5.5. Conclusion

Notably a common retinal signature of altered miR expression in the retinas of two rho- and two rds-linked RP models was revealed in this study (Loscher et al.). Of note this common signature was observed independent of the causative genes or the dominant or recessive mode of action. Significantly the retinal signature of miR expression in RP was also reflected in the rod-specific miR expression profile, confirming the genuine nature of these cellular miR alterations. Likewise, other neurodegenerative disorders may exhibit similar miR profiles largely independent of their genetic origins. Identification of valid retinal mRNA targets and corresponding cellular pathways, would greatly assist in elucidating the role played by the above six

miRs in healthy and diseased retinas. An initial entry into this area of research forms part of the work described in Chapter 7 of this PhD thesis.

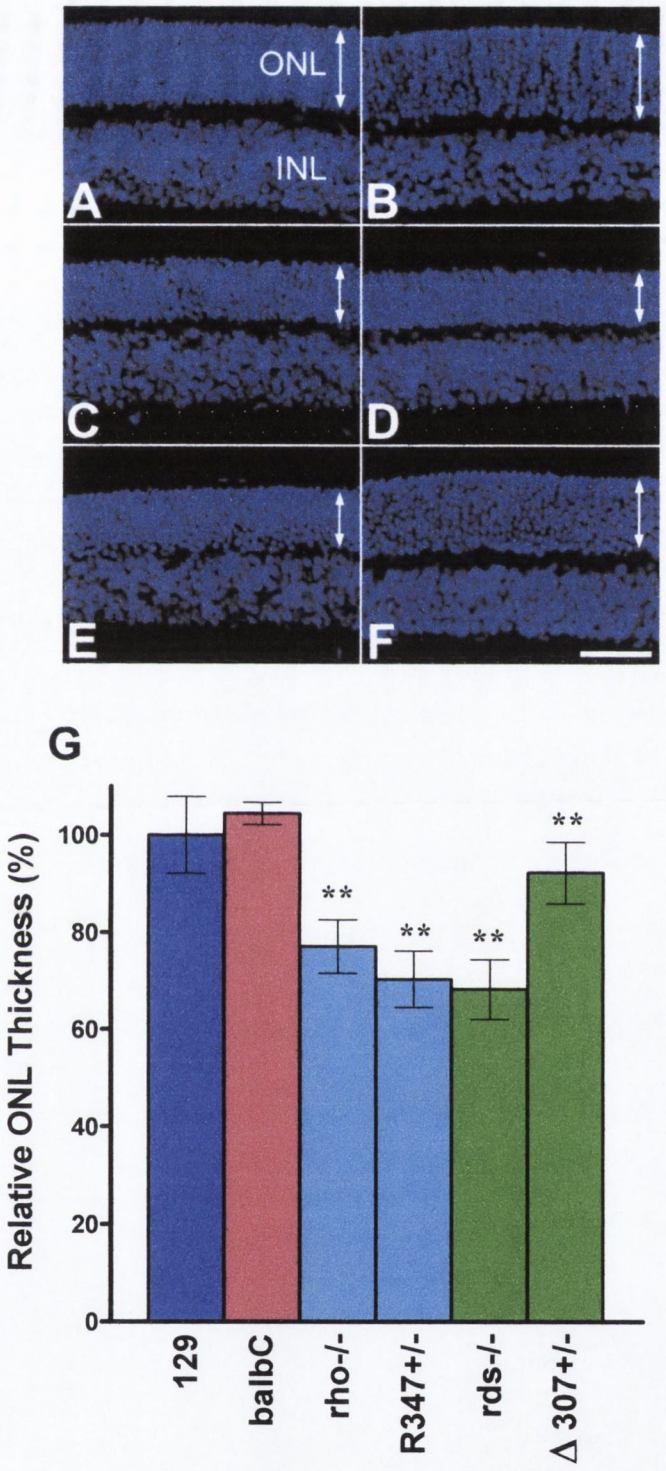

Figure 5.1: Comparative histology of retinas from rho- and rds-linked RP mouse models: Representative microscopic images illustrate retinas of **(A)** 129, **(B)** balbC, **(C)** rho-/-, **(D)** R347+/-, **(E)** rds-/- and **(F)** Δ307+/- mice. Outer nuclear layer (ONL) thickness was measured in microscopic images and corresponding average values plotted **(G).** Arrows indicate the thickness of the ONLs. INL: inner nuclear layer; scale bar represents 25 μm; **: p<0.01Error bars indicate S.E.M.

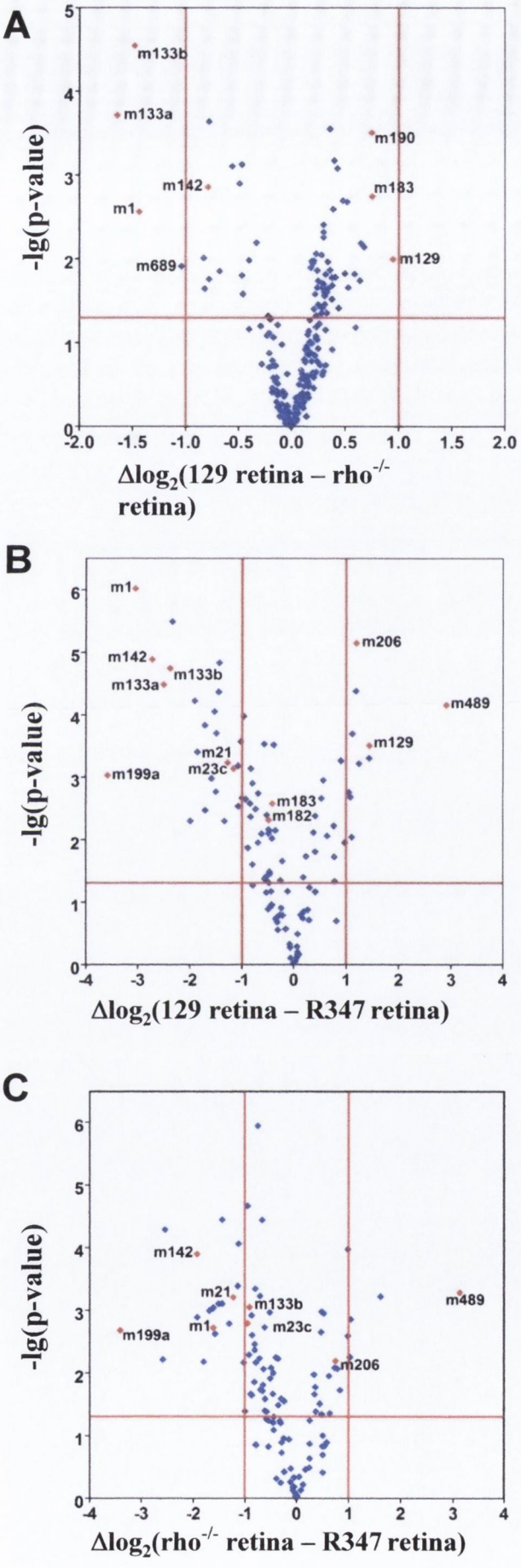

Figure 5.2: Volcano plots of miR expression in Rho-/-, R347 and wild-type retinas. Plots represent comparative miR expression profiles of **(A)** 129 versus rho-/- retinas, **(B)** 129 versus R347 (mutant pro347ser *RHO* transgene) retinas, and **(C)** rho-/- versus R347 retinas using Exiqon miR microarrays. X-axis indicate difference of expression level on a $\log_2$ scale, while Y-axis represents corresponding *p-values* (Student's *t-test*) on a negative log scale. A $-\log_{10}$ *p-value* of 1.30 (highlighted by the red horizontal line) corresponds to a *p-value* of 0.05 on a geometric scale, and therefore points above this line represent statistically significance variations of miR expression. The vertical red line was chosen arbitrarily, and represents differences in expression between samples of ±1 on a $\log_2$scale. Therefore the more lateral points, represent a greater magnitude of miR expression between the two groups analysed, and positive and negative values signify the group with higher or lower expression.

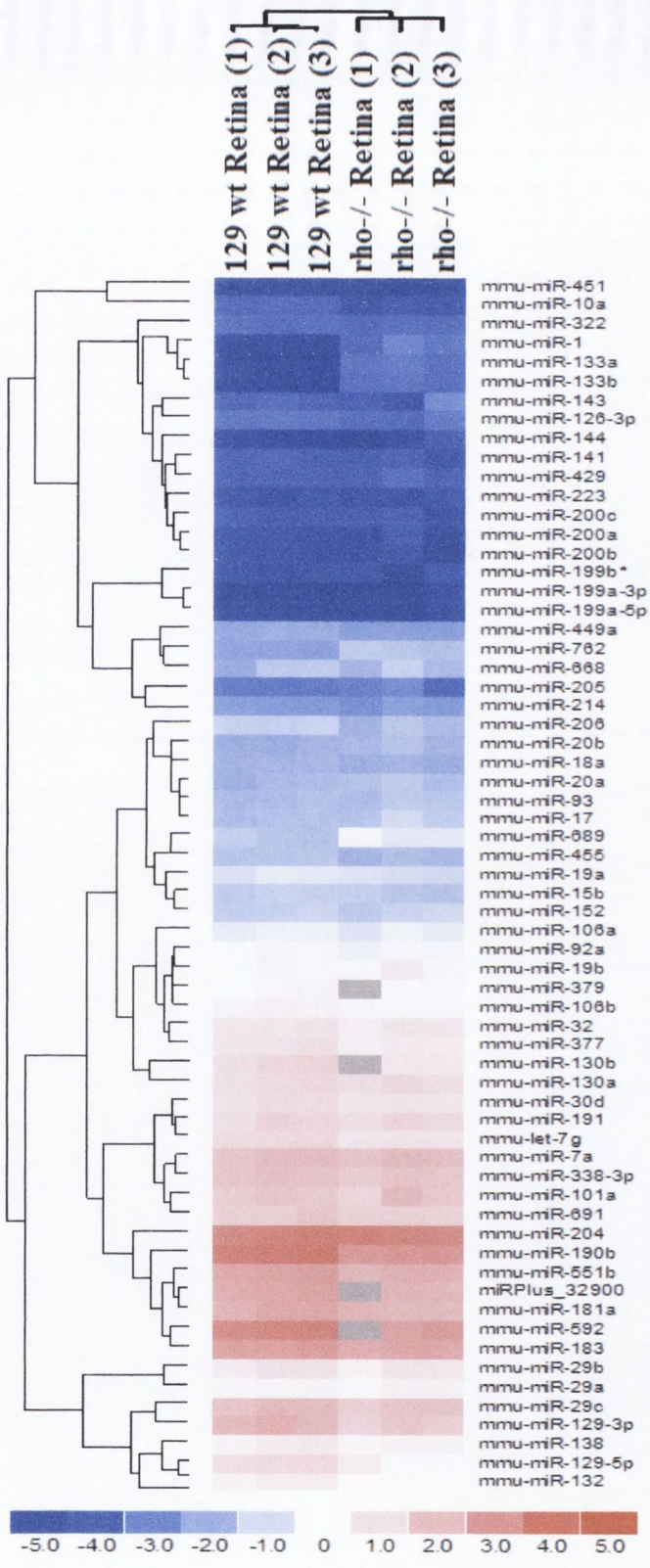

Figure 5.3: Heat Map and Hierarchical clustering of miRs in 129 wild type and Rho-/- retina: The heat map diagram shows the result of the two-way unsupervised hierarchical clustering of miRs and the experimental groups; 129 retina and rho-/- retinas at 1 month, using Exiqon v9.2 microarrays. Each row represents a miR and with clusters indicated on the left, while each column represents a sample with clusters appearing at the top. The clustering was performed on a filtered set of $\log_2$(Cy3/Cy5) ratios, which displayed a high variability across samples (standard deviation >0.5). Clusters were generated using the average linkage method, a method which calculates the distance between clusters. The Cy5 labelled reference was used in each array, and provides a constant baseline to compare samples to. The color scale shown at the bottom illustrates the relative expression level of each miR across all samples ($\log_2$Cy3/Cy5). The red color represents a relative miR expression level greater than the mean, blue color represents a relative expression level lower than the mean. Log_2(Cy3/Cy5) ratios $\pm$ 1 correspond to a more than 2 fold up or down regulation, relative to the miR reference (Cy5).

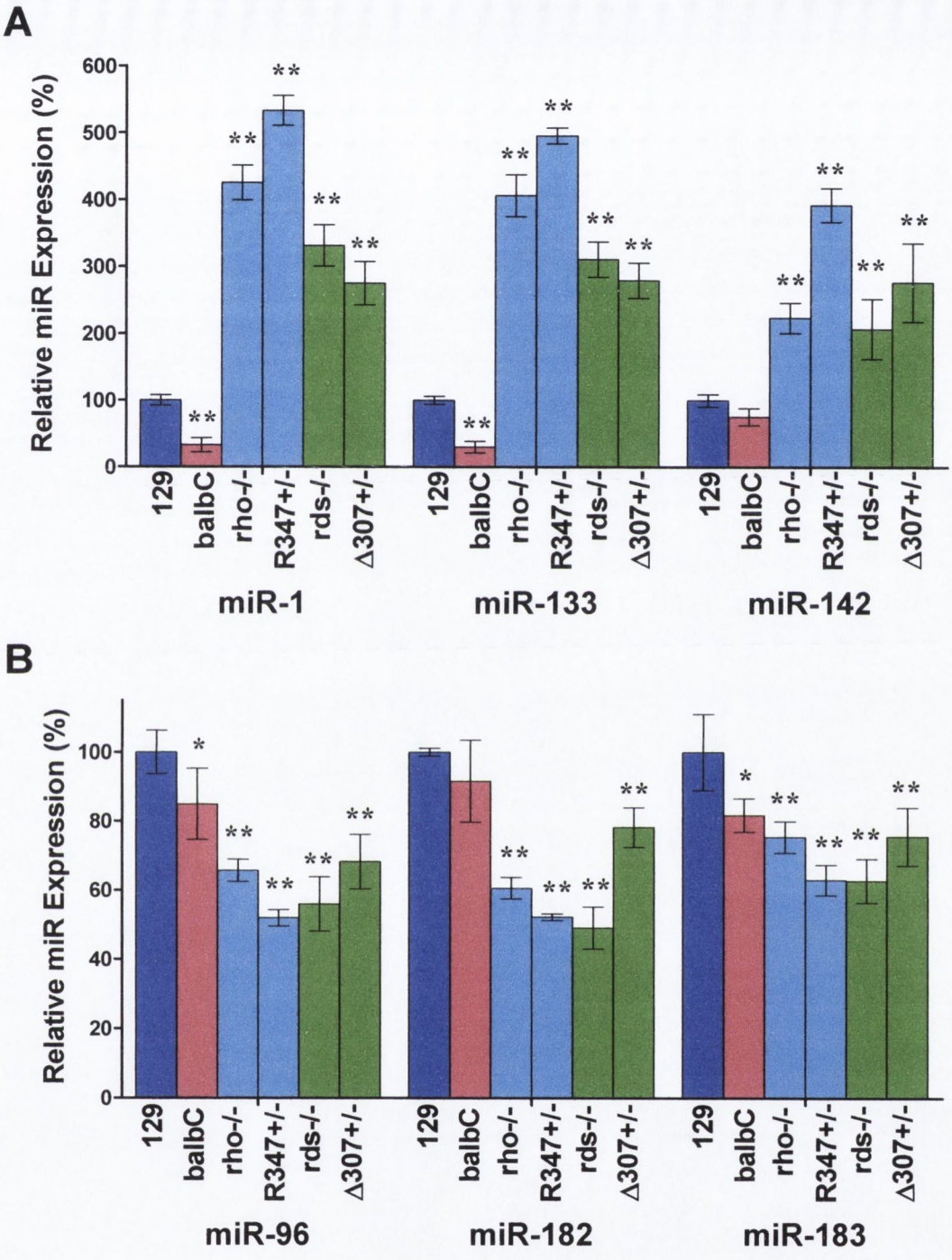

Figure 5.4: Retinal miR expression signature in rho- and rds-linked RP mouse models: Expression levels of miR-1, -133, -142 -96, -182, and -183 were analyzed by qPCR. Note, that as rds-/- mice are on a balb/C background, for *p-value* calculations data from rds-/- mice were compared to those from wild type balbC mice. *: $p<0.05$; **: $p<0.01$; ***: $p<0.001$ using ANOVA (Tukey's Multiple Comparison). Error bars indicate S.E.M.

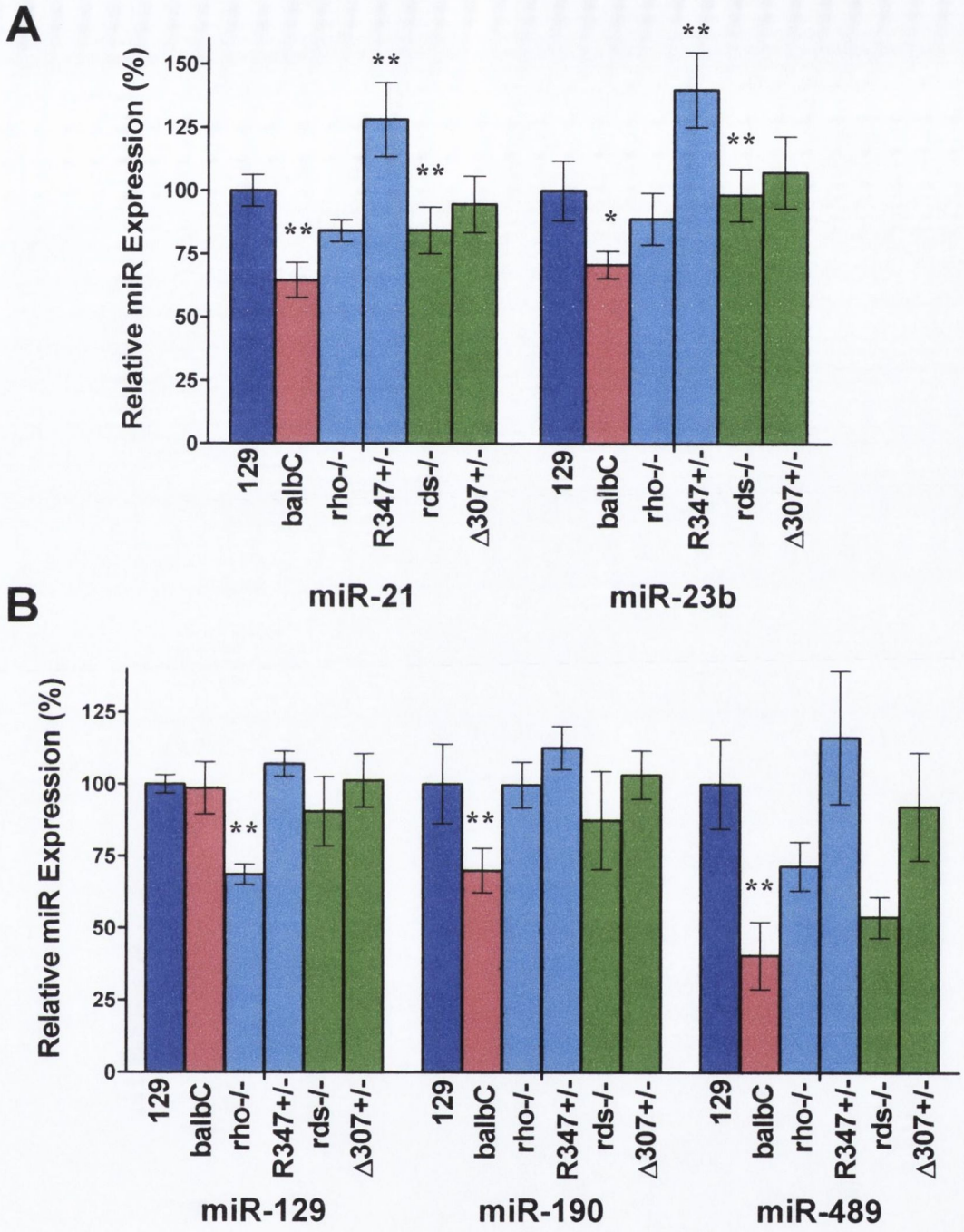

Figure 5.5: Retinal miR expression signature in rho- and rds-linked RP mouse models: Expression levels of miR-21, -23b, -129 -190, and -489 were analyzed by qPCR. Note, that as rds-/- mice are on a balb/C background, for *p-value* calculations data from rds-/- mice were compared to those from wild type balb/C mice. *: $p<0.05$; **: $p<0.01$; using ANOVA (Tukey's Multiple Comparison). Error bars indicate S.E.M.

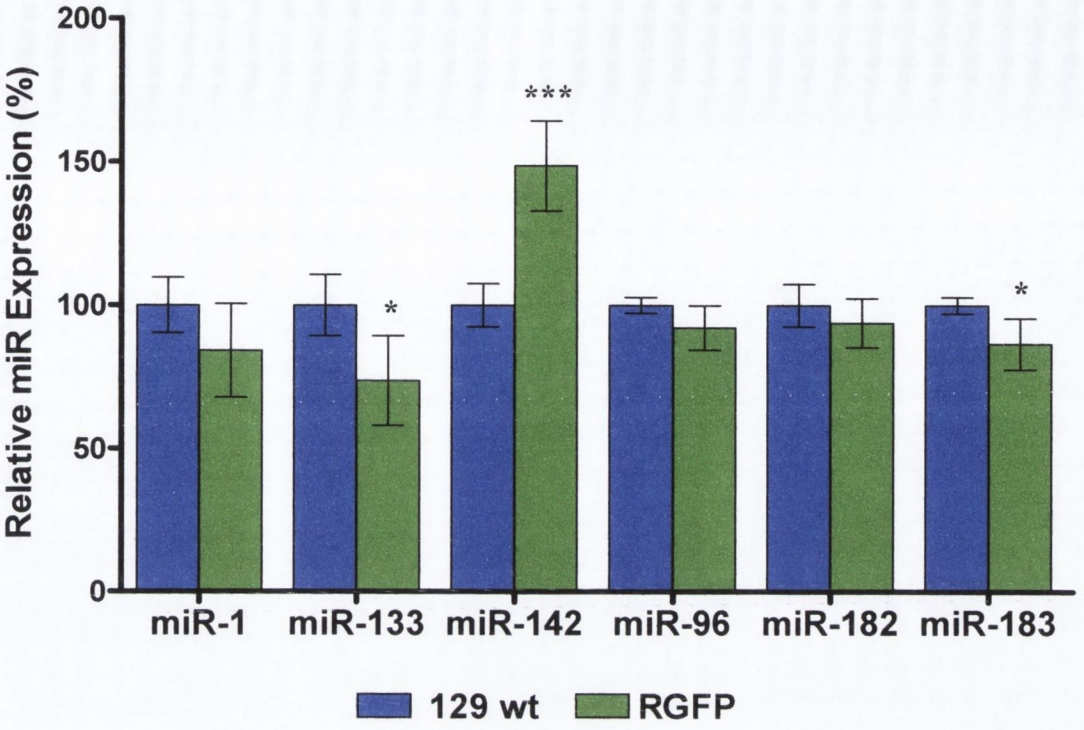

Figure 5.6: MiR expression in the RGFP+/- Retina: Retinal expression levels of miR-1, -133, -142, -96, -182, and -183, were compared using qPCR in wild type 129 mice (blue columns) and RGFP+/- (green columns). Expression levels were normalized to wild type 129 mice. *: $p<0.05$; ***: $p<0.001$ obtained by Student's *t-test*. Error bars indicate S.E.M.

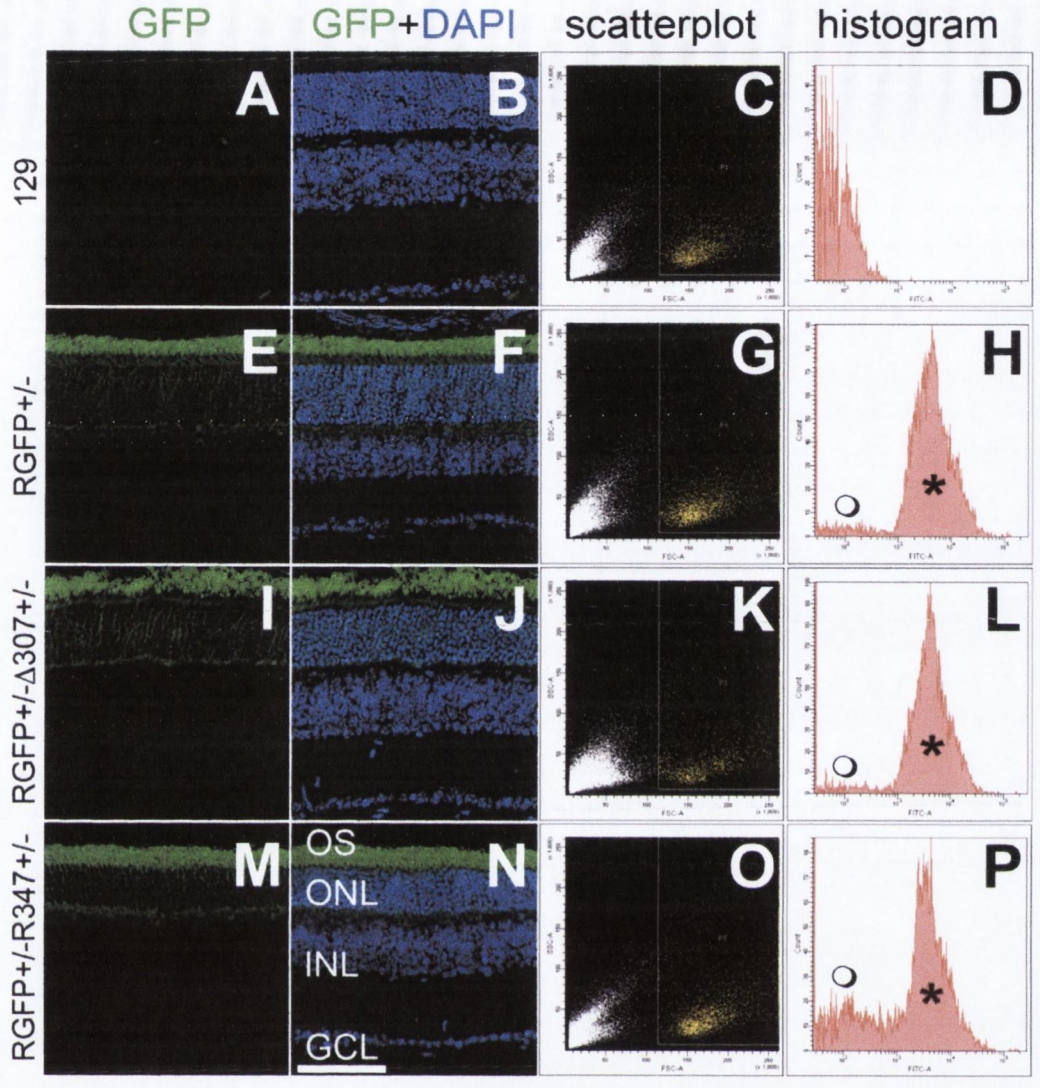

Figure 5.7: Histological and FACS analysis of RGFP-Δ307 and -R347 retinas: Δ307 and R347 mice were crossed onto RGFP background. One month-old wild type 129 (**A** and **B**), RGFP+/- (**E and F**), RGFP+/-Δ307+/- (**I and J**) and RGFP+/-R347+/- (**M and N**) retinas were analyzed for GFP fluorescence; cell nuclei were counterstained with DAPI. Retinas from the above mice were dissociated with trypsin and analyzed by FACS. Forward- versus side-scatter plots of retinal cells are depicted on **C, G, K** and **O**; yellow dots represent the gated populations. GFP fluorescence histograms of the gated populations are given in **D, H, L** and **P;** GFP-positive peak is marked by * in samples from mice on the RGFP background (G, K and O). Also note the GFP-negative populations (❍), which correspond to non-rod cells in the dissociated retinas on the RGFP background (**G**, **K** and **O**). OS: outer segments, ONL: outer nuclear layer: INL: inner nuclear layer; GCL: ganglion cell layer. Scale bar represents 25 μm.

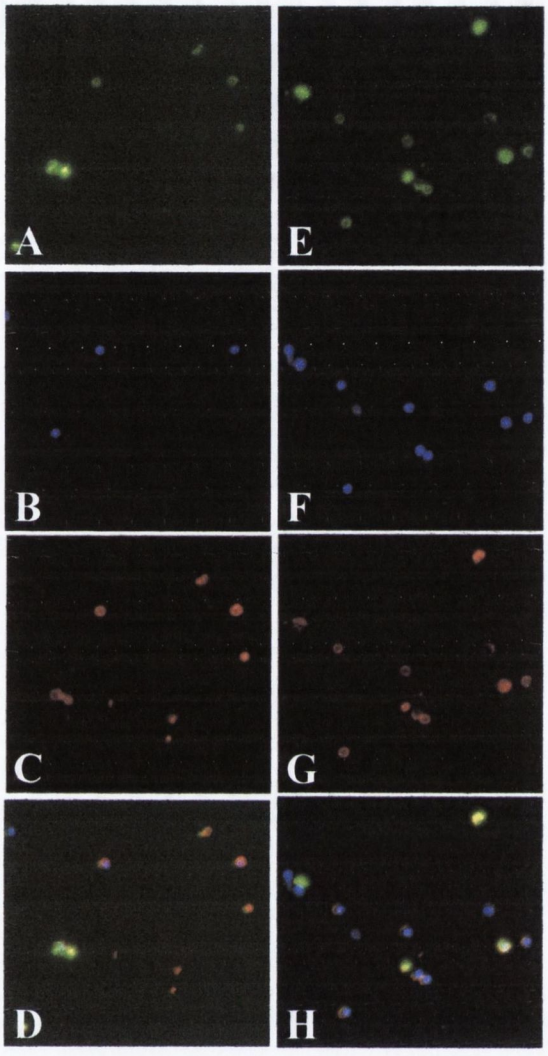

Figure 5.8: Histological analysis of GFP-positive cells from RGFP retina: GFP-positive cells from RGFP+/- mouse retinas were sorted by FACS, fixed in 4% parafomaldehyde and mounted onto glass slides. The expression of the rho-GFP fusion protein is clearly visible (**A**,**E**). The nuclei were stained with 4',6-diamidine-2-phenylindole-dihydrochloride (DAPI) (**B**,**F**) and immunocytochemistry was used to detect rod-transducin-alpha (C) and rhodopsin (G) expression using Cy3-conjugted secondary antibody. Composite images (**D**, **H**) were constructed using the software Adobe Photoshop (Adobe Systems Europe Ltd., Glasgow, UK).

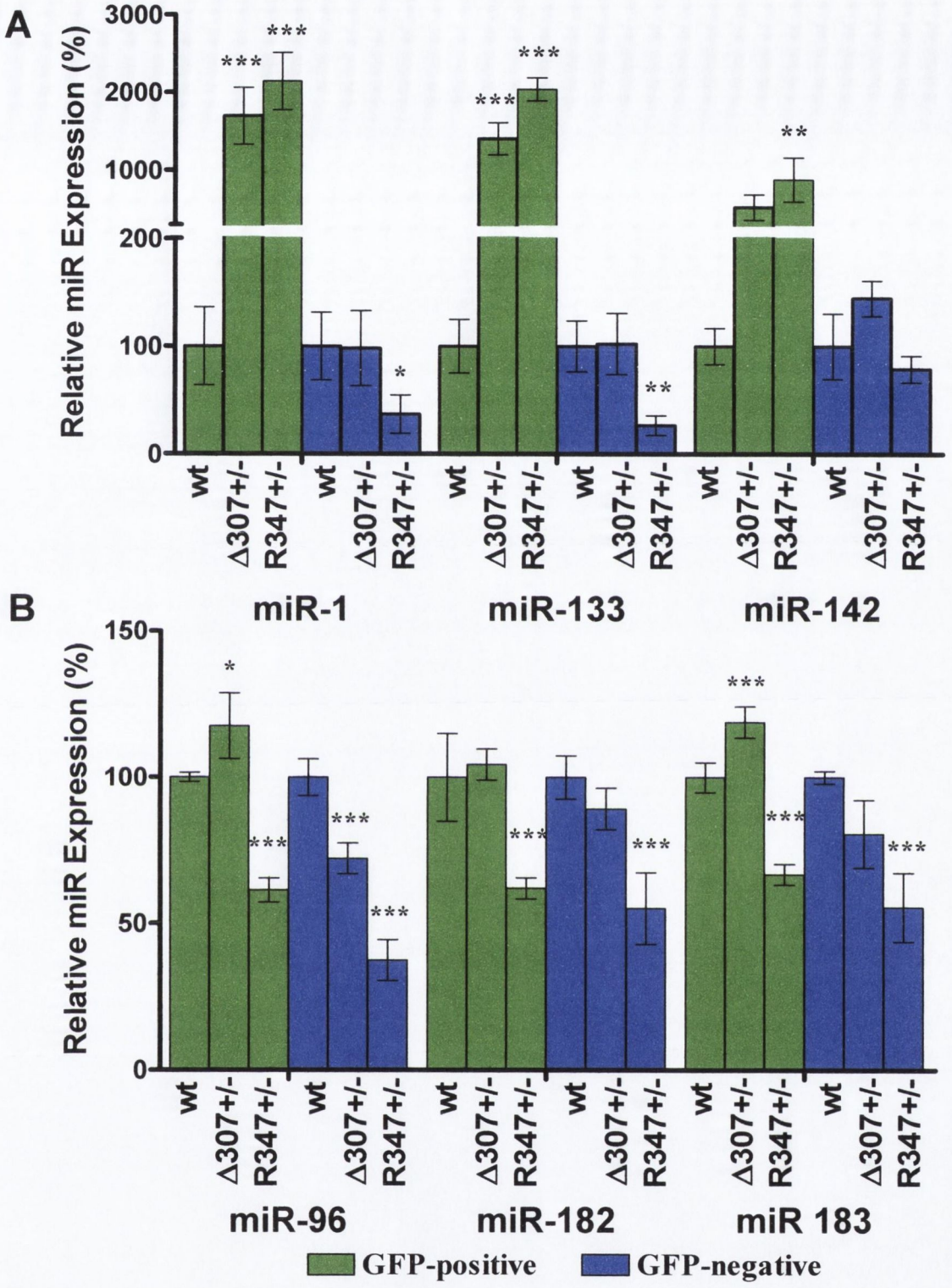

Figure 5.9: MiR expression signature in rod and non-rod cells in Δ307 and R347 retinas: GFP-positive (rods) and GFP-negative (non-rod) cells from RGFP+/- (wild type control), RGFP+/-Δ307+/- and RGFP+/-R347+/- mice were separated by FACS. Expression levels of miR-1, -133 and -142 (**A**) and miR-96, -182, -183 (**B**) in the GFP-positive (green columns) and GFP-negative (blue columns) were analyzed by qPCR. Expression levels were normalized to the wt RGFP+/-. Note, that Y axes are to different scale on **A** and **B** and Y axis is discontinuous on **A**. wt: RGFP+/-; Δ307+/-: RGFP+/-Δ307+/-; R347+/-: RGFP+/- R347+/-; *: $p<0.05$; **: $p<0.01$; ***: $p<0.001$ obtained by ANOVA. Error bars indicate S.E.M.

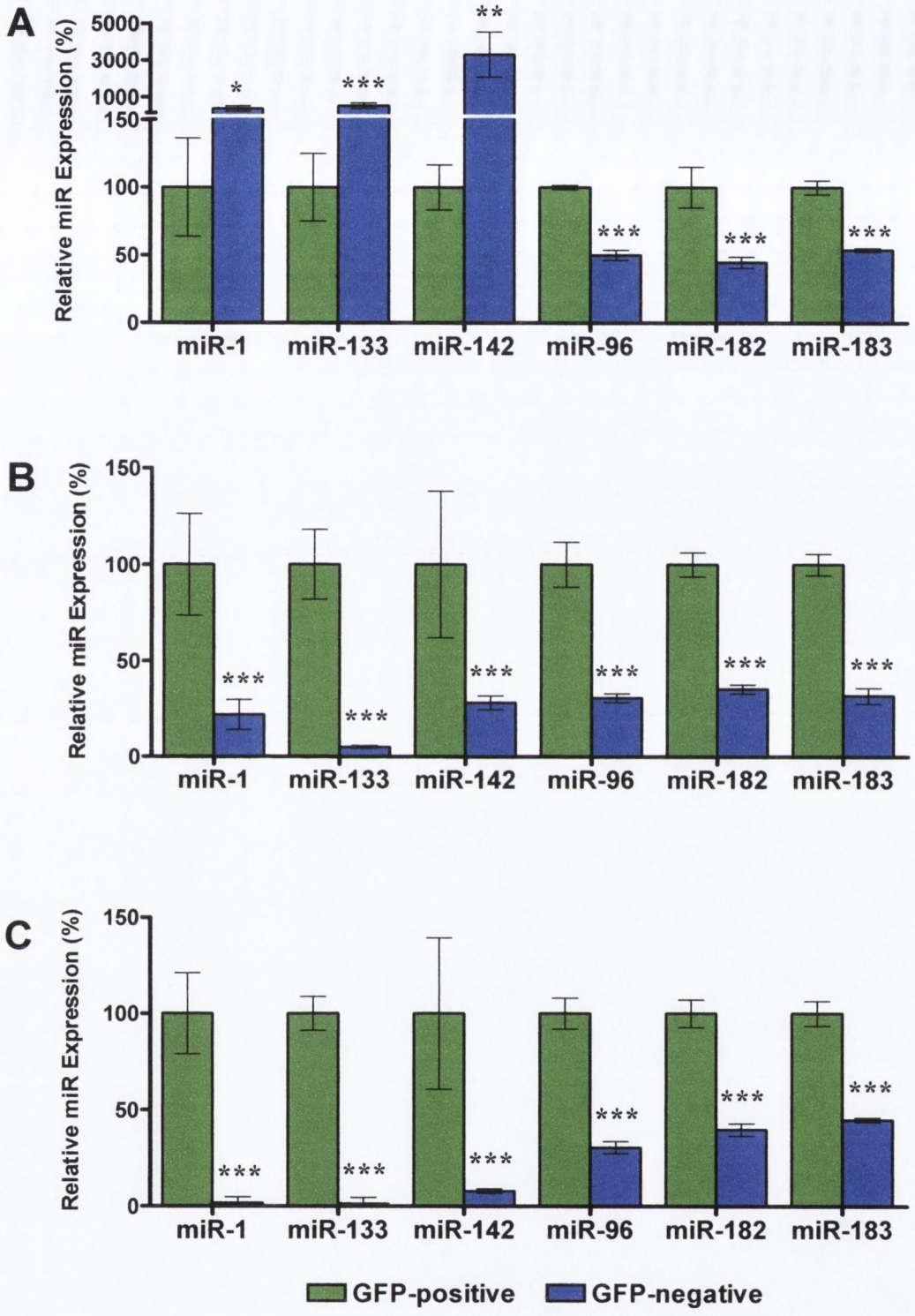

Figure 5.10: Comparative miR expression in rod versus non-rod cells in RGFP retinas: GFP-positive (rod cells) and GFP-negative (non-rod cells) from (**A**) RGFP+/-, (**B**) RGFP+/- Δ307+/-, (**C**) RGFP+/- R347+/-. mice were separated by FACS. Expression levels of miR-1, -133 -142 -96, -182, and -183, in the GFP-positive (green columns) and GFP-negative (blue columns) cells were analyzed by qPCR in (**A**) RGFP+/- (wild type control), (**B**) RGFP+/- Δ307+/- and (**C**) RGFP+/- R347+/-. Expression levels were normalized to that of rods. Note, that Y axis is discontinuous; *: $p<0.05$; **: $p<0.01$; ***: $p<0.001$ obtained by Students t-test analysis. Error bars indicate S.E.M.

Chapter 6

Examination of Retinal miR expression in P23H and *Rd1* mouse models of RP

6.1. Introduction

A common miR expression signature was identified in Chapter 5 in the degenerating retina of two rho-linked and two rds-linked RP mouse models, a finding that was reflected in photoreceptor cells. These results clearly demonstrated that the retinal miR signature identified in RP retinas, represents genuine alterations in cellular miR expression independent of alterations in retinal cell composition.

The regulatory mechanisms and tissue specific factors that are responsible for the altered expression of miR-96, -182, -183 and -1, -133, -142 in RP are ill-defined. Dysregulation of some of these miRs are altered in hypoxic conditions (Kulshreshtha et al. 2007), and are implicated in proliferative and apoptotic processes (Bandres et al. 2006). However the roles played by these miRs in the retina are unknown. In the previous study miR expression was examined in RP models with relatively slow retinal degeneration. However it is of interest to examine if similar alterations of miR expression are also evident in fast degenerating models of RP; in particular, the pro23his (P23H) rhodopsin mutant model (Olsson et al. 1992) and the retinal degeneration 1 (*rd1*) PDE6β null mutant model (Pittler and Baehr 1991).

Analysis of the rho-linked P23H mouse model is significant, as this rhodopsin mutation is the most common form of adRP (autosomal dominant RP) in North America, causative in approximately 12% of human adRP cases (Dryja et al. 1990; Machida et al. 2000), This mouse model undergoes progressive rod degeneration similar to that observed in humans, although displaying a more rapid time course of degeneration (Streichert et al. 1999). As described in Chapter 1, this mutation exists in the N-terminal of the rhodopsin gene, and it is thought that apoptotic photoreceptor death results due to the misfolding and aggregation of the mutant rhodopsin protein in the ER (Roof et al. 1994). Additionally human hereditary mutations in the β subunit of the rod cGMP phosophdiesterase (PDE6β) cause photoreceptor degeneration, accounting for 4% of arRP cases (autosomal recessive RP) (McLaughlin et al. 1995). These mutations are modelled in the naturally occurring null PDE6β mutant originally identified by Keeler as "rodless" in 1924 (Pittler and Baehr 1991; McLaughlin et al. 1995). PDE6β is a rod-specific enzyme, critical in the phototransduction cascade, and in its absence cytoplasmic levels of cGMP are persistently raised resulting in cell

death, due to altered calcium regulation (Fox et al. 1999; Hauck et al. 2006; Sanges et al. 2006). As PDE6β is rod-specific, rods undergo apoptosis initially followed by cones, which do not express PDE6β (Sanges et al. 2006). In both of these mouse RP models, the onset of retinal degeneration is extremely early and degeneration of photoreceptor cell is complete prior to adulthood; by approximately p14 in the P23H model (unpublished data) and p20 in the *rd1* model (Olsson et al. 1992; Takahashi et al. 1999).

In light of the findings presented in Chapter 5, it was of interest to examine whether the characteristic alterations of miR expression observed in the slow degenerative models of RP analysed, were also evident in the retina of the two fast degenerative models, P23H and *rd1*. Indeed due to the fast rate of retinal degeneration in these models a small window of time exists to examine miR expression, preceding alterations of cellular composition due to extensive photoreceptor loss. Specifically, the miR expression profile of the P23H model was obtained by microarray analyses and in addition the expression levels of miR-1, -133, -142, -96, -182, -183 were examined in the P23H and *rd1* mouse models by qPCR. Notably the miR expression signature identified in Chapter 5 does not appear to extend to the P23H and *rd1* mouse models.

6.2. Materials and Methods

6.2.1. Experimental Animals

The following models of retinal degeneration were used in this experiment; P23H (P23H ;(Olsson et al. 1992)), rho knockout ($rho^{-/-}$;(Humphries et al. 1997)), and retinal degeneration 1 (*rd1*: (Pittler and Baehr 1991; Hauck et al. 2006)). The wild type mice, wt 129 and CH3 animals were used as controls as the P23H and rho-/- mice are on a wt 129 backgrounds, while the *rd1* mouse is on a C3H background and contains two mutant *rd1* alleles (Hauck et al. 2006). The P23H mouse is bred on the rho-/- background, therefore only possessing one rhodopsin allele, expressing the P23H mutated rhodopsin transgene (Olsson et al. 1992; Frederick et al. 2001). Animals were bred under specific pathogen free (SPF) housing conditions (see section 2.1.4) and mice at post-natal day 5 (P5) and 11 (P11) were sacrificed by CO_2 asphyxiation.

6.2.2. RNA Extraction

Total RNA from P5 and P11 animals was extracted using the Qiagen miRNeasy Mini Kit as outlined in section 2.3.2.2. Three retinal samples per mouse line were prepared by pooling six retinas per sample.

6.2.3. Micorarray Experiment

Retinal RNA samples from wt 129 retina, rho-/- and P23H at P5 were outsourced to Exiqon for miR profiling. The miRCURY LNA microRNA Array v.9.2 (see section 2.3.5.2) was used in this experiment, which probed for miRs annotated in miRBase v.9.2 (release date May 2007). This array probed specifically for 494 miRs (420 mouse and 74 Exiqon miRs), 74% (431 of 579) of which are annotated in miRBase v.10.0. The total RNA was labelled with the fluor Cy3 while the reference RNA sample was labelled with Cy5. All samples and biological replicates were analysed on separate miR microarrays as outlined in section 2.3.5.4.

6.2.4. Micorarray Data Analysis

Data was pre-processed and normalized using the global Lowess (LOcally WEighted Scatterplot Smoothing) regression algorithm (section 2.3.5.5) by the miR profiling company, Exiqon. Normalised log_2-transformed Cy3/Cy5 ratios were used for further analysis.

6.2.5. Quantitative Real-Time RT-PCR (qPCR)

Two-step qPCR was performed using ABI's TaqMan miR Assay (Applied Biosystems, Foster City, CA, USA) according to manufacturer's instructions (see section 2.3.3.1). The TaqMan miR Assays for the following miRs were used: miR-1, -133, -142, -183, -96, and -182. Equal amounts of RNA (10 ng/reaction) were used in each RT reaction. SnoRNA-202 and -234, with strong correlation in their expressions across all samples (r^2=0.8958 and $p<0.0001$), were used as internal controls.

Expression was examined using primers designed against the human rhodospin mRNA transcript (accession number NM_000539.3; (Genebank)) and diluted in nuclease-free water (250 pmol). The real-time RT-PCR reaction was set up (see section 2.3.3.3.) using the Quantitech Sybr Green RT-PCR Kit, and incubated on the 7300 Real Time PCR System (ABI). 18S rRNA and beta-actin were used as internal controls and a retinal RNA sample from an NHR+/-rho-/- mouse was used as a positive control. This mouse expresses human rhodopsin (RHO), due to the presence of a single wt human rhodopsin allele and does not express mouse rhodopsin.

Cycle Threshold (C_T) data was used for to analyse the RT-PCR data (see section 2.3.3.4) and the log_2-transformed miR/control expression ratios were used for further analysis.

6.2.6. Statistical Analysis

Analysis of statistical significance was performed using ANOVA, Student's t-test and Pearson's correlation by means of the statistical software GraphPad Prism. Differences with $p<0.05$ were considered statistically significant.

6.3. Results

6.3.1. Pro23His and *rd1* RP animal models

It was of interest to examine the miR expression profile in fast degenerative animal models of RP such as the adRP models P23H (Pro23His RHO mutant) and the arRP model *rd1* (homozygous null mutant PDE6β). In order to account for the rapid photoreceptor degeneration observed in these models, an earlier time point of postnatal day 5 (P5) and postnatal day 11 (P11) was chosen for the P23H and *rd1* models respectively (Pittler and Baehr 1991; Olsson et al. 1992). Wild type 129, and CH3 mice were used in this study as controls for the P23H and *rd1* mouse RP model respectively, corresponding to the backgrounds of these mice. Due to the physical limitations in dissecting reliable retinal tissue samples from mouse eyes at P5, the whole-eye was dissected from the P23H and wt 129 samples. In addition miR expression was examined at P5 for the slower degenerative mouse model of RP, rho-/-, and whole-eye samples of this model were also obtained at P5. This contrasts with the examination of miR expression at the later time point of one-month, as presented in Chapter 5, however, the examination of this model at P5 is valuable, providing an additional control for the analysis of miR expression in the P23H+/-rho-/- model. The retinas were dissected from the *rd1* model and corresponding control mouse C3H. Total RNA was extracted from the whole-eye and retina samples using the miRNeasy RNA isolation kit (see section 2.3.2.2). Three biological replicates of total RNA were prepared for each animal model analysed, each sample containing RNA from four retinas/whole-eyes.

6.3.2. Genotyping P23H animals

As the P23H+/-rho-/- model is generated by crossing the P23H+/-rho-/- model with the rho-/- mouse, there is a 50% chance that the resulting offspring will be heterozygous for the mutant P23H RHO allele. Therefore the genotype of these animals was required. Genotyping can be performed using DNA extracted from the tails snips of these mice, however, as retinal RNA samples had already been taken for miR analysis, instead genotyping was performed on these RNA samples by analysing RHO expression by qPCR. QPCR analysis of RHO was performed on the total RNA

samples obtained from the eyes of individual animals. A retinal sample from a previously genotyped NHR+/-rho-/- animal acted as a positive control which expresses the wild type RHO allele (NHR; normal human rhodopsin). Seven of the twelve RNA samples obtained from the putative P5 P23H mouse eyes, were found to be positive for the P23H-RHO transgene. P23H-RHO mRNA was expressed in these RNA samples by an average of 62.8% relative to the NHR control sample (Figure 6.1). In comparison, P23H-RHO expression was undetectable in the remaining five RNA samples, and these samples were eliminated from further analysis (Figure 6.1). As the NHR+/-rho-/- and P23H+/-rho-/- are different transgenic models, the expression level of RHO in these samples cannot be compared directly. The RNA samples from the 7 (P23H+/-rho-/-) animals were pooled to create three independent total RNA samples that were used for all further microarray and qPCR analyses.

6.3.3. Microarray analysis of miR expression in P5 P23H and rho-/- mutant models

Microarray analysis of miR expression was carried out on the P23H, rho-/- and 129 whole-eye P5 RNA samples by the miR profiling company Exiqon, using Exiqon miRCURY LNA microarrays v9.2. These arrays probe for a total of 494 miRs (420 mouse and 74 Exiqon miRs) coverage of the probe set used in this array is 74% (431 of 579) of the miRs annotated in miRBase v10.0. As three whole-eye RNA samples were prepared for each animal model (P23H, rho-/- and wt 129), a total of nine miR arrays were used to analyse miR expression in these RNA samples (labelled with Cy3). In addition a reference RNA sample was provided and labelled with Cy5 (see section 2.3.5.1), thereby permitting the comparison of miR expression profiles between arrays using the Cy3/Cy5 ratio.

Volcano plots were used to display the comparison of miR expression data between animal models (Figure 6.2). These volcano plots were constructed by plotting the $\log_2$ variation of miR expression between two groups on the X-axis (Cy3/Cy5 ratios), and the corresponding statistical significance of these differences on the Y-axis (expressed as the negative $\log_{10}$ of generated p-values). The red vertical line represents a magnitude of variation of miR expression between both groups greater than 1.4-fold (i.e. ± 0.5 on a $\log_2$ scale), while the red horizontal line corresponds to a p-value less

than 0.05 (i.e. 1.3 on a $\log_{10}$ scale). As such, points plotted higher and more lateral than these red lines, indicate miRs which are significantly altered between models by a magnitude greater than 1.4-fold (i.e. a 30-40% increase or decrease) and $p<0.05$ (Figure 6.2). Of the 494 miR probes, data points for 288 and 290 miR probes are plotted representing variations between miR expression in 129 vs. rho-/- whole-eye samples (Figure 6.2A), and of 129 vs. P23H whole-eye (Figure 6.2B),respectively. In the 129 versus rho-/- plot the expression of 10 miRs were significantly altered, however, the magnitudes of these alterations were less than 1.4-fold (±0.5-fold change on a $\log_2$ scale) (Figure 6.2A). In contrast, at a later time point of one-month, the expression levels of 70 miRs were statistically altered between rho-/- and wt 129 models as presented in Chapter 5 (Figure 5.2A), however, of these miRs only the expression of miR-132 was altered in both of these analyses, at one-month and P5. Note however that whole-eye and retinal tissue were used to prepare the RNA samples examined at P5 and one-month respectively in the rho-/- and wt 129 model, and therefore the results from these miR array analyses cannot be directly compared. In addition the miR expression profile in the 129 versus P23H whole-eye samples were also very similar; 25 miRs were significantly altered between these two models, two of which displayed a greater than 1.4-fold alteration in miR expression (Figure 6.2B). Comparison of miR expression in rho-/- versus P23H samples revealed 86 miRs that were differentially expressed between both samples (Figure 6.2C). The expression of miR-1, -133, -206, -183 and -196 appear to be altered between the P23H and rho-/- models at P5 (Figure 6.2C).

Figure 6.4 illustrates the significant alterations of miR expression at P5, between 129 vs. rho-/- (Figure 6.4A) and 129 vs. P23H (Figure 6.4B, 6.4C), determined by microarray analysis (Figure 6.4). In rho-/- eye samples, the expression of miR-465a and -132 was increased by 17.5±4.2% and 6.4±0.7% respectively, while miR-335, -532, -542, -134, -382, -369, and -652 was decreased by an average of 13.4 ± 1.9% ($p<0.05$; Figure 6.2A). In the P23H model the expression of miR-468 was increased by 68±6.4%, while an average increase of expression of 17.7 ±3.5 % was observed for miR-30a, -29c, -183, --184, -289, and -21 (Figure 6.4B, 6.4C). Lower levels of miR-192, -145*, -690, and -326 expression were observed in the P23H whole-eyes by an average of 13.1 ± 1.7 % ($p<0.05$; Figure 6.4C).

Notably, of the altered miRs detected in both the 129 vs. rho-/- and 129 vs. P23H models, no overlapping alterations of miR expression were detected, suggesting that no common alterations of miR expression occurs in both the rho-/- and P23H samples at P5. This is clearly illustrated by the heat map resulting from the unsupervised hierarchal clustering of miRs and whole-eye samples (Figure 6.3), as the nine RNA samples (three biological replicate samples representing each animal model) were not clustered into their representative groups based on their miR expression profiles (Figure 6.3).

6.3.4. qPCR analysis of miR signature in P23H and rho-/- whole-eyes at P5

The expression of miR-1, -133, -142, -96, -182 and -183 was analysed by qPCR in the P23H and rho-/- models of RP at P5 (Figure 6.5), and this analysis also served to validate the microarray data. It was of interest to determine if the altered miR expression profile observed in the one-month study of rho- and rds-linked RP models, extended to the faster degenerative RP models, P23H and rho-/-, at P5. No significant alteration of miR-1, -133 and -142 expression was observed in the P23H and rho-/- models. An increase in miR-182 and -183 expression was observed in the rho-/- model of 23.5±7.9% and 84.5±30.5% respectively, however no variations were observed in the P23H model by qPCR analysis, despite the reported increase in miR-183 expression by microarray analysis. This increase in miR-182 and -183 expression in the rho-/- mice at P5 contrasts with the decrease observed in the one-month rho-/- mouse model (Chapter5). However these expression profiles are not directly comparable, due to the different tissue source of each RNA sample analysed, i.e. whole-eye samples were obtained from P5 animals compared to the retina from the one-month animals. Also it must be noted that there was a large amount of variability within each group of samples, which is clearly illustrated in Figure 6.5. Indeed the miRs that are expressed at a higher absolute level in the retina (i.e. miR-182, -183; Figure 6.5A) display less variability compared to miRs have a low absolute retinal expression (i.e. miR-1, -133; Figure 6.5B).

6.3.5. qPCR analysis of miR signature in *rd1* retinas at P11

A time point of P11 was chosen to analyse the miR expression in the total RNA extracted from the retinas of *rd1* mouse, and compared to retinal samples from C3H and 129 wild type models. The expression levels of miR-1, -133, -142, -96, -182, and -183 were examined in this mouse model (Figure 6.6) and expressed relative to the wt C3H mouse. Of these 6 miRs examined, the expression of miR-96, -182 and -183 did not differ significantly in the *rd1* mouse model (Figure 6.6B). However an increase in expression of miR-1, -133 and –142 was observed, corresponding to 92±51.2 %, 79.4±45.2 % and 30.5±5.8 % (Figure 6.6A). However due to variability within these samples, only the increase of miR-142 expression was statistically significant ($p<0.001$). While miR-142 expression is increased in the retinas of the *rd1* model at P11, the magnitude of this alteration is lower than that observed in the slow degenerative RP mouse models discussed in Chapter 5. Specifically miR-142 expression increased between 207.0±45.0% to 392.3±25.2% in retinal samples of both rho- and rds-linked RP mouse models, which could be specifically attributed to an increase of expression of miR-142 in sorted rod photoreceptor cells from these models, between 527.9±163.3% to 882.8±283.3% (Chapter 5).

6.4. Discussion

The miR signature of retinal degeneration as discussed in Chapter 5 was examined in RP mouse models P23H and *rd1* with a faster retinal degeneration, by microarray analysis and qPCR. However a similar pattern of miR expression was not observed in these mouse models of RP when compared to that observed in the mouse models described in Chapter 5.

The P23H mouse model displays a rapid progression of rod photoreceptor cell death, the severity of degeneration correlating to the ratio of mutant to wild type rhodopsin expression (Olsson et al. 1992). In this study, due to the early age of onset of photoreceptor degeneration in the P23H model and the complete degeneration of photoreceptors by P14, an early time point of P5 was chosen for analysis. Microarray analysis of the P23H and rho-/- models revealed few overall differences in miR expression compared to wt 129 controls, highlighted as the miR expression of the nine RNA samples analysed by microarray were not categorised by hierarchical clustering methods into their corresponding groups (129; P23H; rho-/-) (Figure 6.3.) . On the whole 10 and 25 miRs in the rho-/- and P23H RP mouse models respectively, were differentially expressed compared to wt 129 however, none of these miRs shared a greater than 2-fold alteration in expression. The expression levels of miR-542, -369 and -335 were reduced by up to 26% while miR-465, -132 increased by up to 17% in the rho-/- model (Figure 6.4 A). Significantly in the P23H model, miR-468 expression was increased by 68%, while the degree of up regulation of additional miRs in this model was slighter. For example, the expression levels of miR-30a, -29c, -21, -183, -298 and -184 increased by approximately 16%, while the expression of miR-192, -145, -690, -326 decreased by approximately 13% (Figure 6.3A and C). Notably, at P5 no common alterations of miR expression were observed in the P23H and rho-/- models.

MiR-1, -133, -142 and -96, -182, -183 expression was analysed by qPCR, to determine if the retinal degeneration miR signature described in Chapter 5 extended to the P23H model. Additionally miR expression in the eyes of rho-/- mice was analysed at an earlier timepoint in the degeneration (P5), compared to retinal miR expression in the one-month old rho-/- model, as described in Chapter 5. Expression levels of these miRs were predominantly unchanged, however, the expression of miR-182 and -183 was increased by 23% and 48% respectively in the rho-/- model. The P23H model did not

share this feature. These findings contrast with the decreased expression of miR-182 and -183 observed at 1 month in the rho-/- model, and may reflect both differences in the severity of retinal degeneration and the developmental status of the retina at P5. In addition, it is possible that the degenerative process, resulting from the absence of rhodopsin expression, may not be fully activated by P5 in the rho-/- mouse eye. Indeed rhodopsin expression initiates in mouse photoreceptor cells postnatally, detectable at P3 (McNally et al. 1999), and increases in parallel with rod OS elongation (Fauser et al. 2002). While the rod OSs in the mouse are formed by P10, the rate of rod OS elongation is linear until the full rod OS length is reached by approximately P17-P23 (LaVail 1973; Fauser et al. 2002). In addition, as the source of the RNA samples for the one-month and P5 analysis of rho-/- miR expression differed significantly, the former from the retina and the latter from whole-eye, the miR expression analyses from both of these studies are not directly comparable.

Since the P23H animal is on a rho-/- background, in theory differences in miR expression between the P23H and rho-/- model should represent alterations due to the presence of the mutant rhodopsin transgene. However at the time point examined few alterations in miR expression were observed between the RP models and wt 129 control, and of the miRs which were differentially expressed between models, none of these alterations were common to both P23H and rho-/- degenerations. While the magnitude of miR alterations observed in these models was low, these differences may represent genuine changes in miR expression reflecting the different mechanisms and timeframes of cell death in both models. The expression of the mutant P23H transgene undoubtedly promotes photoreceptor degeneration, as it mediates a severe retinal degeneration in the presence of wt rhodopsin (Olsson et al. 1992). Additionally in comparison to the rho-/- model, the P23H rhodopsin accumulates in the synaptic zone of the OPL and ONL, and the aberrant accumulation of rhodopsin in the ER may mediate cellular responses which vary from the rho-/- model (Portera-Cailliau et al. 1994; Roof et al. 1994).

The broad similarities of miR expression among the P23H, rho-/- and wt 129 models at P5, suggests that miR expression is not altered in these faster degenerative model of RP at the timeframe analysed (P5). Rhodopsin expression in the wt mouse and P23H mouse RP model is demonstrated to steadily increase after P3, in parallel with rod OS elongation (Roof et al. 1994; McNally et al. 1999; Fauser et al. 2002), and indeed RHO expression was detected at P5 in the P23H animals used in the study by qPCR

(Figure 6.1). Consequently the degenerative process may be initiated at the time point analysed in these two models, as degeneration results either due to the expression of the mutant rhodopsin transgene in the P23H model, or the absence of rhodopsin expression in the rho-/- model. However it is possible that the alterations of miR expression observed in the one-month RP models reflect cellular processes which may not be fully activated by P5, for example, the research findings of Hobson *et al.*, (2000) demonstrate that in the rho-/- mouse model, the rate of apoptotic cell death peaks at P24 in the ONL and P8 in the INL (Hobson et al. 2000).

The expression of the six miRs implicated in the signature of retinal degeneration were also examined in the retinas of *rd1* mice, a null mutant of PDE6β. The rapid rate of photoreceptor cell death in this model of RP is similar to that observed in the P23H mouse model (Fauser et al. 2002; Dalke and Graw 2005; Hart et al. 2005). It is thought that apoptosis is activated in the rod photoreceptors of the *rd1* model due to raised levels of intracellular calcium, which results from sustained levels of cytoplasmic cGMP levels and activation of rod cGMP-gated non-selective cation channels (Fox et al. 1999; He et al. 2000). A time point of P11 was chosen for the retinal analysis of miR expression in the *rd1* model, as significant rod photoreceptor apoptosis has been detected at this age with little structural change to the retina (Carter-Dawson et al. 1978; Hauck et al. 2006). Of the 6 miRs analysed by qPCR, only miR-142 was significantly altered, increased by approximately 30% in the *rd1* retina compared to both C3H and wt129 controls. A trend for increased expression of miR-1, and -133 is evident, however due to the variability among samples these results are not significant. The raised expression of miR-142 in the retina of the *rd1* model reflects the increase observed in the slower degenerative rho- and rds-linked models at 1-month (Chapter 4 and 5), however the significance of raised miR-142 expression in the retina is unknown.

Differences in miR expression in the C3H mouse and the wt129 model were also observed in the current study, suggesting that variations in miR expression profiles may exist among mouse strains. Indeed alterations in miR expression were also observed by qPCR analysis, in the retinas of balb/C mice compared to wt 129 mice (Chapter 5), while microarray analysis revealed a markedly similar retinal expression profile of both wt 129 and wt c57 mice (Chapter 4). These findings highlight the importance of using strain-specific animal controls, depending on the background of the mouse model under

investigation, and as such miR microarray analysis of the retinas of both balb/C and *rd1* may be useful to fully ascertain strain-specific alterations in miR expression.

The miR signature of retinal degeneration was not evident in either the P23H, rho-/- or *rd1* models analysed at P5 and P11. It is possible that while rhodopsin is expressed at the time points analysed, the level of expression may not be high enough, or expressed for a sufficient amount of time, for initiation of the degenerative process. Indeed rhodopsin expression is pivotal for OS elongation, and in the P23H model the expression of transgenic rhodopsin correlates with the severity of photoreceptor cell death (Roof et al. 1994) (Olsson et al. 1992). In mice the increase in rhodopsin expression from P3 (McNally et al.; Fauser et al. 2002), parallels the elongation of rod OS (LaVail 1973) and interestingly miR-96, -182, and -183 expression has been demonstrated to increase postnatally from P1 into adulthood (Xu et al. 2007). This correlation suggests that these three miRs may possibly be implicated in photoreceptor maturation, and the predominant localisation of these miRs to photoreceptor cells (Ryan et al. 2006; Karali et al. 2007; Xu et al. 2007) and the co-localisation of miR-182 and rhodopsin, would support this hypothesis (Karali et al. 2007).

In addition the miR signature of retinal degeneration previously observed in slow RP models may reflect common cellular processes resulting from degeneration, such as apoptosis, cell defence mechanisms or indeed neuronal remodelling of the retina. Apoptosis in the rho-/- model is continuous, and maximal at P24 (Hobson et al. 2000), while *in vitro* evidence suggests that P23H photoreceptors readily undergo apoptosis at P7 (Streichert et al. 1999). Neural remodelling of the retina is a lengthy process that occurs in all models of retinal degeneration irrespective of the trigger, in response to photoreceptor loss. Early remodelling events that coincide with initial rod photoreceptor degeneration may be reflected in the miR signature of degeneration; these include progressive shortening of rod OS, slow changes in rhodopsin distribution to rod ISs, and neurite outgrowth of rods into the INL and IPL (Jones et al. 2003; Marc et al. 2003).

6.5. Conclusion

On the whole the study described in this Chapter of the Ph.D. thesis highlights the difficulties that exist in examining retinal degenerations in fast degenerative mouse

models, which potentially limits the use of these models in some areas of ocular research. Indeed the rapid nature of the degeneration of rod photoreceptors in P23H and *rd1* mice severely restricts the timeframe for the appropriate analysis of RP pathogenic mechanisms to after the initial expression of the disease protein and prior to significant alterations in retinal structure or cellular composition, owing to photoreceptor death. Therefore the window of opportunity for experimental analyses is quite narrow in these animal models of RP. Additional issues that also confound the use of these models include the developmental status of the retinas, as the timeframe of the retinal degeneration coincides with the final stages of retinal development, including rhodopsin expression. Furthermore there are some difficulties associated with dissecting reliable retinal tissue from young eyes. Further characterisation of the precise timelines of rod photoreceptor degeneration would be required to derive the full research benefit from RP mouse models such as the P23H model, as variations of the rate of degeneration may be dependent on the background strain used between animal facilities. Therefore elucidating the involvement of miRs in these models is challenging, requiring further examination of the timeframe of retinal degeneration and possibly include the analysis of miR expression in isolated photoreceptor samples, as described in Chapter 5. However, in light of the findings presented in this Chapter, the slower degenerative mouse models of RP appear more advantageous for the miR studies undertaken as these slower degenerating models provide a longer timeframe to examine pathogenic mechanisms of RP and in addition permit the examination of these mechanisms in fully matured photoreceptor cells.

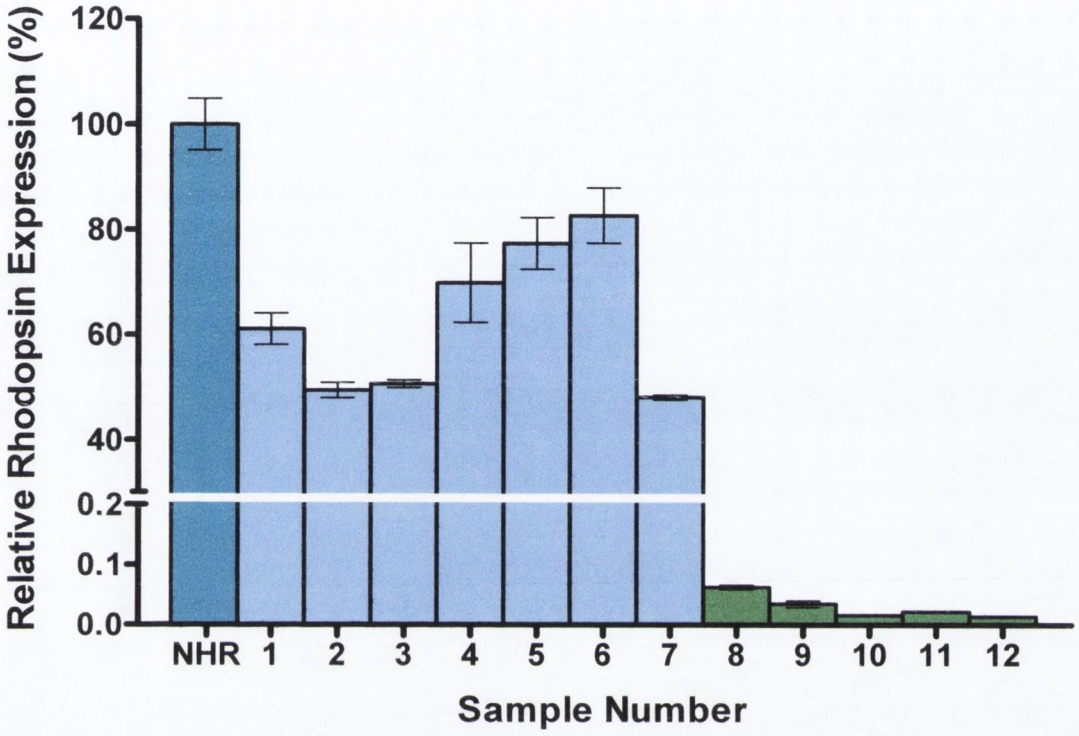

Figure 6.1: Genotype of P23H animals: Total RNA extracted from p5 P23H (pro23his mutant in human RHO) whole-eyes, and genotyped by analysing RHO expression by qPCR. P23H animals were bred on a rho-/- background, and RHO+/- rho-/- (light blue) and RHO-/- rho-/- (green) were discriminated by comparison to RHO expression in NHR transgenic animal (NHR: normal human rhodospin). The NHR model expresses a single wt RHO allele on a rho-/- background (RHO+/-rho-/-).

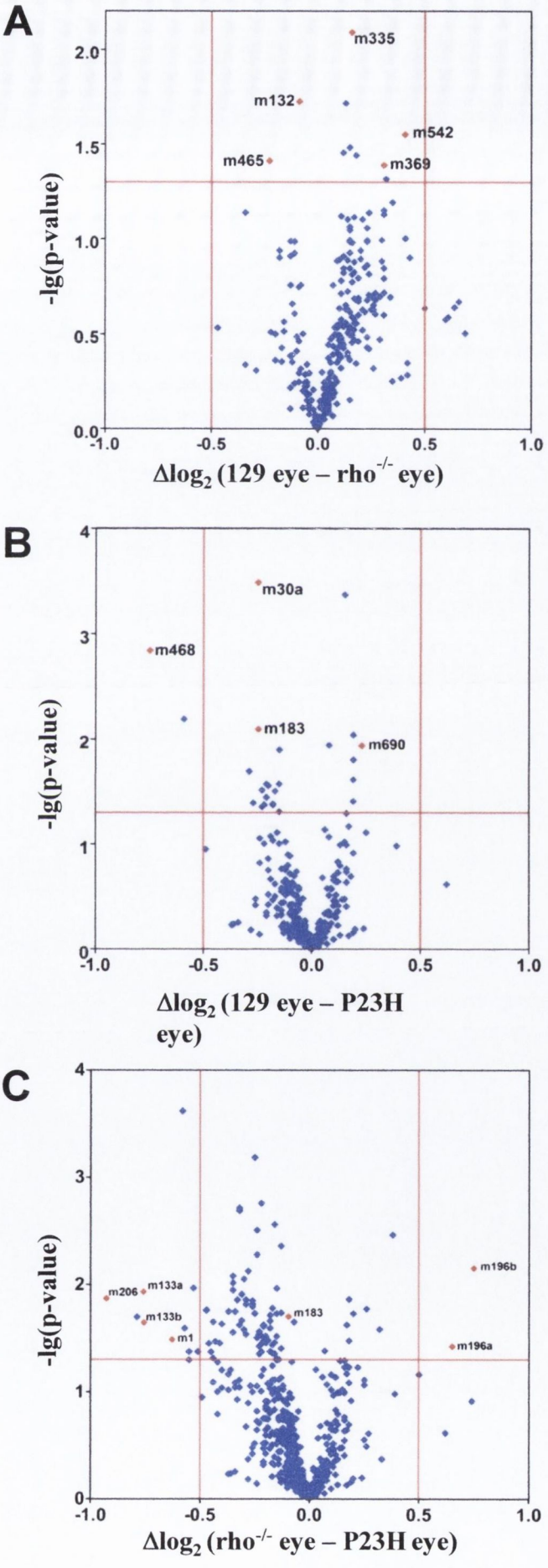

Figure 6.2: Volcano plots of miR expression in Rho-/-, P23H compared to wild-type whole-eyes: Plots represent comparative miR expression profiles of **(A)** 129 versus rho-/- eyes, **(B)** 129 versus P23H (mutant pro23his *RHO* transgene) eyes, and (**C**) rho-/- versus P23H eyes at postnatal day 5 (P5) using Exiqon miR v9.2 microarrays. X-axis indicate difference of expression level on a $\log_2$ scale, while y-axis represents corresponding *p-values* (Student's t-test) on a negative log scale A $-\log_{10}$ *p-value* of 1.30 (highlighted by the red horizontal line) corresponds to a *p-value* of 0.05 on a geometric scale, and therefore points above this line represent statistically significance variations of miR expression. The vertical red line was chosen arbitrarily, and represents differences in expression between samples of ±0.5 on a $\log_2$scale. Therefore the more lateral points, represent a greater magnitude of miR expression between the two groups analysed, and positive and negative values signify the group with higher or lower expression..

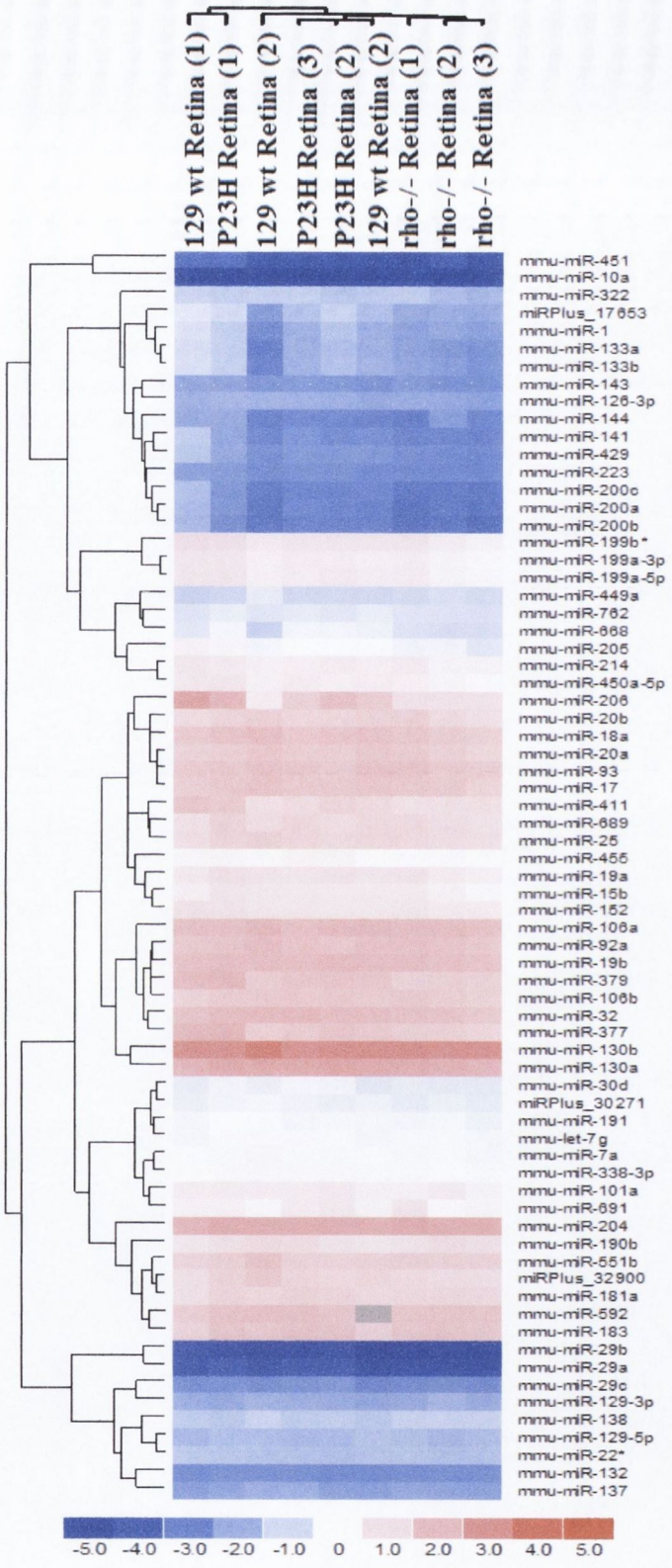

Figure 6.3: Heat Map and Hierarchical clustering of miRNAs in Rho-/- , P23H, and wt 129 whole-eyes at postnatal day 5 (P5): The heat map diagram shows the result of the two-way unsupervised hierarchical clustering of miRs and the experimental groups; 129 eye tissue and rho-/- eyes at postnatal day 5 (P5), using Exiqon v9.2 microarrays. Each row represents a miRNA and with clusters indicated on the left, while each column represents a sample with clusters appearing at the top. The clustering was performed on a filtered set of $\log_2$(Cy3/Cy5) ratios, which displayed a high variability across samples (standard deviation >0.5). Clusters were generated using the average linkage method, a method which calculates the distance between clusters. The Cy5 labeled reference was used in each array, and provides a constant baseline to compare samples to. The color scale shown at the bottom illustrates the relative expression level of each miR across all samples ($\log_2$Cy3/Cy5). The red color represents a relative miR expression level greater than the mean, blue color represents a relative expression level lower than the mean. Log_2(Cy3/Cy5) ratios $\pm$ 1 correspond to a more than 2 fold up or down regulation, relative to the miR reference (Cy5).

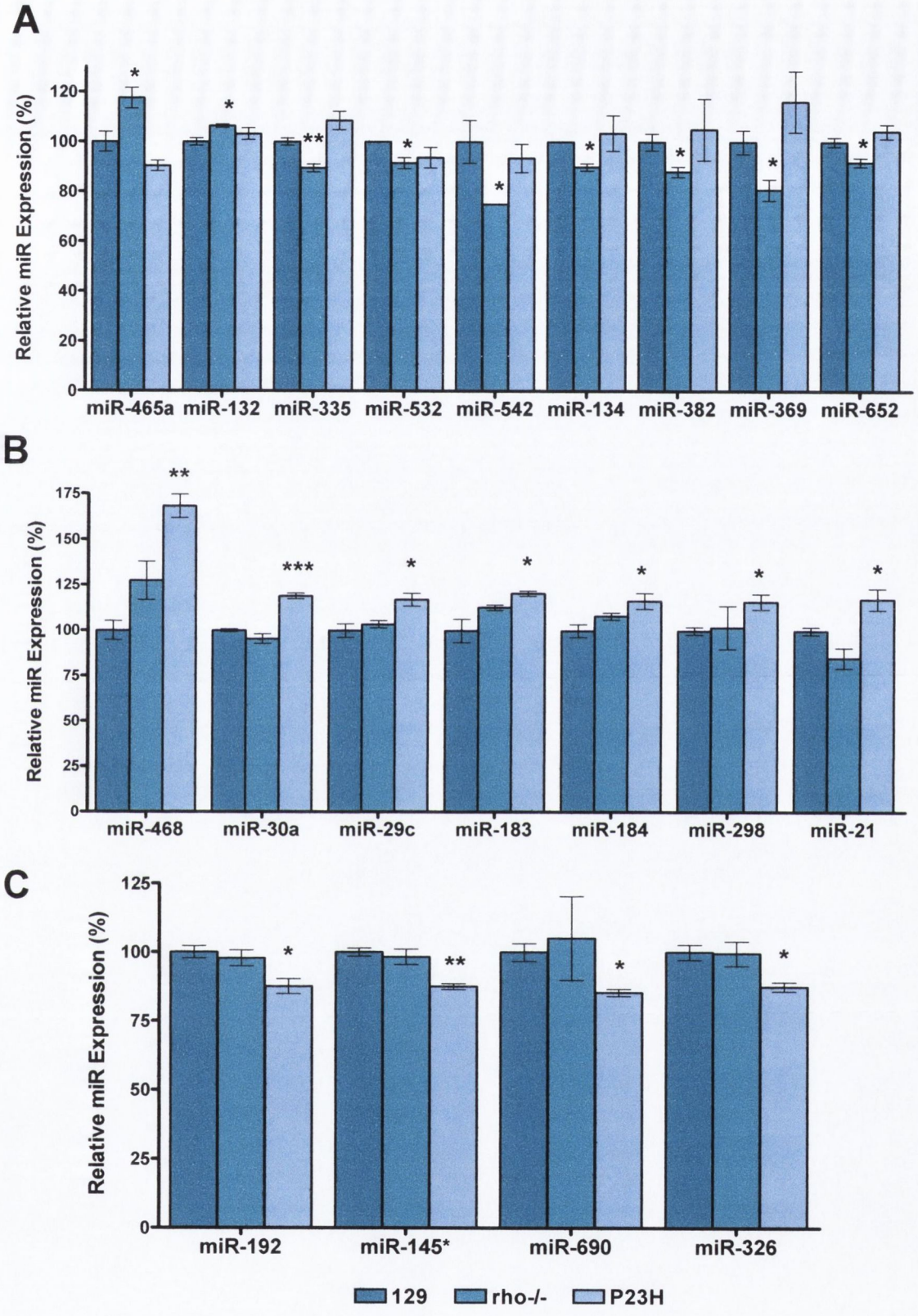

Figure 6.4: Relative miR Expression in wt 129, rho-/- and P23H whole-eyes at P5: Microarray data using Exiqon v9.2 arrays is expressed as relative miR expression (%) in wt 129, rho-/- and P23H eye tissue at postnatal day 5 (p5). Altered miR expression in (**A**) rho-/- model and (**B & C**) P23H models is expressed relative to wild type 129 values, statistically significant variations (Students *t-test*) are represented by; *: $p<0.05$; **: $p<0.01$; ***: $p<0.001$. Error bars indicate S.E.M.

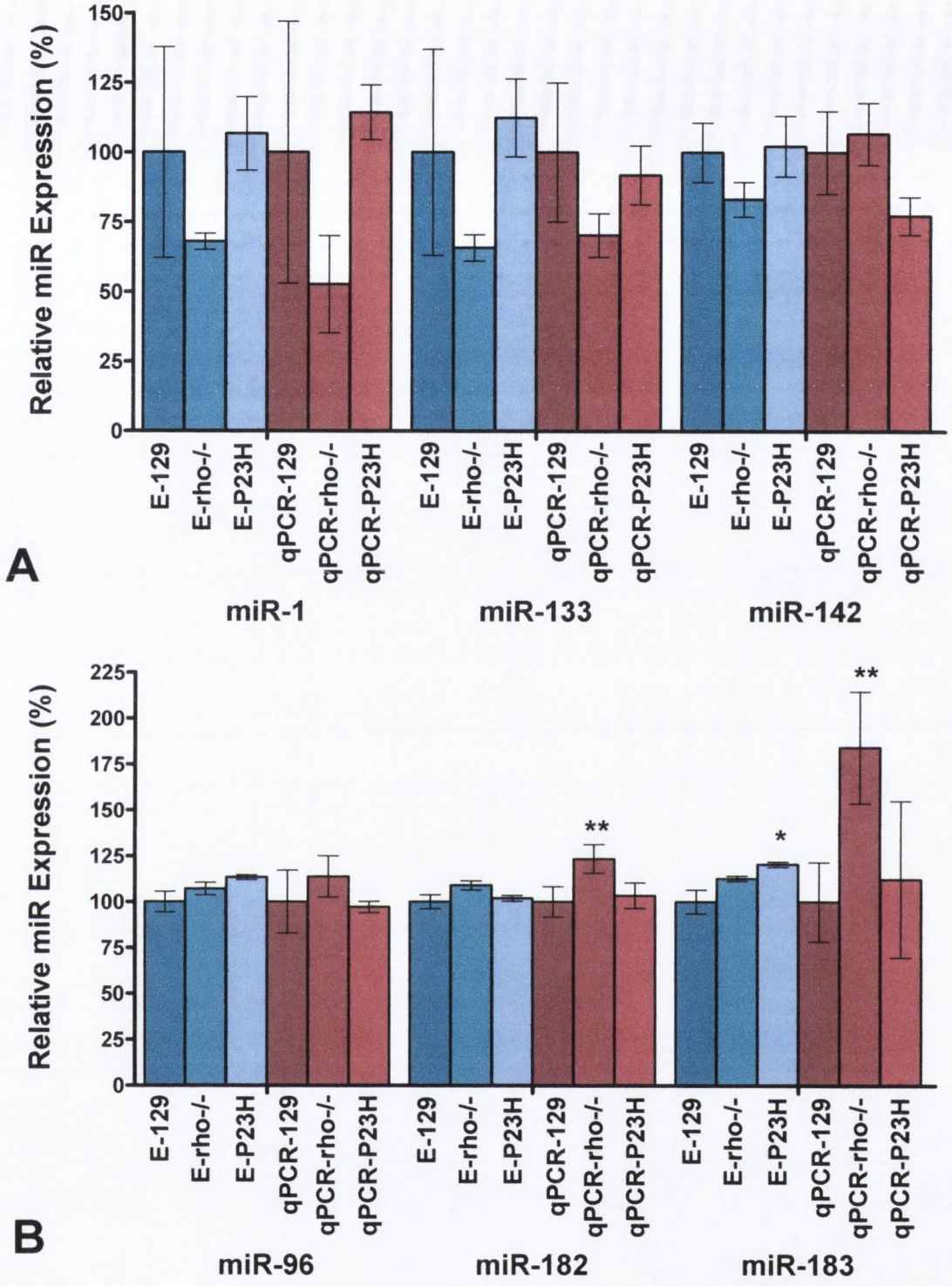

Figure 6.5: qPCR Validation of relative expression of selected miRs in wt 129, rho-/- and P23H whole-eyes at P5: The graph illustrates the relative expression level of miRs from microarray data (blue) and validation by qPCR (magenta). Bars represent miR expression (%) at P5 relative to wt 129 samples (dark blue, dark magenta) in rho-/- eyes (lighter blue, lighter magenta), and P23H eyes (light blue, light magenta). The expression of **A**) miR-1,-133 and –142 and (**B**) miR-96, -182 and –183 are illustrated. Note that the y-axes are to different scales. Comparative miR expression data was analysed by ANOVA (Tukey's Multiple Comparison Test) and the statistical significance is indicated by; *: $p<0.05$; **: $p<0.01$. Error bars indicate S.E.M.

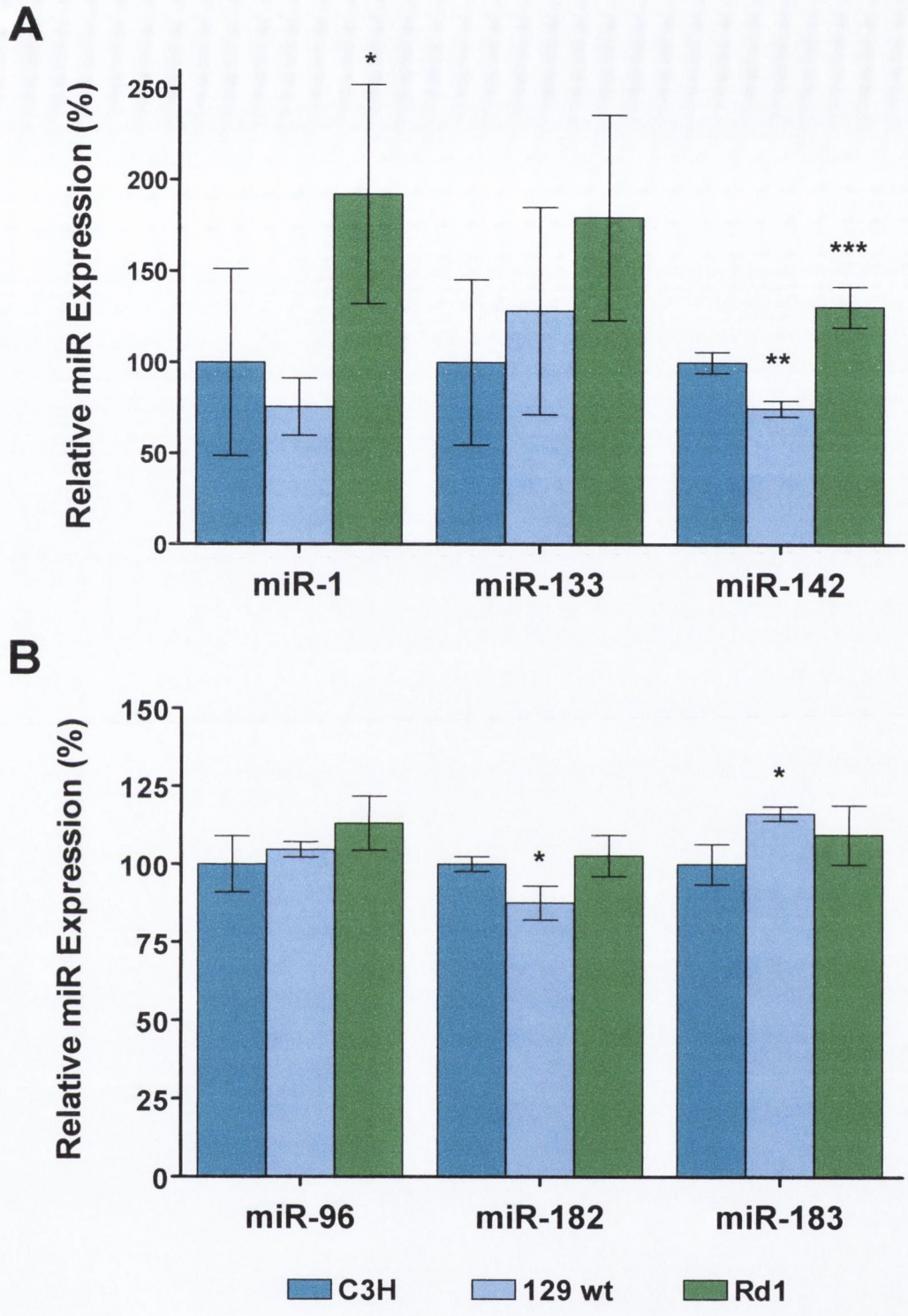

Figure 6.6: Relative expression of selected miRs in wt 129, wt C3H and *rd1* retinas at P11: The graph illustrates the relative expression level of miRs using qPCR. Bars represent miR expression (%) at P11 in *rd1* retinas (light blue), and wt 129 retinas (green) relative to wt C3H wt (dark blue). The expression of **A**) miR-1,-133 and –142 and (**B**) miR-96, -182 and -183 are illustrated. Note that the Y-axes are to different scales. Comparative miR expression data was analysed by *ANOVA* (Tukey's Multiple Comparison Test) and the statistical significance is indicated by; *: $p<0.05$; **: $p<0.01$; ***: $p<0.001$. Error bars indicate S.E.M.

Chapter 7

Target Prediction of Retinal miRs

7.1. Introduction

There are currently 695 and 488 miRs confirmed in humans and mice respectively (miRBase), however recent reports estimate that there may be ~ 1000 miR genes in humans (Bentwich et al. 2005; Berezikov et al. 2006). It is thought that the expression of 30% of genes may be regulated by miRs, with each miR expected to target hundreds of mRNA transcripts (Lewis et al. 2005). Currently, 1094 and 105 miR targets (i.e. proteins whose levels are regulated by miRs) have been experimentally validated in humans and mice respectively (Sethupathy et al. 2006).

Target prediction and validation is a key step to identify the roles played by miRs in physiological processes and disease. It is indeed of great interest to identify retinal targets that may be regulated by differentially expressed miRs in RP, as these targets may potentially be implicated in the disease process. The prediction of miR targets using computational algorithms may prove to be a useful tool to begin to determine the biological functions of miRs. Indeed this has been of great benefit in plants (Rhoades et al. 2002; Bonnet et al. 2004), as miRs interact with mRNA targets with a high degree of sequence complementary, however target prediction in animals is more complex owing to the variability of miR:mRNA interactions. MiRs inhibit gene expression by targeting mRNAs for translational repression or cleavage (Bartel 2004; Behm-Ansmant et al. 2006). MiRs were initially identified to recognise targets based on sequence similarities of the 3'UTR of the mRNA transcript to the 5' seed region (nucleotide 2-8) of the miR, which was reduced by G-U mismatches within this region (Doench and Sharp 2004). However other determinants have since been identified, such as the variance of miR sequence complementarities to their target sites. While the binding of the 5' seed region is critical for target suppression, insufficient 5' base-paring of the miR seed can be compensated by base-pairing of the 3'end (Doench and Sharp 2004; Brennecke et al. 2005; Kiriakidou et al. 2007). Additionally many miR binding sites have bulges in the central or 3' region of the miR that may also be important for target binding (Vella et al. 2004). An added complexity of miR:mRNA interactions is the presence of multiple miR binding sites on target transcripts, which appear to enhance target repression by combinatorial and cooperative interactions of miRs. Recent studies also suggest that the secondary structure of the mRNA target site is an important factor required (Robins et al. 2005). It is theorized that the ability of miRs to interact with mRNA binding sites is

reduced, if the mRNA is folded such that the miR binding site is base-paired with other regions of the mRNA (Robins et al. 2005).

Target prediction algorithms are hampered by the lack of empirical evidence of miR targets, and as such prediction mechanisms are based on anecdotal features of miR:mRNA interactions (Bentwich et al. 2005). Many bioinformatic approaches and the most recognised algorithms, miRanda (John et al. 2004) TargetScan (Lewis et al. 2003) and PicTar (Krek et al. 2005), all focus on the requirement of miR seed base-pairing with the target 3'UTR. However prediction is complex due to the short length of base-pairing of miR and target transcript, and the additional presence of bulges and complementary mismatches. The identification of the 3'UTR of mRNA transcripts is difficult in itself, relying on Ensemble databases to extract 3'UTR regions based on alignments of cDNAs and expressed sequence tags (ESTs) with genomic sequences. Indeed 3'UTR boundaries are not defined for a large percentage of human genes, and therefore only estimates of these regions are used in target predictions which may contribute to false predictions (Maziere and Enright 2007). The thermodynamic stability of the mRNA:miR duplex appears to be important for favourable miR target binding (Zhao et al. 2005). A further complication is the context of miR targeting, as gene regulation by miRs relies on the co-localisation of expressed miRs and target transcripts in the same cellular compartment. Therefore despite experimental validation, these miR target interactions may represent false positive targets, and may not be relevant biologically.

Target prediction by miRanda, TargetScan and PicTar identify targets based on sequence complementarities, favorable thermodynamics and conservation of mRNA target sites in related species, however, differences exist between these prediction methods (Lewis et al. 2003; John et al. 2004; Krek et al. 2005). While all prediction methods focus on strong binding of the seed region to target 3'UTRs they each score this interaction differently and the importance allocated to target conservation varies in each algorithm. For example the PicTar algorithm solely identifies miR targets of phylogenetically conserved 3'UTRs across multiple species, and is the only algorithm to use co-expression criteria of miRs and targets. TargetScan attempts to filter out false negatives at the beginning of the prediction process by requiring a perfect base pairing in the seed region, while miRanda additionally rewards binding in the 3'end of the miR. All prediction methods however examine the thermodynamic stability of miR:mRNA interactions. Nevertheless, as target prediction algorithms attempt to predict miR targets

with a high degree of specificity rather than sensitivity, many genuine miR targets may be lost during the prediction process due to the stringent nature of some of these assumptions. For instance, although miRs potentially target hundreds of conserved targets, it is thought that there may be several hundred more non-conserved targets (Bentwich et al. 2005). In addition to the potential loss of 'real' targets, indeed each miR prediction method has various false positive rates as determined by empirical target validation, resulting from the assumptions used in these predictions (Sethupathy et al. 2006).

Due to the inherent variability of miR target prediction by miRanda, TargetScan and PicTar algorithms, Kuhn *et al.,* (2008) has recently detailed guidelines best suited to the identification and validation of miR targets (Kuhn et al. 2008). This strategy proposed the filtering of overlapping targets predicted using these three algorithms, and in addition determining the accessibility of the 3'UTRs for miR binding by free energy analysis (Kuhn et al. 2008). In the study described in this chapter of the thesis, the miR targets of miR-1, -133, -142 and miR-96, -182, 183 are examined following these guidelines; these miRs are those that were differentially expressed in the retina of RP models as outlined in Chapter 5. Additionally the targets identified are limited to those expressed in the retina, thereby providing biologically relevant predictions. Despite the theoretical nature of target prediction, and the inherent flaws as outlined above, this strategy may offer a feasible approach for examining the potential biological targets and functions of miRs in both healthy and diseased retinal tissue.

7.2. Materials and Methods

While I provided the academic input for the design of the bioinformatic analyses listed below, technical expertise was received to perform these analyses from Dr. Karsten Hokamp of the Smurfit Institute of Genetics, Trinity College Dublin.

7.2.1. Collection of retinal expressed genes

The mouse UniGene repository (Build#175) was downloaded and IDs of genes expressed in the retina of seven selected mouse eye libraries were automatically selected (UniGeneDatabase). As previously mentioned, each UniGene entry represents a group of transcript sequences that appears to be transcribed from the same transcriptional unit (Sayers et al. 2008; UniGeneDatabase).

The following libraries were used:

Lib.8659	NIH_MGC_94
	(23422 ESTs grouped into 7638 UniGene entries)
Lib.6780	NIH_BMAP_Ret4_S2
	(19072 ESTs grouped into 8437 UniGene entries)
Lib.5390	RIKEN full-length enriched, adult retina
	(6089 ESTs grouped into 3452 UniGene entries)
Lib.15224	Mouse retina, unamplified: mk/ml
	(4658 ESTs grouped into 2832 UniGene entries)
Lib.20873	Mouse retina. Y2H (nbk)
	(1843 ESTs grouped into 1290 UniGene entries)
Lib.12980	MOUSE ADULT RETINA
	(1111 ESTs grouped into 872 UniGene entries)
Lib.6773	NIH_BMAP_Ret3
	(961 ESTs grouped into 748 UniGene entries)

Out of 2371 mouse UniGene IDs, 15207 UniGene, 10082 Entrez Gene IDs and 10082 MGI gene symbols were extracted (MGI_Database).

Additionally, genes were retrieved from two SAGE studies (Blackshaw et al. 2001; Blackshaw et al. 2004) that determined genes expressed in the mouse retina (tag levels >2), as follows:

(Blackshaw et al. 2001) **3516 UniGenes (with tag-level>2)**

http://genepath.med.harvard.edu/~cepko/SAGE/Table_S2_1.htm

http://genepath.med.harvard.edu/~cepko/SAGE/Table_S2_51.htm

(Blackshaw et al. 2004) **3475 UniGenes**

http://cepko.med.harvard.edu/table_st3.asp

The addition of the genes identified in these SAGE libraries, increased the number of MGI gene symbols that are expressed in the retina from 10082 to 11858.

Finally, a total number of 509 human eye disease genes were translated into putative mouse homologues and included in the study. These genes were obtained from the following sources:

Cloned and Mapped Retinal Disease Genes **(106 Gene Symbols)**

(Blackshaw et al. 2001)
http://genepath.med.harvard.edu/~cepko/SAGE/Table_S1_Expression_of_previously_mapped_and_cloned_retinal_.htm

NEI Bank: Eye Disease Genes **(445 Gene Symbols)**

(Wistow 2002) http://neibank.nei.nih.gov/cgi-bin/eyeDiseaseGenes.cgi

The addition of these retinal genes from UniGene to the previous retinal list increases the number of retinal genes by 229, from 11,858 to 12,081 genes. This list of 12081 retinal genes from the mouse UniGene repository is used in a later step to filter miR targets expressed in the retina.

7.2.2. MiR Target Prediction

The guidelines for miR target prediction detailed by Kuhn *et al.*, (2008) were followed, in which the miR target predictions are examined using the three algorithms,

miRanda, TargetScan and PicTar and the identified targets are filtered based on the criterion of prediction by 2 or more methods (Kuhn et al. 2008). Using this strategy, targets are predicted for miR-1, -133, -142, -96, -182 and -183 by the 3 prediction programmes listed below.

7.2.2.1. miRanda Target Prediction

Mouse Ensembl transcripts and MGI symbols predicted to be miR targets were retrieved from Sanger's miRBase (version 5) (miRBase), based on Ensembl (version 46), and miR registry (release 10.0). Predictions were computed using miRanda version 3 (John et al. 2004) and filtered for p-orthologous group value <0.05, the probability that a miR-orthologous group value takes the conservation of target 3'UTR into account, and is the probability of a miR to interact with the target transcripts of orthologous species. All targets predicted for *Mus musculus* were downloaded in text format and hits for miR-1, -133, -142, -96, -182, and -183 were identified and the gene symbol extracted. Additionally the positions of the mRNA binding sites were downloaded, which are expressed relative to the start of the chromosome.

miRanda Data source:

(ftp://ftp.sanger.ac.uk/pub/mirbase/targets/v5/arch.v5.txt.mus_musculus.zip).

7.2.2.2. TargetScan Target Prediction

Entrez Gene ID and Gene Symbol data were downloaded from TargetScan (release 4.2) for all targets predicted for conserved miR families (Lewis et al. 2003). The targets predicted for miR-1, -133, -142, -96, -182, and -183 were identified and the gene symbols extracted. Additionally positions of target binding sites were downloaded relative to the 3'UTR of the gene.

TargetScan Data Source:

http://www.targetscan.org/vert_42/vert_42_data_download/Conserved_Family_Info.txt.zip

7.2.2.3. PicTar Target Prediction

As no suitable downloads were offered for this prediction algorithm, a summary page of targets for each miR-1, -133, -142, -96, -182, and -183 was downloaded manually. The hits for each specific miR were extracted as RefSeq IDs, however as MGI gene symbols were not provided, Ensembl BioMart was used to translate RefSeq IDs to MGI gene symbols (Durinck et al. 2005; BioMart). Additional information regarding the mRNA binding sites was extracted, relative to the 3'UTR of the gene by automatically following links to more detailed web-pages contained within the summary pages.

PicTar Data Source:

http://pictar.mdc-berlin.de/cgi-bin/new_PicTar_mouse.cgi

7.2.3. Filtering of Targets

The MGI gene symbol output from each prediction method and UniGene entries from mouse retinal genes, were linked and extracted when gene names were available in both sources (UniGeneDatabase). As recommended, the targets identified for each miR, were filtered for targets which were predicted by 2 or more prediction methods (Kuhn et al. 2008). This list of target genes was further filtered for overlapping miR target sites on the target transcript, prior to mRNA secondary structure analysis (see section 7.2.4).

7.2.4. MiR Accessibility Analysis (ΔG Analysis)

Whereas the miR binding site location reported by miRanda are expressed as chromosome coordinates, TargetScan and PicTar report these distances as coordinates relative to the start of the 3'UTR. As a result the BioMart package was used to retrieve the 3'UTR sequence and chromosomal coordinates of miR target sites from Ensembl (v.46), corresponding to each predicted target gene (Durinck et al. 2005). Target genes were excluded if the miR binding sites, predicted by >2 prediction algorithms, did not overlap. The flanking sequence +70 and -70 nucleotides of the binding site were extracted for further filtering criteria based on the secondary structure of the mRNA binding site.

In order to examine the accessibility of the mRNA target sites for miR binding, the free energy of the target site and 5'- and 3'- flanking sequences were analysed using UNAFold (Markham and Zuker 2005) as previously described (Zhao et al. 2005; Kuhn et al. 2008). This free energy value, ΔG (-kcal/mol), is a measure of amount of free energy lost in the unpairing of the target-site nucleotides and additional flanking sequences. The ΔG values of each target site, was compared to the ΔG value of 13.4 (the ΔG value of 60 random mouse 3'-UTRs of 70 bp each), which has previously been used for such analysis (Zhao et al.; Kuhn et al.). If either the 5'- or 3'- flanking region of the miR binding site had a lower free energy value than the random ΔG value of 13.4, it suggests that local secondary structures are not present at the target site and therefore the target site is thought to be accessible for miR interaction. Note that only one of the 5'- or 3'- flanking sequence is required to fulfill this ΔG criterion to be considered as a candidate for miR binding. However mRNA targets with free energy values higher than 13.4 -kcal/mol on both sides of the predicted binding site were excluded from further target prediction analyses, as these target sites are thought to form secondary structures and therefore may be inaccessible for annealing to the miR/miRNP complex. (Zhao et al. 2005).

7.2.5. Comparison of targets predicted for miR clusters

In silico target predictions using miRanda (John et al. 2004) and PicTar (Krek et al. 2005)were retrieved from miRGator (Nam et al. 2008) for the following clusters, miR-1,-133, -142 and -96, -182, -183. MiR targets were filtered for retinal expressed genes as described above (7.2.1.) and an additional retinal gene list was included in this analysis, which contained 320 retinal genes associated with retinal functions and disease (Arora et al. 2007). The remaining predicted targets of miRs within the same cluster were analysed. Targets which were found to have miR binding sites for two or more miRs within a cluster were identified; i.e. the intersection of predicted miR targets for miR-96, -182, -183 and miR-1, -133, -142.

7.3. Results

7.3.1. miRanda target prediction for miR-1, -133, -96 and -183

Potential target transcripts for miR-96, -183, -1 and -133 predicted by miRanda (John et al. 2004) were retrieved from the Sanger miR Database (Griffiths-Jones et al. 2006). In order to select for targets expressed in the retina, the transcripts were screened against seven Unigene mouse retina libraries and four gene lists derived from NEIBank (Wistow 2002) and serial analysis of gene expression (SAGE) studies in the mouse retina (Blackshaw et al. 2001; Blackshaw et al. 2004). Matches based on gene names were extracted, resulting in a final subset of 1664 miRanda predicted transcripts that are associated with known genes and are present in at least one retinal library or gene list (Table 7.1). The resulting miR targets were sorted by miRanda score, p-orthologous value, presence in the seven retinal libraries and three eye related lists (i.e. a sum from 1 to 10) and predicted miR target sites per transcript. A positive score is given for complementary base-pairing of the miR and target, while a negative score reflects mis-matches. In addition the p-orthologous value is a measure of miR target conservation, the probability of miRs to interact with targets of orthologous species. Table 7.2 lists potential retinal target transcripts with the highest rankings for miR-96, -183, -1 and -133. Notably, transcripts of retinal disease genes, such as *Crb1*, *Abca4*, *Pde6a*, *Prpf8* and *Prpf31*, are predicted to be targeted by these miRs (Table 7.2). Other highly ranked targets sorted by function include proteins involved in the visual cycle (e.g. *Pitpnm1*), transcriptional factors (e.g. *Asb6* and *Ndn*), apoptosis regulators (e.g. *Pdcd6* and *Psen2*), mRNA processing factors (e.g. *Syf11* and *Hnrpl*), intracellular trafficking components (e.g. *Trappc3* and *Ktn1*) and transmembrane signalling molecules (e.g. *Gnb1* and *Gnb 2*) (Table 7.2.).

7.3.2. miR Target Prediction using three prediction methods and ΔG Analysis

Potential target transcripts for miR-1, -133, -142, -96, -182 and -183 were predicted by miRanda (John et al. 2004), TargetScan (Lewis et al. 2003) and PicTar (Krek et al. 2005) and retrieved from the relevant database. Target binding sites predicted by more than one target prediction method were filtered by the corresponding MGI gene symbol. Following recommendations by Kuhn *et al.*, (2008), miR hits predicted by all

three methods were compared and filtered for targets common to at least 2 prediction methods (Kuhn et al. 2008). This necessitated the translation of RefSeq IDs from PicTar predictions into MGI symbols, for comparison with miRanda and TargetScan targets symbols. In order to select for targets expressed in the retina, the transcripts were screened against seven UniGene mouse retina libraries and four gene lists (an additional retinal list was included in this later analysis) derived from NEIBank (Wistow 2002) and serial analysis of gene expression (SAGE) studies in the mouse retina (Blackshaw et al. 2001; Blackshaw et al. 2004). Matches of miR predicted targets and retinal genes were extracted for each miR, resulting is a final subset of targets with potential biological relevance (Table 7.3). This filtering step reduced the total number of overlapping targets by 20.5%, representing miR target transcripts expressed in the retina and predicted by >2 methods (Figure 7.2).

Additionally in order to account for the accessibility of the potential mRNA target sites required for interaction with the miR/mRNP complex, the free energy of the mRNA target binding site sequence and flanking regions (± 70 bp) were obtained from the output of each prediction method. The miR binding site locations on each gene were translated into chromosomal coordinates and the list of miR retinal targets was further filtered for overlapping miR binding sites on the 3'-UTR of each transcript. ΔG analysis of the mRNA binding sites and the flanking regions was performed using UNAFold (Markham and Zuker 2005) (Figure 7.2). This evaluated the predicted local mRNA secondary structure ±70 bp of the proposed miR binding site and the corresponding ΔG (-kcal/mol) values, obtained for each target binding site, were compared to the free energy value randomly expected (ΔG=13.4 -kcal/mol) (Kuhn et al. 2008). MiR predicted targets with a free energy value greater than 13.4 -kcal/mol were excluded from the miR target list, consistent with the idea that RNA secondary structure may play a vital role in miR accessibility to the target binding site (Table 7.3-7.5). This filtering step reduced the total number of target predictions for each miR by an average of 18.5% (Table 7.3; Figure 7.2). Potential miR retinal targets included, transcription and translation regulators (*Ebf3*; *Eif4ebp2*; *Eif5*), intracellular trafficking components (*Sec22b:Myh9*), mRNA processing and splicing factors (*Sf3b4*; *Sfrs12*), apoptosis regulators (*Bcl212*; *Bnip3l*) and solute transporters (*Slc35c1*; *Slc43a2*: *Slc6a6*; *Slc7a8*) (Table 7.4 and 7.5).

7.3.2. Common Targets predicted for clustered miRs using miRanda

In silco target prediction was additionally used to identify overlapping miR targets, predicted by more than one miR for the following groups; miR-1,-133, -142, and -96, -182, -183. As identified in chapter 3 and chapter 4, miR-1-133 and -96-182-183 are clustered miRs, located in close proximity on the genome. Due to the similar expression patterns of these miRs, it was of interest to examine if miR targets predicted by each miR overlapped, thereby suggestive of a cooperative biological function. *In silico* miR target prediction revealed an average number of 846 and 266 targets identified for all miRs by miRanda and PicTar algorithms, 48 of which were predicted by both algorithms (Table 7.6). On average, 48.3% (409 out of 846) of miRanda targets were present in the retinal transcriptome, and 4.2% (17 out of 409) overlapped with retinal disease genes (Table 7.6). The intersection of retinal expressed genes and both target predictions revealed an average of 36 targets/miR. Figure 7.1 summarizes the retinal expressed subset of miRanda target predictions for miR-96, -182 and -183 (Fig. 7.1A) and miR-1, -133 and -142 (Fig. 7.1B). Targets for each miR group, with binding sites for at least two of their miRs ('enriched targets'; intersections in Fig. 7.1.A and 7.1.B). The full list of targets predicted by miRanda for miR-1,-133, -142 and -96, -182 and -18, and overlapping targets are listed in Table 7.7(A-C) and 7.8(A-C).

7.4. Discussion

Using the three main target prediction algorithms, target transcripts were identified for miR-1, -133, -142, -96, -182, and -183. These miRs were altered in expression in the two rds-linked and two rho-linked RP models analysed in chapter 5. The functions of these six miRs in the retina and elsewhere have yet to be fully elucidated. MiR-96, -182 and -183 belong to a sensory organ-specific cluster and have a high relative expression in the retina (Arora et al. 2007; Xu et al. 2007), while miR-1 and -133 have known roles in muscle (Care et al. 2007) and miR-142 is involved in the immune response (Wu et al. 2007). However as observed in Chapter 3, miR-1 -133 and -142 have a low expression in the retina relative to other tissues and to date their roles in the retina are not defined. As miR-96, -182, and -183 are reduced in expression in the retinas of RP models, it is possible that their targets are up regulated. While conversely miR-1, -133 and -142 expression is increased and hence their targets may be suppressed in the RP retinas.

Targets transcripts of these six miRs were predicted using miRanda, TargetScan and PicTar, and a number of filtering steps were applied to these lists, as represented in Figure 7.2. The addition of these filtering steps is aimed to increase the specificity of the target predictions, thereby increasing the probability of predicting genuine miR targets. The first filtering step applied to the targets predicted by each prediction algorithm, involved the filtering of miR targets for those which were identified by two or more target prediction algorithms. The resulting list of targets was additionally filtered for genes expressed in the mouse retina (Blackshaw et al. 2001; Blackshaw et al. 2004) and genes linked with eye diseases (Wistow 2002). This list was further filtered for targets where the same or overlapping sequence is predicted to be used for miR binding. Overall these filtering steps reduced the number of targets for each miR by an average of 57.5% (Table 7.3). Targets predicted by Targetscan and PicTar overlap more frequently, than with targets identified by miRanda, this overlap accounting for approximately 78% of the filtered list of target genes (Table 7.4 and 7.5). This is most likely due to the similar conservation requirements used by both PicTar and TargetScan, in which conservation across 5 species is required in the portion of the target site that binds the miR seed; while in contrast miRanda only requires conservation between human and rodents and 90% identity of miR seed and target binding site. In order to account for the accessibility of the mRNA binding sites, the secondary structure of the predicted miR binding sites and

flanking sequences were analysed, and a free energy value (ΔG) obtained at the miR binding site of each target transcript. In this last step of filtering, an average of 82% of predicted targets appear to have an accessible miR target site, required for interaction with the miR/miRNP complex. These filtered predicted targets, their gene symbol and description are listed in Table 7.4 and 7.5, in addition to the target prediction algorithms that identified each target, and the ΔG value of the target binding site. ΔG values with a higher free energy that the random free energy value of 13.4 -kcal/mol are indicated (Table 7.4 and Table 7.5).

The use of multiple algorithms aims to increase the specificity of target predictions, by reducing the probability of false positive findings. However a sensitivity-specificity trade off naturally exists in target predictions, and by increasing specificity the sensitivity is also reduced likely resulting in more false negative predictions result. In reality, the false positive and negative rates of these target prediction programmes can only be determined by experimental confirmation of miR targets. A recent study compared the sensitivity of a range of prediction methods, including the three used in this study, based on experimentally validated miR targets held in the TarBase repository (Sethupathy et al. 2006; Sethupathy et al. 2006). miRanda, TargetScan and PicTar all displayed the highest sensitivities of between 65-67% when used alone, predicting between 11,259 -18,289 targets each. The sensitivity of target prediction can be increased by combining all of the targets predicted by each method, however, conversely by solely examining the overlapping targets predicted by each algorithm the specificity can be increased. Indeed as examined by Seuthpathy *et al.,* (2006), by increasing the specificity of target prediction methods the sensitivity of these predictions also decreases, for example by examining overlapping predicted targets by these three algorithms, the target prediction sensitivity is estimated to decrease to approximately 40%. However this strategy in addition to increasing the specificity of targets predicted, also dramatically decreases the number of predicted targets to a more manageable number (Sethupathy et al. 2006). This evidence supports the usefulness of the strategy used in this study, in which the overlaps of miR targets predicted by at least 2 programmes are extracted. While indeed some genuine miR targets may be lost in this process, overall it is extremely beneficial to expedite the experimental validation of miR targets, by first reducing the number of predicted targets requiring analysis and increasing the probability of confirming functional miR:mRNA interactions.

The secondary structure of the target site is additionally important for functional miR:mRNA interactions, as self base-pairing of the mRNA target in and near the target site is thought to impede the binding of relevant miRs (Zhao et al. 2005). Most target prediction methods measure the binding energy involved in the interaction of miR and the mRNA target strand. However, as recently examined by Kertesz *et al.*, (2007), this free energy value is not a reliable predictor of miR target interaction, as these values correlate poorly with miR-mediated target suppression (Kertesz et al. 2007), as this prediction fails to account for the impact of the flanking sequence surrounding the target site. As identified by Zhao *et al.,* (2005), most validated miR targets bind to 3'UTR regions which are accessible to miR interaction, reflected by the free energy and secondary structure of the mRNA target site (Zhao et al. 2005) Consequently, the accessibility of the miR target site was examined in this study, by computing the free energy values, ΔG, of the miR binding site and additional flanking sequences on the target transcript. A free energy value higher than 13.4 -kcal/mol represents the existence of stabilising structures in the flanking regions, thereby decreasing the probability of miR interaction with such sites. In contrast, lower ΔG values contain destabilising structure, suggesting that the structure surrounding the miR target site may by linear and therefore accessible to miR/miRNP complex interaction. The filtering of miR targets with inaccessible miR binding sites should therefore be beneficial, to increase the probability of a miR interaction with the predicted target *in vivo*. The ΔG values corresponding to each miR target are listed in Table 7.4 and 7.5, representative of the lowest ΔG values obtained at either the 5'- or 3'-flanking sequence, of any of the predicted miR target sites on an individual transcript. However, without experimental validation of these targets, the benefit of examining the local structure surrounding miR target sites is unknown. While the ΔG values calculated in this study, examines the local secondary structure surrounding the miR target site (± 70 bp), however secondary structures may also form between the target site and more distant parts of the mRNA, which this algorithm does not take into account.

Additionally, two recent studies, by both Kertesz *et al.,* (2007) and Hammell *et al.*, (2008), suggest that the ability of a miR to interact with the target mRNA depends on two free energy requirements; both the stability of the miR:mRNA duplex ΔG_{duplex}, minus the free energy required to alter the structure at the mRNA target site, ΔG_{open}.

Such that:

$$\Delta\Delta G = \Delta G_{duplex} - \Delta G_{open} \text{ (Kertesz et al. 2007; Hammell et al. 2008)}$$

The resulting reaction should be thermodynamically favourable, i.e. the resulting value termed ΔΔG (Kertesz et al. 2007), should be positive, such that a more stable miR:mRNA duplex should have a higher free energy value than the free energy required to alter the mRNA target secondary structure. Indeed the targets predicted in both of these studies analysing this free energy feature, correlate with validated miR targets (Kertesz et al. 2007; Hammell et al. 2008). The ΔG_{open} value, detailed by these two papers, is equivalent to the ΔG values of predicted target binding sites that were obtained in this study and used for filtering predicted gene targets. In addition, a target prediction algorithm is described by Hammel *et al.,* (2008), termed miRWIP, which includes the analysis of ΔΔG values, in addition to other enriched target features observed in targets co-immunoprecipitated with proteins of the miRNP complex (Hammell et al. 2008). Indeed this target prediction algorithm appears to predict miR targets with a lower false positive and negative rate, to individual predictions by miRanda, PicTar, and TargetScan (Hammell et al. 2008).

In addition both *in silico* and experimental evidence indicate that a single miR is capable of targeting hundreds of mRNAs, while several co-expressed miRs may target a single mRNA (Bartel 2004; Krek et al. 2005; Lim et al. 2005). This suggests that the collective action of multiple miRs, expressed in specific spatio-temporal manners, may define miR regulation. This feature may in principle be exploited to characterise relevant gene targets for miRs that are regulated in a similar fashion, by focusing on targets that possess potential binding sites for at least two different miRs. In this vein overlapping miR targets were predicted for miR-1,-133, -142 and miR-96, -182, -183 using miRanda, due to the similar expression of these two sets of miRs, and filtered for retinal expressed genes. Indeed the co-expression of miR-1 and -133 and miR-96, -182 and -183 appears to result from the co-transcription of these miRs due to the close genomic location of these genes (Table 4.1). MiR-96, -182, and -183 are clustered within 3.8kb of each other in the intergenic region on mouse chr6q, while two sets of miR-1 and -133 genes are co-localised on chromosome 18 and 2, within 2.7kb and 9.4kb of each other respectively. Additionally the seed region of miR-96 versus -182 and -183 versus -96 only differ by 1 nt, while a 2nt difference exists between miR-182 versus -183 (Xu et al. 2007). In contrast the sequences of miR-1 and -133 are dissimilar. While the miR-142 gene is not located in a cluster with miR-1 and -133, it was included in the analysis of overlapping miR targets due to the similar expression pattern of these miRs in RP retinas. Due to the similar expression patterns of these miRs, and sequence similarities, it is likely that their targets overlap and may function in a cooperative manner. *In silico* target analysis

adopting this approach was utilized to generate 'enriched' predicted targets for each set of miRs, representing miR targets predicted to contain binding sites for 2 or more miRs in a given cluster using the miRanda algorithm (Figure 7.1 and Table 7.7 and 7.8). A small number of miR targets were predicted to be targeted by three of the clustered miRs, however in line with the sequence similarities of miR-96, -182, and -183, overlapping targets of two of these miRs accounted for 9.7% of all predicted targets, while 2.2% of predicted targets of miR-1, and -133 were shared by these miRs (Figure 7.1). However, this analysis serves to highlight the identification of genes which may be regulated by more than two miRs. 'Enriched targets' identified in this analysis include proteins with various functions, such as transcriptional regulation, signal transduction, RNA/DNA processing, cytoskeletal components, intracellular trafficking, cell cycle regulation and apoptosis (Table 7.7 and 7.8). The relevance of these targets will be discussed later, however the identification of these 'enriched targets' may be significant for future target validation or functional analysis of these miRs.

The top 50 candidate targets identified for miR-1, -133, -96 and -183 by miRanda prediction (Table 7.1), miR targets identified by three target prediction programmes and ΔG analysis (Table 7.4 and Table 7.5) and 'enriched targets' (Table 7.7 and 7.8) correlate to genes that are, among others, involved in the visual cycle, transmembrane and intracellular signalling, mRNA processing and splicing, RNA-binding proteins, and a number of retinal disease genes. Apoptotic genes potentially targeted by these six miRs, include both positive (*Bnip31*) and negative (*Bcl212*, *Api5, Bcl2*) regulators of apoptosis. Additionally cell cycle regulators are also predicted to be targeted by these miRs, specifically the G1/S-specific cyclin-D1/2 (*Ccnd1* and*Ccnd2)* by miR-1, and the cyclin-dependent kinase activator *Cdk5r1* by miR-183. Indeed the regulation of apoptosis and cell-cycle may have important roles in retinal degeneration. In colorectal cancer cell lines, the expression of miR-133, miR-96 and -183 are altered, and these miRs are therefore implicated in cancer biology, suggestive of tumour suppressor and oncogenic effects (Bandres et al. 2006). Without experimental validation, it is difficult to theorise the overall apoptotic outcomes of altered miR expression in RP. Indeed activation of apoptosis genes and suppression of an apoptosis inhibitor would promote apoptotic death of photoreceptor cells, while the opposite actions are also possible, dependant on the influence of miRs over the regulation of these processes. Notably, the identification of apoptotic regulators as potential targets of these miRs, emphasises the role which may be played by miRs in the regulation of apoptosis (Jovanovic and Hengartner 2006).

A number of ubiquitin proteins are also identified as target, proteins involved primarily in proteasomal degradation. Predicted targets of miR-1 and -133 include the E3 ubiquitin-protein ligases (*Ring1*; *Hace*; *Cbl*) and Ubiquitin-conjugating enzyme E2 (*Ube2h*). Interestingly the genomic location of miR-96, -182, and -183 are located in a 60kb intergenic region between the genes encoding *Ubeh2* and nuclear respiratory factor-1 (*Nrf1*). *Ubeh2* is transcribed in the same direction as that of miR-96-182-183 cluster, and is involved in protein degradation by catalysing the covalent attachment of ubiquitin to proteins for degradation (Ravid and Hochstrasser 2008). The relevance of the similar genomic locations of these miRs and *Ubeh2* is not understood (Xu et al. 2007). Additionally, *Ubeh2* is involved in various cellular functions, such as cell-cycle progression and DNA repair (Ravid and Hochstrasser 2008).

Genes encoding cytoskeletal and intracellular transport proteins are chiefly predicted as targets of miR-1 and of miR-133. These include echinoderm mictotubule associated protein (*Eml4*), map/microtubule affinity-regulating kinase 3 (*Mark3*), vesicle-trafficking protein SEC22b (*Sec22b*), trafficking protein particle complex subunit 3 (*Trappc3*) and kinectin (*Ktn1*). MiR-96, -182, and-183 are predicted to target a range of small Ras-GTPase proteins (*Rab10*; *Rab34*; *Rab6b*; *Rab8b*; *Rab21*; *Rap2a*). *Trappc3* is a component of the TRAPP complex involved in anchoring transport vesicles to the Golgi membrane (Turnbull et al. 2005) while *Ktn1* is a membrane anchor for the motor protein kinesin, which is involved in intracellular membrane trafficking (Jimeno et al. 2006). Intriguingly the kinesin-2 motor protein plays a known role in opsin transport, and additionally a loss of function of the kinesin-2 motor protein, *Kif3a,* results in rapid photoreceptor loss and ectopic accumulation of opsin (Jimeno et al. 2006). A number of the predicted Ras-GTPase targets, are involved in vesicle mediated transport, and specifically *Rab6* and *Rab8* regulate the post-Golgi transport of rhodopsin (Deretic et al. 1995; Shetty et al. 1998). In addition, defects in *Rab6* function in *drosophila*, results in altered rhodopsin transport, precipitating a retinal degeneration (Shetty et al. 1998). The potential involvement of intracellular trafficking proteins being targeted by these six miRs, is in agreement with the suggestion that defective transport of rhodopsin in photoreceptor cells may be a possible precursor to cell death in the P347S (R347) mouse RP model (Li et al. 1996).

Additionally, predicted targets may be involved in retinal remodeling due to photoreceptor cell malfunction and death (Marc et al. 2003). The initial phases of retinal

remodeling occur due to stress and defective photoreceptor function, which results in the sprouting of rod neurites into the inner retina and GCL. Both miR-182 and -96 are predicted to target neuroligin-2 precursor (*Nlgn2*), and miR-96 is predicted to target protein phosphatase 1 (*Ppp1r9b*), which interacts with actin and both Neurabin-2 and Spinophilin (Bommer et al. 2007). These elements modulate glutamatergic synaptic transmission and dendritic spine formation, which may be implicated in retinal remodeling (Feng et al. 2000; Marc et al. 2003). MiR-183 is predicted to target SLIT and NTRK-like family, member 3 (*Slitrk3*), a transmembrane protein expressed in neurons, involved in the regulation of neurite outgrowth (Aruga and Mikoshiba 2003). Additionally in relation to the synaptic function of photoreceptor cells, synaptic proteins are also predicted targets of miR-1, -133 and -142, including sytaxin-12 (*Stx12*), Synaptotagmin-1 (*Syt1*), Syntaxia-1A (*stx1a*), Syntaxin-5 (*Stx5a*) and syntaxin-12 (*Stx12*). The synaptic protein, synaptobrevin II (*Vamp2*), expressed in regenerating adult salamander photoreceptors, is also a predicted target of miR-1 and -133 (Yang et al. 2002). Additional targets predicted in this study include a range of transcription factors, including (*Sox6*; *eIF4a-i*; *Foxc1*; *Otx2*; *Elf1*; and *Elof1*) and translation initiators (*Eif5a*; *Eif4ebp2*; *Eif5*).

Results from previous studies have also validated some of the miR targets predicted in this study. Adenylate cyclase type 6 (*Adcy6*) is an experimentally validated target of both miR-182 and -96 where both miRs compete for overlapping binding sites (Xu et al. 2007). Additionally *Adcy6* is predicted in this study to be targeted by miR-133. The circadian locomoter output cycles protein kaput (*Clock*) is a predicted target of both miR-96 and -182, in agreement with findings by Xu *et al.*, (2008), that the expression of these miRs and miR-183 varied diurnally (Xu et al. 2007). In muscle cells, some of the roles of miR-1 and miR-133 and the targets they regulate have been elucidated. Specifically, miR-1 promotes myogenesis by targeting histone deacetylase 4 (*Hdac4*), while miR-133 promotes myoblast proliferation by suppressing serum response factor expression (*Srf*). Additional targets of these miRs have also been validated, including cell division cycle42 (*Cdc42*); cyclin-dependent kinase9 (*Cdk9*); ether-a-go-go-potassium channel (*ERG*); heart and neural crest derivatives expressed 2 (*Hand2*) and heat-shock protein60 (*HSP60*). The retinal disease genes, ATP binding cassette (Abca4; Abcd1) and crumbs homolog 1 (Crb1), involved in transport and photoreceptor polarisation respectively, are also predicted targets for miR-96 (Table 7.1). Additionally the retinal

disease gene retinol dehydrogenase 10 (*Rdh10)* has recently been validated as a target of the neuronal specific miR-124 (Arora et al. 2007).

In silico target predictions inherently contain a high degree of uncertainty, and recent evidence suggests that perfect base-pairing of the gene in the 5' seed region of the miR, may not be a reliable predictor for miR interaction as endogenous miR *lsy-6* can effectively downregulate its target through interactions with the 3' portion of the miR (Didiano and Hobert 2008). However in this study, two main strategies were employed to reduce the false positive rate of target prediction, namely examining overlapping targets predicted for each miR using varying prediction programs, and additionally the identification of enriched targets that are predicted for >2 miRs that reside in a given cluster. Additionally the requirement of retinal expression of these targets, ensures their biological relevance, thereby reduced the number of false positive predictions. These strategies, while greatly increasing the specificity of target prediction also drastically decreases the number of predicted targets, thereby risking the elimination of some noteworthy targets. However, the reliability of these prediction methods will only become evident with experimental confirmation, which is fast emerging owing to the recent use of genome-wide validation methods (Baek et al. 2008; Selbach et al. 2008). These studies examined alterations in global mRNA and protein profiles resulting from overexpression of individual miRs, simultaneously examining 2000-5000 targets (Baek et al. 2008; Selbach et al. 2008). Interestingly, the findings of these studies identified the percentage of validated targets, downregulated at the protein level, that were predicted by miRanda (47%), TargetScan (61%) and PicTar (61%) (Selbach et al. 2008). The findings of these studies and TarBase information will greatly facilitate the understanding of both the requirements for mRNA target recognition, and elucidation of the roles of miRs.

7.5. Conclusion

The miR target transcript predictions revealed in the present study are useful to highlight the possible miR-dependent regulatory mechanisms that underlie retinal degeneration in RP models. However, further studies and experimental evidence is required to validate the predicted miR target transcripts. Such methods may include the examination of miR:mRNA interactions *in vitro* using a luciferase reporter system containing the 3'UTR of predicted target gene. Determining genuine miR targets is

currently the most fundamental challenge in miR research, and will likely require high-throughput screening and validation techniques in wet-lab experiments. Identification of valid retinal mRNA targets and corresponding cellular pathways, would greatly assist in elucidating the role played by the above six miRs in healthy and diseased retinas. Additionally the overexpression or suppression of particular miRs may prove useful in future drug or gene therapies for such disorders. What is clear is that the field of miR based regulation of gene expression is still in its infancy, and undoubtedly the next few years will reveal interesting findings in relation to the roles of miRs in the mammalian retina.

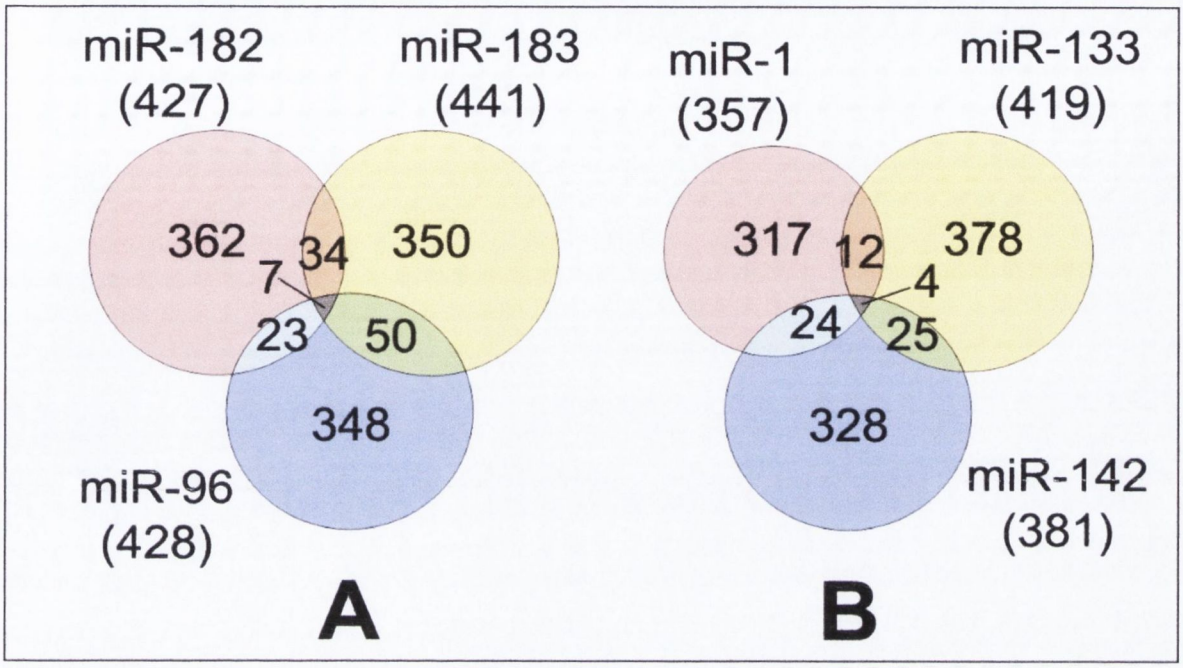

Figure 7.1 : Venn diagrams of miRanda-predicted targets for clustered miRs: Venn diagrams summarise overlapping retinal targets predicted by miRanda for the miR-96-182-183 cluster (**A**) and for the miR-1-133 cluster with miR-142 (**B**).

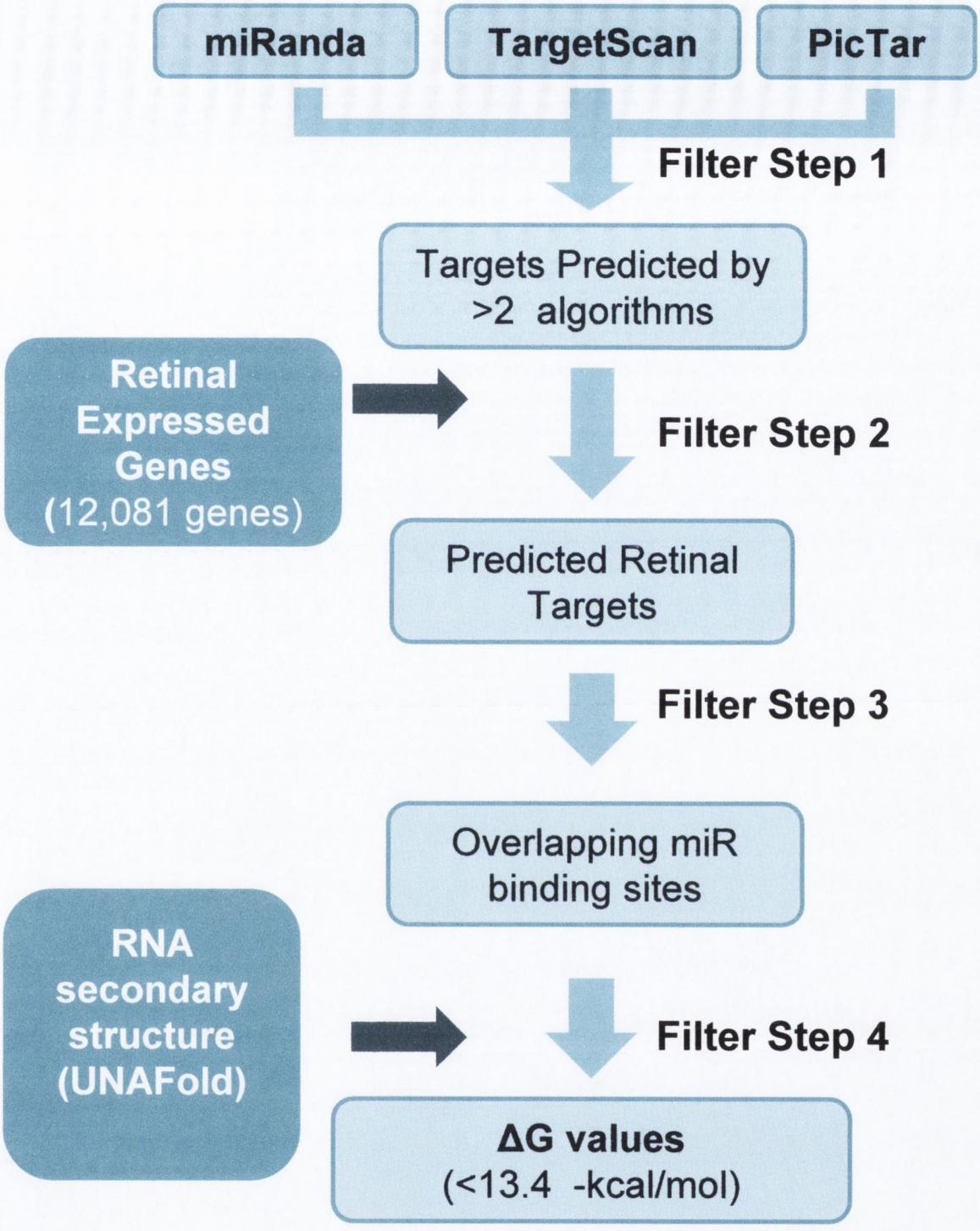

Figure 7.2: Schematic representation of miR target prediction strategy: Putative miR target genes are predicted using three prediction algorithms, and predicted targets are filtered (step 1) for targets predicted by at least 2 prediction models. Putative targets are further filtered (step 2) for genes expressed in the retina, using list of retinal genes obtained from retinal libraries. The filter step 3, eliminates targets if the miR binding site predicted by at least 2 prediction methods, do not overlap. The final filtering step 4 eliminates targets if the local secondary structure of the mRNA is thought to be inaccessible to miR binding, based on free energy values greater than 13.4 –kcal/mol using the software UNAfold.

Table 7.1 Overview of retinal miR target hits predicted by miRanda			
miR	miRanda Total Hits	miRanda Target Genes	Retinal miRanda Target Genes
miR-1	921	760	446
miR-133	1,097	925	592
miR-96	994	857	518
miR-183	1064	902	541

Table 7.1: Overview of retinal miR targets predicted by miRanda: (**column 1**) Total number of target hits predicted for each miR, which includes multiple miR predicted hits on target genes, (**column 2**) total number of predicted genes targeted by miRs, and (**column 3**) filtered target genes expressed in the retina.

Table. 7.2: Potential Retinal Target Transcripts for miR-1, -133, -96 and -183 predicted using miRanda								
miR	Target Gene	Target Gene Description	miRanda Score	P-Orthologous Group Value	Number of Targets/Transcript	Occurrence in Libraries/Lists (1-10)	Eye Diesease Gene	Function
mir-96	*Odf2*	Outer dense fiber of sperm tails 2	19.52	7.50E-04	1	2		
mir-96	*Ndn*	Necdin	18.03	3.26E-03	1	4		transcription factor
mir-96	*Rai12*	Retinoic Acid Induced 12	17.19	2.20E-03	2	2		transcriptional regulation
mir-96	*Crb1*	Crumbs homolog 1 (drosophila)	16.69	4.00E-03	1	5	yes	photoreceptor polarization
mir-96	*Gnb2*	Guanine nucleotide binding protein, beta 2	16.61	4.70E-03	1	6		transmembrane signaling
mir-96	*Stk19*	Serine/threonine kinase 19	16.29	5.15E-05	3	2		nuclear kinase
mir-96	*Asb6*	Ankyrin repeat and SOCS box-containing protein 6	16.10	8.80E-08	2	1		transcription factor
mir-96	*Abca4*	ATP-binding cassette, sub family D (ALD), member 4	15.50	2.60E-02	2	9	yes	visual cycle in photoreceptors
mir-96	*Syt11*	Synaptotagmin XI	15.31	6.81E-06	1	4		synaptic membrane
mir-96	*Abcd1*	ATP-binding cassette, sub family D (ALD), member 1	15.23	1.60E-03	2	2	yes	transporter
mir-96	*Prkar1a*	Protein kinase, cAMP dependent regulatory, type I, alpha	15.07	3.05E-07	1	8	yes	kinase in photoreceptors
mir-183	*Zfp294*	Zinc finger protein 294	18.66	1.40E-03	2	4		
mir-183	*QDRP*	Quinoid dihydropteridine reductase	17.88	8.80E-04	1	6		
mir-183	*Trappc3*	Trafficking protein particle complex 3	17.70	3.50E-07	1	2		vesicular transport
mir-183	*Arhgap21*	Rho GTPase activating protein 21	17.48	1.02E-05	1	4		
mir-183	*Psen2*	Presenilin 2	16.80	3.60E-05	2	1		apoptosis
mir-183	*Nudt4*	Nudix (nucleoside diphospate linked moiety X)- type motif 4	16.52	3.46E-04	1	6		hydrolase
mir-183	*Adck1*	AarF domain containing kinase 1	15.95	4.56E-05	2	2		
mir-183	*Gnb1*	Guanine nucleotide binding protein, beta 1	15.84	3.70E-03	1	8		transmembrane signaling
mir-183	*Pdcd6*	Programmed cell death 6	15.61	2.11E-07	1	4		apoptosis
mir-1	*Ihpk2*	Inositol hexaphosphate kinase 2	19.20	1.67E-08	1	4		kinase
mir-1	*Hnrpu*	Heterogenous nuclear ribonucleoprotein U	18.63	6.37E-05	1	4		pre-mRNA processing
mir-1	*Hspd1*	Chaperone heat shock protein - 1	18.55	3.30E-03	1	6		mitochondrial protein folding
mir-1	*Ktn1*	Kinectin 1	18.15	5.60E-03	1	3		intracellular vesicle transport
mir-1	*Ift140*	Intraflagellar transport 140 homolog	17.63	2.10E-03	2	2		
mir-1	*XRN2*	5'-3' exoribonuclease 2	17.35	7.52E-05	2	2		transcription termination
mir-1	*Wdr61*	WD repeat domain 61	17.03	2.15E-05	1	6		
mir-1	*Hnrpl*	Heterogeneous nuclear ribonucleoprotein L	17.03	1.78E-02	1	6		pre-mRNA processing
mir-1	*Clasp2*	CLIP associating protein 2	16.75	1.99E-03	2	5		cytosceletal polarization
mir-1	*Paics*	Phosphoribosiaminoimidazole carboxylase	16.58	6.79E-05	1	7		IMP biosynthetic process
mir-1	*Auh*	AU RNA binding protein/enoyl-coenzyme A hydratase	16.48	5.29E-05	1	6		RNA binding protein
mir-1	*Clcn3*	Chloride channel 3	16.30	1.82E-09	1	7		ion chanel
mir-1	*Smpd1*	Sphingomyelin phosphodiesterase 1, acid lysosomal	16.29	4.26E-03	1	6	yes	intracellular signaling
mir-1	*Faim*	Fas apoptotic inhibitory molecule	16.26	5.71E-03	1	6		apoptosis
mir-1	*Actr10*	ARP10 actin related protein 10 homologue	16.17	1.96E-05	2	3		cellular motility
mir-1	*Rtbdn*	Retbindin	16.16	4.30E-02	1	7		secreted retina specific
mir-1	*Gngt1*	Guanine nucleotide binding protein (G protein), gamma transducing activity polypeptide 1	16.16	3.36E-03	1	6		transmembrane signaling
mir-1	*Slc25a4*	Solute Carrier family 25, member 4	16.12	1.14E-02	1	7		mitochondrial carrier
mir-1	*Pde6a*	Phosphodiesterase 6A, cGMP-specific, rod, alpha	15.70	3.70E-04	1	6	yes	visual cycle in photoreceptors
mir-1	*Prpf8*	Pre-mRNA processing factor 8	15.54	5.40E-03	1	7	yes	pre-mRNA processing
mir-133	*Odc1*	Ornithine decarboxylase structural - 1	17.62	2.00E-03	2	6		
mir-133	*Elf2*	E74-like factor 2	17.03	9.69E-09	1	4		
mir-133	*Rodgi*	Rodgi homolog (Drosophila)	16.43	4.70E-04	2	6		
mir-133	*Pitpnm1*	Phosphatidylinositol membrane associated 1	16.23	1.10E-02	1	8		visual cycle in photoreceptors
mir-133	*Grina*	Glutamate receptor, ionotropic, N-methyl D-aspartate-associated protein 1	15.54	2.50E-04	1	8		plasmamembrane receptor
mir-133	*Prpf31*	PRP31 pre-mRNA processing factor 31 homolog	15.24	2.29E-04	1	4	yes	pre-mRNA processing
mir-133	*Syf11*	SYF2 homologue RNA splicing factor	15.23	1.18E-05	2	5		mRNA splicing
mir-133	*Myh9*	Myosin, heavy chain 9, non-muscle	15.20	3.80E-05	1	2	yes	cellular motility
mir-133	*Gne*	Glucosamine	14.97	3.69E-03	2	2	yes	sialylation of membrane proteins

Table 7.2: Potential Retinal Target Transcripts for miR-1, -133, -96 and -183 predicted using miRanda: miRanda target prediction was used to generate targets predicted for miR-1, -133, -96 and -183, which were additionally filtered for retinal expressed genes, and p-orthologous group value <0.05. miRanda score reflects the alignment of miR and 3'UTR sequence, a positive score reflecting complementary base pairing.

Table 7.3. Summary of Targets Predicted using miRanda,TargetScan, PicTar and Filtering Steps							
	Prediction Method	**miR-1**	**miR-133**	**miR-142**	**miR-96**	**miR-182**	**miR-183**
1	**miRanda**	783	869	824	881	871	916
2	**TargetScan**	480	351	192	699	672	270
3	**PicTar**	304	238	130	449	408	151
4	**Prediction Overlap (>2)**	248 (38)	199 (37)	113 (22)	360 (52)	321 (49)	140 (30)
5	**Filtered for Retinal Genes**	210 (30)	149 (28)	90 (18)	272 (36)	266 (38)	117 (25)
6	**3'UTR Target Site Overlap**	149 (28)	108 (23)	67 (16)	183 (32)	186 (35)	90 (23)
7	**Filtered by ΔG value**	**123 (26)**	**87 (20)**	**50 (10)**	**151 (29)**	**161 (29)**	**72 (19)**

Table 7.3: Summary of Targets Predicted using miRanda, TargetScan and Pictar Algorithms and the successive filtering steps: (**Row 1-3**) The number of genes predicted as targets by each method are listed for 6 miRs. (**Row 4**) illustrates the overlapping targets predicted by >2 methods, (**Row 5**) lists the number of these overlapping targets also expressed in the retina, (**Row 6**) the targets where the same or overlapping sequence is predicted to be used for miR binding and (**Row 7**) the remaining targets which are thought to be accessible for miR binding based on ΔG analysis. In rows 4-7, the brackets denote the subset of targets predicted by 3 target prediction methods.

Table 7.4. (A) Overlapping Target Predictions for miR-96 using miRanda, TargetScan and PicTar Algorithms

MGI Symbol	Ensembl Gene ID	Description	No. Prediction	Prediction Algorithm (>2)	ΔG (-kcal/mol)
Celsr2	ENSMUSG00000068740	Cadherin EGF LAG seven-pass G-type receptor 2 precursor (Flamingo 1) (mFmi1).	3	miranda|targetscan|pictar	3.0
Tapt1	ENSMUSG00000046985	transmembrane anterior posterior transformation 1	3	miranda|targetscan|pictar	4.0
Sh2d1a	ENSMUSG00000005696	SH2 domain-containing protein 1A (Signaling lymphocytic activation molecule-associated protein)	3	miranda|targetscan|pictar	4.7
Vat1	ENSMUSG00000038429	Ubiquitin carboxyl-terminal hydrolase 5 (Ubiquitin-specific-processing protease 5) (Deubiquitinating enzyme 5)	3	miranda|targetscan|pictar	4.7
Map2k1	ENSMUSG00000004936	Dual specificity mitogen-activated protein kinase kinase 1 (MAP kinase kinase 1) (MAPK/ERK kinase 1) (MEK1).	3	miranda|targetscan|pictar	4.9
Morf4l1	ENSMUSG00000043223	MO4L1_MOUSE Isoform 2 of P60762 - Mus musculus (Mouse)	3	miranda|targetscan|pictar	4.9
Ryk	ENSMUSG00000032547	Tyrosine-protein kinase RYK precursor (Met-related kinase).	3	miranda|targetscan|pictar	5.3
Rnf130	ENSMUSG00000020376	Goliath homolog precursor (RING finger protein 130) (G1-related zinc finger protein).	3	miranda|targetscan|pictar	5.4
Gpc3	ENSMUSG00000055653	Glypican-3 precursor.	3	miranda|targetscan|pictar	7.1
Morf4l2	ENSMUSG00000031422	Mortality factor 4-like protein 2 (MORF-related gene X protein)	3	miranda|targetscan|pictar	7.1
Cugbp2	ENSMUSG00000002107	CUG-BP- and ETR-3-like factor 2 (CELF-2)(Neuroblastoma apoptosis-related RNA-binding protein)	3	miranda|targetscan|pictar	7.2
Klhl7	ENSMUSG00000028986	Kelch-like protein 7.	3	miranda|targetscan|pictar	7.4
Rev1	ENSMUSG00000026082	DNA repair protein REV1 (Rev1-like terminal deoxycytidyl transferase).	3	miranda|targetscan|pictar	7.4
Fyn	ENSMUSG00000019843	Proto-oncogene tyrosine-protein kinase Fyn (p59-Fyn).	3	miranda|targetscan|pictar	7.8
Gpr124	ENSMUSG00000031486	Probable G-protein coupled receptor 124 precursor (Tumor endothelial marker 5).	3	miranda|targetscan|pictar	8.2
Insig2	ENSMUSG00000003721	Insulin-induced gene 2 protein (INSIG-2).	3	miranda|targetscan|pictar	8.4
Uck2	ENSMUSG00000026558	Uridine-cytidine kinase 2 (Uridine monophosphokinase 2) (Cytidine monophosphokinase 2).	3	miranda|targetscan|pictar	8.4
Cnn3	ENSMUSG00000053931	Calponin-3 (Calponin, acidic isoform).	3	miranda|targetscan|pictar	8.5
Tm9sf4	ENSMUSG00000068040	Transmembrane 9 superfamily member 4.	3	miranda|targetscan|pictar	8.8
Yipf4	ENSMUSG00000014932	Proto-oncogene tyrosine-protein kinase Yes (p61-Yes) (c- Yes).	3	miranda|targetscan|pictar	9.6
Hbp1	ENSMUSG00000002996	HMG box-containing protein 1 (High mobility group box transcription factor 1).	3	miranda|targetscan|pictar	10.0
Itpr2	ENSMUSG00000030287	Inositol 1,4,5-trisphosphate receptor type 2 (Type 2 inositol 1,4,5- trisphosphate receptor) (IP3 receptor isoform 2)	3	miranda|targetscan|pictar	10.3

MGI Symbol	Ensembl Gene ID	Description	No. Prediction	Prediction Algorithm (>2)	ΔG (-kcal/mol)
Zhx2	ENSMUSG00000022361	Zinc fingers and homeoboxes protein 1.	3	miranda|targetscan|pictar	10.4
Nlgn2	ENSMUSG00000051790	Neuroligin-2 precursor.	3	miranda|targetscan|pictar	10.7
Ptp4a1	ENSMUSG00000026064	Protein tyrosine phosphatase type IVA protein 1 (Protein-tyrosine phosphatase of regenerating liver 1) (PRL-1).	3	miranda|targetscan|pictar	10.7
Bsdc1	ENSMUSG00000040859	BSD domain-containing protein 1.	3	miranda|targetscan|pictar	11.0
Slc25a1	ENSMUSG00000003528	solute carrier family 25, member 1	3	miranda|targetscan|pictar	11.4
Hbegf	ENSMUSG00000024486	Proheparin-binding EGF-like growth factor precursor	3	miranda|targetscan|pictar	11.9
Ptpn9	ENSMUSG00000032290	Tyrosine-protein phosphatase non-receptor type 9 (Protein-tyrosine phosphatase MEG2)	3	miranda|targetscan|pictar	13.1
Map2k3	ENSMUSG00000018932	Dual specificity mitogen-activated protein kinase kinase 3 (MAP kinase kinase 3) (MAPK/ERK kinase 3).	3	miranda|targetscan|pictar	14.2
Aifm3	ENSMUSG00000022763	Apoptosis-inducing factor 3 (Apoptosis-inducing factor- like protein).	3	miranda|targetscan|pictar	16.0
Tbx1	ENSMUSG00000009097	T-box transcription factor TBX1 (T-box protein 1)	3	miranda|targetscan|pictar	0.0
Cugbp1	ENSMUSG00000005506	CUG-BP- and ETR-3-like factor 1 (CELF-1) (Deadenylation factor CUG-BP) (Deadenylation factor EDEN-BP)	2	pictar|targetscan	-2.4
Nat13	ENSMUSG00000022698	N-acetyltransferase NAT13	2	pictar|targetscan	-2.3
Rac1	ENSMUSG00000001847	Ras-related C3 botulinum toxin substrate 1 precursor (p21-Rac1).	2	pictar|targetscan	0.7
Pcmtd1	ENSMUSG00000051285	Protein-L-isoaspartate O-methyltransferase domain-containing protein 1.	2	pictar|targetscan	2.0
Gad2	ENSMUSG00000026787	Glutamate decarboxylase 2 (Glutamate decarboxylase 65 kDa isoform) (GAD-65)	2	pictar|miranda	2.4
Clic5	ENSMUSG00000023959	Chloride intracellular channel protein 5.	2	pictar|targetscan	3.0
Bcl2	ENSMUSG00000057329	Apoptosis regulator Bcl-2.	2	pictar|targetscan	3.6
Arf4	ENSMUSG00000021877	ADP-ribosylation factor 4.	2	pictar|targetscan	3.7
Pfn1	ENSMUSG00000018293	Profilin-1 (Profilin I).	2	pictar|targetscan	3.8
Fmr1	ENSMUSG00000000838	Fragile X mental retardation protein 1 homolog (FMRP)	2	pictar|targetscan	3.9
Fnta	ENSMUSG00000015994	Protein farnesyltransferase/geranylgeranyltransferase type-1 subunit alpha	2	pictar|targetscan	3.9
Add3	ENSMUSG00000025026	Gamma-adducin (Adducin-like protein 70);Fibroblast growth factor-inducible protein 14 (FIN14).	2	pictar|targetscan	4.1
Amotl2	ENSMUSG00000032531	Angiomotin-like protein 2.	2	pictar|targetscan	4.4
Grb2	ENSMUSG00000059923	Growth factor receptor-bound protein 2 (Adapter protein GRB2);Mortality factor 4-like protein 1 (MORF-related gene 15 protein)	2	pictar|targetscan	4.4
Olfr78	ENSMUSG00000043366	olfactory receptor 78	2	pictar|miranda	4.6
Ebf3	ENSMUSG00000010476	Transcription factor COE3 (Early B-cell factor 3) (EBF-3) (Olf-1/EBF- like 2)	2	pictar|targetscan	4.7

MGI Symbol	Ensembl Gene ID	Description	No. Prediction	Prediction Algorithm (>2)	ΔG (-kcal/mol)
Pcnx	ENSMUSG00000021140	Pecanex-like protein 1 (Pecanex homolog).	2	pictar|targetscan	4.8
Gpr22	ENSMUSG00000044067	Probable G-protein coupled receptor 22.	2	pictar|targetscan	4.9
Axud1	ENSMUSG00000032515	Axin-1 up-regulated gene 1 protein (TGF-beta-induced apoptosis protein 3) (TAIP-3).	2	pictar|targetscan	5.2
Frs2	ENSMUSG00000020170	Fibroblast growth factor receptor substrate 2 (FGFR substrate 2) (FGFR-signaling adaptor SNT) (FRS2 alpha).	2	pictar|targetscan	5.2
Aebp2	ENSMUSG00000030232	AE binding protein 2 isoform 3	2	pictar|targetscan	5.3
Dcun1d3	ENSMUSG00000048787	DCN1, defective in cullin neddylation 1, domain containing 3	2	pictar|targetscan	5.4
Tmem50b	ENSMUSG00000022964	Transmembrane protein 50B.	2	pictar|targetscan	5.4
Col9a1	ENSMUSG00000026147	Collagen alpha-1(IX) chain precursor.	2	pictar|targetscan	5.6
Eif5	ENSMUSG00000021282	Eukaryotic translation initiation factor 5 (eIF-5).	2	pictar|targetscan	5.6
Tpm1	ENSMUSG00000032366	Tropomyosin alpha-1 chain (Tropomyosin-1)	2	pictar|targetscan	5.9
Itpr1	ENSMUSG00000030102	Inositol 1,4,5-trisphosphate receptor type 1	2	pictar|targetscan	6.0
Mtm1	ENSMUSG00000031337	Myotubularin (EC 3.1.3.48).	2	pictar|targetscan	6.1
Zdhhc5	ENSMUSG00000061410	Zinc finger CCHC domain-containing protein 14 (BDG-29).	2	pictar|targetscan	6.1
Slc43a2	ENSMUSG00000038178	Large neutral amino acids transporter small subunit 4; Antisense product of high-affinity glutamate transporter EAAC1 and EAAC2.	2	pictar|targetscan	6.3
Stard7	ENSMUSG00000027367	StAR-related lipid transfer protein 7 (StARD7) (START domain- containing protein 7).	2	pictar|targetscan	6.4
Txndc1	ENSMUSG00000021072	Thioredoxin domain-containing protein 1 precursor.	2	targetscan|miranda	6.4
A130010J15Rik	ENSMUSG00000026638	Interferon regulatory factor 6 (IRF-6).	2	pictar|miranda	6.5
Snap23	ENSMUSG00000027287	Synaptosomal-associated protein 23 (SNAP-23) (Vesicle-membrane fusion protein SNAP-23) (Syndet).	2	pictar|targetscan	6.5
Chst10	ENSMUSG00000026080	Carbohydrate sulfotransferase 10 (HNK-1 sulfotransferase) (HNK1ST) (HNK-1ST).	2	pictar|targetscan	6.7
Dcx	ENSMUSG00000031285	Neuronal migration protein doublecortin (Lissencephalin-X) (Lis-X)	2	pictar|targetscan	6.7
Snx13	ENSMUSG00000020590	Sorting nexin-13.	2	pictar|targetscan	6.7
Elmo1	ENSMUSG00000041112	Engulfment and cell motility protein 1 (CED-12 homolog).	2	pictar|targetscan	6.8
Kpna3	ENSMUSG00000021929	Importin subunit alpha-3 (Karyopherin subunit alpha-3)	2	pictar|targetscan	6.8
Ep300	ENSMUSG00000055024	E1A binding protein p300	2	pictar|targetscan	7.0
Prkar1a	ENSMUSG00000020612	cAMP-dependent protein kinase type I-alpha regulatory subunit.	2	pictar|targetscan	7.1
Mef2c	ENSMUSG00000005583	MEF2C_MOUSE Isoform 4 of Q8CFN5	2	pictar|targetscan	7.2
Pbx2	ENSMUSG00000034673	Pre-B-cell leukemia transcription factor 2 (Homeobox protein PBX2).	2	pictar|targetscan	7.3
Zfand5	ENSMUSG00000034075	Probable palmitoyltransferase ZDHHC5 (Zinc finger DHHC domain-containing protein 5) (DHHC-5).	2	pictar|targetscan	7.3

MGI Symbol	Ensembl Gene ID	Description	No. Prediction	Prediction Algorithm (>2)	ΔG (-kcal/mol)
Zic3	ENSMUSG00000071757	Zinc finger and homeodomain protein 2	2	pictar|targetscan	7.3
Ccdc131	ENSMUSG00000034163	proline/serine-rich coiled-coil 2	2	pictar|targetscan	7.4
Rabgap1	ENSMUSG00000035437	Rab GTPase-activating protein 1 (GAP and centrosome-associated protein).	2	pictar|targetscan	7.6
Cbln4	ENSMUSG00000067578	Cerebellin-4 precursor (Cerebellin-like glycoprotein 1).	2	pictar|targetscan	7.7
Zfp36l1	ENSMUSG00000025255	Zinc finger homeobox protein 4 (Zinc finger homeodomain protein 4) (ZFH-4).	2	pictar|targetscan	7.7
Elavl2	ENSMUSG00000008489	ELAV-like protein 2 (ELAV-like neuronal protein 1)	2	pictar|targetscan	7.9
Rraga	ENSMUSG00000070934	Ras-related GTP-binding protein A (Rag A).	2	pictar|targetscan	8.0
Stc1	ENSMUSG00000014813	Stanniocalcin-1 precursor (STC-1).	2	pictar|targetscan	8.0
Tox	ENSMUSG00000041272	Thymus high mobility group box protein TOX.	2	pictar|targetscan	8.0
Kcnj14	ENSMUSG00000058743	ATP-sensitive inward rectifier potassium channel 14	2	pictar|targetscan	8.1
Rab6b	ENSMUSG00000032549	Ras-related protein Rab-6B.	2	pictar|targetscan	8.1
Tmsb10	ENSMUSG00000079523	Thymosin beta-10.	2	pictar|targetscan	8.2
Cacna2d2	ENSMUSG00000010066	Voltage-dependent calcium channel subunit alpha-2/delta-2 precursor	2	pictar|targetscan	8.3
Gnaq	ENSMUSG00000024639	Guanine nucleotide-binding protein G(q) subunit alpha (Guanine nucleotide-binding protein alpha-q).	2	pictar|targetscan	8.3
Ash1l	ENSMUSG00000028053	Probable histone-lysine N-methyltransferase ASH1L (ASH1- like protein) (Absent small and homeotic disks protein 1 homolog).	2	pictar|targetscan	8.4
Acvr2a	ENSMUSG00000052155	Activin receptor type-2A precursor (Activin receptor type IIA) (ACTR-IIA).	2	pictar|targetscan	8.5
Rftn1	ENSMUSG00000039316	Raftlin (Raft-linking protein).	2	pictar|targetscan	8.5
Dlat	ENSMUSG00000000168	Dihydrolipoamide acetyltransferase component of pyruvate dehydrogenase complex , mitochondrial precursor (PDC-E2).	2	pictar|targetscan	8.8
Slc1a1	ENSMUSG00000024935	Excitatory amino acid transporter 3(Sodium-dependent glutamate/aspartate transporter 3)	2	pictar|targetscan	8.8
Ddx3x	ENSMUSG00000000787	ATP-dependent RNA helicase DDX3X (EC 3.6.1.-) (DEAD box protein 3, X-chromosomal) (DEAD box RNA helicase DEAD3) (mDEAD3	2	pictar|targetscan	8.9
Gria1	ENSMUSG00000020524	Glutamate receptor 1 precursor (GluR-1) (Glutamate receptor ionotropic, AMPA 1)	2	pictar|miranda	8.9
Gnai3	ENSMUSG00000000001	Guanine nucleotide-binding protein G(k) subunit alpha (G(i) alpha-3).	2	pictar|targetscan	9.1
Snx4	ENSMUSG00000022808	Sorting nexin-4.	2	pictar|targetscan	9.1
Stk35	ENSMUSG00000037885	Serine/threonine-protein kinase 35	2	pictar|targetscan	9.1
Rab8b	ENSMUSG00000036943	Ras-related protein Rab-8B.	2	pictar|targetscan	9.2
Snx16	ENSMUSG00000027534	Sorting nexin-16.	2	pictar|targetscan	9.2
Irs1	ENSMUSG00000055980	Insulin receptor substrate 1 (IRS-1).	2	pictar|targetscan	9.3

MGI Symbol	Ensembl Gene ID	Description	No. Prediction	Prediction Algorithm (>2)	ΔG (-kcal/mol)
Phf20l1	ENSMUSG00000072501	PHD finger protein 20-like 1	2	targetscan|miranda	9.3
Acvr1	ENSMUSG00000026836	Activin receptor type-1 precursor (ACTR-I) (Serine/threonine-protein kinase receptor R1) (SKR1) (TGF-B superfamily receptor type I)	2	pictar|targetscan	9.4
Atg9a	ENSMUSG00000033124	autophagy-related 9-like 1	2	pictar|targetscan	9.5
Lcp1	ENSMUSG00000021998	Plastin-2 (L-plastin) (Lymphocyte cytosolic protein 1) (LCP-1)	2	pictar|targetscan	9.5
Sox6	ENSMUSG00000051910	Transcription factor SOX-6 (SOX-LZ).	2	pictar|targetscan	9.5
Creb1	ENSMUSG00000025958	cAMP response element-binding protein (CREB).	2	pictar|targetscan	9.6
Capns1	ENSMUSG00000001794	Calcium-dependent protease small subunit 1 (CDPS) (Calpain regulatory subunit)	2	targetscan|miranda	9.8
Spin1	ENSMUSG00000021395	Spindlin-1 (SSEC P).	2	pictar|targetscan	9.8
Efnb2	ENSMUSG00000001300	Ephrin-B2 precursor (EPH-related receptor tyrosine kinase ligand 5) (HTK-L) (ELF-2).	2	pictar|targetscan	10.1
Phyhipl	ENSMUSG00000037747	phytanoyl-CoA hydroxylase interacting protein-like	2	pictar|targetscan	10.1
Yes1	ENSMUSG00000040389	WD repeat-containing protein 47.	2	pictar|targetscan	10.2
Zcchc14	ENSMUSG00000024072	Protein YIPF4 (YIP1 family member 4).	2	pictar|targetscan	10.2
Prrt3	ENSMUSG00000045009	Proline-rich transmembrane protein 3 precursor.	2	targetscan|miranda	10.3
Denr	ENSMUSG00000023106	Density-regulated protein (DRP).	2	pictar|targetscan	10.4
Sh3kbp1	ENSMUSG00000040990	SH3 domain-containing kinase-binding protein 1 (SH3-containing, expressed in tumorigenic astrocytes)	2	targetscan|miranda	10.5
Srpk1	ENSMUSG00000004865	Serine/threonine-protein kinase SRPK1 (Serine/arginine- rich protein-specific kinase 1)	2	pictar|targetscan	10.5
Dazap2	ENSMUSG00000000346	DAZ-associated protein 2 (Deleted in azoospermia-associated protein 2) (Proline-rich protein expressed in brain).	2	pictar|targetscan	10.6
Slco3a1	ENSMUSG00000025790	Solute carrier organic anion transporter family member 3A1 (Sodium-independent organic anion transporter D)	2	pictar|targetscan	10.6
Rab10	ENSMUSG00000020671	Ras-related protein Rab-10.	2	pictar|targetscan	10.7
Pafah1b1	ENSMUSG00000020745	Platelet-activating factor acetylhydrolase IB subunit alpha	2	pictar|targetscan	10.8
Rdx	ENSMUSG00000032050	Radixin (ESP10).	2	pictar|targetscan	10.8
Usp5	ENSMUSG00000053664	Uck2 protein (Fragment).	2	pictar|targetscan	10.8
Zhx1	ENSMUSG00000021127	Butyrate response factor 1 (Protein TIS11B).	2	pictar|targetscan	10.8
Kctd7	ENSMUSG00000034110	BTB/POZ domain-containing protein KCTD7.	2	pictar|targetscan	10.9
Slc7a8	ENSMUSG00000022180	Large neutral amino acids transporter small subunit 2 (L-type amino acid transporter 2)	2	pictar|targetscan	11.0
Isl1	ENSMUSG00000042258	Insulin gene enhancer protein ISL-1 (Islet-1).	2	pictar|targetscan	11.3
Ncald	ENSMUSG00000051359	Neurocalcin-delta.	2	pictar|targetscan	11.3

MGI Symbol	Ensembl Gene ID	Description	No. Prediction	Prediction Algorithm (>2)	ΔG (-kcal/mol)
Nhlh2	ENSMUSG00000048540	Helix-loop-helix protein 2 (HEN2) (Nescient helix loop helix 2) (NSCL- 2).	2	pictar|targetscan	11.4
Tmem127	ENSMUSG00000034850	Transmembrane protein 127.	2	pictar|targetscan	11.5
Cd164	ENSMUSG00000019818	CD164 antigen	2	pictar|targetscan	11.7
Sort1	ENSMUSG00000068747	Sortilin precursor (Neurotensin receptor 3) (NTR3)	2	pictar|targetscan	11.8
Lass2	ENSMUSG00000015714	LAG1 longevity assurance homolog 2 (Translocating chain-associating membrane protein homolog 3) (TRAM homolog 3).	2	pictar|targetscan	11.9
Oxr1	ENSMUSG00000022307	Oxidation resistance protein 1 (Protein C7).	2	pictar|targetscan	11.9
Tbr1	ENSMUSG00000035033	T-brain-1 protein (T-box brain protein 1) (TBR-1)	2	pictar|miranda	12.0
Cfl1	ENSMUSG00000056201	Cofilin-1 (Cofilin, non-muscle isoform).	2	pictar|targetscan	12.1
Rgs2	ENSMUSG00000026360	Regulator of G-protein signaling 2 (RGS2).	2	pictar|targetscan	12.3
Atg16l1	ENSMUSG00000026289	Autophagy-related protein 16-1 (APG16-like 1).	2	pictar|targetscan	12.4
Ccdc92	ENSMUSG00000037979	Coiled-coil domain-containing protein 92.	2	pictar|targetscan	12.4
Slc35c1	ENSMUSG00000049922	GDP-fucose transporter 1 isoform 2	2	pictar|targetscan	12.4
Smad1	ENSMUSG00000031681	Mothers against decapentaplegic homolog 1 (SMAD 1) (Mad-related protein 1)	2	pictar|targetscan	12.4
Wdr47	ENSMUSG00000034993	Synaptic vesicle membrane protein VAT-1 homolog	2	pictar|targetscan	12.4
Tbc1d22a	ENSMUSG00000051864	TBC1 domain family member 22A.	2	pictar|targetscan	12.5
Kpnb1	ENSMUSG00000001440	Importin subunit beta-1 (Karyopherin subunit beta-1) (Nuclear factor P97)	2	pictar|targetscan	12.6
Pappa	ENSMUSG00000028370	Pappalysin-1 precursor (EC 3.4.24.79) (Insulin-like growth factor-dependent IGF-binding protein 4 protease) (IGF-dependent IGFBP-4 protease)	2	pictar|targetscan	12.8
Ppp1r12c	ENSMUSG00000019254	Protein phosphatase 1 regulatory subunit 12C (Protein phosphatase 1 myosin-binding subunit of 85 kDa)	2	targetscan|miranda	12.8
Prkacb	ENSMUSG00000005034	cAMP-dependent protein kinase, beta-catalytic subunit (PKA C-beta).	2	pictar|targetscan	12.8
Gpr137	ENSMUSG00000024958	Integral membrane protein GPR137 (Transmembrane 7 superfamily member 1-like 1 protein).	2	pictar|miranda	12.9
Cav1	ENSMUSG00000007655	Caveolin-1.	2	pictar|targetscan	13.0
Slc6a6	ENSMUSG00000030096	Sodium- and chloride-dependent taurine and beta-alanine transporter.	2	pictar|targetscan	13.1
Gga2	ENSMUSG00000030872	ADP-ribosylation factor-binding protein GGA2 (Golgi-localized, gamma ear-containing, ARF-binding protein 2)	2	pictar|targetscan	13.2
Evi5	ENSMUSG00000011831	Ecotropic viral integration site 5 protein (EVI-5).	2	pictar|targetscan	13.4
Clock	ENSMUSG00000029238	Circadian locomoter output cycles protein kaput (mCLOCK).	2	pictar|targetscan	14.0
Jazf1	ENSMUSG00000063568	Juxtaposed with another zinc finger protein 1.	2	pictar|targetscan	14.0
Clptm1l	ENSMUSG00000021610	CLPTM1-like	2	pictar|targetscan	14.1

MGI Symbol	Ensembl Gene ID	Description	No. Prediction	Prediction Algorithm (>2)	ΔG (-kcal/mol)
Brpf3	ENSMUSG00000063952	bromodomain and PHD finger containing, 3	2	targetscan|miranda	14.4
Dbc1	ENSMUSG00000028351	Deleted in bladder cancer protein 1 homolog precursor (Protein FAM5A) (BMP/retinoic acid-inducible neural-specific protein 1).	2	pictar|miranda	14.4
Nap1l1	ENSMUSG00000058799	Nucleosome assembly protein 1-like 1 (NAP-1-related protein) (Brain protein DN38).	2	pictar|targetscan	14.4
Plcb4	ENSMUSG00000039943	phospholipase C beta 4	2	targetscan|miranda	14.4
Zfhx4	ENSMUSG00000024750	AN1-type zinc finger protein 5 (Zinc finger A20 domain-containing protein 2)	2	pictar|targetscan	14.4
Map3k7ip3	ENSMUSG00000035476	Mitogen-activated protein kinase kinase kinase 7-interacting protein 3 (TAK1-binding protein 3).	2	pictar|targetscan	14.5
Dhcr24	ENSMUSG00000034926	24-dehydrocholesterol reductase precursor	2	targetscan|miranda	14.6
Esrrg	ENSMUSG00000026610	Estrogen-related receptor gamma (Estrogen receptor-related protein 3)	2	pictar|targetscan	14.8
Smek1	ENSMUSG00000041846	SMEK homolog 1.	2	pictar|targetscan	15.0
Azin1	ENSMUSG00000037458	Antizyme inhibitor 1 (AZI) (Ornithine decarboxylase antizyme inhibitor).	2	pictar|targetscan	15.2
Sh3bgrl3	ENSMUSG00000028843	SH3 domain-binding glutamic acid-rich-like protein 3.	2	pictar|targetscan	16.4
Rab34	ENSMUSG00000002059	Ras-related protein Rab-34 (Ras-related protein Rah)	2	pictar|targetscan	16.9
Rnf208	ENSMUSG00000044628	RING finger protein 208.	2	pictar|targetscan	16.9
Foxk2	ENSMUSG00000039275	Forkhead box protein K2 (Interleukin enhancer-binding factor 1) (Cellular transcription factor ILF-1).	2	targetscan|miranda	17.0
Eif4ebp2	ENSMUSG00000020091	Eukaryotic translation initiation factor 4E-binding protein 2 (4E-BP2) (eIF4E-binding protein 2)	2	pictar|targetscan	17.4
Flot1	ENSMUSG00000059714	Flotillin-1.	2	pictar|targetscan	17.6
Rab35	ENSMUSG00000029518	Ras-related protein Rab-35.	2	pictar|targetscan	17.7
Creb3l2	ENSMUSG00000038648	cAMP responsive element-binding protein 3-like protein 2	2	pictar|targetscan	18.1
Derl2	ENSMUSG00000018442	Derlin-2 (Degradation in endoplasmic reticulum protein 2) (Der1-like protein 2) (F-LANa).	2	pictar|targetscan	18.1
Scyl3	ENSMUSG00000026584	Protein-associating with the carboxyl-terminal domain of ezrin (Ezrin- binding protein PACE-1)	2	pictar|targetscan	18.3
Ctdsp1	ENSMUSG00000026176	Carboxy-terminal domain RNA polymerase II polypeptide A small phosphatase 1 (Golli-interacting protein) (GIP).	2	pictar|targetscan	19.0
Ldb1	ENSMUSG00000025223	LIM domain-binding protein 1 (Nuclear LIM interactor) (Carboxyl- terminal LIM domain-binding protein 2) (CLIM-2).	2	targetscan|miranda	19.6
Slc12a6	ENSMUSG00000027130	Solute carrier family 12 member 6 (K-Cl cotransporter 3).	2	pictar|targetscan	21.3
Ppp1r9b	ENSMUSG00000038976	Neurabin-2 (Neurabin-II) (Spinophilin)	2	pictar|targetscan	22.0
Tspan9	ENSMUSG00000030352	Tetraspanin-9 (Tspan-9)	2	pictar|targetscan	27.5

Table 7.4 (B) Overlapping Target Predictions for miR-182 using miRanda, TargetScan and PicTar Algorithms

MGI Symbol	Ensembl Gene ID	Description	No. Prediction	Prediction Algorithm (>2)	ΔG (-kcal/mol)
Rac1	ENSMUSG00000001847	Ras-related C3 botulinum toxin substrate 1 precursor (p21-Rac1).	3	miranda|targetscan|pictar	0.7
Snap23	ENSMUSG00000027287	Synaptosomal-associated protein 23 (SNAP-23) (Vesicle-membrane fusion protein SNAP-23) (Syndet).	3	miranda|targetscan|pictar	2.5
Flot1	ENSMUSG00000059714	Flotillin-1.	3	miranda|targetscan|pictar	3.3
Tob1	ENSMUSG00000037573	Protein Tob1 (Transducer of erbB-2 1).	3	miranda|targetscan|pictar	3.4
Sh2d1a	ENSMUSG00000005696	Signaling lymphocytic activation molecule-associated protein (SLAM-associated protein)	3	miranda|targetscan|pictar	3.6
Arf4	ENSMUSG00000021877	ADP-ribosylation factor 4.	3	miranda|targetscan|pictar	3.7
Fmr1	ENSMUSG00000000838	Fragile X mental retardation protein 1 homolog (FMRP).	3	miranda|targetscan|pictar	3.9
Isl1	ENSMUSG00000042258	Insulin gene enhancer protein ISL-1 (Islet-1).	3	miranda|targetscan|pictar	4.4
Ccdc131	ENSMUSG00000034163	proline/serine-rich coiled-coil 2	3	miranda|targetscan|pictar	4.5
Khdrbs3	ENSMUSG00000022332	RNA-binding, signal transduction-associated protein 3 (Sam68-like mammalian protein 2)	3	miranda|targetscan|pictar	5.1
Mark3	ENSMUSG00000007411	MAP/microtubule affinity-regulating kinase 3 (MPK-10)	3	miranda|targetscan|pictar	5.8
Kcmf1	ENSMUSG00000055239	potassium channel modulatory factor DEBT-91	3	miranda|targetscan|pictar	6.3
Jazf1	ENSMUSG00000063568	Juxtaposed with another zinc finger protein 1.	3	miranda|targetscan|pictar	6.5
Sh3bp4	ENSMUSG00000036206	SH3 domain-binding protein 4.	3	miranda|targetscan|pictar	6.7
Prdm1	ENSMUSG00000038151	PR domain zinc finger protein 1 (PR domain-containing protein 1)	3	miranda|targetscan|pictar	7.2
Ppil1	ENSMUSG00000024007	Peptidyl-prolyl cis-trans isomerase-like 1 (Rotamase).	3	miranda|targetscan|pictar	7.3
Ppp1r2	ENSMUSG00000047714	Protein phosphatase inhibitor 2 (IPP-2).	3	miranda|targetscan|pictar	7.5
Rnf130	ENSMUSG00000020376	Goliath homolog precursor (RING finger protein 130) (G1-related zinc finger protein).	3	miranda|targetscan|pictar	7.5
Rtn4	ENSMUSG00000020458	Reticulon-4 (Neurite outgrowth inhibitor) (Nogo protein).	3	miranda|targetscan|pictar	7.5
Slc25a1	ENSMUSG00000003528	solute carrier family 25, member 1	3	miranda|targetscan|pictar	8.5
Spin1	ENSMUSG00000021395	Spindlin-1 (30000 Mr metaphase complex) (SSEC P).	3	miranda|targetscan|pictar	9.8
Atp1b3	ENSMUSG00000032412	Sodium/potassium- dependent ATPase subunit beta-3 (ATPB-3)	3	miranda|targetscan|pictar	10.2
Ank3	ENSMUSG00000069601	ankyrin 3, epithelial isoform i	3	miranda|targetscan|pictar	10.4
Dazap2	ENSMUSG00000000346	DAZ-associated protein 2 (Deleted in azoospermia-associated protein 2)	3	miranda|targetscan|pictar	10.6
Paip2	ENSMUSG00000037058	Poly(A)-binding protein-interacting protein 2 (PABP-interacting protein 2)	3	miranda|targetscan|pictar	11.4
Wdr47	ENSMUSG00000040389	WD repeat-containing protein 47.	3	miranda|targetscan|pictar	11.5
Marcks	ENSMUSG00000069662	Myristoylated alanine-rich C-kinase substrate (MARCKS).	3	miranda|targetscan|pictar	11.6
Zfp36	ENSMUSG00000044786	Tristetraproline (TTP) (Zinc finger protein 36) (Growth factor-inducible nuclear protein NUP475)	3	miranda|targetscan|pictar	12.0
Tsnax	ENSMUSG00000047323	Translin-associated protein X (Translin-associated factor X).	3	miranda|targetscan|pictar	12.4
Evi5	ENSMUSG00000011831	Ecotropic viral integration site 5 protein (EVI-5).	3	miranda|targetscan|pictar	13.4
Clptm1l	ENSMUSG00000021610	CLPTM1-like	3	miranda|targetscan|pictar	14.1

MGI Symbol	Ensembl Gene ID	Description	No. Prediction	Prediction Algorithm (>2)	ΔG (-kcal/mol)
Ktn1	ENSMUSG00000021843	Kinectin.	3	miranda|targetscan|pictar	14.4
Lsm14a	ENSMUSG00000066568	LSM14 protein homolog A (Protein FAM61A).	3	miranda|targetscan|pictar	14.4
Rnf208	ENSMUSG00000044628	RING finger protein 208.	3	miranda|targetscan|pictar	14.9
Ctdsp1	ENSMUSG00000026176	Carboxy-terminal domain RNA polymerase II polypeptide A small phosphatase 1	3	miranda|targetscan|pictar	19.0
Xpr1	ENSMUSG00000026469	xenotropic and polytropic retrovirus receptor 1	2	pictar|targetscan	1.5
Pcmtd1	ENSMUSG00000051285	Protein-L-isoaspartate O-methyltransferase domain-containing protein 1.	2	pictar|targetscan	2.0
Cugbp1	ENSMUSG00000005506	CUG-BP- and ETR-3-like factor 1 (CELF-1) (Deadenylation factor CUG-BP)	2	pictar|targetscan	2.4
Clic5	ENSMUSG00000023959	Chloride intracellular channel protein 5.	2	pictar|targetscan	3.0
Frs2	ENSMUSG00000020170	Fibroblast growth factor receptor substrate 2 (FGFR substrate 2) (FGFR-signaling adaptor SNT)	2	pictar|targetscan	3.5
Bcl2	ENSMUSG00000057329	Apoptosis regulator Bcl-2.	2	pictar|targetscan	3.6
Pfn1	ENSMUSG00000018293	Profilin-1 (Profilin I).	2	pictar|targetscan	3.8
Fnta	ENSMUSG00000015994	Protein farnesyltransferase/geranylgeranyltransferase type-1 subunit alpha	2	pictar|targetscan	3.9
Tapt1	ENSMUSG00000046985	transmembrane anterior posterior transformation 1	2	pictar|targetscan	4.0
Add3	ENSMUSG00000025026	Gamma-adducin (Adducin-like protein 70).	2	pictar|targetscan	4.1
Amotl2	ENSMUSG00000032531	Angiomotin-like protein 2.	2	pictar|targetscan	4.4
Grb2	ENSMUSG00000059923	Growth factor receptor-bound protein 2 (SH2/SH3 adapter GRB2).	2	pictar|targetscan	4.4
Vat1	ENSMUSG00000034993	Synaptic vesicle membrane protein VAT-1 homolog	2	pictar|targetscan	4.7
Pcnx	ENSMUSG00000021140	Pecanex-like protein 1 (Pecanex homolog).	2	pictar|targetscan	4.8
Gpr22	ENSMUSG00000044067	Probable G-protein coupled receptor 22.	2	pictar|targetscan	4.9
Morf4l1	ENSMUSG00000043223	MO4L1_MOUSE Isoform 2 of P60762	2	pictar|targetscan	4.9
Chst10	ENSMUSG00000026080	Carbohydrate sulfotransferase 10 (HNK-1 sulfotransferase) (HNK1ST)	2	pictar|targetscan	5.0
Aebp2	ENSMUSG00000030232	AE binding protein 2 isoform 3	2	pictar|targetscan	5.3
Dcun1d3	ENSMUSG00000048787	DCN1, defective in cullin neddylation 1, domain containing 3	2	pictar|targetscan	5.4
Ebf3	ENSMUSG00000010476	Transcription factor COE3 (Early B-cell factor 3) (EBF-3)	2	pictar|targetscan	5.4
Tmem50b	ENSMUSG00000022964	Transmembrane protein 50B.	2	pictar|targetscan	5.4
Eif5	ENSMUSG00000021282	Eukaryotic translation initiation factor 5 (eIF-5).	2	pictar|targetscan	5.6
Mapk9	ENSMUSG00000020366	Mitogen-activated protein kinase 9 (Stress-activated protein kinase JNK2)	2	pictar|targetscan	5.9
Itpr1	ENSMUSG00000030102	Inositol 1,4,5-trisphosphate receptor type 1	2	pictar|targetscan	6.0
Mtm1	ENSMUSG00000031337	Myotubularin (EC 3.1.3.48).	2	pictar|targetscan	6.1
Zdhhc5	ENSMUSG00000034075	Probable palmitoyltransferase ZDHHC5 (Zinc finger DHHC domain-containing protein 5)	2	pictar|targetscan	6.1
Vps26b	ENSMUSG00000031988	Vacuolar protein sorting-associated protein 26B (Vesicle protein sorting 26B)	2	pictar|targetscan	6.2
Rasa1	ENSMUSG00000021549	RAS p21 protein activator 1	2	targetscan|miranda	6.3
Slc43a2	ENSMUSG00000038178	Large neutral amino acids transporter small subunit 4 (L-type amino L- acid transporter 4)	2	pictar|targetscan	6.3
Prpf4b	ENSMUSG00000021413	Serine/threonine-protein kinase PRP4 homolog (PRP4 pre- mRNA-processing factor 4 homolog)	2	pictar|targetscan	6.5

MGI Symbol	Ensembl Gene ID	Description	No. Prediction	Prediction Algorithm (>2)	ΔG (-kcal/mol)
Dcx	ENSMUSG00000031285	Neuronal migration protein doublecortin (Lissencephalin-X)	2	pictar|targetscan	6.7
Klhl7	ENSMUSG00000028986	Kelch-like protein 7.	2	pictar|targetscan	6.7
Snx13	ENSMUSG00000020590	Sorting nexin-13.	2	pictar|targetscan	6.7
Csnk1e	ENSMUSG00000022433	Casein kinase I isoform epsilon (EC 2.7.11.1) (CKI-epsilon) (CKIe).	2	pictar|targetscan	6.8
Elmo1	ENSMUSG00000041112	Engulfment and cell motility protein 1 (CED-12 homolog).	2	pictar|targetscan	6.8
Kpna3	ENSMUSG00000021929	Importin subunit alpha-3	2	pictar|targetscan	6.8
Bhlhb5	ENSMUSG00000025128	Class B basic helix-loop-helix protein 5 (bHLHB5) (Protein BETA3).	2	pictar|targetscan	6.9
Dr1	ENSMUSG00000029265	TATA-binding protein-associated phosphoprotein (Down-regulator of transcription 1)	2	pictar|targetscan	7.0
Ep300	ENSMUSG00000055024	E1A binding protein p300	2	pictar|targetscan	7.0
Gpc3	ENSMUSG00000055653	Glypican-3 precursor.	2	pictar|targetscan	7.1
Ncald	ENSMUSG00000051359	Neurocalcin-delta.	2	pictar|targetscan	7.1
Prkacb	ENSMUSG00000005034	cAMP-dependent protein kinase, beta-catalytic subunit (PKA C-beta).	2	pictar|targetscan	7.1
Prkar1a	ENSMUSG00000020612	cAMP-dependent protein kinase type I-alpha regulatory subunit.	2	pictar|targetscan	7.1
Mef2c	ENSMUSG00000005583	MEF2C_MOUSE Isoform 4 of Q8CFN5	2	pictar|targetscan	7.2
Yaf2	ENSMUSG00000022634	YY1-associated factor 2	2	pictar|targetscan	7.2
Pbx2	ENSMUSG00000034673	Pre-B-cell leukemia transcription factor 2 (Homeobox protein PBX2).	2	pictar|targetscan	7.3
Zfand5	ENSMUSG00000024750	AN1-type zinc finger protein 5 (Zinc finger A20 domain-containing protein 2)	2	pictar|targetscan	7.3
Zic3	ENSMUSG00000067860	Zinc finger protein ZIC 3 (Zinc finger protein of the cerebellum 3).	2	pictar|targetscan	7.3
Morf4l2	ENSMUSG00000062270	Mortality factor 4-like protein 1 (MORF-related gene 15 protein) (Transcription factor-like protein MRG15)	2	pictar|targetscan	7.5
Rev1	ENSMUSG00000026082	DNA repair protein REV1 (Rev1-like terminal deoxycytidyl transferase).	2	pictar|targetscan	7.5
Cacna2d2	ENSMUSG00000010066	Voltage-dependent calcium channel subunit alpha-2/delta-2 precursor	2	pictar|targetscan	7.6
Rabgap1	ENSMUSG00000035437	Rab GTPase-activating protein 1	2	pictar|targetscan	7.6
Cbln4	ENSMUSG00000067578	Cerebellin-4 precursor (Cerebellin-like glycoprotein 1).	2	pictar|targetscan	7.7
Zfp36l1	ENSMUSG00000021127	Butyrate response factor 1 (Protein TIS11B).	2	pictar|targetscan	7.7
Kdelr1	ENSMUSG00000002778	ER lumen protein retaining receptor 1 (KDEL receptor 1)	2	targetscan|miranda	7.9
Rraga	ENSMUSG00000070934	Ras-related GTP-binding protein A (Rag A) (RagA); Echinoderm microtubule-associated protein-like 5-like.	2	pictar|targetscan	8.0
Stc1	ENSMUSG00000014813	Stanniocalcin-1 precursor (STC-1).	2	pictar|targetscan	8.0
Tox	ENSMUSG00000041272	Thymus high mobility group box protein TOX.	2	pictar|targetscan	8.0
Kcnj14	ENSMUSG00000058743	ATP-sensitive inward rectifier potassium channel 14 (Potassium channel, inwardly rectifying subfamily J member 14)	2	pictar|targetscan	8.1
Rab6b	ENSMUSG00000032549	Ras-related protein Rab-6B.	2	pictar|targetscan	8.1
Tmsb10	ENSMUSG00000079523	Thymosin beta-10.	2	pictar|targetscan	8.2
Gnaq	ENSMUSG00000024639	Guanine nucleotide-binding protein G(q) subunit alpha	2	pictar|targetscan	8.3
Dcun1d4	ENSMUSG00000051674	DCN1-like protein 4 (Defective in cullin neddylation protein 1-like protein 4) (DCUN1 domain-containing protein 4).	2	targetscan|miranda	8.4
Elavl2	ENSMUSG00000008489	ELAV-like protein 2 (Nervous system-specific RNA-binding protein Mel-N1).	2	pictar|targetscan	8.4

MGI Symbol	Ensembl Gene ID	Description	No. Prediction	Prediction Algorithm (>2)	ΔG (-kcal/mol)
Nrn1	ENSMUSG00000039114	Neuritin precursor (Candidate plasticity gene 15 protein).	2	pictar|miranda	8.4
Sox6	ENSMUSG00000051910	Transcription factor SOX-6 (SOX-LZ).	2	pictar|targetscan	8.4
Rftn1	ENSMUSG00000039316	Raftlin (Raft-linking protein).	2	pictar|targetscan	8.5
Npm1	ENSMUSG00000057113	Nucleophosmin (NPM) (Nucleolar phosphoprotein B23) (Numatrin)	2	pictar|miranda	8.6
Ppm1e	ENSMUSG00000046442	Protein phosphatase 1E (Ca(2+)/calmodulin-dependent protein kinase phosphatase N)	2	pictar|targetscan	8.6
Acvr1	ENSMUSG00000026836	Activin receptor type-1 precursor (TGF-B superfamily receptor type I)	2	pictar|targetscan	8.8
Slc1a1	ENSMUSG00000024935	Excitatory amino acid transporter 3 (Sodium-dependent glutamate/aspartate transporter 3)	2	pictar|targetscan	8.8
Cacnb4	ENSMUSG00000017412	Voltage-dependent L-type calcium channel subunit beta-4 (CAB4)	2	pictar|targetscan	8.9
Ddx3x	ENSMUSG00000000787	ATP-dependent RNA helicase DDX3X	2	pictar|targetscan	8.9
Fbxw11	ENSMUSG00000020271	F-box and WD-40 domain protein 11	2	pictar|targetscan	8.9
Dlat	ENSMUSG00000000168	Dihydrolipoamide acetyltransferase component of pyruvate dehydrogenase complex (PDC-E2).	2	pictar|targetscan	9.1
Mmd	ENSMUSG00000003948	Monocyte to macrophage differentiation protein	2	pictar|targetscan	9.1
Snx4	ENSMUSG00000022808	Sorting nexin-4.	2	pictar|targetscan	9.1
Sgms1	ENSMUSG00000040451	Phosphatidylcholine:ceramide cholinephosphotransferase 1 (Sphingomyelin synthase 1)	2	pictar|targetscan	9.3
Creb1	ENSMUSG00000025958	cAMP response element-binding protein (CREB).	2	pictar|targetscan	9.6
Stk19	ENSMUSG00000061207	Serine/threonine-protein kinase 19 (RP1 protein).	2	targetscan|miranda	9.7
Yipf4	ENSMUSG00000024072	Protein YIPF4 (YIP1 family member 4).	2	pictar|targetscan	9.8
Hbp1	ENSMUSG00000002996	HMG box-containing protein 1 (High mobility group box transcription factor 1).	2	pictar|targetscan	10.0
Efnb2	ENSMUSG00000001300	Ephrin-B2 precursor (EPH-related receptor tyrosine kinase ligand 5)	2	pictar|targetscan	10.1
Lphn2	ENSMUSG00000028184	Latrophilin-2 (Calcium-independent alpha-latrotoxin receptor 2)	2	targetscan|miranda	10.1
Phyhipl	ENSMUSG00000037747	phytanoyl-CoA hydroxylase interacting protein-like	2	pictar|targetscan	10.1
Yes1	ENSMUSG00000014932	Proto-oncogene tyrosine-protein kinase Yes ((p61-Yes) (c- Yes).	2	pictar|targetscan	10.2
Exoc4	ENSMUSG00000029763	Exocyst complex component 4 (Exocyst complex component Sec8).	2	targetscan|miranda	10.4
Srpk1	ENSMUSG00000004865	Serine/threonine-protein kinase SRPK1.	2	pictar|targetscan	10.5
Txnl1	ENSMUSG00000024583	Thioredoxin-like protein 1	2	pictar|targetscan	10.5
Slco3a1	ENSMUSG00000025790	Solute carrier organic anion transporter family member 3A1; Antisense product of high-affinity glutamate transporter EAAC1 and EAAC2	2	pictar|targetscan	10.6
Zcchc14	ENSMUSG00000061410	Zinc finger CCHC domain-containing protein 14 (BDG-29).	2	pictar|targetscan	10.6
Cited2	ENSMUSG00000039910	Cbp/p300-interacting transactivator 2 (MSG-related protein 1)	2	pictar|targetscan	10.7
Rab10	ENSMUSG00000020671	Ras-related protein Rab-10.	2	pictar|targetscan	10.7
Pafah1b1	ENSMUSG00000020745	Platelet-activating factor acetylhydrolase IB subunit alpha (PAF acetylhydrolase 45 kDa subunit)	2	pictar|targetscan	10.8
Usp5	ENSMUSG00000038429	Ubiquitin carboxyl-terminal hydrolase 5 (Ubiquitin thioesterase 5)	2	pictar|targetscan	10.8
Zhx1	ENSMUSG00000022361	Zinc fingers and homeoboxes protein 1.	2	pictar|targetscan	10.8
Kctd7	ENSMUSG00000034110	BTB/POZ domain-containing protein KCTD7.	2	pictar|targetscan	10.9
Rdx	ENSMUSG00000032050	Radixin (ESP10).	2	pictar|targetscan	10.9

MGI Symbol	Ensembl Gene ID	Description	No. Prediction	Prediction Algorithm (>2)	ΔG (-kcal/mol)
Ptp4a1	ENSMUSG00000026064	Protein tyrosine phosphatase type IVA protein 1	2	pictar|targetscan	11.0
Epas1	ENSMUSG00000024140	Endothelial PAS domain-containing protein 1 (EPAS-1) (Hypoxia- inducible factor 2 alpha) (HIF-2 alpha)	2	targetscan|miranda	11.1
Denr	ENSMUSG00000023106	Density-regulated protein (DRP).	2	pictar|targetscan	11.2
Hbegf	ENSMUSG00000024486	Proheparin-binding EGF-like growth factor precursor	2	pictar|targetscan	11.2
Mtch2	ENSMUSG00000027282	Mitochondrial carrier homolog 2.	2	targetscan|miranda	11.2
Gnai3	ENSMUSG00000000001	Guanine nucleotide-binding protein G(k) subunit alpha (G(i) alpha-3).	2	pictar|targetscan	11.3
Smad1	ENSMUSG00000031681	Mothers against decapentaplegic homolog 1 (SMAD 1) (Mad-related protein 1)	2	pictar|targetscan	11.3
Nlgn2	ENSMUSG00000051790	Neuroligin-2 precursor.	2	pictar|targetscan	11.5
Tmem127	ENSMUSG00000034850	Transmembrane protein 127.	2	pictar|targetscan	11.5
Zhx2	ENSMUSG00000071757	Zinc fingers and homeoboxes protein 2	2	pictar|targetscan	11.7
Coro1c	ENSMUSG00000004530	Coronin-1C (Coronin-3).	2	targetscan|miranda	11.9
Lass2	ENSMUSG00000015714	LAG1 longevity assurance homolog 2 (Translocating chain-associating membrane protein homolog 3)	2	pictar|targetscan	11.9
Mobkl1a	ENSMUSG00000006262	Mps one binder kinase activator-like 1A (Mob1 homolog 1A).	2	targetscan|miranda	11.9
Oxr1	ENSMUSG00000022307	Oxidation resistance protein 1 (Protein C7).	2	pictar|targetscan	11.9
Plch1	ENSMUSG00000036834	phospholipase C, eta 1	2	pictar|targetscan	11.9
Xbp1	ENSMUSG00000020484	X-box-binding protein 1 (XBP-1) (Tax-responsive element-binding protein 5 homolog).	2	pictar|miranda	11.9
Sez6l2	ENSMUSG00000030683	seizure related 6 homolog like 2	2	pictar|miranda	12.0
Cfl1	ENSMUSG00000056201	Cofilin-1 (Cofilin, non-muscle isoform).	2	pictar|targetscan	12.1
Zc3h15	ENSMUSG00000027091	erythropoietin 4 immediate early response	2	pictar|targetscan	12.1
Ccdc117	ENSMUSG00000020482	Coiled-coil domain-containing protein 117.	2	pictar|targetscan	12.2
Rgs2	ENSMUSG00000026360	Regulator of G-protein signaling 2 (RGS2).	2	pictar|targetscan	12.3
Slc1a2	ENSMUSG00000005089	Excitatory amino acid transporter 2 (Sodium-dependent glutamate/aspartate transporter 2)	2	targetscan|miranda	12.3
Ccdc92	ENSMUSG00000037979	Coiled-coil domain-containing protein 92.	2	pictar|targetscan	12.4
Slc35c1	ENSMUSG00000049922	GDP-fucose transporter 1 isoform 2	2	pictar|targetscan	12.4
Ube3c	ENSMUSG00000039000	Ubiquitin-protein ligase E3C	2	pictar|targetscan	12.4
Tbc1d22a	ENSMUSG00000051864	TBC1 domain family member 22A.	2	pictar|targetscan	12.5
Tbx1	ENSMUSG00000009097	T-box transcription factor TBX1 (T-box protein 1)	2	pictar|targetscan	12.5
Stox2	ENSMUSG00000038143	Storkhead-box protein 2.	2	targetscan|miranda	12.6
Rgs17	ENSMUSG00000019775	Regulator of G-protein signaling 17 (RGS17)	2	targetscan|miranda	12.7
Btbd11	ENSMUSG00000020042	BTB (POZ) domain containing 11 isoform 1	2	pictar|targetscan	13.1
Ihpk1	ENSMUSG00000032594	Inositol hexaphosphate kinase 1	2	pictar|targetscan	13.1
Slc6a6	ENSMUSG00000030096	Sodium- and chloride-dependent taurine and beta-alanine transporter.	2	pictar|targetscan	13.1
Sort1	ENSMUSG00000068747	Sortilin precursor (Neurotensin receptor 3) (NTR3).	2	pictar|targetscan	13.2
Kpnb1	ENSMUSG00000001440	Importin subunit beta-1	2	pictar|targetscan	13.3
Ppp1r9b	ENSMUSG00000038976	Neurabin-2 (Neurabin-II) (Spinophilin)	2	pictar|targetscan	13.9
Clock	ENSMUSG00000029238	Circadian locomoter output cycles protein kaput (mCLOCK).	2	pictar|targetscan	14.0

MGI Symbol	Ensembl Gene ID	Description	No. Prediction	Prediction Algorithm (>2)	ΔG (-kcal/mol)
Map2k3	ENSMUSG00000018932	Dual specificity mitogen-activated protein kinase kinase 3 (MAPKK 3) (MAPK/ERK kinase 3).	2	pictar|targetscan	14.2
Ank2	ENSMUSG00000032826	ankyrin 2, brain isoform 2	2	pictar|targetscan	14.4
Nap1l1	ENSMUSG00000058799	Nucleosome assembly protein 1-like 1 (NAP-1-related protein)	2	pictar|targetscan	14.4
Phf21a	ENSMUSG00000058318	PF21A_MOUSE Isoform 4 of Q6ZPK0	2	pictar|targetscan	14.4
Map3k7ip3	ENSMUSG00000035476	Mitogen-activated protein kinase kinase kinase 7-interacting protein 3	2	pictar|targetscan	14.5
Ammecr1l	ENSMUSG00000041915	AMMECR1-like protein.	2	pictar|targetscan	14.7
Esrrg	ENSMUSG00000026610	Estrogen-related receptor gamma	2	pictar|targetscan	14.8
Cttn	ENSMUSG00000031078	Src substrate cortactin.	2	pictar|miranda	15.8
Sh3bgrl3	ENSMUSG00000028843	SH3 domain-binding glutamic acid-rich-like protein 3.	2	pictar|targetscan	16.4
Rab34	ENSMUSG00000002059	Ras-related protein Rab-34 (Rab-39)	2	pictar|targetscan	16.9
Eif4ebp2	ENSMUSG00000020091	Eukaryotic translation initiation factor 4E-binding protein 2 (4E-BP2)	2	pictar|targetscan	17.4
Dcun1d1	ENSMUSG00000027708	DCN1-like protein 1 (Defective in cullin neddylation protein 1-like protein 1)	2	pictar|targetscan	17.6
Ralgds	ENSMUSG00000026821	Ral guanine nucleotide dissociation stimulator (RalGEF)	2	pictar|targetscan	18.7
Dos	ENSMUSG00000035640	Protein Dos (Downstream of Stk11 protein); Fibroblast growth factor-inducible protein 14 (FIN14).	2	pictar|miranda	21.9
Tspan9	ENSMUSG00000030352	Tetraspanin-9 (Tspan-9) (Tetraspan NET-5).; superkiller viralicidic activity 2-like	2	pictar|targetscan	27.5

Table 7.4 (C) Overlapping Target Predictions for miR-183 using miRanda, TargetScan and PicTar Algorithms					
MGI Symbol	**Ensembl Gene ID**	**Description**	**No. Prediction**	**Prediction Algorithm (>2)**	**ΔG (-kcal/mol)**
Dusp10	ENSMUSG00000039384	Dual specificity protein phosphatase 10 (MAP kinase phosphatase 5) (MKP-5).	3	miranda|targetscan|pictar	2.8
Pkp4	ENSMUSG00000026991	Plakophilin-4 (Armadillo-related protein).	3	miranda|targetscan|pictar	5.1
Zmym2	ENSMUSG00000021945	MYM-type zinc finger protein 2 (Zinc finger protein 198).	3	miranda|targetscan|pictar	5.2
Slitrk3	ENSMUSG00000048304	SLIT and NTRK-like protein 3 precursor.	3	miranda|targetscan|pictar	5.6
Laptm4a	ENSMUSG00000020585	Lysosomal-associated transmembrane protein 4A (Golgi 4-transmembrane spanning transporter)	3	miranda|targetscan|pictar	6
Btg1	ENSMUSG00000036478	Protein BTG1 (B-cell translocation gene 1 protein).	3	miranda|targetscan|pictar	6.6
Ppp2cb	ENSMUSG00000009630	Serine/threonine-protein phosphatase 2A catalytic subunit beta isoform (PP2A-beta).	3	miranda|targetscan|pictar	6.6
Psen2	ENSMUSG00000010609	Presenilin-2 (PS-2)	3	miranda|targetscan|pictar	6.6
Sfrs11	ENSMUSG00000055436	splicing factor, arginine/serine-rich 11 isoform 3	3	miranda|targetscan|pictar	6.9
Uchl3	ENSMUSG00000022111	Ubiquitin carboxyl-terminal hydrolase isozyme L3 (UCH- L3) (Ubiquitin thioesterase L3).	3	miranda|targetscan|pictar	7.9
Sfrs2	ENSMUSG00000034120	Splicing factor, arginine/serine-rich 2 (Splicing component, 35 kDa) (Putative myelin regulatory factor 1) (MRF-1).	3	miranda|targetscan|pictar	8
Gng5	ENSMUSG00000068523	Guanine nucleotide-binding protein G(I)/G(S)/G(O) subunit gamma-5 precursor.	3	miranda|targetscan|pictar	8.3
Hbegf	ENSMUSG00000024486	Proheparin-binding EGF-like growth factor precursor	3	miranda|targetscan|pictar	9.3
Pdcd4	ENSMUSG00000024975	Programmed cell death protein 4 (Topoisomerase-inhibitor suppressed protein) (Protein MA-3).	3	miranda|targetscan|pictar	10.1
Snx1	ENSMUSG00000032382	Sorting nexin-1.	3	miranda|targetscan|pictar	10.1
Mtmr6	ENSMUSG00000021987	myotubularin related protein 6	3	miranda|targetscan|pictar	11
L3mbtl3	ENSMUSG00000039089	Lethal(3)malignant brain tumor-like 3 protein (L(3)mbt-like 3 protein).	3	miranda|targetscan|pictar	11.9
Ptdss1	ENSMUSG00000021518	Phosphatidylserine synthase 1 (PtdSer synthase 1) (Serine-exchange enzyme I).	3	miranda|targetscan|pictar	11.9
Hectd2	ENSMUSG00000041180	Probable E3 ubiquitin-protein ligase HECTD2 (HECT domain-containing protein 2).	3	miranda|targetscan|pictar	12

MGI Symbol	Ensembl Gene ID	Description	No. Prediction	Prediction Algorithm (>2)	ΔG (-kcal/mol)
Mapk8ip1	ENSMUSG00000027223	C-jun-amino-terminal kinase-interacting protein 1 (JNK-interacting protein 1) (JIP-1) (JNK MAP kinase scaffold protein 1)	3	miranda|targetscan|pictar	13.5
Itgb1	ENSMUSG00000025809	Integrin beta-1 precursor (Fibronectin receptor subunit beta) (Integrin VLA-4 subunit beta) (CD29 antigen).	3	miranda|targetscan|pictar	14.4
Ralgds	ENSMUSG00000026821	Ral guanine nucleotide dissociation stimulator (RalGEF).	3	miranda|targetscan|pictar	16.2
Clcn3	ENSMUSG00000004319	Chloride channel protein 3 (ClC-3).	3	miranda|targetscan|pictar	16.7
Birc6	ENSMUSG00000024073	baculoviral IAP repeat-containing 6	2	pictar|targetscan	3
Sncb	ENSMUSG00000034891	Beta-synuclein.	2	targetscan|miranda	3.5
Cacnb4	ENSMUSG00000017412	Voltage-dependent L-type calcium channel subunit beta-4 (CAB4) (Calcium channel voltage-dependent subunit beta 4).	2	pictar|targetscan	4.5
Rcn2	ENSMUSG00000032320	Reticulocalbin-2 precursor (Taipoxin-associated calcium-binding protein 49) (TCBP-49).	2	targetscan|miranda	5
Tram1	ENSMUSG00000025935	Translocation-associated membrane protein 1.	2	pictar|targetscan	5.2
Runx1t1	ENSMUSG00000006586	Protein CBFA2T1 (Protein MTG8).	2	pictar|targetscan	5.4
Yes1	ENSMUSG00000014932	Proto-oncogene tyrosine-protein kinase Yes (p61-Yes) (c- Yes).	2	pictar|targetscan	5.6
Scyl3	ENSMUSG00000026584	Protein-associating with the carboxyl-terminal domain of ezrin (Ezrin- binding protein PACE-1) (SCY1-like protein 3).	2	pictar|targetscan	5.8
Slain1	ENSMUSG00000055717	SLAIN motif family, member 1	2	pictar|targetscan	5.8
Ikzf5	ENSMUSG00000040167	Zinc finger protein Pegasus (Ikaros family zinc finger protein 5).	2	pictar|targetscan	5.9
Tpm1	ENSMUSG00000032366	Tropomyosin alpha-1 chain (Tropomyosin-1) (Alpha-tropomyosin).	2	targetscan|miranda	5.9
Acvr2a	ENSMUSG00000052155	Activin receptor type-2A precursor (Activin receptor type IIA) (ACTR-IIA).	2	pictar|targetscan	6.6
Arhgap21	ENSMUSG00000036591	Rho GTPase-activating protein 21 (Rho-type GTPase-activating protein 21) (Rho GTPase-activating protein 10).	2	targetscan|miranda	6.6
Flrt3	ENSMUSG00000079021	fibronectin leucine rich transmembrane protein 3	2	pictar|targetscan	6.7
Rap2c	ENSMUSG00000050029	Ras-related protein Rap-2c precursor.	2	pictar|targetscan	6.7
Smpd3	ENSMUSG00000031906	Sphingomyelin phosphodiesterase 3 (Neutral sphingomyelinase 2)	2	pictar|targetscan	7
Bnip3l	ENSMUSG00000022051	BCL2/adenovirus E1B 19 kDa protein-interacting protein 3-like (NIP3L) (NIP3-like protein X).	2	pictar|targetscan	7.2
Pim1	ENSMUSG00000024014	Proto-oncogene serine/threonine-protein kinase Pim-1 (EC 2.7.11.1).	2	pictar|targetscan	7.5

MGI Symbol	Ensembl Gene ID	Description	No. Prediction	Prediction Algorithm (>2)	ΔG (-kcal/mol)
Ptpn4	ENSMUSG00000026384	protein tyrosine phosphatase, non-receptor type 4	2	targetscan|miranda	7.898
Ppm1e	ENSMUSG00000046442	Protein phosphatase 1E (EC 3.1.3.16) (Ca(2+)/calmodulin-dependent protein kinase phosphatase N) (CaMKP-N) (CaMKP-nucleus) (CaMKN)	2	pictar|targetscan	7.9
Bzw1	ENSMUSG00000051223	Basic leucine zipper and W2 domain-containing protein 1.	2	pictar|targetscan	8
Stc1	ENSMUSG00000014813	Stanniocalcin-1 precursor (STC-1).	2	pictar|targetscan	8
Eml4	ENSMUSG00000032624	Echinoderm microtubule-associated protein-like 4 (EMAP-4).	2	pictar|targetscan	8.2
Rab21	ENSMUSG00000020132	Ras-related protein Rab-21 (Rab-12).	2	pictar|targetscan	8.4
Brms1l	ENSMUSG00000012076	Breast cancer metastasis-suppressor 1-like protein.	2	pictar|targetscan	8.5
Ctdsp1	ENSMUSG00000026176	Carboxy-terminal domain RNA polymerase II polypeptide A small phosphatase 1 (Nuclear LIM interactor-interacting factor 3) (NLI-interacting factor 3) (Golli-interacting protein) (GIP).	2	pictar|targetscan	8.5
Epha4	ENSMUSG00000026235	Ephrin type-A receptor 4 precursor (EC 2.7.10.1) (Tyrosine-protein kinase receptor SEK) (MPK-3).	2	pictar|targetscan	8.8
Ppp2ca	ENSMUSG00000020349	Serine/threonine-protein phosphatase 2A catalytic subunit alpha isoform (EC 3.1.3.16) (PP2A-alpha).	2	pictar|targetscan	8.8
Zdhhc6	ENSMUSG00000024982	Probable palmitoyltransferase ZDHHC6 (Zinc finger DHHC domain-containing protein 6) (DHHC-6)	2	targetscan|miranda	8.8
Zfpm2	ENSMUSG00000022306	Zinc finger protein ZFPM2 (Zinc finger protein multitype 2) (Friend of GATA-2) (FOG-2)	2	targetscan|miranda	8.8
Ap3m1	ENSMUSG00000021824	AP-3 complex subunit mu-1 (Adapter-related protein complex 3 mu-1 subunit) (Mu3A-adaptin)	2	pictar|targetscan	8.9
Rsbn1	ENSMUSG00000044098	Round spermatid basic protein 1 (Rosbin).	2	pictar|targetscan	8.9
Tle4	ENSMUSG00000024642	Transducin-like enhancer protein 4 (Groucho-related protein 4) (Grg- 4).	2	pictar|targetscan	9.2
Tmpo	ENSMUSG00000019961	Lamina-associated polypeptide 2 isoforms beta/delta/epsilon/gamma (Thymopoietin isoforms beta/delta/epsilon/gamma)	2	targetscan|miranda	9.4
Tiam1	ENSMUSG00000002489	T-lymphoma invasion and metastasis-inducing protein 1 (TIAM-1).	2	pictar|targetscan	9.7
Eny2	ENSMUSG00000022338	Enhancer of yellow 2 transcription factor homolog.	2	pictar|targetscan	9.8
Frmd6	ENSMUSG00000048285	FERM domain-containing protein 6.	2	pictar|targetscan	9.8

MGI Symbol	Ensembl Gene ID	Description	No. Prediction	Prediction Algorithm (>2)	ΔG (-kcal/mol)
Sin3a	ENSMUSG00000042557	Paired amphipathic helix protein Sin3a (Transcriptional corepressor Sin3a) (Histone deacetylase complex subunit Sin3a).	2	targetscan|miranda	9.9
Ddx3x	ENSMUSG00000000787	ATP-dependent RNA helicase DDX3X (EC 3.6.1.-) (DEAD box protein 3, X-chromosomal) (DEAD box RNA helicase DEAD3) (mDEAD3)	2	pictar|targetscan	10.6
Ypel5	ENSMUSG00000039770	Protein yippee-like 5.	2	pictar|targetscan	10.8
Nfe2l1	ENSMUSG00000038615	Nuclear factor erythroid 2-related factor 1 (NF-E2-related factor 1) (NFE2-related factor 1)	2	pictar|targetscan	10.9
Irs1	ENSMUSG00000055980	Insulin receptor substrate 1 (IRS-1).	2	pictar|targetscan	11.1
Pdcd6	ENSMUSG00000021576	Programmed cell death protein 6 (Probable calcium-binding protein ALG- 2) (PMP41) (ALG-257).	2	targetscan|miranda	11.1
Cdk5r1	ENSMUSG00000048895	Cyclin-dependent kinase 5 activator 1 precursor (CDK5 activator 1) (Cyclin-dependent kinase 5 regulatory subunit 1)	2	pictar|targetscan	11.2
Unc13b	ENSMUSG00000028456	Protein unc-13 homolog B (Munc13-2) (munc13).	2	targetscan|miranda	11.2
Eif4a2	ENSMUSG00000022884	Eukaryotic initiation factor 4A-II (EC 3.6.1.-) (ATP-dependent RNA helicase eIF4A-2) (eIF4A-II) (eIF-4A-II).	2	pictar|targetscan	12
Mxd4	ENSMUSG00000037235	Max-interacting transcriptional repressor MAD4 (Max-associated protein 4)	2	targetscan|miranda	12.1
Egr1	ENSMUSG00000038418	Early growth response protein 1 (EGR-1) (Protein Krox-24) (Transcription factor Zif268) (Nerve growth factor-induced protein A) (NGFI-A).	2	pictar|targetscan	12.3
Rala	ENSMUSG00000008859	Ras-related protein Ral-A precursor.	2	pictar|targetscan	12.3
Bnc2	ENSMUSG00000028487	Zinc finger protein basonuclin-2.	2	pictar|targetscan	12.4
Sox6	ENSMUSG00000051910	Transcription factor SOX-6 (SOX-LZ).	2	pictar|targetscan	12.4
Kpna4	ENSMUSG00000027782	Importin subunit alpha-4 (Karyopherin subunit alpha-4) (Importin alpha Q1).	2	pictar|targetscan	12.7
AI314180	ENSMUSG00000050812	Proteasome-associated protein ECM29 homolog (Ecm29).	2	pictar|miranda	13
Vdac1	ENSMUSG00000020402	Voltage-dependent anion-selective channel protein 1 (VDAC-1) (mVDAC1) (mVDAC5) (Outer mitochondrial membrane protein porin 1)	2	pictar|targetscan	13.8

MGI Symbol	Ensembl Gene ID	Description	No. Prediction	Prediction Algorithm (>2)	ΔG (-kcal/mol)
Arid4b	ENSMUSG00000039219	AT-rich interactive domain-containing protein 4B (ARID domain- containing protein 4B) (Histone deacetylase complex subunit SAP180)	2	pictar|targetscan	14.4
Cntnap2	ENSMUSG00000039419	Contactin-associated protein-like 2 precursor (Cell recognition molecule Caspr2).	2	pictar|targetscan	14.4
Dtna	ENSMUSG00000024302	Dystrobrevin alpha (Alpha-dystrobrevin).	2	pictar|targetscan	14.4
Plcb4	ENSMUSG00000039943	phospholipase C beta 4	2	targetscan|miranda	14.4
Idh2	ENSMUSG00000030541	Isocitrate dehydrogenase [NADP], mitochondrial precursor (Oxalosuccinate decarboxylase)	2	targetscan|miranda	14.5
Tmem111	ENSMUSG00000030286	Transmembrane protein 111.	2	pictar|miranda	15.9
Stk38l	ENSMUSG00000001630	Serine/threonine-protein kinase 38-like (NDR2 protein kinase) (Nuclear Dbf2-related kinase 2).	2	targetscan|miranda	16
Ppp1r14b	ENSMUSG00000056612	Protein phosphatase 1 regulatory subunit 14B (Phosphatase holoenzyme inhibitor 1) (PHI-1).	2	targetscan|miranda	16.5
Ssrp1	ENSMUSG00000027067	FACT complex subunit SSRP1 (Facilitates chromatin transcription complex subunit SSRP1) (Structure-specific recognition protein 1)	2	targetscan|miranda	18.2
Zfp592	ENSMUSG00000005621	Zinc finger protein 592 (Zfp-592).	2	pictar|miranda	18.8
Usp47	ENSMUSG00000059263	Ubiquitin carboxyl-terminal hydrolase 47 (Ubiquitin-specific-processing protease 47)	2	pictar|targetscan	19.7
Pex19	ENSMUSG00000003464	Peroxisomal biogenesis factor 19 (Peroxin-19) (Peroxisomal farnesylated protein) (PxF).	2	pictar|targetscan	20.6
Ppp2r5c	ENSMUSG00000017843	Serine/threonine-protein phosphatase 2A 56 kDa regulatory subunit gamma isoform (PP2A, B subunit, B' gamma isoform)	2	targetscan|miranda	24.2

Table 7.5 (A) Overlapping Target Predictions for miR-1 using miRanda, TargetScan and PicTar Algorithms					
MGI symbol	**Ensembl Gene ID**	**Description**	**No. Prediction**	**Prediction Algorithm (>2)**	**ΔG (-kcal/mol)**
Cnn3	ENSMUSG00000053931	Calponin-3 (Calponin, acidic isoform).	3	miranda|targetscan|pictar	3.8
Notch3	ENSMUSG00000038146	Neurogenic locus notch homolog protein 3 precursor (Notch 3).	3	miranda|targetscan|pictar	4.0
Dhx15	ENSMUSG00000029169	Putative pre-mRNA-splicing factor ATP-dependent RNA helicase DHX15	3	miranda|targetscan|pictar	4.1
Igf1	ENSMUSG00000020053	Insulin-like growth factor I precursor (IGF-I) (Somatomedin).	3	miranda|targetscan|pictar	4.5
Sfrs9	ENSMUSG00000029538	Splicing factor, arginine/serine-rich 9.	3	miranda|targetscan|pictar	4.8
Hace1	ENSMUSG00000038822	E3 ubiquitin-protein ligase HACE1.	3	miranda|targetscan|pictar	5.1
Clcn3	ENSMUSG00000004319	Chloride channel protein 3 (ClC-3).	3	miranda|targetscan|pictar	6.0
Wdr6	ENSMUSG00000066357	WD repeat domain 6	3	miranda|targetscan|pictar	6.0
Snx2	ENSMUSG00000034484	Sorting nexin-2.	3	miranda|targetscan|pictar	6.5
Mab21l1	ENSMUSG00000056947	Protein mab-21-like 1.	3	miranda|targetscan|pictar	7.1
Ss18	ENSMUSG00000037013	SSXT protein (SYT protein) (Synovial sarcoma-associated Ss18-alpha).	3	miranda|targetscan|pictar	7.1
Cltc	ENSMUSG00000047126	Clathrin heavy chain.	3	miranda|targetscan|pictar	7.2
Trim2	ENSMUSG00000027993	Tripartite motif-containing protein 2 (Neural activity-related RING finger protein).	3	miranda|targetscan|pictar	7.2
Hspd1	ENSMUSG00000025980	60 kDa heat shock protein, mitochondrial precursor (Hsp60) (60 kDa chaperonin).	3	miranda|targetscan|pictar	8.5
Gja1	ENSMUSG00000050953	Gap junction alpha-1 protein (Connexin-43) (Gap junction 43 kDa heart protein).	3	miranda|targetscan|pictar	9.2
Tagln2	ENSMUSG00000026547	Transgelin-2.	3	miranda|targetscan|pictar	9.2
Rnuxa	ENSMUSG00000008301	RNA U small nuclear RNA export adapter protein (Phosphorylated adapter RNA export protein).	3	miranda|targetscan|pictar	9.7
Thrb	ENSMUSG00000021779	Thyroid hormone receptor beta-1	3	miranda|targetscan|pictar	9.9
Gpr85	ENSMUSG00000048216	Probable G-protein coupled receptor 85 (Super conserved receptor expressed in brain 2); Fibroblast growth factor-inducible protein 14 (FIN14).	3	miranda|targetscan|pictar	10.1
Ptpra	ENSMUSG00000027303	Receptor-type tyrosine-protein phosphatase alpha precursor (Protein-tyrosine phosphatase alpha).	3	miranda|targetscan|pictar	10.8
Mea1	ENSMUSG00000002768	Male-enhanced antigen 1 (MEA-1).	3	miranda|targetscan|pictar	11.4
Eml3	ENSMUSG00000071647	Echinoderm microtubule-associated protein-like 3 (EMAP-3).	3	miranda|targetscan|pictar	11.5
Trappc3	ENSMUSG00000028847	Trafficking protein particle complex subunit 3 (BET3 homolog).	3	miranda|targetscan|pictar	11.7
Ppib	ENSMUSG00000032383	Peptidyl-prolyl cis-trans isomerase B precursor (Cyclophilin B) (S-cyclophilin) (SCYLP) (CYP-S1).	3	miranda|targetscan|pictar	12.0
Bscl2	ENSMUSG00000071657	Seipin (Bernardinelli-Seip congenital lipodystrophy type 2 protein homolog).	3	miranda|targetscan|pictar	12.1
Otx2	ENSMUSG00000021848	Homeobox protein OTX2 (Orthodenticle homolog 2).	3	miranda|targetscan|pictar	12.4
Ktn1	ENSMUSG00000021843	Kinectin.	3	miranda|targetscan|pictar	14.4

MGI symbol	Ensembl Gene ID	Description	No. Prediction	Prediction Algorithm (>2)	ΔG (-kcal/mol)
Tmem178	ENSMUSG00000024245	Transmembrane protein 178 precursor.	3	miranda|targetscan|pictar	16.3
Sox6	ENSMUSG00000051910	Transcription factor SOX-6 (SOX-LZ).	2	pictar|targetscan	0.2
Rsbn1	ENSMUSG00000044098	Round spermatid basic protein 1 (Rosbin).	2	pictar|targetscan	0.4
Setbp1	ENSMUSG00000024548	SET-binding protein (SEB).	2	pictar|targetscan	0.5
Yes1	ENSMUSG00000014932	Proto-oncogene tyrosine-protein kinase Yes (EC 2.7.10.2) (p61-Yes) (c- Yes).	2	pictar|targetscan	2.3
Gnpda2	ENSMUSG00000029209	glucosamine-6-phosphate deaminase 2	2	pictar|targetscan	2.6
Matr3	ENSMUSG00000037236	Matrin-3.	2	pictar|targetscan	3.3
Gnptab	ENSMUSG00000035311	N-acetylglucosamine-1-phosphotransferase subunits alpha/beta precursor	2	pictar|targetscan	3.8
Abcb7	ENSMUSG00000031333	ATP-binding cassette sub-family B member 7, mitochondrial (ABC transporter 7 protein).	2	targetscan|miranda	4.3
Smap1	ENSMUSG00000026155	Stromal membrane-associated protein 1.	2	pictar|targetscan	4.9
Pftk1	ENSMUSG00000028926	Serine/threonine-protein kinase PFTAIRE-1.	2	pictar|targetscan	5.9
Kctd13	ENSMUSG00000030685	BTB/POZ domain-containing protein KCTD13	2	targetscan|miranda	6.1
Timp3	ENSMUSG00000020044	Metalloproteinase inhibitor 3 precursor (TIMP-3)	2	pictar|targetscan	6.1
Slc45a4	ENSMUSG00000036649	Adult male diencephalon cDNA, RIKEN full-length enriched library	2	pictar|miranda	6.2
Stard7	ENSMUSG00000027367	StAR-related lipid transfer protein 7 (StARD7); solute carrier family 45, member 4	2	pictar|targetscan	6.4
Hmbox1	ENSMUSG00000021972	Homeobox-containing protein 1.	2	pictar|targetscan	6.5
Sdcbp	ENSMUSG00000028249	Syntenin-1 (Syndecan-binding protein 1) (Scaffold protein Pbp1).	2	pictar|targetscan	6.6
Syt1	ENSMUSG00000035864	Synaptotagmin-1 (Synaptotagmin I) (SytI) (p65).	2	pictar|targetscan	6.6
Ccnd2	ENSMUSG00000000184	G1/S-specific cyclin-D2.	2	pictar|targetscan	6.7
Daam1	ENSMUSG00000034574	Disheveled-associated activator of morphogenesis 1.	2	pictar|targetscan	6.7
Rit2	ENSMUSG00000057455	GTP-binding protein Rit2 (Ras-like protein expressed in neurons)	2	pictar|targetscan	6.9
Prkacb	ENSMUSG00000005034	cAMP-dependent protein kinase, beta-catalytic subunit (PKA C-beta).	2	pictar|targetscan	7.1
Ube2h	ENSMUSG00000039159	Ubiquitin-conjugating enzyme E2 H (Ubiquitin-protein ligase H)	2	pictar|targetscan	7.1
Vamp2	ENSMUSG00000020894	Vesicle-associated membrane protein 2 (VAMP-2) (Synaptobrevin-2).	2	pictar|targetscan	7.2
Usp33	ENSMUSG00000025437	ubiquitin specific protease 33 isoform 1	2	targetscan|miranda	7.3
Anp32b	ENSMUSG00000028333	Acidic leucine-rich nuclear phosphoprotein 32 family member B	2	pictar|targetscan	7.4
Cebpz	ENSMUSG00000024081	CCAAT/enhancer-binding protein zeta (CCAAT-box-binding transcription factor)	2	targetscan|miranda	7.4
H3f3b	ENSMUSG00000060743	Histone H3.3.	2	pictar|targetscan	7.4
Mon2	ENSMUSG00000034602	Protein MON2 homolog (Protein SF21).	2	targetscan|miranda	7.4
Rarb	ENSMUSG00000017491	Retinoic acid receptor beta (RAR-beta)	2	pictar|targetscan	7.4
Pim1	ENSMUSG00000024014	Proto-oncogene serine/threonine-protein kinase Pim-1	2	pictar|targetscan	7.5
Cbl	ENSMUSG00000034342	E3 ubiquitin-protein ligase CBL (Proto-oncogene c-CBL)	2	pictar|targetscan	7.6
Rala	ENSMUSG00000008859	Ras-related protein Ral-A precursor.	2	pictar|targetscan	7.6

MGI symbol	Ensembl Gene ID	Description	No. Prediction	Prediction Algorithm (>2)	ΔG (-kcal/mol)
Pdgfa	ENSMUSG00000025856	Platelet-derived growth factor A chain precursor (PDGF A-chain)	2	targetscan|miranda	7.8
Zfp36l2	ENSMUSG00000045817	Butyrate response factor 2 (Protein TIS11D).	2	pictar|targetscan	7.8
Pafah1b1	ENSMUSG00000020745	Platelet-activating factor acetylhydrolase IB subunit alpha (PAF acetylhydrolase 45 kDa subunit)	2	pictar|targetscan	8.0
Rap1a	ENSMUSG00000068798	Ras-related protein Rap-1A precursor (Ras-related protein Krev-1).	2	pictar|targetscan	8.0
Gpr125	ENSMUSG00000029090	Probable G-protein coupled receptor 125 precursor.	2	targetscan|miranda	8.1
Mmd	ENSMUSG00000003948	Monocyte to macrophage differentiation protein	2	pictar|targetscan	8.1
Azin1	ENSMUSG00000037458	Antizyme inhibitor 1 (AZI) (Ornithine decarboxylase antizyme inhibitor).	2	pictar|targetscan	8.2
Arf4	ENSMUSG00000021877	ADP-ribosylation factor 4.	2	pictar|targetscan	8.3
Twf1	ENSMUSG00000022451	Twinfilin-1 (Protein A6).	2	pictar|targetscan	8.3
Atp6v1a	ENSMUSG00000052459	Vacuolar ATP synthase catalytic subunit A (V-ATPase 69 kDa subunit).	2	pictar|targetscan	8.6
Efnb2	ENSMUSG00000001300	Ephrin-B2 precursor (EPH-related receptor tyrosine kinase ligand 5) (ELF-2).	2	pictar|targetscan	8.6
Ddx5	ENSMUSG00000020719	Probable ATP-dependent RNA helicase DDX5 (EC 3.6.1.-) (DEAD box protein 5)	2	targetscan|miranda	8.7
Rnf38	ENSMUSG00000035696	RING finger protein 38.	2	pictar|targetscan	8.7
Slc25a25	ENSMUSG00000026819	mitochondrial Ca2+-dependent solute carrier	2	pictar|targetscan	8.7
Cap1	ENSMUSG00000028656	Adenylyl cyclase-associated protein 1 (CAP 1).	2	pictar|targetscan	9.0
Eml4	ENSMUSG00000032624	Echinoderm microtubule-associated protein-like 4 (EMAP-4).	2	pictar|targetscan	9.1
Gnb1	ENSMUSG00000029064	Guanine nucleotide-binding protein G(I)/G(S)/G(T) subunit beta-1	2	pictar|targetscan	9.1
Klf4	ENSMUSG00000003032	Krueppel-like factor 4 (Gut-enriched krueppel-like factor) (Epithelial zinc finger protein EZF).	2	pictar|targetscan	9.2
Elf1	ENSMUSG00000036461	ETS-related transcription factor Elf-1 (E74-like factor 1).	2	pictar|targetscan	9.3
Sfrs1	ENSMUSG00000018379	Splicing factor, arginine/serine-rich 1.	2	pictar|targetscan	9.3
Igfbp5	ENSMUSG00000026185	Insulin-like growth factor-binding protein 5 precursor (IGF-binding protein 5).	2	pictar|targetscan	9.4
Wdr61	ENSMUSG00000061559	WD repeat-containing protein 61 (Meiotic recombination REC14 protein homolog).	2	targetscan|miranda	9.4
Ddx3x	ENSMUSG00000000787	ATP-dependent RNA helicase DDX3X (DEAD box RNA helicase DEAD3) (mDEAD3).	2	pictar|targetscan	9.5
Ywhaq	ENSMUSG00000076432	14-3-3 protein theta (14-3-3 protein tau).	2	pictar|targetscan	9.6
BC024479	ENSMUSG00000042138	Uncharacterized protein C11orf61 homolog.	2	pictar|miranda	10.3
Map3k7ip3	ENSMUSG00000035476	Mitogen-activated protein kinase kinase kinase 7-interacting protein 3	2	pictar|targetscan	10.3
Fndc3a	ENSMUSG00000033487	Fibronectin type-III domain-containing protein 3a.	2	pictar|targetscan	10.5
Coro1b	ENSMUSG00000024835	Coronin-1B (Coronin-2).	2	pictar|targetscan	10.6
Rasa1	ENSMUSG00000021549	RAS p21 protein activator 1	2	targetscan|miranda	10.7
Gclc	ENSMUSG00000032350	Glutamate--cysteine ligase catalytic subunit (Gamma- glutamylcysteine synthetase)	2	pictar|targetscan	10.8

MGI symbol	Ensembl Gene ID	Description	No. Prediction	Prediction Algorithm (>2)	ΔG (-kcal/mol)
Sec22b	ENSMUSG00000027879	Vesicle-trafficking protein SEC22b (SEC22 vesicle-trafficking protein homolog B)	2	pictar|targetscan	10.8
Id4	ENSMUSG00000021379	DNA-binding protein inhibitor ID-4 (Inhibitor of DNA binding 4).	2	pictar|targetscan	10.9
Phkg2	ENSMUSG00000030815	Phosphorylase b kinase gamma catalytic chain (PHK-gamma-T)	2	pictar|targetscan	10.9
Lin7c	ENSMUSG00000027162	Lin-7 homolog C (Lin-7C) (Vertebrate lin-7 homolog 3).	2	pictar|targetscan	11.0
Mxd4	ENSMUSG00000037235	Max-interacting transcriptional repressor MAD4 (Max-associated protein 4) (MAX dimerization protein 4).	2	pictar|targetscan	11.0
Otud5	ENSMUSG00000031154	OTU domain-containing protein 5.	2	pictar|targetscan	11.0
Tdg	ENSMUSG00000034674	G/T mismatch-specific thymine DNA glycosylase	2	pictar|targetscan	11.1
Glis2	ENSMUSG00000014303	Zinc finger protein GLIS2 (GLI-similar 2) (Neuronal Krueppel-like protein)	2	pictar|targetscan	11.2
Gtf2b	ENSMUSG00000028271	Transcription initiation factor IIB (General transcription factor TFIIB)	2	pictar|targetscan	11.2
Ccnd1	ENSMUSG00000070348	G1/S-specific cyclin-D1.	2	pictar|targetscan	11.4
Fn1	ENSMUSG00000026193	Fibronectin precursor (FN).	2	targetscan|miranda	11.4
Hmgn1	ENSMUSG00000040681	Non-histone chromosomal protein HMG-14	2	pictar|targetscan	11.5
Pgam1	ENSMUSG00000011752	Phosphoglycerate mutase 1 (Phosphoglycerate mutase isozyme B) (PGAM-B)	2	pictar|targetscan	11.6
Frs2	ENSMUSG00000020170	Fibroblast growth factor receptor substrate 2 (FGFR substrate 2) (FGFR-signaling adaptor SNT)	2	pictar|targetscan	11.7
Spred1	ENSMUSG00000027351	Sprouty-related, EVH1 domain-containing protein 1 (Spred-1).	2	pictar|targetscan	11.7
Atp6v1b2	ENSMUSG00000006273	Vacuolar ATP synthase subunit B, brain isoform (V-ATPase subunit B 2) .	2	pictar|targetscan	11.8
Golph3	ENSMUSG00000022200	Golgi phosphoprotein 3 (Coat protein GPP34).	2	pictar|targetscan	11.8
Rap1b	ENSMUSG00000052681	Ras-related protein Rap-1b precursor (GTP-binding protein smg p21B).	2	pictar|targetscan	11.8
Tmem55b	ENSMUSG00000035953	Transmembrane protein 55B (Type I phosphatidylinositol 4,5-bisphosphate 4-phosphatase)	2	pictar|targetscan	11.8
Zic4	ENSMUSG00000036972	Zinc finger protein ZIC 4 (Zinc finger protein of the cerebellum 4).	2	pictar|targetscan	11.8
Mtpn	ENSMUSG00000029840	Myotrophin (Protein V-1) (Granule cell differentiation protein).	2	pictar|targetscan	11.9
Ptplad1	ENSMUSG00000033629	Protein tyrosine phosphatase-like protein PTPLAD1	2	pictar|targetscan	11.9
Sh3bgrl3	ENSMUSG00000028843	SH3 domain-binding glutamic acid-rich-like protein 3.	2	targetscan|miranda	11.9
Ddx17	ENSMUSG00000055065	Probable ATP-dependent RNA helicase DDX17 (DEAD box protein 17).	2	pictar|targetscan	12.0
Sec61a1	ENSMUSG00000030082	Protein transport protein Sec61 subunit alpha isoform 1 (Sec61 alpha- 1).	2	pictar|targetscan	12.0
Smarca4	ENSMUSG00000032187	SWI/SNF related, matrix associated, actin dependent regulator of chromatin, subfamily a, member 4.	2	pictar|targetscan	12.0
Slc16a3	ENSMUSG00000025161	Monocarboxylate transporter 4 (MCT 4) (Solute carrier family 16 member 3).	2	pictar|targetscan	12.1
Pdcd4	ENSMUSG00000024975	Programmed cell death protein 4 (Topoisomerase-inhibitor suppressed protein)	2	pictar|targetscan	12.2
Vezf1	ENSMUSG00000018377	vascular endothelial zinc finger 1	2	pictar|targetscan	12.3
Wdr1	ENSMUSG00000005103	WD repeat-containing protein 1 (Actin-interacting protein 1) (AIP1).	2	pictar|targetscan	12.3

MGI symbol	Ensembl Gene ID	Description	No. Prediction	Prediction Algorithm (>2)	ΔG (-kcal/mol)
Ihpk2	ENSMUSG00000032599	Inositol hexakisphosphate kinase 2 (InsP6 kinase 2)	2	pictar|miranda	12.5
Hiat1	ENSMUSG00000027958	Hippocampus abundant transcript 1 protein.	2	pictar|targetscan	12.9
Hnrpk	ENSMUSG00000021546	Heterogeneous nuclear ribonucleoprotein K (hnRNP K).	2	pictar|targetscan	13.0
Mtx1	ENSMUSG00000064068	Metaxin-1.	2	pictar|miranda	13.2
Smarcb1	ENSMUSG00000000902	SWI/SNF-related matrix-associated actin-dependent regulator of chromatin subfamily B member 1	2	targetscan|miranda	13.2
Cttnbp2nl	ENSMUSG00000062127	CTTNBP2 N-terminal-like protein.	2	pictar|targetscan	13.5
Rrbp1	ENSMUSG00000027422	RRBP1_MOUSE Isoform RRp47 of Q99PL5 - Mus musculus (Mouse)	2	targetscan|miranda	13.6
Tpm3	ENSMUSG00000027940	Tropomyosin alpha-3 chain (Tropomyosin-3) (Tropomyosin gamma).	2	pictar|miranda	14.0
Nfat5	ENSMUSG00000003847	Nuclear factor of activated T-cells 5 (T-cell transcription factor NFAT5) (NF-AT5)	2	pictar|targetscan	14.4
Xpo6	ENSMUSG00000000131	Exportin-6 (Exp6) (Ran-binding protein 20).	2	pictar|targetscan	14.4
Tppp	ENSMUSG00000021573	Tubulin polymerization-promoting protein (TPPP).	2	pictar|targetscan	14.5
Api5	ENSMUSG00000027193	Apoptosis inhibitor 5 (API-5) (AAC-11).	2	pictar|targetscan	14.8
Cdk9	ENSMUSG00000009555	Cell division protein kinase 9 (Cyclin- dependent kinase 9).	2	targetscan|miranda	15.0
Elof1	ENSMUSG00000013822	Transcription elongation factor 1 homolog.	2	pictar|targetscan	15.0
Dgkz	ENSMUSG00000040479	Diacylglycerol kinase zeta (EC 2.7.1.107) (Diglyceride kinase zeta)	2	pictar|targetscan	15.2
Pias3	ENSMUSG00000028101	E3 SUMO-protein ligase PIAS3 (Protein inhibitor of activated STAT protein 3).	2	pictar|targetscan	16.2
Hp1bp3	ENSMUSG00000028759	heterochromatin protein 1, binding protein 3	2	pictar|targetscan	16.3
Phc2	ENSMUSG00000028796	Polyhomeotic-like protein 2 (mPH2) (Early development regulatory protein 2)	2	pictar|targetscan	16.9
Ubn1	ENSMUSG00000039473	ubinuclein 1	2	pictar|targetscan	17.0
Itsn2	ENSMUSG00000020640	Intersectin-2 (EH and SH3 domains protein 2) (EH domain and SH3 domain regulator of endocytosis 2).	2	pictar|targetscan	17.2
Tex2	ENSMUSG00000040548	Testis-expressed sequence 2 protein.	2	pictar|targetscan	17.2
Tef	ENSMUSG00000022389	Thyrotroph embryonic factor.	2	pictar|targetscan	17.8
Mkrn1	ENSMUSG00000029922	Makorin-1.	2	pictar|targetscan	18.1
Celsr3	ENSMUSG00000023473	Cadherin EGF LAG seven-pass G-type receptor 3 precursor.	2	pictar|targetscan	19.4
Jarid1c	ENSMUSG00000025332	Histone demethylase JARID1C (Jumonji/ARID domain- containing protein 1C).	2	pictar|targetscan	20.4
Tspan4	ENSMUSG00000025511	Tetraspanin-4 (Tspan-4) (Transmembrane 4 superfamily member 7).	2	pictar|targetscan	21.5
Mnt	ENSMUSG00000000282	Max-binding protein MNT (Protein ROX) (Myc antagonist MNT).	2	pictar|targetscan	25.6

Table 7.5 (B) Overlapping Target Predictions for miR-133 using miRanda, TargetScan and PicTar Algorithms					
MGI Symbol	**Ensembl Gene ID**	**Description**	**No. Prediction**	**Prediction Algorithm (>2)**	**ΔG (-kcal/mol)**
Tagln2	ENSMUSG00000026547	Transgelin-2.	3	miranda|targetscan|pictar	3.3
Nrip3	ENSMUSG00000034825	Nuclear receptor-interacting protein 3.	3	miranda|targetscan|pictar	6.2
Whsc2	ENSMUSG00000029111	Negative elongation factor A (NELF-A) (Wolf-Hirschhorn syndrome candidate 2 homolog) (mWHSC2).	3	miranda|targetscan|pictar	6.7
Ppp2ca	ENSMUSG00000020349	Serine/threonine-protein phosphatase 2A catalytic subunit alpha isoform (PP2A-alpha).	3	miranda|targetscan|pictar	7.1
Ppp2cb	ENSMUSG00000009630	Serine/threonine-protein phosphatase 2A catalytic subunit beta isoform (PP2A-beta).	3	miranda|targetscan|pictar	7.1
Elf2	ENSMUSG00000037174	ETS-related transcription factor Elf-2 (E74-like factor 2).	3	miranda|targetscan|pictar	7.3
Timm17a	ENSMUSG00000062580	Mitochondrial import inner membrane translocase subunit Tim17-A	3	miranda|targetscan|pictar	7.3
Foxc1	ENSMUSG00000050295	Forkhead box protein C1 (Forkhead- related transcription factor 3)	3	miranda|targetscan|pictar	7.9
Stx1a	ENSMUSG00000007207	Syntaxin-1A (Neuron-specific antigen HPC-1).	3	miranda|targetscan|pictar	8.4
Sqle	ENSMUSG00000022351	Squalene monooxygenase (Squalene epoxidase)	3	miranda|targetscan|pictar	9.2
B4galt2	ENSMUSG00000028541	Beta-1,4-galactosyltransferase 2 (UDP-galactose:beta-N-acetylglucosamine beta- 1,4-galactosyltransferase 2)	3	miranda|targetscan|pictar	9.3
Appl2	ENSMUSG00000020263	DCC-interacting protein 13-beta (Dip13-beta) (Adapter protein containing PH domain, PTB domain and leucine zipper motif 2).	3	miranda|targetscan|pictar	9.4
Clta	ENSMUSG00000028478	Clathrin light chain A (Lca).	3	miranda|targetscan|pictar	9.4
Eif4a1	ENSMUSG00000059796	Eukaryotic initiation factor 4A-I (ATP-dependent RNA helicase eIF4A-1) (eIF4A-I).	3	miranda|targetscan|pictar	9.4
Coro1b	ENSMUSG00000024835	Coronin-1B (Coronin-2).	3	miranda|targetscan|pictar	10.6
Aftph	ENSMUSG00000049659	Aftiphilin.	3	miranda|targetscan|pictar	11.1
Setd8	ENSMUSG00000049327	Histone-lysine N-methyltransferase, H4 lysine-20 specific	3	miranda|targetscan|pictar	11.2
Cntnap1	ENSMUSG00000017167	Contactin-associated protein 1 precursor (Caspr)	3	miranda|targetscan|pictar	11.8
Brunol4	ENSMUSG00000024268	CUG-BP- and ETR-3-like factor 4 (CELF-4) (RNA- binding protein BRUNOL-4).	3	miranda|targetscan|pictar	12.0
Mllt3	ENSMUSG00000028496	Protein AF-9 (Myeloid/lymphoid or mixed-lineage leukemia translocated to chromosome 3 protein homolog).	3	miranda|targetscan|pictar	12.1
Arfip2	ENSMUSG00000030881	Arfaptin-2 (ADP-ribosylation factor-interacting protein 2).	3	miranda|targetscan|pictar	16.0
Sv2a	ENSMUSG00000038486	Synaptic vesicle glycoprotein 2A (Synaptic vesicle protein 2A) (Synaptic vesicle protein 2)	3	miranda|targetscan|pictar	16.0
Abca2	ENSMUSG00000026944	ATP-binding cassette sub-family A member 2 (ATP-binding cassette transporter 2).	3	miranda|targetscan|pictar	19.0
Slc7a8	ENSMUSG00000022180	Large neutral amino acids transporter small subunit 2 (L-type amino acid transporter 2)	2	pictar|targetscan	0.1

MGI Symbol	Ensembl Gene ID	Description	No. Prediction	Prediction Algorithm (>2)	ΔG (-kcal/mol)
Gabarapl1	ENSMUSG00000030161	Gamma-aminobutyric acid receptor-associated protein-like 1	2	pictar|targetscan	1.4
Yes1	ENSMUSG00000014932	Proto-oncogene tyrosine-protein kinase Yes (EC 2.7.10.2) (p61-Yes) (c- Yes).	2	pictar|targetscan	2.2
Ganab	ENSMUSG00000071650	Neutral alpha-glucosidase AB precursor (Glucosidase II subunit alpha) (Alpha-glucosidase 2).	2	pictar|targetscan	2.9
Sf3b4	ENSMUSG00000068856	splicing factor 3b, subunit 4.	2	pictar|targetscan	3.0
Tram1	ENSMUSG00000025935	Translocation-associated membrane protein 1.	2	pictar|targetscan	3.2
Tmod3	ENSMUSG00000058587	Tropomodulin-3 (Ubiquitous tropomodulin) (U-Tmod).	2	pictar|targetscan	3.5
Casc3	ENSMUSG00000052915	hampin	2	pictar|targetscan	3.8
Prrx1	ENSMUSG00000026586	Paired mesoderm homeobox protein 1 (PRX-1) (Homeobox protein K-2).	2	pictar|targetscan	3.8
Smek1	ENSMUSG00000041846	SMEK homolog 1.	2	pictar|targetscan	3.8
Akap9	ENSMUSG00000040407	A kinase (PRKA) anchor protein (yotiao) 9	2	pictar|miranda	4.0
Lhfp	ENSMUSG00000048332	Lipoma HMGIC fusion partner precursor.	2	pictar|targetscan	4.5
Adcyap1	ENSMUSG00000024256	Pituitary adenylate cyclase-activating polypeptide precursor (PACAP).	2	pictar|targetscan	5.2
Zc3h14	ENSMUSG00000021012	nuclear protein UKp68 isoform b.	2	pictar|targetscan	5.7
Eif5a	ENSMUSG00000078812	Eukaryotic translation initiation factor 5A-1 (eIF-5A-1) (eIF-5A1)	2	pictar|targetscan	6.0
Slc6a1	ENSMUSG00000030310	Sodium- and chloride-dependent GABA transporter 1.	2	pictar|targetscan	6.3
Rap2c	ENSMUSG00000050029	Ras-related protein Rap-2c precursor.	2	pictar|targetscan	6.7
Hmbox1	ENSMUSG00000021972	Homeobox-containing protein 1.	2	pictar|targetscan	6.9
Ccnc	ENSMUSG00000028252	Cyclin-C.	2	pictar|targetscan	7.0
Cdkn2aip	ENSMUSG00000038069	CDKN2A interacting protein	2	pictar|targetscan	7.1
Vamp2	ENSMUSG00000020894	Vesicle-associated membrane protein 2 (VAMP-2) (Synaptobrevin-2).	2	pictar|targetscan	7.2
Rarb	ENSMUSG00000017491	Retinoic acid receptor beta (RAR-beta) (Nuclear receptor subfamily 1 group B member 2).	2	pictar|targetscan	7.4
Azin1	ENSMUSG00000037458	Antizyme inhibitor 1 (AZI) (Ornithine decarboxylase antizyme inhibitor).	2	pictar|targetscan	7.8
Rbmx	ENSMUSG00000031134	RNA binding motif protein, X-linked.	2	pictar|targetscan	7.8
Rapgef6	ENSMUSG00000037533	Rap guanine nucleotide exchange factor (GEF) 6.	2	pictar|targetscan	7.9
Fbxw11	ENSMUSG00000020271	F-box and WD-40 domain protein 11	2	pictar|targetscan	8.0
Stc1	ENSMUSG00000014813	Stanniocalcin-1 precursor (STC-1).	2	pictar|targetscan	8.0
Syt1	ENSMUSG00000035864	Synaptotagmin-1 (Synaptotagmin I) (SytI) (p65).	2	pictar|targetscan	8.0
Tpi1	ENSMUSG00000023456	Triosephosphate isomerase (EC 5.3.1.1) (TIM) (Triose-phosphate isomerase).	2	pictar|targetscan	8.2
Kcna1	ENSMUSG00000047976	Potassium voltage-gated channel subfamily A member 1 (Voltage-gated potassium channel subunit Kv1.1).	2	pictar|targetscan	8.4
Socs5	ENSMUSG00000037104	Suppressor of cytokine signaling 5 (SOCS-5)	2	pictar|targetscan	8.4
Rag1ap1	ENSMUSG00000027953	recombination activating gene 1 activating protein 1	2	targetscan|miranda	8.9
Zmym3	ENSMUSG00000031310	Zinc finger MYM-type protein 3 (Zinc finger protein 261) (DXHXS6673E protein).	2	pictar|targetscan	8.9

MGI Symbol	Ensembl Gene ID	Description	No. Prediction	Prediction Algorithm (>2)	ΔG (-kcal/mol)
Pappa	ENSMUSG00000028370	Pappalysin-1 precursor (EC 3.4.24.79) (Insulin-like growth factor-dependent IGF-binding protein 4 protease) (IGF-dependent IGFBP-4 protease) (IGFBP-4ase).	2	pictar|targetscan	9.1
Gapvd1	ENSMUSG00000026867	GTPase activating protein and VPS9 domains 1	2	pictar|targetscan	9.2
Tmem128	ENSMUSG00000067365	Transmembrane protein 128.	2	targetscan|miranda	9.2
Cltc	ENSMUSG00000047126	Clathrin heavy chain.	2	pictar|targetscan	9.3
Pitx3	ENSMUSG00000025229	Pituitary homeobox 3 (Homeobox protein PITX3).	2	pictar|targetscan	9.4
Ppp1r12c	ENSMUSG00000019254	Protein phosphatase 1 regulatory subunit 12C	2	targetscan|miranda	9.4
Snx1	ENSMUSG00000032382	Sorting nexin-1.	2	targetscan|miranda	9.4
Gdnf	ENSMUSG00000022144	Glial cell line-derived neurotrophic factor precursor (mGDNF)	2	pictar|miranda	9.7
Tbpl1	ENSMUSG00000071359	TATA box-binding protein-like protein 1 (TBP-like protein 1)	2	pictar|targetscan	10.0
Myh9	ENSMUSG00000022443	Myosin-9 (Myosin heavy chain 9) (Myosin heavy chain, non-muscle IIa) (Non-muscle myosin heavy chain IIa) (NMMHC II-a).	2	targetscan|miranda	10.1
Cox6a1	ENSMUSG00000041697	Cytochrome c oxidase polypeptide VIa-liver, mitochondrial precursor.	2	pictar|targetscan	10.3
Vps54	ENSMUSG00000020128	Vacuolar protein sorting-associated protein 54 (Tumor antigen SLP-8p homolog).	2	pictar|targetscan	10.7
Maml1	ENSMUSG00000050567	Mastermind-like protein 1 (Mam-1).	2	pictar|targetscan	10.8
Trhde	ENSMUSG00000050663	Thyrotropin-releasing hormone-degrading ectoenzyme (EC 3.4.19.6) (TRH- degrading ectoenzyme) (TRH-DE).	2	pictar|targetscan	11.1
Bcl2l2	ENSMUSG00000022194	Apoptosis regulator Bcl-W (Bcl-2-like 2 protein) (c98);	2	pictar|targetscan	11.5
Sfrs12	ENSMUSG00000032621	Splicing factor, arginine/serine-rich 12	2	pictar|targetscan	11.5
Rce1	ENSMUSG00000024889	CAAX prenyl protease 2 (Prenyl protein-specific endoprotease 2)	2	targetscan|miranda	11.7
Slc25a25	ENSMUSG00000026819	mitochondrial Ca2+-dependent solute carrier.	2	pictar|targetscan	11.7
Lass2	ENSMUSG00000015714	LAG1 longevity assurance homolog 2 (Translocating chain-associating membrane protein homolog 3) (TRAM homolog 3).	2	pictar|targetscan	11.8
Ccdc117	ENSMUSG00000020482	Coiled-coil domain-containing protein 117.	2	pictar|targetscan	12.0
Ctbp2	ENSMUSG00000030970	C-terminal-binding protein 2 (CtBP2).	2	pictar|miranda	12.0
Trim2	ENSMUSG00000027993	Tripartite motif-containing protein 2 (Neural activity-related RING finger protein).	2	pictar|targetscan	12.0
Ncoa5	ENSMUSG00000039804	Nuclear receptor coactivator 5 (NCoA-5) (Coactivator independent of AF-2).	2	pictar|targetscan	12.2
Sacm1l	ENSMUSG00000025240	SAC1 (supressor of actin mutations 1, homolog)-like.	2	pictar|targetscan	12.4
Exdl2	ENSMUSG00000032705	Exonuclease 3'-5' domain-like-containing protein 2.	2	pictar|targetscan	12.5

MGI Symbol	Ensembl Gene ID	Description	No. Prediction	Prediction Algorithm (>2)	ΔG (-kcal/mol)
Ihpk1	ENSMUSG00000032594	Inositol hexaphosphate kinase 1	2	pictar|targetscan	12.5
Mtmr4	ENSMUSG00000018401	Myotubularin-related protein 4 (EC 3.1.3.48).	2	pictar|targetscan	12.5
Bnip3l	ENSMUSG00000022051	BCL2/adenovirus E1B 19 kDa protein-interacting protein 3-like (NIP3L) (NIP3-like protein X).	2	pictar|targetscan	12.6
Pitpnm2	ENSMUSG00000029406	Membrane-associated phosphatidylinositol transfer protein 2 B	2	pictar|targetscan	12.8
Atp6ap2	ENSMUSG00000031007	Renin receptor precursor (Renin/prorenin receptor)	2	pictar|targetscan	13.1
Numa1	ENSMUSG00000066306	nuclear mitotic apparatus protein 1	2	pictar|targetscan	13.1
Nup153	ENSMUSG00000021374	nucleoporin 153	2	pictar|targetscan	13.1
Kctd20	ENSMUSG00000005936	BTB/POZ domain-containing protein KCTD20.	2	pictar|targetscan	13.2
Jazf1	ENSMUSG00000063568	Juxtaposed with another zinc finger protein 1.	2	pictar|targetscan	13.3
Adcy6	ENSMUSG00000022994	Adenylate cyclase type 6 (Adenylate cyclase type VI)	2	pictar|targetscan	13.7
Ppp1r9b	ENSMUSG00000038976	Neurabin-2 (Neurabin-II) (Spinophilin) (Protein phosphatase 1 regulatory subunit 9B).	2	pictar|targetscan	13.9
Ftl1	ENSMUSG00000050708	Ferritin light chain 1 (Ferritin L subunit 1).	2	pictar|miranda	14.2
Crk	ENSMUSG00000017776	Proto-oncogene C-crk (p38) (Adapter molecule crk).	2	pictar|targetscan	14.3
Nnat	ENSMUSG00000067786	Neuronatin.	2	pictar|targetscan	14.4
Snrk	ENSMUSG00000038145	SNF-related serine/threonine-protein kinase (EC 2.7.11.1) (SNF1- related kinase).	2	pictar|targetscan	14.4
Zc3h10	ENSMUSG00000039810	Zinc finger CCCH domain-containing protein 10.	2	pictar|targetscan	14.8
Gdi2	ENSMUSG00000021218	Rab GDP dissociation inhibitor beta (Rab GDI beta) (Guanosine diphosphate dissociation inhibitor 2)	2	pictar|targetscan	16.8
Zdhhc8	ENSMUSG00000060166	Probable palmitoyltransferase ZDHHC8 (EC 2.3.1.-) (Zinc finger DHHC domain-containing protein 8) (DHHC-8).	2	pictar|targetscan	16.8
Elavl1	ENSMUSG00000040028	ELAV-like protein 1 (Hu-antigen R) (HuR) (Elav-like generic protein) (MelG).	2	pictar|targetscan	18.2
Ring1	ENSMUSG00000024325	E3 ubiquitin-protein ligase RING1 (RING finger protein 1).	2	targetscan|miranda	18.2
Papss1	ENSMUSG00000028032	Bifunctional 3'-phosphoadenosine 5'-phosphosulfate synthetase 1	2	pictar|targetscan	18.3
Ppp2r5d	ENSMUSG00000059409	delta isoform of regulatory subunit B56, protein phosphatase 2A.	2	pictar|targetscan	18.6
Stx5a	ENSMUSG00000010110	Syntaxin-5.	2	pictar|miranda	19.0
Agk	ENSMUSG00000029916	Acylglycerol kinase, mitochondrial precursor (Multiple substrate lipid kinase) (MuLK).	2	pictar|targetscan	19.4
Ndrg1	ENSMUSG00000005125	Protein NDRG1 (N-myc downstream-regulated gene 1 protein) (Protein Ndr1).	2	targetscan|miranda	20.0
Bai1	ENSMUSG00000034730	Brain-specific angiogenesis inhibitor 1 precursor.	2	pictar|targetscan	22.0
Unk	ENSMUSG00000020770	RING finger protein unkempt homolog (Zinc finger CCCH domain- containing protein 5).	2	pictar|targetscan	23.4

Table 7.5 (C) Overlapping Target Predictions for miR-142 using miRanda, TargetScan and PicTar Algorithms					
MGI Symbol	Ensembl Gene ID	Description	No. Prediction	Prediction Algorithm (>2)	ΔG (-kcal/mol)
Marcks	ENSMUSG00000069662	Myristoylated alanine-rich C-kinase substrate (MARCKS).	3	miranda|targetscan|pictar	2.2
Mgat4a	ENSMUSG00000026110	Alpha-1,3-mannosyl-glycoprotein 4-beta-N-acetylglucosaminyltransferase A	3	miranda|targetscan|pictar	4.6
Stam	ENSMUSG00000026718	Signal transducing adapter molecule 1 (STAM-1).	3	miranda|targetscan|pictar	4.7
Ank3	ENSMUSG00000069601	ankyrin 3, epithelial isoform i	3	miranda|targetscan|pictar	5.5
Arntl	ENSMUSG00000055116	Aryl hydrocarbon receptor nuclear translocator-like protein 1	3	miranda|targetscan|pictar	6.2
Mark3	ENSMUSG00000007411	MAP/microtubule affinity-regulating kinase 3	3	miranda|targetscan|pictar	6.4
Atf7ip	ENSMUSG00000030213	Activating transcription factor 7-interacting protein 1 (ATFa- associated modulator)	3	miranda|targetscan|pictar	9.4
Cpeb2	ENSMUSG00000039782	Cytoplasmic polyadenylation element-binding protein 2	3	miranda|targetscan|pictar	9.8
Clta	ENSMUSG00000028478	Clathrin light chain A	3	miranda|targetscan|pictar	12.0
Tmem59	ENSMUSG00000028618	Transmembrane protein 59 precursor (Thymic dendritic cell-derived factor 1).	3	miranda|targetscan|pictar	12.3
Atg16l1	ENSMUSG00000026289	Autophagy-related protein 16-1 (APG16-like 1).	3	miranda|targetscan|pictar	12.4
Rgl2	ENSMUSG00000041354	Ral guanine nucleotide dissociation stimulator-like 2	3	miranda|targetscan|pictar	15.3
Patz1	ENSMUSG00000020453	POZ (BTB) and AT hook containing zinc finger 1	3	miranda|targetscan|pictar	16.1
Inpp5a	ENSMUSG00000025477	inositol polyphosphate-5-phosphatase A	3	miranda|targetscan|pictar	18.9
Llgl2	ENSMUSG00000020782	Lethal(2) giant larvae protein homolog 2 (Lethal giant larvae-like protein 2).	3	miranda|targetscan|pictar	19.2
Gnb2	ENSMUSG00000029713	Guanine nucleotide-binding protein G(I)/G(S)/G(T) subunit beta-2 (Transducin beta chain 2)	3	miranda|targetscan|pictar	0.0
Zeb2	ENSMUSG00000026872	Zinc finger E-box-binding homeobox 2 (Smad-interacting protein 1).	2	pictar|targetscan	0.5
Fbxo3	ENSMUSG00000027180	F-box only protein 3.	2	pictar|targetscan	4.6
Fndc3a	ENSMUSG00000033487	Fibronectin type-III domain-containing protein 3a.	2	pictar|targetscan	4.7
Tfg	ENSMUSG00000022757	Trk-fused	2	targetscan|miranda	5.0
Tsen34	ENSMUSG00000035585	tRNA-splicing endonuclease subunit Sen34 (EC 3.1.27.9) (tRNA-intron endonuclease Sen34)	2	targetscan|miranda	5.1
Nr3c1	ENSMUSG00000024431	Glucocorticoid receptor (GR) (Nuclear receptor subfamily 3 group C member 1).	2	pictar|targetscan	5.9
Twf1	ENSMUSG00000022451	Twinfilin-1 (Protein A6).	2	pictar|targetscan	5.9
Lrrc59	ENSMUSG00000020869	Leucine-rich repeat-containing protein 59.	2	pictar|targetscan	6.5
Tbl1xr1	ENSMUSG00000027630	F-box-like/WD repeat-containing protein TBL1XR1 (Transducin beta-like 1X-related protein 1)	2	pictar|targetscan	6.5
Zeb1	ENSMUSG00000024238	Zinc finger E-box-binding homeobox 1 (Transcription factor 8)	2	pictar|targetscan	6.6
Zfp513	ENSMUSG00000043059	zinc finger protein 513	2	pictar|miranda	6.8
Stau1	ENSMUSG00000039536	Double-stranded RNA-binding protein Staufen homolog 1.	2	pictar|targetscan	6.9
Rab2	ENSMUSG00000047187	Ras-related protein Rab-2A.	2	pictar|miranda	7.7
Stx12	ENSMUSG00000028879	Syntaxin-12.	2	pictar|targetscan	7.7
Aff2	ENSMUSG00000031189	AF4/FMR2 family member 2 (Fragile X mental retardation protein 2 homolog)	2	targetscan|miranda	7.8
Dcun1d4	ENSMUSG00000051674	DCN1-like protein 4 (Defective in cullin neddylation protein 1-like protein 4)	2	targetscan|miranda	7.9

MGI Symbol	Ensembl Gene ID	Description	No. Prediction	Prediction Algorithm (>2)	ΔG (-kcal/mol)
Mmd	ENSMUSG00000003948	Monocyte to macrophage differentiation protein	2	pictar|targetscan	7.9
Sgms1	ENSMUSG00000040451	Phosphatidylcholine:ceramide cholinephosphotransferase 1 (Sphingomyelin synthase 1)	2	pictar|targetscan	8.0
Eml4	ENSMUSG00000032624	Echinoderm microtubule-associated protein-like 4 (EMAP-4).	2	pictar|targetscan	8.2
Xpo1	ENSMUSG00000020290	Exportin-1 (Exp1) (Chromosome region maintenance 1 protein homolog).	2	pictar|targetscan	8.2
Tardbp	ENSMUSG00000041459	TAR DNA-binding protein 43 (TDP-43).	2	pictar|targetscan	8.5
Pmaip1	ENSMUSG00000024521	phorbol-12-myristate-13-acetate-induced protein 1	2	pictar|targetscan	8.6
Morf4l2	ENSMUSG00000031422	Mortality factor 4-like protein 2 (Transcription factor-like protein MRGX)	2	pictar|targetscan	9.4
Myst2	ENSMUSG00000038909	Histone acetyltransferase MYST2	2	pictar|targetscan	9.5
Acvr2a	ENSMUSG00000052155	Activin receptor type-2A precursor (EC 2.7.11.30) (Activin receptor type IIA)	2	pictar|targetscan	9.7
Crk	ENSMUSG00000017776	Proto-oncogene C-crk (p38) (Adapter molecule crk).	2	pictar|targetscan	9.7
Strn3	ENSMUSG00000020954	Striatin-3 (Cell-cycle autoantigen SG2NA) (S/G2 antigen).	2	pictar|miranda	10.1
Dirc2	ENSMUSG00000022848	Disrupted in renal carcinoma protein 2 homolog.	2	pictar|targetscan	10.3
Peli1	ENSMUSG00000020134	Protein pellino homolog 1 (Pellino-1)	2	pictar|targetscan	10.3
Pum1	ENSMUSG00000028580	Pumilio homolog 1.	2	targetscan|miranda	10.3
Tesk2	ENSMUSG00000033985	Dual specificity testis-specific protein kinase 2	2	pictar|targetscan	10.4
Pafah1b2	ENSMUSG00000003131	Platelet-activating factor acetylhydrolase IB subunit beta	2	pictar|targetscan	10.5
Cask	ENSMUSG00000031012	Peripheral plasma membrane protein CASK (Calcium/calmodulin-dependent serine protein kinase).	2	pictar|miranda	11.1
Itgav	ENSMUSG00000027087	Integrin alpha-V precursor (Vitronectin receptor subunit alpha) (CD51 antigen)	2	targetscan|miranda	11.1
Tmem55b	ENSMUSG00000035953	Transmembrane protein 55B (Type I phosphatidylinositol 4,5-bisphosphate 4-phosphatase)	2	pictar|targetscan	11.8
Sox6	ENSMUSG00000051910	Transcription factor SOX-6 (SOX-LZ).	2	pictar|targetscan	11.9
Morf4l1	ENSMUSG00000043223	Mortality factor 4-like protein 1 (Transcription factor-like protein MRG15)	2	pictar|targetscan	12.2
Wasl	ENSMUSG00000029684	Neural Wiskott-Aldrich syndrome protein (N-WASP).	2	pictar|miranda	12.2
Tiparp	ENSMUSG00000034640	TCDD-inducible poly [ADP-ribose] polymerase	2	pictar|targetscan	12.8
Tnks	ENSMUSG00000031529	tankyrase, TRF1-interacting ankyrin-related ADP-ribose polymerase	2	pictar|targetscan	13.7
Ptpn23	ENSMUSG00000036057	Tyrosine-protein phosphatase non-receptor type 23	2	targetscan|miranda	13.9
2310022M17Rik	ENSMUSG00000044502	Protein FAM44B.	2	pictar|miranda	14.4
Gtf2a1	ENSMUSG00000020962	Transcription initiation factor IIA subunit 1 (General transcription factor IIA1)	2	pictar|targetscan	14.4
Vps24	ENSMUSG00000053119	Charged multivesicular body protein 3 (Chromatin-modifying protein 3) (Vacuolar protein-sorting-associated protein 24).	2	targetscan|miranda	14.4
Ppp1r10	ENSMUSG00000039220	Serine/threonine-protein phosphatase 1 regulatory subunit 10	2	pictar|miranda	14.9
Man1a2	ENSMUSG00000008763	Mannosyl-oligosaccharide 1,2-alpha-mannosidase IB	2	pictar|targetscan	15.0
Tmem132e	ENSMUSG00000020701	Transmembrane protein 132E precursor.	2	targetscan|miranda	15.3
Mbd6	ENSMUSG00000025409	methyl-CpG binding domain protein 6	2	pictar|targetscan	16.1
Map3k7ip2	ENSMUSG00000015755	Mitogen-activated protein kinase kinase kinase 7-interacting protein 2	2	targetscan|miranda	16.9
Map3k11	ENSMUSG00000004054	Mitogen-activated protein kinase kinase kinase 11	2	targetscan|miranda	18.4
Spns1	ENSMUSG00000030741	Protein spinster homolog 1.	2	pictar|miranda	18.5

Table 7.6: Summary of *in silico* target predictions for miR-96, -182, -183, -1, -133 and -142			
miR name	**Number of predicted targets** (miRanda/PicTar/intersection)	**Number of miRanda targets** (retinal transcriptome/retinal disease genes)	**Intersection of miRanda and PicTar targets** (retinal transcriptome/retinal disease genes)
miR-96	869 / 435 / 69	428 / 23	43 / 2
miR-182	860 / 396 / 60	427 / 14	50 / 0
miR-183	900 / 143 / 36	441 / 15	30 / 0
miR-1	777 / 289 / 44	357 / 16	34 / 2
miR-133	860 / 207 / 44	419 / 17	32 / 1
miR-142	807 / 125 / 33	381 / 14	28 / 0
Average	**846 / 266 / 48**	**409 / 17**	**36 / <1**

Table 7.6: Summary of *in silico* target predictions for miR-96,-182, -183 and miR-1, 133, and -142 using miRanda and PicTar algorithms: (Column 1) total number of predicted miRanda targets genes using both methods and their intersection, (Column 2) targets expressed in the retina/disease genes and (Column 3) intersection of miRanda and PicTar retinal targets.

miR-1 and miR-133										
GENE	GENE NAME	CHR	DESCRIPTION	FUNCTION	HIT miR-1	HIT miR-133	PVALUE miR-1	PVALUE miR-133	SCORE miR-1	SCORE miR-133
ENSMUSG00000022174	Dad1	14	defender against cell death 1	negative regulator of apoptosis	1	1	7.29E-04	3.28E-04	16.0322	16.3733
ENSMUSG00000022197	Pdzd2	15	PDZ domain containing 2	binding of the C-termini of transmembrane receptors or ion channels, signal transduction	1	1	1.11E-02	3.47E-03	18.0788	15.3018
ENSMUSG00000022656	Pvrl3	16	poliovirus receptor-related 3	interact with afadin, actin cytoskeleton, adherens junctions	1	1	1.16E-03	3.56E-02	17.0362	16.0861
ENSMUSG00000024081	Cebpz	17	CCAAT/enhancer binding protein zeta	regulation of transcription	1	1	2.26E-05	1.90E-02	16.6394	16.7441
ENSMUSG00000024268	Brunol4	18	bruno-like 4, RNA binding protein	pre-mRNA splicing	1	1	4.02E-02	1.49E-03	16.6906	15.9094
ENSMUSG00000024902	Mrpl11	19	mitochondrial ribosomal protein L11	mitochondrial protein synthesis	1	1	1.89E-02	2.84E-03	17.5103	16.9418
ENSMUSG00000026088	Mitd1	1	MIT, microtubule interacting and transport, domain containing 1	protein transport, intracellular trafficking	1	1	5.03E-03	2.44E-02	17.2646	16.4798
ENSMUSG00000026527	Rgs7	1	regulator of G-protein signaling 7	G-protein regulation, signal transduction	1	1	8.24E-03	3.77E-02	15.8019	16.0245
ENSMUSG00000028629	3110037I16Rik	4	RIKEN cDNA 3110037I16 gene	unknown	1	2	1.22E-02	1.09E-05	17.9248	15.8827
ENSMUSG00000032463	Faim	9	Fas apoptotic inhibitory molecule	negative regulator of apoptosis	1	1	1.25E-02	1.02E-03	16.1757	16.8544
ENSMUSG00000033107	Rnf125	18	ring finger protein 125	ubiquitin-proteasome pathway, immune response	2	1	3.49E-03	2.67E-02	15.9902	15.4572
ENSMUSG00000035964	Tmem59l	8	transmembrane protein 59-like	membrane glycoprotein	1	1	8.91E-04	2.76E-02	17.66	16.3519
ENSMUSG00000060279	Ap2a1	7	adaptor-related protein complex 2, alpha 1 subunit	part of the protein coat of coated vesicles, clathrin mediated endocytosis	1	1	3.66E-05	3.74E-03	17.4971	15.2247
ENSMUSG00000066357	Wdr6	9	WD repeat domain 6	may facilitate formation of heterotrimeric or multiprotein complexes	1	1	2.43E-03	7.51E-05	16.7716	16.2475
ENSMUSG00000071647	Eml3	19	echinoderm microtubule associated protein like 3	protein binding, cytoskeleton	1	1	3.72E-06	3.36E-02	17.624	16.1459
ENSMUSG00000078945	Birc1-rs1	13	baculoviral IAP repeat-containing 1, related sequence 1	unknown	1	1	4.83E-02	1.12E-02	16.487	17.2829

Table 7.7.A Common targets predicted for miR-1 and -133: For each target gene corresponding chromosomal location, function, number of target sites/miR (hit), p-value and score associated with miRanda predictions are provided. Common targets shared by all three miRs are highlighted in light blue.

miR-1 and miR-142										
GENE	GENE NAME	CHR	DESCRIPTION	FUNCTION	HIT miR-1	HIT miR-142	PVALUE miR-1	PVALUE miR-142	SCORE miR-1	SCORE miR-142
ENSMUSG00000001482	Def8	8	differentially expressed in FDCP 8 homolog	intracellular signaling	1	1	3.34E-02	1.61E-03	16.8918	16.3799
ENSMUSG00000006373	Pgrmc1	X	progesterone receptor membrane component 1	steroid membrane receptor	1	1	7.01E-06	1.59E-02	15.9341	17.1379
ENSMUSG00000014980	5730449L18Rik	1	RIKEN cDNA 5730449L18 gene	mRNA/tRNA processing	1	1	2.74E-02	3.48E-02	17.1077	16.3882
ENSMUSG00000022708	Zbtb20	16	zinc finger and BTB domain containing 20	regulation of transcription	1	1	4.96E-03	3.86E-02	16.6007	15.499
ENSMUSG00000024076	Vit	17	Vitrin	unknown	1	1	1.39E-03	4.29E-02	17.1431	16.1849
ENSMUSG00000024640	Psat1	19	phosphoserine aminotransferase 1	amino acid biosynthesis	1	1	4.93E-03	8.52E-04	15.761	15.3888
ENSMUSG00000025551	Fgf14	14	fibroblast growth factor 14	cell growth and survival	1	1	1.75E-03	7.47E-03	16.302	15.5328
ENSMUSG00000026088	Mitd1	1	MIT, microtubule interacting and transport, domain containing 1	protein transport, intracellular trafficking	1	1	5.03E-03	4.88E-06	17.2646	16.3981
ENSMUSG00000028580	Pum1	4	pumilio homolog 1	regulation of translation	2	1	3.83E-02	5.06E-04	16.7431	15.7547
ENSMUSG00000029247	Paics	5	phosphoribosylaminoimidazole carboxylase, phosphoribosylaminoimidazole succinocarboxamide synthetase	purine biosynthesis	1	1	1.08E-04	4.60E-02	16.5024	16.1167
ENSMUSG00000029576	D930005D10Rik	5	RIKEN cDNA D930005D10 gene	signal transduction	1	2	6.90E-03	4.43E-02	16.0261	16.1536
ENSMUSG00000029821	Dfna5h	6	Deafness, autosomal dominant 5 homolog	inner ear receptor, cell differentiation	1	1	4.42E-04	2.40E-04	16.2358	15.8401
ENSMUSG00000029924	Slc37a3	6	solute carrier family 37	carbohydrate transport	1	1	2.36E-03	8.65E-05	15.7867	15.4253
ENSMUSG00000030469	Zfp719	7	zinc finger protein 719	zinc ion binding, unknown function	1	1	4.45E-02	3.05E-02	16.5766	15.6027
ENSMUSG00000030724	Cd19	7	CD19 molecule	B-lymphocyte activation	1	2	5.69E-03	2.64E-03	16.156	16.7995
ENSMUSG00000031811	Fbxo31	8	F-box protein 31	ubiquitin-proteasome pathway	1	1	4.70E-03	6.19E-04	16.9418	15.499
ENSMUSG00000031918	Mtmr2	9	myotubularin related protein 2	phospholipid dephosphorylation	1	1	5.77E-03	5.74E-05	16.9418	15.8384
ENSMUSG00000032463	Faim	9	Fas apoptotic inhibitory molecule	negative regulator of apoptosis	1	1	1.25E-02	1.05E-02	16.1757	16.2073
ENSMUSG00000033107	Rnf125	18	ring finger protein 125	ubiquitin-proteasome pathway, immune response	2	2	3.49E-03	3.08E-03	15.9902	15.7026
ENSMUSG00000033703	Fuk	8	fucokinase	cell-cell interactions	1	2	6.08E-03	5.32E-03	16.3202	16.0289
ENSMUSG00000035131	B830045N13Rik	1	RIKEN cDNA B830045N13 gene	unknown	1	1	8.66E-03	3.89E-02	17.3094	15.8904
ENSMUSG00000039671	Prkcbp1	2	zinc finger, MYND-type containing 8	protein and zinc Ion binding, other name: protein kinase C binding protein 1	2	1	3.46E-02	4.32E-02	16.8554	16.1778
ENSMUSG00000041483	Zfp281	1	zinc finger protein 281	unknown	1	1	1.65E-02	4.24E-03	15.8047	15.9515
ENSMUSG00000053119	Vps24	6	vacuolar protein sorting 24 homolog	protein sorting of transmembrane proteins	1	1	4.28E-03	4.85E-02	16.1459	16.0647
ENSMUSG00000060152	Pop5	5	processing of precursor 5, ribonuclease P/MRP subunit	hydrolase, ribonuclease, RNA processing	1	1	6.38E-03	1.53E-05	15.9185	16.0647
ENSMUSG00000060183	Cxcl11	5	chemokine (C-X-C motif) ligand 11	cell - cell signaling	1	1	6.05E-03	2.86E-03	16.5467	17.208
ENSMUSG00000060279	Ap2a1	7	adaptor-related protein complex 2, alpha 1 subunit	part of the protein coat of coated vesicles, clathrin mediated endocytosis	1	1	3.66E-05	3.06E-03	17.4971	15.6004
ENSMUSG00000061911	Myt1l	12	myelin transcription factor 1-like	regulation of transcription	1	1	3.86E-04	2.23E-02	16.7565	15.6832

Table 7.7.B. Common targets predicted for miR-1 and -142: For each target gene corresponding chromosomal location, function, number of target sites/miR (hit), p-value and score associated with miRanda predictions are provided. Common targets shared by all three miRs are highlighted in light blue.

miR-133 and miR-142										
GENE	GENE NAME	CHR	DESCRIPTION	FUNCTION	HIT miR-133	HIT miR-142	PVALUE miR-133	PVALUE miR-142	SCORE miR-133	SCORE miR-142
ENSMUSG00000003527	Es2el	16	xpressed sequence 2 embryonic lethal	mRNA processing	1	1	4.99E-03	3.17E-04	15.3499	15.7253
ENSMUSG00000004054	Map3k11	19	mitogen-activated protein kinase kinase kinase 11	activation of MAP8/JNK kinase	1	1	2.46E-05	2.41E-04	18.402	17.7825
ENSMUSG00000004113	Cacna1b	2	calcium channel, voltage-dependent, N type, alpha 1B subunit	calcium ion transport	1	1	9.61E-05	3.05E-02	15.1155	16.5172
ENSMUSG00000016256	Ctsz	2	cathepsin Z	proteolysis	1	1	3.61E-02	2.65E-02	16.0695	16.6524
ENSMUSG00000018581	Dnahc11	12	dynein, axonemal heavy chain 11	microtubule motor activity	1	2	1.40E-03	3.83E-03	16.0322	18.4844
ENSMUSG00000019710	Mrpl24	3	mitochondrial ribosomal protein L24	mitochondrial protein synthesis	1	1	8.55E-04	7.37E-04	15.3619	16.0718
ENSMUSG00000019889	Ptprk	10	protein tyrosine phosphatase, receptor type, K	protein amino acid dephosphorylation	1	1	6.61E-03	1.20E-02	15.6652	15.4945
ENSMUSG00000020694	Tlk2	11	tousled-like kinase 2	chromatin assembly	1	1	2.91E-02	4.13E-02	16.2964	16.2225
ENSMUSG00000026088	Mitd1	1	MIT, microtubule interacting and transport, domain containing 1	protein transport, intracellular trafficking	1	1	2.44E-02	4.88E-06	16.4798	16.3981
ENSMUSG00000028478	Clta	4	clathrin, light chain (Lca)	clathrin mediated endocytosis	1	1	3.23E-05	1.74E-06	17.0555	18.4404
ENSMUSG00000029066	Mrpl20	4	mitochondrial ribosomal protein L20	mitochondrial ribosome protein	1	1	1.82E-03	2.63E-02	16.294	16.6578
ENSMUSG00000029621	Arpc1a	5	actin related protein 2/3 complex, subunit 1A, 41kDa	actin cytoskeleton organization and biogenesis	1	1	4.26E-02	8.51E-03	15.9185	15.6121
ENSMUSG00000030223	Ptpro	6	protein tyrosine phosphatase, receptor type, O	protein amino acid dephosphorylation	2	1	4.28E-02	4.47E-03	15.8895	15.5253
ENSMUSG00000031840	Rab3a	8	RAB3A, member RAS oncogene family	GTPase activity, regulates synaptic vesicle endocytosis/recycling	1	1	4.49E-05	1.30E-03	16.502	17.2255
ENSMUSG00000032463	Faim	9	Fas apoptotic inhibitory molecule	negative regulator of apoptosis	1	1	1.02E-03	1.05E-02	16.8544	16.2073
ENSMUSG00000033107	Rnf125	18	ring finger protein 12	ubiquitin-proteasome pathway, immune response	1	2	2.67E-02	3.08E-03	15.4572	15.7026
ENSMUSG00000033161	Atp1a1	3	ATPase, Na+/K+ transporting, alpha 1 polypeptide	ATP hydrolysis coupled proton transport	1	1	3.68E-04	3.44E-02	15.961	15.9937
ENSMUSG00000033364	Usp37	1	ubiquitin specific peptidase 37	ubiquitin-proteasome pathway	1	1	7.53E-03	4.24E-03	15.1225	15.6121
ENSMUSG00000034187	Nsf	11	N-ethylmaleimide sensitive fusion protein	ion and protein transport	1	1	4.56E-02	1.94E-02	15.8218	15.4608
ENSMUSG00000037344	Slc12a9	5	solute carrier family 12 (potassium/chloride transporters), member 9	solute transporter	1	1	2.62E-02	3.66E-03	16.3268	16.0276
ENSMUSG00000038387	Rras	7	related RAS viral (r-ras) oncogene homolog	Ras protein signal transduction	2	1	3.88E-03	4.52E-03	16.3733	18.3273
ENSMUSG00000039615	Stub1	17	STIP1 homology and U-Box containing protein 1	protein ubiquitination	1	1	7.53E-03	4.52E-03	15.1225	18.3273
ENSMUSG00000040479	Dgkz	2	diacylglycerol kinase, zeta 104kDa	signal transduction	1	1	8.82E-03	3.30E-02	15.0338	16.4386
ENSMUSG00000040822	1700123O20Rik	14	RIKEN cDNA 1700123O20 gene	unknown	1	1	9.72E-03	6.70E-04	15.0382	15.5012
ENSMUSG00000047557	Lxn	3	latexin	metalloendopeptidase inhibitor activity	1	1	7.24E-03	2.74E-05	15.691	16.6303
ENSMUSG00000052997	Sae2/Uba2	7	ubiquitin-like modifier activating enzyme 2	ubiquitin-proteasome pathway	1	2	2.78E-02	2.55E-02	15.2906	16.6887
ENSMUSG00000060279	Ap2a1	7	adaptor protein complex AP-2, alpha 1 subunit	part of the protein coat of coated vesicles, clathrin mediated endocytosis	1	1	3.74E-03	3.06E-03	15.2247	15.6004
ENSMUSG00000062380	Tubb3	8	tubulin, beta 3	microtubule component	1	1	1.11E-03	1.05E-02	17.7377	15.7253
ENSMUSG00000062480	Acat3	17	acetyl-Coenzyme A acetyltransferase 3	transferase activity	1	1	1.12E-02	4.24E-03	17.2829	15.8384

Table 7.7.C Common targets predicted for miR-133 and -142: For each target gene corresponding chromosomal location, function, number of target sites/miR (hit), p-value and score associated with miRanda predictions are provided. Common targets shared by all three miRs are highlighted in light blue.

miR-96 and miR-182										
GENE	GENE NAME	CHR	DESCRIPTION	FUNCTION	HIT miR-96	HIT miR-182	PVALUE miR-96	PVALUE miR-182	SCORE miR-96	SCORE miR-182
ENSMUSG00000000902	Smarcb1	10	Swi/Snf-Related, Matrix-Associated, Actin-Dependent Regulator of Chromatin, Subfamily B, Member 1; SMARCB1	part of a complex that relieves repressive chromatin structures, allowing the transcriptional machinery to access its targets	1	1	2.61E-02	9.81E-03	16.6303	15.4662
ENSMUSG00000002109	Ddb2	2	damage-specific DNA binding protein 2, 48kDa	DNA repair	2	1	8.67E-04	5.92E-03	16.4828	15.5588
ENSMUSG00000002147	Stat6	10	signal transducer and activator of transcription 6, interleukin-4 induced	regulation of transcription, signal transduction	1	1	4.45E-03	2.74E-02	16.7097	16.6249
ENSMUSG00000003528	Slc25a1	16	solute carrier family 25 (mitochondrial carrier; citrate transporter), member 1	mitochondrial citrate transport	1	1	3.37E-06	4.38E-02	17.1297	16.1475
ENSMUSG00000004031	6430517E21Rik	1	RIKEN cDNA 6430517E21 gene	also called: BMP/retinoic acid-inducible neural-specific protein 2	1	1	2.53E-05	1.29E-02	15.4945	15.6649
ENSMUSG00000005696	Sh2d1a	X	SH2 domain protein 1A, Duncan's disease (lymphoproliferative syndrome)	bidirectional stimulation of T and B cells	1	1	1.96E-04	6.47E-05	17.3424	16.7387
ENSMUSG00000007411	Mark3	12	MAP/microtubule affinity-regulating kinase 3	protein serine/threonine/tyrosine kinase	2	2	8.40E-04	1.24E-02	16.2072	16.4835
ENSMUSG00000020376	Rnf130	11	ring finger protein 130	embryonic development, growth factor withdrawal-induced apoptosis	1	1	3.28E-04	2.74E-03	17.4222	15.6904
ENSMUSG00000020400	Tnip1	11	TNFAIP3 interacting protein 1	protein binding, glycoprotein biosynthetic process	2	1	5.37E-03	1.33E-02	15.7816	15.343
ENSMUSG00000022868	Ahsg	16	alpha-2-HS-glycoprotein	development	1	1	4.72E-04	6.18E-06	16.1685	17.1179
ENSMUSG00000024177	Nme4	17	non-metastatic cells 4, protein expressed in	nucleoside metabolic process	1	1	6.15E-05	4.14E-03	15.6121	16.3628
ENSMUSG00000029022	D4Wsu114e	4	DNA segment, Chr 4, Wayne State University 114, expressed	unknown	1	1	3.83E-03	2.84E-02	18.5536	16.587
ENSMUSG00000029228	Lnx1	5	ligand of numb-protein X 1	ubiquitin cycle	1	1	2.49E-02	1.38E-04	16.6771	15.6904
ENSMUSG00000029472	Anapc5	5	anaphase promoting complex subunit 5	anaphase promoting	1	1	3.70E-02	5.50E-03	16.2741	15.5616
ENSMUSG00000030890	Ilk	7	integrin-linked kinase	integrin-mediated signal transduction	2	2	2.26E-03	1.44E-03	16.0647	16.4749
ENSMUSG00000031169	Porcn	X	porcupine homolog (Drosophila)	endoplasmic reticulum protein	1	1	3.67E-03	2.79E-04	15.9096	16.3173
ENSMUSG00000031918	Mtmr2	9	myotubularin related protein 2	phospholipid dephosphorylation	1	1	6.70E-03	3.01E-03	15.8384	15.9145
ENSMUSG00000032009	Sesn3	9	sestrin 3	cell cycle arrest	1	1	2.86E-04	2.71E-02	16.4989	16.3469
ENSMUSG00000035493	Tgfbi	13	transforming growth factor, beta-induced, 68kDa	inhibitor of cell adhesion	1	1	5.33E-03	8.16E-05	16.5954	16.3472
ENSMUSG00000036206	Sh3bp4	1	SH3-domain binding protein 4	clathrin mediated endocytosis	1	1	1.12E-02	1.72E-05	15.2853	16.3302
ENSMUSG00000038256	Bcl9	3	B-cell CLL/lymphoma 9	protein binding, associated with B-cell acute lymphoblastic leukemia	1	1	1.93E-03	2.33E-02	15.6121	15.8025
ENSMUSG00000040693	Slco4c1	1	solute carrier organic anion transporter family, member 4C1	anion transport	1	1	2.05E-02	1.35E-03	15.8994	15.3809
ENSMUSG00000040907	Atp1a3	7	ATPase, Na+/K+ transporting, alpha 3 polypeptide	potassium and sodium transport	1	1	1.50E-02	3.28E-02	16.2188	16.4414
ENSMUSG00000041650	Pcca	14	propionyl Coenzyme A carboxylase, alpha polypeptide	amino-acid metabolism and fatty acid oxidation	1	1	1.37E-05	2.01E-04	19.5717	15.5783
ENSMUSG00000042655	A930021C24Rik	13	RIKEN cDNA A930021C24 gene	unknown	1	1	5.21E-04	8.20E-03	16.8913	15.3835

ENSMUSG00000041650	Pcca	14	propionyl Coenzyme A carboxylase, alpha polypeptide	component of mitochondrial enzyme propionyl-CoA carboxylase	1	1	2.01E-04	1.16E-03	15.5783	16.2596
ENSMUSG00000048332	Lhfp	3	lipoma HMGIC fusion partner	transmembrane protein	1	1	2.27E-02	4.23E-02	16.8131	15.7326
ENSMUSG00000048756	Foxo3	10	forkhead box O3	transcription factor, regulation of transcription, stimulates apoptosis	1	1	9.20E-03	3.84E-03	15.967	15.439
ENSMUSG00000049686	Tmem142a/ORAT 1	5	ORAI calcium release-activated calcium modulator 1	calcium ion binding/transport	1	1	3.72E-02	2.10E-03	16.3156	15.5477
ENSMUSG00000050812	AI314180	4	expressed sequence AI314180	unkown	2	1	4.86E-02	3.38E-08	16.0391	15.3664
ENSMUSG00000054580	Pla2r1	2	phospholipase A2 receptor 1	receptor, endocytosis	1	1	2.96E-02	2.52E-02	16.5477	16.5593
ENSMUSG00000055319	Sec23ip	7	SEC23 interacting protein	intracellular protein transport	1	1	3.01E-04	3.21E-04	15.8589	15.5292
ENSMUSG00000056310	Tyw1	5	tRNA-yW synthesizing protein 1 homolog	tRNA processing	1	1	1.15E-03	4.10E-02	17.5205	16.2138
ENSMUSG00000058400	Gpr103	3	G protein-coupled receptor 103	signal transduction	1	1	1.24E-02	2.17E-02	15.9468	16.7106
ENSMUSG00000059714	Flot1	17	Flotillin-1.	vesicular trafficking and signal transduction	2	1	6.01E-09	4.52E-02	18.156	15.2362
ENSMUSG00000060475	Wtap	17	Wilms tumor 1 associated protein	mRNA processing	1	1	3.13E-02	4.05E-02	16.4894	16.0777
ENSMUSG00000060679	Mrps9	1	mitochondrial ribosomal protein S9	translation	1	1	4.57E-03	1.14E-02	16.3628	16.8281
ENSMUSG00000061207	Stk19	17	serine/threonine kinase 19	regulation of transcription	1	1	7.32E-05	2.24E-04	17.7077	16.3733
ENSMUSG00000068115	4930519N13Rik	2	RIKEN cDNA 4930519N13 gene	calcium ion binding, cytoskeleton	1	2	4.49E-02	8.30E-04	16.1225	16.3654
ENSMUSG00000070865	6030436E02Rik	5	RIKEN cDNA 6030436E02 gene	electron carrier activity, heme binding	1	1	2.80E-03	4.80E-02	17.3799	15.9019

Table 7.8.A Common targets predicted for miR-96 and -182: For each target gene corresponding chromosomal location, function, number of target sites/miR (hit), p-value and score associated with miRanda predictions are provided. Common targets shared by all three miRs are highlighted in light blue.

miR-96 and miR-183										
GENE	GENE NAME	CHR	DESCRIPTION		HIT miR-96	HIT miR-183	PVALUE miR-96	PVALUE miR-183	SCORE miR-96	SCORE miR-183
ENSMUSG00000000902	Smarcb1	10	Swi/Snf-Related, Matrix-Associated, Actin-Dependent Regulator of Chromatin, Subfamily B, Member 1; SMARCB1	part of a complex that relieves repressive chromatin structures, allowing the transcriptional machinery to access its targets	1	1	2.61E-02	1.09E-02	16.6303	17.3966
ENSMUSG00000001280	Sp1	15	Sp1 transcription factor	RNA polymerase II transcription factor	1	1	8.63E-03	8.97E-03	15.855	15.7284
ENSMUSG00000002833	Hdgfrp2	17	hepatoma-derived growth factor, related protein 2	DNA binding, regulation of transcription	1	1	6.74E-03	1.73E-02	15.499	16.9418
ENSMUSG00000002996	Hbp1	12	HMG-box transcription factor 1 (HBP1)	regulation of transcription	1	1	4.23E-03	1.08E-02	15.5144	16.6821
ENSMUSG00000004936	Map2k1	9	Mitogen-Activated Protein Kinase Kinase 1; MAP2K1	MAP kinase, signal transduction	1	1	2.52E-06	3.51E-04	15.7223	16.0968
ENSMUSG00000005621	Zfp592	7	Zinc finger protein 592 (Zfp592)	DNA binding, regulation of transcription	1	1	6.39E-04	4.96E-02	16.7071	15.8673
ENSMUSG00000005696	Sh2d1a	X	SH2 domain protein 1A, Duncan's disease (lymphoproliferative syndrome)	bidirectional stimulation of T and B cells	1	1	1.96E-04	8.54E-03	17.3424	15.2927
ENSMUSG00000005732	Ranbp1	16	RAN binding protein 1	intracellular transport	1	1	4.41E-04	5.03E-03	16.2251	15.4928
ENSMUSG00000006715	Gmnn	13	Geminin, DNA replication inhibitor (GMNN)	negative regulation of DNA replication	2	1	3.80E-03	1.25E-03	15.499	16.2596
ENSMUSG00000007617	Homer1	13	homer homolog 1	metabolic glutamate receptor function, synaptic transmission	2	2	7.83E-04	1.62E-03	17.3091	17.2829
ENSMUSG00000015476	Prrt1	17	proline-rich transmembrane protein 1	unknown	1	1	7.05E-04	7.71E-04	15.3646	15.2326
ENSMUSG00000017754	Pltp	2	phospholipid transfer protein	lipid metabolic process	1	1	2.01E-02	5.43E-04	15.7253	16.7144
ENSMUSG00000019467	D10Ertd610e	10	DNA segment, Chr 10, ERATO Doi 610	Rho guanyl-nucleotide exchange factor activity	1	2	8.42E-03	3.76E-03	15.5544	15.6328
ENSMUSG00000019785	Rlbp1l2	10	retinaldehyde binding protein 1-like 2	transport	1	1	1.02E-09	2.90E-07	16.1218	15.3846
ENSMUSG00000020524	Gria1	11	glutamate receptor, ionotropic, AMPA 1	synaptic transmission	1	1	8.52E-06	4.89E-05	16.9697	15.3499
ENSMUSG00000021760	2310016C16Rik	13	RIKEN cDNA 2310016C16 gene	glutathione peroxidase activity	1	1	8.52E-03	2.89E-02	16.2304	16.4214
ENSMUSG00000022040	Ephx2	14	epoxide hydrolase 2, cytoplasmic	epoxide - dihydrodiol conversion	1	1	6.81E-03	4.04E-03	15.8088	18.3854
ENSMUSG00000023353	Centg3	5	centaurin, gamma 3	small GTPase mediated signal transduction	1	1	2.09E-02	2.75E-03	16.1407	16.0011
ENSMUSG00000024186	Rgs11	17	regulator of G-protein signaling 11	signal transduction	1	1	7.87E-03	8.55E-03	15.3514	17.642
ENSMUSG00000024486	Hbegf	18	heparin-ninding EGF-like growth factor; HBEGF	growth factor	1	1	6.49E-04	1.50E-02	15.3955	15.9483
ENSMUSG00000024958	Gpr137	19	G protein-coupled receptor 137	signal transduction	2	1	1.04E-03	7.77E-03	16.5172	17.7377
ENSMUSG00000024982	Zdhhc6	19	zinc finger, DHHC-type containing 6	acyltransferase activity, zinc ion binding	1	1	2.58E-06	6.04E-06	17.7962	16.5887
ENSMUSG00000025809	Itgb1	8	integrin, beta-1; ITGB1 (fibronectin receptor, beta subunit; FNRB)	cell adhesion	1	1	1.78E-04	4.72E-02	16.6856	15.9185
ENSMUSG00000025878	Uimc1	13	ubiquitin interaction motif containing 1	regulation of transcription	1	1	2.34E-03	2.39E-02	16.0731	16.6158
ENSMUSG00000026790	Odf2	2	outer dense fiber of sperm tails 2; ODF2	cytoskeletal structure of sperm tail	1	1	1.37E-03	9.76E-03	19.5717	17.5103
ENSMUSG00000027953	Rag1ap1	3	Recombination activating gene 1 activating protein 1 (Rag1ap1)	unknown	1	1	7.67E-04	1.03E-02	16.6303	15.2362
ENSMUSG00000028049	Scamp3	3	secretory carrier membrane protein 3	protein transport	1	1	2.26E-05	7.71E-04	17.1324	15.5195
ENSMUSG00000029022	D4Wsu114e	4	DNA segment, Chr 4, Wayne State University 114, expressed (D4Wsu114e)	unknown	1	1	3.83E-03	5.23E-04	18.5536	18.9884
ENSMUSG00000029474	Rnf34	5	ring finger protein 34; RNF34	protein-protein and protein-DNA interaction, anti-apoptotic	2	1	1.29E-04	8.77E-04	15.8319	17.1439
ENSMUSG00000030189	Csda	6	cold-shock domain protein A; CSDA	DNA/RNA binding	1	1	1.11E-03	2.00E-03	16.3154	15.3345
ENSMUSG00000030287	Itpr2	6	inositol 1,4,5-triphosphate receptor, type 2	calcium ion channel, signal transduction	1	1	1.56E-07	1.80E-02	18.6667	15.4636

ENSMUSG00000030982	9030624J02Rik	7	RIKEN cDNA 9030624J02 gene (9030624J02Rik)	membrane protein	1	1	7.87E-05	5.01E-03	15.499	15.5773
ENSMUSG00000032006	Pdgfd	9	platelet-derived growth factor D; PDGFD	DNA synthesis, cell growth	2	1	9.57E-05	2.87E-06	15.4042	17.735
ENSMUSG00000032009	Sesn3	9	sestrin 3	cell cycle arrest	1	1	2.86E-04	2.62E-04	16.4989	15.2366
ENSMUSG00000036552	9030025P20Rik	17	RIKEN cDNA 9030025P20 gene	unknown	1	1	3.64E-02	1.54E-02	16.2909	17.0564
ENSMUSG00000038156	Spon1	7	spondin 1; SPON1	protein binding, cell adhesion	1	1	3.46E-03	1.00E-02	15.8511	15.8224
ENSMUSG00000039275	Foxk2	11	forkhead box K2	transcription factor, regulation of transcription	1	1	1.77E-08	1.75E-02	15.945	15.412
ENSMUSG00000039943	Plcb4	2	phospholipase C, beta 4	signal transduction	1	1	1.69E-04	4.22E-03	16.2079	15.674
ENSMUSG00000041057	Wdr43	17	WD repeat domain 43	unknown	1	1	4.06E-02	4.28E-03	16.1778	15.5773
ENSMUSG00000041650	Pcca	14	propionyl Coenzyme A carboxylase, alpha polypeptide	component of mitochondrial enzyme propionyl-CoA carboxylase	1	1	1.37E-05	1.16E-03	19.5717	16.2596
ENSMUSG00000042590	Ipo11	13	Importin 11; IPO11	nucleocytoplasmic transport of protein and RNA	1	1	2.92E-02	1.09E-02	16.5172	17.3966
ENSMUSG00000043909	Trp53bp1	2	transformation related protein 53 binding protein 1	DNA repair, transcription factor binding, regulation of transcription	1	1	1.67E-02	2.71E-02	17.0828	16.487
ENSMUSG00000044229	D930028F11Rik	9	RIKEN cDNA D930028F11 gene	unknown	1	1	3.85E-02	4.92E-02	16.2333	15.8768
ENSMUSG00000045576	St7l	3	suppression of tumorigenicity 7 like	unknown	1	1	5.64E-03	4.72E-02	17.196	15.9185
ENSMUSG00000051246	A930005I04Rik	5	RIKEN cDNA A930005I04 gene (A930005I04Rik)	unknown	1	1	2.05E-03	1.40E-04	16.0647	15.4636
ENSMUSG00000052299	Zfp294	16	zinc finger protein 294	zinc ion binding, unknown function	1	1	8.51E-04	5.87E-04	16.5172	18.1925
ENSMUSG00000055523	Gucy2g	19	guanylate cyclase 2G homolog (mouse) pseudogene	protein kinase, intracellular signaling	1	1	8.77E-04	5.58E-03	15.3747	16.3399
ENSMUSG00000056962	Jmjd6	11	jumonji domain containing 6	histone demethylase, oxidoreductase	2	1	4.60E-07	1.33E-03	19.2323	16.3733
ENSMUSG00000058806	Col13a1	10	collagen, type XIII, alpha 1	cell matrix adhesion	1	1	1.70E-02	1.29E-04	17.0656	16.502
ENSMUSG00000060279	Ap2a1	7	adaptor-related protein complex 2, alpha-1 subunit; AP2A1	part of the protein coat of coated vesicles, clathrin mediated endocytosis	1	1	5.34E-03	6.56E-03	16.6178	16.4745
ENSMUSG00000061207	Stk19	17	serine/threonine kinase 19	regulation of transcription	3	1	1.13E-04	2.24E-04	16.2909	16.3733
ENSMUSG00000061455	Stx17	4	syntaxin 17; STX17	membrane trafficking	1	1	3.13E-05	1.79E-02	15.8055	16.902
ENSMUSG00000061755	A230054D04Rik	5	RIKEN cDNA A230054D04 gene	unknown	1	1	2.15E-02	3.79E-02	16.8272	16.1459
ENSMUSG00000062867	Impdh2	9	IMP Dehydrogenase 2; IMPDH2	guanine nucleotide biosynthesis (RNA and DNA synthesis)	1	1	3.41E-02	4.36E-02	16.3574	16.0011
ENSMUSG00000068115	4930519N13Rik	2	RIKEN cDNA 4930519N13 gene	calcium ion binding, cytoskeleton	2	2	2.29E-03	8.30E-04	15.9928	16.3654
ENSMUSG00000068740	Celsr2	3	cadherin, EGF LAG seven-pass G-type receptor 2	cell adhesion	1	1	4.66E-04	4.72E-02	18.2142	15.9185
ENSMUSG00000074622	Mafb	2	v-maf musculoaponeurotic fibrosarcoma oncogene homolog B	regulation of transcription	1	1	2.00E-02	3.84E-03	15.9812	15.2499

Table 7.8.B Common targets predicted for miR-96 and -183: For each target gene corresponding chromosomal location, function, number of target sites/miR (hit), p-value and score associated with miRanda predictions are provided. Common targets shared by all three miRs are highlighted in light blue.

miR-182 and miR-183										
GENE	GENE NAME	CHR	DESCRIPTION		HIT miR-182	HIT miR-183	PVALUE miR-182	PVALUE miR-183	SCORE miR-182	SCORE miR-183
ENSMUSG00000000902	Smarcb1	10	Swi/Snf-Related, Matrix-Associated, Actin-Dependent Regulator of Chromatin, Subfamily B, Member 1; SMARCB1	part of a complex that relieves repressive chromatin structures, allowing the transcriptional machinery to access its targets	1	1	9.81E-03	1.09E-02	15.4662	17.3966
ENSMUSG00000002808	Epdr1	13	ependymin related protein 1	calcium dependent cell adhesion	1	1	2.90E-04	4.74E-02	18.5795	15.915
ENSMUSG00000005696	Sh2d1a	X	SH2 domain protein 1A, Duncan's disease (lymphoproliferative syndrome)	bidirectional stimulation of T and B cells	1	1	6.47E-05	8.54E-03	16.7387	15.2927
ENSMUSG00000009549	Srp14	2	signal recognition particle 14-KD; SRP14	protein transport to ER	1	1	5.51E-03	6.90E-06	15.8917	15.5618
ENSMUSG00000018378	Cuedc1	11	CUE domain containing 1	ubiquitin binding, unknown function	1	1	5.38E-04	8.73E-03	16.3118	15.1958
ENSMUSG00000019775	Rgs17	10	regulator of G-protein signaling 17	regulates G-protein signaling	4	1	6.72E-06	1.91E-04	15.662	15.6622
ENSMUSG00000020412	Ascc2	11	activating signal cointegrator 1 complex subunit 2	regulation of transcription	1	1	3.80E-03	3.26E-03	16.3206	18.5986
ENSMUSG00000020585	Laptm4a	12	Lysosomal-associated protein transmembrane 4 alpha	membrane protein	1	1	1.46E-02	4.54E-03	15.574	15.6797
ENSMUSG00000020801	Med31	11	mediator complex subunit 31	regulation of transcription	1	1	7.04E-03	3.44E-02	15.4662	15.3499
ENSMUSG00000024231	Cul2	18	cullin 2	ubiquitin cycle, induction of apoptosis	1	1	6.38E-03	1.49E-04	15.6177	15.7273
ENSMUSG00000024483	Eif4ebp3	18	eukaryotic translation initiation factor 4E binding protein 3	inhibits translation initiation factor 4E	1	1	1.74E-02	3.79E-02	16.6991	16.1459
ENSMUSG00000025134	Thoc4	11	THO complex 4	molecular chaperone	1	1	7.13E-04	1.66E-02	17.5957	16.1459
ENSMUSG00000029022	D4Wsu114e	4	D4Wsu114e DNA segment, Chr 4, Wayne State University 114	unknown	1	1	2.84E-02	5.23E-04	16.587	18.9884
ENSMUSG00000029064	Gnb1	4	guanine nucleotide binding protein (G protein), beta polypeptide 1	signal transduction	1	1	9.16E-03	3.08E-03	15.5783	15.9185
ENSMUSG00000030067	Foxp1	6	forkhead box P1	transcription factor, regulation of transcription	1	1	5.65E-03	9.16E-07	18.1959	16.2504
ENSMUSG00000030342	Cd9	6	CD9 molecule	modulation of cell adhesion and migration	1	1	2.10E-03	5.39E-03	16.8937	15.4557
ENSMUSG00000030924	2610020H08Rik	7	RIKEN cDNA 2610020H08 gene	hydrolase, nuclease	2	3	1.45E-02	7.45E-04	17.2594	16.502
ENSMUSG00000031295	Phka2	X	phosphorylase kinase, alpha 2	glycogen metabolic process, protein modification process	1	1	2.55E-04	1.25E-04	17.6399	15.3532
ENSMUSG00000032009	Sesn3	9	sestrin 3	cell cycle arrest	1	1	2.71E-02	2.62E-04	16.3469	15.2366
ENSMUSG00000032228	Tcf12	9	transcription factor 12 (HTF4, helix-loop-helix transcription factors 4)	regulation of transcription	1	1	3.55E-02	3.79E-02	16.3628	16.1459
ENSMUSG00000032293	Ireb2	9	iron-responsive element binding protein 2	iron ion binding	2	1	8.82E-06	8.03E-03	17.5957	15.4636
ENSMUSG00000032481	Smarcc1	9	SWI/SNF related, matrix associated, actin dependent regulator of chromatin, subfamily c, member 1	part of a complex that relieves repressive chromatin structures, allowing the transcriptional machinery to access its targets	1	1	1.04E-02	9.66E-03	15.3828	15.1849
ENSMUSG00000032526	Deb1	9	differentially expressed in B16F10 1	unknown	2	2	6.31E-05	3.76E-03	15.4784	15.6826
ENSMUSG00000033392	Clasp2	9	cytoplasmic linker associated protein 2	negative regulation of microtubule depolymerization, cell division/cycle	1	1	5.83E-03	1.40E-05	15.7541	16.6433
ENSMUSG00000036632	Alg5	3	asparagine-linked glycosylation 5 homolog (S. cerevisiae, dolichyl-phosphate beta-glucosyltransferase)	N-linked glycosylation	1	1	1.28E-03	1.12E-02	16.9048	17.0316
ENSMUSG00000040524	Zfp609	9	zinc finger protein 609	zinc ion binding, regulation of transcription	1	1	4.42E-02	1.22E-03	16.1387	18.3062

ENSMUSG00000041650	Pcca	14	propionyl Coenzyme A carboxylase, alpha polypeptide	component of mitochondrial enzyme propionyl-CoA carboxylase	1	1	2.01E-04	1.16E-03	15.5783	16.2596
ENSMUSG00000048332	Lhfp	3	lipoma HMGIC fusion partner	transmembrane protein	1	1	2.27E-02	4.23E-02	16.8131	15.7326
ENSMUSG00000048756	Foxo3	10	forkhead box O3	transcription factor, regulation of transcription, stimulates apoptosis	1	1	9.20E-03	3.84E-03	15.967	15.439
ENSMUSG00000049686	Tmem142a/ORAT 1	5	ORAI calcium release-activated calcium modulator 1	calcium ion binding/transport	1	1	3.72E-02	2.10E-03	16.3156	15.5477
ENSMUSG00000050812	AI314180	4	expressed sequence AI314180	unkown	2	1	4.86E-02	3.38E-08	16.0391	15.3664
ENSMUSG00000054580	Pla2r1	2	phospholipase A2 receptor 1	receptor, endocytosis	1	1	2.96E-02	2.52E-02	16.5477	16.5593
ENSMUSG00000055319	Sec23ip	7	SEC23 interacting protein	intracellular protein transport	1	1	3.01E-04	3.21E-04	15.8589	15.5292
ENSMUSG00000056310	Tyw1	5	tRNA-yW synthesizing protein 1 homolog	tRNA processing	1	1	1.15E-03	4.10E-02	17.5205	16.2138
ENSMUSG00000058400	Gpr103	3	G protein-coupled receptor 103	signal transduction	1	1	1.24E-02	2.17E-02	15.9468	16.7106
ENSMUSG00000059714	Flot1	17	Flotillin-1.	vesicular trafficking and signal transduction	2	1	6.01E-09	4.52E-02	18.156	15.2362
ENSMUSG00000060475	Wtap	17	Wilms tumor 1 associated protein	mRNA processing	1	1	3.13E-02	4.05E-02	16.4894	16.0777
ENSMUSG00000060679	Mrps9	1	mitochondrial ribosomal protein S9	translation	1	1	4.57E-03	1.14E-02	16.3628	16.8281
ENSMUSG00000061207	Stk19	17	serine/threonine kinase 19	regulation of transcription	1	1	7.32E-05	2.24E-04	17.7077	16.3733
ENSMUSG00000068115	4930519N13Rik	2	RIKEN cDNA 4930519N13 gene	calcium ion binding, cytoskeleton	1	2	4.49E-02	8.30E-04	16.1225	16.3654
ENSMUSG00000070865	6030436E02Rik	5	RIKEN cDNA 6030436E02 gene	electron carrier activity, heme binding	1	1	2.80E-03	4.80E-02	17.3799	15.9019

Table 7.8.C Common targets predicted for miR-183 and -182: For each target gene corresponding chromosomal location, function, number of target sites/miR (hit), p-value and score associated with miRanda predictions are provided. Common targets shared by all three miRs are highlighted in light blue.

Chapter 8

Design of miR Expression Vectors and *In Vitro* Analysis

8.1. Introduction

In order to understand how miRs function, as with protein-coding genes, it is vital to determine their spatial and temporal expression. Cloning studies have been used to identify novel miRs, and recently technologies have been developed which greatly enhance the detection of miRs, such as LNA probes for microarray and ISH detection, and stem-loop primers for miR RT-PCR analysis. Additionally in order to identify the roles of endogenous miRs, miR target identification is also vital. As highlighted in chapter 7, *in silico* target prediction methods provide a tool to identify potential gene targets based on the likelihood of miR:mRNA interactions, crucially however these targets require validation in the "wet-lab" environment. The most straightforward and efficient method to identify genuine miR targets is by means of miR overexpression studies, to examine the ability of expressed miRs to interact with, and mediate translational suppression of genuine targets. To validate the targets of the 6 miRs predicted in chapter 7, it is of importance to be able to overexpress these miRs *in vitro* and in *vivo*. Indeed the targets suppressed by these miRs, identified to be dysregulated in mouse models of RP, may play a role in retinal degeneration.

As a result of the expansion of the miR field, commercial miR products have emerged for *in vitro* analysis of miR function, including Pre-miR™ precursor molecules and Anti-miR™ miR inhibitors, chemically modified nucleic acids designed to mimic endogenous mature miRs and to inhibit endogenous miRs respectively. While transfection of these chemically modified nucleic acids is efficient for miR function analysis in cell-based systems, *in vivo* studies generally benefit from longer expression times and thus expression of miRs from vector constructs is highly desirable. Indeed to examine miR function in the retina, *in vivo* or *ex vivo* (organotypic culture) studies are particularly important, as the retinal architecture remains intact. Moreover the lack of reliable retinal/photoreceptor cell lines make *in vitro* analysis difficult (Seigel 1999).

The expression of miRs from vector systems is well established, involving the amplification of the pri-miR sequence by PCR from genomic DNA, and the insertion into the expression vector of choice (Zeng et al. 2002; Chung et al. 2006). RNA Pol II promoters are generally used to drive miR expression constructs as recent bioinformatic searches have identified that the vast majority of human intergenic miRs are transcribed by polymerase II, based on the upstream promoter elements (Lee et al. 2002; Lee et al.

2004). The majority of miR transcription start sites (TSS) appear to locate within 6kb upstream of the pre-miR sequence (Saini et al.; Zhou et al.), and transcribe a pri-miR transcript of 3-4 kb in length (Saini et al. 2007) however, the identification of the 3' and 5' boundaries of the pri-miR sequence is more difficult (Saini et al. 2007). As the pri-miR sequence of the majority of miRs is not defined, determining the required pri-miR length for insertion into miR expression vectors is difficult, but nevertheless required for the correct processing of the mature miR. An alternative method was therefore utilised in this study for the over-expression of retinal miRs, involving a artificial miR expression system originally intended for RNAi applications.

Indeed the development of miR expression vectors has primarily been driven by keen interest from the RNAi research field, for more advantageous vector systems for gene suppression studies (Amarzguioui et al. 2005; Du et al. 2006). The vector based expression of small interfering RNAs (siRNAs) from short hairpin RNA (shRNA) is widely used to examine gene function, shRNAs themselves resembling the pre-miR stem-loop structure and similarly processed by Dicer to produce ~21nt suppressing siRNAs (Amarzguioui et al. 2005). The expression of siRNAs from synthetic pri-miR structures is desired due to the advantages it offers over short-hairpin RNAs (shRNA) as synthetic miR vectors are designed to employ the endogenous miR-processing pathway to produce more efficient RNAi target suppression (Zeng et al. 2002; Chung et al. 2006). Extensive studies expressing miR-30 and miR-155 from vectors, demonstrated that artificial miRs could be expressed from synthetic stem-loop precursors based on the miR-30 and miR-155 pre-miR sequence (Zeng et al. 2002; Stegmeier et al. 2005; Chung et al. 2006). One vector that has emerged from these studies is 'pcDNA 6.2-GW/± EmGFP-miR' construct, which has been used in this study for the expression of endogenous retinal miRs.

pcDNA 6.2-GW/± EmGFP-miR is a vector system based on the endogenous pri-miR-155 sequence (Lagos-Quintana et al. 2002), that mediates the expression of synthetic miRs. The sequence requirements of synthetic pre-miRs have been elucidated sufficiently to ensure the entry of the synthetic pre-miR into the miR Drosha and Dicer processing pathways. The promoter region of miR-155 was previously identified (Tam 2001), and the minimal sequence length of the pre-miR-155 sequence required for efficient production of mature miR-155, was determined to be 108nt, containing both the stem-loop pre-miR and adjacent flanking sequences (Tam 2001; Chen et al. 2004). In general for efficient pri-miR processing by Drosha, a large loop sequence (>10 nt) is

optimal (Zeng and Cullen 2005; Han et al. 2006) and ssRNA flanking sequences at each end of the stem sequence are required (Chen et al. 2004; Zeng and Cullen 2005). The specific sequence of the flanking region appears to be insignificant, provided the sequence is single stranded and of adequate length (>40nt) (Chen et al. 2004; Zeng and Cullen 2005). These important sequence requirements of miR-155 are retained in this vector system, specifically the engineered pre-miR duplex is inserted within the pre-miR-155 sequence, replacing both miR-155 and its complementary strand, while the miR-155 loop and flanking regions are maintained (Figure 8.1). Additionally the expression of this vector is driven by the CMV immediate-early Pol II promoter to provide a high level of expression in various mammalian cells (Boshart et al. 1985), and incorporation of the EmGFP (Emerald Green Fluorescent Protein) gene upstream of the pre-miR sequence to allow efficient tracking of miR expression. In this study endogenous pre-miR sequences are incorporated into this vector, to enable the expression of endogenous miRs. Indeed this use of this pcDNA.6.2 vector to express endogenous miRs represents a novel application of this vector system to our knowledge.

The expression of miRs from expression vectors allows the examination of miR function *in vitro* and *in vivo*. MiR expression vectors have been used in previous studies to examine the effect of miR over-expression. Specifically the functions of miRs in determining cell fate of haematopoietic lineage differentiation has been examined (Chen et al. 2004), in addition to the inhibitory effect of miR-133 on cardiac hypertrophy has also been examined (Care et al. 2007). In order to examine the functions of retinal miRs, including the six miRs identified in the retinal degeneration signature, it is important to explore the effects of miR overexpression in the retina. In this preliminary study miR expression constructs are designed and cloned for a number of retinal miRs (miR-1, -133, -96, -182, -183, -7, -9, -124a, -204, -29c, and –184), using the pcDNA.6.2 vector system, and the ability of these constructs to express miRs is examined *in vitro*. The use of this vector system to overexpress endogenous miR sequences is novel and the findings presented in this Chapter represent an initial study, involving the generation of miR constructs for subsequent detailed analysis *in vitro* and *in vivo*. The rather preliminary results from this study are described in this Chapter, however, it is intended to extend the study significantly in the future.

8.2. Materials and Methods

8.2.1. Vector Construction

The BLOCK-iT™ Pol II miR RNAi Expression Vectors Kit (Invitrogen, Carlsbad, CA, USA), containing the vector pcDNA 6.2-GW/± EmGFP-miR (Appendix 1.2). This construct was originally developed for RNAi applications, to mediate the expression of shRNAs using the miR processing pathways and 'miR-like' structural features. However in this study, this vector construct is used to generate endogenous mature miR expression constructs, and represents the first use of this strategy. Figure 8.1 provides an overview of the steps involved in construction of miR expressing vectors used in this study.

The precursor sequence of endogenous miRs (pre-miR) consists of the antisense miR sequence, loop sequence and the mature sense miR sequence. Upstream flanking sequences determine the pri-miR of endogenous miRs, required for nuclear processing by Drosha. In this vector the pre-miR cassette is based on the mouse miR-155 sequence (Lagos-Quintana et al. 2002), which permits the insertion of an engineered pre-miR ds-oligo between the 5' and 3' flanking regions of miR-155 sequence. The incorporation of the miR-155 flanking sequences facilitates the processing of the inserted pre-miR sequence by Drosha. In this study, miR expression constructs were designed and created to express a total of 13 miRs, using two design methods. The first design incorporates the entire pre-miR sequence of endogenous miRs, including the mature miR, miR loop, and antisense miR endogenous sequences, inserted in between miR-155 flanking regions. These constructs were termed 'endogenous' miR constructs (Figure 8.2) and 11 'endogenous' miR constructs were created, for miR-1, -133, -96, -182, -183, -7, -9, -124a, -204, -29c, and -184. The second design termed 'shRNA' constructs was based on the principles recommended by the manufacturer for RNAi applications. Specifically, the 'shRNA' constructs contain the mature miR sequence the loop-sequence of miR-155, and the antisense miR sequence which is the reverse complement of the mature miR sequence (Figure 8.8 and 8.10) but contains a deletion of two nucleotides at position 9-10. Introduction of this deletion creates an artificial bulge in the secondary structure of the 'shRNA' pre-miR stem, thereby mimicking the structure of possible natural pre-miR stems. shRNA' constructs were made for miR-182 and -29c (Figure 8.8 and 8.10).

The design of these 'shRNA' constructs is to generate shRNA which are processed by the endogenous miR processing pathway. Specifically, the design of 'shRNA' constructs contains the mature miR sequence however features which differ from the 'endogenous miR design' is the insertion of the loop-sequence of miR-155, and the antisense miR sequence is the reverse complement of the mature miR sequence (Figure 8.8 and 8.10). Due to the perfect complementarity of the mature miR and antisense miR sequence, synthetic bulges are introduced into the antisense sequence by deletion of two nucleotides at position 9-10, thereby altering the secondary structure of the transcribed 'shRNA' to reflect that of miRs (Figure 8.8 and 8.10).

8.2.2. DNA dsOligo Design

As detailed above, a total of 13 miR expression constructs were designed, corresponding to 11 mature mouse miRs; namely miR-1, -133, -96, -182, -183, -7, -9, -124a, -204, -29c, and -184. These 'endogenous' miR expression constructs were designed as detailed in Figure 8.2. The top oligo was designed to contain the endogenous pre-miR sequence of these miRs; consisting of the mature miR sequence, hairpin sequence, and the antisense miR sequence. The bottom oligo was designed to be the reverse complement of top oligo strand. Both the top and bottom strands are designed with the appropriate overhangs at the 5' and 3' end, for insertion into the pcDNA.6.2 plasmid. These top and bottom oligos were annealed, prior to ligation into the linearised plasmid (Appendix 1.2) which displays the complementary overhangs for insertion of the engineered sequences. As the complete endogenous pre-miR sequences were inserted into the pcDNA6.2. plasmid, these constructs were termed 'endogenous' miR constructs.

In addition two 'shRNA' miR constructs were designed to express miR-182 and -29c, which are called "pcDNA-6.2-miR-182-shRNA" and "pcDNA-6.2-miR-29c-shRNA" respectively, as detailed in Figures 8.8 and 8.10. The top oligo consisted of the endogenous mature miR sequence, the hairpin sequence of miR-155, and the reverse complement antisense sequence with a 2 nt modification. This alteration of the antisense miR strand involved the deletion of two nucleotides at position 9 and 10, creating bulges that are thought to improve processing by drosha. The bottom oligo was designed to be the reverse complement of the top oligo, containing the necessary overhang sequences.

The top and bottom single stranded HPLC purified DNA oligos were obtained from Sigma-Genosys (Figure 8.3), and used in vector construction.

8.2.3. Vector Construction

In this study circularised pcDNA 6.2-GW/± EmGFP-miR was linearised using the restriction enzyme *Bsa I.* The digest was set up using 1X NEB Buffer 3 (New England Biolabs, Frankfurt, Germany) as outlined in section 2.2.1, at an incubation temperature of 50°C. *Bsa I* cleaved the vector at two sites (5'..GGTCTC$(N)_1$'..3') and excised the 26 bp stuffer sequence (Appendix 1.2). This creates an insertion site for the pre-miR cassette with a 5' TGCTG and 3' GTCC overhang. The digested vector was separated from the 26 bp stuffer insert by gel electrophoresis (1%), the linearised vector was excised from the gel and the DNA extracted using the QIAquick Coulmn (see section 2.2.4).

The top and bottom oligo DNA sequences for each miR expression construct were resuspended in nuclease-free H_2O, and diluted to a concentration of 100 μM. To anneal each pair of top and bottom DNA oligos, 10 μl of each oligo (100 μM) was added to 1X annealing buffer (section 2.1.1.) in a total reaction volume of 30 μl. The reaction was incubated on the T3000 Thermal Cycler (Biometra) at 95°C for 4 minutes, 70°C for 10 minutes, 37°C for 20 minutes, and 10°C for 10 minutes.

The resulting dsDNA stock solution (50 μM) was diluted to 10 nM for ligation into the linearised pcDNA 6.2 vector. The ligation reaction was set up as follows to a final reaction volume of 20 μl using components from the BLOCK-iT™ Pol II miR RNAi Expression Vectors Kit and incubated at 16-18°C overnight; 2 μl of linearised vector, 4 μl ds oligo (10nM), 4 μl 5x ligation buffer (containing T4 DNA ligase), and 7 μl nuclease-free H_20.

For each miR construct, competent *E.coli* strain XL1B bacteria were prepared (see section 2.2.5) and transformed using 10 μl of ligated insert and vector (see section 2.2.6). 200 μl of each transformation was plated onto LB agar plates containing tetracycline (50 μg/ml) and spectinomycin (50 μg/ml) and incubated at 37°C overnight.

Transformants were examined and an agar master plate was created, containing labelled colonies from individual positive clones. Mini plasmid DNA preparations of

positive clones were generated (see section 2.2.7) and the sequence of each plasmid was verified using the recommended forward and reverse primers (Appendix.4.1.) to determine the sequence and orientation of the engineered pre-miR cassette (see section 2.2.11).

Validated positive clones were identified and maintained separately on agar plates containing the appropriate selective antibiotics. The Qiagen High Speed Plasmid Maxi Kit was used for large-scale plasmid purification, as outlined in section 2.2.8. The concentration and purity of the DNA samples was determined using the NanoDrop™ 1000 Spectrophotometer (section 2.2.10), and the constructs were again sequenced as outlined above, to guarantee the expected DNA construct was isolated. Glycerol Stocks of the positive clones for all miR constructs were prepared (see section 2.2.9) for future preparation of DNA stocks.

8.2.4. Transfection of miR Constructs in HeLa cells

The expression of the following 'endogenous' miR constructs were examined in HeLa cells: pcNDA6.2-miR-1, pcNDA6.2-miR-133, pcNDA6.2-miR-96, pcNDA6.2-miR-182, pcNDA6.2-183, miR-124, pcNDA6.2-miR-29c, and pcNDA6.2-miR-184. In addition expression of the 'shRNA' miR-182 and miR-29c constructs were also examined.

Frozen stock of low passage number HeLa cells were thawed and grown in supplemented DMEM (see section 2.1.2) and maintained as outlined in section 2.4.1. HeLa cells were seeded in 6-well plates one day prior to transfection at a concentration of 6.25×10^5 cells per well. 24 hours later, when the cells had reached 90% confluency, 4µg of DNA of each construct was transfected into the cells using LipofectAMINE 2000 as outlined in section 2.4.4. One day later, the transfection efficiency was examined using the fluorescent microscope (Carl Zeiss Ltd., Hertfordshire, UK) and the cells were harvested. The media was removed and 700 µl of the QIAzol Lysis reagent (Qiagen) was added directly to the cells. The cell lysate was transferred to a tube and homogenized by vortexing. The total RNA was isolated and DNase treated using the miRNeasy Mini Kit (Qiagen) as detailed section 2.3.2.2. The pcDNA6.2-EmGFP 'empty vector' was employed as a negative control in these experiments and transfected in parallel with the miR expression constructs. The transfection of each miR construct listed above, was

undertaken in triplicate in 6-well plates, and the experiment was repeated twice. In addition for the analysis of miR-1 mediated suppression of the known target PTK-9 (detailed below), miR-1 and the negative control pcDNA-EmGFP plasmids were transfected in HeLa cells in triplicate and the experiment was repeated four times.

The commercial synthetic miR-1 termed, 'Pre-miR-1', and the negative control 'Pre-miR Negative Control' were purchased from Ambion (Texas, USA). The negative control is designed for use in experiments using Pre-miR miR Precursors, and contains a random sequence that has been tested in cell lines and tissues, and does not appear to alter gene expression. These synthetic miRs were resuspended to 6.25 μM concentration using nuclease-free H_2O and HeLa cells transfected following the manufactures' instructions. A reverse transfection method of dsRNA was carried out in triplicate in 6-well plates using the transfection agent siPORT™ *NeoFX*. Briefly, 9μl of transfection agent was mixed with 300μl of serum free media (Opti-MEM I, Invitrogen) and incubated at room temperature for 10 minutes, and 24 μl of pre-miR-1 and pre-miR negative control were diluted in 300 μl of Opti-MEM I. The transfection agent and DNA mixtures were combined and incubated at room temperature for 10 minutes. To each well, 600 μl of the dsRNA-lipid complexes and $2.4x10^5$ prepared cells were added and gently rocked to evenly distribute the cells and the transfection complex. The cells were incubated at 37°C, fresh media was applied at 24hrs, and the cells were harvested after 48 hours. The total RNA was isolated and DNase treated using the miRNeasy Mini Kit (Qiagen) as detailed in section 2.3.2.2. The transfection of Pre-miR-1 and the Pre-miR Negative Control was carried out in triplicate, and the experiment was repeated twice.

8.2.5. Quantitative real time RT-PCR

Two-step qPCR was performed using ABI's TaqMan miR Assay (Applied Biosystems, Foster City, CA, USA) according to the manufacturer's instructions (see section 2.3.3.1). The TaqMan miR Assays for the following miRs were utilised: miR-1, -133, -96, -182, -183, –184, -124a, and -29c. Equal amounts of RNA (10 ng/reaction) were used in each RT reaction and snoRNA-202 and -234, were used as internal controls.

PTK-9 (TWF1) expression was examined using designed PTK9 primers and TaqMan PTK9 probes (Appendix.1.1). Primers were designed against the human PTK9

mRNA transcript (Genebank ; accession number NM_002822 (Appendix.1.3) and diluted in nuclease-free water (250 pmol). The real-time RT-PCR reaction was set up (see section 2.3.3.3.) using components from the Quantitech Sybr Green RT-PCR Kit, and incubated on the 7300 Real Time PCR System (ABI). 18S rRNA and beta-actin were used as internal controls. PTK9 expression was also examined using TaqMan probes (ABI) for detection of PTK9 mRNA, and 18s rRNA was used as an internal control. The reverse transcription step and the PCR step were carried out as outlined in section 2.3.3.2. Cycle Threshold (C_T) values were used for RNA quantification as outlined in section 2.3.3.4. The log_2-transformed miR/control expression ratios were used for further analysis.

8.2.6. Statistical Analysis

Analysis of statistical significance was performed using Student's *t-test* and the software GraphPad Prism; differences with $p<0.05$ were considered statistically significant.

8.3. Results

8.3.1 miR Expression Vector Design

The vector pcDNA 6.2-GW/± EmGFP-miR, was used to construct the miR expression vectors. The vector system relies on the endogenous processing of miR-155 as the sequence requirements for nuclear and cytoplasmic processing are reported (Chung et al. 2006). The linearised vector contains the terminal regions of the arms of miR-155, and provides an overhang for the insertion of the artificial miR sequences. For each construct a pre-miR cassette was designed as outlined in Figure 8.1.

In this study 'endogenous' miR expression vectors were constructed to express each of the following endogenous miRs; miR-1, -133, -96, -182, -183, -7, -9, -124a, -204, -29c, and –184, while 'shRNA' constructs were additionally made for miR-182 and miR-29c. Figures 8.2 and 8.8 illustrate the design principles used for the construction of both 'endogenous' and 'shRNA' miR expression vectors.

For the construction of the 'endogenous' miR constructs the top oligo strand of each pre-miR cassette, was designed to contain the endogenous sequence of the desired miR, including the sense miR sequence, endogenous miR-loop, and endogenous antisense strand. The bottom oligo sequence was designed as the reverse complement of the top oligo sequence (Figure 8.2). The overhang sequences derived from the flanking regions of miR-155 are present at either end of the strands, to allow for insertion into the linearised pcDNA6.2 vector system. Double stranded oligos were designed and constructed for each miR expression construct (Figure 8.3), annealed and then ligated prior to insertion into the linearised vector. Positive clones were selected and sequenced to ensure the orientation and sequence of the construct was correct. DNA preparations of these miR expression constructs were made for each miR and used in further analysis.

In addition 'shRNA' miR expression constructs were designed for miR-182 and -29c termed 'pcDNA6.2-miR-182sh' and 'pcDNA6.2-miR-29c-sh' based on the design principles recommended by the manufacturer. As previously described, the 'shRNA' pre-miR cassette is designed to incorporate the following features; the mature miR sequence (miR-182, miR-29c); the loop miR-155 sequence; and the reverse complement antisense sequence in which 2nt at position 9-10 are deleted to create a 'miR-like' bulge in the transcribed RNA (Figure 8.8). These 'shRNA' miR expression plasmids were

constructed, transformed, sequenced, and DNA preparations of each construct were completed. Figures 8.8 and 8.10 illustrate the design principles employed in the construction of 'shRNA' miR constructs, pcDNA6.2-miR-182sh and pcDNA6.2-29c-sh respectively. For comparison, Figures 8.7 and 8.9 illustrate the design of the 'endogenous' miR constructs; pcDNA6.2-miR-182 and pcDNA6.2-miR-29c, respectively.

8.3.2 Expression of miR-constructs in HeLa cells

4μg of the following 'endogenous' and 'shRNA' miR expression constructs were transfected into HeLa cells; pcDNA6.2-miR-1, -miR-133, -miR-96, -miR -183, -miR-124, -miR-184, -miR-182, and -miR-29c; and in addition pcDNA-6.4-182-sh and miR-29c-sh. 24-hours post transfection, the HeLa cells were examined using a fluorescent microscope, and an efficient rate of transfection was observed based on the detection of GFP fluorescence (Figure 8.4). Figure 8.4 provides a representative level of transfection achieved in HeLa cells, and indeed future studies are required in which transfection efficiency is fully examined for all miR constructs. The cells were harvested 24-hours after transfection and total RNA was extracted and used for further analysis.

To examine if the miR-expression constructs were indeed over-expressing the mature miR sequence, quantitative RT-PCR (qPCR) was used to examine the expression of the corresponding miRs. The ABI miR TaqMan assays use a specially designed stem-loop primer specific for reverse transcription of each miR, as discussed in Chapter 2. The stem structure of this primer prevents the hybridisation of the primer with miR precursor sequences, and the primer can anneal to the 3' portion of the miR. These primers thereby detect mature miR sequences, displaying strong sequence discrimination and high sensitivity (Schmittgen et al. 2008). HeLa cells were transfected with 'endogenous' and 'shRNA' miR expression constructs, and the over-expression of the corresponding miR was obtained relative to control cells transfected with the empty EmGFP-vector (Figure 8.4).

The expression of all constructs resulted in an increase of miR expression, corresponding to the miR construct transfected ($p>0.01$; Figure 8.5). However the magnitude of this increase of miR expression across two independent experiments differed significantly, possibly due to altered transfection efficiencies in each experiment.

Of the 'endogenous' miR constructs, miR-1, -184, -133 and -182 expression was increased by the greatest magnitude relative to cells transfected with an empty GFP-expression vector; by an average of 653-fold, 1960-fold, 194-fold and 6-fold respectively across two independent experiments (Figure 8.5A). The expression levels of miR-96, -124, -29c and -183 were increased by an average of 20-fold, 3-fold, 8-fold and 16-fold respectively, in transfected HeLa cells (Figure 8.5B). These data represent the average values across both independent experiments, and as can be observed in Figure 8.5 higher and lower levels of expression were observed in individual experiments. Indeed further experiments are required to fully characterise the miR expression levels achieved using these constructs, however, in principle these constructs are capable of overexpressing miRs *in vitro*. In addition, miR expression of miR-182 and -29c from the corresponding 'shRNA' miR constructs was determined by qPCR (Figure 8.11). The expression of miR-29c and miR-182 was significantly increased following transfection of both the 'endogenous' and 'shRNA' construct in two independent experiments, compared to the negative control ($P<0.01$; Figure 8.11). Specifically the expression of miR-29c, from the 'endogenous' and 'shRNA' miR constructs in independent experiments, increased by 4-fold and 0.7-fold and by 13-fold and 3-fold respectively ($p<0.01$; Figure 8.11). The level of miR-182 expression achieved from the 'endogenous' and 'shRNA' constructs in independent experiments increased by 18-fold and 34.4-fold and by 8.7-fold and 15-fold respectively ($p<0.01$; Figure 8.11). The level of expression of miR-182 and -29c achieved from either the 'endogenous' and 'shRNA' construct are similar ($p>0.05$). However it is evident that there is a large degree of variability of expression achieved between transfections, and as such it is not possible to draw any firm conclusion from these findings. Indeed further studies are required to fully examine the transfection efficiency of the constructs in HeLa cells, which may account for some of the variability observed. While it is not possible to determine whether the incorporation of the miR-155 loop and additional features in the 'shRNA' construct affect the level of miR expression from these results, overall the results obtained demonstrate that miR-182 and miR-29c are expressed from either vector design as evaluated by qPCR.

8.3.3. Analysis of PTK9 suppression by miR-1

The ability of miR-1, expressed from the generated 'endogenous' miR-1 construct, to downregulate the expression of PTK9 (TWF1) was evaluated by qPCR

(Figure 8.12). It has previously been demonstrated that PTK9 is a genuine target of miR-1, and that miR-1 downregulates the expression of PTK9 by degradation of mRNA transcript (Figure 8.13). As such, downregulation of PTK9 by the overexpression of miR-1 can be examined by qPCR (Lim et al. 2005). HeLa cells were transfected with pcDNA6.2-miR-1, harvested at 24 hours, and total RNA isolated using the miRNeasy mini kit (Qiagen). This experiment was repeated four times and the expression of PTK-9 was analysed by ABI miR RT-PCR assays using TaqMan probes (Figure 8.12A) and DNA oligo primers (Figure 8.12 B); analysis was undertaken in triplicate. In addition the synthetic Pre-miR-1 double stranded RNA duplex, and a negative control 'Pre-miR Negative Control' were additionally transfected in HeLa cells as outlined in section 8.2.4. The Pre-miR-1 and the negative control dsRNAs were reverse transfected in HeLa cells in triplicate, and the cells were harvested 48 hours post-transfection. This experiment was repeated and total RNA was extracted using the miRNeasy Mini Kit as detailed in section 2.3.2.2. The expression of PTK was suppressed by miR-1 overexpression by up to 21.1% and 30.1% when analysed using TaqMan or SYBR Green qPCR analyses (Figure 8.12A, 8.12B). Expression of the positive control, pre-miR-1 (Ambion), which is a stable double stranded mature miR duplex, reduced the expression of PTK9 by up to 34.5% and 30.09% (Figure 8.12A 8.12B) using TaqMan and SYBR Green probes. These preliminary results demonstrate that miR-1 expressed from the 'endogenous' miR constructs is capable of downregulating the expression of the known target PTK9 at the mRNA level. However further studies are indeed required to fully characterise the degree of suppression achieved by miR-1, as a large degree of variability was observed across independent experiments (Figure 8.12). Indeed the varying degrees of PTK9 suppression achieved in this initial study, may be related to the level of transfection, highlighting the need for the future expansion of this study to fully characterise the ability of miR-1 to downregulate PTK9 expression. Furthermore the functionality of all the other miR constructs generated during the course of the study described in Chapter 8, also needs to be evaluated by assessing suppression of known targets for each miR in a similar manner to that described for miR-1.

8.4. Discussion

MiR expression vectors were designed and constructed as detailed in Figure 8.1 and 8.2 for a number of the retinal specific miRs discussed in Chapter 3, including miR-1, -133, -96, -182, -183, -7, -9, -124a, -204, -29c, and –184. Notably, these include 5 of the miRs altered in retinal degeneration (miR-96, -182, -183, -1, and -133), additional retinal specific miRs (miR-204, -184, -29c), and miRs enriched in neuronal cells (miR-9, -124, -7). Notably, miR-9 and -7 are implicated in *drosophila* sense organ precursor development (Li et al. 2006) and photoreceptor development (Li and Carthew 2005).

The design of the 'endogenous' miR expression constructs (e.g. pcDNA-miR-182) involved the introduction of the endogenous pre-miR sequence into the linearised vector, thereby eliminating the miR-155 loop while maintaining the miR-155 flanking sequences (Section 8.3.1, Figure 8.1). Transfection of these constructs in cell culture demonstrated a marked increase in mature miR expression in two independent experiment ($p<0.01$), as determined by qPCR. Notably, the stem structure of the reverse transcription primers employed prevents the hybridisation with miR precursor sequences, and therefore these primers bind to and detect the mature miR sequence only (Figure 2.1) (Schmittgen et al. 2008). Specifically miR-1, -133, -184, and -182 expression was drastically increased by up to 194.5 - 1960.6 fold, while miR-96, -183, -29c, -124 expression was increased by up 3.1 - 19.6-fold (Figure 8.5). While miR expression was significantly increased in two independent experiments, the degree of miR overexpression varied across experiments.

Additionally 'shRNA' miR expression constructs were designed expressing miR-182 and -29c (pcDNA-miR-29c-sh; pcDNA-miR-182-sh), accurately following design principles examined by Chung *et al.*, (2006) to imitate the secondary structure of pre-miR-155 (Chung et al. 2006). These modifications are thought to enhance the processing of the synthetic miR, and include the insertion of a 2 nt bulge in the antisense strand and preservation of the miR-155 loop sequence (Figures 8.7-8.10). The expression of miR-182 and -29c were significantly raised in HeLa cells following transfection of the 'shRNA' miR constructs, these initial results demonstrating that miRs are successfully expressed from both the 'endogenous' and 'shRNA' constructs. However due to the variation of magnitude of miR expression across independent experiments, the importance of the altered design of these two constructs cannot be ascertained.

The findings from these miR overexpression studies *in vitro* represent preliminary results, and indeed future studies are required specifically examining the transfection efficiency for each miR construct and further optimising transfection conditions. Future studies aim to fully establish any variations which may exist in the level of expression achieved from both the 'endogenous' and 'shRNA' miR constructs.

However in addition, significant variations of miR upregulation were observed from different miR expression constructs, which may reflect the endogenous levels of miR expression in HeLa cells, as miR levels are expressed relative to cells transfected with an empty vector. These findings are supported by the endogenous miR expression profile of untreated HeLa cells generated by Yeung *et al.*, (2005), which illustrate the moderate endogenous expression of miR-182, and -29c compared to the low or absent expression of miR-1, -184, and -183 (Figure 8.6). The differences in endogenous miR expression in HeLa cells reported in this study, appear to correlate with the relative increase in expression of miR, using the artificial miR constructs (Figure 8.6) (Yeung et al. 2005).

In order to facilitate the processing of the artificial miR constructs, the vector system utilises the sequence features of miR-155. The expression of miR-155 is ubiquitous and appears to be regulated at transcription level alone, as a good correlation between pri-miR and mature miR exists in many cell and tissue types (Jiang et al. 2005; Lee et al. 2008). As human pri-mRNA sequences do not appear to contain a common sequence motif, it is thought that structural features are required for the processing of miRs; including the recognition and efficient processing of pri-miR sequences by Drosha, the export of pre-miR by Exportin-5 (Exp5), and Dicer processing of pre-miRs (Zeng and Cullen 2004; Zeng et al. 2005). These structural requirements can account for the successful expression of mature miRs from miR expression constructs. In general a large flexible loop sequence, ideally greater than 10 nt, and a ssRNA flanking sequence are the structural requirements for optimal nuclear processing by Drosha. (Zeng and Cullen 2005; Han et al. 2006). The large loop is thought to be required for the interaction of Drosha and other cellular proteins such as DGRG8, which are thought to determine the cleavage site of the pri-miR at a set distance from the juntion of the stem and terminal loop (Zeng et al. 2005). Indeed DGRG8 is thought to bind to either end of the miR stem extremities at the junction of ssRNA and ddRNA (SD junction), specifically the flanking ssRNA segments at the base of the dsRNA stem, and the ssRNA terminal loop and the top of the dsRNA

stem (Kim 2005; Zeng et al. 2005). Therefore, the replacement of the miR-155 loop with the endogenous miR loop sequences (>10 nt) in the synthetic miR constructs, should not affect miR processing. Additionally the flanking sequence of miR-155 remains intact in these constructs, which provides a 3' 2 nt overhang following Drosha cleavage that is required for nuclear export. Exp5 recognises this structural motif and additional requirements include a stem sequence greater than 16 nt (Zeng and Cullen 2004). The absence of a 2 nt bulge in the pre-miR sequence or alteration of the terminal loop size does not appear to affect export (Zeng and Cullen 2004), supporting the similar expression levels of miR-29c and –182 from both vector constructs. Following export the pre-miR sequence is processed by Dicer, which recognises and binds to the 3' 2 nt overhang, thereby defining the end of the dsRNA fragment and determining the site of RNA cleavage, roughly ~22nt (~2 helical turns) away from the terminus (Lingel et al. 2004; Macrae et al. 2006). On the whole these findings can account for the production of mature miRs from the synthetic miR expression constructs designed in this study, as it appears that structural features rather than sequences are recognised and required. Notably Zeng *et al.*, (2005) successfully applied this theory, by demonstrating that an entirely artificial sequence whose secondary structure fulfilled the structural requirements, was processed correctly by Drosha (Zeng et al. 2005). Consistent with these findings is the utilisation of these vectors in RNAi research, involving the substitution of the stem region of the pre-miRs with varying synthetic sequences (Zeng et al. 2002; Epanchintsev et al. 2006).

In order to examine the ability of miR-1, expressed from the synthetic miR-1 construct, to down-regulate the expression of a target gene, the expression of the gene PTK (TWF1) was examined by qPCR. In the data displayed in Chapter 7, PTK9 is predicted to be a target of miR-1 and -142 (Appendix 1.3) and additionally PTK9 is also an experimentally validated target of miR-1 at the mRNA level (Lim et al. 2005), thereby permitting the assessment of miR-1 mediated suppression of PTK9 expression by qPCR. The miR prediction software TargetScan recognises two binding sites for miR-1 in the 3'UTR of PTK9, both of which demonstrate exact matches to the miR seed region (position 2-7 of the mature miR) and are conserved sites in humans and mice (Figure 8.13) (Lewis et al. 2003).

The suppression of PTK9 by miR-1 overexpression using the miR expression constructs achieved a suppression of up to 30.1% at 24-hours post-transfection. However

in replicates of these experiments suppression of PTK9 was not always detected, despite the raised expression of miR-1. As the efficiency of suppression of the target transcript should be related in part to the transfection efficiency of the plasmid, further studies monitoring the degree of transfection may resolve the observed variability between experiments. Notably the commercial miR-1 mimic displayed a similar level of PTK9 suppression, by up to 34.5%. This moderate reduction in expression is supported by a recent study, in which the observable decrease in expression of targeted mRNAs, following transfection with the synthetic miR-1 mimic, was rarely greater than 1.3-fold (equivalent to a 25% decrease) (Selbach et al. 2008). It is also possible that there is a delay, between the expression of the mature miR-1 and the repression of PTK9 mRNA. Indeed as demonstrated by Selbach *et al.*, (2008), at 8hrs following miR-1 transfection in HeLa cells many genes displayed a decrease in protein production, yet only small alterations of mRNA were detected, however, greater mRNA changes were observed 32hrs post-transfection (Selbach et al. 2008). Further investigation of miR mediated suppression may additionally examine target suppression at varying time points. In addition as miR-1 expression does not appear to be endogenous in HeLa cells, the large increase of miR-1 expression, following transfection of the miR construct, may represent low absolute levels, insufficient to mediate large alterations in PTK9 mRNA levels. While these initial results demonstrate the ability of miR-1, expressed from the miR construct, to moderately downregulate the expression of PTK9, further replication of these experiments is required. In addition, the ability of each miR construct, to express a miR capable of interacting and suppressing target transcripts, needs to be evaluated. Future studies may include luciferase assays for each miR, in which the 3'UTR of a known miR target is incorporated immediately downstream of the luciferase ORF sequence, such that binding of the mRNA transcript to the target site prevents the translation of luciferase.

8.5. Conclusion

MiR expression constructs were generated for a number of retinal miRs, through the application of the pcDNA.6.2 vector system. The preliminary results presented in this Chapter of the Ph.D. thesis demonstrate that miR expression can be achieved from the generated miR expression constructs *in vitro*. The ability of miR-1 to suppress PTK9 mRNA expression was additionally demonstrated, suggesting that the miR-1 is capable of

interacting with their targets. However further investigation is paramount to determine the exact nature of miR expression from the synthetic miR expression constructs. In addition the ability of miRs expressed by each of the generated construct, to interact with, and downregulate the expression of known targets is required. While the results presented in this Chapter are incomplete, they highlight the potential of these constructs to be used in overexpression studies *in vivo* and *in vitro*. In this manner future experiments may utilise such miR expression constructs to examine the function of retinal miRs *in vivo* using either viral or non-viral delivery methods.

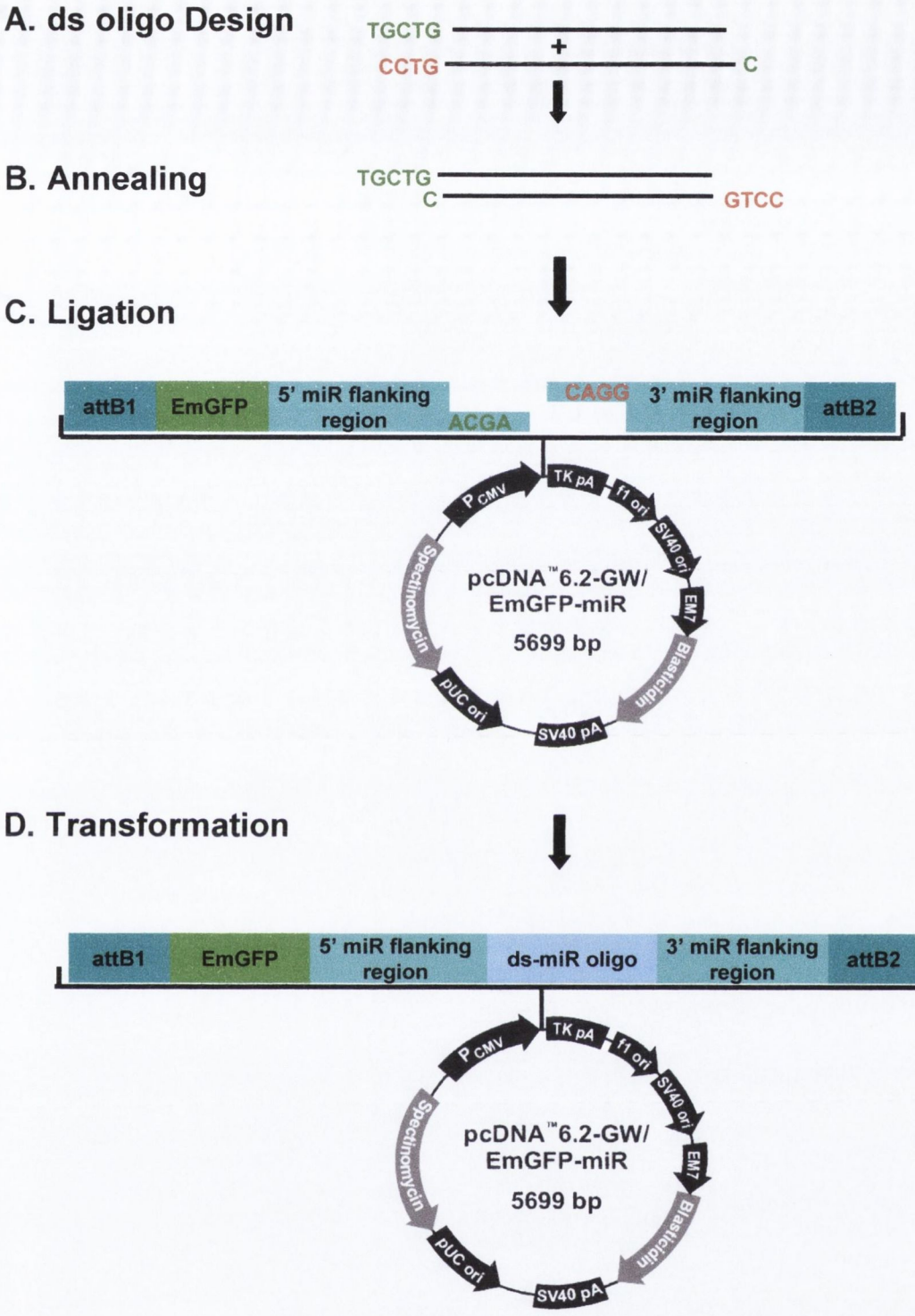

Figure 8.1: Overview of miR Expression Plasmid Construction: (**A**) Double stranded oligos were designed containing the appropriate overhanging sequences (highlighted in green and red) for insertion into the pcDNA6.2-EmGFP-miR vector. Oligos were (**B**) annealed and (**C**) using T4 DNA ligase, the double stranded oligos were inserted into the linearised pcDNA6.2-EmGFP-miR-vector downstream of the CMV-Pol II promoter. (**D**). Transformation of *E.coli* was performed, and the resulting spectinomycin-resistant colonies were screened for the desired expression clone.

Figure 8.3: MiR Oligo Design: The sequences of the top and bottom oligo strands are listed above for the generated miR expression constructs, following the design principles illustrated for miR-1 in **Fig 2.** The 5' and 3' overhang sequences are highlighted in red and green respectively. The ID number relates to the Sanger miR Database identification number.

ID	Name	Strand	Sequence
MI0000139	mmu-mir-1-1	Top	TGCTGCACATACTTCTTTATATGCCCATATGAACCTGCTAAGCTATGGAATGTAAAGAAGTATGTA
	mmu-mir-1-1	Bottom	CCTGTACATACTTCTTTACATTCCATAGCTTAGCAGGTTCATATGGGCATATAAAGAAGTATGTGC
MI0000729	mmu-mir-7-2	Top	TGCTGTGGAAGACTAGTGATTTTGTTGTTGTCTCTGTATCCAACAACAAGTCCCAGTCTGCCA
	mmu-mir-7-2	Bottom	CCTGTGGCAGACTGGGACTTGTTGTTGGATACAGAGACACAACAACAAAATCACTAGTCTTCCAC
MI0000157	mmu-mir-9-2	Top	TGCTGATCTTTGGTTATCTAGCTGTATGAGTGTATTGGTCTTCATAAAGCTAGATAACCGAAAGT
	mmu-mir-9-2	Bottom	CCTGACTTTCGGTTATCTAGCTTTATGAAGACCAATACACTCATACAGCTAGATAACCAAAGATC
MI0000583	mmu-mir-96	Top	TGCTGTTTGGCACTAGCACATTTTTGCTTGTGTCTCTCCGCTGTGAGCAATCATGTGTAGTGCCAAT
	mmu-mir-96	Bottom	CCTGATTGGCACTACACATGATTGCTCACAGCGGAGAGACACAAGCAAAAATGTGCTAGTGCCAAAC
MI0000150	mmu-mir-124a-3	Top	TGCTGGCGTGTTCACAGCGGACCTTGATTTAATGTCTATACAATTAAGGCACGCGGTGAATGCC
	mmu-mir-124a-3	Bottom	CCTGGGCATTCACCGCGTGCCTTAATTGTATAGACATTAAATCAAGGTCCGCTGTGAACACGCC
MI0000159	mmu-mir-133a-1	Top	TGCTGAAAGCTGGTAAAATGGAACCAAATCGCCTCTTCAATGGATTTGGTCCCCTTCAACCAGCTGT
	mmu-mir-133a-1	Bottom	CCTGACAGCTGGTTGAAGGGGACCAAATCCATTGAAGAGGCGATTTGGTTCCATTTTACCAGCTTTC
MI0000225	mmu-mir-183	Top	TGCTGTATGGCACTGGTAGAATTCACTGTGAACAGTCTCAGTCAGTGAATTACCGAAGGGCCATA
	mmu-mir-183	Bottom	CCTGTATGGCCCTTCGGTAATTCACTGACTGAGACTGTTCACAGTGAATTCTACCAGTGCCATAC
MI0000226	mmu-mir-184	Top	TGCTGTTCCTTATCACTTTTCCAGCCAGCTTTGTGACTCTAAGTGTTGGACGGAGAACTGATAAGGGT
	mmu-mir-184	Bottom	CCTGACCCTTATCAGTTCTCCGTCCAACACTTAGAGTCACAAAGCTGGCTGGAAAAGTGATAAGGAAC
MI0000247	mmu-mir-204	Top	TGCTGTTCCCTTTGTCATCCTATGCCTGAGAATATATGAAGGAGGCTGGGAAGGCAAAGGGAC
	mmu-mir-204	Bottom	CCTGGTCCCTTTGCCTTCCCAGCCTCCTTCATATATTCTCAGGCATAGGATGACAAAGGGAAC

MI0000577	mmu-mir-29c	Top	TGCTGACCGATTTCTCCTGGTGTTCAGAGTCTGTTTTTGTCTAGCACCATTTGAAATCGGT
	mmu-mir-29c	Bottom	CCTGACCGATTTCAAATGGTGCTAGACAAAAACAGACTCTGAACACCAGGAGAAATCGGTC
MI0000577	mmu-mir-29c shRNA	Top	TGCTGACCGATTTAATGGTGCTAGTTTTGGCCACTGACTGACTAGCACCATTTGAAATCGGT
	mmu-mir-29c shRNA	Bottom	CCTGACCGATTTCAAATGGTGCTAGTCAGTCAGTGGCCAAAACTAGCACCATTAAATCGGTC
MI0000224	mmu-mir-182	Top	TGCTGTTTGGCAATGGTAGAACTCACACCGGTAAGGTAATGGGACCCGGTGGTTCTAGACTTGCCAAC
	mmu-mir-182	Bottom	CCTGGTTGGCAAGTCTAGAACCACCGGGTCCCATTACCTTACCGGTGTGAGTTCTACCATTGCCAAAC
MI0000224	mmu-mir-182 shRNA	Top	TGCTGTTTGGCAATGGTAGAACTCACAGTTTTGGCCACTGACTGACTGTGAGTTACCATTGCCAAA
	mmu-mir-182 shRNA	Bottom	CCTGTTTGGCAATGGTAACTCACAGTCAGTCAGTGGCCAAAACTGTGAGTTCTACCATTGCCAAAC

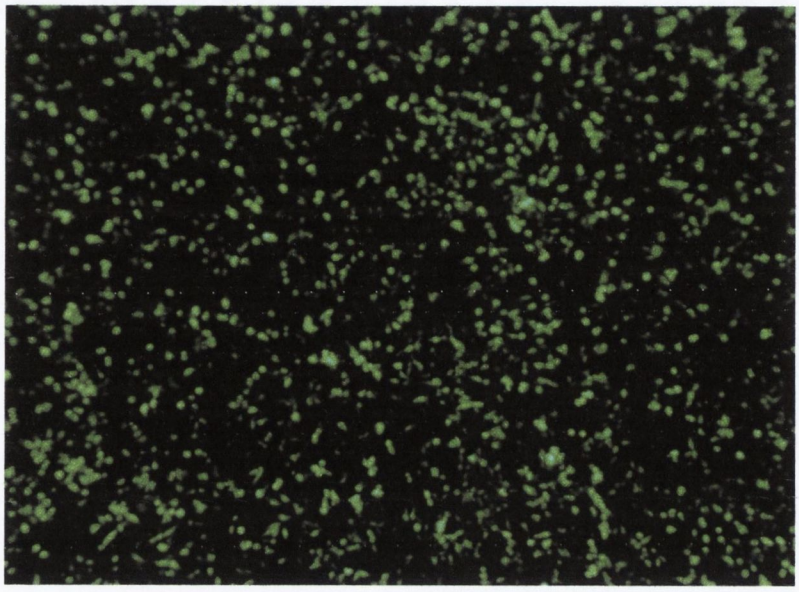

Figure 8.4: Transfection of miRNA Constructs in HeLa cells: The image represents the transfection efficiency achieved with the pcDNA6.2-miR expression constructs. HeLa cells were transfected with 4µg of DNA using lipofectAMINE 2000 and incubated for 24hr. Images were taken at 100X magnification using a fluorescent microscope.

A. Pre-miR-1 Sequence:

Accession: MI0000139
ID:mmu-mir-1-1

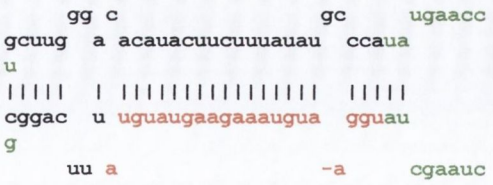

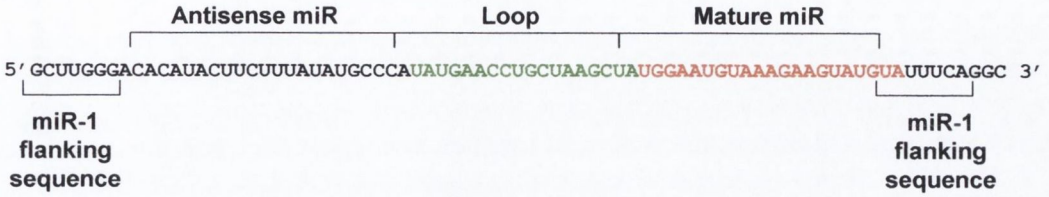

B. Top Strand Oligo:

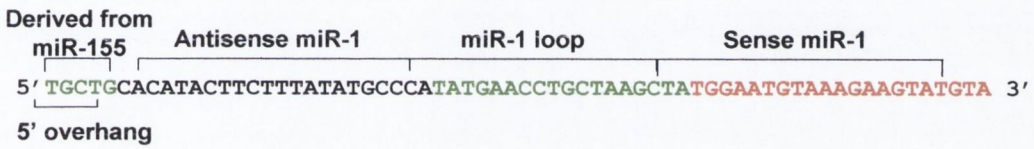

+

C. Bottom Strand Oligo:

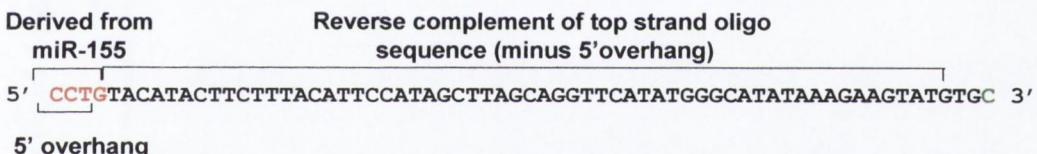



D. ds oligo:

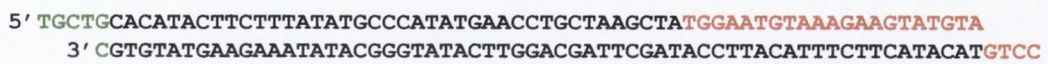

Figure 8.2: Overview of miR vector Design (pcDNA-6.2-EmGFP-miR-1-1 vector): (**A**) The precursor sequence of mmu-miR-1-1 and the secondary structure is illustrated, the mature miR (red) and endogenous loop sequence (green) are highlighted. The top strand oligo (**B**) was designed by deleting the flanking region of miR-1, and inserting the 5'overhang sequence derived from miR-155, for insertion into the linearised pcDNA6.2 vector. The original precursor miR sequence is preserved, including the miR-1-1 loop sequence (green). The bottom strand oligo (**C**) is the reverse complement of the top strand oligo, containing modifications in the 5' and 3' overhang to accommodate insertion into the linearised vector. The annealed ds-oligo is illustrated (**D**) highlighting the overhang sequences allowing insertion into the pcDNA-6.2 vector.

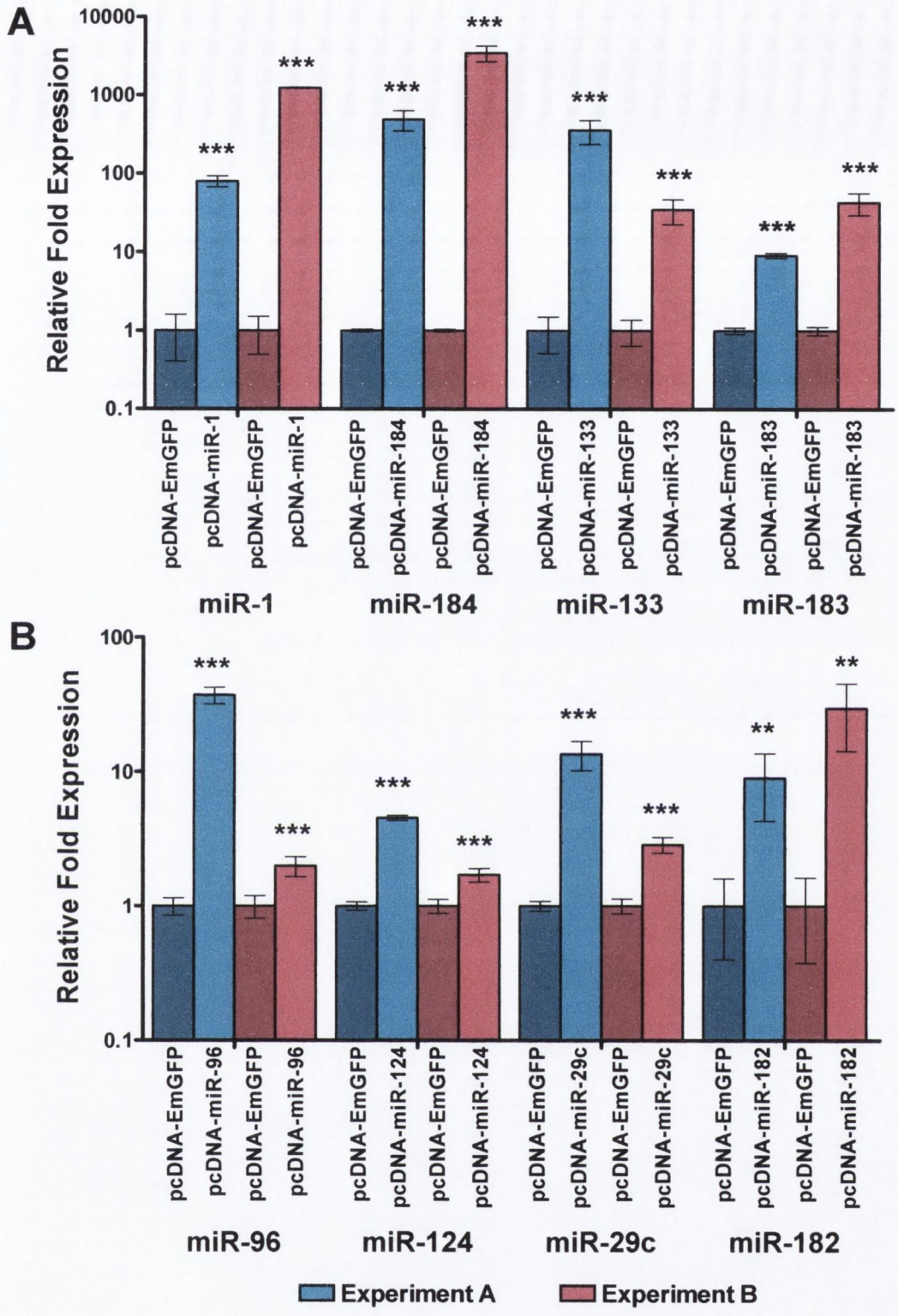

Figure 8.5: Overexpression of pcDNA-miR constructs in HeLa cells: The graph illustrates the relative expression level of selected miRs in experiment A (blue) and experiment B (magenta) following transfection of miR constructs in HeLa cells. Bars represent miR fold expression in cells transfected with pcDNA-miR constructs (light blue, light magenta) relative to cells transfected with empty vectors expressing EGFP (dark blue, dark magenta). The expression of **A**) miR-1,-184, -133 and -183 and (**B**) miR-96, -124, 29c, and -182 are illustrated. Note that the y-axes are on a $\log_{10}$ scale. Comparative miR expression data was analysed by Students t-test and the statistical significance is indicated by; *: $p<0.05$; **: $p<0.01$; ***: $p<0.001$. Error bars indicate S.E.M.

Endogenous miRNA expression in HeLa cell line		
	Yeung *et al.*	
	A	B
hsa-miR-1		
hsa-miR-184		
hsa-miR-204		
hsa-miR-9		
hsa-miR-124a		
hsa-miR-133b		
hsa-miR-183		
hsa-miR-96		
hsa-miR-29c		
hsa-miR-7		
hsa-miR-182		

Figure 8.6: Endogenous miR expression in HeLa cells: The data above is adapted from Yeung *et al*, 2005 **(A and B)**, representing miR expression in un transfected HeLa cells using a RNA-primed, array-based Klenow enzyme (RAKE) assay. The signal strength from the array is allocated a colour where, high signal=red, low signal=black, no signal=green).

A. Pre-miR-182 Sequence:

Accession: MI0000224
ID: mmu-mir-182

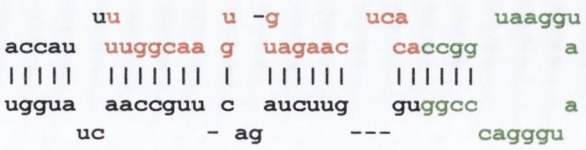

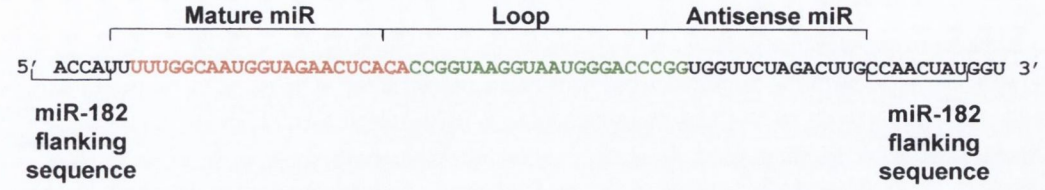

B. Top Strand Oligo:

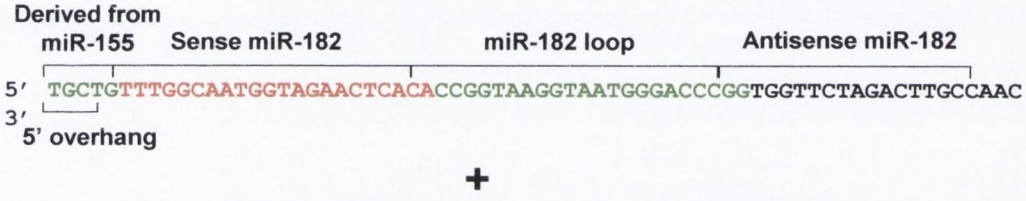

+

C. Bottom Strand Oligo:

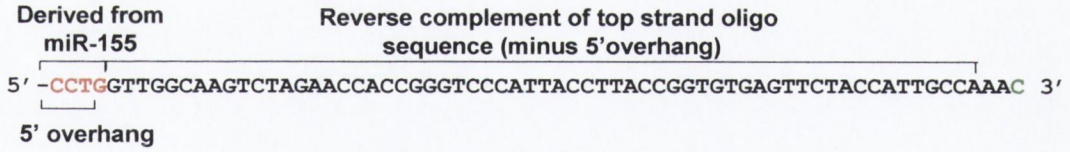

Anneal

D. ds oligo:

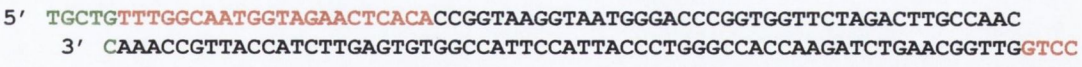

Figure 8.7: Overview of design of pcDNA-6.2-EmGFP-miR-182 vector: (**A**) The precursor sequence of mmu-miR-182 and the secondary structure is illustrated, the mature miR (red) and endogenous loop sequence (green) are highlighted. The top strand oligo (**B**) was designed by deleting the flanking region of miR-182, and inserting the 5' overhang sequence derived from miR-155, for insertion into the linearised pcDNA6.2 vector. The original precursor miR sequence is preserved, including the miR-182 loop sequence (green). The bottom strand oligo (**C**) is the reverse complement of the top strand oligo, containing modifications in the 5' and 3' overhang to accommodate insertion into the linearised vector. The annealed ds-oligo is illustrated (**D**) highlighting the overhang sequences allowing insertion into the pcDNA-6.2 vector.

A. Pre-miR-182 Sequence:

Accession: MI0000224
ID: mmu-mir-182

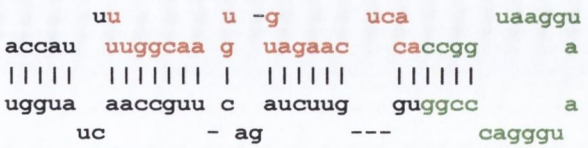

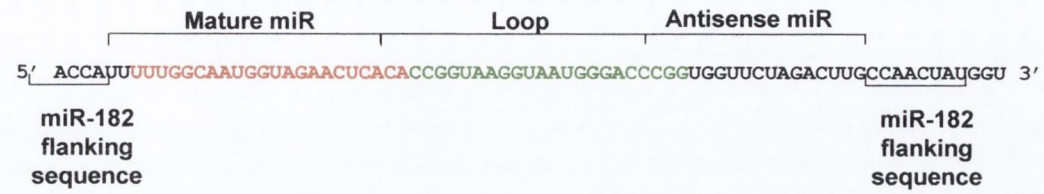

B. Top Strand Oligo:

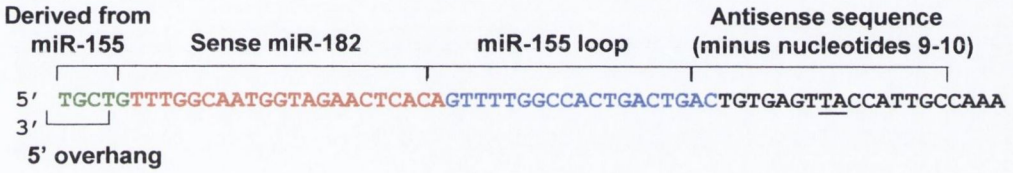

+

C. Bottom Strand Oligo:

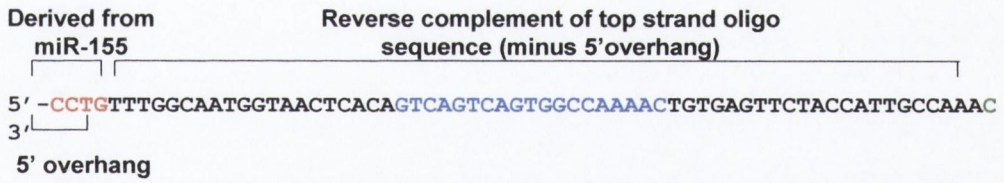

D. ds oligo:

Anneal

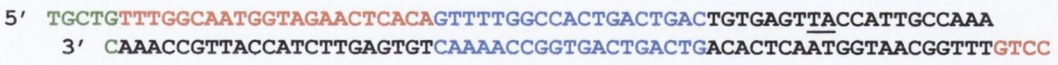

Figure 8.8: Overview of design of pcDNA-6.2-EmGFP-miR-182 shRNA vector: (**A**) The precursor sequence of mmu-miR-182 and the secondary structure is illustrated, the mature miR (red) and endogenous loop sequence (green) are highlighted. The top strand oligo (**B**) was designed by deleting the flanking region of miR-182, and inserting the 5' overhang sequence derived from miR-155, for insertion into the linearised pcDNA6.2 vector. The sense miR-182 sequence is maintained, while the loop sequence is replaced with the loop sequence of miR-155 (blue). The reverse complement of the sense miR-182 strand is inserted in the right arm of the hairpin, minus nucleotides 9-10 (underlined text). The bottom strand oligo (**C**) is the reverse complement of the top strand oligo, containing modifications in the 5' and 3' overhang to accommodate insertion into the linearised vector. The annealed ds-oligo is illustrated (**D**) highlighting the overhang sequences and altered loop sequence (blue)..

A. Pre-miR-29c Sequence:

Accession: MI0000577
ID: mmu-mir-29c

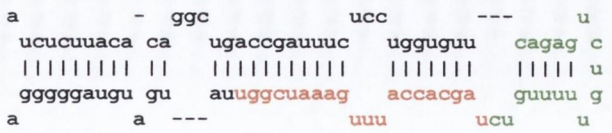

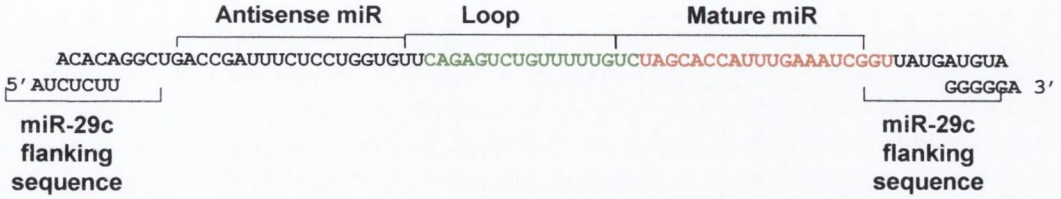

B. Top Strand Oligo:

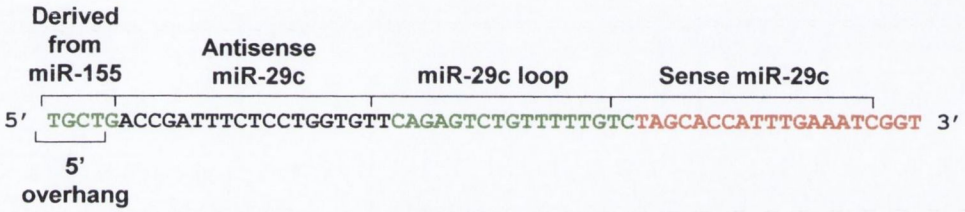

+

C. Bottom Strand Oligo:

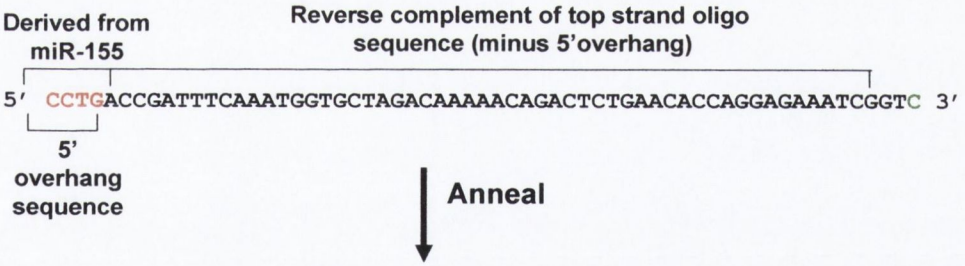

D. ds oligo:

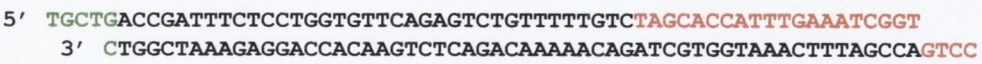

Figure 8.9: Overview of design of pcDNA-6.2-EmGFP-miR-29c vector: (**A**) The precursor sequence of mmu-miR-182 and the secondary structure is illustrated, the mature miR (red) and endogenous loop sequence (green) are highlighted. . The top strand oligo (**B**) was designed by deleting the flanking region of miR-29c, and inserting the 5' overhang sequence derived from miR-155, for insertion into the linearised pcDNA6.2 vector. The original precursor miR sequence is preserved, including the miR-29c loop sequence (green). The bottom strand oligo (**C**) is the reverse complement of the top strand oligo, containing modifications in the 5' and 3' overhang to accommodate insertion into the linearised vector. The annealed ds-oligo is illustrated (**D**) highlighting the overhang sequences allowing insertion into the pcDNA-6.2 vector.

A. Pre-miR-29c Sequence:

Accession: MI0000577
ID: mmu-mir-29c

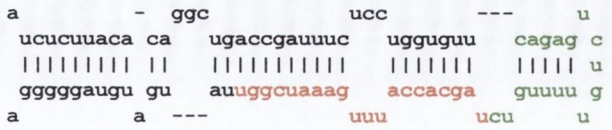

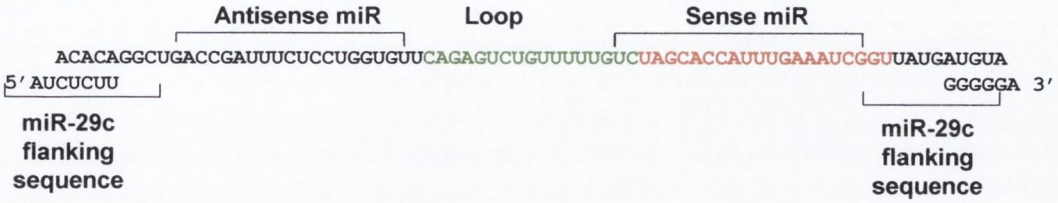

B. Top Strand Oligo:

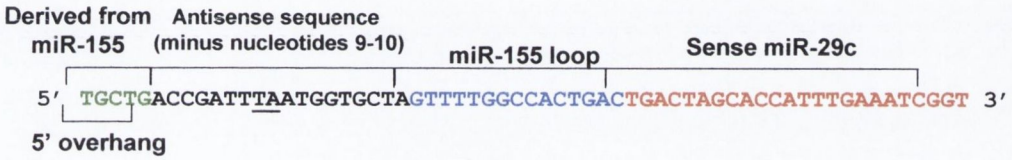

+

C. Bottom Strand Oligo:

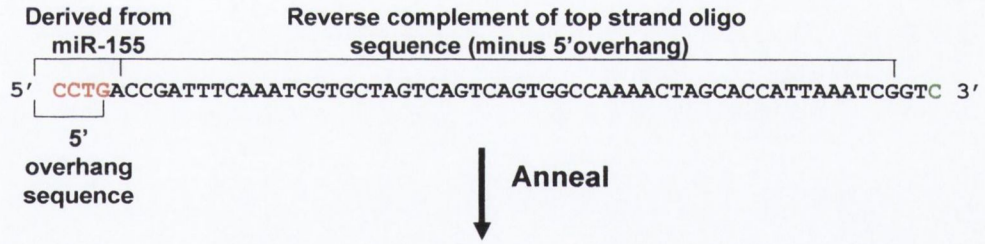

D. ds oligo:

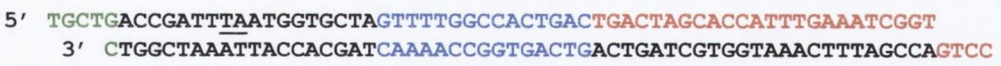

Figure 8.10: Overview of design of pcDNA-6.2-EmGFP-miR-29c shRNA vector: (**A**) The precursor sequence of mmu-miR-182 and the secondary structure is illustrated, the mature miR (red) and endogenous loop sequence (green) are highlighted. The top strand oligo (**B**) was designed by deleting the flanking region of miR-29c, and inserting the 5' overhang sequence derived from miR-155, for insertion into the linearised pcDNA6.2 vector. The sense miR-29c sequence is maintained, while the loop sequence is replaced with the loop sequence of miR-155 (blue). The reverse complement of the sense miR-29c strand is inserted in the left arm of the hairpin, minus nucleotides 9-10 (underlined text). The bottom strand oligo (**C**) is the reverse complement of the top strand oligo, containing modifications in the 5' and 3' overhang to accommodate insertion into the linearised vector. The annealed ds-oligo is illustrated (**D**) highlighting the overhang sequences and altered loop sequence (blue).

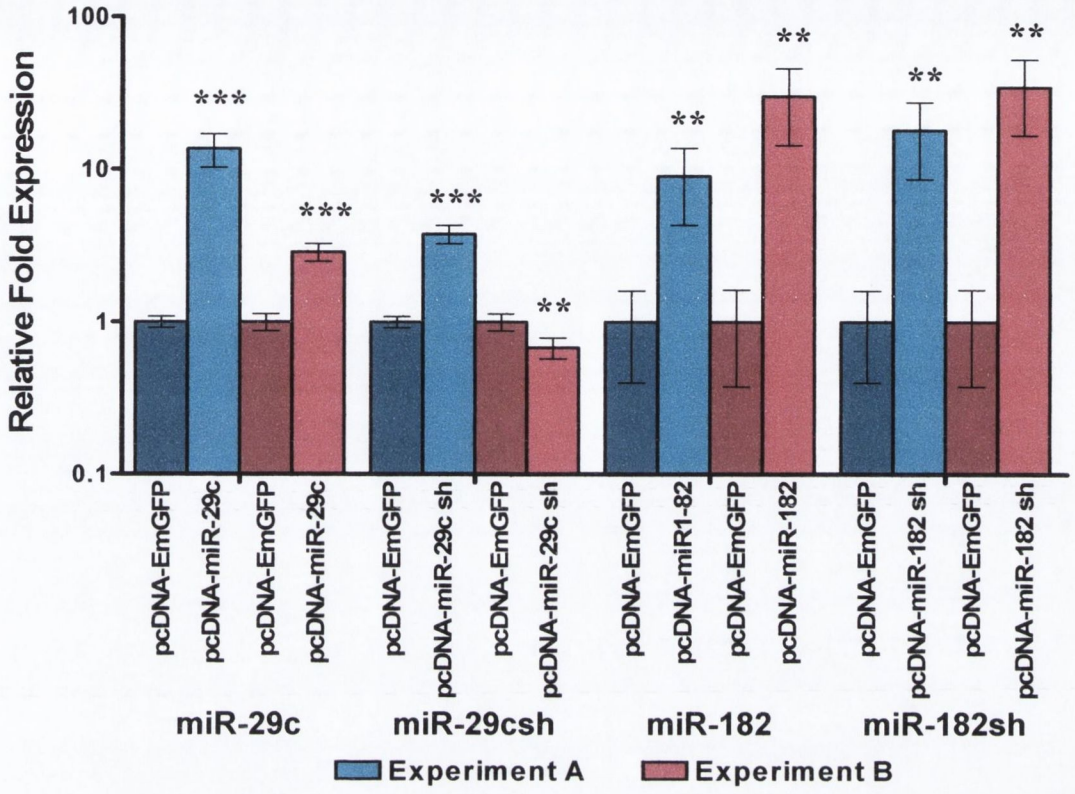

Figure 8.11: Overexpression of pcDNA-miR constructs in HeLa cells: The graph illustrates the relative expression level of selected miRs as detected by quantitative RT-PCR (qPCR). Each miR construct was expressed in HeLa cells in two independent experiments, experiment A (blue) and experiment B (magenta). Bars represent miR fold expression in cells transfected with pcDNA-miR constructs (light blue, light magenta) and the level of miR expression achieved is expressed relative to the negative control (i.e. 1-fold), i.e. cells transfected with empty vectors expressing EGFP (dark blue, dark magenta). The expression of miR-29c, -29c shRNA (-29csh), -182 and -182 shRNA (-182sh) are illustrated. miR expression, relative to the negative control, is analysed for statistical significance for each individual experiment. Statistical analysis by Students *t-test* and is indicated, where; *: $p<0.05$; **: $p<0.01$; ***: $p<0.001$. Error bars indicate S.E.M. Note that the Y-axis is on a $\log_{10}$ scale.

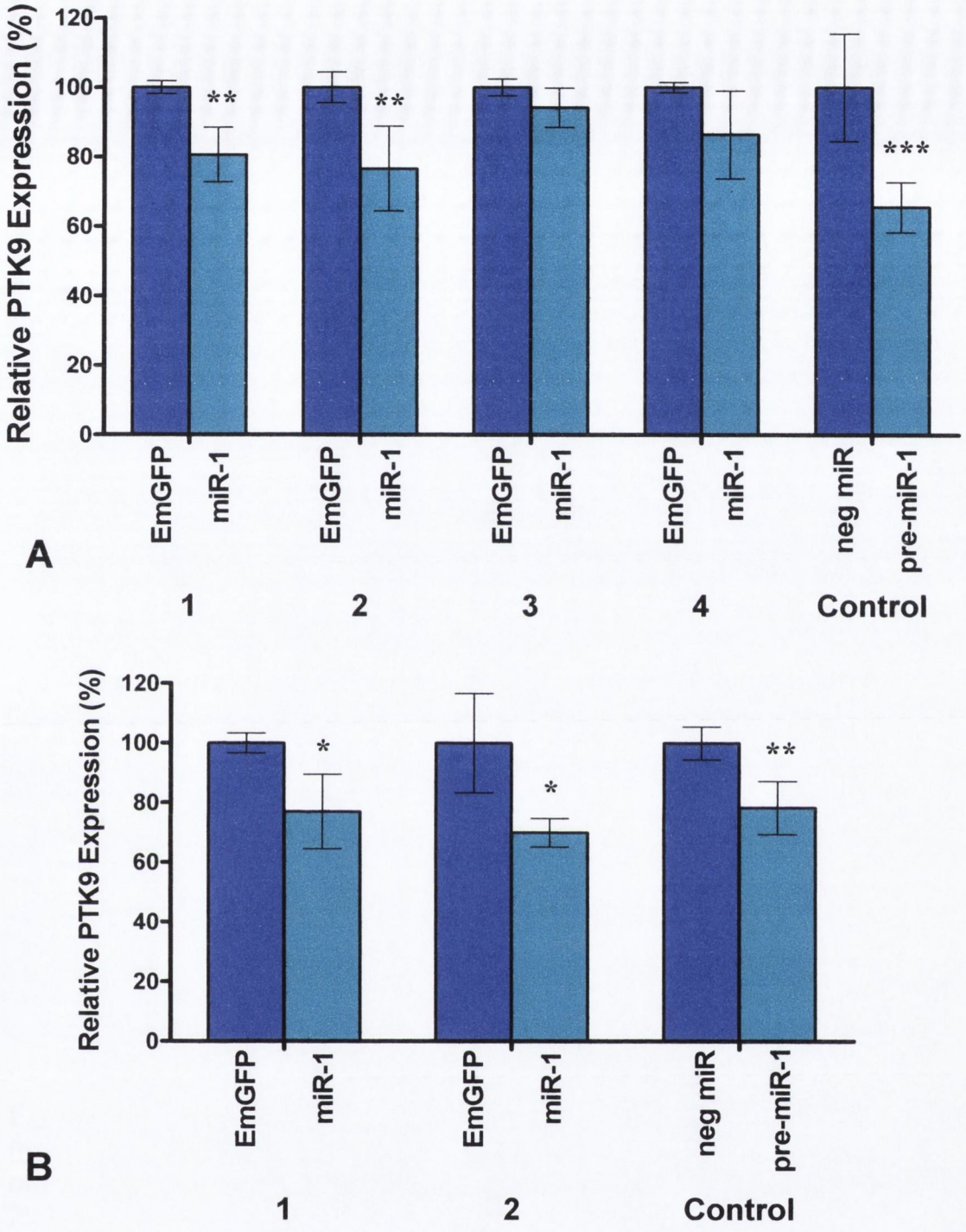

Figure 8.12: PTK9 Suppression in HeLa cells: HeLa cells were transfected with pcDNA-miR-1 and pcDNA-EmGFP (negative control) in four independent transfection experiments (**1-4**). Hela cells were also transfected with (**Control**) pre-miR-1 construct and the negative-pre-miR control, providing a positive control for PTK9 expression analysis. The expression of PTK9 was analysed by quantitative RT-PCR (qPCR) using (**A**) Taqman probes and (**B**) DNA oligo primers. Data is expressed relative PTK9 expression (%), relative to the negative control construct (pcDNA-EmGFP, negative-pre-miR) (i.e. 100%). PTK9 suppression, relative to the negative control, is analysed for statistical significance for each individual experiment. Statistical analysis by Students *t-test* and is indicated, where; *: $p<0.05$; **: $p<0.01$; ***: $p<0.001$. Error bars indicate S.E.M. EmGFP: pcDNA6.2-EmGFP, miR-1; pcDNA.6.2-miR-1, neg miR; negative pre-miR.

TargetScan
Prediction of microRNA targets

Release 4.2: April 2008

Mouse TWF1 3' UTR

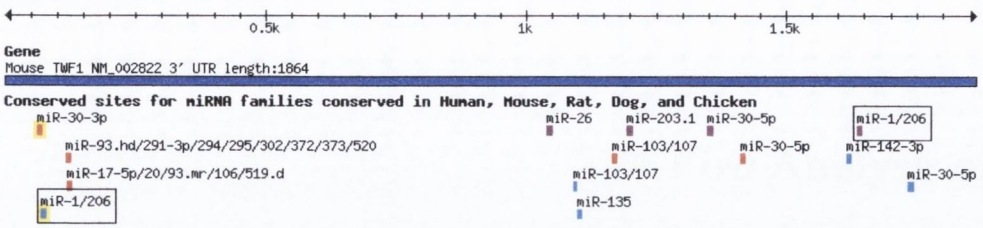

[Show conserved sites for miRNA families conserved in Human, Mouse, Rat, Dog]
[Show poorly conserved sites and sites for poorly conserved miRNA families]
[View SVG image of miRNA sites]
[View table of miRNA sites]
[View mouse genome browser (Feb 06)]

Key:
Sites conserved in Human, Mouse, Rat, Dog, Chicken
8mer 7mer-m8 7mer-1A
Less conserved sites
8mer 7mer-m8 7mer-1A

```
     .........40........50........60........70........80..........90........100.......110.......120.
Mm   -----AAGUUUCCAGCUUUUAGUACAAGGAGAACUGAAAUCAUUCCAUGUUG--AUAGAGUUGGGAGGAAAAUUGUACUUUUUGAAAAAUAGCAC
Hs   -----AAAGU-CCAGCUUUUAGUACA-GGAGAACUGAAAUCAUUCCAUGUUGAUAUAAAGUAGGGAAAAAAAUUGUACUUUUUGGAAAAAUAGCAC
Rn   -----AGAUUUCCAGCUUUUAGUACAAGGAGAACUGAAAUCAUUCCAUGUUG--AUAUAGUUGGGAGGAAAAUUGUACUUUUUGAAAAAUAGCAC
Cf   -----AAAGU-CCAGCUUUUAGUACA-GGAGAACUGAAAUCAUUCCAUGUUGAUACAUAGUAG-GGGAAAAAUUGUACUUUUUGAAAAAUAGCAC
Gg   AAAUGAAAUU-CUGACUUUUG---CC-AAUGAACUGAAACCAUUCCAUUU--AUAGAUGCUAAAGAAAAAAAU-GUUCUUUCU----------AC
                                                    miR-1/206
Con  .....A...U.CcagCUUUUaguaCa.ggaGAACUGAAAuCAUUCCAUgUug..A.A.agU.g.G...AAAAUuGUaCUUUuUg.aaaauagcAC
```

Conserved

	predicted consequential pairing of target region (top) and miRNA (bottom)	seed match	site-type contribution	3' pairing contribution	local AU contribution	position contribution	context score	context score percentile
Position 71-77 of TWF1 3' UTR mmu-miR-1	5' ...AAGGAGAACUGAAAU-CAUUCCAU... 3' AUGUAUGAAGAAAUGUAAGGU	7mer-1A	-0.099	-0.017	-0.051	-0.027	-0.19	71
Position 71-77 of TWF1 3' UTR mmu-miR-206	5' ...AAGGAGAACUGAAAU-CAUUCCAU... 3' GGUGUGUGAAGGAAUGUAAGGU	7mer-1A	-0.099	-0.017	-0.051	-0.027	-0.19	70
Position 1637-1644 of TWF1 3' UTR mmu-miR-206	5' ...CAUCGAAGUCAAUGCACAUUCCA... 3' GGUGUGUGAAGGAA--UGUAAGGU	8mer	-0.310	0.005	0.033	-0.032	-0.30	89
Position 1637-1644 of TWF1 3' UTR mmu-miR-1	5' ...CAUCGAAGUCAAUGCACAUUCCA... 3' AUGUAUGAAGAAA--UGUAAGGU	8mer	-0.310	0.005	0.033	-0.032	-0.30	89

Figure 8.13: PTK9 (TWF1) Target Prediction by TargetSan: The output from TargetScan prediction programme, illustrates the perfect base pairing of the seed region of miR-1 and the 3'-UTR of PTK9 (TWF1). Note: as miR-206 possesses an identical seed region to miR-1, identical targets are predicted for miR-1 and miR-206, as TargetScan exclusively analyses base-pairing with the 5'-seed region of the miR for target predictions.

Chapter 9

In Vivo Analysis of miR Expression Vectors

9.1. Introduction

As described in Chapter 8, miR-constructs can be used to overexpress miRs *in vitro* and overexpression of miR-1 was demonstrated to downregulate the expression of the target gene PTK9. While clearly further work-up is required for these miR constructs as outlined in Chapter 8, in principle these constructs should provide a feasible approach to examine the effects of miR overexpression in the eye.

Cell culture systems can be used to examine the effects of miR overexpression, which offers a practical and versatile system. Validation of predicted miR targets *in vitro* can be achieved by examining the ability of overexpressed miRs to suppress the expression of target 3'UTR-luciferase reporter constructs. Global analysis of miR targets can also be employed, by examining global mRNA and protein suppression by individual miRs. Indeed two recent studies have used this method, and have significantly contributed to our knowledge of miR:mRNA target interactions (Baek et al. 2008; Selbach et al. 2008). The roles of miRs in differentiation and proliferation of progenitor cells have been elucidated by *in vitro* miR overexpression studies involving a number of tissues. Specifically the ectopic expression of miR-181 in hematopoietic progenitor cells drives B-cell differentiation (Chen et al. 2004), while miR-124 overexpression in neuronal progenitor cells promotes neurite outgrowth (Yu et al. 2008). However, as some cell lines may only express a small percentage of the tissue-specific miR targets of interest, potentially important miR:target interactions may go unnoticed depending on the cell lines used for such studies. Additionally, the involvement of miRs in complex tissue-specific interactions, which occur *in vivo*, cannot be examined thoroughly in cell culture. Therefore to gain a comprehensive understanding of the function of miRs in the tissue of interest, *in vivo* analysis is important. Predominantly the main advantage lies in the ability to examine the functions of miRs in context, as tissues comprise of heterogeneous cell types with multiple and complex interactions. Additionally, as the function of miRs is mediated by suppression of target genes, analysis of miR overexpression *in vivo* ensures the expression of the relevant tissue-specific genes.

In vivo miR expression requires the use of expression vectors and an efficient delivery system to the cells of interest. Such expression vectors and delivery systems have been used to examine the gain and loss of function of miRs *in vivo*, during physiological processes and in disease. For example, the *in vivo* overexpression of miR-9

in the embryonic cerebral cortex promotes the differentiation of cortical progenitor cells (Shibata et al. 2008), and in addition the overexpression of miR-133 in the heart, a miR that is reduced in cardiac hypertrophy, successfully inhibited the hallmarks of disease (Care et al. 2007). To gain an understanding of the ocular functions of miRs in physiological conditions or in disease states, *in vivo* examination is particularly important due to the paucity of stable retinal cell lines available for studies, especially photoreceptor cell lines (Seigel 1999). *In vivo* expression studies are advantageous, as the architecture of the retina is maintained, including the complex interactions between multiple cell types.

Viral and non-viral mechanisms can be employed to deliver miR expression vectors to the retina in order to examine the roles of miR expression over a prolonged period of time. Non-viral delivery of naked plasmids to the outer retina can be achieved by injection of the vector into the sub-retinal space (between the retina and RPE) in neonatal eyes followed by electroporation. Electroporation facilitates the delivery of DNA by high voltage electric pulses, which destabilises and permeablises the cell membrane thereby increasing gene transduction (Andrieu-Soler et al. 2006; Bloquel et al. 2006). This delivery method is reasonably efficient, and in the neonatal rodent eye, transgene expression from electroporated vectors can remain up to 50 days post-electroporation (Matsuda and Cepko 2004).

As described in Chapter 3, a number of retinal specific miRs have been identified, and are thought to mediate tissue-specific roles in this tissue. In this study, a number of miRs, miR-7, -182, -183, -96, -133 were injected subretinally in mouse neonatal eyes (at P0) and electroporated into retinal cells, and the expression levels of these miRs were examined 2-weeks post-injection of the constructs. The results from this preliminary study using the miR constructs described in Chapter 8 indicated that while enhanced miR expression was detected in the retina at this time point, structural effects were not observed thus far. This work will be expanded significantly in the future to fully examine the effects of miR overexpression in the retina, from each miR construct.

9.2. Materials and Methods

9.2.1. Concentration of DNA constructs

The following miR expression constructs were concentrated using ethanol precipitation (see section 2.2.3) to a concentration of 3 ng/μl in PBS; pcDNA6.2-miR-133, pcDNA6.2-miR-96, pcDNA6.2-miR-183, pcDNA6.2-miR-182 and pcNDA6.2-miR-7. 0.1% Fast Green dye was added to the DNA as a tracer dye to aid visualisation of retinal detachment during sub-retinal injections.

9.2.2. Sub-retinal Injection and electroporation of miR constructs

All procedures described in this section were performed in a specific pathogen free (SPF) facility with sterile instruments and solutions. Technical expertise was received from Dr. Paul Kenna, a registered ophthalmologist, to facilitate the sub-retinal injections described below.

The following constructs were subretinally injected and electroporated in the right eye at postnatal day zero (P0) mouse pups: pcDNA6.2-miR-133, pcDNA6.2-miR-96, pcDNA6.2-miR-183 and pcNDA6.2-miR-7. Sub-retinal injection and electroporation of DNA was performed as detailed by Matsuda *et al.*, 2004 (Matsuda and Cepko). Newborn mice were anaesthetised by chilling on ice for 6 minutes. A small incision was made in the eyelid to expose the eye, and a 30-gauge needle was used to puncture the eye at the sclera at the edge of the lens. Using a dissecting microscope and a Hamilton syringe with a blunt ended needle (33-gauge), 0.5 μl of the DNA solution (3 ng/μl) was injected to the sub-retinal space of the eye under the central retina. Following injection electrodes were soaked in PBS and placed over the mouse eyes. Five square pulses of 80 V with 50-ms duration with 950-ms intervals were applied using the pulse generator BTX Electroporator ECM 830 (Harvard Apparatus, Holliston, MA, USA). Figure 9.6 provides a schematic representation of the injection and electroporation method. The mice were re-warmed at 33°C for 30 minutes, before being returned to the cage and reunited with their mother.

9.2.3. Histology and Microscopy

Electroporated eyes were dissected and fixed in 4% paraformaldehyde for 4 hours at 4°C (n=3 per miR construct). Cryosections were taken (see section 2.3.4.2) and the nuclei were counterstained by using 4',6-diamidine-2-phenylindole-dihydrochloride (DAPI, Invitrogen) (see section 2.8.). Sections were analysed by bright field normal and phase-contrast as well as fluorescent microscopy using an Axiophot microscope (Carl Zeiss Ltd., Hertfordshire, UK). Composite images were created using Adobe Photoshop software (Adobe Systems Europe Ltd., Glasgow, UK).

9.2.4. miR In Situ Hybridisation

Electroporated eyes were dissected and fixed in 4% paraformaldehyde for 2 hours at 4°C (n=2 per miR construct) (see section 2.3.4.2.). 5'-Digoxigenin (DIG)-labelled LNA-modified oligonucleotide ISH probes were used for the following mouse miRs: miR-96, and -183. ISH probes for miR-181a and sense miR-159 (Exiqon), were used as positive and negative controls respectively. The ISH protocol was carried out as detailed in section 2.3.4.1 using the recommended hybridisation temperature (Table 2.1).

9.2.5. FACS Analysis

2 weeks after electroporation, mice were sacrificed and the electroporated retinas were dissected (n=1 per miR construct). For fluorescence-activated cell sorting (FACS) analysis the retinas were dissociated using trypsin (see section 2.5.1) and cells analyzed and separated by FACS as described in section 2.5.2. Total RNA was extracted from the Ultrafree-MC filter unit (Millipore) by adding 350 µl RNA lysis buffer (see section 2.3.2) to the filter unit. The buffer was passed through the filter by centrifugation at 6600 rpm for 2 minutes, and the filtrate reapplied to the filter unit and eluted 3 times to ensure complete lysis and collection of RNA. The Qiagen miRNeasy Mini Kit was used to extract the RNA from the filtrate according to manufacturers' instructions (see section 2.3.2.2). For quantification of miR expression, two-step qPCR was performed using ABI's TaqMan miR Assay (Applied Biosystems, Foster City, CA, USA) according to manufacturer's instructions (see section 2.3.3.1). The TaqMan miR Assays for the

following miRs were utilised: miR-133, -96, and -183 and normalised to snoRNA-202 and snoRNA-206 controls.

9.2.6. Statistical Analysis

Analysis of statistical significance was performed using Student's t-test and the statistical software, GraphPad Prism, and differences with $p<0.05$ were considered statistically significant.

9.3. Results

9.3.1. Histology of retinas electroporated with miR-expression constructs

The retinal histology of mouse eyes was examined, 2-weeks post-electroporation of the following miR-expression constructs at P0; pcDNA6.2-miR-7, pcDNA6.2-miR-183 and pcDNA6.2-miR-7. An empty emGFP expression vector (pcDNA6.2-EmGFP) was used as a negative control. GFP expression was detected in the retinas of electroporated animals (Figure 9.1 A-D), and DAPI nuclear staining illustrates that the GFP expression was predominantly localised to the outer nuclear layer of the photoreceptor cells (Figure 1 E-H). No structural alterations were observed in these preliminary studies as a result of miR over-expression (Figure 9.1 I-K).

9.3.2 In-Situ Hybridisation of retinas electroporated with miR-expression constructs

In situ hybridisation was carried out probing for miR-96 and miR-183, in retinal sections from mice electroporated at P0 with the miR expression constructs, pcDNA6.2-miR-96 and pcDNA6.2-miR-183(Figure 9.2 I-L). A sense negative control was used (Figure 9.2 D,H,L), nuclear staining was visualised using DAPI (Figure 9.2.E-H) and GFP expression tracked transduced cells (Figure 9.2.A-D). The expression of GFP is predominantly located in the outer nuclear layer of the retina; however, there is no evidence of altered expression of miR-183 in areas of GFP expression detected by ISH using LNA probes. The expression of miR-183 is strongly detected (Figure 9.2.K) in the inner segments (IS) of the rod photoreceptors, and also in the inner nuclear layer (INL). Some miR-96 expression was detected by ISH in the retinas electroporated with the miR-96 expression construct (Figure 9.2 I and 9.2 J), and this expression correlates with the expression of GFP. The expression was most noticeable where GFP expression was strongest in 'rosette-like structures', i.e. ectopic photoreceptors arranged in a tubular pattern and denoted by the arrows in both ISH and GFP images (Figure 9.2 A, I).

9.3.3. FACS analysis of electroporated retinas and miR expression analysis by qPCR

Retinas electroporated at P0 with constructs expressing miR-96, -133 and -183 were harvested at two weeks. The cells of the retina were dissociated and GFP-positive and GFP-negative cells were separated, corresponding to transduced and non-transduced cells respectively (Figure 9.3). Figure 9.3 illustrates the side and forward scatter plots corresponding to a non-electroporated control retina (Figure 9.3A) and those electroporated with miR-expression constructs expressing miR- 96, miR-133 and miR-183 (Figure 9.3 B-D). Total RNA was extracted from the GFP-positive and GFP-negative cell samples, and miR expression was analysed by qPCR. Expression of miR-133 and miR-96 was raised by 642.1 ± 157.1% ($p<0.001$; $n=1$) and 460.9 ± 41.2 % ($p<0.01$; $n=1$) respectively, in retinas electroporated with the corresponding miR-constructs, pcDNA6.2-miR-133 and pcDNA6.2-miR-96. However the expression of miR-183 was not altered in electroporated retinas with the miR construct expressing miR-183 ($n=1$).

9.4. Discussion

It is of particular interest to determine the targets and function of the six miRs differentially expressed in mouse models of RP (Loscher et al. 2008). Specifically, as the expression of miR-96, -182, and -183 is reduced in RP, examining the effects of overexpression may facilitate the elucidation of their roles. Conversely the expression of miR-1, -133, and -142 increased in RP, and over-expression may also provide clues to their roles in disease, by possibly exaggerating their responses *in vivo*. As the expression of miR-96, -182, and -183 in photoreceptors increases postnatally, it may perhaps be involved in the final maturation stages of rod OSs and ISs or the maintenance of photoreceptor cells. Additionally epidermal growth factor receptor (EGFR) signalling in *Drosophila*, promotes miR-7 expression which is thought to stimulate progenitor cells to differentiate into photoreceptors (Li and Carthew 2005). In this initial study expression of miRs *in vivo* is examined utilising the miR expression vectors, described in Chapter 8, and a non-viral delivery mechanism. Indeed as previously discussed, further characterisation and thorough investigation of the miR expression vectors, is required *in vitro*. However while this study is not complete, it represents preliminary experiments which demonstrate the feasibility of expressing miRs in the mouse retina, using a non-viral delivery method. Indeed this strategy may potentially be beneficial for studying miR function in the retina.

The non-viral delivery method of electroporation can be used to deliver naked DNA constructs *in vivo*, involving the electro-transfer of DNA particles to cells by means of high voltage electrical pulses. Indeed this delivery method has been successfully used to deliver DNA constructs *in vivo* to a number of tissues, including the developing mouse brain and skeletal muscle (Tabata and Nakajima 2001; Schertzer and Lynch 2008). Electroporation-mediated delivery has also been used to deliver constructs to various regions of the eye, depending on the site of injection of the DNA solution, prior to electroporation (Kachi et al. 2005). For example, intravitreous injection of the GFP gene followed by electroporation was demonstrated to transduce retinal ganglion cells (Dezawa et al. 2002), while sub-retinal injection facilitates the delivery of DNA constructs to the outer retinal layers and the RPE (Kachi et al. 2005). The delivery of shRNA expression vectors to the outer retinal cells of neonatal rodents has previously been described by Matsuda *et al.*, (2004), involving the sub-retinal injection of the naked plasmid, followed by the electro-transfer of the DNA constructs to retinal cells by means of high voltage

electrical pulses. The success of this method of delivery to the retina was verified *in vivo* by Matsuda *et al.,* (2004), as the delivery of shRNA constructs at P0, targeting two transcription factors *Nrl* and *Crx* with important roles in photoreceptor development, resulted in a phenotypic response similar to those observed in the corresponding knock-out models (Matsuda and Cepko 2004). This delivery method appears to provide an efficient and safe means of gene delivery to the retina, and in principle this strategy can be used for the delivery of miR expression constructs to the retina *in vivo*.

In this study the following miR expression constructs, miR-96, -182, -183, -133, -7, described in Chapter 8, were subretinally injected and electroporated in the eye of P0 mouse pups. Electroporation methods were followed as previously described by Matsuda *et al.*, (2004) (Matsuda and Cepko 2004), this procedure involving the injection of the DNA solutions directly into the sub-retinal space of neonatal mouse eyes, and application of electrical pulses using tweezer-type electrodes (Figure 9.3). This method successfully transduced the miR constructs into the cells of the retina, as GFP expression was observed in the treated retinas by histological examination (Figure 8.1 and 8.2). As the CMV promoter drives vector expression of many mammalian cell types, the expression of the miR expression constructs, as determined by GFP, was not restricted to a particular cell type, however photoreceptor cells of the ONL appear to be predominantly transduced (Figure 9.1) Approximately 10-20% of retinal cells are reported to be transduced using this delivery method, and in this study a significant variation in the number of GFP-positive cells was observed per retina, likely due to the variations in subretinal injections of mouse eyes at P0 and the relative location and distance between the electrodes and the subretinal DNA solution.

Overexpression of these miRs in the P0-P14 mouse retina did not appear to result in any structural effects at 2 weeks, in comparison to retinas transduced with an empty GFP vector (Figure 9.1). It is worth emphasising that this study represents an initial evaluation of the effects of miR overexpression in the murine retina. The numbers of mice used in this study were small and therefore the study needs to be expanded. Further studies involving larger numbers of animals, alternative delivery protocols and multiple time points for evaluation, will be required to fully establish the effects of miR overexpression on retinal structure and function. However, from these preliminary results obtained, it appears that these miRs may not, when delivered at P0 via electroporation (to approximately 10% of retinal cells), alter postnatal physiological processes sufficiently to

result in morphological changes. It is possible that the simultaneous expression of multiple miRs, may have a more noticeable effect resulting from coordinated gene targeting, as a considerable overlap of genes are predicted to be targeted by miR-96, -182, and -183 (Chapter 7). Indeed an advantage of this non-viral delivery method is the ability to transduce a number of constructs simultaneously, into the retina. Of note some alterations of retinal structure were observed in transduced eyes, including 'rosette-like' structures representing ectopic expression of photoreceptors, and altered laminar layers of the retina. However, as these alterations were also observed in the control eyes electroporated with the empty EGFP vector, they cannot be attributed to miR overexpression. These alterations presumably occur due to the invasive nature of sub-retinal injection at a young age (P0), which can result in blebbing and retinal detachment.

FACS analysis was additionally used in order to specifically examine miR expression in transduced cells (i.e. GFP-positive cells), due to the relatively low percentage of total retinal cells transduced using this method. Retinas injected and electroporated with miR constructs expressing, miR-133, -96, and -183 were dissociated and GFP cells were separated by FACS. QPCR analysis of miR-96 and -133 expression demonstrates that effective expression of these miRs in achieved in electroporated cells, notably miR-133 and -96 expression increased by 642% and 460% respectively (Figure 8.4). However no increase in miR-183 expression was observed in retinal cells electroporated with the miR-183 expression construct, in comparison to non-GFP labelled cells. This finding is in contrast to the preliminary results described in Chapter 8, in which transfection of these constructs in HeLa cell resulted in a significantly raised miR-183 expression (Figure 8.5). While further *in vitro* analysis of these miR expression constructs is indeed required to fully characterise miR expression from these constructs, it is possible that high endogenous levels of miR-183 in retinal cells may mask the additional expression achieved from the transduced miR-183 expression vector. While these findings demonstrate that miR-133 and miR-96 are overexpressed in electroporated retinal cells, expansion of this study is required using more animals, which was not possible in this study due to time constraints. Indeed future examinations of gene expression in FACS purified cells, transduced with miR expression constructs is potentially beneficial, in order to examine the functional interaction of the expressed miRs with endogenous retinal targets. Such methods have been applied for RNAi applications by which transduced retinal cells, separated by FACS, were analysed for shRNA-mediated suppression of target transcripts (Matsuda and Cepko).

In situ hybridistaion was additionally employed on sections from eyes transduced with miR-96 and -183, and while positive labelling of these miRs was detected, the signal strength was not explicitly stronger in transduced (GFP) cells (Figure 9.2). As ISH is less sensitive to miR detection than qPCR, it is possible that the alterations of miR expression in absolute levels falls below the discrimination limits of the technique. However, in this regard it is noticeable that no increase in miR-183 expression was observed in transduced retinal cells by FACS analysis and qPCR. Weak ISH labelling of miR-96 however was observed, in comparison to the negative control (Figure 9.2 L), and appeared to specifically label GFP positive inclusions (Figure 9.2. I and J). Note that despite the altered structure of the retina in this figure, similar structural alterations were also observed in retinas electroporated with an empty GFP vector, and as such likely reflect the effect of sub-retinal injection and electroporation at a young age. Notably the mild labelling of miR-96 in these 'rosette-like structures' correlates with the expression with GPF, suggesting that miR-96 is overexpressed *in vivo*. As stated elsewhere, due to the small number of animals used in this preliminary study, the results are inconclusive and further experiments are required to clarify the current observations.

These preliminary *in vivo* results demonstrate that miR expression vectors can be delivered to the retina and expressed, via electroporation. These initial results demonstrate the potential to overexpress miRs *in vivo* from miR expression vectors, which may prove to be beneficial in the future to examine the effects of miRs in the retina. Indeed, a recent study by Shibata *et al.*, (2008), examined the affect of miR-9 overexpression in the developing mouse cerebral cortex, by electroporation of an expression construct overexpressing miR-9 (Shibata et al. 2008). Using a combination of *in vivo* and *in vitro* studies, miR-9 was revealed to regulate cortical development by altering the expression of *Fxog1*, a transcription factor involved in regulating cortical differentiation. Similarly, the effectiveness of *in vivo* electroporation in retinal cells was demonstrated, by the RNAi mediated suppression of two transcription factors involved in photoreceptor development as outlined previously (Matsuda and Cepko 2004).

Notably, in addition to examining the functions of miR overexpression in the retina, suppression of miR expression is also immensely beneficial to both reveal and validate the functional effects of miRs. Tools to suppress miR expression include chemically modified antisense oligonucleotides and decoy vectors ('miR sponges') (Ebert et al. 2007). The latter expression vectors are designed to incorporate multiple miR

binding sites, such that following transcription of the vector miR binding sites sequester endogenous miRs, preventing miRs from interacting with their biological targets (Ebert et al. 2007). Such decoy vectors offer great potential to study loss of function effects of miRs *in vivo,* as demonstrated in cardiac hypertrophy by examining the effect of miR-133 suppression (Care et al. 2007).

In addition to electroporation, other delivery methods also exist which may facilitate the expression, or indeed inhibition, of miRs *in vivo*. Another non-viral delivery method termed iontophoresis, represents a similar technique to electroporation except that a low voltage electric current is applied rather than high-voltage pulses which are used for electroporation. This method of delivery can be used to deliver small nucleic acid fragment such as antisense oligonucleotides, siRNAs, and specifically has been used for the delivery of oligonucleotides to the retina in adult mice (Andrieu-Soler et al. 2006; Bejjani et al. 2007). In addition this non-viral transfer technique may potentially be useful for the delivery of miR mimics and antisense miR inhibitors.

In order to gain greater transduction efficiency by miR expression constructs, the use of viral vectors may be advantageous as approximately 30-40% of the retina can be transduced compared to electroporation (~10%) (Allocca et al. 2007). Indeed a number of viral-vector can be used to deliver constructs *in vivo*, and specifically recombinant AAV2/5 (adeno-associated virus, serotype 2/5) is particularly effective at transducing photoreceptor cells (Yang et al. 2002), which was used previously by the team in Trinity College Dublin for the viral delivery of potential RNAi therapeutics *in vivo* in the mouse (O'Reilly et al. 2007). AAV-based viral delivery may be used in future studies to explore the *in vivo* overexpression and or suppression of miRs of interest.

9.5. Conclusion

miR expression constructs effectively transduced the retina of P0 mouse pups, by a non-viral delivery method and successfully expressed miRs *in vivo,* as traced by GFP labelling and miR detection by qPCR. However no structural effects in the retina were observed which could be conclusively attributed to miR overexpression from this initial study. Clearly, further replication and characterisation of the effects mediated by miR expression is required, including a significant increase in the number of animals

examined, exploration of alternative delivery methods and different time points of analyses. For example viral vectors may be used to achieve a greater coverage of miR overexpression in the retina. The replacement of the CMV promoter with the rod specific rhodopsin promoter in the miR expression cassette may also be beneficial to examine the effects of miR overexpression specifically in rod photoreceptor cells. Therefore while the results from this initial study demonstrate that miR constructs can be delivered *in vivo* to the retina by electroporation, it must be emphasised that extensive further *in vitro* and *in vivo* experiments are necessary, with the miR constructs. Indeed a full examination of the expression of miRs from the miR expression vectors is pivotal for further *in vivo* evaluation of these constructs. Nevertheless, the results from this initial study, demonstrates the type of approach which may be taken in the future to explore the functional roles on miRs in the mammalian retina.

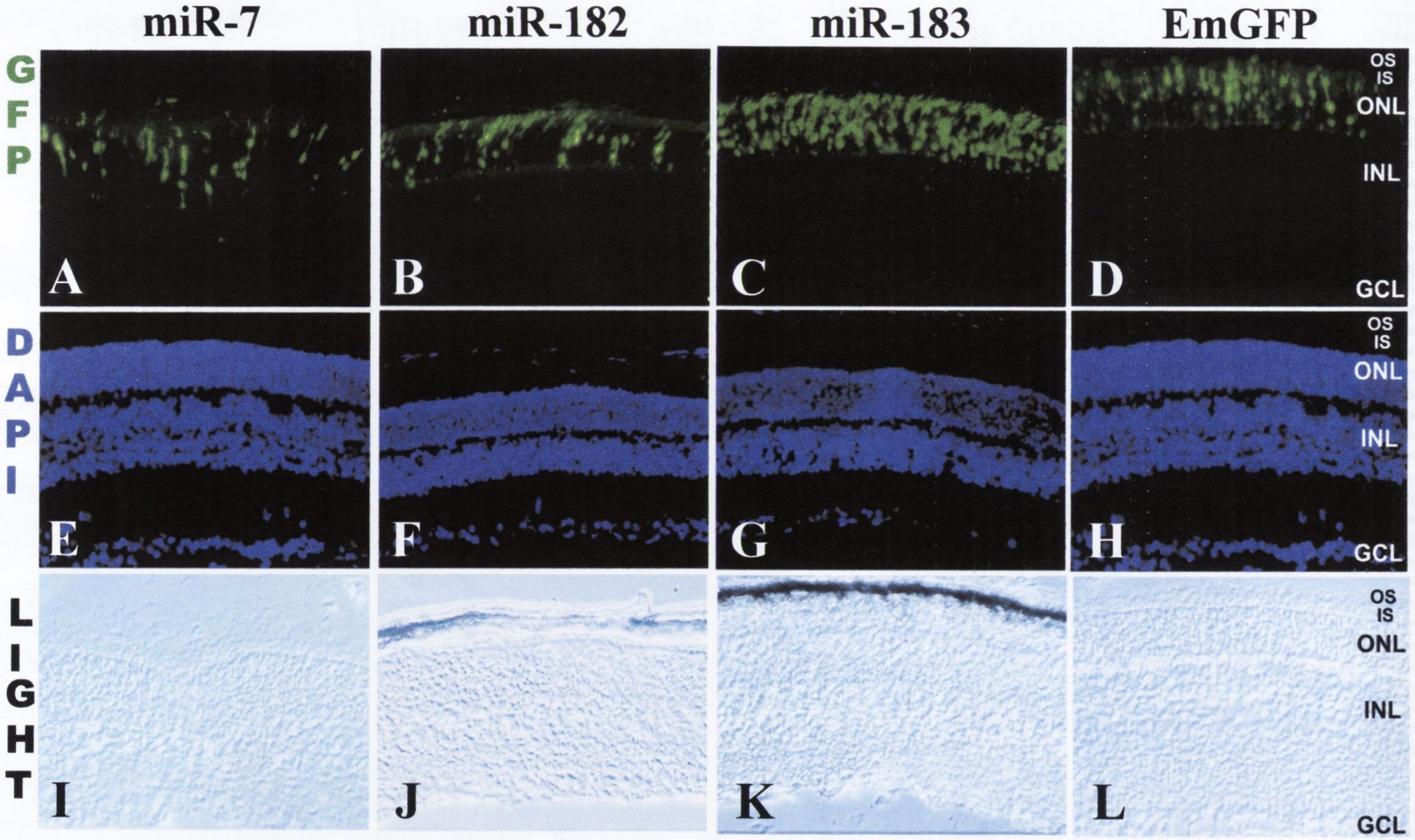

Figure 9.1: Histological sections of retinas electroporated with miRNA constructs: The pcDNA.6.2-miR expression constructs were electroporated into the retinas of P0 mouse eyes. Representative histological images of retinas over-expressing (**A**) miR-7, (**B**) miR-182, (**C**) miR-183, and (**D**) EmGFP empty vector, (**E-H**) and the corresponding nuclear stained sections using DAPI and (**I-L**) light microscope images are displayed. Light microscope and fluorescent microscope images were obtained at 200X magnification. Outer segments (OS), inner segments (IS), outer nuclear layer (ONL), inner nuclear layer (INL), ganglion cell layer (GCL).

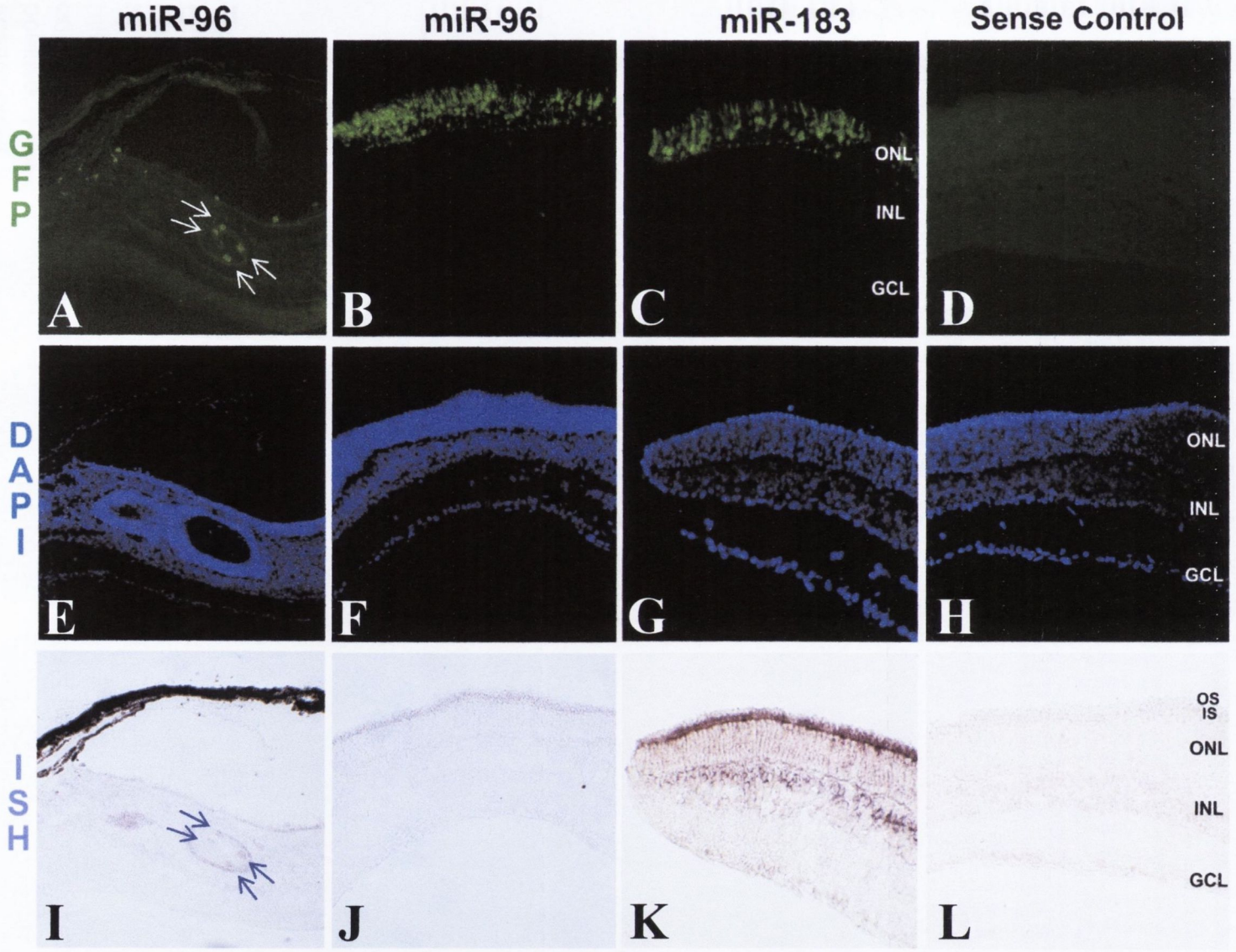

Figure 9.2: miRNA In Situ Hybridisation of electroporated retinas: pcDNA-miR-96 and -183 were subretinally injected and electroporated in the eyes of postnatal day 0 (P0). Sections illustrate GFP expression (**A-D**) DAPI (**E-H**) and in situ hybridisation (**I-L**) for miR-183 and -96 using 5' DIG labelled LNA probes, and the negative sense control, miR-159. Arrows point to GFP positive inclusions (**A**) and corresponding miR-96 labelling (**I**). Bright field light and fluorescent microscopy was used to obtain the images, taken at 200X magnification.; Outer segments (OS), inner segments (IS), outer nuclear layer (ONL), inner nuclear layer (INL), ganglion cell layer (GCL).

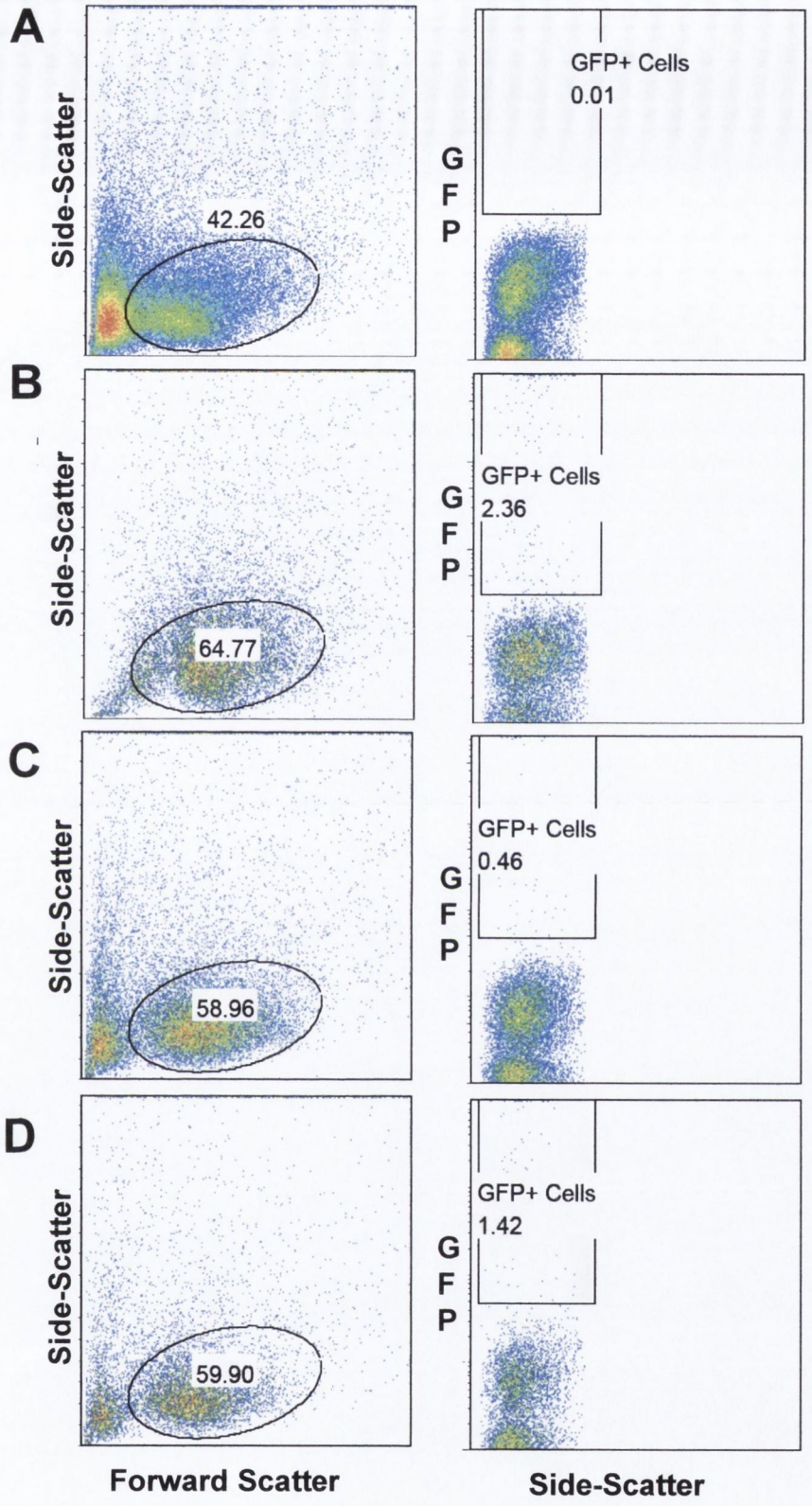

Figure 9.3: FACS Analysis of Electroporated Retinas: Electroporated retinas were harvested at 2 weeks post-electroporation and cells were dissociated by trypsin. GFP-positive and GFP-negative cells were separated by FACS, in (A) control retina and retinas electroporated with (B) miR-96 (C) miR-133 and (D) miR-183 expression constructs. Cells sorted fell within the enclosed area of the side and forward scatter plots (column 1) and GFP-positive cells were sorted which fell into the gated area of FITC and side scatter plot (column 2).

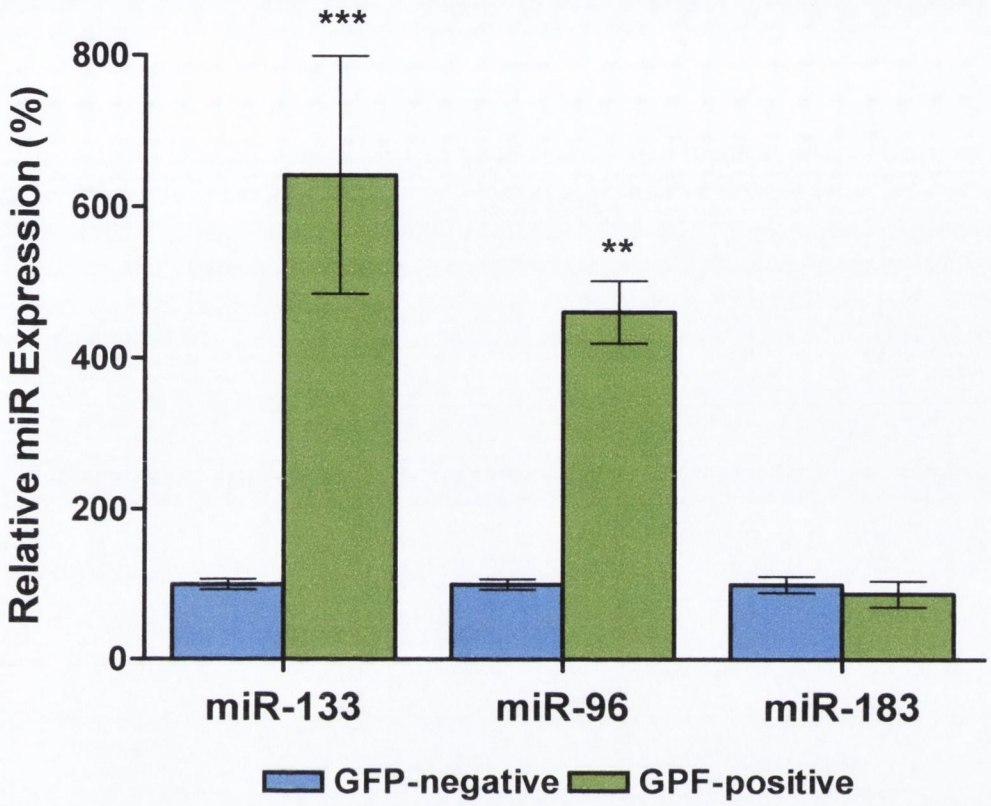

Figure 9.4: qPCR analysis of miR expression: Electroporated retinas with the miR expression constructs, pcDNA6.2-miR-miR-133, -96 and -183, were dissociated and GFP-positive and GFP-negative cells separated by FACS. qPCR analysis of miR expression of the corresponding miRs, miR-133, -96 and -183 was undertaken. Students *t-test* statistical analysis, (n=1), ** $p<0.01$; ***$p<0.001$.

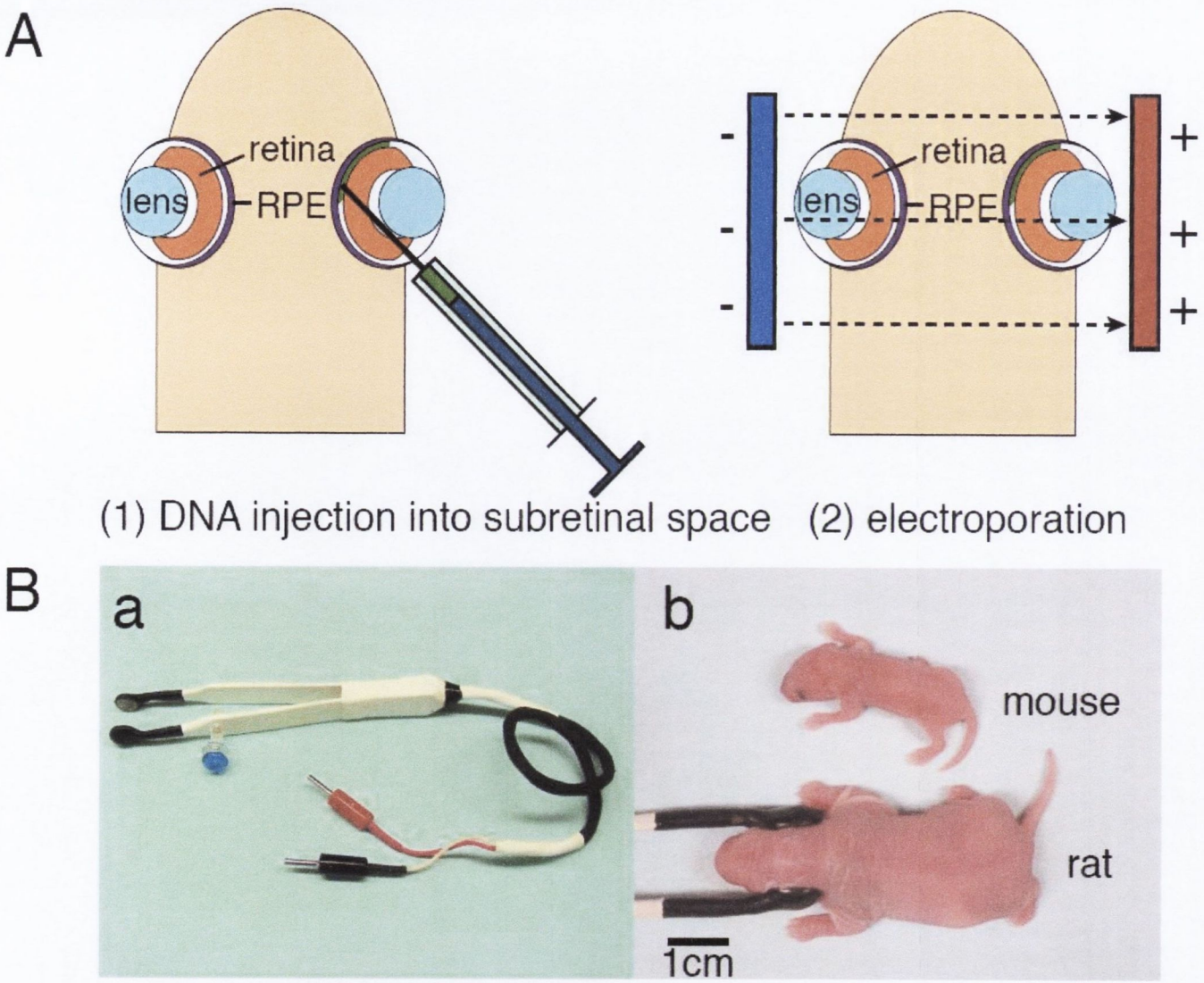

Figure 9.5. Electroporation Procedure and Apparatus for *in vivo* electroporation:. (**A**) Schematic illustration showing the *in vivo* electroporation method. (**B**) The electrodes used in this study are shown. Tweezer-type electrodes (**a**) are placed to hold the head of newborn (P0) rat or mouse (**b**). From Matsuda *et al.*, (2003)

Chapter 10

General Discussion

10.1. General Discussion

In recent years ocular research examining miR expression and function has emerged, aided by increasing knowledge of miR biology and important technological advances (Huang et al. 2008). Overall the findings presented in this thesis contribute to an understanding of miR expression and function, in both healthy and diseased retinas. Specifically the miR expression profile of the retina was examined, and novel retinal preference for a number of miRs was identified. In addition, this study represents the first demonstration of an altered miR expression profile in RP mouse models, making the first connection between altered miR expression and ocular disease (Loscher et al. 2007; Loscher et al. 2008).

The retina expresses a range of miRs and significantly a number of these are preferentially expressed in the retina, while others possess a similar miR expression profile to other neuronal tissues (Ryan et al. 2006; Arora et al. 2007; Karali et al. 2007; Xu et al. 2007). The results described in this thesis confirmed a retinal preference for a number of miRs (miR-204, -31, -29c, -181a, -184, -96, -182, and –183) and notably retinal preference was newly assigned for an additional 7 miRs (miR-335, -31, -106b, -129-3p, -691 and -26b) (Loscher et al. 2007). The functions of these miRs are unknown, however, due to their dominant expression in the retina, these miRs may potentially engage in retinal-specific functions. Evidence for such roles exists, including photoreceptor cell differentiation (Li and Carthew 2005) and the maintenance of adult retinal cells (Damiani et al. 2008). Additionally the spatial and temporal expression pattern of these miRs in the retina, as identified by ISH (Kloosterman et al. 2006; Karali et al. 2007; Xu et al. 2007), is indicative of stage-specific functions in development. For example a number of retinal miRs demonstrate peak expression at embryonic day 14 (E14), while others increase in expression from P1 to adulthood (Xu et al. 2007). Some of these miRs, such as miR-7 and miR-9, may be involved in retinal neurogenesis (Li and Carthew 2005; Li et al. 2006), while other miRs which increase in expression postnatally (miR-96, -182, and -183) may possibly be involved in the terminal differentiation and maintenance of photoreceptor cells, although there is no experimental evidence of this yet.

Perturbed miR expression in retinal degeneration is a key finding of this study, as observed in mouse models of rho-linked and rds-linked RP. Specifically the expression

of miR-1, -133 and -142 are dramatically upregulated in these retinas by up to 5-fold, while the expression of miR-96, -182 and -183 is reduced by up to 2-fold. Pivotally these alterations in expression can be attributed to genuine alterations of miR expression in photoreceptor cells, negating any ambiguity regarding altered cellular composition of the degenerating retina. This signature of retinal degeneration was not observed in the P23H model or the *rd1* retinal degeneration model of RP. This disparity may reflect the developmental status of the retina at the earlier time points analysed for the latter two animal models (P23H and *rd1*). As discussed in Chapter 7, the early time points were chosen due to the rapid nature of the degeneration in these mice, and indeed the rapid degeneration limits the utility of these mouse models for the current study. Notably while this signature of miR expression is not observed in the retinas of all RP models analysed, the findings of perturbed miR profiles in diseased retinas are nevertheless relevant, and may facilitate the elucidation of the most interesting steps in RP pathogenesis. The significance of these alterations of miR expression in the degenerative process are unknown, however it is likely to reflect pathogenic processes common to the models analysed, such as apoptosis, cellular defence mechanisms and retinal remodelling. MiR-1 and -133 appear to exhibit opposing roles in regulating cardiomyocyte apoptosis (Xu et al.), while -182 and -96 overexpression in cell culture inhibits the extrinsic activation of caspase-3 (Ovcharenko et al. 2007). Target prediction of the deregulated miRs in RP mouse models, also implicates a number of pro-apoptotic and anti-apoptotic regulatory genes such as *Binp3*, *Bcl212*, *Api5*. Additionally, alterations of miR expression may represent early events of retinal remodelling in response to ongoing photoreceptor degeneration, such as neurite outgrowth (Jones et al. 2003). In human RP patients, the elongation of rhodopsin-positive neurites has been observed which extends into inner layers of the retina, the sprouting axons immunoreactive for synaptic vesicle proteins (Marc et al. 2003). It is fascinating to suggest, that miR-96, -182, and -183 may be implicated in this process, as expression of these miRs is detected in the rod synapses of the OPL in normal retinas (Karali et al. 2007; Loscher et al. 2007), and indeed predicted targets of these miRs include rod synaptic proteins, such as synaptobrevin (*Vamp*). Although the expression miR-1 and -133 is relatively low in the retina, the upregulation of these miRs in RP models may be significant as these miRs are predicted to target a number of cytoskeletal proteins. The non-motile cilium of photoreceptor cells consists of arranged microtubule proteins, which are vital for intracellular transport of rhodopsin and other protein containing vesicles to the rod OSs. In addition to neurite elongation, slow alterations in the distribution of rhodopsin to the IS precede photoreceptor cell death

(Deretic et al. 1995; Marc et al. 2003). Therefore, the increased expression of miR-1 and -133 in the RP retina may possibly reflect the altered movement of rhodopsin to rod OSs and the aggregation of protein in inclusion bodies in the ISs, both of which are pathophysiological findings observed in mouse models of RP (Li et al. 1996; Illing et al. 2002; Deretic et al. 2005). Moreover cytoskeletal proteins, such as the microfilament actin, and actin associated proteins, are additionally required in the maintenance of photoreceptor cell polarity, essential to sustain contact with supporting Muller cells (Bringmann et al. 2006). MiR-1 is predicted to regulate the expression of the actin interacting protein, WD repeat-containing protein 1 (*Wdr1*). Likewise as miR-96, -182, and -183 expression peaks in adulthood, these miRs may play a role in the maintenance of photoreceptor cell integrity. The role of miR-142 in the retina is undefined and levels are low in the normal retina, however this miR is implicated in regulating the immune response as miR-142 is one of the highest expressed miRs in T-cells and B-cells (Caspi 2006; Wu et al. 2007) and an increased expression of miR-142 is observed during lung inflammation (Moschos et al. 2007). It is important to emphasise that the role of perturbed miR expression profiles in the diseased retina remains unknown and the various hypothesis outlined above require experimental investigation to ascertain if there is any validity associated with them.

In addition to the six miRs described above, the expression levels of additional miRs were altered in specific models of RP. In particular the expression of miR-21 and -23b was increased in the P347S and the rds-/- model, while miR-129 expression was reduced in the rho-/- model alone, and these distinct alterations may possibly represent cellular processes specific to the disease model analysed. Furthermore it would be of benefit to characterise the miR expression profile of a number of additional RP models using miR arrays, in order to comprehensively examine overlapping and non-overlapping miR alterations between models. In this way, miR involvement in both widespread and distinct retinal processes in RP mouse models may be revealed. In this study, the miRs exhibiting the largest relative expression changes in RP models were examined, yet subtle alterations in miR expression may likewise mediate important roles in disease. Indeed, the ability of miRs to mediate a functional response by target downregulation may depend on a range of factors, including the degree of complementary in miR:mRNA base-pairing, the absolute level of miR and target transcript expression, or the role of the suppressed protein (Baek et al. 2008; Selbach et al. 2008). Furthermore, the level of repression of a target protein correlates with the number of miR binding sites on the target transcript, as

recently verified by global target validation (Selbach et al. 2008). It is therefore relevant to consider the biological consequences of subtle alterations in miR expression in disease states.

The difficulty of interpreting the significance of altered miR expression in RP models is exacerbated by the complex nature of miR regulation in which the modification of both transcription and miR processing steps can alter miR expression. Indeed the regulation of pri-miR transcription is thought to be responsible for the tissue-specific expression of miRs, which involves complex negative and positive feedback loops (O'Donnell et al. 2005; Fazi and Nervi 2008). For example miR-133b inhibits the expression of *Pitx3*, which positively regulates miR-133b expression (Kim et al. 2007) and in haematopoietic cells miR -223 expression is regulated by the competitive binding of the two transcription factors NF1-A and C/EBPalpha to the miR promoter, NF1-A itself a target for miR-223 (Fazi and Nervi 2008). However it also appears that miR processing steps, by both Drosha and Dicer, may be additional points of miR regulation accounting for the tissue-specific expression of miRs and altered miR regulation in disease. Indeed cytoplasmic inhibitory factors, were demonstrated to preferentially inhibit Dicer processing of pre-miR-138 (Obernosterer et al. 2006), while previous correlations between pri-miR and mature miR expression in normal tissue, did not exist in primary tumour samples, indicative of altered Drosha processing in cancer (Thomson et al. 2006). Consequently it would be interesting to uncover the nature of regulation imposed on miR expression in the retinas of RP models, by examination of both pri-miR and pre-miR expression levels.

In addition the transcription of miR genes has been demonstrated to be altered by epigenetic modifications, which may alter the transcription of a number of miR genes (Weber et al. 2007). Indeed the deregulated expression of miRs observed in disease may result from abnormal patterns of CpG island methylation of miR genes. The epigenetic silencing of miRs by CpG island hypermethylation appears to be involved in both tumourogenesis and metastasis, as observed in a number of cancers (Datta et al. 2008; Kozaki et al. 2008; Lehmann et al. 2008; Lujambio et al. 2008). For instance, miR-128a, -34b/c and -9 are thought to be hypermethylated in metastatic cancers, as the addition of a DNA demethylating agent to metastatic cancer cell lines, resulted in the reactivation of these miRs. Importantly the reintroduction of these miRs into cancer cells reduced cell

motility and growth, in addition to the downregulation of a number of oncogenes (Lujambio et al. 2008)

In order to elucidate the functions of these miRs, target prediction and validation is important. As the precise manner by which miRs interact with their target mRNAs has not been fully elucidated, prediction algorithms frequently identify false targets and subsequently miR target validation is labour intensive. Targets were predicted for the six miRs altered in expression in RP models following recommendations by Kuhn *et al.* (2008), using a combination of miR prediction methods (Sethupathy et al.; Kuhn et al. 2008) and retinal expression libraries. This approach potentially produces a more robust and specific list of biologically relevant targets, as all targets are reported to be expressed in the retina. In addition the free energy analysis of local RNA secondary structures within or near miR target sites potentially excludes targets that may contain inaccessible binding sites. However other considerations, such as the interaction of miR binding sites with more distant regions of the mRNA and the stability of the miR:mRNA duplex, may provide additional power to miR target prediction methods (Kertesz et al. 2007; Hammell et al. 2008). Nevertheless in order to examine the roles played by these miRs in RP mouse models, future empirical validation of these targets is imperative.

The authenticity of the target may be determined *in vitro*, by demonstrating a miR:mRNA interaction. The most commonly used method to demonstrate target interaction is the use of luciferase reporter plasmids, which express the entire 3'UTR of the target gene immediately downstream of the luciferase ORF sequence. Following concurrent transfection of the target 3'-UTR-luciferase reporter and miR-expression constructs *in vitro*, the ability of specific miRs to inhibit luciferase activity is used as an indicator of successful target suppression. However interaction of these two artificial constructs is insufficient to ensure target validity, and other criteria must be attained including the co-expression of both miR and target and the ability of the miR to regulate endogenous target protein levels. While the *in silico* target prediction used in this study excluded target genes not expressed in the retina, the list of retinal genes screened is obtained from a number of retinal libraries which may contain inaccuracies, therefore experimental validation of miR target interaction in the retina is suggested to ensure retinal expression of predicted miR targets.

Importantly a key indicator for miR:target validation is the ability of miR overexpression and inhibition to suppress and derepress target protein expression,

respectively. While miR overexpression can be achieved using expression constructs, inhibition of miRs generally requires the use of commercial single stranded antisense oligoribonucleotides, chemically modified to improve stability and permeability. In addition miR "miR sponges" or decoy vectors have been designed by insertion of multiple miR binding sites directly downstream of a GFP reporter gene (Ebert et al. 2007). The fused GFP transcript, containing miR binding sites at the 3'UTR acts as a decoy signal and sequesters endogenous miRs (Ebert et al. 2007). Importantly competitive inhibition of endogenous miRs using this method is as effective as antisense technology, while additionally permitting the tracing of miR suppression and expression as demonstrated in the heart (Care et al. 2007). It is anticipated that with further characterisation the *in vitro* miR expression constructs discussed in Chapter 8, can be used to validate the targets predicted for miRs deregulated in RP. A global analysis of proteins repressed following miR overexpression, would provide a more efficient means to validate predicted miR targets. For example, the protein expression could be analysed from cell or retina lysates, using two dimensional differential-in-gel electrophoresis (2D-DIGE) and mass-spectrometry analysis. Two recent studies utilise high throughput miR target validation techniques, thereby offering an efficient means to verify miR targets. In these studies alterations of mRNA and protein expression of 2000 - 5000 targets were analysed simultaneously, in cell lysates following miR overexpression, by labelling proteins during translation via the incorporation of "heavy" amino acids using SILAC (stable-isotope labelling by amino acids in cultured cells) (Baek et al. 2008; Selbach et al. 2008). It is anticipated that these studies, will significantly aid the validation of biologically significant miR targets, and in addition provide valuable insights into the precise nature of miR:target interact, thereby permitting the enhancement of target prediction sensitivity and specificity.

Indeed the pinnacle of miR research is the elucidation of miR function in the tissue of interest, which in principle can be examined by miR overexpression and suppression *in vivo*. It is intriguing to determine the significance of both upregulated and downregulated miRs in RP models and as discussed in chapter 9, the *in vivo* overexpression of miRs in the retina provides a means for this investigation. An initial preliminary study suggested that *in vivo* overexpression of miR-96, -182, and -183 in the retina, did not appear to alter the structure of the retina based on histological analyses. It is important to highlight that this study needs to be significantly expanded, prior to drawing any conclusions concerning the fundamental effects of miR overexpression.

As discussed in Chapter 7, analysis of predicted targets of the miR cluster, miR-96, -182 and -183, reveal overlapping targets, likely due to the close similarities of the seed sequences of these miRs. As these miRs may mediate their effect in a coordinated manner, by regulating the expression of the same proteins, or indeed proteins involved in similar cellular responses, overexpression of these miRs in tandem may be beneficial to examine the functions of these miRs. However, miR-182 and -96 appear to target *Adcy6* independently, as similar levels of target suppression resulted from the overexpression of these miRs individually, suggesting that both miRs compete for the same binding site on the target. In this regard, miR-1 and -133 sequences are not similar and in heart and skeletal muscle, these miRs appear to mediate opposing functions *in vivo* (Chen et al. 2006; Xu et al. 2007). While further characterisation of these expression vectors is required, the non-viral delivery of these miR constructs to the retina was successful as, demonstrated by GFP expression and may provide a means to successfully express miRs *in vivo* over an extended period. Additionally, these constructs can be adapted to improve efficiency and specificity of delivery. For example, the incorporation of a rhodopsin promoter could be used to drive expression of the construct exclusively in rod photoreceptor cells, and the use of viral delivery mechanisms may improve the efficiently of vector delivery in addition to providing a long period of expression. The techniques that have been developed during the course of this study can be utilised in the future to explore the *in vivo* effects of miR overexpression and suppression in the retina.

It would indeed be of interest to suppress the expression of individual miRs in the retina, or indeed in photoreceptors, to exaggerate the functional effects of miR-96, -182, and -183 suppression observed in RP. This would necessitate the construction of "miR sponges" containing specific miR target sites, yet would provide long term miR repression traced by GFP expression. This strategy has been employed by Care *et al.*, (2007), in the examination of miR-133 and its role in cardiac hypertrophy as mentioned previously. MiR-133 expression is reduced in this disease state and interestingly the *in vivo* suppression of endogenous miR-133 expression, using the "miR sponge" vectors, induced cardiac hypertrophy in the absence of the disease stimulus (Care et al. 2007). This highlights the potential of miR expression vectors to examine the functional roles of miRs *in vivo*, and further elucidate miR involvement in disease and examine the potential therapeutic value of modulating miR expression.

The implication of miRs as causative agents of disease, has subsequently led to an explosion of interest in miRs as potential therapeutic targets in a wide range of human disorders. As many disease states display altered miR expression, it is likely the objective of therapeutic strategies involving miRs, would attempt to "normalise" miR expression levels. This strategy would hopefully circumvent disease progression by restoring gene deregulation. Such therapeutic strategies may require *in vivo* miR expression and inhibition, by means of continuous infusion of synthetic miRs and antisense oligoribonucleotides, or miR expression vectors and miR "sponge" vector constructs. While achieving expression of miR constructs in the required spatial and temporal pattern may prove difficult, both viral and non-viral delivery mechanisms currently employed for RNAi applications should be applicable. However, a major difficulty in any therapeutic strategy emanating from miR research is the heterogeneity of miR targets of each miR, and it follows that off-target effects may result from such approaches, as additional genes could be targeted. Indeed prediction of miR action *in vivo* is difficult, due to the large number of unconfirmed miR targets and ideally, a thorough knowledge of genuine targets should be obtained prior to therapeutic use. Another cause for concern is the potential of miR overexpression to saturate endogenous miR processing pathways. Indeed, this has been observed in long-term shRNA expression, which resulted in severe liver toxicity due to a reduction in miR levels (Grimm et al. 2006). Therefore a comprehensive examination of the safety and specificity of any miR therapeutic would be required, including the long-term effects.

As detailed in Chapter 5, a signature of altered miR expression was observed in the retina of RP mouse models. While impractical for retinal disorders, signatures of miR expression in other diseases may additionally act as useful biomarkers for diagnostic purposes potentially permitting the early detection of disease and the ability to distinguish between disease subtypes. Cancer is a heterogeneous disease affecting a multitude of tissue types, with varying levels of growth, metastasis, and prognosis and miRs expression profiles may be used to classify these disease subtypes. Recently the effective use of miRs as biomarkers in cancer has been demonstrated, as the expression of 48 miRs was capable of classifying the tissue origin of primary and metastatic tumours with an accuracy of >90% (Rosenfeld et al. 2008). He *et al.*, (2005) has also demonstrated the usefulness of miRs to discriminate cancerous from healthy thyroid tissue, based on the expression levels of 5 miRs (He et al. 2005). Interestingly, miR levels in serum and other cell-free biological fluids may provide a non-invasive alternative for disease detection.

Indeed circulating miRs in plasma serum can be detected, and raised placental miR expression has successfully been used to distinguish expectant from non-expectant women (Gilad et al. 2008).

A fascinating therapeutic application of the knowledge obtained from miR biology, is the use of tissue-specific miRs to alter tissue tropism of viruses, an approach that has been used in both gene therapy and the delivery of attenuated live virus vaccines. The application involves the incorporation of multiple miR binding sites in the 3'UTR of the transgene or virus, such that tissue-specific miRs prevent the expression of the transgene/virus in undesired tissues. For example, hepatotoxicity resulting from the cancer suicide gene therapy, herpes simplex virus thymidine kinase (HSVtk) gene and ganciclovir, can be prevented by the incorporation of miR-122 binding sites into the 3'UTR of the expression cassette. Expression of the HSVtk virus in the liver is therefore prevented, as expression is suppressed by the endogenous expression of miR-122, a liver-specific miR (Suzuki et al. 2008). Similarly endogenous miR-122 expression in the liver is the basis for the development of a non-hepatotoxic adenovirus, by integration of miR-122 binding sites in the 3'UTR of the early region 1A (E1A) viral gene (Ylosmaki et al. 2008). An interesting use of this strategy is indeed the potential to deliver live attenuated viral vaccines, by preventing viral expression in undesirable tissue. As proof of principle, Barnes *et al.*, (2008) has recently demonstrated in mice that the deleterious expression of the polio virus in neuronal cells can be negated, by incorporation of the binding sites of the neuronal specific miR-124 into non-coding regions of the viral gene (Barnes et al. 2008). While this vaccine is equally as effective in prompting immunity as inactivated vaccines, the ability to create safer live-attenuated viral vaccines may permit the rapid construction of vaccines against emerging viruses (Barnes et al. 2008).

Overall this application of miR technology can be applied to the delivery of RNAi therapeutic strategies, thereby avoiding tissue specific toxicity that was observed by Grim *et al.*, (2002) in the liver (Grimm et al. 2002). While it is possible that the virus may escape miR mediated suppression in the undesired cell type, this has not yet been observed. As discussed in Chapter 8, the expression of RNAi vector constructs can be additionally enhanced by incorporation of the shRNA cassette into the pre-miR-155 sequence, thereby hijacking the miR processing pathway. Indeed it appears that, in the short term at least, the creative applications of knowledge regarding tissue-specific

expression of miRs and miR processing requirements may benefit the development of RNAi gene therapies prior to therapeutics specifically modifying miR expression.

Notably in addition to the implication of altered miR expression in disease and therapeutic interventions, single nucleotide polymorphisms (SNP) of miR binding sites and miRs themselves may additionally affect miR gene regulation (Seuthaphty 2008; Chen, K. 2008). A number of polymorphisms have been identified in the pre-miR loop sequence, and additionally in the mature sequence of miR-125 (Iwai and Naraba 2005; Duan et al. 2007). As the sequence of the loop does not appear to be important for miR processing, most of these SNPs do not have any functional consequence, however the miR-125 SNP appears to inhibit miR-mediated target suppression and additionally the processing of the pri-miR (Duan et al. 2007). While these miR polymorphisms do not appear to have many functional consequences, SNPs within target genes are more likely to occur and affect gene function by altering the ability of miRs to interact with target transcripts. For example a SNP may abolish or weaken miR binding to a target site, or create a miR binding site in a gene that is not normally under the control of the miR in question (Chen et al.). Evidence exists demonstrating both of these effects, tentatively involving a variety of conditions including hypertension (Sethupathy et al. 2007), asthma (Tan et al. 2007), hereditary spastic paraplegia (Beetz et al. 2008) and breast cancer (Adams et al. 2007). The first identified SNP affecting miR function was observed in a small subset of Tourette syndrome patients additionally displaying obsessive-compulsive syndromes. Interestingly, miR-189 target-mediated suppression of a gene involved in regulating dendritic growth (SLITRK1) was prevented by a G→A substitution in the 3'UTR of the gene (Abelson et al. 2005). In contrast in Texel sheep, a miR binding site is created for muscle specific miR-1 and -206, by the G→A substitution in the 3'UTR of the myostatin gene (ovine GDF8). Interestingly this inhibition of myostatin gene expression increases muscle mass, accounting for the phenotypic attributes for which the Texel Sheep is bred (Clop et al. 2006).

In addition to disease, the effect of SNPs on miR function has been implicated in drug resistance of ovarian and breast cancer (Miller et al. 2008; Sorrentino et al. 2008). Specifically raised miR-221/222 expression in tamoxifen resistant breast cancer cells inhibits the expression of p27 (KIP), a cell cycle inhibitor (Miller et al. 2008). Moreover, a SNP (C→T) occurring near the 3'UTR of the dihydrofolate reductase (DHRF) gene was demonstrated to affect miR-24 mediated suppression of DHRF. DHRF is a

pharmacological target of methotrexate a widely used chemotherapeutic agent, and the presence of the SNP results in DHFP overexpression and methotrexate resistance. However as the SNP occurs 15 nt away from the miR-24 binding site, the mechanism by which the SNP alters miR action is not defined. Additionally no direct association of this SNP and methotrexate resistance in patients has been demonstrated. As recently highlighted by *Sethupathy et al.,* (2008) phenotypes that are associated with SNPs in miR target site, are not necessarily causative of that phenotype, and further replication and functional studies are required to eliminate confounding variables (Sethupathy and Collins 2008). Nevertheless SNP databases for miR target sites exit, such as PupaSuite, miRSNP, and Patrocles databases (miRSNP; PupaSuite; Patrocles) demonstrate that SNPs in miR target sites are abundant and may be responsible for phenotypic variation.

While most miRs are thought to regulate gene expression post-transcriptionally, it remains possible that some miRs may regulate gene expression indirectly at the level of DNA transcription, by chromatin remodelling. miRs may mediate this action by regulating the translation of chromatin-modifying enzymes, such as DNA methyltransferases (DNMTs), and indeed some of these enzymes are predicted miR targets (Lewis et al. 2005). Recently a study demonstrated the involvement of miRs in regulating DNA methylation, as global levels of DNA methylation were decreased in the *dicer1* null embryonic stem cells, and similar changes were observed in the *DNMT1* knockout cells (Benetti et al. 2008). Additionally, a study by Wagner *et al.,* (2008) has suggested that miRs may induce epigenetic states, which indeed may be heritable (Wagner et al. 2008). In this study, mice born following microinjection of miR-1 into fertilized mouse oocytes displayed a specific increase in heart size and suggested to result from epigenetic modifications. However intriguingly hypertrophic hearts were observed in the progeny, inherited paternally and maternally and correlated with an increase in expression of miR-1 in the sperm head of these mice, thereby suggesting a miR-mediated paramutation occurs in descendants (Wagner et al. 2008). Recent studies have also alluded to another mechanism of miR mediated effects, by which miRs may upregulate gene expression by activating the translation of target genes (Vasudevan et al. 2007). Specifically, miR-mediated upregulation of target genes was observed in cells during cell-cycle arrest, which did not occur during proliferation (Vasudevan et al. 2007). While miRs may mediate their effects through these alternative mechanisms, further confirmation of these findings are required.

In addition to miRs and siRNAs, another class of small RNA silencing system has recently emerged, called Piwi-associated RNAs (piRNAs) (Pang et al. 2007). piRNAs are 25-30 nt long, present in all animals, and are processed from single stranded precursors using a different biogenesis pathway to miRs, which is as yet undefined. piRNAs are believed to be important for germ cell development, as piRNAs associate with Piwi proteins in their thousands, a subfamily of argonaute proteins involved in the silencing of transposable element during germ cell development (Aravin et al. 2006; Girard et al. 2006; Lau et al. 2006). As 33,051 and 76,385 piRNAs have already been identified in human and mice respectively, the potential involvement of these RNAs in cellular functions is immense. In comparison, 8273 mature miR products have been identified, including 695 miRs confirmed in humans (miRBase). It is clear that ncRNAs play vital roles in regulating the expression of our genomes and that we have only begun to elucidate the nature of such regulation thus far.

10.2. Conclusion

In summary, miRs, a previously unrecognised class of small miRs, are likely to influence various physiological processes and may additionally play significant roles in disease. Significantly, from the findings presented in this PhD thesis, a widespread and intricate pattern of miR expression was identified in the retina. A number of miRs exhibited a high relative expression in the retina compared to other tissues, while the expression of some miRs localise to discrete cellular and subcellular compartments. Knowledge relating to the function of these miRs in the retina is limited; however they may play important roles in the maintenance of both retinal structure and function. Significantly, a common signature of miR deregulation was observed in RP mouse models, independent of the causative gene or the mode of inheritance. While significant progress has been made to characterise miR expression in the healthy and diseased retina, the function of these retinal miRs remains elusive. As recently observed, miR deregulation has been demonstrated to contribute to the pathogenesis of Alzheimer's and Parkinson's disease, and it is hypothesised that the common alterations of retinal miRs in RP may play a role in regulating the pathological process of retinal degeneration. It will be interesting to examine if altering miR expression in RP may modulate the outcome of retinal degeneration. Indeed the findings presented in this thesis, may provide a basis for the future exploration of potential miR-based therapeutic interventions in RP.

While the findings described in this PhD thesis relate to the involvement of miRs in the normal and diseased retinas of RP mouse models, it is likely that other ncRNAs are involved in both normal homeostatic mechanisms of the retina, in addition to disease. While the functions of many non-coding RNAs are unknown, it is becoming increasingly evident that they represent a vital output of the mammalian genome. While the last few decades have focused on elucidating function of the proteome, ncRNAs, previously identified as "junk DNA", are now under the spot-light. Undoubtedly revealing the functions of these ncRNAs in biological and disease processes, including RP, will be invaluable and may be extremely rewarding for the provision of the next generation of endogenous therapeutic targets.

Bibliography

Bibliography

([http://www.ncbi.nlm.nih.gov/Genbank/]). "Genebank."

([http://www.ncbi.nlm.nih.gov/pubmed]). "PubMed."

([http://www.ncbi.nlm.nih.gov/sites/unigene]). "UniGene Database."

Abelson, J. F., K. Y. Kwan, B. J. O'Roak, D. Y. Baek, A. A. Stillman, T. M. Morgan, C. A. Mathews, D. L. Pauls, M. R. Rasin, M. Gunel, N. R. Davis, A. G. Ercan-Sencicek, D. H. Guez, J. A. Spertus, J. F. Leckman, L. S. t. Dure, R. Kurlan, H. S. Singer, D. L. Gilbert, A. Farhi, A. Louvi, R. P. Lifton, N. Sestan and M. W. State (2005). "Sequence variants in SLITRK1 are associated with Tourette's syndrome." Science 310: 317-20.

Abu-Elneel, K., T. Liu, F. S. Gazzaniga, Y. Nishimura, D. P. Wall, D. H. Geschwind, K. Lao and K. S. Kosik (2008). "Heterogeneous dysregulation of microRNAs across the autism spectrum." Neurogenetics 9: 153-61.

Adams, B. D., H. Furneaux and B. A. White (2007). "The micro-ribonucleic acid (miRNA) miR-206 targets the human estrogen receptor-alpha (ERalpha) and represses ERalpha messenger RNA and protein expression in breast cancer cell lines." Mol Endocrinol 21: 1132-47.

Aguirre, G. D., V. Baldwin, S. Pearce-Kelling, K. Narfstrom, K. Ray and G. M. Acland (1998). "Congenital stationary night blindness in the dog: common mutation in the RPE65 gene indicates founder effect." Mol Vis 4: 23.

Aleman, L. M., J. Doench and P. A. Sharp (2007). "Comparison of siRNA-induced off-target RNA and protein effects." Rna 13: 385-95.

Allocca, M., C. Mussolino, M. Garcia-Hoyos, D. Sanges, C. Iodice, M. Petrillo, L. H. Vandenberghe, J. M. Wilson, V. Marigo, E. M. Surace and A. Auricchio (2007). "Novel adeno-associated virus serotypes efficiently transduce murine photoreceptors." J Virol 81: 11372-80.

Alvarez-Garcia, I. and E. A. Miska (2005). "MicroRNA functions in animal development and human disease." Development 132: 4653-62.

Amarzguioui, M., J. J. Rossi and D. Kim (2005). "Approaches for chemically synthesized siRNA and vector-mediated RNAi." FEBS Lett 579: 5974-81.

Ambros, V. (2004). "The functions of animal microRNAs." Nature 431: 350-5.

Ambros, V., B. Bartel, D. P. Bartel, C. B. Burge, J. C. Carrington, X. Chen, G. Dreyfuss, S. R. Eddy, S. Griffiths-Jones, M. Marshall, M. Matzke, G. Ruvkun and T. Tuschl (2003). "A uniform system for microRNA annotation." Rna 9: 277-9.

Ambros, V. and H. R. Horvitz (1984). "Heterochronic mutants of the nematode Caenorhabditis elegans." Science 226: 409-16.

Andrieu-Soler, C., R. A. Bejjani, T. de Bizemont, N. Normand, D. BenEzra and F. Behar-Cohen (2006). "Ocular gene therapy: a review of nonviral strategies." Mol Vis 12: 1334-47.

Andrieu-Soler, C., M. Doat, M. Halhal, N. Keller, L. Jonet, D. BenEzra and F. Behar-Cohen (2006). "Enhanced oligonucleotide delivery to mouse retinal cells using iontophoresis." Mol Vis 12: 1098-107.

Applebury, M. L., M. P. Antoch, L. C. Baxter, L. L. Chun, J. D. Falk, F. Farhangfar, K. Kage, M. G. Krzystolik, L. A. Lyass and J. T. Robbins (2000). "The murine cone photoreceptor: a single cone type expresses both S and M opsins with retinal spatial patterning." Neuron 27: 513-23.

Aquirre, G., D. Farber, R. Lolley, R. T. Fletcher and G. J. Chader (1978). "Rod-cone dysplasia in Irish setters: a defect in cyclic GMP metabolism in visual cells." Science 201: 1133-4.

Aravin, A., D. Gaidatzis, S. Pfeffer, M. Lagos-Quintana, P. Landgraf, N. Iovino, P. Morris, M. J. Brownstein, S. Kuramochi-Miyagawa, T. Nakano, M. Chien, J. J. Russo, J. Ju, R. Sheridan, C. Sander, M. Zavolan and T. Tuschl (2006). "A novel class of small RNAs bind to MILI protein in mouse testes." Nature 442: 203-7.

Arora, A., G. J. McKay and D. A. Simpson (2007). "Prediction and verification of miRNA expression in human and rat retinas." Invest Ophthalmol Vis Sci 48: 3962-7.

Aruga, J. and K. Mikoshiba (2003). "Identification and characterization of Slitrk, a novel neuronal transmembrane protein family controlling neurite outgrowth." Mol Cell Neurosci 24: 117-29.

Ason, B., D. K. Darnell, B. Wittbrodt, E. Berezikov, W. P. Kloosterman, J. Wittbrodt, P. B. Antin and R. H. Plasterk (2006). "Differences in vertebrate microRNA expression." Proc Natl Acad Sci U S A 103: 14385-9.

Babak, T., W. Zhang, Q. Morris, B. J. Blencowe and T. R. Hughes (2004). "Probing microRNAs with microarrays: tissue specificity and functional inference." Rna 10: 1813-9.

Baek, D., J. Villen, C. Shin, F. D. Camargo, S. P. Gygi and D. P. Bartel (2008). "The impact of microRNAs on protein output." Nature 455: 64-71.

Bainbridge, J. W. and R. R. Ali (2008). "Keeping an eye on clinical trials in 2008." Gene Ther 15: 633-4.

Bak, M., A. Silahtaroglu, M. Moller, M. Christensen, M. F. Rath, B. Skryabin, N. Tommerup and S. Kauppinen (2008). "MicroRNA expression in the adult mouse central nervous system." RNA 14: 432-44.

Bandres, E., E. Cubedo, X. Agirre, R. Malumbres, R. Zarate, N. Ramirez, A. Abajo, A. Navarro, I. Moreno, M. Monzo and J. Garcia-Foncillas (2006). "Identification by Real-time PCR of 13 mature microRNAs differentially expressed in colorectal cancer and non-tumoral tissues." Mol Cancer 5: 29.

Barnes, D., M. Kunitomi, M. Vignuzzi, K. Saksela and R. Andino (2008). "Harnessing endogenous miRNAs to control virus tissue tropism as a strategy for developing attenuated virus vaccines." Cell Host Microbe 4: 239-48.

Bartel, D. P. (2004). "MicroRNAs: genomics, biogenesis, mechanism, and function." Cell 116: 281-97.

Baskerville, S. and D. P. Bartel (2005). "Microarray profiling of microRNAs reveals frequent coexpression with neighboring miRNAs and host genes." Rna 11: 241-7.

Baumann, O. and B. Walz (2001). "Endoplasmic reticulum of animal cells and its organization into structural and functional domains." Int Rev Cytol 205: 149-214.

Beetz, C., R. Schule, T. Deconinck, K. N. Tran-Viet, H. Zhu, B. P. Kremer, S. G. Frints, W. A. van Zelst-Stams, P. Byrne, S. Otto, A. O. Nygren, J. Baets, K. Smets, B. Ceulemans, B. Dan, N. Nagan, J. Kassubek, S. Klimpe, T. Klopstock, H. Stolze, H. J. Smeets, C. T. Schrander-Stumpel, M. Hutchinson, B. P. van de Warrenburg, C. Braastad, T. Deufel, M. Pericak-Vance, L. Schols, P. de Jonghe and S. Zuchner (2008). "REEP1 mutation spectrum and genotype/phenotype correlation in hereditary spastic paraplegia type 31." Brain 131: 1078-86.

Behm-Ansmant, I., J. Rehwinkel and E. Izaurralde (2006). "MicroRNAs silence gene expression by repressing protein expression and/or by promoting mRNA decay." Cold Spring Harb Symp Quant Biol 71: 523-30.

Bejjani, R. A., C. Andrieu, C. Bloquel, M. Berdugo, D. BenEzra and F. Behar-Cohen (2007). "Electrically assisted ocular gene therapy." Surv Ophthalmol 52: 196-208.

Bence, N. F., R. M. Sampat and R. R. Kopito (2001). "Impairment of the ubiquitin-proteasome system by protein aggregation." Science 292: 1552-5.

Benetti, R., S. Gonzalo, I. Jaco, P. Munoz, S. Gonzalez, S. Schoeftner, E. Murchison, T. Andl, T. Chen, P. Klatt, E. Li, M. Serrano, S. Millar, G. Hannon and M. A. Blasco

(2008). "A mammalian microRNA cluster controls DNA methylation and telomere recombination via Rbl2-dependent regulation of DNA methyltransferases." Nat Struct Mol Biol 15: 268-79.

Bentwich, I., A. Avniel, Y. Karov, R. Aharonov, S. Gilad, O. Barad, A. Barzilai, P. Einat, U. Einav, E. Meiri, E. Sharon, Y. Spector and Z. Bentwich (2005). "Identification of hundreds of conserved and nonconserved human microRNAs." Nat Genet 37: 766-70.

Berezikov, E., W. J. Chung, J. Willis, E. Cuppen and E. C. Lai (2007). "Mammalian mirtron genes." Mol Cell 28: 328-36.

Berezikov, E., G. van Tetering, M. Verheul, J. van de Belt, L. van Laake, J. Vos, R. Verloop, M. van de Wetering, V. Guryev, S. Takada, A. J. van Zonneveld, H. Mano, R. Plasterk and E. Cuppen (2006). "Many novel mammalian microRNA candidates identified by extensive cloning and RAKE analysis." Genome Res 16: 1289-98.

Bernstein, E., A. M. Denli and G. J. Hannon (2001). "The rest is silence." Rna 7: 1509-21.

Bernstein, E., S. Y. Kim, M. A. Carmell, E. P. Murchison, H. Alcorn, M. Z. Li, A. A. Mills, S. J. Elledge, K. V. Anderson and G. J. Hannon (2003). "Dicer is essential for mouse development." Nat Genet 35: 215-7.

Berson, D. M., F. A. Dunn and M. Takao (2002). "Phototransduction by retinal ganglion cells that set the circadian clock." Science 295: 1070-3.

Berson, E. L. (1996). "Retinitis pigmentosa: unfolding its mystery." Proc Natl Acad Sci U S A 93: 4526-8.

Berson, E. L., B. Rosner, C. Weigel-DiFranco, T. P. Dryja and M. A. Sandberg (2002). "Disease progression in patients with dominant retinitis pigmentosa and rhodopsin mutations." Invest Ophthalmol Vis Sci 43: 3027-36.

Bhattacharya, S. S., A. F. Wright, J. F. Clayton, W. H. Price, C. I. Phillips, C. M. McKeown, M. Jay, A. C. Bird, P. L. Pearson, E. M. Southern and et al. (1984). "Close genetic linkage between X-linked retinitis pigmentosa and a restriction fragment length polymorphism identified by recombinant DNA probe L1.28." Nature 309: 253-5.

Bhattacharyya, S. N., R. Habermacher, U. Martine, E. I. Closs and W. Filipowicz (2006). "Stress-induced reversal of microRNA repression and mRNA P-body localization in human cells." Cold Spring Harb Symp Quant Biol 71: 513-21.

Bilen, J., N. Liu and N. M. Bonini (2006). "A new role for microRNA pathways: modulation of degeneration induced by pathogenic human disease proteins." Cell Cycle 5: 2835-8.

Bilen, J., N. Liu, B. G. Burnett, R. N. Pittman and N. M. Bonini (2006). "MicroRNA pathways modulate polyglutamine-induced neurodegeneration." Mol Cell 24: 157-63.

BioMart ([http://www.ensembl.org/biomart/]).

Blackshaw, S., R. E. Fraioli, T. Furukawa and C. L. Cepko (2001). "Comprehensive analysis of photoreceptor gene expression and the identification of candidate retinal disease genes." Cell 107: 579-89.

Blackshaw, S., S. Harpavat, J. Trimarchi, L. Cai, H. Huang, W. P. Kuo, G. Weber, K. Lee, R. E. Fraioli, S. H. Cho, R. Yung, E. Asch, L. Ohno-Machado, W. H. Wong and C. L. Cepko (2004). "Genomic analysis of mouse retinal development." PLoS Biol 2: E247.

Bloquel, C., R. Bejjani, P. Bigey, F. Bedioui, M. Doat, D. BenEzra, D. Scherman and F. Behar-Cohen (2006). "Plasmid electrotransfer of eye ciliary muscle: principles and therapeutic efficacy using hTNF-alpha soluble receptor in uveitis." FASEB J 20: 389-91.

Bommer, G. T., I. Gerin, Y. Feng, A. J. Kaczorowski, R. Kuick, R. E. Love, Y. Zhai, T. J. Giordano, Z. S. Qin, B. B. Moore, O. A. MacDougald, K. R. Cho and E. R. Fearon (2007). "p53-mediated activation of miRNA34 candidate tumor-suppressor genes." Curr Biol 17: 1298-307.

Bonnet, E., J. Wuyts, P. Rouze and Y. Van de Peer (2004). "Evidence that microRNA precursors, unlike other non-coding RNAs, have lower folding free energies than random sequences." Bioinformatics 20: 2911-7.

Boon, C. J., A. I. den Hollander, C. B. Hoyng, F. P. Cremers, B. J. Klevering and J. E. Keunen (2008). "The spectrum of retinal dystrophies caused by mutations in the peripherin/RDS gene." Prog Retin Eye Res 27: 213-35.

Borchert, G. M., W. Lanier and B. L. Davidson (2006). "RNA polymerase III transcribes human microRNAs." Nat Struct Mol Biol 13: 1097-101.

Boshart, M., F. Weber, G. Jahn, K. Dorsch-Hasler, B. Fleckenstein and W. Schaffner (1985). "A very strong enhancer is located upstream of an immediate early gene of human cytomegalovirus." Cell 41: 521-30.

Bowne, S. J., L. S. Sullivan, S. H. Blanton, C. L. Cepko, S. Blackshaw, D. G. Birch, D. Hughbanks-Wheaton, J. R. Heckenlively and S. P. Daiger (2002). "Mutations in the inosine monophosphate dehydrogenase 1 gene (IMPDH1) cause the RP10 form of autosomal dominant retinitis pigmentosa." Hum Mol Genet 11: 559-68.

Bracht, J., S. Hunter, R. Eachus, P. Weeks and A. E. Pasquinelli (2004). "Trans-splicing and polyadenylation of let-7 microRNA primary transcripts." Rna 10: 1586-94.

Brennecke, J., D. R. Hipfner, A. Stark, R. B. Russell and S. M. Cohen (2003). "bantam encodes a developmentally regulated microRNA that controls cell proliferation and regulates the proapoptotic gene hid in Drosophila." Cell 113: 25-36.

Brennecke, J., A. Stark, R. B. Russell and S. M. Cohen (2005). "Principles of microRNA-target recognition." PLoS Biol 3: e85.

Bringmann, A., T. Pannicke, J. Grosche, M. Francke, P. Wiedemann, S. N. Skatchkov, N. N. Osborne and A. Reichenbach (2006). "Muller cells in the healthy and diseased retina." Prog Retin Eye Res 25: 397-424.

Briscoe, A. D., C. Gaur and S. Kumar (2004). "The spectrum of human rhodopsin disease mutations through the lens of interspecific variation." Gene 332: 107-18.

Burt, D. W., D. R. Morrice, D. H. Lester, G. W. Robertson, M. D. Mohamed, I. Simmons, L. M. Downey, C. Thaung, L. R. Bridges, I. R. Paton, M. Gentle, J. Smith, P. M. Hocking and C. F. Inglehearn (2003). "Analysis of the rdd locus in chicken: a model for human retinitis pigmentosa." Mol Vis 9: 164-70.

Bussing, I., F. J. Slack and H. Grosshans (2008). "let-7 microRNAs in development, stem cells and cancer." Trends Mol Med 14: 400-409.

Cai, X., C. H. Hagedorn and B. R. Cullen (2004). "Human microRNAs are processed from capped, polyadenylated transcripts that can also function as mRNAs." Rna 10: 1957-66.

Callis, T. E. and D. Z. Wang (2008). "Taking microRNAs to heart." Trends Mol Med 14: 254-60.

Care, A., D. Catalucci, F. Felicetti, D. Bonci, A. Addario, P. Gallo, M. L. Bang, P. Segnalini, Y. Gu, N. D. Dalton, L. Elia, M. V. Latronico, M. Hoydal, C. Autore, M. A. Russo, G. W. Dorn, 2nd, O. Ellingsen, P. Ruiz-Lozano, K. L. Peterson, C. M. Croce, C. Peschle and G. Condorelli (2007). "MicroRNA-133 controls cardiac hypertrophy." Nat Med 13: 613-8.

Carninci, P., T. Kasukawa, S. Katayama, J. Gough, M. C. Frith, N. Maeda, R. Oyama, T. Ravasi, B. Lenhard, C. Wells, R. Kodzius, K. Shimokawa, V. B. Bajic, S. E. Brenner, S. Batalov, A. R. Forrest, M. Zavolan, M. J. Davis, L. G. Wilming, V. Aidinis, J. E. Allen, A. Ambesi-Impiombato, R. Apweiler, R. N. Aturaliya, T. L. Bailey, M. Bansal, L. Baxter, K. W. Beisel, T. Bersano, H. Bono, A. M. Chalk, K.

P. Chiu, V. Choudhary, A. Christoffels, D. R. Clutterbuck, M. L. Crowe, E. Dalla, B. P. Dalrymple, B. de Bono, G. Della Gatta, D. di Bernardo, T. Down, P. Engstrom, M. Fagiolini, G. Faulkner, C. F. Fletcher, T. Fukushima, M. Furuno, S. Futaki, M. Gariboldi, P. Georgii-Hemming, T. R. Gingeras, T. Gojobori, R. E. Green, S. Gustincich, M. Harbers, Y. Hayashi, T. K. Hensch, N. Hirokawa, D. Hill, L. Huminiecki, M. Iacono, K. Ikeo, A. Iwama, T. Ishikawa, M. Jakt, A. Kanapin, M. Katoh, Y. Kawasawa, J. Kelso, H. Kitamura, H. Kitano, G. Kollias, S. P. Krishnan, A. Kruger, S. K. Kummerfeld, I. V. Kurochkin, L. F. Lareau, D. Lazarevic, L. Lipovich, J. Liu, S. Liuni, S. McWilliam, M. Madan Babu, M. Madera, L. Marchionni, H. Matsuda, S. Matsuzawa, H. Miki, F. Mignone, S. Miyake, K. Morris, S. Mottagui-Tabar, N. Mulder, N. Nakano, H. Nakauchi, P. Ng, R. Nilsson, S. Nishiguchi, S. Nishikawa, F. Nori, O. Ohara, Y. Okazaki, V. Orlando, K. C. Pang, W. J. Pavan, G. Pavesi, G. Pesole, N. Petrovsky, S. Piazza, J. Reed, J. F. Reid, B. Z. Ring, M. Ringwald, B. Rost, Y. Ruan, S. L. Salzberg, A. Sandelin, C. Schneider, C. Schonbach, K. Sekiguchi, C. A. Semple, S. Seno, L. Sessa, Y. Sheng, Y. Shibata, H. Shimada, K. Shimada, D. Silva, B. Sinclair, S. Sperling, E. Stupka, K. Sugiura, R. Sultana, Y. Takenaka, K. Taki, K. Tammoja, S. L. Tan, S. Tang, M. S. Taylor, J. Tegner, S. A. Teichmann, H. R. Ueda, E. van Nimwegen, R. Verardo, C. L. Wei, K. Yagi, H. Yamanishi, E. Zabarovsky, S. Zhu, A. Zimmer, W. Hide, C. Bult, S. M. Grimmond, R. D. Teasdale, E. T. Liu, V. Brusic, J. Quackenbush, C. Wahlestedt, J. S. Mattick, D. A. Hume, C. Kai, D. Sasaki, Y. Tomaru, S. Fukuda, M. Kanamori-Katayama, M. Suzuki, J. Aoki, T. Arakawa, J. Iida, K. Imamura, M. Itoh, T. Kato, H. Kawaji, N. Kawagashira, T. Kawashima, M. Kojima, S. Kondo, H. Konno, K. Nakano, N. Ninomiya, T. Nishio, M. Okada, C. Plessy, K. Shibata, T. Shiraki, S. Suzuki, M. Tagami, K. Waki, A. Watahiki, Y. Okamura-Oho, H. Suzuki, J. Kawai and Y. Hayashizaki (2005). "The transcriptional landscape of the mammalian genome." Science 309: 1559-63.

Carter-Dawson, L. D., M. M. LaVail and R. L. Sidman (1978). "Differential effect of the rd mutation on rods and cones in the mouse retina." Invest Ophthalmol Vis Sci 17: 489-98.

Caspi, R. R. (2006). "Ocular autoimmunity: the price of privilege?" Immunol Rev 213: 23-35.

Cepko, C. L., C. P. Austin, X. Yang, M. Alexiades and D. Ezzeddine (1996). "Cell fate determination in the vertebrate retina." Proc Natl Acad Sci U S A 93: 589-95.

Chader, G. J. (2002). "Animal models in research on retinal degenerations: past progress and future hope." Vision Res 42: 393-9.

Chakarova, C. F., M. M. Hims, H. Bolz, L. Abu-Safieh, R. J. Patel, M. G. Papaioannou, C. F. Inglehearn, T. J. Keen, C. Willis, A. T. Moore, T. Rosenberg, A. R. Webster, A. C. Bird, A. Gal, D. Hunt, E. N. Vithana and S. S. Bhattacharya (2002). "Mutations in HPRP3, a third member of pre-mRNA splicing factor genes, implicated in autosomal dominant retinitis pigmentosa." Hum Mol Genet 11: 87-92.

Chan, F., A. Bradley, T. G. Wensel and J. H. Wilson (2004). "Knock-in human rhodopsin-GFP fusions as mouse models for human disease and targets for gene therapy." Proc Natl Acad Sci U S A 101: 9109-14.

Chan, J. A., A. M. Krichevsky and K. S. Kosik (2005). "MicroRNA-21 is an antiapoptotic factor in human glioblastoma cells." Cancer Res 65: 6029-33.

Chang, B., N. L. Hawes, R. E. Hurd, M. T. Davisson, S. Nusinowitz and J. R. Heckenlively (2002). "Retinal degeneration mutants in the mouse." Vision Res 42: 517-25.

Chang, G. Q., Y. Hao and F. Wong (1993). "Apoptosis: final common pathway of photoreceptor death in rd, rds, and rhodopsin mutant mice." Neuron 11: 595-605.

Chang, T. C., E. A. Wentzel, O. A. Kent, K. Ramachandran, M. Mullendore, K. H. Lee, G. Feldmann, M. Yamakuchi, M. Ferlito, C. J. Lowenstein, D. E. Arking, M. A. Beer, A. Maitra and J. T. Mendell (2007). "Transactivation of miR-34a by p53 broadly influences gene expression and promotes apoptosis." Mol Cell 26: 745-52.

Chen, C., D. Ridzon, C. T. Lee, J. Blake, Y. Sun and W. M. Strauss (2007). "Defining embryonic stem cell identity using differentiation-related microRNAs and their potential targets." Mamm Genome 18: 316-27.

Chen, C., D. A. Ridzon, A. J. Broomer, Z. Zhou, D. H. Lee, J. T. Nguyen, M. Barbisin, N. L. Xu, V. R. Mahuvakar, M. R. Andersen, K. Q. Lao, K. J. Livak and K. J. Guegler (2005). "Real-time quantification of microRNAs by stem-loop RT-PCR." Nucleic Acids Res 33: e179.

Chen, C. Z., L. Li, H. F. Lodish and D. P. Bartel (2004). "MicroRNAs modulate hematopoietic lineage differentiation." Science 303: 83-6.

Chen, J. F., E. M. Mandel, J. M. Thomson, Q. Wu, T. E. Callis, S. M. Hammond, F. L. Conlon and D. Z. Wang (2006). "The role of microRNA-1 and microRNA-133 in skeletal muscle proliferation and differentiation." Nat Genet 38: 228-33.

Chendrimada, T. P., R. I. Gregory, E. Kumaraswamy, J. Norman, N. Cooch, K. Nishikura and R. Shiekhattar (2005). "TRBP recruits the Dicer complex to Ago2 for microRNA processing and gene silencing." Nature 436: 740-4.

Cheng, A. M., M. W. Byrom, J. Shelton and L. P. Ford (2005). "Antisense inhibition of human miRNAs and indications for an involvement of miRNA in cell growth and apoptosis." Nucleic Acids Res 33: 1290-7.

Cheng, H. Y., J. W. Papp, O. Varlamova, H. Dziema, B. Russell, J. P. Curfman, T. Nakazawa, K. Shimizu, H. Okamura, S. Impey and K. Obrietan (2007). "microRNA modulation of circadian-clock period and entrainment." Neuron 54: 813-29.

Chung, K. H., C. C. Hart, S. Al-Bassam, A. Avery, J. Taylor, P. D. Patel, A. B. Vojtek and D. L. Turner (2006). "Polycistronic RNA polymerase II expression vectors for RNA interference based on BIC/miR-155." Nucleic Acids Res 34: e53.

Cimmino, A., G. A. Calin, M. Fabbri, M. V. Iorio, M. Ferracin, M. Shimizu, S. E. Wojcik, R. I. Aqeilan, S. Zupo, M. Dono, L. Rassenti, H. Alder, S. Volinia, C. G. Liu, T. J. Kipps, M. Negrini and C. M. Croce (2005). "miR-15 and miR-16 induce apoptosis by targeting BCL2." Proc Natl Acad Sci U S A 102: 13944-9.

Clop, A., F. Marcq, H. Takeda, D. Pirottin, X. Tordoir, B. Bibe, J. Bouix, F. Caiment, J. M. Elsen, F. Eychenne, C. Larzul, E. Laville, F. Meish, D. Milenkovic, J. Tobin, C. Charlier and M. Georges (2006). "A mutation creating a potential illegitimate microRNA target site in the myostatin gene affects muscularity in sheep." Nat Genet 38: 813-8.

Cuellar, T. L., T. H. Davis, P. T. Nelson, G. B. Loeb, B. D. Harfe, E. Ullian and M. T. McManus (2008). "Dicer loss in striatal neurons produces behavioral and neuroanatomical phenotypes in the absence of neurodegeneration." Proc Natl Acad Sci U S A 105: 5614-9.

Curcio, C. A., K. R. Sloan, R. E. Kalina and A. E. Hendrickson (1990). "Human photoreceptor topography." J Comp Neurol 292: 497-523.

Dalke, C. and J. Graw (2005). "Mouse mutants as models for congenital retinal disorders." Exp Eye Res 81: 503-12.

Damiani, D., J. J. Alexander, J. R. O'Rourke, M. McManus, A. P. Jadhav, C. L. Cepko, W. W. Hauswirth, B. D. Harfe and E. Strettoi (2008). "Dicer inactivation leads to progressive functional and structural degeneration of the mouse retina." J Neurosci 28: 4878-87.

Danial, N. N. and S. J. Korsmeyer (2004). "Cell death: critical control points." Cell 116: 205-19.

Datta, J., H. Kutay, M. W. Nasser, G. J. Nuovo, B. Wang, S. Majumder, C. G. Liu, S. Volinia, C. M. Croce, T. D. Schmittgen, K. Ghoshal and S. T. Jacob (2008). "Methylation mediated silencing of MicroRNA-1 gene and its role in hepatocellular carcinogenesis." Cancer Res 68: 5049-58.

Davis, T. H., T. L. Cuellar, S. M. Koch, A. J. Barker, B. D. Harfe, M. T. McManus and E. M. Ullian (2008). "Conditional loss of Dicer disrupts cellular and tissue morphogenesis in the cortex and hippocampus." J Neurosci 28: 4322-30.

Davson, H. (1980). Physiology of the eye. Edinburgh, Churchill Livingstone.

Delori, F. C., C. K. Dorey, G. Staurenghi, O. Arend, D. G. Goger and J. J. Weiter (1995). "In vivo fluorescence of the ocular fundus exhibits retinal pigment epithelium lipofuscin characteristics." Invest Ophthalmol Vis Sci 36: 718-29.

Denli, A. M., B. B. Tops, R. H. Plasterk, R. F. Ketting and G. J. Hannon (2004). "Processing of primary microRNAs by the Microprocessor complex." Nature 432: 231-5.

Deo, M., J. Y. Yu, K. H. Chung, M. Tippens and D. L. Turner (2006). "Detection of mammalian microRNA expression by in situ hybridization with RNA oligonucleotides." Dev Dyn 235: 2538-48.

Deretic, D., L. A. Huber, N. Ransom, M. Mancini, K. Simons and D. S. Papermaster (1995). "rab8 in retinal photoreceptors may participate in rhodopsin transport and in rod outer segment disk morphogenesis." J Cell Sci 108 (Pt 1): 215-24.

Deretic, D., S. Schmerl, P. A. Hargrave, A. Arendt and J. H. McDowell (1998). "Regulation of sorting and post-Golgi trafficking of rhodopsin by its C-terminal sequence QVS(A)PA." Proc Natl Acad Sci U S A 95: 10620-5.

Deretic, D., A. H. Williams, N. Ransom, V. Morel, P. A. Hargrave and A. Arendt (2005). "Rhodopsin C terminus, the site of mutations causing retinal disease, regulates trafficking by binding to ADP-ribosylation factor 4 (ARF4)." Proc Natl Acad Sci U S A 102: 3301-6.

Dezawa, M., M. Takano, H. Negishi, X. Mo, T. Oshitari and H. Sawada (2002). "Gene transfer into retinal ganglion cells by in vivo electroporation: a new approach." Micron 33: 1-6.

Didiano, D. and O. Hobert (2008). "Molecular architecture of a miRNA-regulated 3' UTR." RNA 14: 1297-317.

Doench, J. G. and P. A. Sharp (2004). "Specificity of microRNA target selection in translational repression." Genes Dev 18: 504-11.

Doi, N., S. Zenno, R. Ueda, H. Ohki-Hamazaki, K. Ui-Tei and K. Saigo (2003). "Short-interfering-RNA-mediated gene silencing in mammalian cells requires Dicer and eIF2C translation initiation factors." Curr Biol 13: 41-6.

Doonan, F., M. Donovan and T. G. Cotter (2005). "Activation of multiple pathways during photoreceptor apoptosis in the rd mouse." Invest Ophthalmol Vis Sci 46: 3530-8.

Dostie, J., Z. Mourelatos, M. Yang, A. Sharma and G. Dreyfuss (2003). "Numerous microRNPs in neuronal cells containing novel microRNAs." Rna 9: 180-6.

Dryja, T. P., J. T. Finn, Y. W. Peng, T. L. McGee, E. L. Berson and K. W. Yau (1995). "Mutations in the gene encoding the alpha subunit of the rod cGMP-gated channel in autosomal recessive retinitis pigmentosa." Proc Natl Acad Sci U S A 92: 10177-81.

Dryja, T. P., T. L. McGee, L. B. Hahn, G. S. Cowley, J. E. Olsson, E. Reichel, M. A. Sandberg and E. L. Berson (1990). "Mutations within the rhodopsin gene in patients with autosomal dominant retinitis pigmentosa." N Engl J Med 323: 1302-7.

Du, G., J. Yonekubo, Y. Zeng, M. Osisami and M. A. Frohman (2006). "Design of expression vectors for RNA interference based on miRNAs and RNA splicing." Febs J 273: 5421-7.

Duan, R., C. Pak and P. Jin (2007). "Single nucleotide polymorphism associated with mature miR-125a alters the processing of pri-miRNA." Hum Mol Genet 16: 1124-31.

Durinck, S., Y. Moreau, A. Kasprzyk, S. Davis, B. De Moor, A. Brazma and W. Huber (2005). "BioMart and Bioconductor: a powerful link between biological databases and microarray data analysis." Bioinformatics 21: 3439-40.

Ebert, M. S., J. R. Neilson and P. A. Sharp (2007). "MicroRNA sponges: competitive inhibitors of small RNAs in mammalian cells." Nat Methods 4: 721-6.

Eisen, M. B., P. T. Spellman, P. O. Brown and D. Botstein (1998). "Cluster analysis and display of genome-wide expression patterns." Proc Natl Acad Sci U S A 95: 14863-8.

Eisenberg, I., A. Eran, I. Nishino, M. Moggio, C. Lamperti, A. A. Amato, H. G. Lidov, P. B. Kang, K. N. North, S. Mitrani-Rosenbaum, K. M. Flanigan, L. A. Neely, D. Whitney, A. H. Beggs, I. S. Kohane and L. M. Kunkel (2007). "Distinctive patterns of microRNA expression in primary muscular disorders." Proc Natl Acad Sci U S A 104: 17016-21.

Elbashir, S. M., J. Harborth, W. Lendeckel, A. Yalcin, K. Weber and T. Tuschl (2001). "Duplexes of 21-nucleotide RNAs mediate RNA interference in cultured mammalian cells." Nature 411: 494-8.

Engels, B. M. and G. Hutvagner (2006). "Principles and effects of microRNA-mediated post-transcriptional gene regulation." Oncogene 25: 6163-9.

Enright, A. J., B. John, U. Gaul, T. Tuschl, C. Sander and D. S. Marks (2003). "MicroRNA targets in Drosophila." Genome Biol 5: R1.

Epanchintsev, A., P. Jung, A. Menssen and H. Hermeking (2006). "Inducible microRNA expression by an all-in-one episomal vector system." Nucleic Acids Res 34: e119.

Esquela-Kerscher, A. and F. J. Slack (2006). "Oncomirs - microRNAs with a role in cancer." Nat Rev Cancer 6: 259-69.

Farh, K. K., A. Grimson, C. Jan, B. P. Lewis, W. K. Johnston, L. P. Lim, C. B. Burge and D. P. Bartel (2005). "The widespread impact of mammalian MicroRNAs on mRNA repression and evolution." Science 310: 1817-21.

Farjo, R. and M. I. Naash (2006). "The role of Rds in outer segment morphogenesis and human retinal disease." Ophthalmic Genet 27: 117-22.

Farrar, G. J., P. Kenna, S. A. Jordan, R. Kumar-Singh, M. M. Humphries, E. M. Sharp, D. M. Sheils and P. Humphries (1991). "A three-base-pair deletion in the peripherin-RDS gene in one form of retinitis pigmentosa." Nature 354: 478-80.

Farrar, G. J., P. Kenna, S. A. Jordan, R. Kumar-Singh and P. Humphries (1991). "A sequence polymorphism in the human peripherin/RDS gene." Nucleic Acids Res 19: 6982.

Farrar, G. J., P. F. Kenna and P. Humphries (2002). "On the genetics of retinitis pigmentosa and on mutation-independent approaches to therapeutic intervention." Embo J 21: 857-64.

Farrar, G. J., P. McWilliam, D. G. Bradley, P. Kenna, M. Lawler, E. M. Sharp, M. M. Humphries, H. Eiberg, P. M. Conneally, J. A. Trofatter and et al. (1990). "Autosomal dominant retinitis pigmentosa: linkage to rhodopsin and evidence for genetic heterogeneity." Genomics 8: 35-40.

Fauser, S., J. Luberichs and F. Schuttauf (2002). "Genetic animal models for retinal degeneration." Surv Ophthalmol 47: 357-67.

Fazi, F. and C. Nervi (2008). "MicroRNA: basic mechanisms and transcriptional regulatory networks for cell fate determination." Cardiovasc Res 79: 553-61.

Fazi, F., A. Rosa, A. Fatica, V. Gelmetti, M. L. De Marchis, C. Nervi and I. Bozzoni (2005). "A minicircuitry comprised of microRNA-223 and transcription factors NFI-A and C/EBPalpha regulates human granulopoiesis." Cell 123: 819-31.

Feng, J., Z. Yan, A. Ferreira, K. Tomizawa, J. A. Liauw, M. Zhuo, P. B. Allen, C. C. Ouimet and P. Greengard (2000). "Spinophilin regulates the formation and function of dendritic spines." Proc Natl Acad Sci U S A 97: 9287-92.

Finger, S. (2001). Origins of Neuroscience : A History of Explorations into Brain Function.

Forstemann, K., M. D. Horwich, L. Wee, Y. Tomari and P. D. Zamore (2007). "Drosophila microRNAs are sorted into functionally distinct argonaute complexes after production by dicer-1." Cell 130: 287-97.

Fox, D. A., A. T. Poblenz and L. He (1999). "Calcium overload triggers rod photoreceptor apoptotic cell death in chemical-induced and inherited retinal degenerations." Ann N Y Acad Sci 893: 282-5.

Frederick, J. M., N. V. Krasnoperova, K. Hoffmann, J. Church-Kopish, K. Ruther, K. Howes, J. Lem and W. Baehr (2001). "Mutant rhodopsin transgene expression on a null background." Invest Ophthalmol Vis Sci 42: 826-33.

Fu, Y. and K. W. Yau (2007). "Phototransduction in mouse rods and cones." Pflugers Arch 454: 805-19.

Galy, A., M. J. Roux, J. A. Sahel, T. Leveillard and A. Giangrande (2005). "Rhodopsin maturation defects induce photoreceptor death by apoptosis: a fly model for RhodopsinPro23His human retinitis pigmentosa." Hum Mol Genet 14: 2547-57.

Garzon, R., F. Pichiorri, T. Palumbo, R. Iuliano, A. Cimmino, R. Aqeilan, S. Volinia, D. Bhatt, H. Alder, G. Marcucci, G. A. Calin, C. G. Liu, C. D. Bloomfield, M. Andreeff and C. M. Croce (2006). "MicroRNA fingerprints during human megakaryocytopoiesis." Proc Natl Acad Sci U S A 103: 5078-83.

Genebank ([http://www.ncbi.nlm.nih.gov/Genbank/]).

Ghobrial, I. M., T. E. Witzig and A. A. Adjei (2005). "Targeting apoptosis pathways in cancer therapy." CA Cancer J Clin 55: 178-94.

Gilad, S., E. Meiri, Y. Yogev, S. Benjamin, D. Lebanony, N. Yerushalmi, H. Benjamin, M. Kushnir, H. Cholakh, N. Melamed, Z. Bentwich, M. Hod, Y. Goren and A. Chajut (2008). "Serum microRNAs are promising novel biomarkers." PLoS ONE 3: e3148.

Giraldez, A. J., R. M. Cinalli, M. E. Glasner, A. J. Enright, J. M. Thomson, S. Baskerville, S. M. Hammond, D. P. Bartel and A. F. Schier (2005). "MicroRNAs regulate brain morphogenesis in zebrafish." Science 308: 833-8.

Girard, A., R. Sachidanandam, G. J. Hannon and M. A. Carmell (2006). "A germline-specific class of small RNAs binds mammalian Piwi proteins." Nature 442: 199-202.

Gregory, R. I., K. P. Yan, G. Amuthan, T. Chendrimada, B. Doratotaj, N. Cooch and R. Shiekhattar (2004). "The Microprocessor complex mediates the genesis of microRNAs." Nature 432: 235-40.

Griffiths-Jones, S. (2004). "The microRNA Registry." Nucleic Acids Res 32: D109-11.

Griffiths-Jones, S., R. J. Grocock, S. van Dongen, A. Bateman and A. J. Enright (2006). "miRBase: microRNA sequences, targets and gene nomenclature." Nucleic Acids Res 34: D140-4.

Grimm, C., A. Wenzel, M. Groszer, H. Mayser, M. Seeliger, M. Samardzija, C. Bauer, M. Gassmann and C. E. Reme (2002). "HIF-1-induced erythropoietin in the hypoxic retina protects against light-induced retinal degeneration." Nat Med 8: 718-24.

Grimm, D., K. L. Streetz, C. L. Jopling, T. A. Storm, K. Pandey, C. R. Davis, P. Marion, F. Salazar and M. A. Kay (2006). "Fatality in mice due to oversaturation of cellular microRNA/short hairpin RNA pathways." Nature 441: 537-41.

Grimson, A., K. K. Farh, W. K. Johnston, P. Garrett-Engele, L. P. Lim and D. P. Bartel (2007). "MicroRNA targeting specificity in mammals: determinants beyond seed pairing." Mol Cell 27: 91-105.

Grishok, A., A. E. Pasquinelli, D. Conte, N. Li, S. Parrish, I. Ha, D. L. Baillie, A. Fire, G. Ruvkun and C. C. Mello (2001). "Genes and mechanisms related to RNA interference regulate expression of the small temporal RNAs that control C. elegans developmental timing." Cell 106: 23-34.

Grun, D., Y. L. Wang, D. Langenberger, K. C. Gunsalus and N. Rajewsky (2005). "microRNA target predictions across seven Drosophila species and comparison to mammalian targets." PLoS Comput Biol 1: e13.

Hammell, M., D. Long, L. Zhang, A. Lee, C. S. Carmack, M. Han, Y. Ding and V. Ambros (2008). "mirWIP: microRNA target prediction based on microRNA-containing ribonucleoprotein-enriched transcripts." Nat Methods.

Hammond, S. M. (2007). "MicroRNAs as tumor suppressors." Nat Genet 39: 582-3.

Hammond, S. M., S. Boettcher, A. A. Caudy, R. Kobayashi and G. J. Hannon (2001). "Argonaute2, a link between genetic and biochemical analyses of RNAi." Science 293: 1146-50.

Han, J., Y. Lee, K. H. Yeom, J. W. Nam, I. Heo, J. K. Rhee, S. Y. Sohn, Y. Cho, B. T. Zhang and V. N. Kim (2006). "Molecular basis for the recognition of primary microRNAs by the Drosha-DGCR8 complex." Cell 125: 887-901.

Hanahan, D. and R. A. Weinberg (2000). "The hallmarks of cancer." Cell 100: 57-70.

Harfe, B. D. (2005). "MicroRNAs in vertebrate development." Curr Opin Genet Dev 15: 410-5.

Hart, A. W., L. McKie, J. E. Morgan, P. Gautier, K. West, I. J. Jackson and S. H. Cross (2005). "Genotype-phenotype correlation of mouse pde6b mutations." Invest Ophthalmol Vis Sci 46: 3443-50.

Hartong, D. T., E. L. Berson and T. P. Dryja (2006). "Retinitis pigmentosa." Lancet 368: 1795-809.

Hauck, S. M., P. A. Ekstrom, P. Ahuja-Jensen, S. Suppmann, F. Paquet-Durand, T. van Veen and M. Ueffing (2006). "Differential modification of phosducin protein in degenerating rd1 retina is associated with constitutively active Ca2+/calmodulin kinase II in rod outer segments." Mol Cell Proteomics 5: 324-36.

Hauswirth, W., T. S. Aleman, S. Kaushal, A. V. Cideciyan, S. B. Schwartz, L. Wang, T. Conlon, S. L. Boye, T. R. Flotte, B. Byrne and S. G. Jacobson (2008). "Phase I Trial of Leber Congenital Amaurosis due to RPE65 Mutations by Ocular Subretinal Injection of Adeno-Associated Virus Gene Vector: Short-Term Results." Hum Gene Ther.

He, H., K. Jazdzewski, W. Li, S. Liyanarachchi, R. Nagy, S. Volinia, G. A. Calin, C. G. Liu, K. Franssila, S. Suster, R. T. Kloos, C. M. Croce and A. de la Chapelle (2005). "The role of microRNA genes in papillary thyroid carcinoma." Proc Natl Acad Sci U S A 102: 19075-80.

He, L., A. T. Poblenz, C. J. Medrano and D. A. Fox (2000). "Lead and calcium produce rod photoreceptor cell apoptosis by opening the mitochondrial permeability transition pore." J Biol Chem 275: 12175-84.

He, L., J. M. Thomson, M. T. Hemann, E. Hernando-Monge, D. Mu, S. Goodson, S. Powers, C. Cordon-Cardo, S. W. Lowe, G. J. Hannon and S. M. Hammond (2005). "A microRNA polycistron as a potential human oncogene." Nature 435: 828-33.

Hebert, S. S. and B. De Strooper (2007). "Molecular biology. miRNAs in neurodegeneration." Science 317: 1179-80.

Hebert, S. S., K. Horre, L. Nicolai, A. S. Papadopoulou, W. Mandemakers, A. N. Silahtaroglu, S. Kauppinen, A. Delacourte and B. De Strooper (2008). "Loss of

microRNA cluster miR-29a/b-1 in sporadic Alzheimer's disease correlates with increased BACE1/beta-secretase expression." Proc Natl Acad Sci U S A 105: 6415-20.

Heckenlively, J. R. (1988). Retinitis pigmentosa.

Hennig, A. K., G. H. Peng and S. Chen (2008). "Regulation of photoreceptor gene expression by Crx-associated transcription factor network." Brain Res 1192: 114-33.

Hobson, A. H., M. Donovan, M. M. Humphries, G. Tuohy, N. McNally, R. Carmody, T. Cotter, G. J. Farrar, P. F. Kenna and P. Humphries (2000). "Apoptotic photoreceptor death in the rhodopsin knockout mouse in the presence and absence of c-fos." Exp Eye Res 71: 247-54.

Houbaviy, H. B., L. Dennis, R. Jaenisch and P. A. Sharp (2005). "Characterization of a highly variable eutherian microRNA gene." RNA 11: 1245-57.

Huang, K. M., T. Dentchev and D. Stambolian (2008). "MiRNA expression in the eye." Mamm Genome.

Huang, S. H., S. J. Pittler, X. Huang, L. Oliveira, E. L. Berson and T. P. Dryja (1995). "Autosomal recessive retinitis pigmentosa caused by mutations in the alpha subunit of rod cGMP phosphodiesterase." Nat Genet 11: 468-71.

Huber, W., A. von Heydebreck, H. Sultmann, A. Poustka and M. Vingron (2002). "Variance stabilization applied to microarray data calibration and to the quantification of differential expression." Bioinformatics 18 Suppl 1: S96-104.

Humphries, M. M., D. Rancourt, G. J. Farrar, P. Kenna, M. Hazel, R. A. Bush, P. A. Sieving, D. M. Sheils, N. McNally, P. Creighton, A. Erven, A. Boros, K. Gulya, M. R. Capecchi and P. Humphries (1997). "Retinopathy induced in mice by targeted disruption of the rhodopsin gene." Nat Genet 15: 216-9.

Hutvagner, G. and P. D. Zamore (2002). "A microRNA in a multiple-turnover RNAi enzyme complex." Science 297: 2056-60.

Hwang, H. W. and J. T. Mendell (2006). "MicroRNAs in cell proliferation, cell death, and tumorigenesis." Br J Cancer 94: 776-80.

Illing, M. E., R. S. Rajan, N. F. Bence and R. R. Kopito (2002). "A rhodopsin mutant linked to autosomal dominant retinitis pigmentosa is prone to aggregate and interacts with the ubiquitin proteasome system." J Biol Chem 277: 34150-60.

Iwai, N. and H. Naraba (2005). "Polymorphisms in human pre-miRNAs." Biochem Biophys Res Commun 331: 1439-44.

Jacobson, M. D., M. Weil and M. C. Raff (1997). "Programmed cell death in animal development." Cell 88: 347-54.

Jiang, J., E. J. Lee, Y. Gusev and T. D. Schmittgen (2005). "Real-time expression profiling of microRNA precursors in human cancer cell lines." Nucleic Acids Res 33: 5394-403.

Jimeno, D., C. Lillo, E. A. Roberts, L. S. Goldstein and D. S. Williams (2006). "Kinesin-2 and photoreceptor cell death: requirement of motor subunits." Exp Eye Res 82: 351-3.

Jin, P., R. S. Alisch and S. T. Warren (2004). "RNA and microRNAs in fragile X mental retardation." Nat Cell Biol 6: 1048-53.

John, B., A. J. Enright, A. Aravin, T. Tuschl, C. Sander and D. S. Marks (2004). "Human MicroRNA targets." PLoS Biol 2: e363.

Johnson, C. D., A. Esquela-Kerscher, G. Stefani, M. Byrom, K. Kelnar, D. Ovcharenko, M. Wilson, X. Wang, J. Shelton, J. Shingara, L. Chin, D. Brown and F. J. Slack (2007). "The let-7 microRNA represses cell proliferation pathways in human cells." Cancer Res 67: 7713-22.

Jones, B. W., C. B. Watt, J. M. Frederick, W. Baehr, C. K. Chen, E. M. Levine, A. H. Milam, M. M. Lavail and R. E. Marc (2003). "Retinal remodeling triggered by photoreceptor degenerations." J Comp Neurol 464: 1-16.

Jovanovic, M. and M. O. Hengartner (2006). "miRNAs and apoptosis: RNAs to die for." Oncogene 25: 6176-87.

Junk, A. K., A. Mammis, S. I. Savitz, M. Singh, S. Roth, S. Malhotra, P. S. Rosenbaum, A. Cerami, M. Brines and D. M. Rosenbaum (2002). "Erythropoietin administration protects retinal neurons from acute ischemia-reperfusion injury." Proc Natl Acad Sci U S A 99: 10659-64.

Kachi, S., Y. Oshima, N. Esumi, M. Kachi, B. Rogers, D. J. Zack and P. A. Campochiaro (2005). "Nonviral ocular gene transfer." Gene Ther 12: 843-51.

Kalloniatis, M. and E. L. Fletcher (2004). "Retinitis pigmentosa: understanding the clinical presentation, mechanisms and treatment options." Clin Exp Optom 87: 65-80.

Kanno, R., H. Janakiraman and M. Kanno (2008). "Epigenetic regulator polycomb group protein complexes control cell fate and cancer." Cancer Sci 99: 1077-84.

Karali, M., I. Peluso, V. Marigo and S. Banfi (2007). "Identification and characterization of microRNAs expressed in the mouse eye." Invest Ophthalmol Vis Sci 48: 509-15.

Keeler, C. E. (1924). "The Inheritance of a Retinal Abnormality in White Mice." Proc Natl Acad Sci U S A 10: 329-33.

Kennan, A., A. Aherne and P. Humphries (2005). "Light in retinitis pigmentosa." Trends Genet 21: 103-10.

Kennan, A., A. Aherne, A. Palfi, M. Humphries, A. McKee, A. Stitt, D. A. Simpson, K. Demtroder, T. Orntoft, C. Ayuso, P. F. Kenna, G. J. Farrar and P. Humphries (2002). "Identification of an IMPDH1 mutation in autosomal dominant retinitis pigmentosa (RP10) revealed following comparative microarray analysis of transcripts derived from retinas of wild-type and Rho(-/-) mice." Hum Mol Genet 11: 547-57.

Kertesz, M., N. Iovino, U. Unnerstall, U. Gaul and E. Segal (2007). "The role of site accessibility in microRNA target recognition." Nat Genet 39: 1278-84.

Ketting, R. F., S. E. Fischer, E. Bernstein, T. Sijen, G. J. Hannon and R. H. Plasterk (2001). "Dicer functions in RNA interference and in synthesis of small RNA involved in developmental timing in C. elegans." Genes Dev 15: 2654-9.

Khvorova, A., A. Reynolds and S. D. Jayasena (2003). "Functional siRNAs and miRNAs exhibit strand bias." Cell 115: 209-16.

Kim, J., K. Inoue, J. Ishii, W. B. Vanti, S. V. Voronov, E. Murchison, G. Hannon and A. Abeliovich (2007). "A MicroRNA feedback circuit in midbrain dopamine neurons." Science 317: 1220-4.

Kim, J., A. Krichevsky, Y. Grad, G. D. Hayes, K. S. Kosik, G. M. Church and G. Ruvkun (2004). "Identification of many microRNAs that copurify with polyribosomes in mammalian neurons." Proc Natl Acad Sci U S A 101: 360-5.

Kim, V. N. (2005). "MicroRNA biogenesis: coordinated cropping and dicing." Nat Rev Mol Cell Biol 6: 376-85.

Kim, V. N. and J. W. Nam (2006). "Genomics of microRNA." Trends Genet 22: 165-73.

Kim, Y. K. and V. N. Kim (2007). "Processing of intronic microRNAs." Embo J 26: 775-83.

Kiriakidou, M., G. S. Tan, S. Lamprinaki, M. De Planell-Saguer, P. T. Nelson and Z. Mourelatos (2007). "An mRNA m7G cap binding-like motif within human Ago2 represses translation." Cell 129: 1141-51.

Kirino, Y. and Z. Mourelatos (2008). "Site-specific crosslinking of human microRNPs to RNA targets." Rna 14: 2254-9.

Kloosterman, W. P., F. A. Steiner, E. Berezikov, E. de Bruijn, J. van de Belt, M. Verheul, E. Cuppen and R. H. Plasterk (2006). "Cloning and expression of new microRNAs from zebrafish." Nucleic Acids Res 34: 2558-69.

Kloosterman, W. P., E. Wienholds, E. de Bruijn, S. Kauppinen and R. H. Plasterk (2006). "In situ detection of miRNAs in animal embryos using LNA-modified oligonucleotide probes." Nat Methods 3: 27-9.

Komeima, K., B. S. Rogers and P. A. Campochiaro (2007). "Antioxidants slow photoreceptor cell death in mouse models of retinitis pigmentosa." J Cell Physiol 213: 809-15.

Komeima, K., B. S. Rogers, L. Lu and P. A. Campochiaro (2006). "Antioxidants reduce cone cell death in a model of retinitis pigmentosa." Proc Natl Acad Sci U S A 103: 11300-5.

Kosik, K. S. (2006). "The neuronal microRNA system." Nat Rev Neurosci 7: 911-20.

Kosik, K. S. and A. M. Krichevsky (2005). "The Elegance of the MicroRNAs: A Neuronal Perspective." Neuron 47: 779-82.

Kozaki, K., I. Imoto, S. Mogi, K. Omura and J. Inazawa (2008). "Exploration of tumor-suppressive microRNAs silenced by DNA hypermethylation in oral cancer." Cancer Res 68: 2094-105.

Krek, A., D. Grun, M. N. Poy, R. Wolf, L. Rosenberg, E. J. Epstein, P. MacMenamin, I. da Piedade, K. C. Gunsalus, M. Stoffel and N. Rajewsky (2005). "Combinatorial microRNA target predictions." Nat Genet 37: 495-500.

Krichevsky, A. M., K. S. King, C. P. Donahue, K. Khrapko and K. S. Kosik (2003). "A microRNA array reveals extensive regulation of microRNAs during brain development." Rna 9: 1274-81.

Krichevsky, A. M., K. C. Sonntag, O. Isacson and K. S. Kosik (2006). "Specific microRNAs modulate embryonic stem cell-derived neurogenesis." Stem Cells 24: 857-64.

Kuhn, D. E., M. M. Martin, D. S. Feldman, A. V. Terry, Jr., G. J. Nuovo and T. S. Elton (2008). "Experimental validation of miRNA targets." Methods 44: 47-54.

Kulshreshtha, R., M. Ferracin, S. E. Wojcik, R. Garzon, H. Alder, F. J. Agosto-Perez, R. Davuluri, C. G. Liu, C. M. Croce, M. Negrini, G. A. Calin and M. Ivan (2007). "A microRNA signature of hypoxia." Mol Cell Biol 27: 1859-67.

Lagos-Quintana, M., R. Rauhut, W. Lendeckel and T. Tuschl (2001). "Identification of novel genes coding for small expressed RNAs." Science 294: 853-8.

Lagos-Quintana, M., R. Rauhut, J. Meyer, A. Borkhardt and T. Tuschl (2003). "New microRNAs from mouse and human." Rna 9: 175-9.

Lagos-Quintana, M., R. Rauhut, A. Yalcin, J. Meyer, W. Lendeckel and T. Tuschl (2002). "Identification of tissue-specific microRNAs from mouse." Curr Biol 12: 735-9.

Lai, E. C., P. Tomancak, R. W. Williams and G. M. Rubin (2003). "Computational identification of Drosophila microRNA genes." Genome Biol 4: R42.

Landgraf, P., M. Rusu, R. Sheridan, A. Sewer, N. Iovino, A. Aravin, S. Pfeffer, A. Rice, A. O. Kamphorst, M. Landthaler, C. Lin, N. D. Socci, L. Hermida, V. Fulci, S. Chiaretti, R. Foa, J. Schliwka, U. Fuchs, A. Novosel, R. U. Muller, B. Schermer, U. Bissels, J. Inman, Q. Phan, M. Chien, D. B. Weir, R. Choksi, G. De Vita, D. Frezzetti, H. I. Trompeter, V. Hornung, G. Teng, G. Hartmann, M. Palkovits, R. Di Lauro, P. Wernet, G. Macino, C. E. Rogler, J. W. Nagle, J. Ju, F. N. Papavasiliou, T. Benzing, P. Lichter, W. Tam, M. J. Brownstein, A. Bosio, A. Borkhardt, J. J. Russo, C. Sander, M. Zavolan and T. Tuschl (2007). "A mammalian microRNA expression atlas based on small RNA library sequencing." Cell 129: 1401-14.

Landgraf, P., M. Rusu, R. Sheridan, A. Sewer, N. LIovino, A. Aravin, S. Pfeffer, A. Rice, A. O. Kamphorst, M. Landthaler, C. Lin, N. D. Socci, L. Herminda, V. Fulci, S.

Chiaretti, R. Foa, J. Schliwka, U. Fuchs, A. Novosel, R. U. Muller, B. Schermer, U. Bilssels, J. Inman, Q. Phan, M. Chien, D. B. Weir, R. Choksi, G. De Vita, D. Frezzetti, H. I. Trompeter, V. Hornung, G. Teng, G. Hartman, M. Palkovits, R. Di Lauro, P. Wernet, G. Macino, C. E. Rogler, J. W. Nagle, J. Ju, F. N. Papavasiliou, T. Benzing, P. Lichter, W. Tam, M. J. Brownstein, A. Bosio, A. Borkhardt, J. J. Russo, C. Sander, M. Zavolan and T. Tuschl (2007). "A Mammalian microRNA Expression Atlas Based on Small RNA Library Sequencing." Cell 129: 1401-1414.

Lau, N. C., L. P. Lim, E. G. Weinstein and D. P. Bartel (2001). "An abundant class of tiny RNAs with probable regulatory roles in Caenorhabditis elegans." Science 294: 858-62.

Lau, N. C., A. G. Seto, J. Kim, S. Kuramochi-Miyagawa, T. Nakano, D. P. Bartel and R. E. Kingston (2006). "Characterization of the piRNA complex from rat testes." Science 313: 363-7.

LaVail, M. M. (1973). "Kinetics of rod outer segment renewal in the developing mouse retina." J Cell Biol 58: 650-61.

Le Meur, G., K. Stieger, A. J. Smith, M. Weber, J. Y. Deschamps, D. Nivard, A. Mendes-Madeira, N. Provost, Y. Pereon, Y. Cherel, R. R. Ali, C. Hamel, P. Moullier and F. Rolling (2007). "Restoration of vision in RPE65-deficient Briard dogs using an AAV serotype 4 vector that specifically targets the retinal pigmented epithelium." Gene Ther 14: 292-303.

Leaman, D., P. Y. Chen, J. Fak, A. Yalcin, M. Pearce, U. Unnerstall, D. S. Marks, C. Sander, T. Tuschl and U. Gaul (2005). "Antisense-mediated depletion reveals essential and specific functions of microRNAs in Drosophila development." Cell 121: 1097-108.

Lee, E. J., M. Baek, Y. Gusev, D. J. Brackett, G. J. Nuovo and T. D. Schmittgen (2008). "Systematic evaluation of microRNA processing patterns in tissues, cell lines, and tumors." Rna 14: 35-42.

Lee, R. C. and V. Ambros (2001). "An extensive class of small RNAs in Caenorhabditis elegans." Science 294: 862-4.

Lee, R. C., R. L. Feinbaum and V. Ambros (1993). "The C. elegans heterochronic gene lin-4 encodes small RNAs with antisense complementarity to lin-14." Cell 75: 843-54.

Lee, Y., K. Jeon, J. T. Lee, S. Kim and V. N. Kim (2002). "MicroRNA maturation: stepwise processing and subcellular localization." Embo J 21: 4663-70.

Lee, Y., M. Kim, J. Han, K. H. Yeom, S. Lee, S. H. Baek and V. N. Kim (2004). "MicroRNA genes are transcribed by RNA polymerase II." Embo J 23: 4051-60.

Lee, Y., R. C. Samaco, J. R. Gatchel, C. Thaller, H. T. Orr and H. Y. Zoghbi (2008). "miR-19, miR-101 and miR-130 co-regulate ATXN1 levels to potentially modulate SCA1 pathogenesis." Nat Neurosci 11: 1137-9.

Lee, Y. S., K. Nakahara, J. W. Pham, K. Kim, Z. He, E. J. Sontheimer and R. W. Carthew (2004). "Distinct roles for Drosophila Dicer-1 and Dicer-2 in the siRNA/miRNA silencing pathways." Cell 117: 69-81.

Lehmann, U., B. Hasemeier, M. Christgen, M. Muller, D. Romermann, F. Langer and H. Kreipe (2008). "Epigenetic inactivation of microRNA gene hsa-mir-9-1 in human breast cancer." J Pathol 214: 17-24.

Leucht, C., C. Stigloher, A. Wizenmann, R. Klafke, A. Folchert and L. Bally-Cuif (2008). "MicroRNA-9 directs late organizer activity of the midbrain-hindbrain boundary." Nat Neurosci 11: 641-8.

Lewis, B. P., C. B. Burge and D. P. Bartel (2005). "Conserved seed pairing, often flanked by adenosines, indicates that thousands of human genes are microRNA targets." Cell 120: 15-20.

Lewis, B. P., I. H. Shih, M. W. Jones-Rhoades, D. P. Bartel and C. B. Burge (2003). "Prediction of mammalian microRNA targets." Cell 115: 787-98.

Li, T., W. K. Snyder, J. E. Olsson and T. P. Dryja (1996). "Transgenic mice carrying the dominant rhodopsin mutation P347S: evidence for defective vectorial transport of rhodopsin to the outer segments." Proc Natl Acad Sci U S A 93: 14176-81.

Li, X. and R. W. Carthew (2005). "A microRNA mediates EGF receptor signaling and promotes photoreceptor differentiation in the Drosophila eye." Cell 123: 1267-77.

Li, Y., L. Lin and P. Jin (2008). "The microRNA pathway and fragile X mental retardation protein." Biochim Biophys Acta.

Li, Y., F. Wang, J. A. Lee and F. B. Gao (2006). "MicroRNA-9a ensures the precise specification of sensory organ precursors in Drosophila." Genes Dev 20: 2793-805.

Liang, Y., D. Fotiadis, T. Maeda, A. Maeda, A. Modzelewska, S. Filipek, D. A. Saperstein, A. Engel and K. Palczewski (2004). "Rhodopsin signaling and organization in heterozygote rhodopsin knockout mice." J Biol Chem 279: 48189-96.

Lim, L. P., N. C. Lau, P. Garrett-Engele, A. Grimson, J. M. Schelter, J. Castle, D. P. Bartel, P. S. Linsley and J. M. Johnson (2005). "Microarray analysis shows that some microRNAs downregulate large numbers of target mRNAs." Nature 433: 769-73.

Lin, S. M., P. Du, W. Huber and W. A. Kibbe (2008). "Model-based variance-stabilizing transformation for Illumina microarray data." Nucleic Acids Res 36: e11.

Lingel, A., B. Simon, E. Izaurralde and M. Sattler (2004). "Nucleic acid 3'-end recognition by the Argonaute2 PAZ domain." Nat Struct Mol Biol 11: 576-7.

Liu, C. G., G. A. Calin, B. Meloon, N. Gamliel, C. Sevignani, M. Ferracin, C. D. Dumitru, M. Shimizu, S. Zupo, M. Dono, H. Alder, F. Bullrich, M. Negrini and C. M. Croce (2004). "An oligonucleotide microchip for genome-wide microRNA profiling in human and mouse tissues." Proc Natl Acad Sci U S A 101: 9740-4.

Liu, J., F. V. Rivas, J. Wohlschlegel, J. R. Yates, 3rd, R. Parker and G. J. Hannon (2005). "A role for the P-body component GW182 in microRNA function." Nat Cell Biol 7: 1261-6.

Liu, J., M. A. Valencia-Sanchez, G. J. Hannon and R. Parker (2005). "MicroRNA-dependent localization of targeted mRNAs to mammalian P-bodies." Nat Cell Biol 7: 719-23.

Livak, K. J. and T. D. Schmittgen (2001). "Analysis of relative gene expression data using real-time quantitative PCR and the 2(-Delta Delta C(T)) Method." Methods 25: 402-8.

Loscher, C., K. Hokamp, P. Humphries, G. J. Farrar and A. Palfi (2008). "Common microRNA signature in mouse models of retinal degeneration." Exp Eye Res.

Loscher, C. J., K. Hokamp, P. F. Kenna, A. C. Ivens, P. Humphries, A. Palfi and G. J. Farrar (2007). "Altered retinal microRNA expression profile in a mouse model of retinitis pigmentosa." Genome Biol 8: R248.

Lujambio, A., G. A. Calin, A. Villanueva, S. Ropero, M. Sanchez-Cespedes, D. Blanco, L. M. Montuenga, S. Rossi, M. S. Nicoloso, W. J. Faller, W. M. Gallagher, S. A. Eccles, C. M. Croce and M. Esteller (2008). "A microRNA DNA methylation signature for human cancer metastasis." Proc Natl Acad Sci U S A 105: 13556-61.

Lund, E., S. Guttinger, A. Calado, J. E. Dahlberg and U. Kutay (2004). "Nuclear export of microRNA precursors." Science 303: 95-8.

Luo, D. G., T. Xue and K. W. Yau (2008). "How vision begins: an odyssey." Proc Natl Acad Sci U S A 105: 9855-62.

MacDonald, I. M., Y. Sauve and P. A. Sieving (2007). "Preventing blindness in retinal disease: ciliary neurotrophic factor intraocular implants." Can J Ophthalmol 42: 399-402.

Machida, S., M. Kondo, J. A. Jamison, N. W. Khan, L. T. Kononen, T. Sugawara, R. A. Bush and P. A. Sieving (2000). "P23H rhodopsin transgenic rat: correlation of retinal function with histopathology." Invest Ophthalmol Vis Sci 41: 3200-9.

Macrae, I. J., K. Zhou, F. Li, A. Repic, A. N. Brooks, W. Z. Cande, P. D. Adams and J. A. Doudna (2006). "Structural basis for double-stranded RNA processing by Dicer." Science 311: 195-8.

Maglott, D., J. Ostell, K. D. Pruitt and T. Tatusova (2005). "Entrez Gene: gene-centered information at NCBI." Nucleic Acids Res 33: D54-8.

Maguire, A. M., F. Simonelli, E. A. Pierce, E. N. Pugh, Jr., F. Mingozzi, J. Bennicelli, S. Banfi, K. A. Marshall, F. Testa, E. M. Surace, S. Rossi, A. Lyubarsky, V. R. Arruda, B. Konkle, E. Stone, J. Sun, J. Jacobs, L. Dell'Osso, R. Hertle, J. X. Ma, T. M. Redmond, X. Zhu, B. Hauck, O. Zelenaia, K. S. Shindler, M. G. Maguire, J. F. Wright, N. J. Volpe, J. W. McDonnell, A. Auricchio, K. A. High and J. Bennett (2008). "Safety and efficacy of gene transfer for Leber's congenital amaurosis." N Engl J Med 358: 2240-8.

Makarev, E., J. R. Spence, K. Del Rio-Tsonis and P. A. Tsonis (2006). "Identification of microRNAs and other small RNAs from the adult newt eye." Mol Vis 12: 1386-91.

Maniataki, E. and Z. Mourelatos (2005). "Human mitochondrial tRNAMet is exported to the cytoplasm and associates with the Argonaute 2 protein." Rna 11: 849-52.

Marc, R. E., B. W. Jones, C. B. Watt and E. Strettoi (2003). "Neural remodeling in retinal degeneration." Prog Retin Eye Res 22: 607-55.

Marigo, V. (2007). "Programmed cell death in retinal degeneration: targeting apoptosis in photoreceptors as potential therapy for retinal degeneration." Cell Cycle 6: 652-5.

Markham, N. R. and M. Zuker (2005). "DINAMelt web server for nucleic acid melting prediction." Nucleic Acids Res 33: W577-81.

Mathonnet, G., M. R. Fabian, Y. V. Svitkin, A. Parsyan, L. Huck, T. Murata, S. Biffo, W. C. Merrick, E. Darzynkiewicz, R. S. Pillai, W. Filipowicz, T. F. Duchaine and N. Sonenberg (2007). "MicroRNA inhibition of translation initiation in vitro by targeting the cap-binding complex eIF4F." Science 317: 1764-7.

Matsuda, T. and C. L. Cepko (2004). "Electroporation and RNA interference in the rodent retina in vivo and in vitro." Proc Natl Acad Sci U S A 101: 16-22.

Mattick, J. S. and I. V. Makunin (2005). "Small regulatory RNAs in mammals." Hum Mol Genet 14 Spec No 1: R121-32.

Mattick, J. S. and I. V. Makunin (2006). "Non-coding RNA." Hum Mol Genet 15 Spec No 1: R17-29.

Maziere, P. and A. J. Enright (2007). "Prediction of microRNA targets." Drug Discov Today 12: 452-8.

McCabe, K. L., C. McGuire and T. A. Reh (2006). "Pea3 expression is regulated by FGF signaling in developing retina." Dev Dyn 235: 327-35.

McCracken, A. A. and J. L. Brodsky (2000). "A molecular portrait of the response to unfolded proteins." Genome Biol 1: REVIEWS1013.

McKie, A. B., J. C. McHale, T. J. Keen, E. E. Tarttelin, R. Goliath, J. J. van Lith-Verhoeven, J. Greenberg, R. S. Ramesar, C. B. Hoyng, F. P. Cremers, D. A. Mackey, S. S. Bhattacharya, A. C. Bird, A. F. Markham and C. F. Inglehearn (2001). "Mutations in the pre-mRNA splicing factor gene PRPC8 in autosomal dominant retinitis pigmentosa (RP13)." Hum Mol Genet 10: 1555-62.

McLaughlin, M. E., T. L. Ehrhart, E. L. Berson and T. P. Dryja (1995). "Mutation spectrum of the gene encoding the beta subunit of rod phosphodiesterase among

patients with autosomal recessive retinitis pigmentosa." Proc Natl Acad Sci U S A 92: 3249-53.
McNally, N., P. Kenna, M. M. Humphries, A. H. Hobson, N. W. Khan, R. A. Bush, P. A. Sieving, P. Humphries and G. J. Farrar (1999). "Structural and functional rescue of murine rod photoreceptors by human rhodopsin transgene." Hum Mol Genet 8: 1309-12.
McNally, N., P. F. Kenna, D. Rancourt, T. Ahmed, A. Stitt, W. H. Colledge, D. G. Lloyd, A. Palfi, B. O'Neill, M. M. Humphries, P. Humphries and G. J. Farrar (2002). "Murine model of autosomal dominant retinitis pigmentosa generated by targeted deletion at codon 307 of the rds-peripherin gene." Hum Mol Genet 11: 1005-16.
McWilliam, P., G. J. Farrar, P. Kenna, D. G. Bradley, M. M. Humphries, E. M. Sharp, D. J. McConnell, M. Lawler, D. Sheils, C. Ryan and et al. (1989). "Autosomal dominant retinitis pigmentosa (ADRP): localization of an ADRP gene to the long arm of chromosome 3." Genomics 5: 619-22.
Megraw, M., P. Sethupathy, B. Corda and A. G. Hatzigeorgiou (2007). "miRGen: a database for the study of animal microRNA genomic organization and function." Nucleic Acids Res 35: D149-55.
Meister, G., M. Landthaler, A. Patkaniowska, Y. Dorsett, G. Teng and T. Tuschl (2004). "Human Argonaute2 mediates RNA cleavage targeted by miRNAs and siRNAs." Mol Cell 15: 185-97.
Mendell, J. T. (2008). "miRiad roles for the miR-17-92 cluster in development and disease." Cell 133: 217-22.
Mendes, H. F., J. van der Spuy, J. P. Chapple and M. E. Cheetham (2005). "Mechanisms of cell death in rhodopsin retinitis pigmentosa: implications for therapy." Trends Mol Med 11: 177-85.
MGI_Database ([http://www.informatics.jax.org/mgihome/nomen/]).
Miller, T. E., K. Ghoshal, B. Ramaswamy, S. Roy, J. Datta, C. L. Shapiro, S. Jacob and S. Majumder (2008). "MicroRNA-221/222 confers tamoxifen resistance in breast cancer by targeting p27(Kip1)." J Biol Chem.
Mineno, J., S. Okamoto, T. Ando, M. Sato, H. Chono, H. Izu, M. Takayama, K. Asada, O. Mirochnitchenko, M. Inouye and I. Kato (2006). "The expression profile of microRNAs in mouse embryos." Nucleic Acids Res 34: 1765-71.
"Sanger miR Database "[http://microrna.sanger.ac.uk/].
miRSNP ([http://compbio.utmem.edu/miRSNP/]).
Mishima, T., Y. Mizuguchi, Y. Kawahigashi, T. Takizawa and T. Takizawa (2007). "RT-PCR-based analysis of microRNA (miR-1 and -124) expression in mouse CNS." Brain Res 1131: 37-43.
Miska, E. A., E. Alvarez-Saavedra, M. Townsend, A. Yoshii, N. Sestan, P. Rakic, M. Constantine-Paton and H. R. Horvitz (2004). "Microarray analysis of microRNA expression in the developing mammalian brain." Genome Biol 5: R68.
Molday, R. S. (1998). "Photoreceptor membrane proteins, phototransduction, and retinal degenerative diseases. The Friedenwald Lecture." Invest Ophthalmol Vis Sci 39: 2491-513.
Monticelli, S., K. M. Ansel, C. Xiao, N. D. Socci, A. M. Krichevsky, T. H. Thai, N. Rajewsky, D. S. Marks, C. Sander, K. Rajewsky, A. Rao and K. S. Kosik (2005). "MicroRNA profiling of the murine hematopoietic system." Genome Biol 6: R71.
Moschos, S. A., A. E. Williams, M. M. Perry, M. A. Birrell, M. G. Belvisi and M. A. Lindsay (2007). "Expression profiling in vivo demonstrates rapid changes in lung microRNA levels following lipopolysaccharide-induced inflammation but not in the anti-inflammatory action of glucocorticoids." BMC Genomics 8: 240.

Mourelatos, Z., J. Dostie, S. Paushkin, A. Sharma, B. Charroux, L. Abel, J. Rappsilber, M. Mann and G. Dreyfuss (2002). "miRNPs: a novel class of ribonucleoproteins containing numerous microRNAs." Genes Dev 16: 720-8.

Nairz, K., C. Rottig, F. Rintelen, E. Zdobnov, M. Moser and E. Hafen (2006). "Overgrowth caused by misexpression of a microRNA with dispensable wild-type function." Dev Biol 291: 314-24.

Nam, S., B. Kim, S. Shin and S. Lee (2008). "miRGator: an integrated system for functional annotation of microRNAs." Nucleic Acids Res 36: D159-64.

Narfstrom, K. and S. E. Nilsson (1987). "Hereditary rod-cone degeneration in a strain of Abyssinian cats." Prog Clin Biol Res 247: 349-68.

Nathans, J. (1992). "Rhodopsin: structure, function, and genetics." Biochemistry 31: 4923-31.

Neely, L. A., K. M. Rieger-Christ, B. S. Neto, A. Eroshkin, J. Garver, S. Patel, N. A. Phung, S. McLaughlin, J. A. Libertino, D. Whitney and I. C. Summerhayes (2008). "A microRNA expression ratio defining the invasive phenotype in bladder tumors." Urol Oncol.

NEIBank ([http://neibank.nei.nih.gov/index.shtml]).

Nelson, P. T., A. G. Hatzigeorgiou and Z. Mourelatos (2004). "miRNP:mRNA association in polyribosomes in a human neuronal cell line." Rna 10: 387-94.

Newell, F. W. (1996). Ophthalmology : principles and concepts. St. Louis ; London, Mosby.

Nilsen, T. W. (2007). "Mechanisms of microRNA-mediated gene regulation in animal cells." Trends Genet 23: 243-9.

O'Donnell, K. A., E. A. Wentzel, K. I. Zeller, C. V. Dang and J. T. Mendell (2005). "c-Myc-regulated microRNAs modulate E2F1 expression." Nature 435: 839-43.

O'Reilly, M., A. Palfi, N. Chadderton, S. Millington-Ward, M. Ader, T. Cronin, T. Tuohy, A. Auricchio, M. Hildinger, A. Tivnan, N. McNally, M. M. Humphries, A. S. Kiang, P. Humphries, P. F. Kenna and G. J. Farrar (2007). "RNA interference-mediated suppression and replacement of human rhodopsin in vivo." Am J Hum Genet 81: 127-35.

Obernosterer, G., P. J. Leuschner, M. Alenius and J. Martinez (2006). "Post-transcriptional regulation of microRNA expression." Rna 12: 1161-7.

Obernosterer, G., J. Martinez and M. Alenius (2007). "Locked nucleic acid-based in situ detection of microRNAs in mouse tissue sections." Nat Protoc 2: 1508-14.

Okamura, K., J. W. Hagen, H. Duan, D. M. Tyler and E. C. Lai (2007). "The mirtron pathway generates microRNA-class regulatory RNAs in Drosophila." Cell 130: 89-100.

Olsen, P. H. and V. Ambros (1999). "The lin-4 regulatory RNA controls developmental timing in Caenorhabditis elegans by blocking LIN-14 protein synthesis after the initiation of translation." Dev Biol 216: 671-80.

Olsson, J. E., J. W. Gordon, B. S. Pawlyk, D. Roof, A. Hayes, R. S. Molday, S. Mukai, G. S. Cowley, E. L. Berson and T. P. Dryja (1992). "Transgenic mice with a rhodopsin mutation (Pro23His): a mouse model of autosomal dominant retinitis pigmentosa." Neuron 9: 815-30.

Organisciak, D. T., R. M. Darrow, L. Barsalou, R. K. Kutty and B. Wiggert (2003). "Susceptibility to retinal light damage in transgenic rats with rhodopsin mutations." Invest Ophthalmol Vis Sci 44: 486-92.

Ovcharenko, D., K. Kelnar, C. Johnson, N. Leng and D. Brown (2007). "Genome-scale microRNA and small interfering RNA screens identify small RNA modulators of TRAIL-induced apoptosis pathway." Cancer Res 67: 10782-8.

Pang, K. C., S. Stephen, M. E. Dinger, P. G. Engstrom, B. Lenhard and J. S. Mattick (2007). "RNAdb 2.0--an expanded database of mammalian non-coding RNAs." Nucleic Acids Res 35: D178-82.

Papagiannakopoulos, T., A. Shapiro and K. S. Kosik (2008). "MicroRNA-21 targets a network of key tumor-suppressive pathways in glioblastoma cells." Cancer Res 68: 8164-72.

Parker, R. and H. Song (2004). "The enzymes and control of eukaryotic mRNA turnover." Nat Struct Mol Biol 11: 121-7.

Pasquinelli, A. E., B. J. Reinhart, F. Slack, M. Q. Martindale, M. I. Kuroda, B. Maller, D. C. Hayward, E. E. Ball, B. Degnan, P. Muller, J. Spring, A. Srinivasan, M. Fishman, J. Finnerty, J. Corbo, M. Levine, P. Leahy, E. Davidson and G. Ruvkun (2000). "Conservation of the sequence and temporal expression of let-7 heterochronic regulatory RNA." Nature 408: 86-9.

Patrocles ([http://www.patrocles.org/Patrocles.htm]).

Penn, J. S., S. Li and M. I. Naash (2000). "Ambient hypoxia reverses retinal vascular attenuation in a transgenic mouse model of autosomal dominant retinitis pigmentosa." Invest Ophthalmol Vis Sci 41: 4007-13.

Petersen, C. P., M. E. Bordeleau, J. Pelletier and P. A. Sharp (2006). "Short RNAs repress translation after initiation in mammalian cells." Mol Cell 21: 533-42.

Petters, R. M., C. A. Alexander, K. D. Wells, E. B. Collins, J. R. Sommer, M. R. Blanton, G. Rojas, Y. Hao, W. L. Flowers, E. Banin, A. V. Cideciyan, S. G. Jacobson and F. Wong (1997). "Genetically engineered large animal model for studying cone photoreceptor survival and degeneration in retinitis pigmentosa." Nat Biotechnol 15: 965-70.

Phelan, J. K. and D. Bok (2000). "A brief review of retinitis pigmentosa and the identified retinitis pigmentosa genes." Mol Vis 6: 116-24.

Pillai, R. S. (2005). "MicroRNA function: multiple mechanisms for a tiny RNA?" Rna 11: 1753-61.

Pillai, R. S., C. G. Artus and W. Filipowicz (2004). "Tethering of human Ago proteins to mRNA mimics the miRNA-mediated repression of protein synthesis." Rna 10: 1518-25.

Pillai, R. S., S. N. Bhattacharyya and W. Filipowicz (2007). "Repression of protein synthesis by miRNAs: how many mechanisms?" Trends Cell Biol 17: 118-26.

Pittler, S. J. and W. Baehr (1991). "Identification of a nonsense mutation in the rod photoreceptor cGMP phosphodiesterase beta-subunit gene of the rd mouse." Proc Natl Acad Sci U S A 88: 8322-6.

Pittler, S. J., C. E. Keeler, R. L. Sidman and W. Baehr (1993). "PCR analysis of DNA from 70-year-old sections of rodless retina demonstrates identity with the mouse rd defect." Proc Natl Acad Sci U S A 90: 9616-9.

Ponjavic, J., C. P. Ponting and G. Lunter (2007). "Functionality or transcriptional noise? Evidence for selection within long noncoding RNAs." Genome Res 17: 556-65.

Portera-Cailliau, C., C. H. Sung, J. Nathans and R. Adler (1994). "Apoptotic photoreceptor cell death in mouse models of retinitis pigmentosa." Proc Natl Acad Sci U S A 91: 974-8.

Poy, M. N., L. Eliasson, J. Krutzfeldt, S. Kuwajima, X. Ma, P. E. Macdonald, S. Pfeffer, T. Tuschl, N. Rajewsky, P. Rorsman and M. Stoffel (2004). "A pancreatic islet-specific microRNA regulates insulin secretion." Nature 432: 226-30.

PupaSuite ([http://pupasuite.bioinfo.cipf.es/]).

Ramirez, C. V., C. Vilela, K. Berthelot and J. E. McCarthy (2002). "Modulation of eukaryotic mRNA stability via the cap-binding translation complex eIF4F." J Mol Biol 318: 951-62.

Ramkissoon, S. H., L. A. Mainwaring, Y. Ogasawara, K. Keyvanfar, J. P. McCoy, Jr., E. M. Sloand, S. Kajigaya and N. S. Young (2006). "Hematopoietic-specific microRNA expression in human cells." Leuk Res 30: 643-7.

Ravid, T. and M. Hochstrasser (2008). "Diversity of degradation signals in the ubiquitin-proteasome system." Nat Rev Mol Cell Biol 9: 679-90.

http://www.sph.uth.tmc.edu/Retnet/http://www.sph.uth.tmc.edu/Retnet/.

Reuter, J. H. and S. Sanyal (1984). "Development and degeneration of retina in rds mutant mice: the electroretinogram." Neurosci Lett 48: 231-7.

Rhoades, M. W., B. J. Reinhart, L. P. Lim, C. B. Burge, B. Bartel and D. P. Bartel (2002). "Prediction of plant microRNA targets." Cell 110: 513-20.

Robins, H., Y. Li and R. W. Padgett (2005). "Incorporating structure to predict microRNA targets." Proc Natl Acad Sci U S A 102: 4006-9.

Rodriguez, A., S. Griffiths-Jones, J. L. Ashurst and A. Bradley (2004). "Identification of mammalian microRNA host genes and transcription units." Genome Res 14: 1902-10.

Roof, D. J., M. Adamian and A. Hayes (1994). "Rhodopsin accumulation at abnormal sites in retinas of mice with a human P23H rhodopsin transgene." Invest Ophthalmol Vis Sci 35: 4049-62.

Rosenfeld, N., R. Aharonov, E. Meiri, S. Rosenwald, Y. Spector, M. Zepeniuk, H. Benjamin, N. Shabes, S. Tabak, A. Levy, D. Lebanony, Y. Goren, E. Silberschein, N. Targan, A. Ben-Ari, S. Gilad, N. Sion-Vardy, A. Tobar, M. Feinmesser, O. Kharenko, O. Nativ, D. Nass, M. Perelman, A. Yosepovich, B. Shalmon, S. Polak-Charcon, E. Fridman, A. Avniel, I. Bentwich, Z. Bentwich, D. Cohen, A. Chajut and I. Barshack (2008). "MicroRNAs accurately identify cancer tissue origin." Nat Biotechnol 26: 462-9.

Roush, S. and F. J. Slack (2008). "The let-7 family of microRNAs." Trends Cell Biol.

Rowan, S. and C. L. Cepko (2004). "Genetic analysis of the homeodomain transcription factor Chx10 in the retina using a novel multifunctional BAC transgenic mouse reporter." Dev Biol 271: 388-402.

Ruby, J. G., C. H. Jan and D. P. Bartel (2007). "Intronic microRNA precursors that bypass Drosha processing." Nature 448: 83-6.

Rutkowski, D. T. and R. J. Kaufman (2004). "A trip to the ER: coping with stress." Trends Cell Biol 14: 20-8.

Ryan, D. G., M. Oliveira-Fernandes and R. M. Lavker (2006). "MicroRNAs of the mammalian eye display distinct and overlapping tissue specificity." Mol Vis 12: 1175-84.

Saini, H. K., S. Griffiths-Jones and A. J. Enright (2007). "Genomic analysis of human microRNA transcripts." Proc Natl Acad Sci U S A 104: 17719-24.

Sambrook, J., E. F. Fritsch and T. Maniatis (1989). Molecular cloning : a laboratory manual. Cold Spring Harbor, N.Y., Cold Spring Harbor Laboratory.

Sanges, D., A. Comitato, R. Tammaro and V. Marigo (2006). "Apoptosis in retinal degeneration involves cross-talk between apoptosis-inducing factor (AIF) and caspase-12 and is blocked by calpain inhibitors." Proc Natl Acad Sci U S A 103: 17366-71.

Sanyal, S., A. De Ruiter and R. K. Hawkins (1980). "Development and degeneration of retina in rds mutant mice: light microscopy." J Comp Neurol 194: 193-207.

Sathyan, P., H. B. Golden and R. C. Miranda (2007). "Competing interactions between micro-RNAs determine neural progenitor survival and proliferation after ethanol exposure: evidence from an ex vivo model of the fetal cerebral cortical neuroepithelium." J Neurosci 27: 8546-57.

Sayers, E. W., T. Barrett, D. A. Benson, S. H. Bryant, K. Canese, V. Chetvernin, D. M. Church, M. Dicuccio, R. Edgar, S. Federhen, M. Feolo, L. Y. Geer, W. Helmberg,

Y. Kapustin, D. Landsman, D. J. Lipman, T. L. Madden, D. R. Maglott, V. Miller, I. Mizrachi, J. Ostell, K. D. Pruitt, G. D. Schuler, E. Sequeira, S. T. Sherry, M. Shumway, K. Sirotkin, A. Souvorov, G. Starchenko, T. A. Tatusova, L. Wagner, E. Yaschenko and J. Ye (2008). "Database resources of the National Center for Biotechnology Information." Nucleic Acids Res.

Schaefer, A., D. O'Carroll, C. L. Tan, D. Hillman, M. Sugimori, R. Llinas and P. Greengard (2007). "Cerebellar neurodegeneration in the absence of microRNAs." J Exp Med 204: 1553-8.

Schertzer, J. D. and G. S. Lynch (2008). "Plasmid-based gene transfer in mouse skeletal muscle by electroporation." Methods Mol Biol 433: 115-25.

Schmittgen, T. D., E. J. Lee, J. Jiang, A. Sarkar, L. Yang, T. S. Elton and C. Chen (2008). "Real-time PCR quantification of precursor and mature microRNA." Methods 44: 31-8.

Schratt, G. M., F. Tuebing, E. A. Nigh, C. G. Kane, M. E. Sabatini, M. Kiebler and M. E. Greenberg (2006). "A brain-specific microRNA regulates dendritic spine development." Nature 439: 283-9.

Schwarz, D. S., G. Hutvagner, T. Du, Z. Xu, N. Aronin and P. D. Zamore (2003). "Asymmetry in the assembly of the RNAi enzyme complex." Cell 115: 199-208.

Seigel, G. M. (1999). "The golden age of retinal cell culture." Mol Vis 5: 4.

Selbach, M., B. Schwanhausser, N. Thierfelder, Z. Fang, R. Khanin and N. Rajewsky (2008). "Widespread changes in protein synthesis induced by microRNAs." Nature 455: 58-63.

Sempere, L. F., S. Freemantle, I. Pitha-Rowe, E. Moss, E. Dmitrovsky and V. Ambros (2004). "Expression profiling of mammalian microRNAs uncovers a subset of brain-expressed microRNAs with possible roles in murine and human neuronal differentiation." Genome Biol 5: R13.

Sethupathy, P., C. Borel, M. Gagnebin, G. R. Grant, S. Deutsch, T. S. Elton, A. G. Hatzigeorgiou and S. E. Antonarakis (2007). "Human microRNA-155 on chromosome 21 differentially interacts with its polymorphic target in the AGTR1 3' untranslated region: a mechanism for functional single-nucleotide polymorphisms related to phenotypes." Am J Hum Genet 81: 405-13.

Sethupathy, P. and F. S. Collins (2008). "MicroRNA target site polymorphisms and human disease." Trends Genet 24: 489-97.

Sethupathy, P., B. Corda and A. G. Hatzigeorgiou (2006). "TarBase: A comprehensive database of experimentally supported animal microRNA targets." Rna 12: 192-7.

Sethupathy, P., M. Megraw and A. G. Hatzigeorgiou (2006). "A guide through present computational approaches for the identification of mammalian microRNA targets." Nat Methods 3: 881-6.

Shen, J., X. Yang, B. Xie, Y. Chen, M. Swaim, S. F. Hackett and P. A. Campochiaro (2008). "MicroRNAs regulate ocular neovascularization." Mol Ther 16: 1208-16.

Shetty, K. M., P. Kurada and J. E. O'Tousa (1998). "Rab6 regulation of rhodopsin transport in Drosophila." J Biol Chem 273: 20425-30.

Shibata, M., D. Kurokawa, H. Nakao, T. Ohmura and S. Aizawa (2008). "MicroRNA-9 modulates Cajal-Retzius cell differentiation by suppressing Foxg1 expression in mouse medial pallium." J Neurosci 28: 10415-21.

Shichida, Y. and T. Morizumi (2007). "Mechanism of G-protein activation by rhodopsin." Photochem Photobiol 83: 70-5.

Shingara, J., K. Keiger, J. Shelton, W. Laosinchai-Wolf, P. Powers, R. Conrad, D. Brown and E. Labourier (2005). "An optimized isolation and labeling platform for accurate microRNA expression profiling." Rna 11: 1461-70.

Smirnova, L., A. Grafe, A. Seiler, S. Schumacher, R. Nitsch and F. G. Wulczyn (2005). "Regulation of miRNA expression during neural cell specification." Eur J Neurosci 21: 1469-77.
Sonkoly, E., M. Stahle and A. Pivarcsi (2008). "MicroRNAs: novel regulators in skin inflammation." Clin Exp Dermatol 33: 312-5.
Sorrentino, A., C. G. Liu, A. Addario, C. Peschle, G. Scambia and C. Ferlini (2008). "Role of microRNAs in drug-resistant ovarian cancer cells." Gynecol Oncol.
Soto, C. and L. D. Estrada (2008). "Protein misfolding and neurodegeneration." Arch Neurol 65: 184-9.
Standart, N. and R. J. Jackson (2007). "MicroRNAs repress translation of m7Gppp-capped target mRNAs in vitro by inhibiting initiation and promoting deadenylation." Genes Dev 21: 1975-82.
Stanelle, J. and B. M. Putzer (2006). "E2F1-induced apoptosis: turning killers into therapeutics." Trends Mol Med 12: 177-85.
Stark, A., P. Kheradpour, L. Parts, J. Brennecke, E. Hodges, G. J. Hannon and M. Kellis (2007). "Systematic discovery and characterization of fly microRNAs using 12 Drosophila genomes." Genome Res 17: 1865-79.
Stark, K. L., B. Xu, A. Bagchi, W. S. Lai, H. Liu, R. Hsu, X. Wan, P. Pavlidis, A. A. Mills, M. Karayiorgou and J. A. Gogos (2008). "Altered brain microRNA biogenesis contributes to phenotypic deficits in a 22q11-deletion mouse model." Nat Genet 40: 751-60.
Stefani, G. and F. J. Slack (2008). "Small non-coding RNAs in animal development." Nat Rev Mol Cell Biol 9: 219-30.
Stegmeier, F., G. Hu, R. J. Rickles, G. J. Hannon and S. J. Elledge (2005). "A lentiviral microRNA-based system for single-copy polymerase II-regulated RNA interference in mammalian cells." Proc Natl Acad Sci U S A 102: 13212-7.
Streichert, L. C., C. D. Birnbach and T. A. Reh (1999). "A diffusible factor from normal retinal cells promotes rod photoreceptor survival in an in vitro model of retinitis pigmentosa." J Neurobiol 39: 475-90.
Suarez, Y., C. Fernandez-Hernando, J. Yu, S. A. Gerber, K. D. Harrison, J. S. Pober, M. L. Iruela-Arispe, M. Merkenschlager and W. C. Sessa (2008). "Dicer-dependent endothelial microRNAs are necessary for postnatal angiogenesis." Proc Natl Acad Sci U S A 105: 14082-7.
Sullivan, L. S., S. J. Bowne, C. R. Seaman, S. H. Blanton, R. A. Lewis, J. R. Heckenlively, D. G. Birch, D. Hughbanks-Wheaton and S. P. Daiger (2006). "Genomic rearrangements of the PRPF31 gene account for 2.5% of autosomal dominant retinitis pigmentosa." Invest Ophthalmol Vis Sci 47: 4579-88.
Sun, Y., S. Koo, N. White, E. Peralta, C. Esau, N. M. Dean and R. J. Perera (2004). "Development of a micro-array to detect human and mouse microRNAs and characterization of expression in human organs." Nucleic Acids Res 32: e188.
Sung, C. H., C. Makino, D. Baylor and J. Nathans (1994). "A rhodopsin gene mutation responsible for autosomal dominant retinitis pigmentosa results in a protein that is defective in localization to the photoreceptor outer segment." J Neurosci 14: 5818-33.
Susin, S. A., H. K. Lorenzo, N. Zamzami, I. Marzo, B. E. Snow, G. M. Brothers, J. Mangion, E. Jacotot, P. Costantini, M. Loeffler, N. Larochette, D. R. Goodlett, R. Aebersold, D. P. Siderovski, J. M. Penninger and G. Kroemer (1999). "Molecular characterization of mitochondrial apoptosis-inducing factor." Nature 397: 441-6.
Suzuki, T., F. Sakurai, S. Nakamura, E. Kouyama, K. Kawabata, M. Kondoh, K. Yagi and H. Mizuguchi (2008). "miR-122a-regulated expression of a suicide gene prevents hepatotoxicity without altering antitumor effects in suicide gene therapy." Mol Ther 16: 1719-26.

Tabata, H. and K. Nakajima (2001). "Efficient in utero gene transfer system to the developing mouse brain using electroporation: visualization of neuronal migration in the developing cortex." Neuroscience 103: 865-72.

Taganov, K. D., M. P. Boldin, K. J. Chang and D. Baltimore (2006). "NF-kappaB-dependent induction of microRNA miR-146, an inhibitor targeted to signaling proteins of innate immune responses." Proc Natl Acad Sci U S A 103: 12481-6.

Tahbaz, N., F. A. Kolb, H. Zhang, K. Jaronczyk, W. Filipowicz and T. C. Hobman (2004). "Characterization of the interactions between mammalian PAZ PIWI domain proteins and Dicer." EMBO Rep 5: 189-94.

Takahashi, M., H. Miyoshi, I. M. Verma and F. H. Gage (1999). "Rescue from photoreceptor degeneration in the rd mouse by human immunodeficiency virus vector-mediated gene transfer." J Virol 73: 7812-6.

Tam, L. C., A. S. Kiang, A. Kennan, P. F. Kenna, N. Chadderton, M. Ader, A. Palfi, A. Aherne, C. Ayuso, M. Campbell, A. Reynolds, A. McKee, M. M. Humphries, G. J. Farrar and P. Humphries (2008). "Therapeutic benefit derived from RNAi-mediated ablation of IMPDH1 transcripts in a murine model of autosomal dominant retinitis pigmentosa (RP10)." Hum Mol Genet 17: 2084-100.

Tam, W. (2001). "Identification and characterization of human BIC, a gene on chromosome 21 that encodes a noncoding RNA." Gene 274: 157-67.

Tan, Z., G. Randall, J. Fan, B. Camoretti-Mercado, R. Brockman-Schneider, L. Pan, J. Solway, J. E. Gern, R. F. Lemanske, D. Nicolae and C. Ober (2007). "Allele-specific targeting of microRNAs to HLA-G and risk of asthma." Am J Hum Genet 81: 829-34.

Tang, G. (2005). "siRNA and miRNA: an insight into RISCs." Trends Biochem Sci 30: 106-14.

Thanos, C. and D. Emerich (2005). "Delivery of neurotrophic factors and therapeutic proteins for retinal diseases." Expert Opin Biol Ther 5: 1443-52.

Thomson, J. M., M. Newman, J. S. Parker, E. M. Morin-Kensicki, T. Wright and S. M. Hammond (2006). "Extensive post-transcriptional regulation of microRNAs and its implications for cancer." Genes Dev 20: 2202-7.

Thornberry, N. A. (1998). "Caspases: key mediators of apoptosis." Chem Biol 5: R97-103.

Tijsterman, M. and R. H. Plasterk (2004). "Dicers at RISC; the mechanism of RNAi." Cell 117: 1-3.

Tokumaru, S., M. Suzuki, H. Yamada, M. Nagino and T. Takahashi (2008). "let-7 regulates Dicer expression and constitutes a negative feedback loop." Carcinogenesis.

Tomita, K., S. Nakanishi, F. Guillemot and R. Kageyama (1996). "Mash1 promotes neuronal differentiation in the retina." Genes Cells 1: 765-74.

Tsonis, P. A., M. Madhavan, E. E. Tancous and K. Del Rio-Tsonis (2004). "A newt's eye view of lens regeneration." Int J Dev Biol 48: 975-80.

Turnbull, A. P., D. Kummel, B. Prinz, C. Holz, J. Schultchen, C. Lang, F. H. Niesen, K. P. Hofmann, H. Delbruck, J. Behlke, E. C. Muller, E. Jarosch, T. Sommer and U. Heinemann (2005). "Structure of palmitoylated BET3: insights into TRAPP complex assembly and membrane localization." EMBO J 24: 875-84.

Valencia-Sanchez, M. A., J. Liu, G. J. Hannon and R. Parker (2006). "Control of translation and mRNA degradation by miRNAs and siRNAs." Genes Dev 20: 515-24.

van Rooij, E., L. B. Sutherland, N. Liu, A. H. Williams, J. McAnally, R. D. Gerard, J. A. Richardson and E. N. Olson (2006). "A signature pattern of stress-responsive

microRNAs that can evoke cardiac hypertrophy and heart failure." Proc Natl Acad Sci U S A 103: 18255-60.
Vasudevan, S., Y. Tong and J. A. Steitz (2007). "Switching from repression to activation: microRNAs can up-regulate translation." Science 318: 1931-4.
Vella, M. C., E. Y. Choi, S. Y. Lin, K. Reinert and F. J. Slack (2004). "The C. elegans microRNA let-7 binds to imperfect let-7 complementary sites from the lin-41 3'UTR." Genes Dev 18: 132-7.
Vester, B. and J. Wengel (2004). "LNA (locked nucleic acid): high-affinity targeting of complementary RNA and DNA." Biochemistry 43: 13233-41.
Vithana, E. N., L. Abu-Safieh, M. J. Allen, A. Carey, M. Papaioannou, C. Chakarova, M. Al-Maghtheh, N. D. Ebenezer, C. Willis, A. T. Moore, A. C. Bird, D. M. Hunt and S. S. Bhattacharya (2001). "A human homolog of yeast pre-mRNA splicing gene, PRP31, underlies autosomal dominant retinitis pigmentosa on chromosome 19q13.4 (RP11)." Mol Cell 8: 375-81.
Volinia, S., G. A. Calin, C. G. Liu, S. Ambs, A. Cimmino, F. Petrocca, R. Visone, M. Iorio, C. Roldo, M. Ferracin, R. L. Prueitt, N. Yanaihara, G. Lanza, A. Scarpa, A. Vecchione, M. Negrini, C. C. Harris and C. M. Croce (2006). "A microRNA expression signature of human solid tumors defines cancer gene targets." Proc Natl Acad Sci U S A 103: 2257-61.
Wagner, K. D., N. Wagner, H. Ghanbarian, V. Grandjean, P. Gounon, F. Cuzin and M. Rassoulzadegan (2008). "RNA induction and inheritance of epigenetic cardiac hypertrophy in the mouse." Dev Cell 14: 962-9.
Weber, B., C. Stresemann, B. Brueckner and F. Lyko (2007). "Methylation of human microRNA genes in normal and neoplastic cells." Cell Cycle 6: 1001-5.
Weleber, R. G. and K. Gregory-Evans (2001). Retinitis pigmentosa and allied disorders. In Retina. S. J. Ryan. St Louis, Missouri, USA Mosby, Inc: 362-460.
Weston, M. D., M. L. Pierce, S. Rocha-Sanchez, K. W. Beisel and G. A. Soukup (2006). "MicroRNA gene expression in the mouse inner ear." Brain Res 1111: 95-104.
Wienholds, E., W. P. Kloosterman, E. Miska, E. Alvarez-Saavedra, E. Berezikov, E. de Bruijn, H. R. Horvitz, S. Kauppinen and R. H. Plasterk (2005). "MicroRNA expression in zebrafish embryonic development." Science 309: 310-1.
Wienholds, E., M. J. Koudijs, F. J. van Eeden, E. Cuppen and R. H. Plasterk (2003). "The microRNA-producing enzyme Dicer1 is essential for zebrafish development." Nat Genet 35: 217-8.
Wienholds, E. and R. H. Plasterk (2005). "MicroRNA function in animal development." FEBS Lett 579: 5911-22.
Wightman, B., I. Ha and G. Ruvkun (1993). "Posttranscriptional regulation of the heterochronic gene lin-14 by lin-4 mediates temporal pattern formation in C. elegans." Cell 75: 855-62.
Wilson, J. H. and T. G. Wensel (2003). "The nature of dominant mutations of rhodopsin and implications for gene therapy." Mol Neurobiol 28: 149-58.
Winderickx, J., C. Delay, A. De Vos, H. Klinger, K. Pellens, T. Vanhelmont, F. Van Leuven and P. Zabrocki (2008). "Protein folding diseases and neurodegeneration: lessons learned from yeast." Biochim Biophys Acta 1783: 1381-95.
Winstanley, J. (2001). "Dr. William Briggs: ophthalmic physician at St. Thomas' Hospital, London." Surv Ophthalmol 46: 81-8.
Wistow, G. (2002). "A project for ocular bioinformatics: NEIBank." Mol Vis 8: 161-3.
Wistow, G., K. Peterson, J. Gao, P. Buchoff, C. Jaworski, C. Bowes-Rickman, J. N. Ebright, M. A. Hauser and D. Hoover (2008). "NEIBank: genomics and bioinformatics resources for vision research." Mol Vis 14: 1327-37.
Wolfensohn, S. and M. Lloyd (2003). Handbook of laboratory animal management and welfare. Oxford, U.K. ; Ames, Iowa, Blackwell Pub.

Wu, H., J. R. Neilson, P. Kumar, M. Manocha, P. Shankar, P. A. Sharp and N. Manjunath (2007). "miRNA Profiling of Naive, Effector and Memory CD8 T Cells." PLoS ONE 2: e1020.

Wu, L., J. Fan and J. G. Belasco (2006). "MicroRNAs direct rapid deadenylation of mRNA." Proc Natl Acad Sci U S A 103: 4034-9.

Xu, C., Y. Lu, Z. Pan, W. Chu, X. Luo, H. Lin, J. Xiao, H. Shan, Z. Wang and B. Yang (2007). "The muscle-specific microRNAs miR-1 and miR-133 produce opposing effects on apoptosis by targeting HSP60, HSP70 and caspase-9 in cardiomyocytes." J Cell Sci 120: 3045-52.

Xu, P., S. Y. Vernooy, M. Guo and B. A. Hay (2003). "The Drosophila microRNA Mir-14 suppresses cell death and is required for normal fat metabolism." Curr Biol 13: 790-5.

Xu, S., P. D. Witmer, S. Lumayag, B. Kovacs and D. Valle (2007). "MicroRNA (miRNA) Transcriptome of Mouse Retina and Identification of a Sensory Organ-specific miRNA Cluster." J Biol Chem 282: 25053-25066.

Yang, B., Y. Lu and Z. Wang (2008). "Control of cardiac excitability by microRNAs." Cardiovasc Res 79: 571-80.

Yang, G. S., M. Schmidt, Z. Yan, J. D. Lindbloom, T. C. Harding, B. A. Donahue, J. F. Engelhardt, R. Kotin and B. L. Davidson (2002). "Virus-mediated transduction of murine retina with adeno-associated virus: effects of viral capsid and genome size." J Virol 76: 7651-60.

Yang, H., K. M. Standifer and D. M. Sherry (2002). "Synaptic protein expression by regenerating adult photoreceptors." J Comp Neurol 443: 275-88.

Yang, L. P., L. M. Wu, X. J. Guo and M. O. Tso (2007). "Activation of endoplasmic reticulum stress in degenerating photoreceptors of the rd1 mouse." Invest Ophthalmol Vis Sci 48: 5191-8.

Yang, Y. H., S. Dudoit, P. Luu, D. M. Lin, V. Peng, J. Ngai and T. P. Speed (2002). "Normalization for cDNA microarray data: a robust composite method addressing single and multiple slide systematic variation." Nucleic Acids Res 30: e15.

Yeung, M. L., Y. Bennasser, T. G. Myers, G. Jiang, M. Benkirane and K. T. Jeang (2005). "Changes in microRNA expression profiles in HIV-1-transfected human cells." Retrovirology 2: 81.

Ylosmaki, E., T. Hakkarainen, A. Hemminki, T. Visakorpi, R. Andino and K. Saksela (2008). "Generation of a conditionally replicating adenovirus based on targeted destruction of E1A mRNA by a cell type-specific microRNA." J Virol.

Yoon, K. J., B. K. Koo, S. K. Im, H. W. Jeong, J. Ghim, M. C. Kwon, J. S. Moon, T. Miyata and Y. Y. Kong (2008). "Mind bomb 1-expressing intermediate progenitors generate notch signaling to maintain radial glial cells." Neuron 58: 519-31.

Yu, J. Y., K. H. Chung, M. Deo, R. C. Thompson and D. L. Turner (2008). "MicroRNA miR-124 regulates neurite outgrowth during neuronal differentiation." Exp Cell Res 314: 2618-33.

Yu, S. L., H. Y. Chen, G. C. Chang, C. Y. Chen, H. W. Chen, S. Singh, C. L. Cheng, C. J. Yu, Y. C. Lee, H. S. Chen, T. J. Su, C. C. Chiang, H. N. Li, Q. S. Hong, H. Y. Su, C. C. Chen, W. J. Chen, C. C. Liu, W. K. Chan, K. C. Li, J. J. Chen and P. C. Yang (2008). "MicroRNA signature predicts survival and relapse in lung cancer." Cancer Cell 13: 48-57.

Yuan, J. and B. A. Yankner (2000). "Apoptosis in the nervous system." Nature 407: 802-9.

Yuan, L., M. Kawada, N. Havlioglu, H. Tang and J. Y. Wu (2005). "Mutations in PRPF31 inhibit pre-mRNA splicing of rhodopsin gene and cause apoptosis of retinal cells." J Neurosci 25: 748-57.

Zeng, Y. (2006). "Principles of micro-RNA production and maturation." Oncogene 25: 6156-62.
Zeng, Y. and B. R. Cullen (2004). "Structural requirements for pre-microRNA binding and nuclear export by Exportin 5." Nucleic Acids Res 32: 4776-85.
Zeng, Y. and B. R. Cullen (2005). "Efficient processing of primary microRNA hairpins by Drosha requires flanking nonstructured RNA sequences." J Biol Chem 280: 27595-603.
Zeng, Y., E. J. Wagner and B. R. Cullen (2002). "Both natural and designed micro RNAs can inhibit the expression of cognate mRNAs when expressed in human cells." Mol Cell 9: 1327-33.
Zeng, Y., R. Yi and B. R. Cullen (2005). "Recognition and cleavage of primary microRNA precursors by the nuclear processing enzyme Drosha." Embo J 24: 138-48.
Zhang, B., X. Pan, G. P. Cobb and T. A. Anderson (2007). "microRNAs as oncogenes and tumor suppressors." Dev Biol 302: 1-12.
Zhang, H., F. A. Kolb, V. Brondani, E. Billy and W. Filipowicz (2002). "Human Dicer preferentially cleaves dsRNAs at their termini without a requirement for ATP." Embo J 21: 5875-85.
Zhao, Y., E. Samal and D. Srivastava (2005). "Serum response factor regulates a muscle-specific microRNA that targets Hand2 during cardiogenesis." Nature 436: 214-20.
Zhou, X., J. Ruan, G. Wang and W. Zhang (2007). "Characterization and identification of microRNA core promoters in four model species." PLoS Comput Biol 3: e37.

Appendices

Appendix I

A.1.1. Primer Sequences:

PTK9 Forward Primer:	5′- TGTTGGAGGACAAACAACCA
PTK9 Reverse Primer:	5′- TCTGGAGACCATGCAATGAA
RHO Forward Primer:	5′- CTGGTCCAGGTAATGGCACT
RHO Reverse Primer:	5′- CCAGCCCTTGTAGCAACATT
18S Forward Primer:	5′- CAAGAACGAAAGTCGGAGGT
18S Reverse Primer:	5′- CGGGTCATGGGAATAACG
EmGFP Forward Primer:	5′- TCCCAAGCTGGCTAGTTAAG
EmGFP Reverse Primer:	5′- CTCTAGATCAACCACTTTGT

A.1.2. pcDNA6.2-EmGFP Construct

A.1.2.1. pcDNA6.2-EmGFP-miR expression construct sequence:

GTTGACATTGATTATTGACTAGTTATTAATAGTAATCAATTACGGGGTCATTAGTTCATAGCCCATATAT
GGAGTTCCGCGTTACATAACTTACGGTAAATGGCCCGCCTGGCTGACCGCCCAACGACCCCCGCCCATTG
ACGTCAATAATGACGTATGTTCCCATAGTAACGCCAATAGGGACTTTCCATTGACGTCAATGGGTGGAGT
ATTTACGGTAAACTGCCCACTTGGCAGTACATCAAGTGTATCATATGCCAAGTACGCCCCCTATTGACGT
CAATGACGGTAAATGGCCCGCCTGGCATTATGCCCAGTACATGACCTTATGGGACTTTCCTACTTGGCAG
TACATCTACGTATTAGTCATCGCTATTACCATGGTGATGCGGTTTTGGCAGTACATCAATGGGCGTGGAT
AGCGGTTTGACTCACGGGGATTTCCAAGTCTCCACCCCATTGACGTCAATGGGAGTTTGTTTTGGCACCA
AAATCAACGGGACTTTCCAAAATGTCGTAACAACTCCGCCCCATTGACGCAAATGGGCGGTAGGCGTGTA
CGGTGGGAGGTCTATATAAGCAGAGCTCTCTGGCTAACTAGAGAACCCACTGCTTACTGGCTTATCGAAA
TTAATACGACTCACTATAGGGAGTCCCAAGCTGGCTAGTTAAGCTATCAACAAGTTTGTACAAAAAAGCA
GGCTTTAAAACCATGGTGAGCAAGGGCGAGGAGCTGTTCACCGGGGTGGTGCCCATCCTGGTCGAGCTGG
ACGGCGACGTAAACGGCCACAAGTTCAGCGTGTCCGGCGAGGGCGAGGGCGATGCCACCTACGGCAAGCT
GACCCTGAAGTTCATCTGCACCACCGGCAAGCTGCCCGTGCCCTGGCCCACCCTCGTGACCACCTTCACC
TACGGCGTGCAGTGCTTCGCCCGCTACCCCGACCACATGAAGCAGCACGACTTCTTCAAGTCCGCCATGC
CCGAAGGCTACGTCCAGGAGCGCACCATCTTCTTCAAGGACGACGGCAACTACAAGACCCGCGCCGAGGT
GAAGTTCGAGGGCGACACCCTGGTGAACCGCATCGAGCTGAAGGGCATCGACTTCAAGGAGGACGGCAAC
ATCCTGGGGCACAAGCTGGAGTACAACTACAACAGCCACAAGGTCTATATCACCGCCGACAAGCAGAAGA
ACGGCATCAAGGTGAACTTCAAGACCCGCCACAACATCGAGGACGGCAGCGTGCAGCTCGCCGACCACTA
CCAGCAGAACACCCCCATCGGCGACGGCCCCGTGCTGCTGCCCGACAACCACTACCTGAGCACCCAGTCC
GCCCTGAGCAAAGACCCCAACGAGAAGCGCGATCACATGGTCCTGCTGGAGTTCGTGACCGCCGCCGGGA
TCACTCTCGGCATGGACGAGCTGTACAAGTAAGCTAAGCACTTCGTGGCCGTCGATCGTTTAAAGGGAGG
TAGTGAGTCGACCAGTGGATCCTGGAGGCTTGCTGAAGGCTGTATGCTTGAGACCAAAAAAAAGGTCTCA
CAGGACACAAGGCCTGTTACTAGCACTCACATGGAACAAATGGCCCAGATCTGGCCGCACTCGAGATATC
TAGACCCAGCTTTCTTGTACAAAGTGGTTGATCTAGAGGGCCCGCGGTTCGCTGATGGGGGAGGCTAACT
GAAACACGGAAGGAGACAATACCGGAAGGAACCCGCGCTATGACGGCAATAAAAAGACAGAATAAAACGC
ACGGGTGTTGGGTCGTTTGTTCATAAACGCGGGGTTCGGTCCCAGGGCTGGCACTCTGTCGATACCCCAC
CGTGACCCCATTGGGGCCAATACGCCCGCGTTTCTTCCTTTTCCCCACCCCACCCCCCAAGTTCGGGTGA
AGGCCCAGGGCTCGCAGCCAACGTCGGGGCGGCAGGCCCTGCCATAGCATCCCCTATAGTGAGTCGTATT
ACATGGTCATAGCTGTTTCCTGGCAGCTCTGGCCCGTGTCTCAAAATCTCTGATGGATCTGCGCAGCTGG
GGCTCTAGGGGGTATCCCCACGCGCCCTGTAGCGGCGCATTAAGCGCGGCGGGTGTGGTGGTTACGCGCA
GCGTGACCGCTACACTTGCCAGCGCCCTAGCGCCCGCTCCTTTCGCTTTCTTCCCTTCCTTTCTCGCCAC
GTTCGCCGGCTTTCCCCGTCAAGCTCTAAATCGGGGGCTCCCTTTAGGGTTCCGATTTAGTGCTTTACGG
CACCTCGACCCCAAAAAACTTGATTAGGGTGATGGTTCACGTAGTGGGCCATCGCCCTGATAGACGGTTT
TTCGCCCTTTGACGTTGGAGTCCACGTTCTTTAATAGTGGACTCTTGTTCCAAACTGGAACAACACTCAA
CCCTATCTCGGTCTATTCTTTTGATTTATAAGGGATTTTGCCGATTTCGGCCTATTGGTTAAAAAATGAG
CTGATTTAACAAAAATTTAACGCGAATTAATTCTGTGGAATGTGTGTCAGTTAGGGTGTGGAAAGTCCCC
AGGCTCCCCAGCAGGCAGAAGTATGCAAAGCATGCATCTCAATTAGTCAGCAACCAGGTGTGGAAAGTCC
CCAGGCTCCCCAGCAGGCAGAAGTATGCAAAGCATGCATCTCAATTAGTCAGCAACCATAGTCCCGCCCC
TAACTCCGCCCATCCCGCCCCTAACTCCGCCCAGTTCCGCCCATTCTCCGCCCCATGGCTGACTAATTTT
TTTTATTTATGCAGAGGCCGAGGCCGCCTCTGCCTCTGAGCTATTCCAGAAGTAGTGAGGAGGCTTTTTT
GGAGGCCTAGGCTTTTGCAAAAAGCTCCCGGGAGCTTGTATATCCATTTTCGGATCTGATCAGCACGTGT
TGACAATTAATCATCGGCATAGTATATCGGCATAGTATAATACGACAAGGTGAGGAACTAAACCATGGCC
AAGCCTTTGTCTCAAGAAGAATCCACCCTCATTGAAAGAGCAACGGCTACAATCAACAGCATCCCCATCT
CTGAAGACTACAGCGTCGCCAGCGCAGCTCTCTCTAGCGACGGCCGCATCTTCACTGGTGTCAATGTATA
TCATTTTACTGGGGGACCTTGTGCAGAACTCGTGGTGCTGGGCACTGCTGCTGCTGCGGCAGCTGGCAAC
CTGACTTGTATCGTCGCGATCGGAAATGAGAACAGGGGCATCTTGAGCCCCTGCGGACGGTGCCGACAGG
TGCTTCTCGATCTGCATCCTGGGATCAAAGCCATAGTGAAGGACAGTGATGGACAGCCGACGGCAGTTGG
GATTCGTGAATTGCTGCCCTCTGGTTATGTGTGGGAGGGCTAAGCACTTCGTGGCCGAGGAGCAGGACTG
ACACGTGCTACGAGATTTCGATTCCACCGCCGCCTTCTATGAAAGGTTGGGCTTCGGAATCGTTTTCCGG
GACGCCGGCTGGATGATCCTCCAGCGCGGGGATCTCATGCTGGAGTTCTTCGCCCACCCCAACTTGTTTA
TTGCAGCTTATAATGGTTACAAATAAAGCAATAGCATCACAAATTTCACAAATAAAGCATTTTTTTCACT
GCATTCTAGTTGTGGTTTGTCCAAACTCATCAATGTATCTTATCATGTCTGTATACCGTCGCTCTTCCGC
TGCTTCCTCGCTCACTGACTCGCTGCGCTCGGTCGTTCGGCTGCGGCGAGCGGTATCAGCTCACTCAAAG
GCGGTAATACGGTTATCCACAGAATCAGGGGATAACGCAGGAAAGAACATGTGAGCAAAAGGCCAGCAAA
AGGCCAGGAACCGTAAAAAGGCCGCGTTGCTGGCGTTTTTCCATAGGCTCCGCCCCCCTGACGAGCATCA
CAAAAATCGACGCTCAAGTCAGAGGTGGCGAAACCCGACAGGACTATAAAGATACCAGGCGTTTCCCCCT
GGAAGCTCCCTCGTGCGCTCTCCTGTTCCGACCCTGCCGCTTACCGGATACCTGTCCGCCTTTCTCCCTT
CGGGAAGCGTGGCGCTTTCTCATAGCTCACGCTGTAGGTATCTCAGTTCGGTGTAGGTCGTTCGCTCCAA
GCTGGGCTGTGTGCACGAACCCCCCGTTCAGCCCGACCGCTGCGCCTTATCCGGTAACTATCGTCTTGAG
TCCAACCCGGTAAGACACGACTTATCGCCACTGGCAGCAGCCACTGGTAACAGGATTAGCAGAGCGAGGT
ATGTAGGCGGTGCTACAGAGTT0CTTGAAGTGGTGGCCTAACTACGGCTACACTAGAAGAACAGTATTTG
GTATCTGCGCTCTGCTGAAGCCAGTTACCTTCGGAAAAAGAGTTGGTAGCTCTTGATCCGGCAAACAAAC
CACCGCTGGTAGCGGTGGTTTTTTTGTTTGCAAGCAGCAGATTACGCGCAGAAAAAAAGGATCTCAAGAA

GATCCTTTGATCTTTTCTACGGGGTCTGACGCTCAGTGGAACGACGCGTAACTCACGTTAAGGGATTTTG
GTCATGGGTGGCTCGACGAGGGTTATTTGCCGACTACCTTGGTGATCTCGCCTTTCACGTAGTGGACAAA
TTCTTCCAACTGATCTGCGCGCGAGGCCAAGCGATCTTCTTCTTGTCCAAGATAAGCCTGTCTAGCTTCA
AGTATGACGGGCTGATACTGGGCCGGCAGGCGCTCCATTGCCCAGTCGGCAGCGACATCCTTCGGCGCGA
TTTTGCCGGTTACTGCGCTGTACCAAATGCGGGACAACGTAAGCACTACATTTCGCTCATCGCCAGCCCA
GTCGGGCGGCGAGTTCCATAGCGTTAAGGTTTCATTTAGCGCCTCAAATAGATCCTGTTCAGGAACCGGA
TCAAAGAGTTCCTCCGCCGCTGGACCTACCAAGGCAACGCTATGTTCTCTTGCTTTTGTCAGCAAGATAG
CCAGATCAATGTCGATCGTGGCTGGCTCGAAGATACCTGCAAGAATGTCATTGCGCTGCCATTCTCCAAA
TTGCAGTTCGCGCTTAGCTGGATAACGCCACGGAATGATGTCGTCGTGCACAACAATGGTGACTTCTACA
GCGCGGAGAATCTCGCTCTCTCCAGGGGAAGCCGAAGTTTCCAAAAGGTCGTTGATCAAAGCTCGCCGCG
TTGTTTCATCAAGCCTTACGGTCACCGTAACCAGCAAATCAATATCACTGTGTGGCTTCAGGCCGCCATC
CACTGCGGAGCCGTACAAATGTACGGCCAGCAACGTCGGTTCGAGATGGCGCTCGATGACGCCAACTACC
TCTGATAGTTGAGTCGATACTTCGGCGATCACCGCTTCCCTCATAATGTTTAACTTTGTTTTAGGGCGAC
TGCCCTGCTGCGTAACATCGTTGCTGCTCCATAACATCAAACATCGACCCACGGCGTAACGCGCTTGCTG
CTTGGATGCCCGAGGCATAGACTGTACCCCAAAAAAACAGTCATAACAAGCCATGAAAACCGCCACTGCG
CCGTTACCACCGCTGCGTTCGGTCAAGGTTCTGGACCAGTTGCGTGAGCGCATACGCTACTTGCATTACA
GCTTACGAACCGAACAGGCTTATGTCCACTGGGTTCGTGCCTTCATCCGTTTCCACGGTGTGCGTCACCC
GGCAACCTTGGGTAGCAGCGAAGTCGAGGCATTTCTGTCCTGGCTGGTCTAGAATTGCATGAAGAATCTG
CTTAGGGTTAGGCGTTTTGCGCTGCTTCGCGATGTACGGGCCAGATATACGC

A.1.2.1. pcDNA6.2 Stuffer Sequence:

In the above sequence, the underlined sequence is a stuffer sequence (see below) which was inserted to circularise the plasmid and in addition provide two restriction sites for the restriction enzyme BsaI within this region for linearization of the plasmid for cloning (see section 8.2.3.).

Forward Sequence Insert: 5'- TGCTTGAGACCAAAAAAAAGGTCTCA
Reverse Sequence Insert: 5'- CCTGTGAGACCTTTTTTTTGGTCTCA

A.1.3. Human PTK 9 (Protein tyrosine kinase 9) mRNA transcript sequence:
(TWF1; twinfilin, actin-binding protein, homolog 1)
Ensembl Transcript ID: ENST00000325127

GGGCGGGGCGGCCGCGGGTCGCGGGCGGATGACGCGCCGGGGCCGGCGGAGGAGCAGCCA
CTTCCTGGGGCCGCCGGCCGGGGCCGCTGGCTGCACTCAGCGCCGGAGCCGGGAGCTAGC
GGCCGCCGCCATGTCCCACCAGACCGGCATCCAAGCAAGTGAAGATGTTAAAGAGATCTT
TGCCAGAGCCAGAAATGGAAAGTACAGACTTCTGAAAATATCTATTGAAAATGAGCAACT
TGTGATTGGATCATATAGTCAGCCTTCAGATTCCTGGGATAAGGATTATGATTCCTTTGT
TTTACCCCTGTTGGAGGACAAACAACCATGCTATATATTATTCAGGTTAGATTCTCAGAA
TGCCCAGGGATATGAATGGATATTCATTGCATGGTCTCCAGATCATTCTCATGTTCGTCA
AAAAATGTTGTATGCAGCAACAAGAGCAACTCTGAAGAAGGAATTTGGAGGTGGCCACAT
TAAAGATGAAGTATTTGGAACAGTAAAGGAAGATGTATCATTACATGGATATAAAAAATA
CTTGCTGTCACAATCTTCCCCTGCCCCACTGACTGCAGCTGAGGAAGAACTACGACAGAT
TAAAATCAATGAGGTACAGACTGACGTGGGTGTGGACACTAAGCATCAAACACTACAAGG
AGTAGCATTTCCCATTTCTCGAGAAGCCTTTCAGGCTTTGGAAAAATTGAATAATAGACA
GCTCAACTATGTGCAGTTGGAAATAGATATAAAAAATGAAATTATAATTTTGGCCAACAC
AACAAATACAGAACTGAAAGATTTGCCAAAGAGGATTCCCAAGGATTCAGCTCGTTACCA
TTTCTTTCTGTATAAACATTCCCATGAAGGAGACTATTTAGAGTCCATAGTTTTTATTTA
TTCAATGCCTGGATACACATGCAGTATAAGAGAGCGGATGCTGTATTCTAGCTGCAAGAG
CCGTCTGCTAGAAATTGTAGAAAGACAACTACAAATGGATGTAATTAGAAAGATCGAGAT
AGACAATGGGGATGAGTTGACTGCAGACTTCCTTTATGAAGAAGTACATCCCAAGCAGCA
TGCACACAAGCAAAGTTTTGCAAAACCAAAAGGTCCTGCAGGAAAAAGAGGAATTCGAAG
ACTAATTAGGGGCCCAGCGGAAACTGAAGCTACTACTGATTAAAGTCATCACATTAAACA
TTGTAATACTAGTTTTTTAAAAGTCCAGCTTTTAGTACAGGAGAACTGAAATCATTCCAT
GTTGATATAAAGTAGGGAAAAAAATTGTACTTTTTGGAAAATAGCACTTTTCACTTCTGT
GTGTTTTTAAAATTAATGTTATAGAAGACTCATGATTTCTATTTTTGAGTTAAAGCTAGA
AAAGGGTTCAACATAATGTTTAATTTTGTCACACTGTTTTCATAGCGTTGATTCCACACT
TCAAATACTTCTTAAAATTTTATACAGTTGGGCCAGTTCTAGAAAGTCTGATGTCTCAAA
GGGTAAACTTACTACTTTCTTGTGGGACAGAAAGACCTTAAAATATTCATATTACTTAAT
GAATATGTTAAGGACCAGGCTAGAGTATTTTCTAAGCTGGAAACTTAGTGTGCCTTGGAA
AAGGCCGCAAGTTGCTTACTCCGAGTAGCTGTGCTAGCTCTGTCAGACTGTAGGATCATG
TCTGCAACTTTTAGAAATAGTGCTTTATATTGCAGCAGTCTTTTATATTTGACTTTTTTT
TAATAGCATTAAAATTGCAGATCAGCTCACTCTGAAACTTTAAGGGTACCAGATATTTTC
TATACTGCAGGATTTCTGATGACATTGAAAGACTTTAAACAGCCTTAGTAAATTATCTTT
CTAATGCTCTGTGAGGCCAAACATTTATGTTCAGATTGAAATTTAAATTAATATCATTCA
AAAGGAAACAAAAAATGTTGAGTTTTAAAAATCAGGATTGACTTTTTTCTCCAAAACCAT
ACATTTATGGGCAAATTGTGTTCTTTATCACTTCCGAGCAAATACTCAGATTTAAAATTA
CTTTAAAGTCCTGGTACTTAACAGGCTAACGTAGATAAACACCTTAATAATCTCAGTTAA
TACTGTATTTCAAAACACATTTAACTGTTTTCTAATGCTTTGCATTATCAGTTACAACCT
AGAGAGATTTTGAGCCTCATATTTCTTTGATACTTGAAATAGAGGGAGCTAGAACACTTA
ATGTTTAATCTGTTAAACCTGCTGCAAGAGCCATAACTTTGAGGCATTTTCTAAATGAAC
TGTGGGGATCCAGGATTTGTAATTTCTTGATCTAAACTTTATGCTGCATAAATCACTTAT
CGGAAATGCACATTTCATAGTGTGAAGCACTCATTTCTAAACCTTATTATCTAAGGTAAT
ATATGCACCTTTCAGAAATTTGTGTTCGAGTAAGTAAAGCATATTAGAATAATTGTGGGT
TGACAGATTTTTAAAATAGAATTTAGAGTATTTGGGGTTTTGTTTGTTTACAAATAATCA
GACTATAATATTTAAACATGCAAAATAACTGACAATAATGTTGCACTTGTTTACTAAAGA
TATAAGTTGTTCCATGGGTGTACACGTAGACAGACACACATACACCCAAATTATTGCATT
AAGAATCCTGGAGCAGACCATAGCTGAAGCTGTTATTTTCAGTCAGGAAGACTACCTGTC
ATGAAGGTATAAAATAATTTAGAAGTGAATGTTTTTCTGTACCATCTATGTGCAATTATA
CTCTAAATTCCACTACACTACATTAAAGTAAATGGACATTCCAGAATATAGATGTGATTA
TAGTCTTAAACTAATTATTATTAAACCAATGATTGCTGAAAATCAGTGATGCATTTGTTA
TAGAGTATAACTCATCGTTTACAGTATGTTTTAGTTGGCAGTATCATACCTAGATGGTGA
ATAACATATTCCCAGTAAATTTATATAGCAGTGAAGAATTACATGCCTTCTGGTGGACAT
TTTATAAGTGCATTTTATATCACAATAAAAATTTTTTCTCTTT